VOLUME 107 PART C NUMBER 12 SEPTEMBER 1960

The Proceedings

OF

THE INSTITUTION OF ELECTRICAL ENGINEERS

FOUNDED 1871: INCORPORATED BY ROYAL CHARTER 1921

PART C

MONOGRAPHS Nos. 354–386

SAVOY PLACE · LONDON W.C.2

Price Fifteen Shillings

The Institution of Electrical Engineers

FOUNDED 1871
INCORPORATED BY ROYAL CHARTER 1921

PATRON: HER MAJESTY THE QUEEN

COUNCIL 1959–1960

President

SIR WILLIS JACKSON, D.Sc., F.R.S.

Past-Presidents

W. H. ECCLES, D.Sc., F.R.S.
THE RT. HON. THE EARL OF MOUNT EDGCUMBE, T.D.
J. M. DONALDSON, M.C.
PROF. E. W. MARCHANT, D.Sc.
H. T. YOUNG.
SIR GEORGE LEE, O.B.E., M.C.
SIR ARTHUR P. M. FLEMING, C.B.E., D.Eng., LL.D.
J. R. BEARD, C.B.E., M.Sc.
SIR NOEL ASHBRIDGE, B.Sc.(Eng.).
SIR HARRY RAILING, D.Eng.
P. DUNSHEATH, C.B.E., M.A., D.Sc.(Eng.), LL.D.
SIR VINCENT Z. DE FERRANTI, M.C.
T. G. N. HALDANE, M.A.
PROF. E. B. MOULLIN, M.A., Sc.D., LL.D.
SIR ARCHIBALD J. GILL, B.Sc.(Eng.).
SIR JOHN HACKING.
COL. B. H. LEESON, C.B.E., T.D.
SIR HAROLD BISHOP, C.B.E., B.Sc.(Eng.), F.C.G.I.
SIR JOSIAH ECCLES, C.B.E., D.Sc.
THE RT. HON. THE LORD NELSON OF STAFFORD.
SIR GORDON RADLEY, K.C.B., C.B.E., Ph.D.(Eng.).
S. E. GOODALL, M.Sc.(Eng.), F.Q.M.C.

Vice-Presidents

O. W. HUMPHREYS, C.B.E., B.Sc.
G. S. C. LUCAS, O.B.E., F.C.G.I.
SIR HAMISH D. MACLAREN, K.B.E., C.B., D.F.C.,* LL.D., B.Sc.
C. T. MELLING, C.B.E., M.Sc.Tech.
A. H. MUMFORD, O.B.E., B.Sc.(Eng.).

Honorary Treasurer

E. LEETE.

Ordinary Members of Council

PROF. H. E. M. BARLOW, Ph.D., B.Sc.(Eng.).
C. O. BOYSE, B.Sc.(Eng.).
PROF. M. W. HUMPHREY DAVIES, M.Sc.
SIR JOHN DEAN, B.Sc.
L. DRUCQUER.
J. M. FERGUSON, B.Sc.(Eng.).
D. C. FLACK, B.Sc.(Eng.), Ph.D.
J. S. FORREST, D.Sc., M.A.
R. J. HALSEY, C.M.G., B.Sc.(Eng.), F.C.G.I.
J. B. HIGHAM, Ph.D., B.Sc.
R. A. HORE, M.A., B.Sc.
F. C. MCLEAN, C.B.E., B.Sc.
B. L. METCALF, B.Sc.(Eng.).
J. R. MORTLOCK, Ph.D., B.Sc.(Eng.).
THE HON. H. G. NELSON, M.A.
R. H. PHILLIPS, T.D.
H. V. PUGH.
J. R. RYLANDS, M.Sc., J.P.
G. A. V. SOWTER, Ph.D., B.Sc.(Eng.).
C. E. STRONG, O.B.E., B.A., B.A.I.
D. H. TOMPSETT, B.Sc.(Eng.).

Chairmen and Past-Chairmen of Sections

Electronics and Communications:
M. J. L. PULLING, C.B.E., M.A.
†G. MILLINGTON, M.A., B.Sc.

Measurement and Control:
PROF. A. TUSTIN, M.Sc.
†J. K. WEBB, M.Sc.(Eng.), B.Sc.Tech.

Supply:
J. R. MORTLOCK, Ph.D., B.Sc.(Eng.).
†D. P. SAYERS, B.Sc.

Utilization:
T. E. HOUGHTON, M.Eng.
†R. A. MARRYAT, B.Sc.(Eng.).

Chairmen and Past-Chairmen of Local Centres

East Midland Centre:
D. H. PARRY, B.Sc.
†D. E. LAMBERT, B.Sc.(Eng.).

Mersey and North Wales Centre:
†T. A. P. COLLEDGE, B.Sc.(Eng.).
J. COLLINS.

North Midland Centre:
PROF. G. W. CARTER, M.A.
†J. D. NICHOLSON, B.Sc.

North-Eastern Centre:
H. WATSON-JONES, M.Eng.
†A. T. CRAWFORD, B.Sc.

North-Western Centre:
F. J. HUTCHINSON, M.Eng.
†PROF. F. C. WILLIAMS, O.B.E., D.Sc., D.Phil., F.R.S.

Northern Ireland Centre:
T. S. WYLIE.
†D. S. MCILLHAGGER, Ph.D., M.Sc.

Western Centre:
H. JACKSON, B.Sc.(Eng.).
†R. W. STEEL.

Scottish Centre:
J. A. AKED, M.B.E.
†R. J. RENNIE, B.Sc.

South Midland Centre:
G. F. PEIRSON.
†L. L. TOLLEY, B.Sc.(Eng.).

Southern Centre:
W. D. MALLINSON, B.Sc.(Eng.).
†G. BISHOP, B.Sc.

† Past Chairman.

Secretary

W. K. BRASHER, C.B.E., M.A., M.I.E.E.

Deputy Secretary

F. JERVIS SMITH, M.I.E.E.

Principal Assistant Secretary

F. C. HARRIS.

Editor-in-Chief

G. E. WILLIAMS, B.Sc.(Eng.), M.I.E.E.

The Institution is not, as a body, responsible for the opinions expressed by individual authors or speakers.
An example of the preferred form of bibliographical references will be found beneath the list of contents.

THE PROCEEDINGS OF
THE INSTITUTION OF ELECTRICAL ENGINEERS

EDITED UNDER THE SUPERINTENDENCE OF W. K. BRASHER, C.B.E., M.A., M.I.E.E., SECRETARY

VOL. 107. PART C. NO. 12. SEPTEMBER 1960

621.313.1

The Institution of Electrical Engineers
Monograph No. 354 U
Feb. 1960
©

LIFE EXPECTANCY OF ELECTRICAL MACHINES WITH VARIABLE LOADS

By JOSEPH BEN URI, Dr.Ing., Associate Member.

(*The paper was first received 20th May, and in revised form 8th August*, 1959. *It was published as an* INSTITUTION MONOGRAPH *in February*, 1960.)

SUMMARY

Modern economics demand a reduction in costs and prices, and this usually means reduction in the amount of materials used. The danger is that some of the insulation materials in use have a cellulose base, which means that their ageing may be endangered if the temperature is higher than the 110°C, since, above this temperature, the cellulose materials tend to change quickly their consistency and mechanical strength.

It has been generally agreed that the life expectancy of electrical machines should be seven years when continuously under rated load. General equations for change in life expectancy with temperature have been experimentally and partly deductively found and presented by Montsinger and Bussing, and experiments show that the equations are correct for continuous loads. But when the load changes the heating and cooling periods must be taken into consideration. Short-circuits or heavy overloads can be very dangerous.

Equations have been developed for load changes and for straight-line and exponential temperature changes, and it is shown that the cooling-off period especially can be very dangerous and take a very appreciable part of the life expectancy of the electrical equipment in question. Sample calculations on transformer and intermittent motor loads are included.

LIST OF SYMBOLS

A and k = Constants [see eqn. (1*c*)].
B = Constant [see eqn. (2)].
C = Constant [see eqn. (11)].
C_0 = Constant [see eqn. (12)].
D_1 = Variable factor [see eqn. (11*a*)].
D_2 = Variable factor [see eqn. (12*a*)].
h = Constant [see eqn. (16)].
T = Temperature, deg K.
T_0 = Ambient or lowest steady-state temperature under load, deg K.
T_f = Final steady-state temperature under load increase, deg K.
L = Life expectancy for temperature.
L_0 = Life expectancy for temperature θ_0.
$N = B/378$ = Constant [see eqn. (3*c*)].
p = Percentage ageing factor [see eqn. (3)].
t = Time, sec.
τ = Thermal time-constant of the machine.
θ = Temperature, deg C.
θ_0 = Ambient or lowest steady-state temperature under load, deg C.
θ_f = Final steady-state temperature under load increase, deg C.
$\Delta\theta$ = Temperature rise, i.e. $(\theta_2 - \theta_1)$, or temperature difference between two specific temperatures under consideration, deg C or deg K.
$v = 378/T$, which is a variable [see eqn. (3*c*)].
$\alpha = t/\tau$, relative time factor.

(1) INTRODUCTION

The latest developments in insulation materials for electrical machines make it possible to increase the maximum temperature and tend, therefore, to reduce the amount of material (copper and iron) used. This question is very important from the economic point of view, but it is not advisable to increase the maximum temperature too much and to reduce the amount of the materials used in such a way that the normal life expectancy of the equipment may suffer.

All metal parts used in electrical machines, whether iron or copper, will withstand quite high temperatures; the most vulnerable part of the equipment is the insulation material. The actual changes that take place in the insulation material during the heating periods of electrical equipment are still under study by chemists, physicists and machine engineers. In order to obtain smooth temperature distribution within the machine and as few 'hot spots' as possible the effective cooling of electrical equipment is of great importance, as is the proper construction and the general layout. Such hot spots tend locally to change the chemical structure of the insulation material, and it is there that we obtain the first sparking and damage to the material itself. There are two factors of great importance which tend to change the chemical consistency of the insulation material—first, the temperature of the hot spots and, secondly, the times of heating

Correspondence on Monographs is invited for consideration with a view to publication.
Dr. Ben Uri is at the Israel Institute of Technology, Israel, and is, at present, visiting Associate Professor, Carnegie Institute of Technology, Pittsburgh, Pennsylvania, U.S.A.

© 1960: The Institution of Electrical Engineers

and cooling. We shall see that the cooling period may be the more dangerous. It is therefore of great importance to provide adequate construction and design, in order to avoid hot spots and to shorten the cooling time.

Both the above-mentioned factors tend to influence the ageing of the insulation material and thereby limit the life expectancy of the electrical machine in question. Many papers have been published on the subject, and many different insulation materials have been tested under varying conditions. It is obvious that, by permitting higher temperatures in the copper windings and the iron, we reduce the price of the equipment, but we endanger the insulation material and shorten its life expectancy. It has been agreed and accepted that, on the average, the life expectancy of any electrical machine should be seven years at continuous full rated load.

Since the beginning of the present century formulae have been found, based mostly on experimental data, which enable us to calculate the life expectancy of electrical machines. This work was crowned by Montsinger[10] in his law, which expresses the generally accepted view proved experimentally that increasing or decreasing the temperature above or below the normal by $\Delta\theta = 8°\,C$ will halve or double the life expectancy of the machine. This means that for synthetic-enamel-covered wire, where the maximum permissible temperature is $\theta_{max} = 105°C$, the life expectancy will change: thus

$$L = L_{105}2^{(105-\theta)/\Delta\theta} \quad . \quad . \quad . \quad . \quad . \quad (1a)$$

According to the generally accepted rule $L_{105} = 7$ years and $\Delta\theta = 8°\,C$,

i.e.
$$L_0 = 7 \cdot 2^{(105-\theta)/\Delta\theta} \quad . \quad . \quad . \quad . \quad . \quad (1b)$$

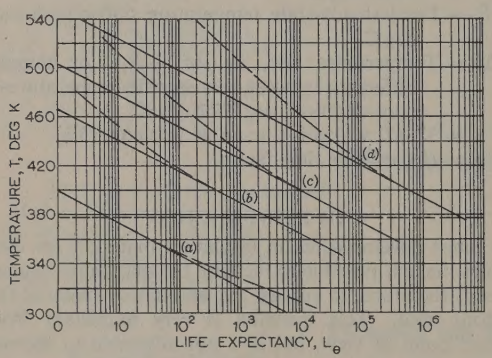

Fig. 1.—Life expectancy as a function of continuous temperature

——— Montsinger equation.
-·-·-·- Bussing equation.

(*a*) In years. (*c*) In days.
(*b*) In months. (*d*) In minutes.

On half-log paper this equation is a straight line, as shown in Fig. 1. We usually transform this equation into an exponential since this is the more familiar form. We then have

$$L_\theta = L_{105}\varepsilon^{A-k\theta} \quad . \quad . \quad . \quad . \quad . \quad (1)$$

from which

$$\left.\begin{aligned} &L_{105} = 7 \text{ years} \\ &A = \frac{\theta_{max}}{\Delta\theta}\log 2 = 9{\cdot}1 \text{ as } \theta_{max} = 105°\,C,\ \Delta\theta = 8°\,C \\ &k = \log 2/\Delta\theta = 0{\cdot}087 \end{aligned}\right\} \quad (1c)$$

Latest tests and theoretical considerations by Stager, Hess and Bussing[5, 6, 14] show that eqn. (1) requires a correction, and the latest generally adopted equation by Bussing is

$$L = L_{378}\varepsilon^{(B/T-B/378)} \quad . \quad . \quad . \quad . \quad . \quad (2$$

where B is 12 500 for synthetic-enamel-covered wire and is a function of the insulating material used. The maximum permissible temperature for the enamel-covered wire is

$$T_{max} = 273 + 105 = 378°\,K$$

The curves of the Bussing equation are also shown as dashed lines in Fig. 1.

The above data were taken from various experiments on synthetic-enamel-covered wire embedded in presspan insulation. B will vary for other insulation materials, but this does not alter the main point of our considerations.

(2) VARIABLE LOADS

Owing to the change in the load with time, the temperature rise of any transformer or electrical machine will also change with time. We are obviously interested in calculating the average life expectancy of the equipment in question, taking into consideration these changing load conditions. Assuming that the standard life expectancy under rated load is seven years, we have to evaluate the percentage factor of the machine under the variable load conditions. This can be defined as

$$p = 100\int_0^t \frac{dt}{L_\theta} \text{ per cent} \quad . \quad . \quad . \quad . \quad (3$$

where L_θ is the life expectancy under the variable load condition during time t. Using eqn. (1) of Reference 10 we can write

$$p = 100\int_0^t \frac{dt}{L_{105}\varepsilon^{A-k\theta}} \text{ per cent} \quad . \quad . \quad . \quad (3$$

which means, for $L_{105} = 7$ years, that

$$p = 14{\cdot}3\int_0^t \varepsilon^{k\theta-A}dt \quad . \quad . \quad . \quad . \quad (3$$

Using the life-expectancy equation of Bussing[14]

$$p = 14{\cdot}3\int_0^t \varepsilon^{N(1-\nu)}dt \quad . \quad . \quad . \quad . \quad (3$$

where $N = B/378 = 33$ for synthetic-enamel-covered wire and $\nu = 378/T$.

In eqns. (3*b*) and (3*c*) the load and also the temperature change with time. It is customary to adopt certain simple modes for such changes, i.e. linear temperature rise or fall of short duration or exponential temperature changes for long time periods. These two temperature-change conditions are the most acceptable, but, as we shall see later, linear changes in load can also be evaluated.

(2.1) Linear Temperature Changes

Let us first assume that, owing to a short-circuit or a very high overload, the temperature of the effected electrical machine will rise steeply during a very short time period. Obviously such a temperature rise will be linear with time, i.e. in eqn. (3*b*),

$$\theta = f(t) = a + bt \quad . \quad . \quad . \quad . \quad . \quad (4$$

where $a = \theta_0$ is the temperature of the machine before the overload and

$$b = (\theta_m - \theta_0)/t_m = \Delta\theta_m/t_m$$

where θ_m is the maximum temperature achieved before cut-off; this is reached at time t_m. It means that the life-expectancy equation will be

$$L_\theta = L_{105}\varepsilon^{A-kf(t)} \quad . \quad . \quad . \quad . \quad . \quad (5a)$$

and the percentage ageing factor is

$$p = 14{\cdot}3\int_0^{t_m} \varepsilon^{k(a+bt)-A}dt \quad . \quad . \quad . \quad . \quad (5b)$$

Evaluating this integral equation, using the Montsinger[10] base eqn. (1), we obtain the percentage ageing factor

$$p = \frac{100}{k\Delta\theta_m} t_m(1/L_{\theta m} - 1/L_{\theta 0}) \quad . \quad . \quad . \quad (5)$$

where $L_{\theta m}$ = Life expectancy for the continuous temperature θ_m.

$L_{\theta 0}$ = Life expectancy for continuous temperature θ_0.

Both of these are taken from Fig. 1.

For higher temperature differences the Bussing equation seems to be more accurate, and using this base eqn. (2) or (3*a*) the percentage ageing factor is

$$p = 14{\cdot}3\int_0^t \varepsilon^{N(1-\nu)}dt$$

where $\nu = 378/T$

and $T = a' + bt$

with $a' = 273 + \theta_0 = T_0 \quad . \quad . \quad . \quad . \quad . \quad . \quad . \quad . \quad . \quad (6)$

$$b = (T_m - T_0)/t_m = (\theta_m - \theta_0)/t_m = \Delta\theta_m/t_m$$

In spite of the fact that it is possible to evaluate such integrals, as we shall see later, the final equation is quite complicated, and we can choose a simpler method by assuming that

$$1 - \nu = 1 - 378/(a' + bt) = 1 - \frac{378/a'}{1 + tb/a'}$$

and $$1 - \nu \simeq 1 - \frac{378}{a}0{\cdot}975\left(1 - 0{\cdot}67\frac{b}{a'}t\right) = c + dt \quad (7)$$

using the well-known assumption that, for small values of $x < 0{\cdot}5$,

$$1/(1 + x) = 0{\cdot}975(1 - 0{\cdot}67x) \quad . \quad . \quad . \quad . \quad (7a)$$

and now

$$c = 1 - 0{\cdot}975\frac{378}{a'} \text{ and } d = 0{\cdot}975 \times 0{\cdot}67 \times \frac{378}{a'} \times \frac{b}{a'} \quad (7b)$$

The above simplification means that

$$N(1 - \nu) = N(c + dt)$$

We can easily evaluate the integral and the percentage ageing factor

$$p = \frac{100a'^2}{8\,100}\frac{t_m}{\Delta\theta_m}(1/L_{\theta m} - 1/L_{\theta 0})$$

$$p = 0{\cdot}0124a'^2\frac{t_m}{\Delta\theta_m}(1/L_{\theta m} - 1/L_{\theta 0}) \quad . \quad . \quad . \quad (8)$$

As an example, an oil-cooled transformer with percentage short-circuit voltage $V_k = 7{\cdot}15\%$ and rated current density, J_n, of $4{\cdot}3\,\text{amp/mm}^2$ is working under full load at a constant temperature of 105° C. A direct short-circuit is cut off after 5·5 sec. The current density rises to $J_m = J_n 100/V_k\% = 60\,\text{amp/mm}^2$, and we can now calculate the maximum temperature rise after 5·5 sec for $J_m^2 t_m = 1{\cdot}88 \times 10^4$ to be $\Delta\theta_m = 158°\,\text{C}$ (see, for example, Fig. 53 of Reference 1), i.e. $\theta_m = 263°\,\text{C}$ and $T_m = 536°\,\text{K}$.

Using eqn. (8), since, for high temperature difference, the Bussing equation seems to be more accurate, we can evaluate the percentage ageing factor, p, as 0·004 2%, which means 2·58 hours of the life of the transformer compared with 5·5 sec, the duration of the short circuit. This was expected since the maximum temperature $\theta_m = 263°\,\text{C}$ was unusually high.

(2.2) Exponential Temperature Changes

It is well known that the temperature transient of electrical machines is an exponential function, the heating equation being

$$\theta = \theta_0 + (\theta_f - \theta_0)(1 - \varepsilon^{-\alpha}) \quad . \quad . \quad . \quad (9)$$

The equation for the cooling period is

$$\theta = \theta_0 + (\theta_m - \theta_0)\varepsilon^{-\alpha} \quad . \quad . \quad . \quad . \quad (10)$$

where θ_m is the temperature at time $t = 0$.

Let us first calculate the percentage ageing factor of the machine for the heating period, which has an exponential temperature rise.

We have to use the Montsinger[10] eqns. (1) and (3*b*) for the variable temperature θ, and eqn. (9), and to evaluate the integral.

This is shown in Section 6.1, and we obtain, as the final equation for the percentage ageing factor,

$$p = 14{\cdot}3\alpha\tau\varepsilon^C D_1 \quad . \quad . \quad . \quad . \quad . \quad (11)$$

where $C = 0{\cdot}087(\theta_f - 105)$

and

$$D_1 = 1 - \frac{a(1 - \varepsilon^{-\alpha})}{\alpha \times 1 \times 1!} + \frac{a^2(1 - \varepsilon^{-2\alpha})}{\alpha \times 2 \times 2!} - \frac{a^3(1 - \varepsilon^{-3\alpha})}{\alpha \times 3 \times 3!} + - \ldots \quad (11a)$$

and $$a = 0{\cdot}087(\theta_f - \theta_0)$$

D_1 can be evaluated since, even for high temperature rises, up to $a = 15{\cdot}0$, and for values of $a^2/nn! < 1{\cdot}0$ the series starts to converge very quickly. The factor D_1 has been calculated for different values of α as shown in Fig. 2.

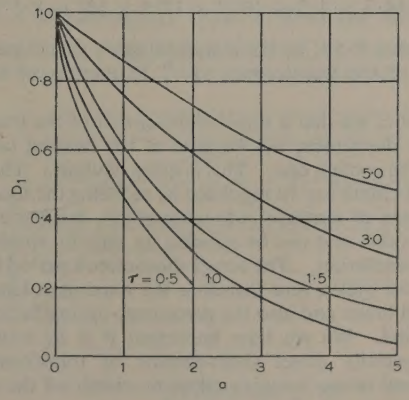

Fig. 2.—Heating-period factor.

The same procedure can be adopted for the cooling period. It now means, from eqns. (10) and (3*b*), that for

$$\theta = \theta_0 + (\theta_m - \theta_0)\varepsilon^{-\alpha}$$

the percentage ageing factor will be (see Section 6.2)

$$p = 14{\cdot}3\alpha\tau\varepsilon^{C_0}D_2 \quad . \quad . \quad . \quad . \quad . \quad (12)$$

where $C_0 = 0{\cdot}087(\theta_0 - 105)$

and

$$D_2 = 1 + \frac{a(1-\varepsilon^{-\alpha})}{\alpha \times 1 \times 1!} + \frac{a^2(1-\varepsilon^{-2\alpha})}{\alpha \times 2 \times 2!} + \frac{a^3(1-\varepsilon^{-3\alpha})}{\alpha \times 3 \times 3!} + \ldots$$

$$. \quad . \quad . \quad . \quad (12a)$$

for $a = 0{\cdot}087(\theta_m - \theta_0)$

The factor D_2 is also convergent and can be evaluated for various values of α, as shown in Figs. 3(*a*) and 3(*b*).

Whenever the temperature changes are 30° C or more it seems advisable to use the Bussing equation as the basis. For this purpose the integrals can be evaluated as shown in Sections 6.3 and 6.4, the final percentage ageing factor for the heating period being

$$p = 14{\cdot}3\alpha\tau\varepsilon^{N(1-378/T_f)}D_1 \quad . \quad . \quad . \quad . \quad (13)$$

where D_1 has to be taken from Fig. 2 for

$$d = a = N\frac{378}{T_f}\frac{\Delta\theta_m}{T_f}$$

For the cooling period the percentage ageing factor is

$$p = 14{\cdot}3\alpha\tau\varepsilon^{N(1-378/T_0)}D_2 \quad . \quad . \quad . \quad . \quad (14)$$

where D_2 is taken from Fig. 3(*a*) or 3(*b*) for

$$d' = a = N\frac{378}{T_0}\frac{\Delta\theta_m}{T_0}$$

Let us now use the above method to calculate the percentage ageing factor for the cooling period in the case of the above-mentioned transformer, assuming that the short-circuit was lifted immediately and the transformer was continuously loaded at the rated value, i.e. $\theta_0 = 105°$ C and $T_0 = 378°$ K. The thermal time-constant of the transformer is $\tau = 5$ min ($=9{\cdot}5 \times 10^{-6}$ years), and we assume that the total cooling has been effected for $\alpha = 5$, i.e. after 25 min. We calculate $d' = 13{\cdot}7$, and from Fig. 3(*a*), $D_2 = 12{\cdot}5 \times 10^3$,

i.e. $p = 14{\cdot}3 \times 9{\cdot}5 \times 10^{-6} \times 12{\cdot}5 \times 10^3 = 8{\cdot}5\%$

and this means 8·5% of the standard seven years' average life expectancy of the transformer, i.e. 7·12 months of its life at rated load.

We therefore see that a direct short-circuit of the transformer can be very dangerous, not because of the heating period but because of the cooling one. This is quite obvious. The heating during short-circuit can be regulated by reducing the short-circuit time by means of sensitive automatic relays, but the cooling is a natural process and can be speeded up only by special design and forced ventilation. The actual short-circuit period is usually limited to 2–3 cycles, and therefore the maximum temperature will be much lower and also the percentage ageing factor for the cooling period. We see how important it is to avoid short-circuits, especially direct short-circuits of transformers and generators and to use sensitive relays to switch off the overload very quickly.

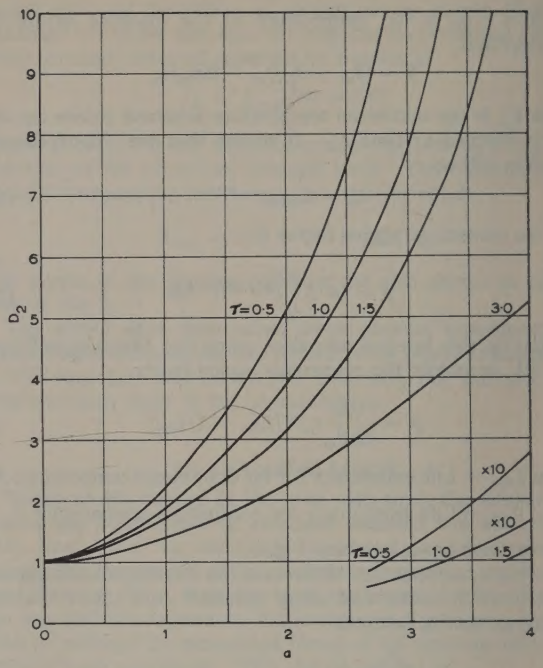

(*a*)

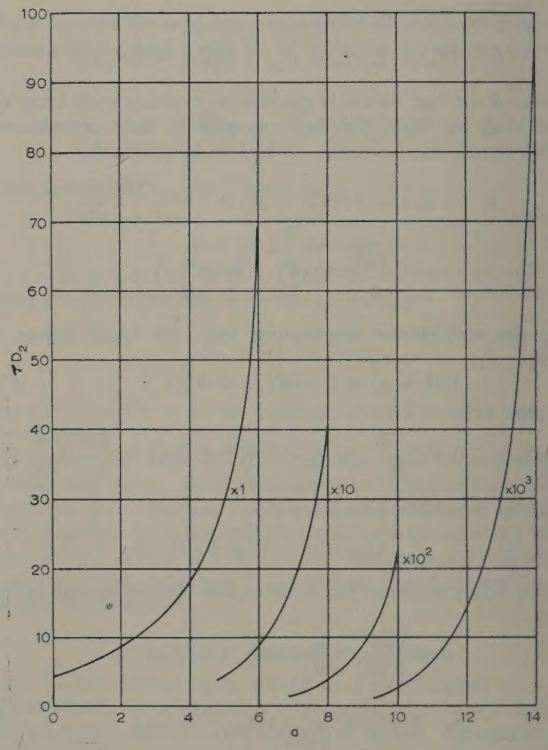

(*b*)

Fig. 3.—Cooling-period factor.

(2.3) Linear Changes of Losses during the Heat-Transient Period

Herczog and Richter[7, 4] developed an equation for the slow temperature rise and cooling when the losses of the machine change linearly with time. The starting point is the standard equation for heat equivalence, used for all heating and cooling of electrical machines:

$$Pdt = A\gamma dt + Cd\theta$$

where P = Losses, watts.
C = Heat capacity of the machine, watt-sec/deg C.
A = Cooling surface, m^2.
γ = Heat transfer factor, watts/deg C-m^2.

Until now we have assumed that, during the time in question, the losses producing the heat effect are constant. Now P is not constant, but changes linearly with time. We have

$$P = P_0 + \frac{P_1 - P_0}{t_m} t \quad . \quad . \quad . \quad . \quad . \quad (15)$$

Fig. 4 shows an average daily load curve of a transformer or generator together with the respective losses of the machine, and

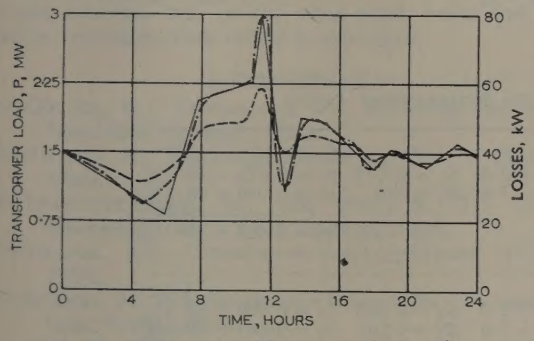

Fig. 4.—Daily load and loss curve of a transformer.
—·— Load curve.
---- Loss curve.

it is shown that, when accuracy is required, it may be of advantage to apply this method, since the difference between the straight lines and the actual curve is very slight.

Evaluating the final temperature difference for P_0 for $t = 0$, we have $\Delta\theta_{0f} = P_0/\gamma A$, and the corresponding final temperature difference for P_1 for $t = t_m$ is $\Delta\theta_{1f} = P_1/\gamma A$. The solution of eqns. (4) and (15) for variable losses during the period is

$$\Delta\theta = \Delta\theta_0\varepsilon^{-\alpha} + (\Delta\theta_{0f} - h)(1 - \varepsilon^{-\alpha}) + h\alpha \quad . \quad (16)$$

where $\alpha = t/\tau$ and $h = (\Delta\theta_{1f} - \Delta\theta_{0f})\tau/t_m$ . . . (16*a*)

Using eqn. (16) as the $\theta = f(t)$ in the Montsinger eqns. (1) and (3*b*) we can evaluate the integral. The actual solution is obtained on the lines shown in Sections 1 and 2. The final equation is

$$p = 14{\cdot}3\tau\alpha\varepsilon^{Ch}\left[\varepsilon^h(1-h) - \frac{a}{h-1}\frac{1-\varepsilon^{(h-1)\alpha}}{\alpha\times 1\times 1!} - \frac{2a^2}{h-2}\frac{1-\varepsilon^{(h-2)}}{\alpha\times 2\times 2!} - \ldots\right] \quad (17)$$

where $C_h = \Delta\theta_{0f} - h - 9{\cdot}1$
and $a = \Delta\theta_0 - \Delta\theta_{0f} + h$ . . . . . (17*a*)

This equation can be used for the temperature rise and the cooling period, but the values of D_1 and D_2 cannot be taken from charts and must be evaluated for each value of $h = (\Delta\theta_{1f} - \Delta\theta_{0f})\tau/t_m$, which differs for each individual case. These elaborate calculations may sometimes be necessary, but they are very lengthy and in most cases the method described in Sections 2.1 and 2.2 will be sufficiently accurate.

(3) CALCULATIONS

(3.1) Life Expectancy of a Transformer with Changing Daily Load

An oil-filled transformer of 1·5 MVA rated size has a daily load curve as shown in Fig. 4, which also gives the loss curve (see Fig. 5) due to the load in question. From transformer data we

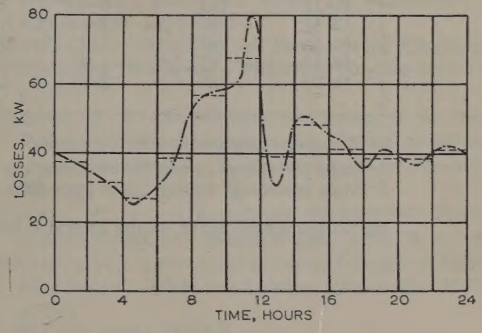

Fig. 5.—Daily loss curve of a transformer.

calculate the thermal time-constant, τ, as 10 min. We divide the load periods into equal 2-hour stretches of constant load and assume that $\tau\alpha = 5\tau = 50$ min each time is the temperature transient period, and during the remaining 70 min the temperature is assumed to be constant. We take for granted that, for $\alpha = t/\tau = 5$, the steady-state temperature has been achieved, and this is always the case. The percentage ageing factor has been calculated for each period (see Table 1), and the total percentage ageing factor during one day is $11{\cdot}385 \times 10^{-3}$ per cent of 7 years, i.e. approximately 7 hours. This means that the life expectancy of the transformer with a daily assumed load distribution will be $7 \times 24/7 = 24$ years.

From the same Table we can calculate the average temperature during the load period of 24 hours, and we find it to be 84° C. From Fig. 1 we see that the life expectancy for this average temperature is 33 years. This shows that the method of average temperature is incorrect, as has already been found by many workers.

(3.2) Intermittent Loads of Electrical Motors

Let us assume some kind of electrical drive with intermittent load, as shown in Fig. 6. We calculate the thermal time-constant

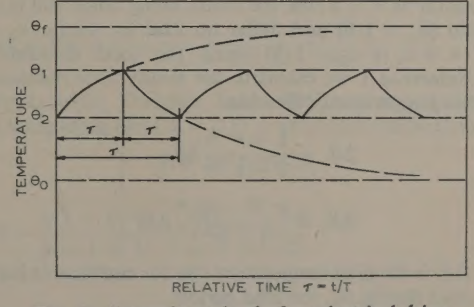

Fig. 6.—Intermittent load of an electrical drive.

Table 1

CALCULATION OF THE PERCENTAGE AGEING FACTOR FOR A TRANSFORMER

The load distribution is as shown in Fig. 5.

Time	θ	C	ε^{α}	a	D_1/D_2	p_1	p_2
hours	°C					$\times 10^{-3}$	$\times 10^{-3}$
20–22	80	−2·17	0·115	0	1·000	0·157	0·218
22–24	83	−1·91	0·150	+0·260	0·946	0·193	0·284
0–2	78	−2·35	0·095	−0·435	1·080	0·140	0·180
2–4	71	−2·95	0·052	−0·610	1·130	0·080	0·100
4–6	66	−3·40	0·033	−0·435	1·080	0·048	0·062
6–8	80	−2·17	0·115	+1·220	0·820	0·129	0·218
8–10	102	−0·26	0·771	+1·910	0·740	0·078	1·470
10–12	113	+0·70	2·014	+0·950	0·853	2·330	3·820
12–14	80	−2·17	0·115	−2·880	2·220	0·347	0·218
14–16	91	−1·22	0·295	+0·780	0·870	0·350	0·560
16–18	83	−1·91	0·150	0·700	1·175	0·240	0·284
18–20	80	−2·17	0·115	−0·260	1·050	0·165	0·218

84° C *average temperature over the cycle.*

Average percentage ageing factor during the transient period of 50 min, p_1 .. .. .. $4{\cdot}257 \times 10^{-3}$
Average percentage ageing factor during the steady-state period of 70 min, p_2 .. .. $7{\cdot}128 \times 10^{-3}$

Percentage ageing factor during 24 hours' load cycle, $p = p_1 + p_2$ .. .. $11{\cdot}385 \times 10^{-3}$

Table 2

CALCULATION OF LIFE EXPECTANCY ON INTERMITTENT LOADS

(*a*)
$\Delta\theta_f = 80°\text{C}$ $T_f = 388°\text{K}$ $d_1' = 4{\cdot}40$ $N(1\text{–}378/T_f) = +0{\cdot}8$ $D_1' = 0{\cdot}075$ $p_1 = 0{\cdot}023 \times 10^{-3}\%$
$\Delta\theta_1 = 61°\text{C}$ $T_1 = 369°\text{K}$ $d_2' = 7{\cdot}95$ $N(1\text{–}378/T_0) = -7{\cdot}6$ $D_2' = 550$ $p_2 = 0{\cdot}030 \times 10^{-3}\%$
$\Delta\theta_2 = 27°\text{C}$ $T_2 = 335°\text{K}$
$p = p_1 + p_2 = 0{\cdot}053 \times 10^{-3}\%$
i.e. 32 years

(*b*)
$\Delta\theta_f = 95°\text{C}$ $T_f = 403°\text{K}$ $d_1' = 4{\cdot}85$ $N(1\text{–}378/T_f) = +2{\cdot}0$ $D_2' = 0{\cdot}060$ $p_1 = 0{\cdot}060 \times 10^{-3}\%$
$\Delta\theta_1 = 71°\text{C}$ $T_1 = 379°\text{K}$ $d_2' = 9{\cdot}35$ $N(1\text{–}378/T_0) = -7{\cdot}6$ $D_2' = 1\,530$ $p_2 = 0{\cdot}083 \times 10^{-3}\%$
$\Delta\theta_2 = 32°\text{C}$ $T_2 = 340°\text{K}$
$p = p_1 + p_2 = 0{\cdot}143 \times 10^{-3}\%$
i.e. 12 years

(*c*)
$\Delta\theta_f = 110°\text{C}$ $T_f = 418°\text{K}$ $d_1' = 5{\cdot}15$ $N(1\text{–}378/T_f) = +3{\cdot}1$ $D' = 0{\cdot}040$ $p_1 = 0{\cdot}120 \times 10^{-3}\%$
$\Delta\theta_1 = 84°\text{C}$ $T_1 = 392°\text{K}$ $d_2' = 11$ $N(1\text{–}378/T_0) = -7{\cdot}6$ $D_2' = 8\,100$ $p_2 = 0{\cdot}0465 \times 10^{-3}\%$
$\Delta\theta_2 = 38°\text{C}$ $T_2 = 346°\text{K}$
$p = p_1 + p_2 = 0{\cdot}1665 \times 10^{-3}\%$
i.e. 2·95 years

and interpolating

(*d*)
$\Delta\theta_f = 102°\text{C}$ $T_f = 137°\text{K}$ for 7 years' life expectancy
$\Delta\theta_1 = 77°\text{C}$ $T_1 = 385°\text{K}$ $\theta_1 = 112°\text{C}$
$\Delta\theta_2 = 35°\text{C}$ $T_2 = 243°\text{K}$ $\theta_2 = 70°\text{C}$

of the motor as $\tau = 5$ min, the motor being under full rated load for 5 min ($\alpha_1 = 1{\cdot}0$) and under no load for 4 min ($\alpha_2 = 0{\cdot}8$), 9 min ($\alpha = \alpha_1 + \alpha_2 = 1{\cdot}8$) being the total recurrent cycle. From Reference 1 we calculate the steady-state maximum and minimum temperature differences

$$\left.\begin{aligned} \Delta\theta_1 &= \frac{1-\varepsilon^{-\alpha_1}}{1-\varepsilon^{-\alpha_2}}\Delta\theta_f \\ \text{and} \quad \Delta\theta_2 &= \frac{\varepsilon^{-\alpha_2}-\varepsilon^{-\alpha_1}}{1-\varepsilon^{-\alpha}}\Delta\theta_f \end{aligned}\right\} \quad \ldots\ldots \quad (18)$$

where $\Delta\theta_f$ is the final temperature rise for continuous load equal to the load during α_1, the load period.

Using the modified Bussing eqns. (13) and (14) we calculate the percentage ageing factor for different values of $\Delta\theta_f$, i.e. for different loads of the same motor or for different motor sizes as the case may be, and from the interpolation we evaluate $\theta_1 = 112°\text{C}$ and $\theta_2 = 70°\text{C}$ for seven years' average life expectancy. This means that we are permitted to overheat the winding by 7° C only (above the standard $\theta_{max} = 105°\text{C}$ for synthetic-enamel-covered wire) in spite of the fact that the lowest temperature is 70° C. As mentioned previously, the cooling period is dangerous.

Calculating the same case in accordance with the until now accepted method, i.e. using the r.m.s. value of the current distribution, the average temperature would be 93·5° C and the life expectancy approximately 18 years instead of 7 years as calculated above.

(3.3) Short-Cycle Loads

For short-cycle loads, where $\alpha = t/\tau < 1{\cdot}0$, straight-line temperature rise and cooling can be assumed. In such cases the accepted method, using the r.m.s. value of the current distribution for temperature calculations, should be sufficient.

(4) CONCLUSIONS

Our knowledge of the heating effect in electrical machines is still in its infancy. It is obvious that, under normal conditions of daily work, the loading curves change from day to day and even from cycle to cycle. On the other hand, it has not been proved that the maximum temperatures suggested by standards committees in Europe and the United States are correct for the different materials used for insulation purposes. We must be grateful to the members of these committees for fixing very low maximum permitted temperatures, since it is clear that present methods of calculation are very inadequate and we obtain life expectancy figures some 40% above the 'true' ones.

Extensive chemical, physical, mechanical and electrical tests should be carried out for different insulation materials and for different combination of insulation materials used in transformers and machines under various intermittent load conditions. The theory suggested by Bussing[14] and others should be followed up and extended, but, on the other hand, better and more effective cooling methods should be developed.

(5) REFERENCES

(1) GOTTER, G.: 'Erwaermung und Kuehlung Elektrischer Maschinen' (Springer, 1954).

(2) RICHTER, R.: 'Elektrische Maschinen. Vol. 1' (Springer, 1924).

(3) LIWSCHITZ-GARIK, M., and WEIL, R. T.: 'Electric Machinery. Vol. I' (Van Nostrand, 1946).

(4) VIDMAR, M.: 'Transformatorenkurzschluesse' (Vieweg, 1953).

(5) STAEGER, J.: 'Elektrotechnische Isolierstoffe' (Wissenschaftlicher Verlag, 1952).

(6) HESS, M.: 'Isolierstoffe Elektrischer Maschinen' (Vieweg, 1942).

(7) HERCZEG, M.: 'Erwaermungskurve bei beliebiger Belastung', *Elektrotechnische Zeitschrift*, 1923, **44**, p. 916.

(8) DETTMAR, H.: 'Notwendigkeit von Normen fuer die Angabe von Leistung und Erwaermung elektrischer Maschinen', *ibid.*, 1900, **21**, p. 720.

(9) SCHUELER, J.: 'Waermebestaendigkeit von Baumwolle und Papier', *ibid.*, 1916, **37**, p. 535.

(10) MONTSINGER, V. M.: 'Loading Transformers by Temperature', *Transactions of the American I.E.E.*, 1930, **49**, p. 776.

(11) MONTSINGER, V. M.: 'Temperature Limits for Short-Time Overloads for Oil-Insulated Neutral Grounding Reactors and Transformers', *ibid.*, 1938, **57**, p. 39.

(12) HILL, M.: 'Temperature Limits set by Oil and Cellulose Insulation', *ibid.*, 1939, **58**, p. 484.

(13) CLARK, T.: 'Factors affecting the Mechanical Deterioration of Cellulose Insulation', American I.E.E. Technical Papers Nos. 42–98.

(14) BUSSING, W.: 'Beitraege zum Lebensdauergesetz elektrischer Maschinen', *Archiv für Elektrotechnik*, 1942, **36**, p. 333.

(15) MOSES, G. L.: 'Synthetic Insulation and the 10-Degree Rule', *Westinghouse Engineering*, 1945, p. 106.

(16) MOSES, G. L.: 'Synthetic Insulation and the 10-Degree Rule', *ibid.*, 1946, p. 80.

(17) DAKIN, T. W.: 'Electrical Insulation Deterioration Treated as a Chemical Rate Phenomenon', *Transactions of the American I.E.E.*, 1948, **67**, p. 113.

(18) STEWART, H. C., and WHITMAN, L. C.: 'Ageing Characteristics of Dry Type Transformer Insulation of High Temperature', *ibid.*, 1948, **67**, Part II, p. 1600.

(19) STEWART, H. C., and WHITMAN, L. C.: 'Ageing of Class B Insulation Material in Nitrogen', *ibid.*, 1951, **70**, Part I, p. 436.

(20) STEWART, H. C., WHITMAN, L. C., and SCHEIDELER, A. L.: 'Ageing of Dry Type Transformer Insulating System', *ibid.*, 1953, **72**, Part I, p. 480.

(21) STEWART, H. C., WHITMAN, L. C., and SCHEIDELER, A. L.: 'Ageing Evaluation of Dry Type Transformer Insulating System', *ibid.*, 1953, **72**, Part I, p. 267.

(22) IMHOFF, O.: 'Temperaturbestaendigkeit der Elektrischen Isolierstoffe', *Schweizer Archiv für angewandte Wissenschaft*, 1953, **19**, p. 355.

(23) MATHES, L.: 'Principles of Temperature Classification of Insulating Materials', *Electrical Engineering*, 1954, **73**, p. 243.

(24) FRENTZ, H. J.: 'Berechnung der Lebensdauer elektrischer Isolierstoffe bei konstantem und veraenderlichen Alterungstemperaturen', *Elektrotechnische Zeitschrift*, 1957, **78** A, p. 156.

(25) FRENTZ, H. J.: 'Lebensdauer Elektrischer Isolierstoffe', *Elektrotechnik und Maschinenbau*, 1958, **75**, p. 485.

(26) INGLISCH, W.: 'Lebensdaueruntersuchungen an Elektrischen Maschinen', *Elektrotechnische Zeitschrift*, 1958, **79** A, p. 693.

(6) APPENDICES

(6.1) Evaluation of the Percentage Ageing Factor from the Montsinger[10] Equation for the Exponential Heating Period

From the Montsinger eqn. (3*b*) the percentage ageing factor is

$$p = 14{\cdot}3\int_0^{(t)-t} \varepsilon^{kf(t)-A}dt \quad . \quad . \quad . \quad . \quad (3b)$$

and $$f(t) = \theta_0 + (\theta_f - \theta_0)(1 - \varepsilon^{-\alpha}) \quad . \quad . \quad . \quad (19)$$

where $$\alpha = t/\tau \text{ and } \Delta\theta_f = \theta_f - \theta_0$$

i.e. $$f(t) = \theta_f - (\theta_f - \theta_0)\varepsilon^{-\alpha} \quad . \quad . \quad . \quad . \quad (20)$$

and now $$p = 14{\cdot}3\tau\int_0^{\alpha} \exp(k\theta_f - k\Delta\theta_f\varepsilon^{-\alpha} - A)d\alpha \quad . \quad (21)$$

and assuming $$C = k\theta_f - A = 0{\cdot}087(\theta_f - 105) \quad . \quad . \quad (22)$$

$$p = 14{\cdot}3\tau\int_0^{\alpha} \varepsilon^{C-k\Delta\theta_f\varepsilon^{-\alpha}}d\alpha = 14{\cdot}3\tau\varepsilon^{C}\int_0^{\alpha} \varepsilon^{-k\theta_f\varepsilon^{-\alpha}}d\alpha \quad (23)$$

Taking $$-\varepsilon^{-\alpha} = x \text{ and } d\alpha = -dx/x$$

we can find the integral

$$\int \frac{ax}{x}dx = \log x + \frac{ax}{1\times 1!} + \frac{a^2x^2}{2\times 2!} + \frac{a^3x^3}{3\times 3!} + \ldots \quad . \quad (24)$$

[see, for example, Dwight's Tables of Integrals—eqn. (568.1)], and by integrating from $\alpha = 0$ to α we obtain the final equation

$$p = 14{\cdot}3\alpha\tau\varepsilon^{C}D_1 \quad . \quad . \quad . \quad . \quad . \quad (11)$$

where

$$D_1 = 1 - \frac{a(1-\varepsilon^{-\alpha})}{\alpha\times 1\times 1!} + \frac{a^2(1-\varepsilon^{-2\alpha})}{\alpha\times 2\times 2!} - \frac{a^3(1-\varepsilon^{-3\alpha})}{\alpha\times 3\times 3!} + - \ldots \quad (11a)$$

for $a = k\Delta\theta_f = 0{\cdot}087(\theta_f - \theta_0)$

and the series converges quickly for $a/n < 1{\cdot}0$.

(6.2) Evaluation of the Percentage Ageing Factor from the Montsinger Equation for the exponential Cooling Period

In similar way eqn. (3*b*),

i.e. $$p = 14{\cdot}3\int_0^t \varepsilon^{kf(t)-A}dt \quad . \; . \; . \; . \quad (3b)$$

can be used for the cooling period, where

$$f(t) = \theta_0 + (\theta_m - \theta_0)\varepsilon^{-\alpha} \quad . \; . \; . \; . \quad (25)$$

in which $$k\theta_0 + k\Delta\theta_m\varepsilon^{-\alpha} - A = k\Delta\theta_m\varepsilon^{-\alpha} + C_0 \quad . \quad (26)$$

It is assumed that

$$a' = k\Delta\theta_m \quad \Delta\theta_m = \theta_m - \theta_0 \quad C_0 = 0{\cdot}087(\theta_0 - 105) \quad (27)$$

i.e. for $\theta_0 = 105°C$ being the final cooling temperature for $C_0 = 0°C$. Now

$$p = 14{\cdot}3\tau\varepsilon^{C_0}\int_0^\alpha \varepsilon^{+\alpha'\varepsilon^{-\alpha}}d\alpha \quad . \; . \; . \quad (28)$$

and using the same method as above

$$p = 14{\cdot}3\tau\varepsilon^{C_0}\alpha D_2 \quad . \; . \; . \; . \; . \; . \quad (29)$$

where

$$D_2 = 1 + \frac{a'(1-\varepsilon^{-\alpha})}{\alpha \times 1 \times 1!} + \frac{a'^2(1-\varepsilon^{-2\alpha})}{\alpha \times 2 \times 2!} + \frac{a'^3(1-\varepsilon^{-3\alpha})}{\alpha \times 3 \times 3!} + \ldots \quad (30)$$

This series converges quickly for $a/n < 1{\cdot}0$.

It should be noted that, for the heating period, $a = 0{\cdot}087\,(\theta_f - \theta_0)$ and for the cooling period $a = 0{\cdot}087\,(\theta_m - \theta_0)$

(6.3) Evaluation of the Percentage Ageing Factor from the Bussing Equation for the Heating Exponential Period.

From the Bussing eqn. (3*c*)

$$p = 14{\cdot}3\int_0^t \varepsilon^{N(1-\nu)}dt \quad . \; . \; . \; . \quad (3c)$$

where

$$N = B/378 = 33 \text{ and } \nu = 378/f(t) \quad . \; . \; . \quad (31)$$

Now

$$f(t) = T_0 + (T_f - T_0)(1 - \varepsilon^{-\alpha}) = T_f - (T_f - T_0)\varepsilon^{-\alpha} \quad (32)$$

and as $$\Delta\theta_m = T_f - T_0 = \theta_f - \theta_0 \quad . \; . \; . \quad (33)$$

and usually $$h = \Delta\theta_m/T_f \ll 1{\cdot}0 \quad . \; . \; . \; . \; . \quad (34)$$

we can assume

$$\nu = 378/f(t) = 378/T_f(1 - h\varepsilon^{-\alpha}) \simeq (1 + h\varepsilon^{-\alpha})378/T_f \quad (35)$$

We evaluate the integral

$$p = 14{\cdot}3\tau\varepsilon^{N(1-378/T_f)}\int_0^\alpha \varepsilon^{-d\varepsilon^{-\alpha}}d\alpha \quad . \; . \quad (36)$$

where $$d = N\frac{378}{T_f}h = N\frac{378}{T_f}\frac{\Delta\theta_m}{T_f} \quad . \; . \; . \; . \quad (37)$$

We obtain

$$p = 14{\cdot}3\alpha\tau\varepsilon^{N(1-378/T_f)}D_1 \quad . \; . \; . \; . \; . \quad (13)$$

where

$$D_1 = 1 - \frac{d(1-\varepsilon^{-\alpha})}{\alpha \times 1 \times 1!} + \frac{d^2(1-\varepsilon^{-2\alpha})}{\alpha \times 2 \times 2!} - \frac{d^3(1-\varepsilon^{-3\alpha})}{\alpha \times 3 \times 3!} + - \ldots \quad (13a)$$

and can be read from Fig. 2 for

$$d = N\frac{378}{T_f}\frac{\Delta\theta_m}{T_f}$$

(6.4) Evaluation of the Percentage Ageing Factor from the Bussing Equation for the Exponential Cooling Period

In similar way, from eqn. (3*c*),

i.e. $$p = 14{\cdot}3\int_0^t \varepsilon^{N(1-\nu)}dt \quad . \; . \; . \; . \quad (3c)$$

where, for the cooling period,

$$f(t) = T = T_0 + (T_f - T_0)\varepsilon^{-\alpha} = T_0 + \Delta\theta_m\varepsilon^{-\alpha} \quad (38)$$

and

$$\nu = 378/f(t) = 378/(T_0 + \Delta\theta_m\varepsilon^{-\alpha}) \simeq (1 - h_0\varepsilon^{-\alpha})378/T_0 \quad (39)$$

where $$h_0 = \Delta\theta_m/T_0$$

and now $$p = 14{\cdot}3\tau\varepsilon^{N(1-378/T_0)}\int_2^\alpha \varepsilon^{+d'\varepsilon^{-\alpha}}d\alpha \quad . \; . \; . \quad (40)$$

where $$d' = N\frac{378}{T_0}h_0 = N\frac{378}{T_0}\frac{\Delta\theta_m}{T_0} \quad . \; . \; . \; . \quad (41)$$

The final solution can be found in similar way as above

$$p = 14{\cdot}3\tau\alpha\varepsilon^{N(1-378/T_0)}D_2 \quad . \; . \; . \; . \quad (14)$$

where

$$D_2 = 1 + \frac{d'(1-\varepsilon^{-\alpha})}{\alpha \times 1 \times 1!} + \frac{d'^2(1-\varepsilon^{-2\alpha})}{\alpha \times 2 \times 2!} + \frac{d'^3(1-\varepsilon^{-3\alpha})}{\alpha \times 3 \times 3!} + \ldots \quad (14a)$$

and can be taken from Fig. 3 or 3(*a*) for $d' = N\frac{378}{T_0}\frac{\Delta\theta_m}{T_0}$.

621.372.6.011.1

The Institution of Electrical Engineers
Monograph No. 355 E
Feb. 1960
©

VOLTAGE AND CURRENT TRANSFORMATION MATRICES

By I. CEDERBAUM, Ph.D.

(*The paper was first received* 24*th March, and in revised form* 21*st September*, 1959. *It will be published as an* INSTITUTION MONOGRAPH *in February*, 1960.)

SUMMARY

Transformation matrices relating two adequate systems of simple network co-ordinates such as node-pair voltages or link currents belong to the class of unimodular or E-matrices. The paper makes a distinction between the matrices corresponding to such voltage and current transformations, and different sets of necessary conditions are derived for each type.

Since the loop- and cut-set-to-branch incidence matrices are closely related to transformation matrices, the discussion proposes new sets of necessary conditions for incidence matrices corresponding to systems of node-pair voltages or link currents. Examples are given of matrices which whilst representing a voltage transformation cannot represent a current transformation and vice versa. Another example shows an E-matrix which can represent neither a voltage nor a current transformation.

(1) INTRODUCTION

In a recent paper (see Reference 1, Section 2) it has been shown that transformation matrices relating two adequate systems of node-pair voltages or link currents necessarily have all their subdeterminants (and the elements among them) equal to 1, −1 or 0. Such matrices are called unimodular[2] or E-matrices[1,3] and one may ask whether any non-singular E-matrix represents some transformation of voltage or current co-ordinates of a network and whether there is any difference between matrices representing voltage and current transformations. These questions are answered, and it is shown that not every voltage transformation matrix may represent a current transformation and vice versa. Moreover, there exist E-matrices which can represent neither a voltage nor a current transformation.

The interesting point is that the loop- and cut-set-to-branch* incidence matrices for links and node-pair systems, respectively, are submatrices of such transformation matrices. The necessary and sufficient conditions for such matrices are well known[1] but they are, in general, difficult to apply. The following discussion offers a new set of necessary conditions which give additional information on the structure of those matrices and may be helpful in some instances.

(2) INCIDENCE CONDITIONS FOR TWO ADEQUATE SYSTEMS OF NODE-PAIR VOLTAGES

Consider some connected network N with t nodes and b branches and choose on it two adequate systems of $s(=t-1)$ node-pair voltages U_i and V_i $(i=1, 2, \ldots s)$ forming the vectors U and V.

If each voltage of such a system is regarded as a fictitious branch joining the nodes of the corresponding pair, the system is represented by a tree on the network, although, of course, the network branches which correspond to all or some of these voltages need not exist.

* For the definitions of the basic topological concepts see Reference 5, Chapter 1.

Correspondence on Monographs is invited for consideration with a view to publication.

Dr. Cederbaum is in the Scientific Department, Ministry of Defence, Israel.

In the following the elements of the vectors U and V will be referred to, somewhat indiscriminately, as either voltages or tree branches.

Let
$$V = AU \quad . \quad . \quad . \quad . \quad . \quad . \quad . \quad (1)$$
be the relation between U and V involving the non-singular $s \times s$ matrix A. The same state of the network may be considered as being caused by s voltage generators, U, applied to the node-pairs of the U-system or by s voltage generators, V, defined by eqn. (1) and applied to the node-pairs V. Let the vectors of currents supplied by the generators U and V be I and J, respectively. The relation between I and J corresponding to eqn. (1)—the so-called contragredient transformation[4]—is
$$I = A'J \quad . \quad . \quad . \quad . \quad . \quad . \quad . \quad (2)$$
In the further discussion the inverse relations corresponding to eqns. (1) and (2)
$$U = A^{-1}V \quad . \quad . \quad . \quad . \quad . \quad . \quad (3)$$
and
$$J = (A')^{-1}I \quad . \quad . \quad . \quad . \quad . \quad . \quad (4)$$
will sometimes be used.

The non-zero elements of some row of A (or A^{-1}) correspond to the branches of the set U (or V) which build an arch spanned by a branch of V (or U), whereas the relation between the currents is somewhat more complicated. However, if some k branches of one system meet at one node a single branch of the other system, the current of that branch is equal to the algebraic sum of the currents of those k branches. In this case the corresponding row of the matrix A′ or $(A')^{-1}$ contains exactly k non-zero elements.

Consider the incidence conditions between the nodes of the network and the branches of both systems U and V. Since the branches U and V form trees on the network, each node is necessarily incident with at least one branch of each system. But both trees U and V comprise together $2s$ branches based on $t = s + 1$ nodes. These branches have $4s$ ends and therefore the 'mean' incidence number of branches meeting at one node is
$$m = \frac{4s}{s+1} < 4 \quad . \quad . \quad . \quad . \quad . \quad . \quad (5)$$

Thus in the network there are necessarily some nodes where only two or three branches meet. Let the minimum number of such 2- or 3-branch nodes be found. Denoting by k_2 and k_3 the numbers of nodes with 2 and 3 incident branches, respectively, and by p the number of branches incident with those nodes (the p's not necessarily all different),
$$p = 2k_2 + 3k_3 \quad . \quad . \quad . \quad . \quad . \quad . \quad (6)$$
The remaining mean incidence number at other nodes,
$$\bar{m} = \frac{4s - p}{s + 1 - (k_2 + k_3)} \quad . \quad . \quad . \quad . \quad (7)$$
is necessarily not less than 4, so that $2k_2 + k_3 \leqslant 4$. Evidently the minimum number of deficient nodes corresponds to the equality sign, and Table 1 may be obtained by putting $k_2 = 0, 1, 2$.

Table 1

MINIMUM NUMBER OF DEFICIENT NODES

k_2	k_3	$k = k_2 + k_3$	$p = 2k_2 + 3k_3$
0	4	4	12
1	2	3	8
2	0	2	4

If a node is incident with only two branches, then necessarily one, U_q, belongs to the set U and the other, V_r, to V. Considering some state of the network as being caused by the currents I or J, one realizes that the magnitude of the qth component of I is equal to the magnitude of the rth component of J. Since this is true for arbitrary excitation conditions, it follows from eqn. (2) that the qth row of A′ has a single non-zero element located in the rth column, and similarly from eqn. (4) that the rth row of $(A')^{-1}$ has a single non-zero element located in the qth column.

If a node is incident with three branches, this triplet may be composed of one branch U and two branches V, or vice versa. In the first case the matrix A′ has only two non-zero elements in the corresponding row and in the second case the same is true for the matrix $(A')^{-1}$. It may be remarked that it is impossible to predict how the number k_3 is subdivided between the triplets of both kinds. To demonstrate this, three different cases with $k_3 = 4$ have been shown in Fig. 1. The node-pair

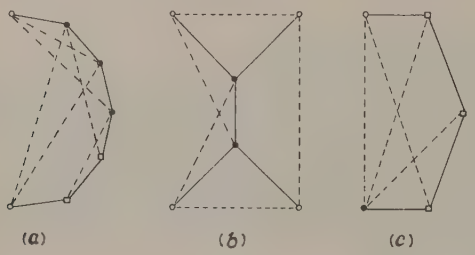

Fig. 1.—2-tree networks, each having four 3-branch nodes.

(*a*) Two 3-branch nodes of each kind.
(*b*) Four 3-branch nodes of the first kind and none of the second kind.
(*c*) One 3-branch node of the first kind and three of the second kind.

voltages U and V have been shown with full and broken lines, respectively, the 'physical' network branches being omitted as irrelevant to the discussion. The nodes of the first kind have been denoted by circles and of the second kind by squares. It can be seen that there are in (*a*) two nodes of each kind, in (*b*) four nodes of the first kind and none of the second and in (*c*) one node of the first kind and three nodes of the second. This implies that the further discussion need be related only to the pair $[A', (A')^{-1}]$ or $[A, A^{-1}]$ rather than individually to each of the matrices.

(3) E-MATRICES REPRESENTING VOLTAGE TRANSFORMATIONS

Consider the pair of matrices (A, A^{-1}). Since each node incident with only two branches corresponds to a column with a single non-zero element in both A and A^{-1}, whereas a 3-branch node corresponds to a column with two non-zero elements in only one of the matrices, Theorem 1 follows readily from Table 1.

Theorem 1.—If A is a transformation matrix from one system of s independent node-pair voltages to another ($s \geqslant 2$), the pair of matrices (A, A^{-1}) has at least four columns, each with not more than two non-zero elements.

Consider the case of a 2-branch node. Since this node is incident with only one branch of each system it is an end-node for each voltage tree. Let it be removed together with the two branches incident with it leaving two connected graphs of $s - 1$ voltage branches based on s nodes. Assume that these two branches be the first in their respective systems. In that case the first columns of A and A^{-1} have each a single non-zero element which is the first element of those columns. Thus

$$A = \begin{bmatrix} a_{11} & a_1 \\ 0 & A_1 \end{bmatrix} \quad A^{-1} = \begin{bmatrix} a_{11}^{-1} & b_1 \\ 0 & A_1^{-1} \end{bmatrix} \quad . \quad . \quad (8)$$

where a_1, b_1 are $1 \times (s-1)$ row vectors and A_1 is a square non-singular matrix of order $s - 1$. Let the reduced $(s-1) \times 1$ voltage vectors by $\bar{U}$ and $\bar{V}$. From eqns. (1), (3) and (8) it follows that

$$\bar{V} = A_1 \bar{U} \quad . \quad . \quad . \quad . \quad . \quad . \quad . \quad (9)$$

and

$$\bar{U} = A_1^{-1} \bar{V} \quad . \quad . \quad . \quad . \quad . \quad . \quad . \quad (10)$$

Thus the matrix pair relating the reduced vectors $\bar{U}$ and $\bar{V}$ may be obtained simply by crossing out the rows and columns corresponding to the deleted branches. Such a combined operation on a graph and on the transformation matrix will be referred to as an α-operation. Of course, since the reduced matrix pair (A_1, A_1^{-1}) relates two sets of $s - 1$ independent node-pair voltages based on s nodes, the Theorem 1 is valid for it as well.

In the case of a 3-branch node, assume that this node is incident with the first of the U-system and with the first two branches of the V-system, as shown for node B in Fig. 2(*a*).

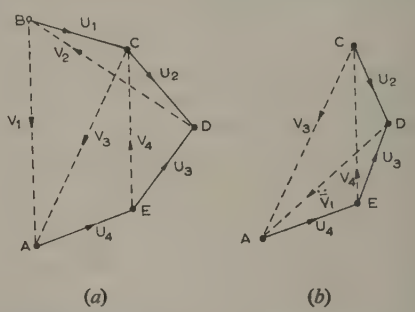

Fig. 2.—Removal of the 3-branch node B.

(*a*) Original network.
(*b*) Reduced network: branches V_1 and V_2 are replaced by $\bar{V}_1$.

Node B is an end-node for graph U but not for graph V. It may therefore be removed together with branch U_1 leaving both graphs connected if the two branches V_1 and V_2 are replaced by one branch $\bar{V}_1$, as shown in Fig. 2(*b*). The orientation of $\bar{V}_1$ may be chosen arbitrarily; let it, for instance, be directed with relation to the node previously incident with V_1 as was the removed branch V_1.

Since $\bar{V}_1 = V_1 \pm V_2$, according as the quantities a_{21}, a_{11}, of unit magnitude, are of the same or opposite sign, these changes of the graphs lead to the following changes of the transformation matrices. In the matrix A the first row needs to be augmented by the second row multiplied by $-a_{11}a_{21}$, and the first column and second row should be deleted. The transformation of the matrix A^{-1} amounts to deleting the first row and second column.

For general indices this procedure may be summarized as follows: In the graphs of two independent node-pair voltages U and V let U_k, V_m and V_p be the three branches meeting at some

node. The removal of this node from the graph in the way explained above results in

(*a*) deleting the kth column of matrix A and adding the pth row multiplied by $-a_{mk}a_{pk}$ to the mth row, followed by deleting the pth row, and

(*b*) deleting the kth row and pth column of matrix A^{-1}.

If the triplet consists of V_k, U_m and U_p the procedures applied to A and A^{-1} are reversed.

Such a combined operation on both graphs and corresponding matrices caused by the removal of a 3-branch node will be referred to as a β-operation.

After performing an α- or β-operation on two graphs of s independent node-pair voltages one is left with two graphs of $s-1$ independent node-pair voltages based on s nodes. Thus the reduced matrix-pair (A_1, A_1^{-1}) for $s \geqslant 2$ necessarily has at least four columns with not more than two non-zero elements and the α- and β-operations may be performed further until one arrives at two graphs consisting each of one branch based on two nodes with the transformation matrix equal to $[\pm 1]$.

It may be shown that, although a 3-branch node incident, say, with U_k, V_m and V_p corresponds necessarily to the case that in the kth column of A the only non-zero elements are in the mth and pth rows, the inverse statement is not necessarily true. As shown in Fig. 3(*a*) the second column in matrix A does not

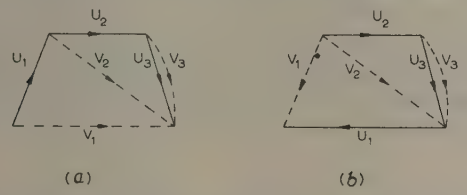

Fig. 3.—Two pairs of voltages (U, V) related by the same matrix A (V = AU).

$$(a)\ A = \begin{bmatrix} 1 & 1 & 1 \\ 0 & 1 & 1 \\ 0 & 0 & 1 \end{bmatrix} \quad (b)\ A^{-1} = \begin{bmatrix} 1 & -1 & 0 \\ 0 & 1 & -1 \\ 0 & 0 & 1 \end{bmatrix}$$

correspond to a 3-branch node incident with the branches U_2, V_1 and V_2. A closer inspection reveals that this follows from the fact that the same matrix A corresponds to the network shown in Fig. 3(*b*), where the branches U_2, V_1 and V_2 in fact form a triplet. Such a situation may, however, arise only if besides a 3-branch node there also exists in the network a 2-branch node [the node incident with the branches U_1 and V_1 in Fig. 3(*a*)]. Thus the reduction process of a matrix needs at any stage to give preference to an α- before a β-operation.

Moreover, since every non-singular submatrix of A may be interpreted as a transformation matrix relating two adequate sets of independent node-pair voltages,[1] each such submatrix necessarily shares with A the above properties. Thus the following theorem is true:

Theorem 2.—The necessary conditions for a matrix A to be a transformation matrix relating two sets of s independent node-pair voltages based on a network with $s+1$ nodes are that:

(*a*) Matrix A is a non-singular E-matrix.

(*b*) The matrix-pair (A, A^{-1}) can be reduced to the elementary form $([\pm 1], [\pm 1])$ by a sequence of α- and β-operations.

(*c*) At each stage of the reduction process (with the evident exception of the last stage) the pair (A_i, A_i^{-1}) has at least four columns with not more than two non-zero elements.

(*d*) The reduction process may proceed by any of the α- or β-operations possible at the given stage with the preference given always to α-operations.

(*e*) Every non-singular submatrix of the matrix A shares with A properties (*b*)–(*d*).

Let all square or rectangular E-matrices whose non-singular submatrices of order $m \geqslant 2$ satisfy the above conditions be, for brevity, called E_1-matrices. Thus according to Theorem 2 every transformation matrix between two adequate systems of node-pair voltages is necessarily a square non-singular E_1-matrix.

(4) CURRENT TRANSFORMATION MATRICES

Consider two adequate systems of link currents I and J corresponding to trees T_I and T_J, respectively. Since the network has b branches and $t\,(=s+1)$ nodes, each of the systems considered consists of $f\,(=b-s)$ link currents.

Let $$J = BI \quad . \quad . \quad . \quad . \quad . \quad . \quad . \quad (11)$$

be the relation between I and J involving matrix B which is a non-singular E-matrix of order f.

The trees T_I and T_J may have some m branches in common. Let these common branches be short-circuited and the 'new' network be called N_1. N_1 has $t-m$ nodes and the link systems I and J on N_1 correspond to trees $T_I^{(1)}$ and $T_J^{(1)}$ which have no branches in common. Evidently eqns. (11) have not been influenced by the above operation.

The systems I and J may as well have some p links in common. Let p new nodes be created, one in the middle of each of the common links. The 'new' network having $t-m+p$ nodes and $b-m+p$ branches may be called N_2. The tree $T_I^{(1)}$ on N_1 may be now augumented to form a tree $T_I^{(2)}$ on N_2 by adding to it p new branches each of which is a part of one of the p common links. The other tree, $T_J^{(1)}$, is augmented by the remaining parts of the common links to form the tree $T_J^{(2)}$ on N_2. The corresponding link systems may be called $\bar{I}$ and $\bar{J}$, respectively.

The trees $T_I^{(2)}$ and $T_J^{(2)}$ and the link systems $\bar{I}$ and $\bar{J}$ are, of course, alien to each other. However, since each branch is necessarily either a tree branch or a link, the links $\bar{I}$ are the branches of the tree $T_J^{(2)}$ and the links $\bar{J}$ are the branches of the tree $T_I^{(2)}$. This shows that N_2 represents a 2-tree structure. It may readily be recognized that eqns. (11) remain valid if I and J are replaced by $\bar{I}$ and $\bar{J}$, respectively.

The system of current generators, $\bar{I}$, placed in the $\bar{I}$ links generates a system of voltages U across these links, and the system of equivalent current generators, $\bar{J}$, placed in the $\bar{J}$ links generates an equivalent system of voltages V. The (contragredient) relation between U and V is given by

$$U = B'V \quad . \quad . \quad . \quad . \quad . \quad . \quad (12)$$

But U and V may be looked on as systems of tree voltages. Hence B′ necessarily satisfies the conditions of Theorem 2 and is a non-singular E_1-matrix. Let the transpose of an E_1-matrix be called, for brevity, an E_2-matrix. Thus the above results may be summarized as follows:

The necessary condition for a matrix B to be a transformation matrix relating two adequate systems of link currents is that B be a non-singular E_2-matrix.

An interesting property of a matrix B satisfying this is that the composite $2f \times f$ matrix

$$\begin{bmatrix} B \\ B^{-1} \end{bmatrix}$$

has necessarily at least four rows with not more than two non-zero elements.

(5) NODE-PAIRS AND LINKS INCIDENCE MATRICES

The above results may be applied to the incidence matrices corresponding to adequate systems of node-pairs or links on a network.

It has been shown[1] that the transpose of the incidence matrix of an adequate system of node-pair voltages may be identified as a submatrix of a transformation matrix relating two adequate systems of node-pair voltages. This shows that such an incidence matrix is necessarily an E_2-matrix.

Dually, the transpose of the incidence matrix corresponding to an adequate system of link currents is a submatrix of a transformation matrix between two adequate systems of link currents. Thus this incidence matrix is necessarily of the E_1-kind. This may be summarized as follows:

The incidence matrices of adequate systems of link currents or node-pair voltages are necessarily E_1- or E_2-matrices, respectively.

(6) EXAMPLES

Some examples of various kinds of E-matrices will be given.

Example 1.—Fig. 4(*a*) shows the eight nodes of a network and two systems of seven independent node-pair voltages based on

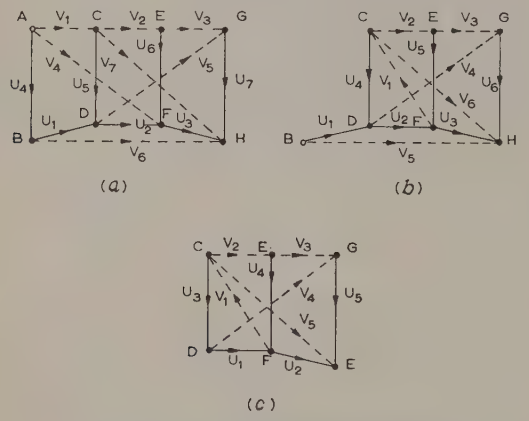

Fig. 4.—8-node network of Example 1.

(*a*) Original network.
(*b*) Network reduced by removal of the 3-branch node A.
(*c*) Network (*b*) reduced by removal of 2-branch node B.

these nodes. The systems U and V have been shown with full and broken lines, respectively. The square non-singular matrix A corresponding to the transformation from the system U to V($V = AU$) is an E_1-matrix.

$$A = \begin{bmatrix} 1 & 0 & 0 & 1 & -1 & 0 & 0 \\ 0 & 1 & 0 & 0 & 1 & -1 & 0 \\ 0 & 0 & 1 & 0 & 0 & 1 & -1 \\ 1 & 1 & 0 & 1 & 0 & 0 & 0 \\ 0 & 1 & 1 & 0 & 0 & 0 & -1 \\ 1 & 1 & 1 & 0 & 0 & 0 & 0 \\ 0 & 1 & 1 & 0 & 1 & 0 & 0 \end{bmatrix}.$$

$$A^{-1} = \begin{bmatrix} 0 & 1 & 1 & 0 & -1 & 1 & -1 \\ -1 & -1 & -1 & 1 & 1 & 0 & 0 \\ 1 & 0 & 0 & -1 & 0 & 0 & 1 \\ 1 & 0 & 0 & 0 & 0 & -1 & 1 \\ 0 & 1 & 1 & 0 & -1 & 0 & 0 \\ -1 & -1 & 0 & 1 & 0 & 0 & 0 \\ 0 & -1 & -1 & 0 & 0 & 0 & 1 \end{bmatrix}$$

In the matrix pair (A, A^{-1}) there are no columns with a single non-zero element and exactly four columns with two non-zero elements, namely columns 4, 6 and 7 of A and column 6 of A^{-1}, which correspond to the 3-branch nodes, A, E, G and B, respectively. The matrix pair may be accordingly reduced in four different ways by β-operations, e.g. by deleting the node A. This leads to the network shown in Fig. 4(*b*), and the reduced pair is

$$A_1 = \begin{bmatrix} 0 & -1 & 0 & -1 & 0 & 0 \\ 0 & 1 & 0 & 1 & -1 & 0 \\ 0 & 0 & 1 & 0 & 1 & -1 \\ 0 & 1 & 1 & 0 & 0 & -1 \\ 1 & 1 & 1 & 0 & 0 & 0 \\ 0 & 1 & 1 & 1 & 0 & 0 \end{bmatrix}$$

$$A_1^{-1} = \begin{bmatrix} 0 & 1 & 1 & -1 & 1 & -1 \\ -1 & -1 & -1 & 1 & 0 & 0 \\ 1 & 0 & 0 & 0 & 0 & 1 \\ 0 & 1 & 1 & -1 & 0 & 0 \\ -1 & -1 & 0 & 0 & 0 & 0 \\ 0 & -1 & -1 & 0 & 0 & 1 \end{bmatrix}$$

In the reduced pair we find two columns with a single element, namely columns 1 of A_1 and 5 of A_1^{-1}, and two columns with two elements, namely columns 5 and 6 of A_1, which correspond to nodes B, E and G of the reduced network in Fig. 4(*b*). Further reduction may be achieved by an α-operation or by one of two possible β-operations. The α-operation is achieved by removing the node B and leads to the network shown in Fig. 4(*c*). The reduced matrix pair is

$$A_2 = \begin{bmatrix} -1 & 0 & -1 & 0 & 0 \\ 1 & 0 & 1 & -1 & 0 \\ 0 & 1 & 0 & 1 & -1 \\ 1 & 1 & 0 & 0 & -1 \\ 1 & 1 & 1 & 0 & 0 \end{bmatrix} \quad A_2^{-1} = \begin{bmatrix} -1 & -1 & -1 & 1 & 0 \\ 1 & 0 & 0 & 0 & 1 \\ 0 & 1 & 1 & -1 & 0 \\ -1 & -1 & 0 & 0 & 0 \\ 0 & -1 & -1 & 0 & 1 \end{bmatrix}$$

Here we find four columns with two non-zero elements, and further reduction may proceed by applying one of four possible β-operations.

Example 2.—The square non-singular matrix A′ corresponding to the current transformation, $I = A'J$, in Fig. 4(*a*), being the transpose of an E_1-matrix, is an E_2-matrix.

$$A' = \begin{bmatrix} 1 & 0 & 0 & 1 & 0 & 1 & 0 \\ 0 & 1 & 0 & 1 & 1 & 1 & 1 \\ 0 & 0 & 1 & 0 & 1 & 1 & 1 \\ 1 & 0 & 0 & 1 & 0 & 0 & 0 \\ -1 & 1 & 0 & 0 & 0 & 0 & 1 \\ 0 & -1 & 1 & 0 & 0 & 0 & 0 \\ 0 & 0 & -1 & 0 & -1 & 0 & 0 \end{bmatrix}$$

$$(A')^{-1} = \begin{bmatrix} 0 & -1 & 1 & 1 & 0 & -1 & 0 \\ 1 & -1 & 0 & 0 & 1 & -1 & -1 \\ 1 & -1 & 0 & 0 & 1 & 0 & -1 \\ 0 & 1 & -1 & 0 & 0 & 1 & 0 \\ -1 & 1 & 0 & 0 & -1 & 0 & 0 \\ 1 & 0 & 0 & -1 & 0 & 0 & 0 \\ -1 & 0 & 1 & 1 & 0 & 0 & 1 \end{bmatrix}$$

As may be seen in the pair $[A', (A')^{-1}]$ there is no column with less than three non-zero elements. This shows that A′ is not an E_1-matrix and that A is not an E_2-matrix.

Example 3.—Consider the E-matrix

$$A = \begin{bmatrix} 1 & 1 & 1 \\ 1 & 1 & 0 \\ 0 & 1 & 0 \end{bmatrix}$$

Then $$A^{-1} = \begin{bmatrix} 1 & 0 & -1 \\ -1 & 1 & 1 \\ 1 & -1 & 0 \end{bmatrix} \quad A' = \begin{bmatrix} 1 & 1 & 0 \\ 1 & 1 & 1 \\ 1 & 0 & 1 \end{bmatrix}$$

and $$(A')^{-1} = \begin{bmatrix} 1 & -1 & 1 \\ 0 & 1 & -1 \\ -1 & 1 & 0 \end{bmatrix}$$

The matrix pairs (A, A^{-1}) and $[A', (A')^{-1}]$ both have four columns with only two non-zero elements and they may both be reduced to the elementary form by one β- and one α-operation. Thus A and A′ are both E_1- and E_2-matrices. This proves that the conditions for E_1- and E_2-matrices are not mutually exclusive.

Example 4.—Take the sum $A \dot{+} A'$,* where A is the matrix of Example 1. This matrix, according to Reference 3, Section 2, is an E-matrix. However, it cannot be either an E_1- or an E_2-matrix, since after reducing, for example, A by α- and β-operations A′ is left which cannot be further reduced. This shows that there are E-matrices which are neither E_1- nor E_2-matrices.

* The direct sum $A \dot{+} B$ of two matrices is defined by

$$A \dot{+} B = \begin{bmatrix} A & O \\ O & B \end{bmatrix}$$

From the above examples it follows that E-matrices can be subdivided into four (non-empty) groups:

(*a*) E_1-matrices which are not E_2-matrices.
(*b*) E_2-matrices which are not E_1-matrices.
(*c*) Matrices which are E_1- and E_2-matrices.
(*d*) E-matrices which are neither E_1- nor E_2-matrices.

(7) ACKNOWLEDGMENT

The author wishes to express his thanks to the Scientific Department, Ministry of Defence, Israel, under whose auspices this research was done.

(8) REFERENCES

(1) CEDERBAUM, I.: 'Conditions for the Impedance and Admittance Matrices of *n*-Ports without Ideal Transformers', *Proceedings I.E.E.*, Monograph No. 276 R, January, 1958 (**105** C, p. 245).
(2) KUHN, H. W., and TUCKER, A. W. (Editors): 'Linear Inequalities and Related Systems' (Princeton University, 1956), p. 223.
(3) CEDERBAUM, I.: 'Matrices All of Whose Elements and Subdeterminants are 1, −1 or 0', *Journal of Mathematics and Physics*, 1958, **36**, p. 351.
(4) CAUER, W.: 'Theorie der linearem Wechselstromschaltungen' (Akademie-Verlag, Berlin, 1954).
(5) GUILLEMIN, E. A.: 'Introductory Circuit Theory' (John Wiley, 1953).

621.52

The Institution of Electrical Engineers
Monograph No. 356 M
Feb. 1960

©

THE STABILIZATION OF CONTROL SYSTEMS WITH BACKLASH USING A HIGH-FREQUENCY ON-OFF LOOP

By E. A. FREEMAN, B.Sc., Ph.D., Graduate.

(*The paper was first received 26th June, and in revised form 29th September*, 1959. *It was published as an* INSTITUTION MONOGRAPH *in February*, 1960.)

SUMMARY

The paper introduces a method of stabilizing control systems which have backlash in their control sequence. The technique described employs an auxiliary loop to drive the motor across the backlash whenever the motor and load tend to separate. Requirements of the auxiliary loop are deduced and a phase-plane analysis is developed for a second-order position-control system with this loop operative. Analysis shows that the system with backlash is effectively linearized. It is also shown that impacts between motor and load are avoided.

To establish the feasibility of the method an analogue computer study is presented. Results from the analogue show that the technique leads to considerable improvement in the step-function response. Variation of the system damping and of the ratio of inertias is also investigated. It is found that the system stabilized by the technique behaves essentially as a linear system.

LIST OF PRINCIPAL SYMBOLS

ψ = Amplitude of step-function disturbance.
θ_{BL} = Angle of backlash referred to the output shaft.
θ_o = Output position of load indicated by resetter.
θ_M = Position of the motor.
α = Gain of auxiliary-loop amplifier.
$f(s)$ = Frequency-dependent part of auxiliary-loop amplifier transfer function.
T_d = Phase-advance time-constant of auxiliary loop.
$T_q(M)$ = Torque developed by the motor.
I_M = Moment of inertia of motor.
K_{VM} = Viscous friction coefficient for the motor side of the backlash.
K_g = Tachogenerator output velocity feedback constant.
K = Normal-loop amplifier gain.
θ_i = Demanded output position from normal loop.
n = Ratio of the amplitude of the input step applied to the auxiliary loop to the amplitude which just causes saturation.
I_L = Moment of inertia on resetter side of backlash.
$I = I_M + I_L$ = Total moment of inertia.
K_{VL} = Viscous friction coefficient for the resetter side of the backlash.
$K_V = K_{VM} + K_{VL} + K_g$.
$\omega_n = \sqrt{\frac{K}{I}}$ = Undamped natural frequency of servo mechanism.
$\zeta = \frac{K_V}{2\omega_n I}$ = Damping factor of servo mechanism.
$\sigma = \omega_n\zeta$ = Logarithmic decrement of transient oscillations.
$\omega = \omega_n\sqrt{(1 - \zeta^2)}$ = Angular frequency of damped oscillations.
r, ρ = Polar co-ordinates of point on the phase-plane trajectory in the uv-plane.
$\zeta_L = K_{VL}/2\omega_n I_L$.
τ = Period of separation or transit time.

Correspondence on Monographs is invited for consideration with a view to publication.
Dr. Freeman is at Sunderland Technical College.

(1) INTRODUCTION

The occurrence of backlash in the gearing or linkages present in many control systems generally gives rise to certain undesirable performance characteristics. It may, for example, lead to sustained oscillations of the output, an excessively oscillatory transient response or a positional error greater than that of the linear system. To overcome these disadvantages a method of stabilizing servo systems with backlash, namely divided reset, has been suggested and examined by certain workers.[1,2] It has been indicated that if the positional reset, taken partly from the motor side of the backlash and partly from the load side of the backlash, is divided in the ratio of inertias the transient response will be the same as that of the linear system. Experimental work by Liversedge[1] does not, however, verify this theoretical conclusion. In a recent paper by the author[3] it has been shown that the presence of friction on either side of the backlash invalidates the theoretical conclusion and that, if the coefficients of friction for the two sides of the backlash are not in the ratio of inertias, it is not possible to obtain a transient response identical with that of the linear system. In such cases the transient response may be 'linearized' if divided velocity-feedback is employed for stabilization.[3] However, servo systems stabilized in this manner still suffer two principal drawbacks.

First, positional error is increased because all of the reset signal is not taken from the load or output side of the backlash. Secondly, the increased mechanical wear, occasioned by the repeated impacts between motor and load which take place during each oscillatory transient, is reduced but little.

An alternative method of stabilization, transient divided reset, has the advantage that under steady-state conditions there is no positional feedback from the motor side of the backlash. This would seem to imply improved positional accuracy. However, according to Liversedge[1] the static stiffness of such servo systems is low, and this gives rise to larger errors under constant load-torque conditions.

The paper presents a new method of improving system performance which results in dynamic characteristics almost identical with those obtained in the absence of backlash. Furthermore, because positional reset may be taken entirely from the output member, the steady-state accuracy is not impaired. Finally, the technique is such that impacts between motor and load are avoided, which gives rise to an appreciable reduction in the wear of mechanical parts.

An understanding of the method is best gained by considering its application to a second-order position-control system. The phase-plane method of analysis may then be used to derive the important characteristics of the step-function response.

Experimental work is carried out on an analogue computer. Transients thus recorded provide a means of understanding the technique and of assessing the improvement in performance effected. In concluding the paper some of the difficulties experienced in realizing the technique in a practical position-control system, employing a type 73 split-field motor with field control, are discussed.

(2) TRANSIENT RESPONSE WITH BACKLASH

In order to deduce the requirements of the stabilizing technique we shall first examine the response of a position-control system, shown schematically in Fig. 1, which has backlash.

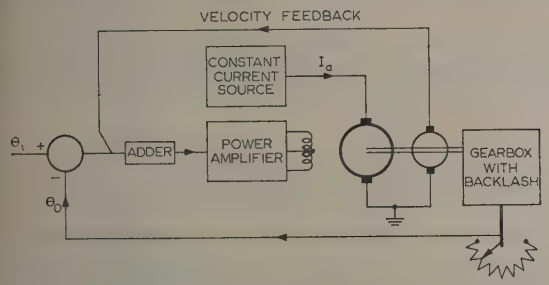

Fig. 1.—Position-control servo system with backlash in the gearing.

The backlash is assumed to occur in the gearing connecting the output measuring device, or resetter, to the motor. We shall suppose that the ratio of friction force to moment of inertia for the resetter side of the backlash is finite. This means that the resetter will cease to be driven by the motor whenever its deceleration, caused by friction, is less than that of the motor.

The waveforms of Fig. 2 illustrate the response of the servo

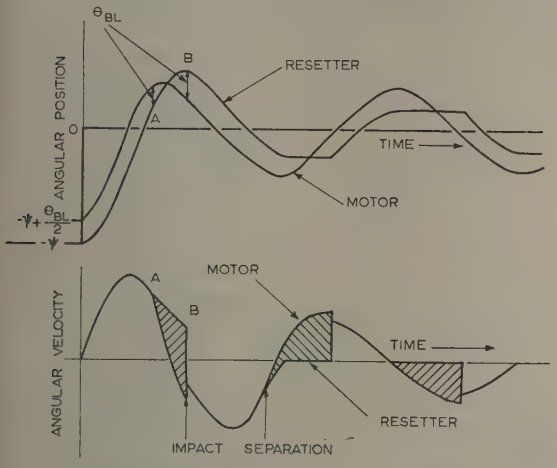

Fig. 2.—Step-function response waveforms of position servo system with backlash.

system when subjected to a step-function disturbance of amplitude ψ. It is assumed that the system is initially at rest with the output at an angular position $-\psi$, and that the motor and resetter are in contact through the gearing. Application of the step tends to drive the output to the zero position.

Fig. 2 shows that as the motor accelerates it maintains contact with the resetter; this is evidenced by the velocity waveforms showing the velocities of the motor and resetter to be equal. When the output approaches the zero position, however, the motor starts to decelerate. During this period of deceleration the resetter maintains contact with the motor because frictional forces attempt to cause a greater resetter deceleration. Eventually, the deceleration of the motor exceeds that of the resetter, point A in Fig. 2, at which point the two members lose contact. The motor then continues to move relative to the resetter whilst the latter coasts towards standstill. When the distance moved by the motor relative to the resetter is equal to the backlash angle, θ_{BL}, the motor makes contact with the resetter and an impact takes place.

It is assumed that the two members move on together with a common velocity after this impact (Fig. 2). The entire cycle of events is then repeated.

As the oscillation proceeds and the amplitude of the overshoot falls the torque driving the motor across the backlash during a period of separation decreases and hence the period of separation increases. This effect eventually allows the resetter to be brought to rest during a period of separation. As a result, the maximum overshoot persists for a prolonged period. Ultimately the amplitude of overshoot is so small that the deceleration of the motor never exceeds that of the resetter and the two only become separated when the velocity of the motor changes sign. Under these latter conditions the half periodic time of the transient becomes extremely large, so that the peak overshoot persists for a prohibitively long period.[4]

(3) REQUIREMENTS OF THE STABILIZING TECHNIQUE

In this Section we shall deduce the requirements of the method of stabilization. To this end let us examine the effects which backlash has had on the transient response just described.

First, it may be seen from Fig. 2 that backlash increases the amplitude of the first overshoot of the response. This increase is caused by the increased velocity of the resetter during the first period of separation. Clearly, reducing the period of separation will minimize this effect.

Secondly, had we assumed the motor to be on the wrong side of the backlash at the instant of applying the step the response would have shown an initial delay, the delay being the time taken for the motor to cross the backlash.

Thirdly, as the error in the system is reduced the frequency of the transient oscillation falls and eventually low-frequency sustained oscillations may exist. This low-frequency oscillation, transient or otherwise, is made possible because of the lag between the resetter position and the motor position (Fig. 2). The lag is greater the longer the period of separation.

Finally, it may be observed that an impact takes place during each half cycle of the transient. The magnitude of the impact depends on the relative velocity of the two members.

It will be apparent that all four effects stem from the lack of control of the output member during a period of separation, and, as the backlash prevents control of the output, one is naturally led to thinking of controlling the position of the motor in some beneficial way during a period of separation. First thoughts may suggest that one need only increase the acceleration (or deceleration) of the motor when a separation commences and so race the motor across the backlash. This would certainly reduce the period of separation but, since additional energy would then effectively be given to the system during each half cycle of the transient, the possibility of sustained oscillations would be aggravated. In addition, a greater impact at recontact would take place and therefore wear and fatigue due to mechanical shock would be increased.

Thus the requirements of the stabilizer are twofold. It must race the motor across the backlash in a minimum of time whilst also ensuring that the motor comes into contact with the output member with zero relative velocity. These requirements are suggestive of an auxiliary control loop, to be actuated only for the period of separation and to be supplied with input information to enable the above requirements to be satisfied.

(3.1) The Auxiliary Control Loop

The requirements stated above imply that the auxiliary loop should control the position of the motor and should be in

equilibrium with the motor on either side of the backlash. An input step applied to this auxiliary loop at the instant of separation must then disturb the equilibrium position of the motor from one side of the backlash to the other. Also, if the motor must traverse the backlash in a short time, the natural frequency of the auxiliary loop must be high compared with that of the normal loop. This means that the auxiliary-loop gain must be comparatively high.

Consider now the arrangement shown schematically in Fig. 3.

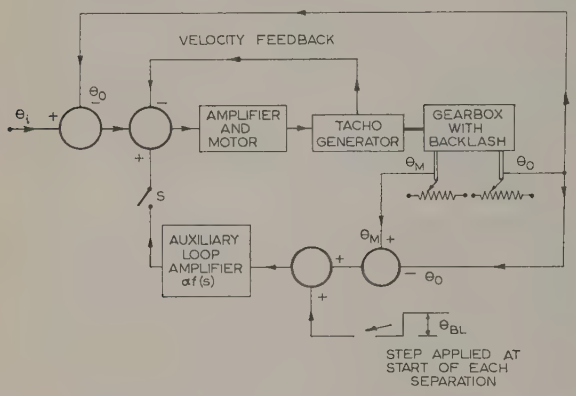

Fig. 3.—Schematic of position servo system using the auxiliary-loop method of stabilization.

The amplifier and motor receive signals from the auxiliary loop via a switch S which is closed only for the period of separation. An auxiliary-loop amplifier having a transfer function $\alpha f(s)$ is supplied with a voltage signal $\theta_M - \theta_0$ and one which changes by an amount θ_{BL} at the instant of separation. The sense of this step-change is such as to cause the motor to move to the required side of the backlash.

We shall now assume that the basic system is of second order and that $f(s)$ is, in this case, given by $f(s) = 1 + sT_d$. The equations defining the position of the motor during a period of separation, with switch S closed, are therefore

$$T_q(M) = I_M\ddot{\theta}_M + K_{VM}\dot{\theta}_M \quad . \quad . \quad . \quad (1)$$

coulomb friction having been neglected,

$$\text{and } T_q(M) = \underbrace{K[(\theta_i - \theta_0) - K_g\dot{\theta}_M]}_{\text{Normal loop signals}}$$

$$\underbrace{- K\alpha\left(1 + T_d\frac{d}{dt}\right)[(\theta_M - \theta_0) \pm \theta_{BL}]}_{\text{Auxiliary loop signals}} \quad (2)$$

In eqn. (2) the lag in the motor field has been neglected and the $\pm$ sign associated with the term θ_{BL} is included to indicate that either sense of step may be applied. The system will, of course, select the correct sense.

If the auxiliary amplifier gain, α, is made large the auxiliary-loop signals will predominate and the normal-loop signals may be neglected without introducing much error.

The equation defining the response during a period of separation is then obtained from eqns. (1) and (2) as

$$I_M\ddot{\theta}_M + K_{VM}\dot{\theta}_M = -K\alpha\left(1 + T_d\frac{d}{dt}\right)[(\theta_M - \theta_0) \pm \theta_{BL}] \quad (3)$$

which may be written in the form

$$\frac{I_M}{K\alpha}\ddot{\theta}_M + T_d\left(1 + \frac{K_{VM}}{K\alpha T_d}\right)\dot{\theta}_M + \theta_M = (\theta_0 \mp \theta_{BL}) + T_d\frac{d}{dt}(\theta_0 \mp \theta_{BL}) \quad (4)$$

If we now make the reasonable supposition that the term $(I_M/K\alpha)\ddot{\theta}_M$ is very nearly zero in the steady state, the steady-state solution of eqn. (4) is

$$\theta_M = \theta_0 \pm \theta_{BL} \quad . \quad . \quad . \quad . \quad . \quad . \quad . \quad (5)$$

$$\text{and} \qquad \dot{\theta}_M = \frac{\dot{\theta}_0}{(1 + K_{VM}/K\alpha T_d)} \quad . \quad . \quad . \quad . \quad (6)$$

This means that, when the steady state is reached, the motor has moved across the backlash and is travelling with virtually the same velocity as the resetter. The shape of the transient leading to this steady state is most important, for we must ensure that the motor never exceeds the position $\theta_0 \pm \theta_{BL}$ during the entire transient; if it did it would attempt to pass through this position with a velocity greater than $\dot{\theta}_0$ and an impact would take place.

The desired form of response is shown in Fig. 4.

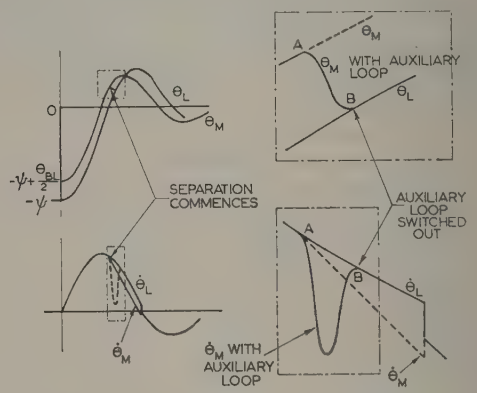

Fig. 4.—Step-function response waveforms showing the effect of the auxiliary loop.

In the case of a linear second-order system, critical damping of the auxiliary loop would give the required result. However, the requirement of minimum backlash transit time, and hence high gain, results in saturation of the power element and, if the gain is increased too much, the response exhibits overshoot even with critical damping.[5] Accordingly the damping of the auxiliary loop must be greater than critical.

Fig. 5 gives a comparison between the calculated and measured values of the damping factor and transit time as a function of n for a second-order system. The servo system used for the measurement employed a type 73 servo-motor with field control, and backlash of 3° amplitude was introduced intentionally. The theoretical curves were obtained from a phase-plane analysis which took account of coulomb friction and saturation.[6] It should also be pointed out that the noise in the system was purposely increased by using poorly filtered position signals from synchro receivers. This procedure was adopted to introduce the effect present in higher-order systems which have lags in the power-amplifying stages. Such systems may be stabilized by electrical networks inserted before the power amplifier, and the noisy signal, fed into the first power stage, is filtered but little before reaching the saturating element.

It has been deduced[6] that the discrepancy between the cal-

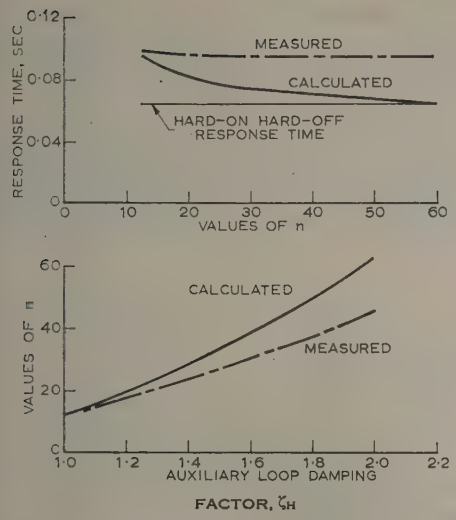

Fig. 5.—Comparison between the calculated and measured auxiliary-loop step-function response time and damping factor for zero overshoot.

culated and measured curves of Fig. 5 is due to the presence of noise. The curves do show, however, that with very large values of n sensibly practical damping factors prevent overshoot. Nevertheless, it is apparent that the presence of noise prevents any appreciable reduction in the transit time. Even so, a transit time of 0·1 sec with the large backlash angle of 3° is quite satisfactory for this servo system whose normal-loop natural frequency would be about 1–2 c/s.

Reduction of the transit time may not, therefore, be the deciding factor in choosing the gain of the auxiliary loop. This must also be chosen so as to make the auxiliary-loop signals predominate during the periods of separation. If this is not achieved the response during a separation period becomes dependent on the position and velocity of the resetter, and the transit time then depends on the amplitude of the overshoot of the normal loop. When examining the technique on the test rig it was found possible to satisfy this condition, and recordings of the transit response showed that the transit time was independent of the normal-loop signals. In the analysis which follows we shall assume, therefore, that the transit time is constant and a function only of the auxiliary-loop design. Transit times for a practical servo system will be deduced later.

(4) PHASE-PLANE ANALYSIS OF A SECOND-ORDER POSITION-CONTROL SYSTEM USING THE STABILIZING TECHNIQUE

From the discussion given above it may be observed that the suggested technique will minimize the last three effects attributed to backlash in Section 3.1. In this Section a phase-plane analysis will be outlined with the object of determining how well the technique reduces the overshoot of the servo mechanism. For this purpose we consider the second-order position-control system shown schematically in Fig. 3, stabilized partly by output velocity feedback and partly by viscous friction applied to the motor and resetter. Positional reset is taken from the load side of the backlash as shown.

When the motor is in contact with the load and resetter through the gearing, the equation defining the system is

$$I\ddot{\theta}_0 + K_V\dot{\theta}_0 + K\theta_0 = K\theta_i \quad . \quad . \quad . \quad (7)$$

If θ_i is a step-function input of amplitude ψ which reaches zero at time $t = 0$, eqn. (7) becomes

$$I\ddot{\theta}_0 + K_V\dot{\theta}_0 + K\theta_0 = 0 \quad . \quad . \quad . \quad . \quad . \quad (8)$$

The solution of this equation is well known and is

$$\theta_0 = -\frac{\psi\varepsilon^{-\sigma t}}{\sqrt{(1-\zeta^2)}}[\zeta \sin \omega t + \sqrt{(1-\zeta^2)} \cos \omega t] \quad (9)$$

and

$$\dot{\theta}_0 = \frac{\omega_n\psi\varepsilon^{-\sigma t}}{\sqrt{(1-\zeta^2)}} \sin \omega t \quad . \quad . \quad . \quad . \quad (10)$$

If we now make the substitutions

$$v = \dot{\theta}_0/\omega_n \quad . \quad . \quad . \quad . \quad . \quad (11)$$

and

$$u = \frac{\theta_0}{\sqrt{(1-\zeta^2)}} + \frac{\dot{\theta}_0}{\omega_n}\frac{\zeta}{\sqrt{(1-\zeta^2)}} \quad . \quad . \quad . \quad (12)$$

we obtain

$$v = \frac{\psi\varepsilon^{-\sigma t}}{\sqrt{(1-\zeta^2)}} \sin \omega t \quad . \quad . \quad . \quad . \quad (13)$$

and

$$u = -\frac{\psi\varepsilon^{-\sigma t}}{\sqrt{(1-\zeta^2)}} \cos \omega t \quad . \quad . \quad . \quad . \quad (14)$$

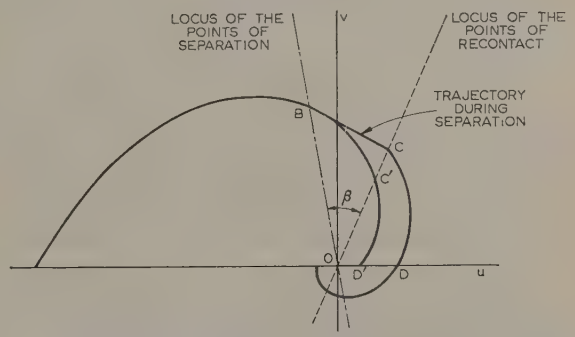

Fig. 6.—Phase-plane trajectories in the uv-plane for the linear system and the system with backlash using the auxiliary loop.

Thus, if we plot the trajectory representing the transient in the uv-plane, as in Fig. 6, the polar co-ordinates of any point (u, v) are

$$r = \sqrt{(u^2 + v^2)} \quad . \quad . \quad . \quad . \quad . \quad (15)$$

and

$$\rho = \arctan (v/u) \quad . \quad . \quad . \quad . \quad . \quad (16)$$

so that from eqns. (13) and (14) we have

$$r = \frac{\psi}{\sqrt{(1-\zeta^2)}} \exp\left[\frac{-\zeta(\pi-\rho)}{\sqrt{(1-\zeta^2)}}\right] \quad . \quad . \quad (17)$$

Eqns. (16) and (17) represent a logarithmic spiral in the uv-plane.

(4.1) Points of Separation on the uv-Plane

Eqns. (16) and (17) describe the motion of the output so long as it maintains contact with the motor. During the period of deceleration a point is reached when the deceleration of the motor exceeds that of the resetter. At this point the two members separate.

The decleration of the motor just before separation is obtained from eqn. (8) as

$$\ddot{\theta}_0 = -\frac{K_V\dot{\theta}_0 + K\theta_0}{I} \quad . \quad . \quad . \quad . \quad (18)$$

The motion of the load and resetter during a separation is defined by

$$I_L\ddot{\theta}_0 + K_{VL}\dot{\theta}_0 = 0 \quad . \quad . \quad . \quad . \quad (19)$$

Thus the load deceleration is given by

$$\ddot{\theta}_0 = -\frac{K_{VL}}{I_L}\dot{\theta}_0 \quad . \quad . \quad . \quad . \quad . \quad . \quad (20)$$

At the point of separation the deceleration of the motor just equals that of the load. Thus the instant of separation is obtained by equating eqns. (19) and (20). Therefore

$$\frac{-K_{VL}}{I_L}\dot{\theta}_0 = -\frac{K_V\dot{\theta}_0 + K\theta_0}{I} \quad . \quad . \quad . \quad (21)$$

for a separation.

By transforming eqn. (21) through eqns. (11) and (12), points of separation in the *uv*-plane are characterized by

$$v_s = \frac{\sqrt{(1-\zeta^2)}}{2\zeta_L - \zeta}u_s \quad . \quad . \quad . \quad . \quad . \quad (22)$$

where the subscript s indicates the beginning of a separation. The point of separation on any particular trajectory occurs at the intersection of that trajectory with the locus defined by eqn. (22) (point B, Fig. 6).

(4.2) Points of Recontact in the *uv*-Plane

We have already seen that, provided that the gain of the auxiliary amplifier is made sufficiently large, the period of separation is constant. After this fixed period of separation, τ, therefore, the auxiliary loop is switched out of circuit and the trajectory in the *uv*-plane is once more defined by eqn. (8). The initial conditions to be substituted into eqn. (8) are those existing at the instant of recontact. Since the motor is brought into contact with the load with zero relative velocity the initial conditions are the velocity and position of the load at the end of the separation period. These conditions are obtained by solving eqn. (19). They are $\dot{\theta}_{oc}$ and θ_{oc} and are given by

$$\dot{\theta}_{oc} = \dot{\theta}_{os}\exp(-2\zeta_L\omega_n\tau) \quad . \quad . \quad . \quad . \quad (23)$$

and

$$2\zeta_L\omega_n(\theta_{oc} - \theta_{os}) = \dot{\theta}_{os} - \dot{\theta}_{oc} \quad . \quad . \quad . \quad (24)$$

where the subscripts c and s indicate the instants of contact and separation, respectively. After transforming eqns. (23) and (24) through eqns. (11) and (12) and eliminating the initial conditions by substituting from eqn. (22), the relation between v_c and u_c may be simplified to give

$$v_c = \frac{2\zeta_L\sqrt{(1-\zeta^2)}u_c}{[2\zeta\zeta_L - 1 + \exp(2\zeta_L\omega_n\tau)(1 + 4\zeta_L^2 - 4\zeta\zeta_L)]} \quad (25)$$

Points of recontact occur where the trajectory representing the motion during a period of separation intersects the locus defined by eqn. (25). A more direct method of determining the point of recontact is to use eqn. (23) to obtain

$$v_c = v_s\exp(-2\zeta_L\omega_n\tau). \quad . \quad . \quad . \quad . \quad (26)$$

and then by measuring v_s from the trajectory to compute v_c. This value of v_c must then lie on the locus of the points of recontact. Having thus plotted the trajectory up to the point of recontact (point C, Fig. 6) the trajectory from C to the next point of separation can be drawn, since it takes the form of a logarithmic spiral. Fig. 6 shows the complete trajectory and also the trajectory obtained in the absence of backlash.

(4.3) Overshoot of the Transient Oscillation

In this Section we shall be concerned with the question: how closely does the overshoot approach that of the linear system? Maximum overshoot occurs when $\dot{\theta}_0 = 0$, or in the *uv*-plane shown in Fig. 6, when $v = 0$. Thus the overshoot of the non-linear system is OD whilst that of the linear system is OD′. Now both trajectories, C′D′ and CD, turn through the same angle in moving from the locus of the points of recontact to the axis $v = 0$ and both are logarithmic spirals with the same decrement; therefore

$$\frac{\text{OD}}{\text{OD}'} = \frac{\text{OC}}{\text{OC}'} \quad . \quad . \quad . \quad . \quad . \quad . \quad (27)$$

Now $$\text{OC} = \sqrt{(v_c^2 + \mu_c^2)} = v_c\sqrt{(1 + u_c^2/v_c^2)} \quad . \quad . \quad (28)$$

Using eqn. (23) we obtain

$$\text{OC} = v_s\exp(-2\zeta_L\omega_n\tau)\sqrt{(1 + u_c^2/v_c^2)} \quad . \quad . \quad (29)$$

The ratio u_c/v_c depends only on the system parameters and may be calculated directly from eqn. (25).

Using eqn. (17) we have

$$\text{OC}' = \text{OB}\exp\left[\frac{-\zeta\beta}{\sqrt{(1-\zeta^2)}}\right] \quad . \quad . \quad . \quad (30)$$

where $$\beta = \arctan(v_s/u_s) - \arctan(v_c/u_c)$$

But $$\text{OB} = \sqrt{(v_s^2 + u_s^2)} = v_s\sqrt{(1 + u_s^2/v_s^2)} \quad . \quad . \quad (31)$$

Therefore $$\text{OC}' = v_s\exp\left[\frac{-\zeta\beta}{\sqrt{(1-\zeta^2)}}\right]\sqrt{(1 + u_s^2/v_s^2)} \quad . \quad (32)$$

The ratio u_s/v_s may be calculated directly from eqn. (22):

$$\frac{\text{OD}}{\text{OD}'} = \Gamma = \frac{\exp(-2\zeta_L\omega_n\tau)\sqrt{(1 + u_c^2/v_c^2)}}{\exp\left[\frac{-\zeta\beta}{\sqrt{(1-\zeta^2)}}\right]\sqrt{(1 + u_s^2/v_s^2)}} \quad . \quad (33)$$

Eqn. (33) defines the ratio of the percentage overshoot for the non-linear system to the percentage overshoot for the linear system. It will be apparent that this ratio, Γ, is dependent on system parameters and, in particular, on the transit time, τ. Before going on to discuss the ratio Γ, therefore, it is necessary to make an estimate of the value of τ obtainable in practice.

(4.4) Estimating the Transit Time

The transit time depends on the gain of the auxiliary loop. Increasing the gain reduces the transit time provided that the power element does not limit. Ultimately, saturation prevents appreciable reduction in transit time, and the minimum time is obtained with virtually 'hard-on, hard-off' control. Under these conditions τ is given by[7]

$$\tau_{min} = 2\sqrt{\left(\frac{I_M\theta_{BL}}{T_{qmax}}\right)} \quad . \quad . \quad . \quad . \quad (34)$$

where T_{qmax} is the maximum torque available. If we now assume that a step of amplitude θ_s demands maximum torque we have

$$T_{qmax} = K\theta_s \quad . \quad . \quad . \quad . \quad . \quad (35)$$

and therefore

$$\tau_{min} = 2\sqrt{\left(\frac{I_M\theta_{BL}}{K\theta_s}\right)}$$

$$= \frac{2}{\omega_n}\sqrt{\left(\frac{I_M}{I}\frac{\theta_{BL}}{\theta_s}\right)} \quad . \quad . \quad . \quad . \quad (36)$$

To obtain an estimate of the maximum value of τ we assume that the gain of the auxiliary amplifier is so low that it just fails to saturate the motor when the step θ_{BL} is applied to the auxiliary loop. This means that

$$K\alpha\theta_{BL} = K\theta_s \quad . \quad . \quad . \quad . \quad . \quad . \quad (37)$$

If we examine the transient response of a reasonably well-damped servo mechanism with natural frequency ω_n, it is found that the response time is approximately $3/\omega_n$. Hence the response time of the auxiliary loop is

$$\tau_{max} = 3/\omega_H \quad . \quad . \quad . \quad . \quad . \quad . \quad (38)$$

where ω_H is the natural frequency of this loop.

But

$$\frac{\omega_H}{\omega_n} = \sqrt{\left(\frac{K\alpha/I_M}{K/I}\right)}$$

which, on substituting for α from eqn. (37), gives

$$\frac{\omega_H}{\omega_n} = \sqrt{\left(\frac{I}{I_M}\frac{\theta_s}{\theta_{BL}}\right)} \quad . \quad . \quad . \quad . \quad (39)$$

Thus

$$\tau_{max} = \frac{3}{\omega_n}\sqrt{\left(\frac{I_M}{I}\frac{\theta_{BL}}{\theta_s}\right)} \quad . \quad . \quad . \quad (40)$$

Comparing τ_{max} and τ_{min} it is seen that varying the auxiliary-loop gain over the entire practical range does not give appreciable change in the transit time. Thus we shall assume a value for τ of

$$\tau = \frac{2{\cdot}5}{\omega_n}\sqrt{\left(\frac{I_M}{I}\frac{\theta_{BL}}{\theta_s}\right)}$$

when calculating the overshoot. Furthermore we shall assume that $I_M = I_L = I/2$ and $\theta_s = 20\theta_{BL}$.

This latter assumption means that a step of 20 times the backlash angle just causes saturation of the normal loop. With these assumptions, $\omega_n\tau = 0{\cdot}4$. Fig. 7 shows how the ratio Γ

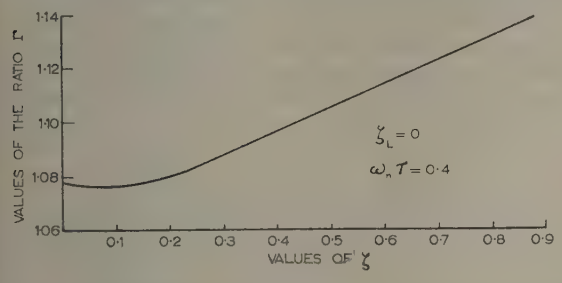

Fig. 7.—Comparison of overshoot of servo system with the auxiliary loop and that of the linear system for the case where $\zeta_L = 0$ and $\omega_n\tau = 0{\cdot}4$.

varies with ζ for the worst possible case, namely $\zeta_L = 0$. It may be seen that the overshoot of the non-linear transient is never appreciably greater than that exhibited by the servo mechanism without backlash. Furthermore, since Γ is independent of overshoot the non-linear transient is identical with a linear transient with slightly smaller damping. For example, suppose $\zeta = 0{\cdot}5$ and $\zeta_L = 0$. Fig. 7 shows that $\Gamma = 1{\cdot}106$. A linear system showing the same overshoot would have a damping factor $\zeta = 0{\cdot}48$. In other words, the method of stabilization linearizes the step-function response but results in very slightly reduced damping.

(5) ANALOGUE COMPUTER STUDY

The servo system examined with the computer is one in which the friction/inertia ratio for the load side of the backlash is very large. This implies that the motor and load separate only when the velocity of the motor changes sign. Such systems receive no assistance from the motion of the load when transporting the motor across the backlash. Accordingly they present the most difficult conditions under which the auxiliary loop has to operate. Fig. 8 shows the schematic arrangement of the additional circuits required for the auxiliary loop in the analogue study. The circuits have also been used to realize the technique on a test rig.

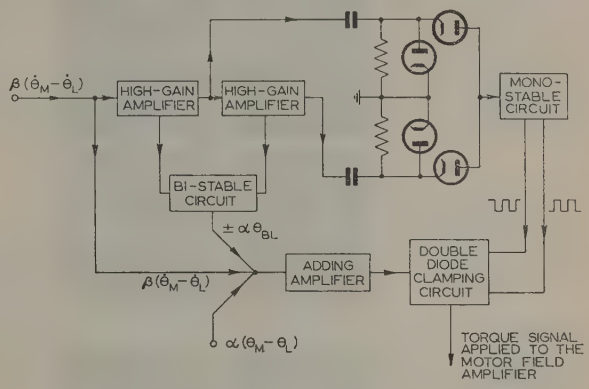

Fig. 8.—Schematic of circuit-elements employed by the auxiliary loop.

Separation is detected by feeding a signal $\beta(\dot{\theta}_M - \dot{\theta}_L)$ into a high-gain amplifier. Pulses thus produced are supplied to bistable and monostable circuits. The bistable circuit provides the step output $\alpha\theta_{BL}$ whenever a pulse is received, the sense of the step being determined by the sense of $\frac{d}{dt}(\dot{\theta}_M - \dot{\theta}_L)$. By adding this output to signals $\alpha(\theta_M - \theta_L)$ and $\beta(\dot{\theta}_M - \dot{\theta}_L)$ the error signal for the auxiliary loop is obtained. The monostable circuit provides the gating waveform for the auxiliary-loop error signal; its recovery time-constant being adjusted so that the gate is opened for the time taken by the motor to move across the backlash.

(5.1) Transient Response from the Analogue Computer

Waveforms showing the transient response of a second-order linear system, the system with backlash and the system stabilized by the auxiliary loop are shown in Figs. 9(*a*), (*b*) and (*c*). The most undesirable features of the response with backlash are the increase in rise time and settling time. It may be recalled that settling time is increased because the motor takes longer to traverse the backlash when the overshoot becomes small. With the auxiliary loop correctly adjusted, the separation period remains constant and the transient response is thereby improved. Measurement of the transient also indicates that the overshoot with the auxiliary loop is the same as that of the linear system.

Examination of the motor-velocity waveforms reveals that, at the instant of separation, the motor velocity rises instantaneously and then, as the motor approaches the other side of the backlash, falls to become almost equal to the load velocity.

The instantaneous rise in motor velocity is effected by stabilizing the auxiliary loop with derivative of error. Had output-velocity feedback been used, the rise in motor velocity would have been more gradual and thus the time to cross the backlash would have been increased.

In a practical system, saturation of the power element limits the rate of change of velocity still further.

Another interesting possibility in practical systems is that of

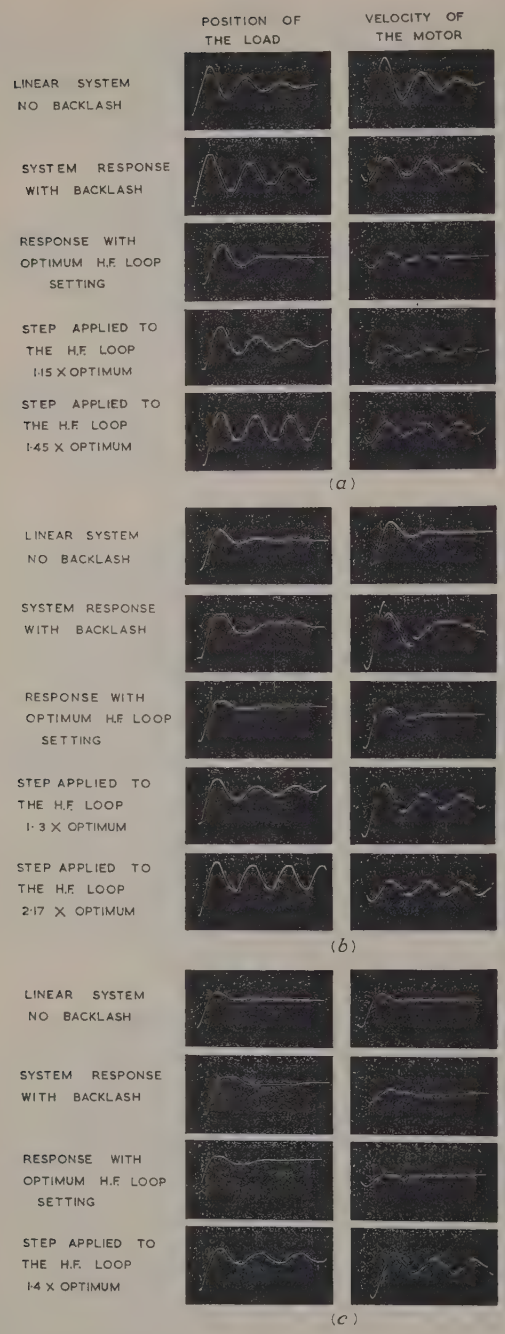

Fig. 9.—Transient response with the auxiliary loop, illustrating the effect of reducing the amount of backlash.
All velocity feedback from the motor. $I_L/I_M = 1{\cdot}36$; $\psi/\theta_{BL} = 1{\cdot}64$.
(*a*) $K_V/\omega_n I = 0{\cdot}34$. (*b*) $K_V/\omega_n I = 0{\cdot}73$. (*c*) $K_V/\omega_n I = 1{\cdot}06$.

changes in the amount of backlash present. The effect of reduced backlash, the worst case, is illustrated in Figs. 9(*a*), (*b*) and (*c*). It is apparent that, if the backlash decreases sufficiently without adjustment of the auxiliary loop, sustained oscillations may result. Fortunately, backlash in practical systems tends to increase with time, and, in this case, oscillations will only result when the increase in the backlash is equal to the amount likely to cause oscillations in the absence of the auxiliary loop. In any event the simple re-adjustment of the signal $\alpha\theta_{BL}$ will compensate for changes in the amplitude of the backlash.

Comparison of Figs. 9(*a*), (*b*) and (*c*) will also show the improvement in response obtained when the low-frequency loop damping is increased. It is apparent that, whilst the response with backlash is not improved satisfactorily, the auxiliary loop results in the same improvement as is shown by the linear servo system.

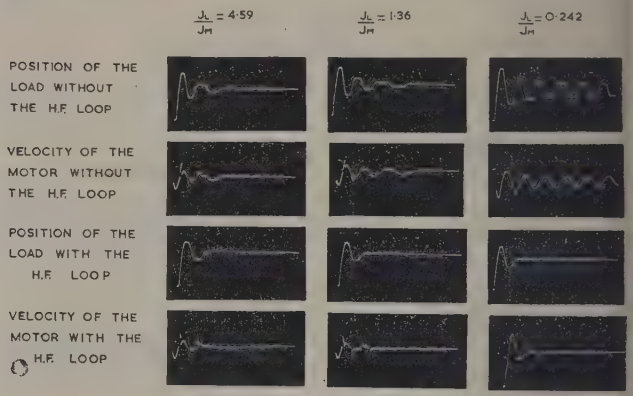

Fig. 10.—Effect of varying the ratio of inertias I_L/I_M.
$\frac{K_V}{\omega_n I} = 0{\cdot}48 \quad \frac{\psi}{\theta_{BL}} = 3{\cdot}33$
All positional reset taken from the load.
All velocity feedback taken from the motor.

Finally, Fig. 10 illustrates the effect of varying the ratio of inertias. It may be seen that the auxiliary loop removes the dependence of the step-function response on this ratio. It should be borne in mind that the analogue computer gives only an approximate representation of the actual system, for it assumes that separations take place as the motor velocity changes sign. However, it has been shown[4] that the analogue computer gives a pessimistic estimate of the servo system's transient response.

(6) DISCUSSION AND CONCLUSIONS

A method of stabilizing control systems with backlash has been introduced which requires an auxiliary control loop. This drives the motor across the backlash, in the appropriate direction, whenever the motor and load tend to separate. It has been shown that the method improves the step-function response to that of the servo mechanism without backlash. Also, since the motor is always controlled to one side of the backlash, the dead space is effectively removed and the positional accuracy is thereby improved. Mechanical wear is reduced because the auxiliary loop minimizes the impacts which tend to occur between motor and load.

The analogue computer study has illustrated the degree of improvement effected, and it has been shown schematically how one may realize the desired switching sequence. Certain difficulties encountered in the practical application have been omitted from this introduction, however, for the sake of a clear presentation of the basic idea, a simplified though adequate analysis and the requirements of the auxiliary loop. Some of the difficulties experienced when realizing the technique on a test rig of a second-order position-control servo mechanism will now be outlined.

The first problem arises in the accurate measurement of the

difference between motor position and output position in servo systems with small amounts of backlash. For, if we suppose that the servo system will be satisfactory when the backlash is virtually reduced by a factor of ten, we require that the inaccuracy in the measuring instrument shall not be greater than $\theta_{BL}/10$. Since the most accurate synchro has a maximum error of about 3′ the minimum amount of backlash that can be overcome is 30′. In large servos this restriction may be eased by using highly accurate instrument gears to amplify the difference position, although it is as well to point out that, when the amount of backlash present is small, dry friction, inherent in many servo systems, tends to damp out small-amplitude oscillations.

Coupled with the measurement difficulty is the detection of the instant of separation. Differentiation of the difference-position signal provides a suitable voltage from which to derive the pulse indicating separation. However, with this method, if the motor should start from rest in the middle of the backlash the first separation is not detected. To overcome this, detection may be achieved by interrupting the light incident on a photo-transistor with two toothed discs mounted on both the driving and driven shafts. Any relative motion between the two shafts then produces a pulsed output from the photo-transistor.

A further complication may arise if the backlash present is a function of the angular position of the gear wheels. Such a dependence may be caused by variations in the dimensions of individual teeth or eccentricities in the gear mounting and shafts. The former of these causes is not so important, for the variations tend to decrease as the gears are run in. The latter, however, is more serious because the step applied to the auxiliary loop at the start of a separation may be greater than the actual backlash for that particular angular position. As a result, an increased impact may take place and, because the auxiliary loop has not removed all of the additional energy given to the system at separation, sustained oscillations may result. These oscillations can only be excited for certain angular positions of the output. Figs. 9(*a*), (*b*) and (*c*) from the analogue computer study illustrate this possibility. This drawback may be overcome by making the step applied to the auxiliary loop dependent on angular position, using a function generator supplied with θ_0 or θ_M to generate the appropriate value of the step θ_{BL}.

The transient response of the auxiliary loop is of fundamental importance to the method, and the design of this loop may prove difficult in higher-order systems. The test rig used by the author is basically second order with a field lag. Saturation, noise and the presence of coulomb friction limit the response time of the auxiliary loop.

A phase-plane analysis based on the assumption that a phase-advance network cancels the field lag may be used to design the auxiliary loop for zero impact.[6] The response time and damping factor thus obtained compare favourably with measurements from the rig. Discrepancies arise because noise and saturation prevent complete cancellation of the field lag and also reduce the effective gain of the loop.

In higher-order systems it is probably more expedient to derive the best damping by a combination of describing-function analysis[8] and test-rig measurement. However, although it may be possible to design the auxiliary loop so as to prevent impact, the time of response may be so impaired that the improvement effected does not justify the extra equipment except when mechanical wear is the prime consideration. An estimate of the degree of linearization for the step-function response may be made from the analysis already given, once the response time of the auxiliary loop is known. Further, because of the nature of the technique, the system behaves as a linear one for any type of input. Measured frequency/response characteristics compare with those from the rig without backlash and with reduced damping.

(7) ACKNOWLEDGMENTS

The author is indebted to the Governors and Principal of Sunderland Technical College for the special facilities placed at his disposal during the preparation of this work. Thanks are due to Dr. M. Hutton, Vice-Principal, for his advice and encouragement.

In addition, the author is grateful to Professor J. C. Prescott of King's College, Newcastle upon Tyne, for the facilities placed at his disposal. Useful discussions also took place with Mr. F. J. U. Ritson and Dr. C. A. Walley, both of King's College.

(8) REFERENCES

(1) LIVERSEDGE, J. H.: 'Backlash and Resilience within the Closed Loop of Automatic Control Systems', from TUSTIN, A. (Ed.): 'Automatic and Manual Control' (Butterworths Scientific Publications, 1952), p. 343.

(2) CHESTNUT, H., and MAYER, R. W.: 'Servomechanisms and Regulating System Design' (Chapman and Hall, 1955), Vol. II, p. 301.

(3) FREEMAN, E. A.: 'The Effect of Speed-Dependent Friction and Backlash on the Stability of Automatic Control Systems', *Transactions of the American I.E.E.*, 1958, **77**, p. 680.

(4) FREEMAN, E. A.: 'An Approximate Transient Analysis of a Second-Order Position-Control System when Backlash is Present', *Proceedings I.E.E.*, Monograph No. 254 M, September, 1957 (**105** C, p. 61).

(5) WEST, J. C., and DALTON, I. R.: 'The Step-Function Response of an R.P.C. Servo Mechanism possessing Torque Limitation', *ibid.*, Paper No. 1576 M, November, 1953 (**101**, Part II, p. 166).

(6) FREEMAN, E. A.: 'An Investigation of Some Non-Linear Phenomena affecting the Performance of Automatic Control Systems', Ph.D. Thesis, King's College, University of Durham, November, 1958.

(7) MCDONALD, D.: 'Nonlinear Techniques for Improving Servo Performance', *Proceedings of the National Electronics Conference*, 1950, **16**, p. 413.

(8) KOCHENBURGER, R. J.: 'A Frequency Response Method for Analyzing and Synthesizing Contactor Servomechanisms', *Transactions of the American I.E.E.*, **69**, p. 270.

621.385:032.213.13

The Institution of Electrical Engineers
Monograph No. 357 E
Feb. 1960
©

THE CONDUCTIVITY OF OXIDE CATHODES

Part 8. Current-Dependent Matrix Dissociation

By G. H. METSON, M.C., D.Sc., Ph.D., M.Sc., B.Sc.(Eng.), Member, and EDITH MACARTNEY, M.Sc., B.Sc.

(*The paper was first received 7th July, and in revised form 24th September*, 1959. *It was published as an* INSTITUTION MONOGRAPH *in February* 1960.)

SUMMARY

In the present Part an attempt is made to determine the nature of the dissociative action which accompanies the passage of a current through a barium-strontium-oxide matrix at 1 020° K. Two identical oxide systems operating at a common temperature and passing the same quantity of electricity but at different rates might be expected to suffer the same mass of oxide dissociation. Experiment shows, however, that such is not necessarily the case and that dissociation mass is determined by rate of application of electricity rather than by the total quantity of electricity.

The products of dissociation are shown to be in ionic form, and experimental arrangements are made for the separate collection of the ions in chemical form on a relatively massive scale.

A working hypothesis is offered in explanation of the experimental observations.

(1) INTRODUCTION

The present Part examines the circumstances under which a passage of current causes the chemical dissociation of the barium-strontium-oxide matrix. That such dissociation occurs has been known since the earliest days of the art, and it has long been assumed that the phenomenon is a solid-state electrolytic one determined in magnitude by the laws of Faraday. Following the contemporary view of the cathode as two parallel conducting elements—one solid and the other vacuum—it would seem that the electrolytic phenomenon must be associated with the solid-conduction phase and be largely independent of the vacuum flight of electrons through the matrix. Until recently the authors would themselves have held this conventional view, but as a result of experiments to be described in the present Part, they now have reservations as to the basic nature of the dissociation. According to the evidence set out in the paper it would seem that the dissociation is not of a Faradaic nature, is associated primarily with the vacuum passage of electrons through the porous matrix, and is markedly dependent on electron flight velocity. Such an action cannot be appropriately described as electrolytic, and it is for this reason that an apparently prolix sub-title has been chosen for the paper.

(2) EXPERIMENTAL PROCEDURE

(2.1) Development of an Experimental Method

The primary object of the present exercise is to demonstrate first in direct and convincing fashion the act of current-dependent dissociation, and then to see whether the Faradaic law of proportionality between quantities of current and dissociated oxide is obeyed.

Fig. 1 shows a typical conductivity/temperature characteristic for an oxide matrix held between parallel plane electrodes. At the conventional operating temperature of 1 020° K conduction is partly by way of a solid conductivity, σ_{sol}, and partly by way of a parallel vacuum conductivity, σ_{vac}, where $\sigma_{vac} \gg \sigma_{sol}$.

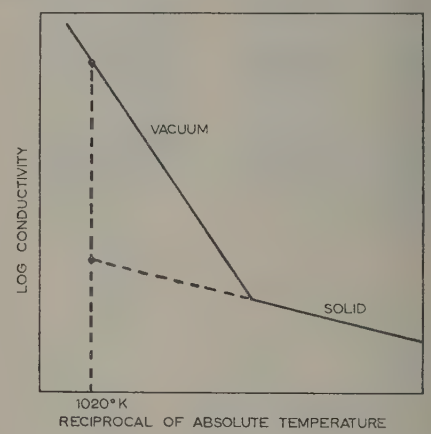

Fig. 1.—Typical conductivity/temperature characteristic.

Both of these conductivities have been shown to obey Ohm's law in their current/voltage relationships. For any applied voltage V_A it follows that

$$V_A = I_{sol}/\sigma_{sol} = I_{vac}/\sigma_{vac}$$

or

$$I_{vac}/I_{sol} = \sigma_{vac}/\sigma_{sol} = \text{constant}$$

or

$$I_{sol} \propto I_{vac}$$

The current, I_{sol}, carried by the contiguous chains of solid particles is therefore always proportional to the current, I_{vac}, passing vacuum-wise through the hollow pores. Furthermore, since $I_{vac} \gg I_{sol}$ we can write $I_{sol} \propto I_A$ without sensible error, where I_A is the total current carried by the matrix, measured with an external ammeter.

Suppose now that I_{sol} has an electronic component I_e and an ionic component I_i in fixed ratio to each other. Then

$$I_A \propto I_e + I_i$$
$$\propto I_i$$
$$\propto m$$

where m is, by Faraday's law, the quantity of oxygen or barium liberated per second at the appropriate electrode by I_i. At constant temperature, therefore, the rate of dissociation of the oxide matrix should be proportional to the current I_A traversing the matrix. In other words, a certain quantity of electricity will

The paper is a continuation of Monographs Nos. 221 R and 243 R, published in February and June, 1957 (see 104 C, pp. 316 and 496), Nos. 268 R, 269 R and 289 R, published in December, 1957, and February, 1958 (see 105 C, pp. 183, 189 and 374), No. 317 R, published in November, 1958 (see 106 C, p. 55) and No. 347 E, published in October, 1959 (see 107 C).

Correspondence on Monographs is invited for consideration with a view to publication.

Dr. Metson and Miss Macartney are at the Post Office Research Station.

roduce a fixed amount of oxygen and barium irrespective of the ate at which it is applied.

Fig. 2 shows two identical S-assembly systems working at a ommon temperature $T°$; one system carries a current I_{A1} for

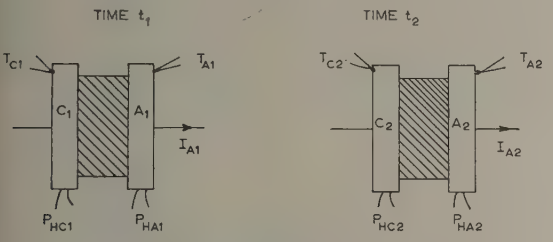

Fig. 2.—Representation of the basic experiment.

ime t_1 and the other a current I_{A2} for time t_2 such that both ystems pass the same quantity of electricity, Q, i.e.

$$Q = I_{A1}t_1 = I_{A2}t_2$$

On the assumption that the oxide matrix does indeed possess an ionic conductivity at temperature $T°$, the total quantity of oxygen delivered at each anode will be the same—as, of course, will be the total quantity of barium metal at each cathode. All that is now required is a means of storing and subsequently comparing the quantities of oxygen delivered to the anodes. If the same end can be achieved with barium delivered to the cathodes, so much the better—although this is not essential. In respect of oxygen released at the anodes, the most convenient method of storage is chemical in the form of black oxide of nickel, NiO_2 of Ni_2O_3. Barium metal released at the cathode can be stored in platinum as a solid solution or alloy.

The experimental plan can thus be summed up in the following terms. Two identical systems (Fig. 2) are run at the same temperature and pass the same total quantity of electricity but at different current levels. The products of matrix dissociation are stored at the electrodes by either chemical or alloying action. By comparing the quantities stored in the two cases it is hoped that a conclusion can be reached as to the nature of the dissociative action.

(2.2) Experimental Arrangements

A schematic of the experimental valve is set out in Fig. 2 and this is seen to be a standard S-type assembly* with certain additional facilities. Each electrode is provided with an individual thermocouple and the insulated internal heaters for each core are brought out of the vacuum envelope separately. The cores may be both nickel, both platinum or one nickel and one platinum, according to the requirements of a particular experiment. The valves are vacuum-processed in the standard manner described in Part 1 of the paper, except that carbonate decomposition is effected rather more slowly to avoid a tendency to core oxidation by carbon dioxide. After activation to bring the matrix resistance at 1 020° K down to the minimum R_0 level, the valves are ready for the proposed experiment.

In order to set up a valve for measurement, certain essential precautions are necessary, and these will be described. Suppose that it is decided to conduct an experiment at a constant temperature of 1 020° K. A valve is set up with $I_{A1} = 0$ and its two heater inputs adjusted individually to give $T_{C1} = T_{A1} = 1\,020°$ K. The current I_{A1} is now increased from zero to its predetermined value by adjusting a voltage V_A between the electrodes. This current flow immediately alters the individual electrode temperatures in the manner described in Part 4 of the paper. By simultaneous adjustment of V_A and the two core inputs P_{HC} and P_{HA}, the system is brought back into the desired temperature condition $T_{C1} = T_{A1} = 1\,020°$ K, while carrying the required current I_{A1}. This condition is held for time t_1 to complete the passage of a quantity of electricity $Q = I_{A1}t_1$. A companion is next taken and adjusted in the same way but to a different current level, I_{A2}, with $T_{C2} = T_{A2} = 1\,020°$ K and held for time t_2 such that $Q = I_{A1}t_1 = I_{A2}t_2$. This completes a single experimental run and the pair of valves are now ready for comparison of the quantities of dissociated ions on a pair of electrodes.

* Specification of standard S-type assembly:
Cores: Active nickel or pure platinum.
Matrix: Co-precipitated equimolar barium-strontium oxide.
Matrix density: About 1·0.
Matrix thickness: 150μ.
Matrix Area: 0·25 cm².
Erratum: In previous Parts the area has been quoted in error as 0·45 cm².

(2.3) The Basic Experiment

In a system with both cathode and anode cores of nickel, it is possible only to collect and store oxygen. The bulk of effort has been put into this system. In a typical experiment two identical valves are set up for the following condition:

Common temperature, $T = 1\,020°$ K
$I_{A1} = 50$ mA
$t_1 = 40$ hours
$I_{A2} = 500$ mA
$t_2 = 4$ hours

$$Q = I_{A1}t_1 = I_{A2}t_2 = 2\,000 \text{ mAh}$$

The two valves have now passed a common quantity of electricity at a common temperature, but at rates of transfer of charge differing by a factor of ten. After the valves are opened the four electrodes are carefully lixiviated with distilled water, dried and laid out for comparison.

The two cathodic cores C_1 and C_2 are identical in appearance, with their working surfaces showing a light grey colour with the usual etched finish. The anodic core A_1, which has received 50 mA for 40 hours, is hardly distinguishable in appearance from the two cathodic cores C_1 and C_2. The anodic core A_2, which has carried the higher level of current, is, however, strikingly different and is coated with a layer of dense black oxide of nickel. The difference in appearance of A_1 and A_2 is, in fact, so marked that any anticipated difficulty in comparison does not arise. If the A_2 core is, for example, wiped with a wet filter paper, the outer layers of oxide are removed as a black smear on the paper. This description covers the basic experiment of the paper, and it has been repeated ten times with unvarying result.

The basic experiment can now be summed-up in the following terms. The mass of the matrix dissociated by a fixed quantity of electricity at a fixed temperature is dependent on the rate of application of electricity. The rate of variation of dissociated mass with magnitude of current is great and comfortably within the sensitivity range of the black-oxide method of detection.

(2.4) Dissociation Modes

Let the mass of matrix dissociated per second by a current 1 mA be denoted by M. Then the observed mode of matrix dissociation can be compared with the Faradaic mode in the following terms:

Faradaic mode: M = Constant and invariant with I_A.
Observed mode: $M = f(I_A)$.

The two modes are therefore essentially different, and the observed matrix dissociation cannot be regarded as being due to electrolysis in the accepted sense of the word.

The manner in which M varies with I_A can be appreciated in a qualitative way by observing the change of density of the black oxide over a range of I_A at constant temperature and constant charge quantity Q. The relationship appears to take the general form shown in Fig. 3, in which the Faradaic mode is included for comparison.

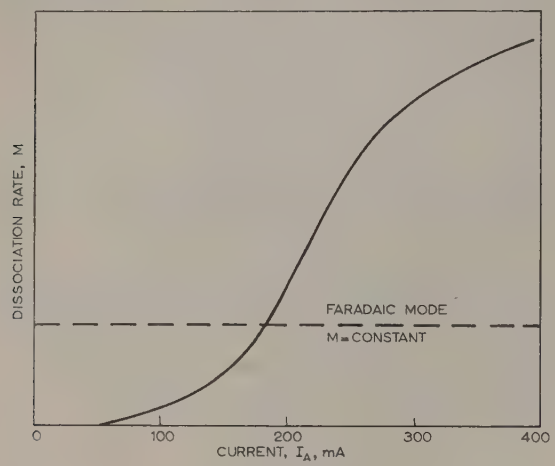

Fig. 3.—Probable form of the relationship between dissociation rate and current.

(2.5) Dissociation at Low Current Level

At a current of less than 50 mA at 1 050° K there is no visible oxidation of the anodic nickel core in 2 000 mAh. The rate of dissociation has fallen either to zero or to a magnitude that is too small to give rise to any observable anodic oxide film. This lack of sensitivity of the detection method can be overcome to some extent by increasing Q, and experiments to this end have been undertaken. Keeping $I_A = 50$ mA at 1 020° K the value of Q has been extended from 2 000 to 80 000 mAh, whereafter it is just possible to recognize a black oxide film on the cooler parts of the anode core face. This experiment seems to have extended the method to its useful limit. The impression thus gained by the authors is that, within the context of the experimental method, the dissociation rate is vanishingly small with $I_A < 50$ mA but increases with progressing rapidity as I_A increases. The current density at $I_A = 50$ mA is about $0{\cdot}2$ amp/cm^2.

(2.6) Working Hypothesis

It will be useful at this stage to set out the working hypothesis which the authors have adopted to explain the mechanism of the dissociation. At constant temperature the S-type assembly is ohmic in character and we can therefore write

$$M = f(I_A) = F(V_A)$$

where V_A is the voltage across the electrodes. This change gives a distinctive property to the electron—its speed of passage through the matrix.

The basic assumption of the hypothesis is that of the current elements in the equation

$$I_A = I_{vac} + I_{sol} \simeq I_{vac}$$

it is the vacuum element, I_{vac}, which causes the dissociation. This element is emitted thermionically at the cathode core face and proceeds vacuum-wise through the matrix on a start-stop basis, with electrons dissipating energy in the form of heat i successive non-elastic collisions with the impeding oxide particle It is a basic assumption of the hypothesis that these collisio are the sites at which dissociation occurs.

Consider an idealized matrix of thickness d and consisting uniformly spaced identical oxide particles of separation l su that $d = nl$. During passage of a current I_A under a potenti V_A each electron will make vacuum flights of length l and suff n non-elastic collisions with the impeding oxide particles. If is the power delivered to each particle and there are a total of particles in the matrix, $P = V_A I_A/N$, and this accession of pow will cause each particle to rise in temperature until it comes in equilibrium with its surroundings. It will be supposed now th as the electron bombardment power P is steadily increased the comes eventually a critical temperature, T_{crit}, at which a partic dissociates and its ions separate in the electric field V_A/d. Th is our elementary model, and in its present state it clearly suffe from two defects, namely

(*a*) The onset of dissociation is sudden and complete at son critical value of I_A corresponding to T_{crit}: in practice there is critical value of I_A.

(*b*) The model will work only if its temperature as a whole allowed to rise to T_{crit}, whereas in practice dissociation is shown be a function of I_A at constant temperature.

The first defect of the model is readily overcome by rearrangi the distribution of particles. Suppose in one part of the matr the particles have a spacing $2l$ in the direction of electron flo instead of the standard spacing l. Electrons passing throu this low-density section will make only $n/2$ flights and collisio and will in consequence deliver twice the power P to ea bombarded particle. Assuming uniform current density in t matrix, it is then clear that the lower-density section will arri at the critical temperature T_{crit} before the high-density sectio There will thus be two critical values of I_A at which dissociati will occur. If now the process is taken to the limit and t separation distance l made random, then, so far as the matr as a whole is concerned, the critical condition is eliminated a M will become a continuous function of I_A. The general conce will be clear from Fig. 4, which shows a matrix cross-section wi

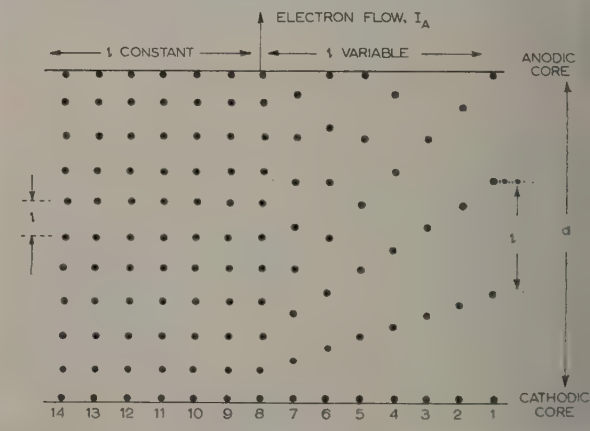

Fig. 4.—Model of cross-section of the matrix, showing the distributio of oxide particles.

dots representing oxide particles. Under a steadily increasir value of I_A the column of particles marked 1 will be the first reach the critical temperature and to dissociate. Columns 2- will follow at discrete intervals of I_A and columns 8–14 wi disintegrate simultaneously shortly after the disappearance

column 7. Assuming a permanent separation in the electric field of the dissociated ions, the model obviously implies the ultimate disappearance of the matrix.

The randomization of the particle-separation distance, l, gives, not only the required form of continuous relationship $M = f(I_A)$, but also avoids the temperature difficulty mentioned in (*b*) above. The matrix as a whole can now be kept at a constant mean temperature while allowing small numbers of individual particles, sited at the end of long electron runs, to come up to the critical temperature. In other words, the condition

$$T_{crit} \gg T_C = T_A = 1\,020^\circ\,\mathrm{K}$$

is quite compatible with the conditions under which the basic experiment of Section 2.3 was performed.

Further consideration will now be given to an individual particle which is about to arrive at the critical temperature. As I_A and V_A are steadily increased the core temperatures, T_C and T_A, can each be maintained at 1 020° K by adjustment of the core heater inputs P_{HC} and P_{HA}. Somewhere within the randomly arranged reticule of particles will be a longest electron run and the particle at its terminus will be the one to receive bombardment power at the fastest rate. As the particle reaches the critical temperature its constituent ions separate in the electric field, with the negative oxygen ions migrating to the anode and the positive barium ions to the cathode. The picture so far images the disintegration of the particle as a whole, but such a large-scale event is not essential. A stream of high-velocity electrons may strike one particular oxide molecule of a particle, giving to it sufficient vibrational energy to dissociate in the field. Such a piecemeal destruction is perhaps more credible than disintegration of the particle as a whole. In other words, a small finite point on a particle may come up to the critical temperature without the necessity for bringing the particle as a whole up to the required temperature. The relative functions of I_A and V_A emerge clearly from the picture: below some critical value of V_A there will be no dissociation, but above this value the rate of dissociation will increase with increase of both V_A and I_A.

(2.7) Bulk Separation of the Ions

A return will now be made to experimental observation. A group of standard S-type assemblies is prepared with pure platinum cathode cores and active-nickel anodic cores. One such valve is operated at 800 mA for 4 hours, and then opened for examination of the core surfaces. After removal of the barium-strontium-oxide matrix by lixiviation in distilled water, the two cores are dried and laid out for inspection. The nickel anodic core is coated with the usual layer of black nickel oxide, but interest now centres on the platinum core. The working or current-carrying surface of the platinum is quite distinctive in appearance compared with the non-working surface. It shows no signs of crystal boundaries, is of a characteristic matt finish, and is very hard compared with the non-working surface. At this stage the platinum core is washed in dilute hydrochloric acid, refitted with a new interior heater and remounted in a glass envelope. After the usual vacuum-processing the valve is sealed from the pump and the core set at 1 400° K for 70 hours. At the end of the experimental run the glass wall of the envelope opposite the non-working surface of the rectangular core is quite clear, showing a negligible evaporation of platinum metal, but the glass wall opposite the working surface is covered with a dense black metallic deposit of sufficient thickness to obscure all sight through the wall. When the envelope is opened to atmosphere the black deposit disappears instantly, leaving a white film which is found by spectrographic analysis to be a mixture of barium and strontium radicles.

In another experiment a tube is run at 1 100° K with a current of 170 mA for 2 000 hours. After opening the tube the platinum cathodic core is lixiviated in dilute acetic acid to remove the matrix from the inner current-carrying surface and the outer non-working surface. Photographs at a magnification factor of 200 show the typical appearances of the two surfaces. The non-working surface, which has been covered with barium-strontium during the test run, is shown in Fig. 5 and the crystal

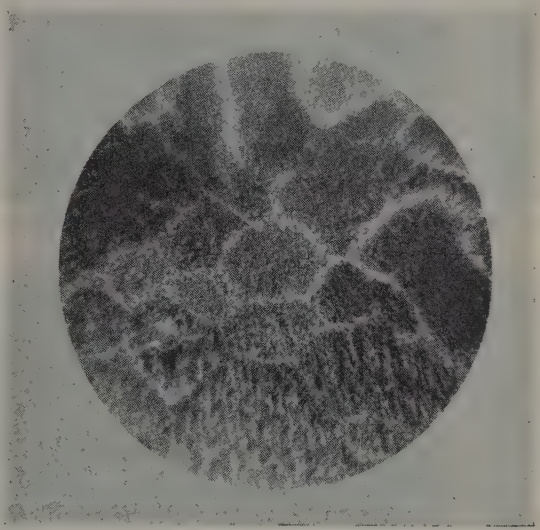

Fig. 5.—Non-working surface of platinum cathode core (×200).

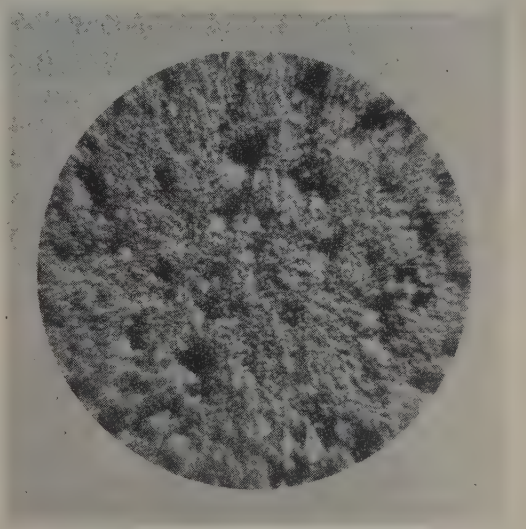

Fig. 6.—Working surface of platinum cathode core (×200).

boundaries of the platinum core are clearly visible. Fig. 6 shows the working surface, with its characteristic matt finish covered with irregularly spaced promontories of barium-platinum alloy. Fig. 7 is a cross-section of the core wall with a magnification of 1 000 and gives an idea of the magnitude of the alloy promontories in relation to the thickness of the core wall. Fig. 8 is a cross-section with a magnification of 1 000 at a point where barium alloying has been particularly deep. Over areas of the working surface where substantial alloying has occurred it is

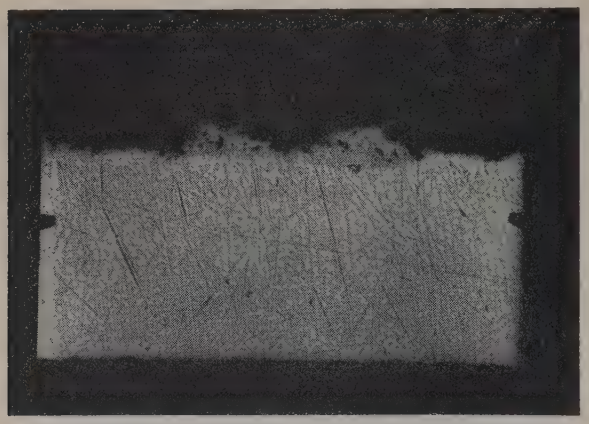

Fig. 7.—Cross-section of working surface of platinum core (×1 000).

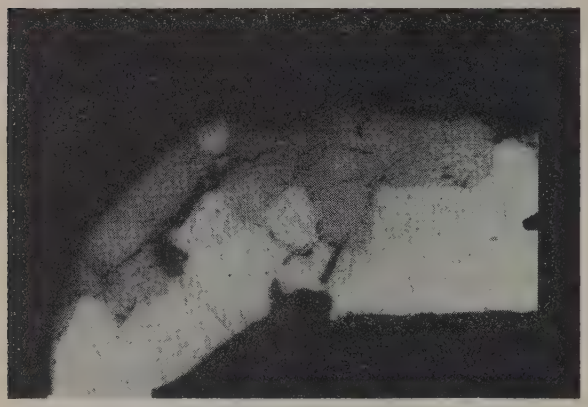

Fig. 8.—Cross-section of working surface of platinum core showing area of deep alloying (×1 000).

observed that mechanical buckling is present. This is doubtless due to a bimetallic-strip action with the alloy developing a different coefficient of thermal expansion from that of the underlying pure platinum.

The two experiments taken together show ion separation on a relatively massive scale.

(2.8) Oxygen Action on the Matrix

The behaviour of a standard S-type assembly fitted with platinum cathode and anode cores was studied in some detail in Part 2 of the paper. Under direct-current flow at 1 020° K it was shown that the system has an inherent tendency to self-deactivation and that this tendency increases with increase of current level. The phenomenon is explained in terms of a current-dependent matrix dissociation with concurrent loss of barium by solution into the platinum cathode core. Since the oxygen ions find no chemical 'sink' at the platinum anode, the gas tends to accumulate in the vacuum pores of the matrix which suffers progressive deactivation:

$$BaO \rightarrow Ba + O \downarrow Pt$$

Suppose such a platinum system is operated at 1 020° K at a constant current of 100 mA. The resistance of the device rises from the initial value $R_0 \simeq 20$ ohms to some maximum value in the range 200–500 ohms, where it is held for a period of 20 hours. At the end of the test run the valve is opened and the two core pieces are separated with as little disturbance to the matrix as possible, i.e. each working core face is left with its white coating adhering to it. The cathode-core coating has changed little in appearance and retains its original white opaque powdery characteristic. The anode-core coating, however, is strikingly different and a proportion of the coating has apparently disappeared. What remains of the coating has lost its opaque and powder-like quality and is now translucent and glittering in appearance. Under a magnification of 300 the particles appear fused and glass-like in character.

An explanation of the change in matrix structure in the layer adjacent to the anode core must clearly be based on some interaction between the discharged oxygen atoms and the matrix itself. The most obvious reaction is the formation of barium strontium peroxide, which could reasonably be expected to fuse at the operating temperature of the system.

(3) CONCLUSIONS

The following conclusions may now be drawn from the experimental evidence:

(*a*) At 1 020° K a dissociation of the oxide matrix occurs for current densities greater than 200 mA/cm².

(*b*) The mass of oxide matrix dissociated is not proportional to the quantity of electricity passed through the matrix. The dissociative action is therefore dissimilar to a classical electrolytic action.

(*c*) At constant temperature the rate of dissociation is a direct but complex function of current density.

(*d*) The products of dissociation are in ionic form.

(*e*) Negative ions of oxygen can be collected in bulk as black nickel oxide on a nickel anode.

(*f*) Positive ions of both barium and strontium can be collected in bulk in solution or alloy form in a platinum cathode.

The observations are explained in terms of a model in which isolated oxide particles are brought up to some critical temperature, T_{crit}, at which they dissociate thermally into their constituent ions. After this thermal dissociation the ions drift apart in the applied electric field. The increase in temperature of particular particles is due to their acceptance of impact energy from a stream of free-flying electrons, and preferred particles are probably those lying at the termini of long electron runs.

(4) ACKNOWLEDGMENTS

Acknowledgment is made to the Engineer-in-Chief of the Post Office for permission to use the information contained in the paper. The senior author also wishes to thank Mr. H. Bate for skilled assistance in parts of the work.

621.372.821

The Institution of Electrical Engineers
Monograph No. 358 E
Feb. 1960
©

RADIATION FROM DISCONTINUITIES IN STRIP-LINE

By L. LEWIN, Associate Member.

(*The paper was first received* 19*th June, and in revised form* 4*th September*, 1959. *It was published as an* INSTITUTION MONOGRAPH *in February*, 1960.)

SUMMARY

A method of calculation, which should be adequate for strip-lines of small spacing, is proposed for the evaluation of the radiation of line-above-ground configurations. It is shown that an open-circuit is appreciably worse, from the point of view of radiation loss, than a short-circuit with a right-angle corner at an intermediate level. The radiation from a matched post is slightly worse than from the short-circuit, but it should be capable of considerable improvement by the use of a terminating frame antenna. Formulae are also given for the effects of reactive posts, with applications to a simple resonator.

LIST OF SYMBOLS

E = Electric field.
f = Geometric form factor for strip-line characteristic impedance.
F = Radiation factor (= Radiated power for unit incident current wave divided by $60(kt)^2$).
F_1 = Radiation factor for open-circuit.
F_2 = Radiation factor for matched termination.
F_3 = Radiation factor for general termination.
F_4 = Radiation factor for short-circuit.
F_5 = Radiation factor for general parallel stub.
F_6 = Radiation factor for reactive parallel stub.
F_7 = Radiation factor for two-stub resonator.
F_8 = Radiation factor for right-angle corner.
F_9 = Radiation factor for compensated matched termination.
i_x, i_y, i_z = Unit vectors.
I = Strip-line current.
I_f = Frame-antenna current.
I_s = Post current.
I_p = Effective polarization current.
J = Current density.
$k = 2\pi/\lambda$.
$k' = k\sqrt{\epsilon}$.
L = Loop perimeter.
p = Frame-antenna parameter.
P = Radiated power for unit incident current wave.
Q = Resonator Q-factor.
r_0 = Distance between current and field points.
r = Radial distance from origin.
$R, Re^{j\psi}$ = Current reflection coefficient.
t = Dielectric thickness.
T = Current transmission coefficient.
V = Voltage.
w = Strip width.
X = Stub reactance.
x, y, z = Rectangular co-ordinates.
Z_s = Strip-line characteristic impedance.
Z_f = Frame-aerial characteristic impedance.
Z = Post impedance.
ϵ = Effective permittivity.
ϵ' = Permittivity of spacing material.
λ = Free-space wavelength.
Π = Hertzian vector.
ζ = Current co-ordinate in z-direction.
θ, ϕ = Spherical co-ordinate angles.

Correspondence on Monographs is invited for consideration with a view to publication.
Mr. Lewin is with Standard Telecommunication Laboratories, Ltd.

(1) INTRODUCTION

The use of line-above-ground printed-circuit configurations for microwave applications is limited by a number of factors, including line attenuation due to metallic and dielectric loss, breakdown effects at high power levels and radiation from discontinuities. The latter constitutes one of the major limiting features at the higher frequencies, and, in order to permit the extension of the technique into this range, it is necessary to understand, and ultimately to control, this radiation. The purpose of the paper is to explain a method of calculation which should contain all the essential features of strip-line radiation. Its application to any particular case is then mainly a matter of evaluating the appropriate expressions, which may be done analytically or by numerical calculation. The method is illustrated by a variety of examples.

(2) METHOD OF CALCULATION

(2.1) Field Under the Strip

Fig. 1(*a*) illustrates a strip-above-ground configuration located along the z-axis of a co-ordinate system. The strip, of width w, is spaced a distance t from the ground-plane, or, alternatively,

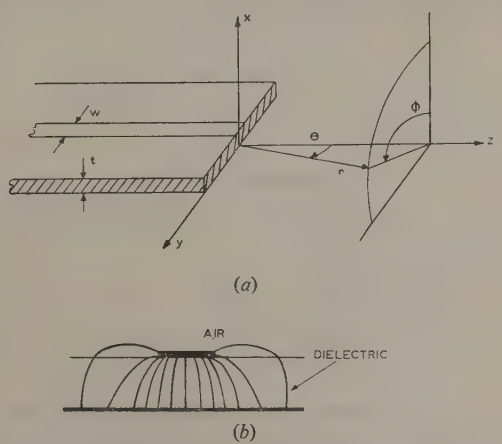

Fig. 1.—(*a*) Strip above ground and co-ordinate system.
(*b*) Lines of electric force under the strip.

a distance $2t$ from its image therein. The spacing material has a permittivity ϵ'.

Fig. 1(*b*) shows the lines of electric force in a cross-section of the strip-line. Immediately beneath the centre of the strip they

pass uniformly to the ground-plane. Near the edges they bow away somewhat, and a small fringe field 'leaks' into the air surrounding the upper part of the strip. If it were not for this leakage the wave under the strip would be of the transverse electromagnetic type. In fact, such a field form is a close approximation to the actual strip-line mode and is commonly used for most theoretical investigations on strip-line. This approximation will be adopted here. Its main shortcoming is the incorrect propagation velocity which it predicts. The measured effective permittivity as determined by the strip wavelength is about $\epsilon = 2{\cdot}25$, whereas the measured permittivity of the spacing material (Teflon-impregnated fibre glass) is about $2{\cdot}8$. This discrepancy can be allowed for by using for the permittivity the empirically determined value rather than the material permittivity. This same value also occurs in the formula for the wave impedance of the strip, since the voltage and current are related by $\partial V/\partial z = -j\omega\mathscr{L}I$, and the z-differentiation introduces into the formula the quantity $k' = k\sqrt{\epsilon}$ (where $k = 2\pi/\lambda$ and λ is the free-space wavelength). Accordingly we write for the wave impedance of the strip

$$Z_s = \frac{120\pi}{\sqrt{\epsilon}}\,\frac{\tau}{w}f \quad . \quad . \quad . \quad . \quad . \quad . \quad (1)$$

where ϵ, as indicated above, is the empirically determined or effective permittivity and f is a geometric factor, different from unity because of the bowing out of the lines of force near the edges of the strip. For a $\frac{1}{4}$in strip with $\frac{1}{16}$in strip–ground spacing its numerical value, as determined by measurements of the strip impedance, is about two thirds. Since Z_s is inversely proportional to capacitance per unit length, f is equal to the voltage/charge ratio divided by the same quantity for an assumed uniform field concentrated under the strip.

Hence
$$f = \frac{\int_0^t (E_x)_{y=0}dx}{\int_{-\infty}^{\infty}(E_x)_{x=0}dy}\;\frac{\int_{-w/2}^{w/2}{}_0E_x dy}{\int_0^t {}_0E_x dx} \quad . \quad . \quad . \quad . \quad (2)$$

where ${}_0E_x$ is the uniform field under the strip and equals $-V/t$, minus the voltage divided by the spacing. Eqn. (2) simplifies to

$$f = -wV/t\int Eds \quad . \quad . \quad . \quad . \quad . \quad (3)$$

where E is the field normal to any equipotential of which ds is an element.

(2.2) Dielectric Polarization

Maxwell's second equation for the magnetic field can be written as

$$\text{Curl } H = \frac{jk}{300}\epsilon E + \frac{4\pi J}{10}$$

$$= \frac{jk}{300}E + \frac{4\pi}{10}\left[J + \frac{jk(\epsilon-1)}{120\pi}E\right] \quad . \quad . \quad (4)$$

This equation shows that the dielectric polarization acts as an impressed current of density $jk(\epsilon - 1)E/120\pi$. Applying this to the field around the strip we see that, for $0 < x < t$, ϵ is the material permittivity, whilst, above the strip, the contribution is zero. If we take instead ϵ to be everywhere the effective permittivity, as defined earlier, the contribution below the strip is under-valued and that above is over-valued. As an approximation this may be justifiable, and it becomes increasingly more correct the closer is the strip–ground spacing.

If we integrate the polarization over the cross-section we get the effective impressed current, I_p, per unit length of strip. It is

$$I_p = \frac{2jk(\epsilon-1)}{120\pi}\int EdS \quad . \quad . \quad . \quad . \quad . \quad (5)$$

where dS is an element of area of cross-section. The factor 2 arises from the positive image of the polarization currents in the ground plane. E in eqn. (5) is a vector with E_x and E_y components. The E_y components are due to the bowing out of the lines of force and are oppositely directed on either side of the strip. Moreover, their images in the ground plane are also oppositely directed. There is therefore a high degree of cancellation of effects, and the E_y components will henceforth be ignored. The integral in eqn. (5) is accordingly replaced by $\int\int E_x dxdy$ and approximately equals the integral $t\int Eds$ appearing in eqn. (3). If the two are identified, eqn. (5) simplifies to

$$I_p = \frac{-2jk(\epsilon-1)}{120\pi}\,\frac{wV}{f} \quad . \quad . \quad . \quad . \quad . \quad (6)$$

Moreover, the voltage V and the strip current I are related by

$$V = Z_s\partial I/\partial z(j/k') = j\frac{120\pi tf}{\epsilon wk}\,\frac{\partial I}{\partial z} \text{ from eqn. (1)}$$

Substituting in eqn. (6) we have

$$I_p = \frac{\epsilon-1}{\epsilon}2t\frac{\partial I}{\partial z} \quad . \quad . \quad . \quad . \quad . \quad . \quad (7)$$

This formula will henceforth be used for the effect of the polarization of the dielectric under the strip. It is not rigorous, but it becomes so in the limit of very close strip–ground spacing in terms of the strip width. Although it seems very difficult to assess the numerical errors introduced it appears likely that good order-of-magnitude results can be obtained from eqn. (7). The approximations used are as follows:

(*a*) TEM transmission.
(*b*) Uniform dielectric in the neighbourhood of the strip, equal in magnitude to the value empirically determined from the measured propagation coefficient.
(*c*) Neglect of the radiation from the E_y-component of the bowed lines of force near the strip.
(*d*) Identity of geometric form factors for the wave impedance and for the radiation from the E_x-component of field near the strip.

A further approximation, used in the subsequent analysis, is that t is much less than the free-space wavelength. This will be so for all practical strip-line arrangements. Hence the radiated field from eqn. (7) will be proportional to t. This field will set up a further dielectric polarization in the thin dielectric covering of the ground-plane, causing a radiation field proportional to t^2. This effect will be ignored, so that the calculations may be expected to give the field correct to the order t, and therefore the power to the order t^2.

(2.3) Hertzian Vector

In terms of the Hertzian vector

$$\Pi = \frac{-j30}{k}\int\frac{\varepsilon^{-jkr}}{r}id\tau$$

($d\tau$ is an element of volume) the electric field is given by

$$E = \text{grad div } \Pi + k^2\Pi$$

For the strip-line configuration the integration with respect to $d\tau$ can be replaced by an integration over the cross-section and an integration with respect to dz. The cross-section integration

gives a current from the current density J, which is either the current I_p of eqn. (7) or the strip current I. These are directed in the x and z directions, respectively. Moreover, associated with I is its negative image in the ground plane. For an infinite strip-line the Hertzian vector is accordingly

$$\Pi = \frac{-j30i_x}{k}\int_{-\infty}^{\infty}\frac{\varepsilon^{-jkr_0}}{r_0}\,\frac{\epsilon-1}{\epsilon}2t\frac{\partial I}{\partial\zeta}d\zeta$$

$$-\frac{j30i_z}{k}\int_{-\infty}^{\infty}\left(\frac{\varepsilon^{-jkr_1}}{r_1}-\frac{\varepsilon^{-jkr_2}}{r_2}\right)Id\zeta \quad . \quad (8)$$

where i_x and i_z are unit vectors in the x and z directions, ζ is the variable of integration and

$$\begin{aligned} r_0 &= \sqrt{[x^2+y^2+(z-\zeta)^2]} \\ r_{1,2} &= \sqrt{[(x\mp t)^2+y^2+(z-\zeta)^2]} \\ &\simeq r_0 \mp t\partial r_0/\partial x \text{ if } t \text{ is small} \\ &= r_0 \mp tx/r_0 \end{aligned}$$

Let us put $r=\sqrt{(x^2+y^2+z^2)}$, the radial distance from the origin, so that, sufficiently far from the strip, we can put $r_0 \simeq r - z\zeta/r = r - \zeta\cos\theta$ where θ is the angle between z and r (this is the usual far-field approximation). The integrals in eqn. (8) both involve

$$J_0 = \int_{-\infty}^{\infty}\varepsilon^{-j(k'-k\cos\theta)\zeta}d\zeta \quad . \quad . \quad . \quad . \quad (9)$$

since $I=\varepsilon^{-jk'\zeta}$ for an assumed current wave from the left of the origin. Because the radiation from an undisturbed or infinite strip-line should be zero, it is necessary to see how eqn. (9) is to be interpreted. We assume that the dielectric is very slightly lossy, so that there is a small attenuation coefficient. Putting $k'-k\cos\theta=c$ for brevity, we get

$$J_0 = \varepsilon^{-jc\zeta}/-jc\Big|_{-\infty}^{+\infty} \to \varepsilon^{jc\infty}/jc$$

This is infinite if c contains a small negative imaginary part corresponding to the strip-current attenuation.

The reason for this result is as follows. Seen from the origin, the strip current in the negative direction appears to increase exponentially with distance, the integration to $\zeta=-L$ giving an infinite contribution in the limit. Since it is commonly assumed that the infinitely distant parts of the line can have no physical effect at the origin, it has been customary in analyses of this sort to ignore this contribution as being physically meaningless. This procedure is not, however, satisfactory, and, in the case of strip-line, it actually gives wrong results.

If the limit is taken only to $\zeta=-L$ it is apparent that the strip-line cannot be excited unless a generator is provided there. This could take the form, for instance, of an impressed current across the line at $\zeta=-L$. The current will radiate in its own right, giving a term of the form $\varepsilon^{j(k'-k)L}/L$, and, together with the contribution from the integral at $\zeta=-L$, gives the radiation at the feed. With an enclosed system this radiation vanishes, so that a proper consideration of the conditions at the input can, in fact, justify the neglect of the contribution of the integral at the lower limit. (This aspect is pursued in more detail elsewhere,* where a similar situation occurs in the analysis of the radiation from an open-ended waveguide.) In the case of strip-line the system is not enclosed and the impressed current of the feed merely augments the contribution of the integral to give the radiation from the input.

Anticipating the results of Section 3.2, where the radiation pattern of a matched coaxial termination is investigated, it is apparent that the feed radiation will take a similar form (depending on the details of the input), and will not therefore be negligible in its effect. For example, suppose that we have a strip-line 20 m long with an attenuation of 1 dB/m, and we are interested in the radiation 2 m from the origin. The radiation from the feed will be reduced by a tenth due to the distance factor, but increased ten times because the current there will be ten times larger. Thus the two radiations are of comparable magnitude. This is an unusual situation because such long lengths of strip-line are not normally used: it is discussed here mainly to show how the attenuation factor can be responsible for a non-negligible feed contribution to the radiation.

In practice the lengths are very much shorter, so that the exponential factor hardly enters, but the distance factors will then be comparable. Therefore, as workers in the field are well aware, the feed radiation can be a problem, and the design of transitions from waveguide or coaxial to strip-line with reduced radiation characteristics has been one of the problems to be solved in the utilization of the strip-line medium.

If the feed radiation is significant, what could be the justification for ignoring it? The radiation of two aerials, as a function of their distance apart, varies rapidly when they are in close proximity, approaches its asymptotic value when the distance is about one quarter to one half a wavelength, and thereafter fluctuates with ripples of smaller and smaller amplitude about the asymptotic value as the distance increases. For distances in excess of about one to two wavelengths the mutual impedance of two aerials can usually be neglected. This means that they radiate substantially independently so far as the power output is concerned, although the shape of the radiation pattern will depend, of course, very markedly on the details of the arrangement. Thus, for strip-line configurations other than those in which the element of interest is extremely close to the feed, it may be assumed that the feed radiation, although of non-negligible magnitude, is independent of, and does not affect, the radiation of the component under investigation. It may therefore be investigated without the complication of adding on the feed field. Since this comes from the contribution of the integral at $\zeta=-L$, the latter may therefore also be neglected. This really amounts to ignoring the attenuation factor altogether, and treating the contribution at infinity of exponentials with imaginary arguments as zero. This will now be done.

We therefore return to eqn. (8), which can now be simplified to

$$\Pi \simeq -\frac{j60t}{k}\,\frac{\varepsilon^{-jkr}}{r}\int_{-\infty}^{\infty}\left(i_x\frac{\epsilon-1}{\epsilon}\frac{\partial I}{\partial\zeta}-i_z jk\sin\theta\cos\phi I\right)$$

$$\varepsilon^{jk\zeta\cos\theta}d\zeta \quad . \quad (10)$$

Here $\sin\theta\cos\phi = x/r$, which is the cosine of the angle between the x-axis and the radial vector from the origin. The approximation in eqn. (10) refers to the far field, and we have taken $\varepsilon^{-jkt}\simeq 1-jkt$.

To find the electric field the vector operator (grad div $+k^2$) must be applied to the Hertzian vector. It is readily found, using spherical co-ordinates, that $E_r=0$ to the far-field approximation, whilst the θ and ϕ components are

$$\left.\begin{aligned} E_\theta &= k^2(\cos\theta\cos\phi\,\Pi_x - \sin\theta\,\Pi_z) \\ E_\phi &= -k^2\sin\phi\,\Pi_x \end{aligned}\right\} \quad . \quad . \quad (11)$$

again to the far-field approximation.

In order to evaluate the radiation in any particular case it is therefore necessary to calculate Π_x and Π_z, substitute in eqn. (11), form the Poynting vector, which is proportional to $|E_\theta|^2+|E_\phi|^2$, and integrate over a hemisphere. The method will be illustrated by a number of examples.

* LEWIN, L.: 'Advanced Theory of Waveguides' (Iliffe, 1951, p. 137).

(3) APPLICATION TO SOME STRIP-LINE CONFIGURATIONS

(3.1) Open-Circuit

The arrangement is shown schematically in Fig. 2(*a*). We consider the Hertzian vector in eqn. (10) but take the upper limit to $\zeta = 0$ instead of infinity. The current is $\varepsilon^{-jk'\zeta} - \varepsilon^{jk'\zeta}$, corresponding to a unit current wave reflected at the open-circuit. (The incomplete reflection of the current due to the

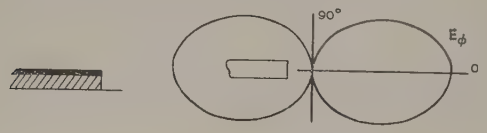

(*a*) (*b*)

Fig. 2.—(*a*) Strip-line open-circuit.
(*b*) Field pattern in plane of strip.

radiation from the open end constitutes only a second-order correction and is ignored.) The integration is readily carried out, and substitution in eqn. (11) gives

$$\left.\begin{aligned} E_\theta &= \frac{-j\varepsilon^{-jkr}}{r}\,\frac{120kt}{\sqrt{\epsilon}}\cos\phi \\ E_\phi &= \frac{j\varepsilon^{-jkr}}{r}\,\frac{120kt}{\sqrt{\epsilon}}\,\frac{\epsilon-1}{\epsilon-\cos^2\theta}\cos\theta\sin\phi \end{aligned}\right\} \quad . \quad (12)$$

The radiated power is

$$P = \frac{1}{120\pi}\int_{-\pi/2}^{\pi/2} d\phi \int_0^{\pi} |E|^2 r^2 \sin\theta d\theta$$

and on putting $\cos\theta = c$ and carrying out the ϕ integration we have

$$P = 60\frac{(kt)^2}{\epsilon}\int_{-1}^{1}\left[1 + \frac{c^2(\epsilon-1)^2}{(\epsilon-c^2)^2}\right]dc$$

$$= 60(kt)^2F_1(\epsilon) \quad . \quad . \quad . \quad . \quad . \quad . \quad . \quad . \quad . \quad (13)$$

where $$F_1(\epsilon) = \frac{\epsilon+1}{\epsilon} - \frac{(\epsilon-1)^2}{2\epsilon\sqrt{\epsilon}}\log\frac{\sqrt{\epsilon}+1}{\sqrt{\epsilon}-1} \quad . \quad . \quad (14)$$

In order to assess the meaning of these formulae, consider first the radiated power. The factor $60(kt)^2$ is common to all the configurations we shall examine. For example, when $t = \frac{1}{16}$ in and the frequency is 4 Gc/s its value is about 1 ohm, the strip impedance being about 50 ohms. Thus, if F_1 is unity, we can say that 2% of the power incident on the open-circuit is radiated, and, according to the values reached by the radiation factor F, we can judge the radiation of the configuration. F will henceforth be evaluated at $\epsilon = 2{\cdot}25$, the value of F_1 being actually $1{\cdot}07$. Since $Z_s \propto t$ (apart from a small correction due to the geometric factor f discussed in Section 2.1) the *fractional* radiated power will be approximately proportional to t—at least for small thicknesses of dielectric.

The E_θ field in eqn. (12) is similar to that of a magnetic dipole or frame aerial. From the ϕ component it is seen that the vertical field (i.e. perpendicular to the ground-plane) in the plane of the strip is of figure-of-eight form, the loops being circular for large permittivities, and progressively more elongated as $\epsilon \to 1$. It is shown in Fig. 2(*b*) for the case $\epsilon = 2{\cdot}25$.

A power loss of 2% of the incident wave means that the reflection coefficient (current or voltage) is $0{\cdot}99$, so that the voltage standing-wave ratio is 200 : 1. Line attenuation will, of course, reduce this value in practice.

(3.2) Matched Co-axial Termination

The arrangement is shown in Fig. 3(*a*), the strip terminating in a short post of height t. Either the post is lossy, of resistance equal to the strip-line impedance, or it could enter a coaxial

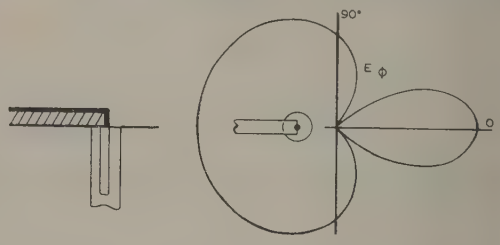

(*a*) (*b*)

Fig. 3.—(*a*) Strip-line matched into coaxial cable.
(*b*) Field pattern in plane of strip.

line. In the latter case it is assumed that the coaxial line is matched and that the termination matches the strip. In either case the strip current is $I = \varepsilon^{-jk'\zeta}$ and a current of unity value flows in the negative x-direction down the post. There are therefore two contributions to the Hertzian vector. Eqn. (10), with the upper limit at $\zeta = 0$, gives one part. The effect of the current in the post together with its image in the ground plane gives

$$\Pi = \frac{j60t}{k}\,i_x\,\frac{\varepsilon^{-jkr}}{r}$$

as the other. The total electric far field becomes

$$\left.\begin{aligned} E_\theta &= \frac{-j\varepsilon^{-jkr}}{r}\,\frac{60kt}{\sqrt{\epsilon}}\cos\phi \\ E_\phi &= \frac{j\varepsilon^{-jkr}}{r}\,\frac{60kt}{\sqrt{\epsilon}}\left(\frac{\epsilon-1}{\sqrt{\epsilon}-\cos\theta} - \sqrt{\epsilon}\right)\sin\phi \end{aligned}\right\} \quad . \quad (15)$$

The radiated power is $P = 60(kt)^2F_2(\epsilon)$ where

$$F_2(\epsilon) = 1 - \frac{\epsilon-1}{2\sqrt{\epsilon}}\log\frac{\sqrt{\epsilon}+1}{\sqrt{\epsilon}-1} \quad . \quad . \quad . \quad (16)$$

When $\epsilon = 2{\cdot}25$, then $F_2 = 0{\cdot}33$. This gives rise only to a third of the radiation compared with that from an open-circuit. To some extent, however, this reduction may be a question of definition. From eqn. (15) it is seen that E_θ is half that given by eqn. (12), and the absence of a reflected wave is mainly the cause. In the open-circuit case, owing to the reflected wave, the maximum voltage and current are double those from the matched termination. If we compare the radiation, not for the same incoming current wave but for the same maximum, eqn. (14) would need to be quartered and the matched termination would then appear to be the heavier radiator.

The identity in form of E_θ in eqns. (12) and (15) is surprising. Both are as from a frame aerial, although the form taken mathematically depends on a number of contributions of different functional dependence. The same result also follows in some further examples.

The vertical component of field in the plane of the strip is shown for the case $\epsilon = 2{\cdot}25$ in Fig. 3(*b*). It is of figure-of-eight form with unequal loops, the fatter loop being in the direction opposite to the propagated current wave.

(3.3) Mismatched Termination

If a general termination is used, with a reflection coefficient $R\varepsilon^{j\psi}$ to the current wave, then $I = \varepsilon^{-jk'\zeta} + R\varepsilon^{j\psi}\varepsilon^{jk'\zeta}$ and a

current $1 + R\varepsilon^{j\psi}$ flows in the negative x-direction in the termination. The calculation is similar to that of Section 3.2 and gives

$$\left.\begin{aligned} E_\theta &= -j\frac{\varepsilon^{-jkr}}{r}\frac{60kt}{\sqrt{\epsilon}}(1 - R\varepsilon^{j\psi})\cos\phi \\ E_\phi &= j\frac{\varepsilon^{-jkr}}{r}\frac{60kt}{\sqrt{\epsilon}}\left[\left(\frac{\epsilon - 1}{\sqrt{\epsilon} - \cos\theta} - \sqrt{\epsilon}\right)\right. \\ &\qquad \left. + R\varepsilon^{j\psi}\left(\frac{\epsilon - 1}{\sqrt{\epsilon} + \cos\theta} - \sqrt{\epsilon}\right)\sin\phi\right] \end{aligned}\right\} \quad . \quad (17)$$

Eqns. (15) and (12) follow as the special cases $R = 0$ and $R = 1$, $\psi = \pi$. The radiated power is $P = 60(kt)^2F_3(\epsilon)$ with

$$F_3 = 1 + R^2 + R\cos\psi(1 - 1/\epsilon) - \frac{\epsilon - 1}{2\sqrt{\epsilon}}[1 + R^2 + R\cos\psi(1 + 1/\epsilon)]\log\frac{\sqrt{\epsilon} + 1}{\sqrt{\epsilon} - 1} \quad . \quad (18)$$

When $R = 1$, $\psi = 0$, the arrangement is a short-circuit, as shown in Fig. 4(*a*). The radiation factor is then

$$F_4 = 3 - 1/\epsilon - (3 + 1/\epsilon)\frac{\epsilon - 1}{2\sqrt{\epsilon}}\log\frac{\sqrt{\epsilon} + 1}{\sqrt{\epsilon} - 1} \quad . \quad . \quad (19)$$

and takes the value 0·25 when $\epsilon = 2{\cdot}25$. In this case comparison with an open-circuit gives rise to no ambiguity, whichever basis of comparison is used, and the short-circuit radiates something less than a quarter that of the open-circuit.

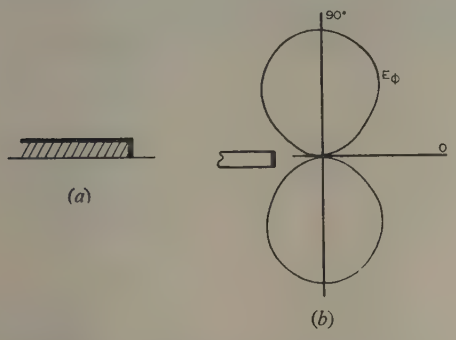

Fig. 4.—(*a*) Strip-line short-circuited to earth.
(*b*) Field pattern in plane of strip.

From eqn. (17) E_θ is identically zero for the short-circuit and E_ϕ becomes

$$E_\phi = -j\frac{\varepsilon^{-jkr}}{r}120kt\frac{\sin^2\theta\sin\phi}{\epsilon - \cos^2\theta} \quad . \quad . \quad . \quad (20)$$

The vertical field in the plane of the strip is shown in Fig. 4(*b*) for the case $\epsilon = 2{\cdot}25$. The forward and backward radiation is zero, and there is a slightly unsymmetrical loop on either side of the strip.

As a matter of interest, eqn. (18) has a minimum (for $\epsilon = 2{\cdot}25$) at $R = 0{\cdot}62$, $\psi = 0$, when F_{min} takes the value 0·2.

(3.4) Parallel Post

The short-circuit, treated in Section 3.3 as a particular case of a general termination, can also be considered a particular case of a general parallel impedance or post, as shown in Fig. 5. The post may be purely reactive or it may contain a resistive component. In either case the current to the left will be of the form $I = \varepsilon^{-jk'\zeta} + R\varepsilon^{jk'\zeta}$, and to the right it will be of the form

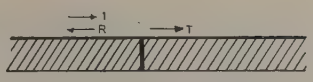

Fig. 5.—Post in parallel across the strip-line.

$I = T\varepsilon^{-jk'\zeta}$, with the difference current, $I_s = 1 + R - T$, flowing down the post in the negative x-direction. The current reflection and transmission coefficients are related, from circuit considerations, by

$$\left.\begin{aligned} T &= 1 - R \\ R &= \frac{1}{1 + 2Z/Z_s} \\ T &= \frac{2Z/Z_s}{1 + 2Z/Z_s} \end{aligned}\right\} \quad . \quad . \quad . \quad . \quad . \quad (21)$$

Z is the impedance of the post, and equals jX if the post is purely reactive. The Hertzian vector is made up from three parts, two being as in eqn. (10) with limits $\zeta = -\infty$ to 0, and $\zeta = 0$ to ∞ respectively, and the third, as in Section 3.2, coming from the current in the post.

The E_θ field takes the same form as in eqn. (17) but with a coefficient $1 - R - T$. In view of the first of relations (21) it is therefore identically zero. The E_ϕ field becomes, on using this same relation,

$$E_\phi = -j\frac{\varepsilon^{-jkr}}{r}120(kt)R\frac{\sin^2\theta\sin\phi}{\epsilon - \cos^2\theta} \quad . \quad . \quad . \quad (22)$$

and is of the same form as eqn. (20), apart from the multiplying coefficient R. Hence the radiation is given by F_4 in eqn. (19) multiplied by $|R|^2$.

$$F_5 = \left|\frac{1}{1 + 2Z/Z_s}\right|^2F_4 \quad . \quad . \quad . \quad . \quad . \quad (23)$$

If the post is a reactive one this becomes

$$F_6 = \frac{1}{1 + 4X^2/Z_s^2}F_4 \quad . \quad . \quad . \quad . \quad . \quad (24)$$

Eqn. (19) is recovered by putting $X = 0$ (short-circuit). In the absence of the post ($X = \infty$) F_6 becomes zero, confirming the absence of radiation from an undisturbed line.

(3.5) Resonator Formed by Two Parallel Posts

Two posts, each of reactance X and spaced apart a distance L, given by $\tan k'L = -2X/Z_s$, behave like a resonator of Q-factor, as loaded by the line, given (approximately) by*

$$Q = \pi Z_s^2/4X^2 \quad . \quad . \quad . \quad . \quad . \quad (25)$$

In this equation X is assumed small, so that the Q-factor is high, and the spacing will be nearly half a wavelength in the line.

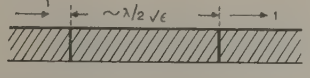

Fig. 6.—Two-post resonant cavity.

Resistive and radiation losses are ignored. The device is shown in Fig. 6.

Each post, and the strip-line in its neighbourhood, will radiate. This radiation can be calculated in detail using the preceding methods, but the analysis is quite unnecessarily lengthy if order-

* MUMFORD, W. W.: 'Maximally Flat Filters in Waveguide', *Bell System Technical Journal*, 1948, 27, p. 684, Eqn. (A13).

of-magnitude results only are needed. The radiation of two antennae, as a function of their separation, undergoes slight fluctuations about the asymptotic value for infinite spacing, except when the spacing is very close (say less than an eighth of a wavelength), in which case the radiation decreases to zero or increases to double, depending on the relative phase. In the present case, with a separation of half the strip-wavelength, or about one-third of the free-space wavelength, the value attained at large spacing should be quite an accurate measure of the radiation. We will therefore consider the radiation of one post in isolation, and double it for the complete resonator. In this way the results of Section 3.4 can be utilized with very little extra labour.

Let us consider the currents at the first post in more detail. If the resonator is on tune, a unit current will be incident on the left, there will be no reflection at the post, and to its right there will be a current incident towards the post and a reflected current. These latter will both be rather large, since they are the currents in the resonator. A similar set of currents occurs at the second post, the unit current wave leaving it being the current transmitted past the resonator.

The situation at the first post is practically that of Section 3.4 if the sign of j is reversed. A current wave of magnitude T is incident on the post without reflection, and past the post is an incident wave of magnitude R and a wave leaving of unit magnitude. If all the currents are increased in the ratio $1 : T$, the incident wave becomes of unit magnitude and the resonator condition is realized.

Hence if eqn. (24) be doubled (for the two posts) and divided by $|T|^2$ the radiation factor for the resonator results.

$$F_7 = (Z_s^2/2X^2)F_4 \quad . \quad . \quad . \quad . \quad . \quad . \quad (26)$$

In this equation we can put Z_s^2/X^2 in terms of Q by means of eqn. (25), giving

$$F_7 = (2Q/\pi)F_4 \quad . \quad . \quad . \quad . \quad . \quad . \quad . \quad (27)$$

The significance of this equation can be seen more readily if numerical values are inserted. Thus, with a 50-ohm line at 4 Gc/s using a $\frac{1}{16}$ in spacing, and an effective permittivity of 2·25, we find that a fraction, $Q/300$, of the power is radiated. Of course, the formula breaks down as soon as an appreciable amount of power is lost, but it reveals in a striking way the penalty to be paid for a high-Q-factor cavity of the type described in strip-line. And since open-circuits radiate more than short-circuits, a similar limitation is also to be expected there.

(3.6) Right-Angle Corner

Configurations in which the strip-line itself changes direction are difficult to analyse, and the right-angle corner is the only one for which it proved possible to obtain a simple result. The arrangement is shown in Fig. 7, with the second leg of the corner along the y-axis. In terms of spherical co-ordinate angles θ and ϕ, the cosine of the angle between the x-axis and the radial vector from the origin is $\sin\theta\cos\phi$, and for the angle between the y-axis and the radial vector, it is $\sin\theta\sin\phi$. The Hertzian vector consists of two parts, from $\zeta = -\infty$ to 0, as from eqn. (10), and a similar part for the contribution along the y-axis. It is assumed that there is no reflection of the current at the corner.

After calculation it is found that, far from the origin,

$$\Pi = -j60\frac{t}{k}\frac{\varepsilon^{-jkr}}{r}\left\{i_x\frac{\epsilon-1}{\sqrt{\epsilon}}\left[\frac{1}{\sqrt{\epsilon}-\cos\theta}-\frac{1}{\sqrt{\epsilon}-\sin\theta\sin\phi}\right]\right.$$
$$\left. + i_y\frac{\sin\theta\cos\phi}{\sqrt{\epsilon}-\sin\theta\sin\phi} - i_z\frac{\sin\theta\cos\phi}{\sqrt{\epsilon}-\cos\theta}\right\} \quad . \quad (28)$$

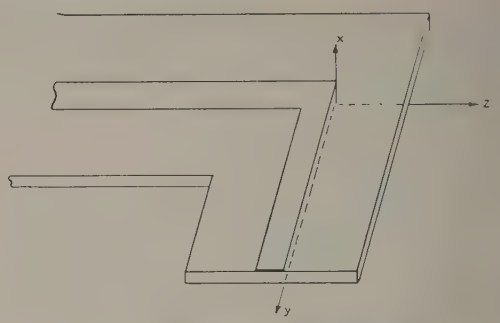

Fig. 7.—Right-angle corner in strip-line.

which gives rise to field components

$$E_\theta = \frac{-j\varepsilon^{-jkr}}{r}\frac{60kt}{\sqrt{\epsilon}}\left[1+\frac{\cos\theta}{\sqrt{\epsilon}-\sin\theta\sin\phi}\right]\cos\phi \quad . \quad (29)$$

$$E_\phi = \frac{j\varepsilon^{-jkr}}{r}\frac{60kt}{\sqrt{\epsilon}}$$
$$\left[\frac{(\epsilon-1)\sin\phi}{\sqrt{\epsilon}-\cos\theta} - \frac{(\epsilon-1)\sin\phi+\sqrt{\epsilon}\sin\theta\cos^2\phi}{\sqrt{\epsilon}-\sin\theta\sin\phi}\right] \quad . \quad (30)$$

The field-pattern formulae are more complicated than those encountered previously. The vertical component in the plane of the strip is shown in Fig. 8(*a*) for the case $\epsilon = 2{\cdot}25$. Fig. 8(*b*) shows, in the xz-plane, the E_θ and E_ϕ components.

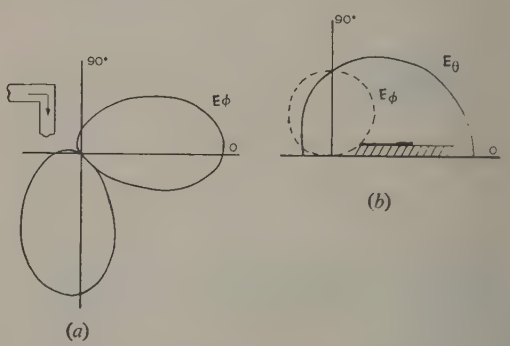

Fig. 8.—(*a*) Field pattern in plane of strip for right-angle corner.
(*b*) Field pattern in xz plane for right-angle corner.

The calculation of the radiation factor is somewhat involved. It is outlined in Section 6 where it is shown that $P = 60(kt)^2F_8$, where

$$\left.\begin{aligned} F_8 &= F(\epsilon) - F(2\epsilon-1) \\ F(\epsilon) &= \frac{\epsilon+1}{\sqrt{\epsilon}}\log\frac{\sqrt{\epsilon}+1}{\sqrt{\epsilon}-1} \end{aligned}\right\} \quad . \quad . \quad . \quad . \quad (31)$$

F_8 takes the value 0·61 when $\epsilon = 2{\cdot}25$, so that the corner radiates about twice as much as a matched termination.

Because of the logarithmic singularity at $\epsilon = 1$, eqn. (31) does not indicate, as might have appeared at first sight, a lack of radiation in the absence of a dielectric. The limiting value as $\epsilon \to 1$ is $F_8 = 2\log 2 = 1{\cdot}4$. For large permittivities $F_8 \to 4/(3\epsilon)$, which is a form that holds to a fair degree of approximation over the entire range.

(4) APPLICATIONS

(4.1) Comparison of Radiation Levels

The possible applications of the preceding results, apart from their acting as a guide to probable radiation levels, do not seem very numerous. Other things being equal one would choose a short-circuited line rather than an open-circuited one for a reactive element. Information on circular bends is not yet forthcoming, but when it is, a comparison with the right-angle corner can be made. High-Q-factor elements must be made from other than open- or short-circuited lengths of line. These trends seem fairly definitely indicated by the formulae. More speculatively, one might consider configurations in which the radiation from the discontinuity is reduced or cancelled by some compensating element. Bearing in mind that the discontinuity is there for a purpose, the possibility of doing this appears to be severely circumscribed. However, the matched termination appears to be suited to this treatment. In the next Section a possible solution is outlined.

(4.2) Matched Load with Compensating Frame Aerial

The radiation of the matched termination itself is given by eqn. (15), and the radiation factor by eqn. (16). It is seen that the E_θ field is as from a frame antenna. In fact, this form of E_θ field is common to most of the arrangements examined. A compensating frame is suggested, and if this can be located at the same position as the entry to the load from the strip, and fed with a current of the correct magnitude and phase, a substantial cancellation may be envisaged. The cancellation will not be complete because of the form of the E_ϕ component—a frame antenna giving a field proportional to $\cos\theta \sin\phi$. However, a partial cancellation would occur with this form, provided that the correct current amplitude could be obtained.

It will now be shown that, if the feed for the frame is taken directly from the strip-line, the phases of the currents are suitable for cancellation, and a variation of frame perimeter will then enable the currents to be adjusted as desired.

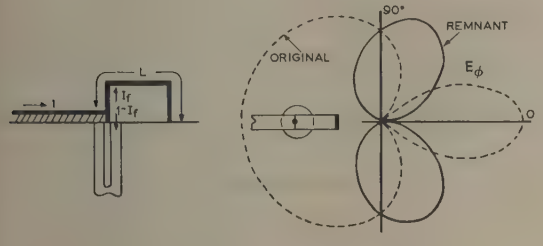

(*a*) (*b*)

Fig. 9.—(*a*) Matched load with compensating frame antenna.
(*b*) Remnant field pattern in plane of strip.

Fig. 9(*a*) shows the termination and frame. The frame and load are assumed to be matched as a combination. This means that somewhere (not shown), but possibly within the coaxial line, matching elements are inserted. The strip current, of unit magnitude, will not be reflected, a current I_f entering the frame and $1 - I_f$ the post to the coaxial line. Noting that the current $-I_f$ flowing down the post is equivalent to a current $+I_f$ flowing up it, this part of the post current completes the 'missing' part of the frame antenna, corresponding to the dielectric thickness. If the frame perimeter is L and its wave impedance is Z_f the relation between the voltage at the feed point and the frame current is

$$I_f = V/(jZ_f \tan kL) \quad . \quad . \quad . \quad . \quad . \quad (32)$$

Since V is the strip voltage for unit current wave we have simply $V = Z_s$, and if we take $\tan kL = kL$ for an assumed small frame perimeter, eqn. (32) simplifies to

$$I_f = Z_s/(jkLZ_f) \quad . \quad . \quad . \quad . \quad . \quad (33)$$

We now assume that the frame is twice as long as its height, so that, with its image in the ground-plane, it appears as a square frame. Accordingly, the effective vertical current element produced by the frame is

$$2I_f(L/4)[1 - \varepsilon^{(jkL\cos\theta)/2}] \simeq -(jkL^2 I_f \cos\theta)/4$$
$$= -L\cos\theta(Z_s/4Z_f)$$

Similarly the equivalent horizontal current is $L\sin\theta\cos\phi\,(Z_s/4Z_f)$. Both formulae assume that $kL \ll 1$ and that t can be neglected with respect to L. If the contribution of these currents is added to eqn. (15) we get

$$E_\theta = -j\frac{\varepsilon^{-jkr}}{r}60kt\frac{1-p}{\sqrt{\epsilon}}\cos\phi \quad . \quad . \quad . \quad (34)$$

$$E_\phi = j\frac{\varepsilon^{-jkr}}{r}\frac{60kt}{\sqrt{\epsilon}}\left(\frac{\epsilon-1}{\sqrt{\epsilon}-\cos\theta} - \sqrt{\epsilon} - p\cos\theta\right)\sin\phi$$

where

$$p = \frac{L}{8t}\frac{\sqrt{\epsilon}Z_s}{Z_f} \quad . \quad . \quad . \quad . \quad . \quad . \quad (35)$$

The parameter p measures the strength of the radiation of the frame relative to the strip-line. Since we have, very approximately, $\sqrt{\epsilon}Z_s = Z_f$, provided that the frame is made from a conductor of the same width as the strip, and not too far removed from the ground-plane, we see that $p = 1$ when $L \simeq 8t$. This is the condition for complete cancellation of the E_θ component, and for near cancellation of the E_ϕ component. It is subject to some slight modification as a result of the approximations made, but it gives a good order-of-magnitude estimate of the necessary perimeter. For $t = \frac{1}{16}$ in and $\lambda = 7{\cdot}5$ cm L is about one eighth of a wavelength. The mismatch is a drawback for broadband work, but a combination of series capacitance in the line and shunt capacitance at the entry of the post into the coaxial line can be used partially to compensate for the inductive effect of the frame.

The radiation factor of the modified termination is

$$F_9 = 1 + p + \frac{2p^2}{3\epsilon} - \frac{2p}{\epsilon} - \frac{\epsilon-1}{2\sqrt{\epsilon}}(1+p)\log\frac{\sqrt{\epsilon}+1}{\sqrt{\epsilon}-1} \quad . \quad (36)$$

When $\epsilon = 2{\cdot}25$ and $p = 1$, then $F_9 = 0{\cdot}07$. The minimum is actually at $p = 0{\cdot}945$ with $F_{9(min)} = 0{\cdot}067$, but it is fairly broad. It is concluded that the radiation can be cut to one fifth in this way, since $F_2 = 0{\cdot}33$ for the uncompensated termination.

Fig. 9(*b*) shows the remnant (with $p = 1$) of the vertical component of field in the plane of the strip. For comparison the uncompensated field is shown dotted.

(4.3) Experimental Confirmation

In general, it is difficult to obtain a reliable estimate of the total radiation from a strip-line discontinuity. What can be measured with slightly more facility are the relative fields of different configurations in various directions. Unfortunately reflection from nearby objects complicates matters, and if the line already contains a discontinuity in the form of a feed, the separation of the contribution from a second radiating region is not too straightforward. Qualitatively the open-circuit is found to radiate more than the short-circuit, in confirmation of the prediction made in Section 4.1.

A compensated termination as described in Section 4.2 has been tested for radiation. A reduction in the E_θ field of between 8 to 16dB was achieved, showing a considerable degree of cancellation. However, no absolute measurements of radiation loss have, as yet, been made.

(5) ACKNOWLEDGMENT

Acknowledgments are due to Standard Telecommunication Laboratories, Ltd., for facilities to prepare, and permission to publish, the paper.

(6) APPENDIX

The radiation factor for the corner is found to be

$$F_8 = \frac{1}{2\pi\epsilon}\int_{-\pi/2}^{\pi/2} d\phi \int_0^{\pi} d\theta \left\{\left(1 + \frac{\cos\theta}{\sqrt{\epsilon} - \sin\theta\sin\phi}\right)^2 \cos^2\phi + \left[\frac{(\epsilon-1)\sin\phi}{\sqrt{\epsilon}-\cos\theta} - \frac{(\epsilon-1)\sin\phi + \sqrt{\epsilon}\sin\theta\cos^2\phi}{\sqrt{\epsilon}-\sin\theta\sin\phi}\right]^2\right\}$$

The ϕ integration is first carried out using the result

$$\int_{-\pi/2}^{\pi/2} \frac{d\phi}{1 + g\sin\phi} = \frac{\pi}{\sqrt{(1-g^2)}}$$

where g is a constant parameter.

Similar results are obtained either by algebraic manipulatio or by differentiating with respect to g. A typical one is

$$\int_{-\pi/2}^{\pi/2} \frac{\cos^2\phi\sin\phi d\phi}{(1+g\sin\phi)^2} = \frac{\pi}{g^3}\left[2 - \frac{2-g^2}{\sqrt{(1-g^2)}}\right]$$

The result of the ϕ integration, on changing the variable t $c = \cos\theta$ is

$$F_8 = \frac{1-\epsilon}{\epsilon} + \int_0^1 \left\{\frac{\epsilon+1}{\epsilon-c^2} + \frac{\sqrt{\epsilon}}{\sqrt{(\epsilon-1+c^2)}}\left[\frac{1+\epsilon}{\epsilon} - \frac{2\epsilon}{\epsilon-c^2} + \frac{(\epsilon-1)^2/\epsilon}{\epsilon-1+c^2}\right]\right\} d$$

The integrations are now straightforward, $\sqrt{[(\epsilon-1+c^2)/(\epsilon-c^2)}$ being taken as a new variable in the third term. Eqn. (31 follows after some simplification.

621.372.83

The Institution of Electrical Engineers
Monograph No. 359 E
Feb. 1960
©

SOME OBSERVATIONS ON WAVEGUIDE COUPLING THROUGH MEDIUM-SIZED SLOTS

By L. LEWIN, Associate Member.

(*The paper was first received 22nd June, and in revised form 5th September*, 1959. *It was published as an* INSTITUTION MONOGRAPH *in February*, 1960.)

SUMMARY

A quasi-static transmission-line method, as used in antenna theory, and modified to take into account effects of radiation damping, is applied to the problem of waveguide coupling through slots which may be large enough to exhibit resonance effects. It is shown that the waveguide environment significantly alters the value to be used for the slot characteristic impedance, although this quantity cannot itself be calculated by the present analysis. The method is applied in detail to the case of axially-coupled waveguides and to guides coupled, via a common broad wall, through crossed slots. It is shown that a narrow slot needs to be very near resonance to give a coupling as large as that from a circular hole of comparable dimensions.

LIST OF SYMBOLS

a, b = Rectangular-waveguide cross-sectional dimensions.
A, B (Section 3) = Large rectangular-waveguide cross-sectional dimensions.
A, B (Section 4) = Forward and reverse wave amplitudes.
C_a = Capacitance per unit length of wire aerial.
C_s = Capacitance per unit length of slot aerial.
C_0 [eqn. (23)] = Radiation damping-field component for slot aerial.
C_1, C_2 [eqn. (32)] = Radiation damping field components for slot aerial.
C, D, E, F = Functions defined by eqn. (36).
C_+, C_- [eqn. (48)] = Forward and backward scattered field amplitudes.
C, D (Section 4) = Difference and sum of normalized scatter amplitudes.
C_0, D_0 (Section 4) = Values of C and D obtained from eqn. (48) in the absence of radiation damping.
$\bar{C}_+$, $\bar{C}_-$ = Side scattered field amplitudes into cross guide.
c_s = $(\lambda_g/2a)\cos(\pi\eta/a)$.
c = Velocity of light.
E = Electric field strength.
E_a = Antenna radiation field strength.
E_i = Impressed electric field on antenna.
E_0 = Incident electric-field amplitude.
E_r = Reflected electric-field amplitude.
E_1, E_2 [eqn. (21)] = Dominant-mode electric-field components at slot.
$E = E(y, z)$ = z-component of prescribed electric field.
$e_n = e_n(z)$ = Fourier component of $E(y, z)$.
F_n, G_n [eqn. (40)] = Functions determining Fourier coefficients.
$F = F(y, z)$ = y-component of prescribed electric field.
$f_n = f_n(z)$ = Fourier component of $F(y, z)$.
$f(\theta, \phi)$ = Function defined by eqn. (35).
H = Magnetic field strength.
H_i = Impressed magnetic field on slot antenna.
H_s = Slot radiation field.
H_{y0}, H_{z0} [eqn. (58)] = y and z components of magnetic field calculated in the absence of radiation damping.
I = Aerial current.
I_0 = Aerial-current maximum (zero-order approximation).
k = $2\pi/\lambda$ (free-space propagation coefficient).
k' = $2\pi/\lambda_g$ (rectangular-waveguide propagation coefficient).
K = Large rectangular-waveguide propagation coefficient.
l = Slot length.
l_a = Wire-antenna length.
L_a = Inductance per unit length of wire aerial.
L_s = Inductance per unit length of slot aerial.
M, N, P [eqn. (33)] = Slot voltage components.
n = Mode number.
r = Wire-aerial radius.
s = $\sin(\pi\eta/a)$.
S = Slot co-ordinate.
t = Time.
V = Aerial or slot voltage.
V_0 = Impressed voltage amplitude.
w = Slot width.
w' = Average slot width.
x, y, z = Rectangular co-ordinates.
X_1, X_2 = Slot reactances [eqns. (27) and (56)].
X, Y [eqn. (37)] = Slot reactance and susceptance components.
Z_0 = Impedance of free space.
Z_a = Wire aerial wave impedance.
Z_s = Slot aerial wave impedance.
Z_{ab}, Z_{AB} = Rectangular-waveguide characteristic impedance, for dimensions a, b and A, B, respectively.
Z_t = Normalized terminating impedance.
β [eqn. (40)] = Variable of integration.
Γ_n = Propagation coefficient of nth order made.
λ = Free-space wavelength.
λ_g = Rectangular guide wavelength.
θ, ϕ, ψ = Electrical angles associated with the slot.
η, ζ = Running co-ordinates in the slot.
ζ_m = Maximum value of ζ.
ω = Angular frequency.

(1) INTRODUCTION

Bethe,[1] in a classic paper, produced a number of very general formulae for coupling through small slots. The essence of the method is to treat the slot as a small perturbation in an otherwise perfectly conducting and infinite plane boundary, and to express the effect of the slot in terms of the fields which would have been present in the absence of the slot. The problem is reduced to an electrostatic or magnetostatic one by ignoring retardation effects in the neighbourhood of the slot, and the results are expressed in terms of lumped constants known as 'polariza-

Correspondence on Monographs is invited for consideration with a view to publication.
Mr. Lewin is with Standard Telecommunication Laboratories, Ltd.

bilities', which can be obtained from the solution of known electrostatic problems for a few simple shapes like circular holes, or long elliptical slots as an approximation to rectangular slots.

At the other extreme, Stevenson[2] set up rigorous equations for the fields in the guides and slot for a waveguide arrangement in which the size of the slot is not restricted. An integral equation, similar in nature to Hallén's integral equation for a cylindrical antenna, is obtained, and the usual iteration procedure of antenna theory is used to obtain approximations to the solution. The problem is complicated by the waveguide environment, which, from the antenna point of view, produces a doubly infinite series of images, and which, from the point of view of the mathematics, introduces awkward double infinite series into an already difficult analysis. Ordinary antenna theory and design would have been severely circumscribed if there had not existed some intermediate procedures between the infinitesimal dipole analysis, on the one hand, and Hallén's rigorous formulation on the other. In fact, workers in the field have long utilized a transmission-line approach, with various refinements according to circumstances, and some such approach is obviously desirable to handle the numerous slot-coupling arrangements which can arise from time to time in waveguide technique. It is the purpose of this paper to indicate how a usable intermediate process can be achieved.

(2) ANTENNA IN FREE SPACE

Since the methods to be expounded have some affinity to those used with antennae, we shall begin with a few introductory remarks on the latter.

A straight cylindrical rod, fed at the centre, is the simplest type of antenna from the point of view of the transmission-line approach. It is characterized by a wave-impedance Z_a given approximately by the equation

$$Z_a = 60\left(\log\frac{2l_a}{r} - 1\right) \quad . \quad . \quad . \quad . \quad (1)$$

where l_a is the total length of the antenna and r is its radius (the subscript a refers to the antenna). Alternative forms of eqn. (1) exist according to approximations made in the theory, the above form being valid for a short antenna. For a long wire the asymptotic form is

$$Z_a = 60\left(\log\frac{\lambda}{2\pi r} + 0{\cdot}116\right) \quad . \quad . \quad . \quad . \quad (2)$$

λ being the free space wavelength, and is the preferred form when the length is about half a wavelength or more. At a quarter wavelength the two formulae are in error by about the same amount, the constants in the two cases being too large by about 0·18. In general, this indeterminacy amounts to the introduction of only small errors, and merely reflects the approximations inherent in the method. Further details are given by Schelkunoff and Friis.[3]

In a later Section, we shall be using Babinet's principle,[4] which relates to the interchange of a slot and a *strip* antenna of equal size. To relate a strip and cylinder we use a result[5] according to which a strip of width w has the same inductance as a cylinder of radius $r = w/4$. Hence, for a short strip, eqn. (1) would give

$$Z_a = 60\left(\log\frac{8l_a}{w} - 1\right) \quad . \quad . \quad . \quad . \quad (3)$$

Surdin[6] gives results for a short elongated elliptical slot of length l and (maximum) width w involving a factor $\log(4l_a/w) - 1$. The breadth varies along the length, on account of the elliptical shape. If we define an average breadth w' by

$$\log w' = \int_0^1 \log\left[w\sqrt{(1-x^2)}\right]dx$$

then $w' = 2w/e$. (The ordinary linear average would have given $w' = \pi w/4$, which does not differ significantly from the above result.) Substituting for w in Surdin's formula gives a form $\log(8l/w') - 2$, differing from eqn. (3) by having the additive constant doubled. It might have been expected that agreement between the two methods would have been closer than this, but the discrepancy is not large, and will be ignored in what follows.

After this preliminary discussion on the characteristic impedance of the antenna, we note the following pair of equations for the voltage, V, and current, I, on the line

$$\frac{\partial V}{\partial x} = -L_a\frac{\partial I}{\partial t} \quad . \quad . \quad . \quad . \quad . \quad . \quad (4)$$

$$\frac{\partial I}{\partial x} = -C_a\frac{\partial V}{\partial t} \quad . \quad . \quad . \quad . \quad . \quad . \quad (5)$$

L_a and C_a are related by $Z_a = \sqrt{(L_a/C_a)}$ and $c = 1/\sqrt{(L_aC_a)}$.

Eqn. (4) relates the potential drop, dV, in a short length, dx, of line with the reverse voltage $-(L_a dx)\partial I/\partial t$ arising from the rate of current change in the inductance $L_a dx$. In a similar way, eqn. (5) relates the change of current, dI, with the rate of change of charge, $-(C_a dx)\partial V/\partial t$, due to a changing potential in a capacitance $C_a dx$. If there is an *impressed* electric field E_i the voltage and current in the line distribute themselves to give a field $-E_i$ at the surface of the antenna, and eqn. (4) is modified to

$$\frac{\partial V}{\partial x} = -L_a\frac{\partial I}{\partial t} + E_i \quad . \quad . \quad . \quad . \quad . \quad (6)$$

Eliminating V between eqns. (5) and (6), expressing L_a and C_a in terms of Z_a and c, and putting $j\omega \equiv \partial/\partial t$, we have

$$\frac{\partial^2 I}{\partial x^2} + k^2 I = -j\omega C_a E_i$$
$$= -jkE_i/Z_a \quad . \quad . \quad . \quad . \quad . \quad (7)$$

where $k = 2\pi/\lambda$.

When E_i is constant and the antenna is free from end loading, so that $I(x = \pm l_a/2) = 0$, the solution to eqn. (7) is

$$I = \frac{-jE_i\left[\cos(\frac{1}{2}kl_a) - \cos(kx)\right]}{kZ_a\cos(\frac{1}{2}kl_a)} \quad . \quad . \quad . \quad (8)$$

When the length is very small, an approximation to eqn. (8) is

$$I = (jkE_i/2Z_a)(l_a^2/4 - x^2) \quad . \quad . \quad . \quad . \quad (9)$$

Eqn. (8) fails when $l_a \simeq \lambda/2$, since the denominator becomes zero. The reason is that the field produced at the surface of the antenna, in addition to the externally impressed field E_i, should also contain the radiated field of the antenna itself, which is proportional to I. This can often be neglected, but near resonance, when the current becomes large, it makes itself felt. There are two components of this field—an in-phase component, responsible for the antenna radiation, and a quadrature component, whose main effect is to alter the tuning length slightly from the half-wave position. If this antenna field is denoted by E_a, eqn. (7) must be modified to

$$\frac{\partial^2 I}{\partial x^2} + k^2 I = -jk(E_i + E_a)/Z_a \quad . \quad . \quad . \quad (10)$$

The solution is found by assuming a sinusoidal current, calculating E_a, inserting this value into eqn. (10) and solving that equation for the current. As an indication of the method, take the case of a dipole fed by an impressed voltage V_0 at the centre. Then $E_i = -V_0\delta(x)$. We first ignore E_a in eqn. (10). The sinusoidal approximation is readily found to be

$$I = \frac{jV_0}{2Z_a}\frac{\sin(k|x| - \frac{1}{2}kl_a)}{\cos(\frac{1}{2}kl_a)} \quad . \quad . \quad . \quad . \quad (11)$$

The input impedance is $-V_0/I(x=0) = -j2Z_a \cot(\frac{1}{2}kl_a)$, or just the impedance to be expected from a transmission line of length $\frac{1}{2}l_a$ and characteristic impedance $2Z_a$. The correction to the impedance to take account of radiation requires the calculation of E_a from a current of the form given by eqn. (11), its insertion into eqn. (10) and the solution of eqn. (10). The rigorous process is quite lengthy and will not be pursued. However, as an indication of what can be achieved by quite approximate methods, let us take the case of the half-wave dipole and use Reference 3 [eqn. (18), Chapter 13) for the field produced. The real part of this radiation field is the source of the main correction sought, and this field is fairly constant over the length of the wire. Its value at the centre of the antenna is found to be $E_a = -240I_0/\lambda$, and eqn. (10) becomes

$$\frac{\partial^2 I}{\partial x^2} + k^2 I = \frac{-jk}{Z_a}[-V_0\delta(x) - 240I_0/\lambda] \quad . \quad . \quad (12)$$

which has the solution

$$I = \frac{jV_0}{2Z_a}\sin k|x| + \frac{j240I_0}{Z_a\lambda k} + I_0 \cos kx \quad . \quad . \quad (13)$$

At $x = l_a/2 = \lambda/4$ we require $I = 0$, whence $I_0 = -\pi V_0/240$. Apart from a small reactive term (which vanishes for large values of Z_a), this current gives an input impedance $-V_0/I_0 = 240/\pi = 76$ ohms, compared with the accurate value of 73 ohms for a half-wave dipole. Since the main objection to eqn. (11) is the absence of any limit to the current at resonance, it is seen that a simple consideration of the real part of the radiation field can supply an adequate correction. (A more detailed analysis would also give the end correction for tuning, but this aspect will not be pursued in the paper.)

(3) SLOT ANTENNA IN AN INFINITE PERFECTLY CONDUCTING PLANE

Fig. 1 shows a slot of total length l and width w. Babinet's principle asserts that the distribution of electric and magnetic

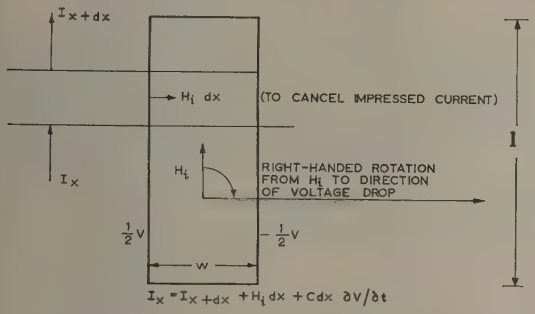

Fig. 1.—Current and voltage relations for slot in an infinite plane.

fields can be obtained from that of the corresponding strip antenna if electric and magnetic quantities are interchanged and the fields rotated through a right angle. This means a voltage V exists across the slot, with a variation along the length of the same character as that of the current in the strip antenna; whilst a current I in the plane, flowing parallel to the slot, will correspond to the antenna voltage.

Analogously to eqns. (5) and (6) we have

$$\frac{\partial V}{\partial x} = -L_s\frac{\partial I}{\partial t} \quad . \quad . \quad . \quad . \quad . \quad . \quad . \quad (14)$$

$$\frac{\partial I}{\partial x} = -C_s\frac{\partial V}{\partial t} - H_i \quad . \quad . \quad . \quad . \quad (15)$$

and, corresponding to eqn. (7),

$$\frac{\partial^2 V}{dx^2} + k^2 V = jkH_iZ_s \quad . \quad . \quad . \quad . \quad (16)$$

In eqn. (15) we use the convention that a right-handed rotation takes the direction of magnetic field to that of the voltage drop.

Z_s $[=\sqrt{(L_s/C_s)}]$ is the characteristic impedance of the slot, and it is related, through Babinet's principle, to the characteristic impedance of the corresponding strip antenna by

$$Z_sZ_a = (Z_0/2)^2 \quad . \quad . \quad . \quad . \quad . \quad (17)$$

where Z_0 $(=120\pi$ ohms) is the impedance of free space.

Eqn. (14) states that the change in potential across the slot in a length dx is equal to the back voltage due to the change of current in an inductance $L_s dx$. Similarly, eqn. (15) states that the change in current flow in the plane, parallel to the slot, is equal to the difference between the charge stored at a voltage V in a capacitance $C_s dx$ and the current needed to cancel at the slot the impressed current $H_i dx$ arising from the driving field H_i. H_i is the field, parallel to the slot, which would have existed in the absence of the slot. As with eqn. (10), it needs to be augmented by a field H_s arising from the radiation of the slot itself. As in the case of the antenna, this additional field has the two main effects of limiting the resonance voltage and of altering the tuning length. The former effect is the more important, and can be catered for by approximate, though adequate, means without involving long and complicated analyses. Like the antenna current, the slot voltage has to be zero at the ends of the slot.

However, there are some differences between the strip antenna in free space and the slot in an infinite plane. In the former the incident field is usually taken as that of a freely propagating wave, whilst in the latter, in the absence of the slot, the wave will be completely reflected, doubling the magnetic field at the boundary. It is this doubled field which appears in eqn. (15). Similarly the field H_s due to the slot itself consists of two fields, due to the excitation by the slot of the two sides of the plane. The currents on the two sides will be the same, and hence the associated magnetic fields are equal but of opposite sign. Since the currents are primarily of concern here, it is the *difference* in the two magnetic fields which is used to augment H_i. With these alterations the analyses of Section 1 may be used for the slot, utilizing eqn. (17), in conjunction with eqn. (3) or an equivalent, for Z_s.

The following Sections provide examples of this method.

(4) SLOT COUPLING OF AXIALLY ALIGNED GUIDES

(4.1) General Equations

Fig. 2 shows a waveguide of dimensions a and b abutting axially and symmetrically to a guide of dimensions A and B

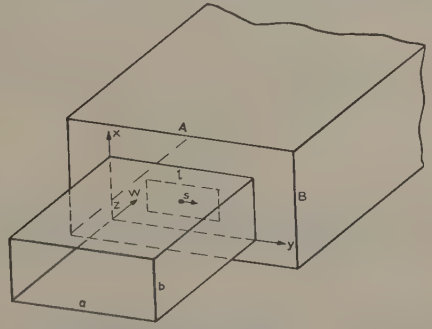

Fig. 2.—Slot-coupled axially abutting rectangular waveguides.

through a common end-wall with a slot of dimensions l and w. The incident electric field is reflected at the end-wall, giving rise, in the absence of the slot, to a field

$$\left.\begin{aligned}(E_i)_x &= E_0(\varepsilon^{-jk'z} - \varepsilon^{jk'z})\sin(\pi y/a)\\ (H_i)_y &= E_0(\varepsilon^{-jk'z} + \varepsilon^{jk'z})(k'/kZ_0)\sin(\pi y/a)\end{aligned}\right\} \quad . \quad (18)$$

where $k' = 2\pi/\lambda_g$ and $\lambda_g = \lambda/(1 - \lambda^2/4a^2)^{1/2}$

H_i (with $z = 0$) is the exciting field, for insertion into eqn. (16), which, in the present instance, takes the form

$$\frac{\partial^2 V}{\partial y^2} + k^2 V = jkZ_s\left[2E_0\frac{k'}{kZ_0}\sin(\pi y/a) + H_s\right] \quad . \quad (19)$$

A voltage V over a slot of width w corresponds to an electric field strength over the slot of $E = -V/w$, and this radiates into the two waveguides waves whose amplitudes can be determined by Fourier analysis. For $z < 0$ the dominant mode is

$$\left.\begin{aligned}E_x &= \varepsilon^{jk'z}\sin(\pi y/a)(2/ab)\int(-V/w)\sin(\pi y/a)dxdy\\ H_y &= -E_x(k'/kZ_0)\end{aligned}\right\} \quad (20)$$

For $z > 0$ the sign of z, and of H_y, is reversed, A and B replacing a and b. $K = \lambda/(1 - \lambda^2/4A^2)^{1/2}$ replaces k'. Now H_s is the difference between these magnetic fields, and therefore it takes the form

$$H_s = -E_1k'/(kZ_0) - E_2K/(kZ_0) \quad . \quad . \quad (21)$$

where E_1 and E_2 are the fields at $z = 0$ given by eqn. (20) and its equivalent for the second guide. Eqn. (21) represents actually the contribution to H_s from the dominant waves only, but assuming that these are the only ones propagating, this is all that is needed to account for the radiation component from the slot. The remaining (evanescent) part of the field determines the slot reactance and tuning length, but if these are to be examined it is better to proceed with the rigorous analysis, as on page 88 of Reference 7, where the case of two equal guides is treated in detail.

(4.2) Equal Guides

Returning now to eqn. (19) we consider first the case of equal guides. The equation is

$$\partial^2 V/\partial y^2 + k^2 V = 2jk'\sin(\pi y/a)(E_0 - C_0)Z_s/Z_0 \quad . \quad (22)$$

where $$C_0 = (2/ab)\int(-V/w)\sin(\pi y/a)dxdy \quad . \quad . \quad (23)$$

A simple case, for which a known solution exists, is the capacitive diaphragm, for which the slot extends right across the guide. In this case a solution of eqn. (22), zero at the ends of the slot, is $V = V_0\sin(\pi y/a)$ with

$$(k')^2V_0 = 2jk'(E_0 - C_0)Z_s/Z_0 \quad . \quad . \quad . \quad (24)$$

where $C_0 = -V_0/b$ from eqn. (23).

Solving eqn. (24) for V_0 and introducing $Z_a = (Z_0/2)^2/Z_s$ from eqn. (17) we have

$$V_0 = \frac{\frac{1}{2}j(Z_0/Z_a)E_0}{k' - \frac{1}{2}j(Z_0/Z_ab)} \quad . \quad . \quad . \quad . \quad (25)$$

From eqn. (20) we deduce the field radiated by the slot back into the guide. From eqn. (18) the total reflection coefficient is given by adding $-E_0$ to this field and dividing throughout by E_0. The result of the calculation is

$$\frac{E_r}{E_0} = -1 - \frac{V_0}{E_0b} = \frac{-1}{1 - \frac{1}{2}jZ_0/Z_ak'b} \quad . \quad . \quad (26)$$

A normalized reactance jX_1 across the guide would cause a reflection given by the formula $-1/(1 + 2jX_1)$, and on comparison with eqn. (26) we have

$$X_1 = -\tfrac{1}{4}Z_0/Z_ak'b \quad . \quad . \quad . \quad . \quad . \quad (27)$$

The known solution (see Reference 7, page 72) can be put in the above form if, for Z_a, we take

$$Z_a = 60\log\operatorname{cosec}\tfrac{1}{2}\pi w/b \quad . \quad . \quad . \quad . \quad (28)$$

From a comparison of this with, say, eqn. (3), we see that the form for Z_a is somewhat different from that of the equivalent strip antenna in free space. In fact, the dominant length involved is b rather than a, showing that the images of the slot in the waveguide walls are all-important in determining the effective characteristic impedance. It is, perhaps, a shortcoming of the present analysis that it introduces the quantity Z_a in an extraneous way, rather than producing it as a consequence of the calculations. Of course, in the limiting case of very small values of w all the forms are equivalent, but in many applications it is intermediate values of w which are of consequence, and the differences between the various formulae, though not excessive, are not so small that they can be overlooked entirely. Until this situation is remedied perhaps the best we can do is to make contact with known solutions at various points, as in eqn. (28), and in this way to obtain some guide as to the appropriate values to use. It should be noted that the full form for the impressed magnetic field, properly augmented by the slot radiation, was needed in order to get the form of eqn. (26) for comparison with other solutions.

(4.3) Unequal Guides of Same Width

A case of unequal guides in which $a = A$ but $b \neq B$ can be solved in a similar way. In eqn. (23) instead of the factor $(2/ab)$ we now have $1/ab + 1/aB$. The rest of the calculation proceeds as before, eqn. (26) becoming

$$\frac{E_r}{E_0} = -\frac{1 - (1 - b/B)jX_1}{1 + (1 + b/B)jX_1} \quad . \quad . \quad . \quad . \quad (29)$$

where X_1 is as in eqn. (27). This reflection is precisely the form to be expected from a reactance across a guide of characteristic impedance proportional to b feeding into a guide of impedance given by B. When the slot width is equal to the width of the narrower guide, b say, the arrangement becomes simply an E-plane step with a known solution. The reactance is then very close to half the corresponding capacitive diaphragm as seen by the broader guide,[8] which suggests the following general formula for the wave impedance in this arrangement:

$$Z_a = 30\log[\operatorname{cosec}(\tfrac{1}{2}\pi w/b)\operatorname{cosec}(\tfrac{1}{2}\pi w/B)] \quad . \quad (30)$$

(4.4) General Unequal Guides

Finally, we consider the very general case of a central slot of length l in an end-wall between two unequal guides. Instead of eqn. (22) we have, on introducing a co-ordinate $S = y - a/2$ measured from the centre of the slot,

$$\begin{aligned}\partial^2 V/\partial S^2 + k^2 V = {} & (2jk'Z_s/Z_0)(E_0 - C_1)\cos(\pi S/a)\\ & + (2jKZ_s/Z_0)(-C_2)\cos(\pi S/A) \quad (31)\end{aligned}$$

where

$$\left.\begin{aligned}C_1 &= (1/ab)\int_{-l/2}^{l/2}(-V)\cos(\pi S/a)dS\\ C_2 &= (1/AB)\int_{-l/2}^{l/2}(-V)\cos(\pi S/A)dS\end{aligned}\right\} \quad . \quad . \quad (32)$$

The total reflection coefficient into the first guide is $-1+2C_1/E_0$ whilst the transmission coefficient in the second is similarly $2C_2/E_0$. A solution of eqn. (31) is

$$V = M\cos(\pi S/a) + N\cos(\pi S/A) + P\cos(kS)\,. \quad (33)$$

where

$$\left.\begin{aligned} M &= (2jZ_s/k'Z_0)(E_0 - C_1)\\ N &= (2jZ_s/KZ_0)(-C_2)\\ P &= -\sec(\tfrac{1}{2}kl)[M\cos(\pi l/2a) + N\cos(\pi l/2A)] \end{aligned}\right\} \quad (34)$$

The last equation comes from the requirement that the voltage is to be zero at the ends of the slot.

From eqn. (32) we have

$$C_1 = (-2/ab)\int_0^{l/2}\cos(\pi S/a)[M\cos(\pi S/a) + N\cos(\pi S/A) + P\cos(kS)]dS$$

$$C_2 = (-2/AB)\int_0^{l/2}\cos(\pi S/A)[M\cos(\pi S/a) + N\cos(\pi SA) + P\cos(kS)]dS$$

The integrations involved are all elementary, and after substituting for M, N and P in terms of C_1 and C_2 from eqn. (34), C_2 can be eliminated from the resulting equations, and C_1, and hence the reflection coefficient, can be calculated. The algebra is rather lengthy, though quite straightforward. We introduce the angles $\theta = \pi l/2a$, $\phi = \pi l/2A$ and $\psi = kl/2 = \pi l/\lambda$. The integrations involve the functions

$$\mathrm{f}(\theta,\phi) = \frac{\sin(\theta+\phi)}{\theta+\phi} + \frac{\sin(\theta-\phi)}{\theta-\phi} \quad . \quad . \quad (35)$$

in the following combinations

$$\left.\begin{aligned} C &= \mathrm{f}(\theta,\theta) - \mathrm{f}(\theta,\psi)\cos\theta\sec\psi\\ D &= \mathrm{f}(\theta,\phi) - \mathrm{f}(\theta,\psi)\cos\phi\sec\psi\\ E &= \mathrm{f}(\theta.\phi) - \mathrm{f}(\phi,\psi)\cos\theta\sec\psi\\ F &= \mathrm{f}(\phi,\phi) - \mathrm{f}(\phi,\psi)\cos\phi\sec\psi \end{aligned}\right\} \quad . \quad . \quad . \quad (36)$$

If the reflection coefficient is put in the form $(Z_t-1)/(Z_t+1)$, then Z_t is the (normalized) terminating impedance for the first guide. Introducing, for brevity, the notation

$$\left.\begin{aligned} X &= lZ_s/k'abZ_0\\ Y &= KABZ_0/lZ_s \end{aligned}\right\} \quad . \quad . \quad . \quad . \quad . \quad (37)$$

Z_t can be written in the form

$$Z_t = \frac{jX}{F}(DE - CF) + \frac{-j(XDE/F)}{1 - j(XDE/F)/(XYDE/F^2)} \quad (38)$$

The interpretation of this expression is fairly straightforward. Z_t consists of a reactance $jX(DE-CF)/F$ in series with an impedance consisting of a further reactance $-jXDE/F$ in parallel with a resistance $XYDE/F^2$, all normalized with respect to the first guide. We expect, for the resistive term, a contribution $Z_{AB}/Z_{ab} = (B/b)(k'a/KA)$, and if we extract this form, the remaining factor is $DE(KA/Fk'a)^2$. This factor respresents the *radiative coupling* from one guide to the other through the slot, and is given in eqn. (5.8) of Reference 7 for the simplest case of the H-plane step. The slot, in addition to presenting a reactance to the guide, acts as a transformer with a ratio as given above. When $a = A$, then $\theta = \phi$ and all the expressions in eqn. (36) become equal. The transformer ratio is then unity, the series reactance vanishes, whilst the parallel reactance becomes simply $-jXF$. For a slot equal in length to the guide width, $F = 1$, and we recover the case leading to eqn. (29). Thus eqn. (30) for the characteristic impedance of the slot seems to be indicated, at least for slots which are not too short.

Although the above calculations may appear a little complicated, the point to be stressed is that a solution by elementary means has been found for a relatively intricate waveguide configuration. To have provided a rigorous solution would have been quite a formidable task. About the only aspect not completely resolved is the value to be used for the characteristic impedance for short slots, the free-space value of Surdin's formulation presumably needing some minor modification for the waveguide environment.

(5) SLOT COUPLING THROUGH THE BROAD WALL OF A WAVEGUIDE

(5.1) Field from an Arbitrary Wall Source

In order to solve problems involving broad-wall coupling it is first necessary to have an explicit formula for the field in the guide generated by a prescribed field over the guide surface. Fig. 3 shows a waveguide with a hole in which impressed fields

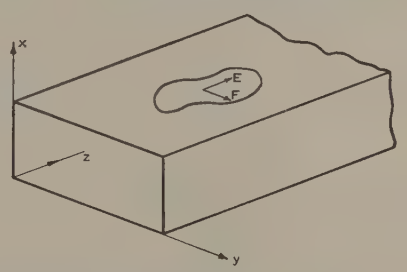

Fig. 3.—Rectangular waveguide excited by arbitrary electric field in broad wall.

E and F in the z and y directions are excited. (Excitation by a normal component of electric field is also possible but is not considered in this Section.) In the guide a field with electric components E_x, E_y, and E_z will be produced, and this will satisfy the following conditions:

$$\left.\begin{aligned} E_x = E_z &= 0 \text{ at } y = 0,\ a\\ E_y = E_z &= 0 \text{ at } x = 0\\ E_z = E,\ E_y &= F \text{ at } x = b\\ \operatorname{div} E &= 0\\ \nabla^2 + k^2 &= 0 \text{ for } E_x,\ E_y \text{ and } E_z \end{aligned}\right\} \quad . \quad . \quad . \quad (39)$$

Expressing the fields as a sum of modes in the broad dimension, the following forms can be written in terms of as yet undetermined functions F_n and G_n.

$$E_x = \sum_1^\infty \sin(n\pi y/a)\int_{-\infty}^{\infty}\varepsilon^{j\beta z}\frac{\cos(x\Gamma_n)}{\sin(b\Gamma_n)}\frac{F_n(\beta) - G_n(\beta)}{\Gamma_n}d\beta + \sin(\pi y/a)(A\varepsilon^{-jk'z} + B\varepsilon^{jk'z}) \quad (40)$$

$$E_y = \sum_0^\infty \cos(n\pi y/a)\int_{-\infty}^{\infty}\varepsilon^{j\beta z}\frac{\sin(x\Gamma_n)}{\sin(b\Gamma_n)}\frac{G_n(\beta)}{n\pi/a}d\beta \quad . \quad (41)$$

$$E_z = \sum_1^\infty \sin(n\pi y/a)\int_{-\infty}^{\infty}\varepsilon^{j\beta z}\frac{\sin(x\Gamma_n)}{\sin(b\Gamma_n)}\frac{F_n(\beta)}{j\beta}d\beta \quad . \quad (42)$$

where $\Gamma_n = (k^2 - n^2\pi^2/a^2 - \beta^2)^{1/2}$ and β is a variable of

integration. It is readily verified that these forms satisfy $\text{div}\, E = 0$ and the wave equation, and all the boundary conditions (39) except that relating to the prescribed fields at $x = b$. This condition can be met by determining F_n and G_n by a Fourier analysis and Fourier integral inversion.

If $E = E(y, z) = \sum_1^\infty \sin(n\pi y/a)e_n(z)$ is the prescribed field in the z-direction, then

$$e_n(z) = \frac{2}{a}\int_0^a E(\eta, z)\sin(n\pi\eta/a)d\eta$$

and $$\mathrm{F}_n(\beta) = \frac{j\beta}{2\pi}\int_{-\infty}^{\infty}\varepsilon^{-j\beta\zeta}e_n(\zeta)d\zeta$$

$$= \frac{j\beta}{a\pi}\int_0^a\int_{-\infty}^{\infty}\varepsilon^{-j\beta\zeta}\sin(n\pi\eta/a)E(\eta, \zeta)d\eta d\zeta \quad . \quad . \quad (43)$$

on substituting for e_n.

Similarly, if $\mathrm{F}(y, z) = \sum_0^\infty \cos(n\pi y/a)\mathrm{f}_n(z)$ is the y-component of the prescribed field, then

$$\mathrm{G}_n(\beta) = \frac{n}{a^2}\int_0^a\int_{-\infty}^{\infty}\varepsilon^{-j\beta\zeta}\cos(n\pi\eta/a)\mathrm{F}(\eta, \zeta)d\eta d\zeta \quad . \quad (44)$$

The $n = 0$ term is anomalous and has $\mathrm{G}_n(\beta)/(n\pi/a)$ replaced by $\mathrm{G}_0(\beta)$ where

$$\mathrm{G}_0(\beta) = \frac{1}{2\pi a}\int_0^a\int_{-\infty}^{\infty}\varepsilon^{-j\beta\zeta}\mathrm{F}(\eta, \zeta)d\eta d\zeta \quad . \quad . \quad (45)$$

From these expressions the dominant mode contribution arising from the integral in eqn. (40) is

$$E_x = \sin(\pi y/a)\int_{-\infty}^{\infty}\varepsilon^{j\beta z}\frac{\cos(x\Gamma_1)}{\sin(b\Gamma_1)}\frac{\mathrm{F}_1(\beta) - \mathrm{G}_1(\beta)}{\Gamma_1}d\beta \quad (46)$$

From eqn. (43) we see that $\mathrm{F}_n(\beta)$ involves the integration of $\varepsilon^{-j\beta\zeta}$ over an infinite range of ζ; but if $E(\eta, \zeta)$ is limited in range to some maximum value ζ_m, say, the dominant contribution for large values of β cannot exceed some constant multiplied by $\varepsilon^{-j\beta\zeta_m}$. Hence, from eqn. (46) we see that, for $z > \zeta_m$, the coefficient multiplying β in the exponent is positive imaginary, so that, if the contour is deformed into the upper half of the complex plane, the real part of the exponent becomes negative, and the integrand vanishes if the deformation is taken to the semicircle at infinity. Hence the integral in eqn. (46) for large values of z becomes equal to the sum of the contributions from the residues in the upper half of the complex plane.

In a similar way it may be shown that, for large negative values of z, the integral is the sum of the contributions from the residues in the lower half of the complex plane. Of all these residues, for a guide possessing only a single propagating mode, all except two occur on the imaginary axis and correspond to evanescent waves. The residues corresponding to the dominant mode occur at values of β given by $\Gamma_1 = 0$, or $k^2 - \pi^2/a^2 - \beta^2 = 0$. Hence β equals $\pm k'$. If the medium in the guide possesses a very slight attenuation, so that k contains a small negative imaginary part, the pole at $\beta = -k'$ will lie above the real axis and that at $\beta = +k'$ below it. This determines which pole contributes in each part of the plane.

The evaluation at the residues is quite straightforward, and gives, after some calculation,

$$E_x = \sin(\pi y/a)(A\varepsilon^{-jk'z} + B\varepsilon^{jk'z} + C_\pm\varepsilon^{-jk'|z|}) \quad . \quad (47)$$

where

$$\left.\begin{aligned} C_+ &= \frac{1}{ab}\int_0^a\int_{-\infty}^{\infty}\varepsilon^{jk'\zeta}\left[E\sin(\pi\eta/a) - \frac{j\lambda_g}{2a}F\cos(\pi\eta/a)\right]d\eta d\zeta, \quad z \gg 0 \\ C_- &= -\frac{1}{ab}\int_0^a\int_{-\infty}^{\infty}\varepsilon^{-jk'\zeta}\left[E\sin(\pi\eta/a) + \frac{j\lambda_g}{2a}F\cos(\pi\eta/a)\right]d\eta d\zeta, \quad z \ll 0 \end{aligned}\right\} \quad (48)$$

(5.2) Parallel Guides. Small Slots

Let us consider the case of the reflection due to a small crossed slot, as used in the crossed-slot directive coupler. If the slot is small enough, a number of approximations can be made. Thus in eqn. (48) the functions $\sin(\pi\eta/a)$ and $\cos(\pi\eta/a)$ can be given their mean values at the centre of the slots. The retardation implicit in the factors $\varepsilon^{\pm jk'\zeta}$ can be ignored. E and F are determined by the slot analogue of eqn. (7), i.e. eqn. (16), in which the impressed fields may also be given their values at the slot centres. Finally the influence of the radiation field of the slots on the distribution of slot voltages may be ignored, since small slots will be well below resonance.

The *impressed* fields corresponding to E and F are, respectively, $-H_y$ and H_z where

$$\left.\begin{aligned} H_y &= \frac{\lambda}{Z_0\lambda_g}A\sin(\pi\eta/a)\varepsilon^{-jk'z} \\ H_z &= \frac{\lambda}{Z_0\lambda_g}A\cos(\pi\eta/a)\varepsilon^{-jk'z}(-j\lambda_g/2a) \end{aligned}\right\} \quad . \quad . \quad (49)$$

[The coefficient B in eqn. (47) is taken to be zero for a wave incident in a guide which is matched in the absence of the disturbance from the slots.] The solution to eqn. (16), valid for small slots, is the equivalent of eqn. (9) for the small antenna, and is

$$V = (jH_iZ_sk/2)(S^2 - l^2/4) \quad . \quad . \quad . \quad (50)$$

where H_i is the value of $-H_y$ or H_z at the slot centre from eqn. (49), and S is the co-ordinate in the slots in the direction of η or ζ.

Since the integrals of E or F with respect to $d\zeta$ or $d\eta$ are minus their respective voltages, eqn. (48) for C_-/A, the reflection coefficient, becomes

$$C_-/A = \frac{jZ_s\pi}{ab\lambda_gZ_0}[(\lambda_g/2a)^2\cos^2(\pi\eta/a) - \sin^2(\pi\eta/a)]\int_{-l/2}^{l/2}(S^2 - l^2/4)dS$$

$$= \frac{j\pi l^3Z_0}{24ab\lambda_gZ_a}[\sin^2(\pi\eta/a) - (\lambda_g/2a)^2\cos^2(\pi\eta/a)] \quad (51)$$

Thus the reflection coefficient is zero when $\tan(\pi\eta/a) = \pm\lambda_g/2a$, the well-known condition for circular polarization of the magnetic field at the guide wall. [In eqn. (51) we have introduced the characteristic impedance Z_a of the equivalent antenna, which takes the value $60[\log(8l/w) - 1]$ for a small antenna in free space.]

If instead of taking for E and F the fields derived from the field in the guide we had taken the fields derived from a second guide of the same dimensions with a common broad wall, eqn. (51) would represent the reverse-coupled wave, whilst a similar equation with the trigonometrical terms added rather than subtracted would give the forward-coupling coefficient. The results may be compared with Surdin's eqn. (23), the only difference

being the small discrepancy already discussed in the characteristic impedance.

(5.3) Crossed Guides. Small Slots

If the second guide is rotated through a right angle the roles of E and F are interchanged, the coupling coefficients being now

$$\frac{Z_s\pi}{ab\lambda_g Z_0}\frac{\lambda_g}{2a}[(\cos\pi\eta/a)\sin(\pi\eta/a) \pm \cos(\pi\eta/a)\sin(\pi\eta/a)]\int_{-l/2}^{l/2}(S^2-l^2/4)dS = \frac{\pi l^3 Z_0}{48a^2bZ_a}[\sin(2\pi\eta/a),\,0] \quad . \; . \; . \quad (52)$$

From this, the well-known frequency-independent coupling and perfect directivity for small crossed-slot coupling can be readily seen. However, for large slots these properties are only approximated, the main disturbance being the effect of the approach to resonance on the coupling. In the first instance this requires the use of the form of eqn. (8) instead of eqn. (9), leading to the replacement of l^3 in eqn. (52) by

$$\frac{24}{k^2}\int_0^{l/2}\frac{\cos(kS)-\cos(\frac{1}{2}kl)}{\cos(\frac{1}{2}kl)}dS = \frac{24}{k^3}[\tan(\tfrac{1}{2}kl)-\tfrac{1}{2}kl]$$

Eqn. (52) is therefore to be multiplied by the factor

$$\frac{3}{\psi^3}(\tan\psi-\psi) \text{ where } \psi = kl/2 \quad . \; . \; . \quad (53)$$

This factor increases rapidly as resonance ($\psi=\pi/2$) is approached. Eqn. (51) is also modified by the same factor.

As an example, a quarter-wave slot has a factor 1·33, whilst, for a length of one third of a wavelength, it has increased to 1·79. As against a circular hole of diameter l with a quasi-static polarizability of $l^3/6$, the slot has only $l^3\pi/(24\log 4l/we)$ so that a factor of magnitude $\frac{4}{\pi}\log 4l/we$ has to be obtained via eqn. (53). Typically this may be of the order of 5 or 6, so that a very close approach to resonance is indicated. The conclusion appears to be that circular holes are more appropriate for large coupling than tuned slots, unless the selectivity of the tuning is desired.

(5.4) Parallel Guides. Effect of Radiation Damping

Although infinite coupling at resonance is indicated by eqn. (53), it must ultimately be limited by radiation effects. These are taken into account by augmenting eqn. (49) by the contributions from the slots. We shall indicate how this is done for parallel guide coupling whilst still retaining the small-slot approximations which permit the use of the fields at the slot centres. For a more accurate formulation the integrals in eqn. (48) would need to be evaluated, leading to the occurrence of the functions introduced in eqn. (35).

In the first instance we note that C_+/A and C_-/A are the relative amplitudes of the dominant modes of the electric fields radiated by the slots in the positive and negative directions in the guide. So far as the slot itself is concerned the dominant-mode magnetic fields are those associated with the waves C_+ and C_- on either side of the slot, the *effective* field being the average, at the slot, of the relevant components. Thus the induced H_y field relative to the exciting H_y field is $\frac{1}{2}(C_+ - C_-)/A$, this being the average of the two H_y components, whilst the relative H_z field is similarly $\frac{1}{2}(C_+ + C_-)/A$. These values need to be doubled on account of the equal magnetic fields produced in the coupled guides, so that the impressed H_y and H_z fields in eqn. (50) need to be multiplied by $1+(C_+ - C_-)/A$ and $1+(C_+ + C_-)/A$, respectively. Hence E and F in eqn. (48) have to be multiplied by the same factors. Putting $(C_+ - C_-)/A = C$ and $(C_+ + C_-)/A = D$, with a subscript zero for the corresponding quantities deduced from eqn. (48) in the absence of a consideration of the slot radiation correction, we get, by adding and subtracting the two equations in eqn. (48),

$$\left.\begin{aligned} C &= C_0(1+C)\\ D &= D_0(1+D)\end{aligned}\right\} \quad . \; . \; . \; . \; . \; . \quad (54)$$

$$\text{Hence} \quad C_+/A = (C+D)/2 = \frac{1}{2}\left(\frac{C_0}{1-C_0}+\frac{D_0}{1-D_0}\right)$$

Substituting for C_- and C_+ from eqn. (51) and its equivalent for the forward-coupled wave, both being modified by the tuning factor in eqn. (53), we have

$$\left.\begin{aligned} C_+/A &= \frac{s^2}{jX_2-2s^2}+\frac{c_s^2}{jX_2-2c_s^2}\\ C_-/A &= -\frac{s^2}{jX_2-2s^2}+\frac{c_s^2}{jX_2-2c_s^2}\end{aligned}\right\} \quad . \; . \quad (55)$$

where $s = \sin(\pi\eta/a)$

$$c_s = (\lambda_g/2a)\cos(\pi\eta/a)$$

and X_2 is a term related to the slot reactance.

$$X_2 = \frac{24ab\lambda_g Z_a}{Z_0\pi l^3 3\,(\tan\psi-\psi)/\psi^3} \quad . \; . \; . \quad (56)$$

At resonance $X_2 = 0$ and eqn. (55) becomes simply $C_+/A = -1$, $C_-/A = 0$, with similar coefficients for the waves in the coupled guide.

Thus the reflected wave, which depends on the circular polarization condition for its cancellation in the small-slot case, becomes accurately zero at resonance.

(5.5) Crossed Guides. Effect of Radiation Damping

In the case of crossed guides a similar type of conclusion is reached, although the mathematics is different. If we put $s = \sin(\pi\eta/a)$ and $c_s = (\lambda_g/2a)\cos(\pi\eta/a)$ as before and define $\bar{C}_+$ and $\bar{C}_-$ as the coupled waves into the two arms of the crossed guide, eqn. (48) and its equivalents give

$$\left.\begin{aligned} C_+ &= Es - jFc_s\\ C_- &= -Es - jFc_s\\ \bar{C}_+ &= jEc_s + Fs\\ \bar{C}_- &= jEc_s - Fs\end{aligned}\right\} \quad . \; . \; . \; . \quad (57)$$

where a constant of proportionality has been omitted.

The H_y component of field, in addition to being augmented by $(C_+ - C_-)/2A$, will also be augmented by the appropriate field from the crossed guide, in this case $(-jc_s/s)\times(\bar{C}_+ - \bar{C}_-)/2A$, the initial factor arising from the interchanging roles of the y and z components in the two guides. Thus we find

$$\left.\begin{aligned} H_y &\to H_{y0}\left[1+\frac{C_+-C_-}{2A}-(jc_s/s)\frac{(\bar{C}_+-\bar{C}_-)}{2A}\right]\\ \text{and} \quad H_z &\to H_{z0}\left[1+\frac{C_++C_-}{2A}-(js/c_s)\frac{(\bar{C}_++\bar{C}_-)}{2A}\right]\end{aligned}\right\} \quad (58)$$

From eqn. (57) we have $\bar{C}_+ - \bar{C}_- = (C_+ + C_-)(s/-jc_s)$ and $\bar{C}_+ + \bar{C}_- = (C_+ - C_-)(jc_s/s)$. Hence eqn. (58) becomes

simply

$$H_y \rightarrow H_{y0}\left(1 + \frac{C_+}{A}\right)$$

$$H_z \rightarrow H_{z0}\left(1 + \frac{C_+}{A}\right)$$

Defining C_0 and D_0 as the same quantities as before, we have, instead of eqn. (54),

$$(C_+ - C_-)/A = C_0\left(1 + \frac{C_+}{A}\right)$$

$$(C_+ + C_-)/A = D_0\left(1 + \frac{C_+}{A}\right)$$

Hence

$$\left.\begin{aligned} C_+/A &= \frac{C_0 + D_0}{2 - C_0 - D_0} \\ C_-/A &= \frac{D_0 - C_0}{2 - C_0 - D_0} \end{aligned}\right\} \quad . \quad . \quad . \quad . \quad (59)$$

C_0 and D_0 are, respectively, $4s^2/jX_2$ and $4c_s^2/jX_2$ with X_2 as in eqn. (56). It is seen that at resonance, when C_0 and D_0 become infinite, C_+/A becomes -1, exactly cancelling the forward wave, whilst C_-/A becomes $(s^2 - c_s^2)/(s^2 + c_s^2)$, which vanishes when the circular-polarization condition $s = \pm c_s$ is satisfied, although not otherise. Similarly we find

$$\left.\begin{aligned} \bar{C}_+ &= \frac{C_0c^2 + D_0s^2}{-jc_s s(2 - C_0 - D_0)} \\ \bar{C}_- &= \frac{C_0c^2 - D_0s^2}{-jc_s s(2 - C_0 - D_0)} \end{aligned}\right\} \quad . \quad . \quad . \quad (60)$$

and since C_0 and D_0 are, respectively, proportional to s^2 and c_s^2 we see that $\bar{C}_-$ vanishes identically under all conditions, i.e. perfect directivity is forecast irrespective of tuning conditions.

Slight modifications of these results are to be expected as a consequence of the finite extension of the slots, but their basic character should not be altered.

As confirmation of these results we note that

$$|C_-|^2 + |\bar{C}_-|^2 + |\bar{C}_+|^2 + |A + C_+|^2 = |A|^2 \quad . \quad (61)$$

which correctly states the conservation law that the energy flowing away from the slot equals that flowing to it.

(6) CONCLUSIONS

The quasi-static antenna method can be applied to the calculation of the properties of slots of medium size in order to give corrections to the quasi-static polarizability. The approach to resonance is covered, and also the development of the relevant equivalent circuit, in which the radiation damping of the slot plays an important role. The end correction to the resonant length is not, however, treated by this method. A shortcoming of the method is its inability to obtain from the analysis the accurate slot wave impedance to be used. This is partly determined by proximity effects, and can be approximated in many cases by comparison with some known configurations. However, a small discrepancy remains in the treatment of the free-space rectangular slot.

The crossed-slot directional coupler, with the slots near resonance, is examined in some detail. In the case of coupled parallel or crossed guides, it is concluded that the circular-polarization condition, necessary in the small-slot configuration for perfect directivity, is not required at resonance. This result may seem unexpected, since, for central slots, it would be contradicted by the symmetry. But with the axial slot just off centre [a double limit is involved in eqn. (55)] the very weak coupling to the slot is compensated by the very weak radiation damping it suffers, so that its effect is comparable to that of the other slot because of the high resonance field it can support (ohmic losses are neglected).

The case of two unequal coaxial guides coupled through a symmetrical slot is treated, and through a comparison with known special solutions, suitable values are obtained for the slot wave impedance.

(7) ACKNOWLEDGMENT

Acknowledgment is due to Standard Telecommunication Laboratories, Ltd., for facilities to prepare, and permission to publish, the paper.

(8) REFERENCES

(1) BETHE, H. A.: 'Theory of Diffraction by Small Holes', *Physical Review*, 1944, **66**, p. 163.
(2) STEVENSON, A. F.: 'Theory of Slots in Rectangular Waveguides', *Journal of Applied Physics*, 1948, **19**, p. 24.
(3) SCHELKUNOFF, S. A., and FRIIS, H. T.: 'Antennas, Theory and Practice' (Wiley, 1952), p. 236.
(4) BOOKER, H. G.: 'Slot Aerials and their Relation to Complementary Wire Aerials (Babinet's Principle)', *Journal I.E.E.*, 1946, **93**, Part IIIA, p. 621.
(5) BAILEY, C. E. G.: 'Slot Feeders and Slot Aerials', *ibid.*, p. 616.
(6) SURDIN, M.: 'Directive Couplers in Waveguides', *ibid.*, p. 728.
(7) LEWIN, L.: 'Advanced Theory of Waveguides' (Iliffe, 1951).
(8) MACFARLANE, G. G.: 'Quasi-Stationary Field Theory and its Applications to Diaphragms and Junctions in Transmission Lines and Waveguides', *Journal I.E.E.*, 1946, **93**, Part IIIA, p. 708.

621.396.677.833

The Institution of Electrical Engineers
Monograph No. 360 E
Feb. 1960
©

A NEW DESIGN METHOD FOR PHASE-CORRECTED REFLECTORS AT MICROWAVE FREQUENCIES

By S. CORNBLEET, B.Sc.

(*The paper was first received 8th September, and in revised form 5th November*, 1959. *It was published as an* INSTITUTION MONOGRAPH *in February*, 1960.)

SUMMARY

A method is given for the design of a class of wide-angle reflectors in which the aberrations are reduced by coating the reflector surface with a dielectric. At microwave frequencies this dielectric may take the form of an array of metal plates or waveguides and the constraint imposed by this form greatly simplifies the analysis. The path of the feed point is chosen so that only selected rays from it are equally phased. It is then found that both of the reflector's profiles and the path of the feed point can be described by a single parameter. The residual aberrations of several cylindrical systems, including the corrected parabola and circle, are analysed to find a reflector for which the scanning arc is the circle with centre at the vertex of the reflector. A refocusing procedure, which is found to be necessary, produces this scanning arc. Experimental results in agreement with the theory are given.

It is shown that the design principle can be used to programme a step-wise procedure for the design of corrected surfaces using non-constrained natural dielectric coatings.

(1) INTRODUCTION

The first mirror to be designed with a correcting coating of dielectric consisted of a negative meniscus lens with two spherical surfaces, the convex one of which was silvered (Fig. 1). Such a

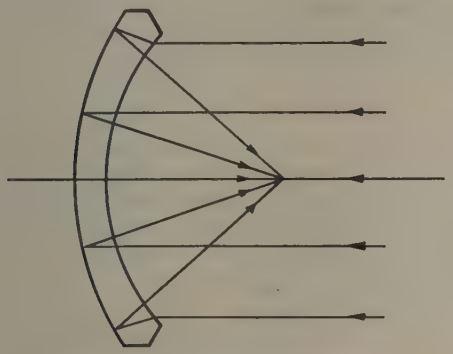

Fig. 1.—The Mangin mirror system.

mirror, described by Mangin in 1876, is free from coma and spherical aberration.[1] It will thus satisfactorily collimate the radiation from a point source when this is displaced from the axis of the mirror along a path termed the 'scanning arc'. Conversely, if the feeding source is kept stationary, an angular tilt of the mirror, such that the position of the feed relative to the axis of the mirror is always on this scanning arc, will cause the collimated beam to scan a line in space. The simplest mechanical operation of this nature is a rotation about a single axis. This requires, therefore, that the scanning arc be a circle with its centre on the axis about which the mirror is tilted. With the Mangin mirror, however, such a scanning arc is not obtainable and so the angle of scan of the beam by this method is limited. An improvement in performance can best be sought by constructing a similar mirror in which one or both of the surfaces are aspherical. Such aspheric surfaces with wide-angle optical properties are used in microwave lenses in which the material of the lens is formed by an array of metal plates or waveguides. This array constrains each ray to be parallel to the lens axis within the material of the lens, with a resulting simplification in the ray-tracing procedure needed for the design. It is to be expected, therefore, that, given such a lens, the introduction of a reflecting surface somewhere in the interior will convert it into a reflector with a correcting layer of this type of material, without disturbing too greatly the wide-angle properties of the lens and still retaining the scanning arc in its circular form. This would then provide a first approximation to the design of a similar reflector using unconstrained natural dielectric to form the correcting surface.

Microwave lenses for wide-angle scanning are designed by a 2-point correction method.[2,3] In this, two given points which are symmetrically displaced from the axis of the system are made to be points of perfect focus. These may be as widely displaced in angle as required to cover a given angle of scan, provided that focusing at the points intermediate between the two perfect foci does not deteriorate beyond an acceptable limit.

The specification of two perfect foci establishes conditions upon the path lengths of the rays from them, thus determining the shape of the first refracting surface and giving one relation between the refractive index (possibly variable) and the thickness at any point of the lens. A second condition between these two variables, e.g. constancy of refractive index or constancy of thickness, can then be applied. For any such condition a third point of minimum or zero aberration is defined on the axis of the system. The scanning arc is then taken to be the circle through this point and the two perfect foci. This assumption is unsupported by any analysis, and in fact some refocusing may be desirable at intermediate points along the scanning arc. A particular lens of this type, termed the 'triple corrected point lens', has zero aberration at the axial position and has a circular scanning arc with centre at the centre of the reflector (Fig. 2). The first refracting profile of this and all such lenses is the ellipse whose foci are the two outer corrected points. Such a lens is converted into a reflector with a phase-correcting layer by interposing a reflecting layer in the refracting medium. In so doing, a degree of freedom that was associated with the independent surface of the lens is lost and so is not available for the choice of the third point on the axis. Thus, although the complete reflecting and refracting surfaces are defined, only the two fixed points exist to determine the scanning arc.

A new method for the design of lenses and phase-corrected reflectors is proposed in which three rays are correctly phased for every point on an arc, instead of correctly phasing all the rays at three points on the arc. The three rays which have been chosen are (Fig. 3):

(*a*) The main ray PO to the centre of the system, where P is any point on the scanning arc.

Correspondence on Monographs is invited for consideration with a view to publication.

The paper is a communication from the Staff of the Applied Electronics Laboratories of The General Electric Company, Limited, Stanmore, England.

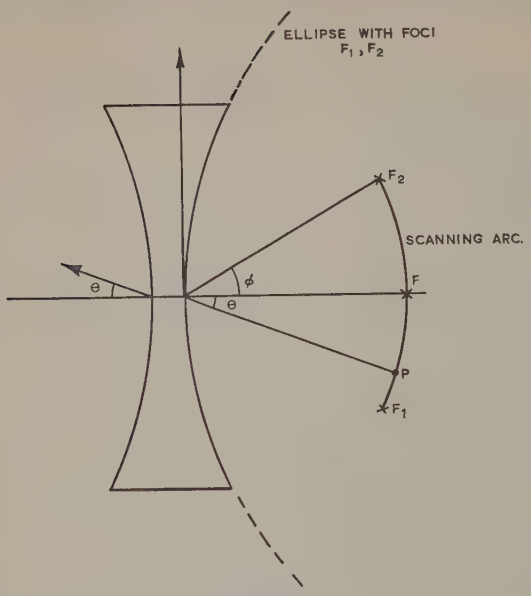

Fig. 2.—Two-point correction principle.

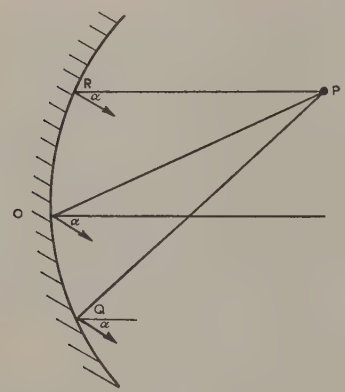

Fig. 3.—Selection of equi-phased rays.

(*b*) The ray PR parallel to the axis of the system.

(*c*) The ray PQ meeting the refracting surface at a point Q diametrically opposite R.

These rays have been chosen to simplify the form of the subsequent analysis. Other systems may be obtained by the choice of other variable rays, or rays that meet the refracting surface, say, at fixed points. Such systems bear a similar relationship to each other as do lenses with different third correcting points.

With the above choice of rays, the profile is defined point by point as the feed moves over any given path that is essentially smooth and symmetrical about the axis. It is apparent that, in positions close to the axis, the feed is at a paraxial focus, whereas at wider angles of scan the feed moves to a position of marginal focus. This effect cannot be taken into account in the first stages of the design but can be overcome for certain systems by eventual refocusing. Several reflectors are investigated to discover which are suitable for this refocusing procedure. Systems which have the required circular scanning arc are then selected.

(2) THE PHASE-CORRECTED REFLECTOR

Only symmetrical cylindrical phase-corrected reflectors with correcting layers of the metal-plate constrained form used in microwave lenses are considered in the analysis. For these, the rays are constrained to travel parallel to the axis of the system on entering the refracting medium. In Fig. 4, (x, y) are co-ordinates axes with origin at the centre of the refracting profile; λ_0 is the free-space wavelength and λ_g is the wavelength within the refracting medium. With the notation of the Figure the condition for a linear phase front, QNM, is

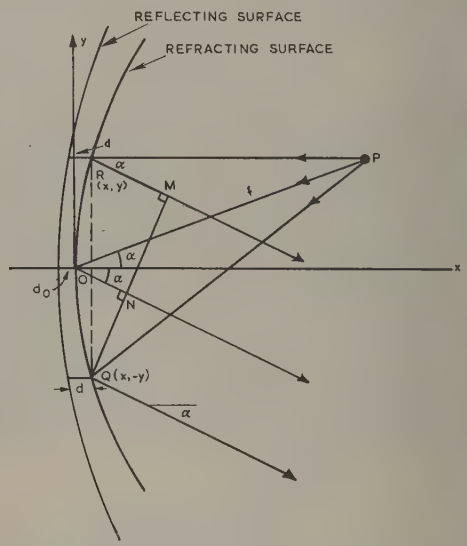

Fig. 4.—Three-ray correction principle.

$$\frac{PO}{\lambda_0}+\frac{NO}{\lambda_0}+\frac{2d_0}{\lambda_g}=\frac{PR}{\lambda_0}+\frac{MR}{\lambda_0}+\frac{2d(y)}{\lambda_g}=\frac{PQ}{\lambda_0}+\frac{2d(y)}{\lambda_g} \quad . \quad (1)$$

where d_0 is the thickness of the refracting layer at the centre and $d(y)$ is the thickness at R, which is the point (x, y).

Since R has co-ordinates (x, y), Q has co-ordinates $(x, -y)$ and $y = f \sin \alpha$, where $OP = f$.

Therefore, from eqn. (1),

$$PQ = PR + MR$$

whence $PQ^2 = PR^2 + MR^2 + 2PR \,.\, MR = PR^2 + QR^2$

Therefore

$$QR^2 = MR^2 + 2PR \,.\, MR$$

i.e. $QM^2 = 2PR \,.\, MR$

$$(2f \sin \alpha \cos \alpha)^2 = 2(f \cos \alpha - x) \,.\, 2f \sin^2 \alpha$$

i.e.
$$\left.\begin{aligned} x &= f \cos \alpha (1 - \cos \alpha) \\ y &= f \sin \alpha \end{aligned}\right\} \quad . \quad . \quad . \quad . \quad (2)$$

If f is now made to vary with α, P describes the arc whose polar co-ordinates are (f, α), and (x, y) describes a curve that determines the refracting profile.

Solving the remaining pair of equations in (1) one obtains

$$2\mu[d(y) - d_0] = x \cos \alpha \quad . \quad . \quad . \quad . \quad (3)$$

where $\mu = \lambda_0/\lambda_g$ = refractive index of the medium.

In addition to the variable thickness $d(y)$ used above, a

medium with variable refractive index $\mu(y)$ could be used and eqn. (3) becomes more generally

$$2[d(y)\mu(y) - d_0\mu_0] = x\cos\alpha \quad . \quad . \quad . \quad . \quad (4)$$

where μ_0 is the refractive index at the centre.

For example, with d constant,

$$2d[\mu(y) - \mu_0] = x\cos\alpha \quad . \quad . \quad . \quad . \quad (5)$$

Eqns. (2) and (3) completely specify the phase-corrected reflector system. Since y is given by $f\sin\alpha$, where f is now a function of α, properties such as thickness or refractive index which vary with y can now be considered as varying with α and thus the complete reflector and scanning arc are expressed as functions of this parameter.

(2.1) Residual Phase Distribution

Since only three of the rays from each point are correctly phased, it is important to obtain expressions from the phase distribution for the other rays. Let the feed be in any angular position θ. We now require the difference in path length between the main ray to the centre and any other ray meeting the system at a point of parameter α. With the surfaces of the system given in terms of α by eqns. (2) and (3), this path-length difference, E_p, is

$$E_p = f(\theta) - f(\alpha)\sin\alpha\sin\theta + f(\alpha)\cos\alpha\cos\theta(1 - \cos\alpha) - f(\alpha)\cos^2\alpha(1 - \cos\alpha) - \{[f(\theta)\cos\theta - f(\alpha)\cos\alpha(1 - \cos\alpha)]^2 + [f(\theta)\sin\theta - f(\alpha)\sin\alpha]^2\}^{1/2} \quad . \quad . \quad . \quad . \quad (6)$$

where the sign of α is the same as or opposite to that of θ, according as the surface point α is on the side adjacent to, or remote from, the displaced feed at θ. From this it can be seen that $E_p = 0$ when $\alpha = \pm\theta$ and when $\alpha = 0$, in accordance with the choice of the three focused rays.

(3) COMPARISON WITH THE 2-POINT CORRECTED SURFACE

Given this parametric notation, it is of interest to compare these results with those of a reflector designed from the 2-point correction principle. The refracting profile for this reflector, using the two foci F_1 and F_2, is the same as the first surface of the lens of Fig. 2, i.e. the ellipse $x^2 - 2f_0x\cos\phi + y^2\cos^2\phi = 0$ where $(f_0, \pm\phi)$ are the polar co-ordinates of F_1 and F_2.

This can be written parametrically as

$$\left.\begin{aligned} x &= f_0\cos\phi(1 - \cos\alpha) \\ y &= f_0\sin\alpha \end{aligned}\right\} \quad . \quad . \quad . \quad . \quad (7)$$

where f_0 and ϕ are essentially constant.

The thickness is given by

$$2\mu[d(y) - d_0] = x\cos\phi \quad . \quad . \quad . \quad . \quad . \quad (8)$$

[cf. eqns. (2) and (3)].

A comparison of the curves given by eqn. (2) (keeping f constant) and eqn. (7) with the circle $x = r(1 - \cos\alpha)$, $y = r\sin\alpha$ (Fig. 5) shows that the central portion of the former closely approximates to the circle. Now the circle is the profile which would fulfil the sine condition for minimum coma for small displacements about the axis.[4] In the 2-point correction case, however, the wider the scan angle required, i.e. the greater the displacement of the foci from the axis, the flatter the ellipse about the axis and the greater the departure from the sine condition.

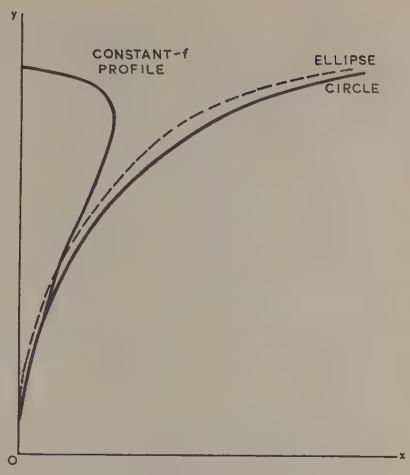

Fig. 5.—Comparison of refracting profiles.

(4) INVESTIGATION OF THE SCANNING PROPERTIES

From the parametric expressions of eqns. (2) and (3) (with constant refractive index) and the phase distribution given by eqn. (6) we can analyse systems which are specified in one of three different ways:

(*a*) Definition of f in terms of α. This specifies the scanning arc and hence the two profiles.

(*b*) Specification of the refracting profile. Comparison of the equation to this curve with the parametric form required provides a definition of f in terms of α and hence the scanning arc and the reflecting surface.

(*c*) Specification of the reflecting profile. When this profile is given, it is apparent that the shape of the refracting profile is dependent upon the refractive index of the surface coating. Thus, since the scanning arc depends on the shape of the refracting profile, it too contains terms involving the refractive index. In this case, if the refractive index is given, the refracting profile can be obtained and the procedure is then the same as in (*b*).

(4.1) Specification of Scanning Arc

Two scanning arcs are of interest, the circle with centre at the reflector centre, and the straight line perpendicular to the axis. The former provides a scan motion which is mechanically simple to perform either for movement of the feed or for tilt of the reflector. The latter focuses plane waves arriving at an angle to the axis into points of a plane, which, in pure optics, is a requirement for astronomical photographic processes.

Circular Scanning Arc.—Until a later investigation revealed other refocused systems with a circular scanning arc (see Section 5), the first experiments were carried out with a reflector designed from eqns. (2) and (3) with f = constant, c.

This gives

$$\left.\begin{aligned} x &= c\cos\alpha(1 - \cos\alpha) \\ y &= c\sin\alpha \\ d &= \frac{x\cos\alpha}{2\mu} \end{aligned}\right\} \quad . \quad . \quad . \quad . \quad (9)$$

the centre thickness, d_0, being zero.

The residual phase distribution is shown in Fig. 6.

Straight Line Scanning Arc.—To obtain a straight scanning

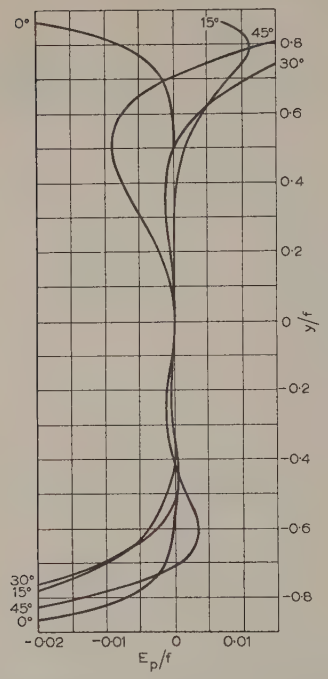

Fig. 6.—Phase error for constant-f scanning arc.

arc at right angles to the axis, put $f = c/\cos\alpha$. The system is thus defined by

$$\left.\begin{aligned} x &= c(1-\cos\alpha) \\ y &= c\tan\alpha \\ d &= \frac{x\cos\alpha}{2\mu} \end{aligned}\right\} \quad . \quad . \quad . \quad . \quad . \quad (10)$$

the centre thickness being zero.

The residual phase distribution is given in Fig. 7. The high degree of asymmetry greatly limits the achievable angular aperture.

(4.2) Specification of the Refracting Profile

Let $y^2 = \mathrm{F}(x)$ be the equation of the refracting profile.

If this profile is also to be given by the parametric form of eqn. (2),

$$f^2\sin^2\alpha = \mathrm{F}[f\cos\alpha(1-\cos\alpha)]$$

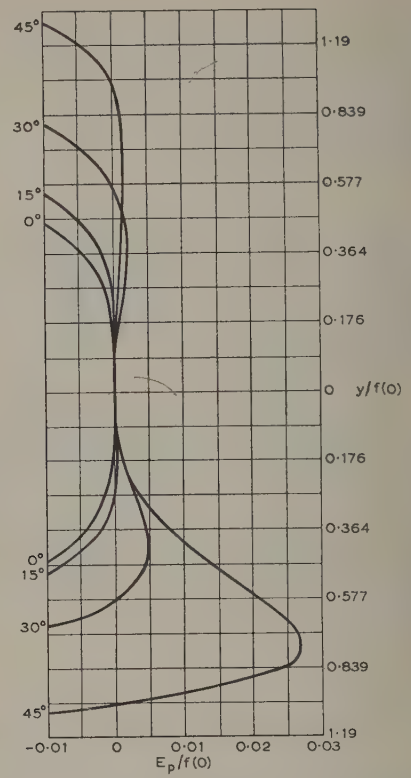

Fig. 7.—Phase error for straight-line scanning arc.

and thus f can be obtained as a function of α, defining the required scanning arc.

For example, if the refracting profile is a circle of radius r defined by the equation $x^2 + y^2 - 2rx = 0$, substituting for x and y from eqn. (2) gives

$$f^2\cos^2\alpha(1-\cos\alpha)^2 + f^2\sin^2\alpha - 2rf\cos\alpha(1-\cos\alpha) = 0$$

i.e.
$$f = \frac{2r\cos\alpha}{\cos^2\alpha(1-\cos\alpha) + (1+\cos\alpha)}$$

This equation defines the scanning arc for a circular cylindrical refracting surface. The residual phase error for the 3-ray method is then given by eqn. (6).

The results of this operation for several refracting profiles are given in Table 1. The phase distributions given in Figs. 8–11

Table 1

Refracting profile	Equation of profile	Polar equation of scanning arc	Axial focal length $f(0)$	Phase distribution and scanning arc reference
Circle (radius r)	$x^2 + y^2 - 2rx = 0$	$f = \dfrac{2r\cos\alpha}{\cos^2\alpha(1-\cos\alpha) + (1+\cos\alpha)}$	r	Fig. 8
Ellipse (semi-axes a, b) ..	$x^2 + \dfrac{a^2}{b^2}y^2 - 2ax = 0$	$f = \dfrac{2a\cos\alpha}{\cos^2\alpha(1-\cos\alpha) + \dfrac{a^2}{b^2}(1+\cos\alpha)}$	$\dfrac{b^2}{a}$	Fig. 9 $a = \frac{1}{3}\ b = \dfrac{1}{\sqrt{3}}$
Parabola (focal length a) ..	$y^2 = 4ax$	$f = \dfrac{4a\cos\alpha}{1+\cos\alpha}$	$2a$	Fig. 10
Two-point correction. Ellipse [foci $(f_0, \pm\phi)$]	$x^2 + y^2\cos^2\phi - 2f_0x\cos\phi = 0$	$f = \dfrac{2f_0\cos\phi\cos\alpha}{\cos^2\alpha(1-\cos\alpha) + \cos^2\phi(1+\cos\alpha)}$	$\dfrac{f_0}{\cos\phi}$	Fig. 11 $\phi = 30°$

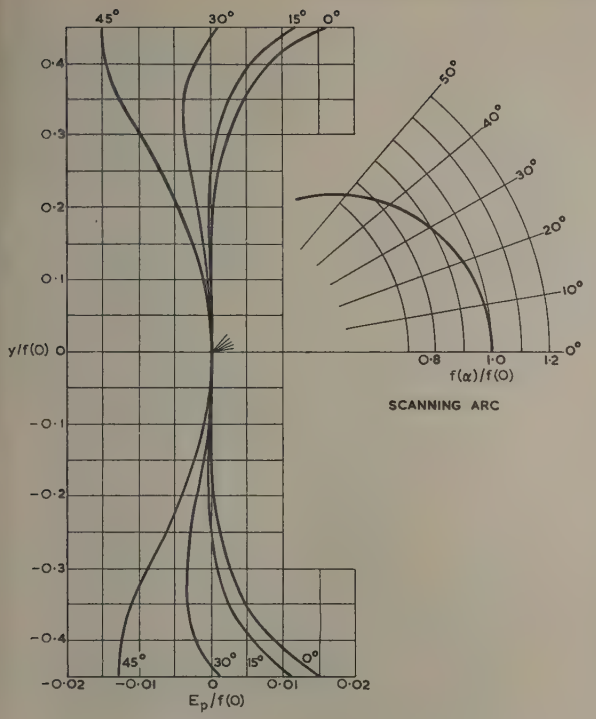

Fig. 8.—Circular refracting profile.

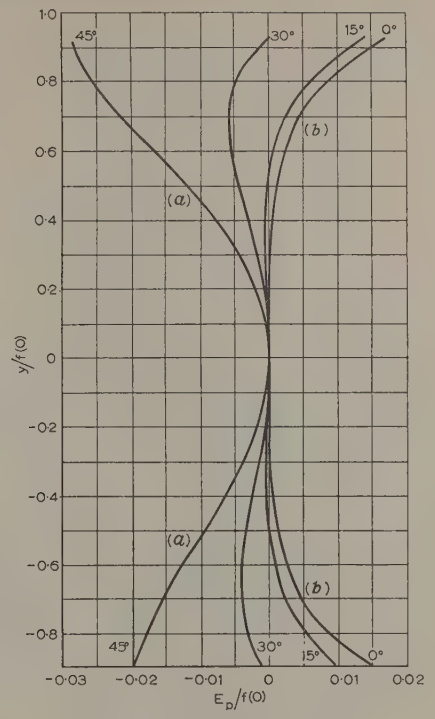

Fig. 10.—Parabolic refracting profile.

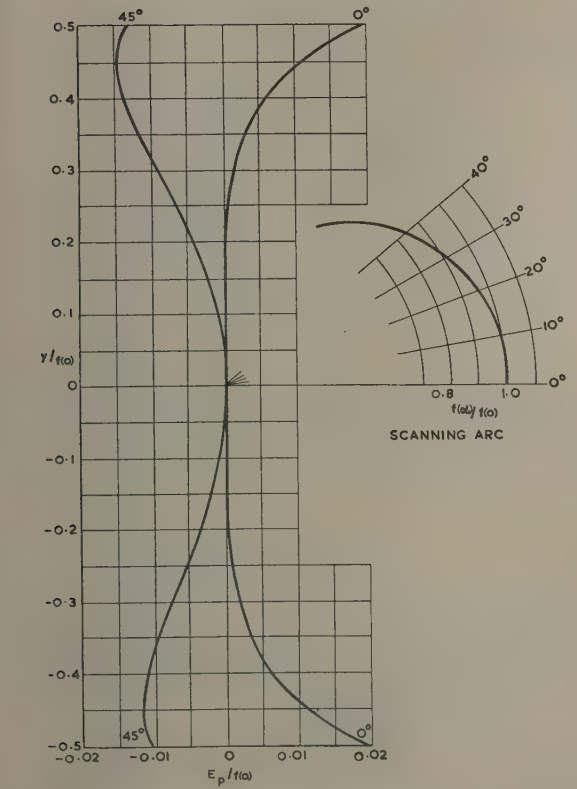

Fig. 9.—Elliptic refracting profile.

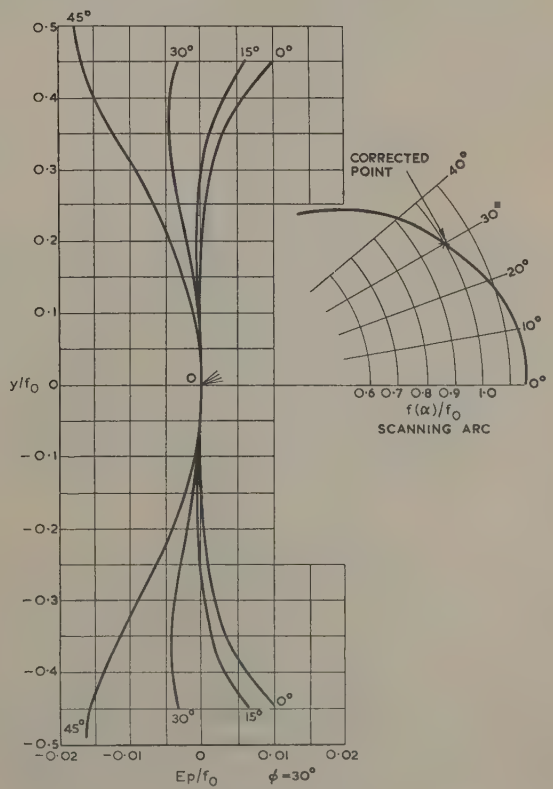

Fig. 11.—Two-point corrected refracting profile.

Table 2

Reflecting profile	Equation of profile	Polar equation of scanning arc	Axial focal length $f(0)$	Phase distribution and scanning arc reference
Parabola	$y_1^2 = 4ax_1$	$f = \dfrac{4a\cos\alpha\left(1-\dfrac{\cos\alpha}{2\mu}\right)}{1+\cos\alpha}$	$a\left(2-\dfrac{1}{\mu}\right)$	$\mu = 0{\cdot}75$ Fig. 12 $\mu = 1{\cdot}6$ Fig. 13
Circle	$x_1^2 + y_1^2 - 2ax_1 = 0$	$f = \dfrac{2a\cos\alpha\left(1-\dfrac{\cos\alpha}{2\mu}\right)}{1+\cos\alpha+\cos^2\alpha\left(1-\dfrac{\cos\alpha}{2\mu}\right)^2(1-\cos\alpha)}$	$\dfrac{a}{2}\left(2-\dfrac{1}{\mu}\right)$	$\mu = 1{\cdot}6$ Fig. 14

have a high degree of symmetry about the main ray for offset angles up to 45°. The similarity between these curves and the profiles of Schmidt correcting plates for spherical mirrors is marked[5] since the main residual phase error is spherical aberration. Such systems may be refocused with advantage, and this will be dealt with in Section 5.

The scanning arc for the 2-point corrected profile (Fig. 11) passes through the two correcting points as expected. It is not, however, the anticipated circle centred on the reflector centre. Since the thickness of this reflector was derived from eqn. (3) and not from eqn. (8), this fact cannot be taken as conclusive.

It may be noted that attempts to design a reflector with a tapered or plane refracting surface proved to be impossible. If the apex is at the origin no solution for f in terms of α can be obtained. If the apex is behind the origin the distance f becomes infinite.

(4.3) Specification of the Reflecting Profile

We assume the systems to have zero thickness at the centre and constant refractive index. From eqns. (2) and (3) the reflecting surface has equations

$$y_1 = y = f\sin\alpha$$

$$x_1 = x - d = x\left(1-\frac{\cos\alpha}{2\mu}\right) = f\cos\alpha(1-\cos\alpha)\left(1-\frac{\cos\alpha}{2\mu}\right) \quad . \quad . \quad . \quad . \quad (11)$$

When this is expressed as $y_1^2 = \mathrm{F}(x_1)$, the same analysis can be made as in the previous Section. This method has been applied to the design of the corrected parabola and corrected circle, with the results as shown in Table 2 and Figs. 12–14. In both cases the axial focal length $f(0)$ contains a factor $2 - 1/\mu$ which gives a lower limit of 0·5 to the possible range of refractive indices that can be used for the correcting layers. Furthermore, the axial focal length of a corrected parabola of focal length a is double that of a corrected circle of radius a, as is the case for uncorrected reflectors. In both cases a valid solution is obtained for $\mu = 1$. This means that the constraint alone enables phase correction to be obtained.

(5) REFOCUSING

Those systems exhibiting large symmetrical or nearly symmetrical aberrations about the main ray can be refocused to a certain extent in off-axis positions by a radial movement of the source.

The effect of refocusing is to introduce a quadratic phase error which can be made equal and opposite to the quadratic component of the symmetrical phase distribution. The phase-distribution diagrams for the conic-section refracting profiles (Figs. 8–11) show that the central portions of the symmetrical phase-error curves can be adequately approximated by a quadratic term.

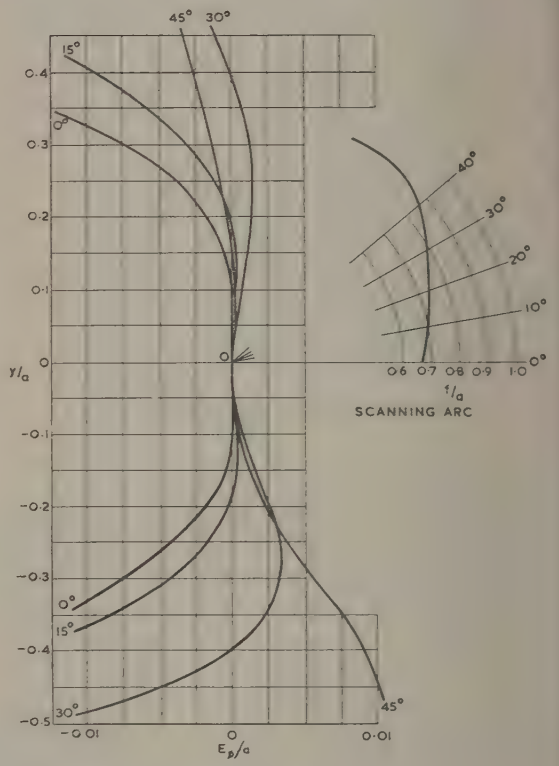

Fig. 12.—Corrected parabola, $\mu = 0{\cdot}75$.

If the feed is at a position F (Fig. 15) on the scanning arc of one of these reflectors, a displacement inward along FO by an amount $\varepsilon f(\theta)$ where $\mathrm{FO} = f(\theta)$ results in a change in the path length relative to the central ray of

$$\Delta E_p = r' - r'' - \varepsilon f(\theta)$$

$$\simeq -\frac{\varepsilon}{2}\left[\frac{y^2}{f(\theta)} - \frac{\theta y^3}{f(\theta)^2}\right] \quad . \quad . \quad . \quad . \quad (12)$$

which is correct to the first order in ε and θ and to the third order[2] in $y/f(\theta)$.

If ΔE_p is then taken as the value of the quadratic approximation to the phase error at any intermediate value of α, the refocusing increment ε is given by

$$\Delta E_p = \frac{-\varepsilon}{2f(\theta)}[f(\alpha)\sin\alpha]^2(1-\theta\sin\alpha) \quad . \quad . \quad (13)$$

This can be calculated for several values of θ, with α and E_p

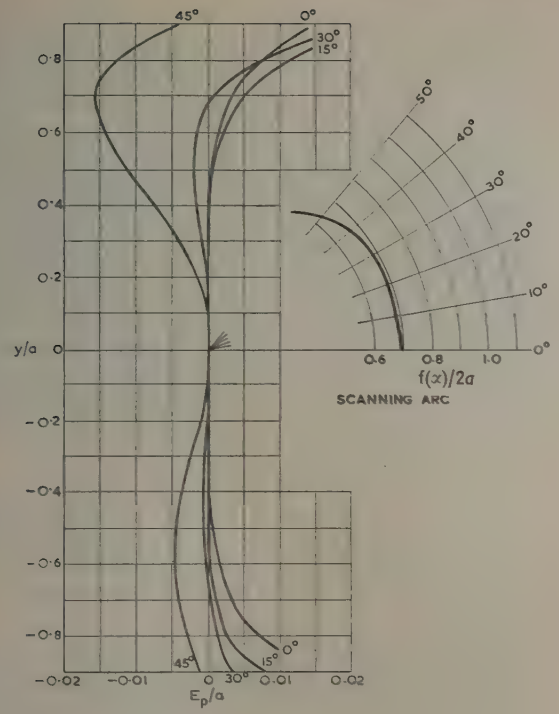

Fig. 13.—Corrected parabola, $\mu = 1{\cdot}6$.

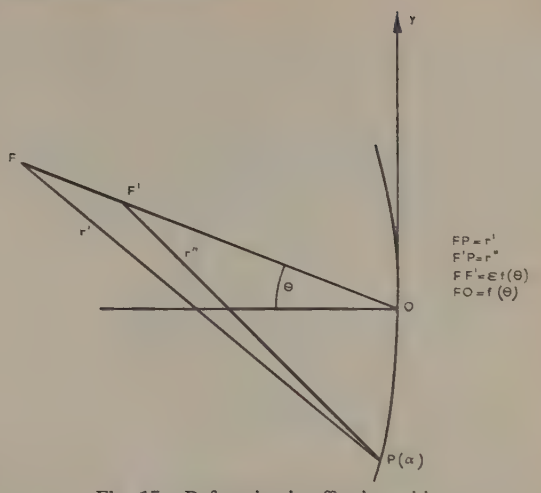

Fig. 15.—Refocusing in off-axis positions.

given by the phase-error curve corresponding to the particular value of θ. With appropriate sign, this adjusts the scanning arc to a best-focal-position arc.

The cubic term of eqn. (12) introduces some asymmetry, particularly at the larger values of θ. The refocusing increments, calculated for the reflector with a circular refracting profile, are shown in Fig. 16. After removing the quadratic component a small residual phase error remains and a slight asymmetry, consisting mainly of the cubic component, is observed. The refocusing results in a best-focus arc which is circular with radius 0·94 of the original axial focal length.

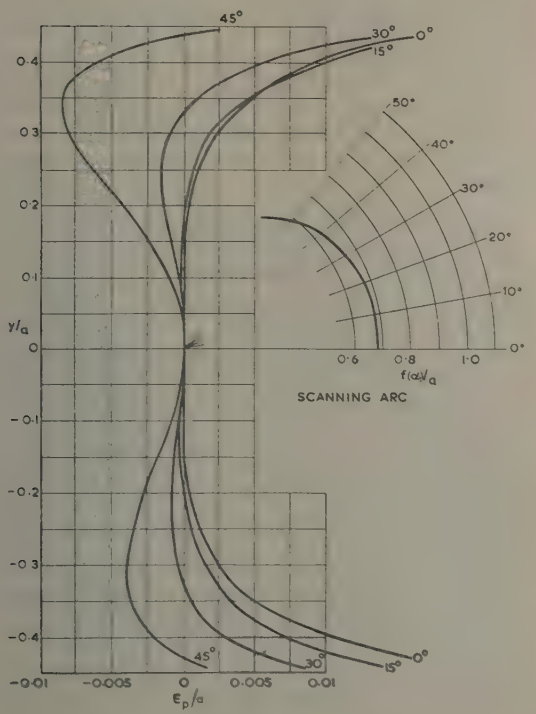

Fig. 14.—Corrected circle, $\mu = 1{\cdot}6$.

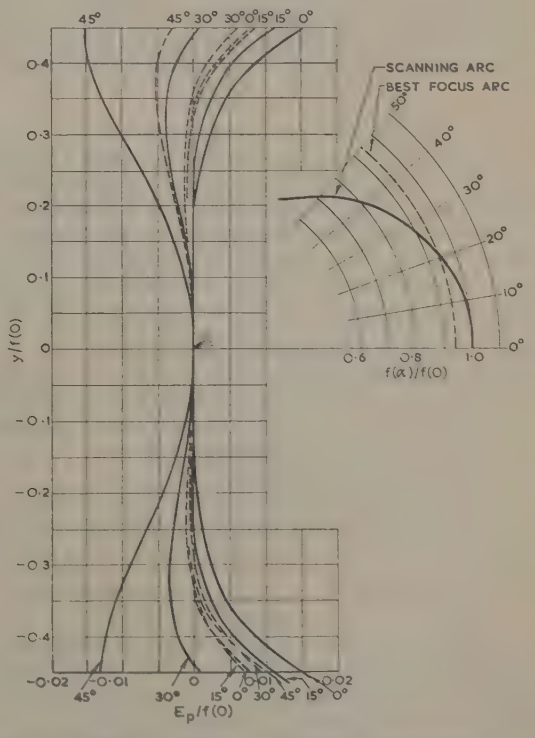

Fig. 16.—Effect of refocusing on reflector with circular refracting profile.

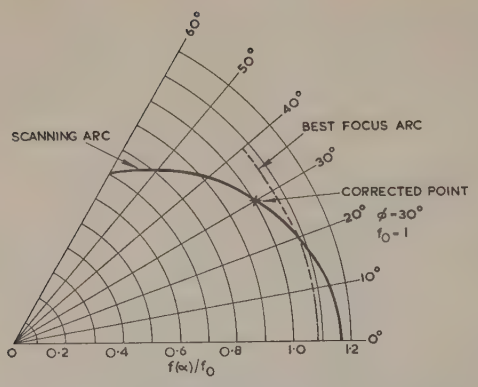

Fig. 17.—Refocused scanning arc of 2-point corrected refracting profile.

When this method is applied to the 2-point corrected profile and scanning arc, as in Fig. 17, the scanning arc once more becomes circular but with radius $1{\cdot}09f_0$, and hence it no longer passes through the two correction points.

From the similarity of the parametric description of the scanning arcs and the phase-error distribution curves between these two systems and the other systems given in Table 1, it can be expected that refocusing these also produces circular scanning arcs. This has been shown to be the case, but a complete analysis has not been made. These systems have in common the fact that the refracting profile is given by a curve that is a conic section. Hence these refracting-reflecting combinations constitute a class whose best-focus scanning arc is the circle with centre at the centre of the system. Although this refocusing procedure has destroyed the *a priori* relationship between the refracting profile and scanning arc, the discovery of this class of related curves provides a basis for the iterative design of similar coated reflectors with a natural dielectric correcting layer.

(6) THE ANGULAR APERTURE

From the diagrams of the residual phase error it is possible to determine either the maximum angular displacement that a system with a given numerical aperture can permit or, for a maximum required angular displacement, the numerical aperture that will allow it. This can be done by defining the maximum permissible residual phase error and offsetting the feed along the scanning arc to the angle at which this maximum occurs; or, conversely, by offsetting the feed to the maximum angle required and limiting the aperture to the point at which the maximum permissible error is obtained.

For example, with the system illustrated in Fig. 10 (parabolic refracting profile, not refocused), let the axial focal length, $2a$, be 20λ and the permissible quadratic error $\lambda/10$.

Then $E_{p\,max}/a = (\lambda/10)/(10\lambda) = 0{\cdot}01$.

The line $|E_p/a| = 0{\cdot}01$ gives a maximum aperture of $0{\cdot}9a$ for a scan of 0–45° [curve (*a*)] and of $1{\cdot}66a$ for scan of 0–30° [curve (*b*)].

(7) PHASE CORRECTION WITH A NATURAL DIELECTRIC MEDIUM

It may be noted that the shape of the reflectors so far considered, for which the correcting layer is an array of metal waveguides, is, in general, the same as that of the original negative meniscus lens of Mangin, i.e. concavo-convex. This fact is contrary to the usual experience when comparing microwave with optical lenses. It means that, for these reflectors at least, the shape with a constrained refractive medium is in itself a satisfactory first approximation to a natural dielectric unconstrained correcting layer. This is particularly so in fully stepped systems, in which the thickness of the correcting layer need never be greater than half the wavelength in the medium used. The approximation involved in assuming that the rays are still parallel to the axis when they are within the correcting medium causes the quadratic error of the system to increase slightly. This can be cancelled, therefore, by further focusing.

A better approximation for the natural dielectric medium can be made by calculating the refracting profile from the original formula [eqn. (2)] and then calculating the reflecting profile on the assumption that the rays in the correcting layer travel along the normals to the refracting profile. In this case, the path length along each normal has to be the value of d calculated from eqn. (3). This approximation is particularly appropriate to the circular refracting profile, where, in the axial position, the rays do, in fact, travel along these normals. The approximation here also results in an increase in the residual quadratic error and may similarly be corrected.

However, in all natural dielectric systems a further parameter is available in the thickness of the corrected reflector at its centre. It is found that variation of this parameter too gives rise mainly to a quadratic component of phase error which could possibly be used for the cancellation of the above two effects.

Finally, the 3-ray principle itself can be used directly for the natural dielectric case. Apart from the necessity of refocusing which has been demonstrated, the method by which the movement of the feed over a given arc describes both this arc and the refracting profile is a step-wise procedure suitable for programming a computer. To do this, one establishes the phase equality of the three rays concerned by considering the localities at which the outer two rays meet the reflector to be sections of thin reflecting prisms, similar in shape and symmetrical with respect to the axis. The 3-ray principle, however, does not give a defined axial focal position. The scanning arc limits towards a point on the axis at which, of course, the three rays coincide. This point cannot therefore be taken as a starting-point for the step-wise procedure. This means that a guess has to be made at the thickness at the starting-point, the guess being acceptable if, on reaching the axial position, a zero thickness has not been passed.

(8) EXPERIMENTAL RESULTS

The analysis presented in the previous Sections has dealt with 2-dimensional or cylindrically symmetrical reflectors. The profiles concerned could, however, also be considered as cross-sections of a rotationally symmetrical reflector. Where such a reflector is required it is constructed by the rotation of the profiles about its axis. This, of course, introduces the further aberration of astigmatism which limits the angle of scan of rotationally symmetrical reflectors to a much lower value than cylindrically symmetrical ones. With the type of construction possible at microwave frequencies, namely a 2-dimensional array of waveguides, systems with rectangular symmetry can be considered. In these the surfaces would be formed by the translation across a profile of a similar profile at right angles to it. The astigmatism of such systems, however, is still to be investigated.

Experimental work so far has been concerned with the construction of systems to test the elementary theory and to assess the limitations imposed on the scanning properties by the astigmatism of the rotationally symmetrical reflector and the dielectric approximation of the previous Section.

To test the basic theory a linear reflector (cylindrical system) was constructed for which the correcting layer was a parallel

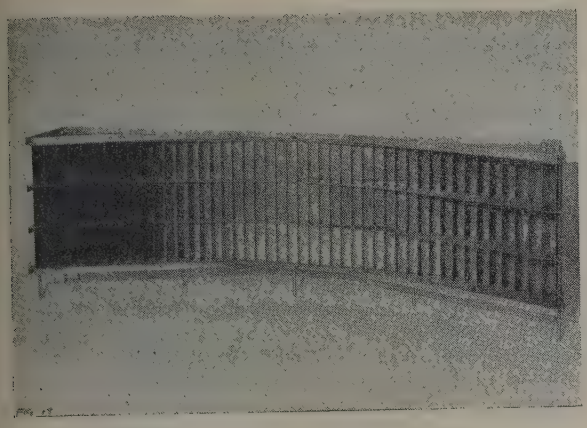

Fig. 18.—Cylindrical constant-f reflector.

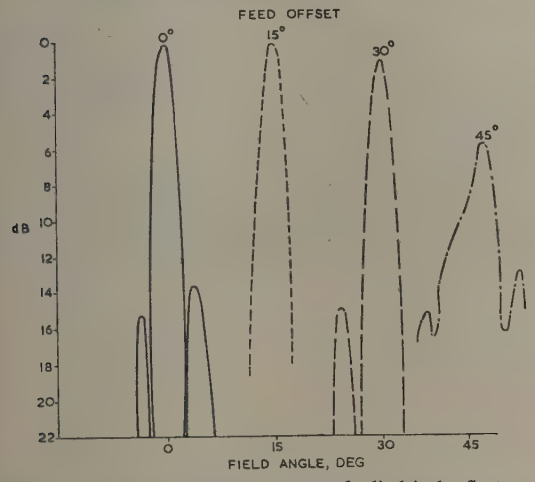

Fig. 19.—Polar diagrams of constant-f cylindrical reflector at different offset angles.

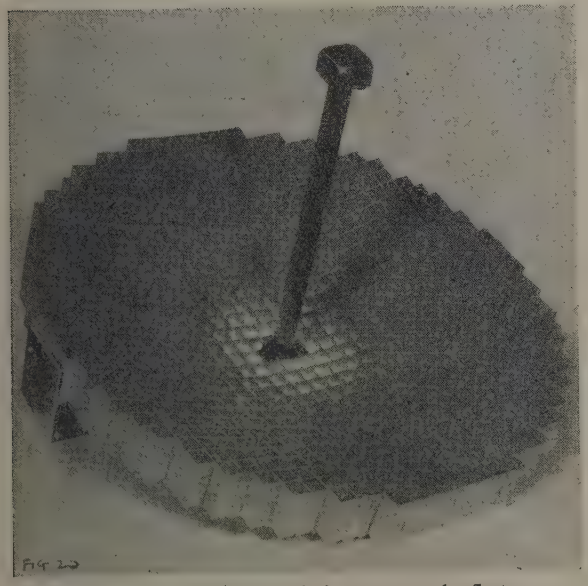

Fig. 20.—Constant-f spherical phase-corrected reflector.

array of metal plates so spaced that the effective refractive index, λ_0/λ_g, at the frequency of operation was 0·6. The profiles were determined from eqns. (2) and (3) with f constant: this gives the uncorrected scanning arc as the circle $f = c$ (Section 4.1). The reflector, shown in Fig. 18, is 36 in long and has a focal length of 30 in operating at a frequency of 9·375 Gc/s. The f/D ratio is 0·83. From the residual phase-error curves (Fig. 6) it is to be expected that coma effects will become noticeable

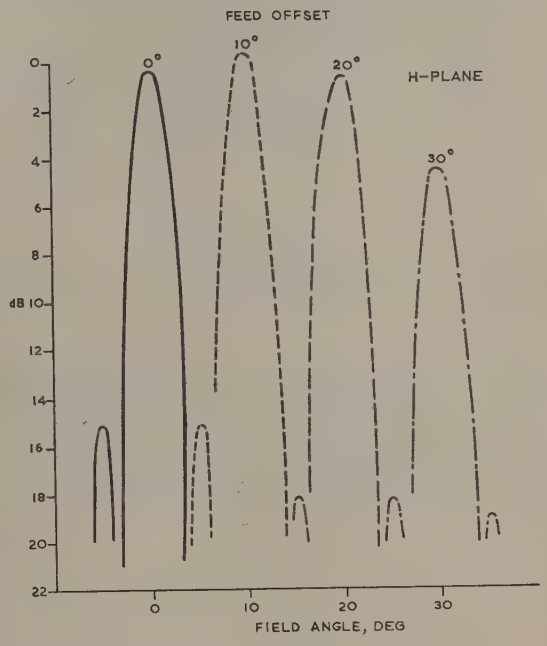

(*a*)

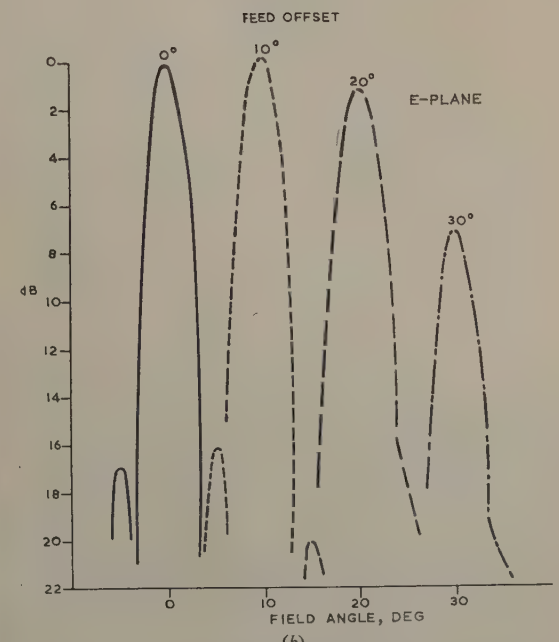

(*b*)

Fig. 21.—Polar diagrams of constant-f reflector at different offset angles.

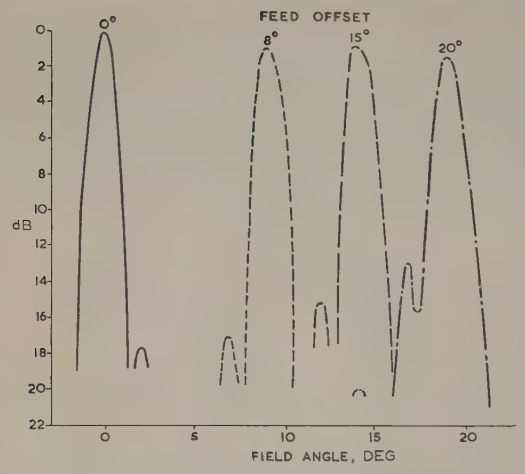

Fig. 22.—Polar diagrams of constant-f dielectric reflector at different offset angles.

beyond 30° of angular displacement, because of the asymmetry in the phase-error curve. This is found to be the case, as shown by the scan patterns of Fig. 19. A beam displacement of 30° (approximately 15 beam widths) is achieved without any observable deterioration in the beam shape, and is followed quite suddenly by a decrease in gain and a large increase in the coma lobe. In this case no attempt has been made to improve the side-lobe level by tapering the illumination, an open-ended waveguide being used to provide the primary source.

The rotationally symmetrical system (Fig. 20) is constructed from square-section metal tubes giving a refractive index of 0·6 at 9·375 Gc/s. The surfaces thus have the same basic profiles as the cylindrical system. This reflector was 2 ft in diameter with an f/D ratio of 1. The scan patterns shown in Fig. 21 demonstrate that the gain and beam shape deteriorate steadily on displacing the feed source along the scanning arc. A decrease of 1 dB in gain at an angle of 20° is observed, this forming an arbitrary limit to the useful scan. Very similar results are achieved with a 9 in-diameter dielectric-coated reflector at a frequency of 36 Gc/s (Fig. 22). The approximation used is to make the refracting profile as for a constrained system and the normals to it of the correct phase length. A useful scan of 20° is obtained with this reflector.

The above three systems are all based on the constant-f scanning arc and profile. The conclusions that can be drawn are, first, that a rotationally symmetrical reflector has about two-thirds the useful scan of a cylindrical reflector. Secondly, the dielectric approximation for the rotationally symmetrical system is satisfactory in that the same useful scan is achieved as for the reflector with a constrained refracting surface.

Examination of the residual phase-error curves of Fig. 16 shows that an expected scan angle of 45° should be achieved with a cylindrical reflector having a circular refracting profile. A system for which $r = 20\lambda$ is possible with the maximum permissible phase error equal to $\lambda/10$.

This gives $E_{p\,max}/r = 0{\cdot}005$, which is not exceeded by the phase-error curves up to 45° of scan within the aperture $2y = 0{\cdot}8$. This reflector has for its corrected scanning arc the circle $f = 0{\cdot}94r$, giving for the f/D ratio the value $0{\cdot}94/0{\cdot}8 \simeq 1{\cdot}2$.

A spherical natural dielectric system with the same aperture thus has an expected useful scan approaching 30°. A reflector of this type has been constructed. The meniscus lens is machined from a sheet of Perspex after a pre-moulding operation and the reflecting surface is copper-gauze. The refracting surface is purely spherical with a radius of 24 in ($f = 22{\cdot}5$ in), and the diameter of the reflector is 20 in. The reflecting surface is obtained by the 'normal' approximation and the edge of the lens was then $\frac{7}{8}$ in thick. The scan patterns achieved, shown in Fig. 23, give a useful scan of 30°, at which point the gain has decreased by 2 dB without any great deterioration in the main beam shape and before the coma lobe level has become pronounced. Here again no attempt was made at illumination tapering or side-lobe reduction.

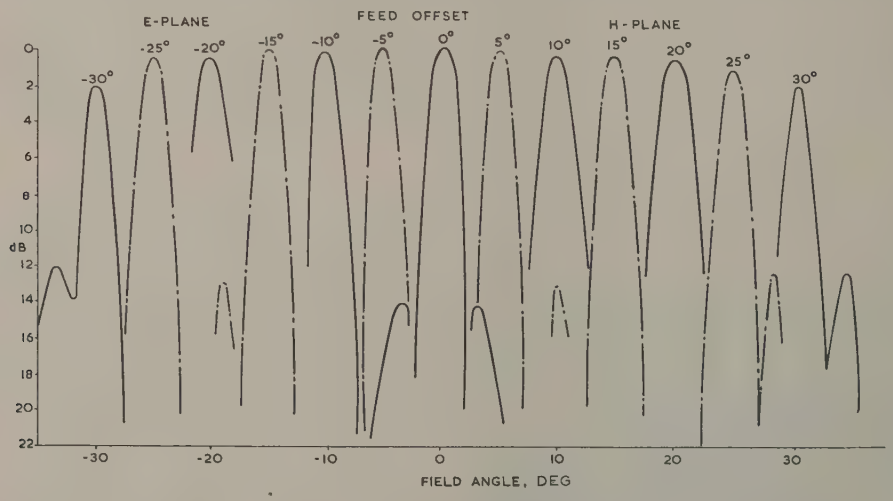

Fig. 23.—Polar diagram of refocused spherical dielectric reflector at different offset angles.

The achievement of these results with a circular scanning arc makes possible the design of radar systems in which a feed or cluster of feeds is kept stationary and the beam is scanned in space by the rotation of the reflector about transverse axes through its vertex. Under these circumstances the beam can be deflected twice as far as the permissible angular offset of the system and it moves at double the rate of the moving mirror. The mechanical advantage of such a system, depending as it does upon the shape of the scanning arc, has been the main reason for this investigation. The results achieved show that it

is possible in this manner to scan a beam linearly with a cylindrical reflector through angles approaching $\pm 90°$, and volumetrically with a spherical reflector through a cone of half-angle 60°.

(9) CONCLUSIONS

The design procedure, whereby three rays from every point of a specified scanning arc are kept equi-phased, gives rise to a class of phase-corrected reflectors with the following properties:

(*a*) The refracting profile is a conic section and can, for simplicity, be circular.

(*b*) The residual phase errors at angles of scan up to 45° are largely symmetrical about the main ray.

(*c*) Refocusing the system at angles off-axis makes the scanning arc circular.

With such systems used as beam-scanning devices, i.e. with stationary feed and mechanical scan of the reflector, linear scans approaching $\pm 90°$ can be achieved with cylindrical reflectors, and a cone of semi-angle 60° can be scanned with spherical reflectors.

(10) REFERENCES

(1) MARTIN, L. C.: 'Technical Optics' (Pitman, 1954), Vol. II, p. 253.

(2) RUZE, J.: 'Wide-Angle Metal-Plate Optics', *Proceedings of the Institute of Radio Engineers*, 1950, **38**, p. 53.

(3) BROWN, J.: 'Microwave Lenses' (Methuen, 1953), p. 69.

(4) CONRADY, A. E.: 'Applied Optics and Optical Design' (Dover Publications, 1957), p. 376.

(5) LINFOOT, E. H.: 'Recent Advances in Optics' (Oxford University Press, 1955), p. 182.

621–526

The Institution of Electrical Engineers
Monograph No. 361 M
Feb. 1960
©

THE EFFECT OF AN ADDITIONAL NON-LINEARITY ON THE PERFORMANCE OF TORQUE-LIMITED CONTROL SYSTEMS SUBJECTED TO RANDOM INPUTS

By J. L. DOUCE, M.Sc., Ph.D., Graduate, and R. E. KING, M.Sc., Student.

(*The paper was first received 26th June, and in revised form 15th October*, 1959. *It was published as an* INSTITUTION MONOGRAPH *in February*, 1960.)

SUMMARY

The paper discusses a technique for improving the response of a saturating servo mechanism subjected to random signals. It is shown that a non-linear error detector gives a considerable reduction in error magnitude for a large range of input signals. It is possible to design the additional non-linearity to optimize the performance of the system for all input magnitudes. This form of non-linearity has previously been shown to effect improvement in the response of such systems to step-function and sinusoidal inputs.

Experimental work verifies the predicted results for a particular system, and shows that considerable latitude is permitted for the characteristic of the additional non-linearity.

LIST OF PRINCIPAL SYMBOLS

x_i = Input signal.
x_o = Output signal.
$x_e = x_i - x_o$ = Error signal.
x_c = Control signal.
$\mathscr{L}(p)$ = Laplace transform.
$f_1(x_e)/x_e$ = Gain of error-processing non-linearity.
$f_2(x_c)/x_c$ = Gain of torque limiter.
K = Booton's equivalent gain.
σ^2 = Mean-square power.
$\Phi_i(j\omega)$ = Input r.m.s. voltage spectrum.
$\Phi_i(0)$ = Input zero-frequency r.m.s. voltage per unit bandwidth.
$\omega_0 = 1/T$ = Servo linear undamped resonant frequency.
ζ = Servo damping factor.
$Y(p, \sigma_i)$ = Closed-loop transfer function.
$E(p, \sigma_i)$ = Error-ratio transfer function.
$C(p, \sigma_i)$ = Control-ratio transfer function.
μ = Ratio of servo resonant frequency ω_0 to input spectrum half-power frequency.

(1) INTRODUCTION

Previous work has shown how the response of a feedback control system may be determined in the presence of saturation of some element. When the maximum motor torque is limited, the non-linear system exhibits a more oscillatory step-function response than the linear system and a closed-loop frequency response with a more pronounced resonance.

When such a non-linear system is subjected to a random signal, the bandwidth of the system is reduced as the input power is increased, and the response is degraded owing to distortion in the saturating element.

By the correct design procedure, a less powerful motor may satisfy the requirements of the system provided that saturation of the motor is compensated for by special techniques. In particular, it has been shown[1, 2] that a non-linear error detector can give optimum transient response for a system possessing torque limitation for all sizes of input step by applying full accelerating motor torque until the system comes to rest with zero error. Further work shows that this system possesses in addition a better frequency response than the initial non-linear system.[3]

It is possible to extend previous analysis to show that a similar system can be constructed which has a greatly reduced error when the input is a random signal, approximating to the operating conditions normally encountered in practice.

Linear theory based on the mean-square-error criterion[4–7] enables the best possible linear system to be designed, given certain specified elements; this system will be the optimum for any input provided that the form of the frequency spectrum of the input signal remains constant. When motor saturation is considered, this technique enables the system to be optimized for one particular input spectrum and one input power: the parameters must be adjusted for any change in the input, to maintain the best operation.[8]

Combining the optimization procedure of Wiener[9] with the quasi-linearizing technique due to Booton,[10] the paper shows that it is possible to design non-linearities to optimize a particular inherently non-linear system for a class of random signals, giving considerable reduction in error magnitude compared with the initial non-linear systems.

The presence of a non-linear element in a feedback system gives rise to two effects. First, the gain of the loop, neglecting any distortion, will vary with the amplitude of the signal applied to the non-linearity. Where the system is designed on the basis of small-signal operation, the behaviour for large signals will, in general, be slower and more oscillatory. The effect of the gain variation can be evaluated readily, using known techniques. An extension to the theory enables the best linear gain for the error detector to be found for each equivalent gain of the inherent non-linearity. The best value of error-detector gain now depends on the magnitude of the error signal, and it is shown possible to produce the desired variation by introducing a non-linear unit following the error detector. Secondly, distortion of a signal occurs when the signal passes through a non-linear element.[11] When the non-linear characteristic is included in a feedback system, the system will endeavour to follow the distorted signal, increasing the error between input and output.

For sinusoidal signals, the distortion consists of harmonics of the input frequency. Since the response of electro-mechanical systems inevitably falls with increasing frequency, the effect of the harmonics can normally be neglected.

A random signal may be considered as the sum of a very large number of small sinusoidal signals of different frequencies. Thus, when such a signal is applied to a non-linearity, the output consists of a 'fundamental' component, harmonics of each input frequency and intermodulation terms. As before, the harmonic terms will be of relatively high frequency so that their effect is not important. The intermodulation terms, however, extend down to very low frequencies where the loop gain is high. Hence the overall system will respond readily to these

Correspondence on Monographs is invited for consideration with a view to publication.
Dr. Douce and Mr. King are in the Electrical Engineering Department, Queen's University, Belfast.

signals, producing a spurious output and increasing the error magnitude. Furthermore, this error will be appreciable at low frequencies where good performance is required.

After a non-linear system has been designed and analysed by neglecting distortion, the effect of distortion must then be considered. In particular, when an additional non-linearity is suggested to improve the performance of a control system, the change in total distortion power must be evaluated.

(2) BASIC SYSTEM

The basic system to be considered is a simple remote-position-control servo mechanism possessing velocity-feedback stabilization, as shown in Fig. 1. The linear elements comprising the

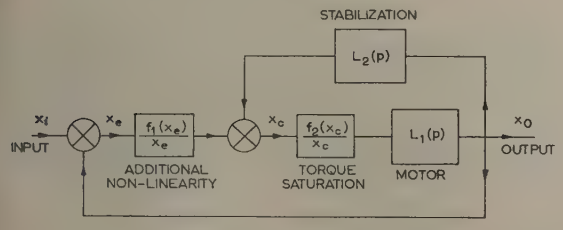

Fig. 1.—Basic system.

servo motor and the stabilization network are described by the transfer functions $L_1(p)$ and $L_2(p)$, respectively. The control signal $x_c(t)$ produces an acceleration $f_2(x_c)$ whose maximum magnitude is limited.

The intentionally introduced non-linearity $f_1(x_e)$ immediately follows the error detector.

The error signal is

$$x_e(t) = x_i(t) - x_o(t)$$

the control signal

$$\mathscr{L}[x_c(t)] = \mathscr{L}\{f_1[x_e(t)]\} - L_2(p)\mathscr{L}[x_o(t)]$$

and the output signal

$$\begin{aligned}\mathscr{L}[x_o(t)] &= L_1(p)\mathscr{L}\{f_2[x_c(t)]\} \\ &= L_1(p)\mathscr{L}\{f_1[x_i(t) - x_o(t)] - \mathscr{L}^{-1}\{L_2(p)\mathscr{L}[x_o(t)]\}\}\end{aligned}$$

These expressions cannot be evaluated explicitly.

An approximate analysis is possible if distortion due to the non-linear elements is neglected, each non-linearity being replaced by a linear amplifier whose gain depends on the power of the signal applied to it. Booton[10] has shown that the best gain, K, to replace a non-linearity $f(x)$ is given by

$$K = \frac{1}{\sigma^2}\int_{-\infty}^{+\infty} xf(x)p_1(x)dx \quad . \quad . \quad . \quad . \quad . \quad (1)$$

This value of equivalent gain minimizes the mean-square difference between the output of the non-linearity and that of the linear amplifier, where σ^2 is the power of the signal applied to the non-linearity and $p_1(x)$ is the amplitude probability density distribution of this signal. The random signal applied to the system input is assumed to have a Gaussian amplitude distribution. Any amplitude non-linearity changes the probability distribution in a characteristic manner, but it has been shown[12] that any narrow-band filter, e.g. a servo motor, following the non-linearity tends to restore the Gaussian distribution. Thus the equivalent gain K, as defined by eqn. (1), can be evaluated, for a given non-linear function, in terms of the input power to the element. When two non-linear elements are present, this approximation is clearly less accurate.

However, it has been observed that the equivalent gain of a saturating-type non-linearity is relatively insensitive to the form of the probability distribution of its input signal, as demonstrated in Reference 17 for three widely different probability distributions. To a first approximation, therefore, it may be assumed that the inputs to both non-linearities have a Gaussian distribution.

For the system with only one non-linear element, $f_2(x_c)$ in Fig. 1 [i.e. $f_1(x_e)/x_e = K_1$], the equivalent-gain technique enables the steady-state operating conditions to be evaluated graphically. When the non-linearity is replaced by a linear amplifier of gain K_2, two relationships can be obtained between K_2 and the signal power applied to this element.

Linear theory gives the control signal, x_c, in terms of the input signal and the equivalent gain of the second non-linearity to be

$$x_c = \frac{K_1}{1 + K_1K_2L_1(p) + K_2L_1(p)L_2(p)}x_i$$

where x_i is a random signal having a voltage spectrum $\Phi_i(p)$.

The total control power is

$$\begin{aligned}\overline{x_c^2} &= \sigma_c^2 \\ &= \frac{1}{2\pi j}\int_{-j\infty}^{j\infty}\left|\frac{K_1}{1 + K_1K_2L_1(p) + K_2L_1(p)L_2(p)}\Phi_i(p)\right|^2 dp \quad . \quad (2)\end{aligned}$$

For a given input-signal power, σ_c^2 is a function of K_1 and K_2.

The equivalent gain of the torque-limiting device varies in a known way with σ_c^2, from eqn. (1). Hence two expressions are obtained relating K_2 and σ_c^2, both of which must hold simultaneously. Thus if the two relationships are plotted on the same graph, the point of intersection gives the operating conditions.

Knowing the operating value of K_2, the error power σ_e^2 can be found directly, since

$$\overline{x_e^2} = \sigma_e^2 = \frac{1}{2\pi j}\int_{-j\infty}^{+j\infty}\left|\frac{1 + K_2L_1(p)L_2(p)}{1 + K_1K_2L_1(p) + K_2L_1(p)L_2(p)}\Phi_i(p)\right|^2 dp$$

. . . . (3)

The error power, as given in eqn. (3), provides a convenient measure of the performance of the system. It is a relatively simple function to measure experimentally, using a wattmeter type of instrument, and is readily evaluated theoretically.

For any given input power and K_1, the error power can be found by using a graphical technique to determine K_2 and by substitution in eqn. (3). Integrals of the form of eqn. (3) are fully tabulated in References 4 and 7. This procedure can be repeated for the same input signal and different values of K_1. Thus a relationship between error power and K_1 can be obtained, and in general, there will be a value of K_1 giving minimum error power, equivalent to optimizing the system for the particular applied signal.

When this technique is applied repeatedly for a range of input powers, a relationship is obtained between error power and K_1 corresponding to minimum error power for any input power. If the gain of the error detector is related to the error power in the derived manner, the predicted mean-square error is the minimum possible with the given system. Hence the desired system is defined by a known relationship between error power and error detector gain. A non-linearity can now be found giving this relationship, producing a system in which the gain of the error detector is optimum for any input power, allowing for inherent motor saturation. It will also be shown that the dis-

tortion produced in the new system, with two non-linearities, is less than that in the initial system possessing torque limitation, for the particular example considered.

(3) PARTICULAR SYSTEM

The system considered is one of second order. In the linear regime $K_1 = K_2 = 1$, the damped resonant angular frequency is $\omega_0 = 1/T$ and the damping factor is ζ. Thus the transfer functions are

$$L_1(p) = \frac{1}{T^2p^2}$$

and

$$L_2(p) = 2\zeta Tp$$

The overall closed-loop transfer function using the Booton equivalent gains K_1 and K_2 is

$$Y(p, \sigma_i) = \frac{x_o}{x_i} = \frac{K_1K_2}{T^2p^2 + 2\zeta K_2Tp + K_1K_2}$$

the error ratio is

$$E(p, \sigma_i) = \frac{x_e}{x_i} = \frac{T^2p^2 + 2\zeta K_2Tp}{T^2p^2 + 2\zeta K_2Tp + K_1K_2}$$

and the control ratio

$$C(p, \sigma_i) = \frac{x_c}{x_i} = \frac{K_1T^2p^2}{T^2p^2 + 2\zeta K_2Tp + K_1K_2}$$

For non-linear operation it is seen that the undamped natural frequency reduces to

$$\omega_0 = \frac{1}{T}\sqrt{(K_1K_2)}$$

and the effective damping factor is modified to

$$\zeta_{eff} = \zeta\sqrt{\frac{K_2}{K_1}}$$

For a conventional torque-limited system with no error processing, i.e. $K_1 = 1$, the effect of torque limitation is to reduce K_2 so that both the resonant frequency and damping factor are reduced with increasing signal amplitude. However, in the case of the processed system, this reduction in damping factor is counteracted to a great extent by a corresponding reduction in the gain, K_1, of the error-processing element.

The input-signal power spectrum to the control system is taken for mathematical simplicity to be of the form

$$G_i(\omega) = \frac{\Phi_i^2(0)}{1 + \mu^2\omega^2T^2}$$

which has 6 dB/octave high-frequency fall-off and a half-power angular frequency of $1/\mu T$. This spectrum can alternatively be considered as being the result of white noise having a power per unit bandwidth of $\Phi_i^2(0)$ being passed through a filter of transfer function $1/(1 + \mu Tp)$.

The total input power to the system is therefore

$$\overline{x_i^2} = \sigma_i^2 = \frac{\Phi_i^2(0)}{2\pi j}\int_{-j\infty}^{j\infty}\left|\frac{1}{1 + \mu Tp}\right|^2 dp$$

$$= \frac{\Phi_i^2(0)}{2\mu T} \quad . \quad . \quad . \quad . \quad . \quad . \quad . \quad . \quad (4)$$

and the control and error powers as functions of this input power and the system parameters are given respectively by

$$\overline{x_c^2} = \sigma_c^2 = \frac{1}{2\pi j}\int_{-j\infty}^{j\infty}|C(p, \sigma_i)\Phi_i(p)|^2 dp$$

$$= \frac{\sigma_i^2}{2\zeta}\,\frac{K_1^2(2\zeta + \mu K_1)}{1 + 2\mu\zeta K_2 + \mu^2K_1K_2} \quad . \quad . \quad . \quad . \quad (5)$$

and from Reference 7,

$$\overline{x_e^2} = \sigma_e^2 = \frac{1}{2\pi j}\int_{-j\infty}^{j\infty}|E(p, \sigma_i)\Phi_i(p)|^2 dp$$

$$= \frac{\sigma_i^2}{2\zeta}\,\frac{2\zeta + \mu K_1 + 4\zeta^2\mu K_2}{1 + 2\mu\zeta K_2 + \mu^2K_1K_2} \quad . \quad . \quad . \quad . \quad (6)$$

The torque-limiting non-linearity $f_2(x_c)$ is taken to have unity slope within the limits $\pm h$ and zero slope outside this range; the equivalent gain of such a function is given by

$$K_2 = \text{erf}\left[\frac{h}{\sqrt{(2\sigma_c)}}\right] \text{ from eqn. (1) and Reference 10}$$

$$= \text{erf}\left(\frac{1}{\sigma_{cN}}\right) \quad . \quad . \quad . \quad . \quad . \quad . \quad . \quad . \quad . \quad . \quad (7)$$

where $\sigma_{cN} = \sigma_c(\sqrt{2})/h$ is the normalized r.m.s. voltage.

The particular system considered has damping one-half critical for small-signal operation, i.e. $\zeta = 0{\cdot}5$. An input signal with cut-off frequency $\frac{1}{8}\omega_0$ (i.e. $\mu = 8$) is considered, corresponding to acceptable operation in the linear regime. Other cases ($\mu = 2$ and 4) have also been evaluated and are considered later.

To obtain the variation of error power as a function of K_1 for all input powers to the system using eqn. (6), it is first necessary to plot eqn. (5) relating control-signal power, σ_c^2, to K_2, as shown in Fig. 2. The second relationship between K_2, the gain of the

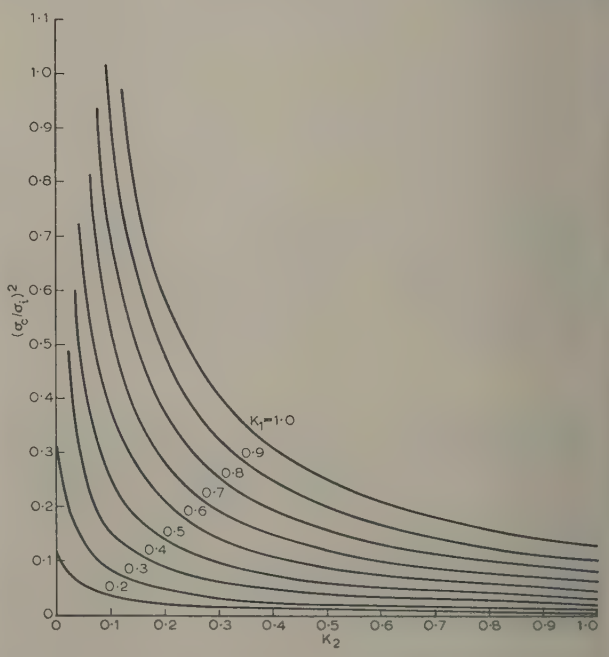

Fig. 2.—Derivation of closed-loop response for different values of K_1.
$\mu = 8 \quad \zeta = 0{\cdot}5$

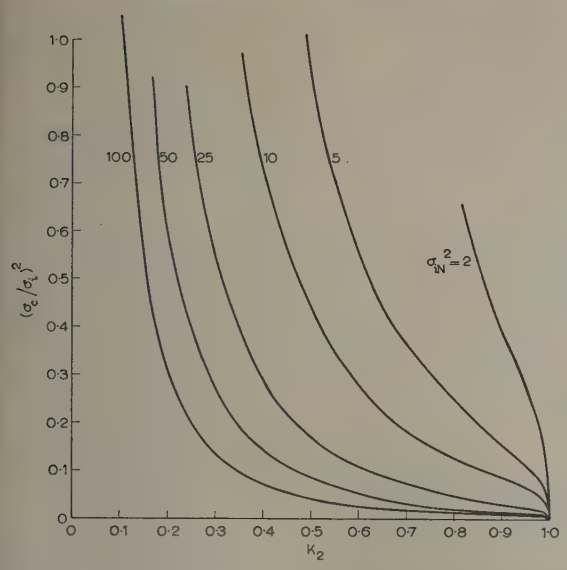

Fig. 3.—Derivation of closed-loop response for different values of σ_{iN}^2.

non-linearity, and σ_e^2, as derived from eqn. (7), is shown in Fig. 3. Plotting $(\sigma_e/\sigma_i)^2$ against K_2 gives loci which are dependent on the input power to the system, σ_i^2.

Superimposing the loci of Figs. 2 and 3 enables the operating value of K_2, for any input power σ_i^2 and any value of K_1, to be determined.

By substitution in eqn. (6), σ_e^2 can be obtained as a function of K_1 for any input power. This relationship is plotted in Fig. 4 for a range of input-signal powers. In general a minimum will be observed, corresponding to a minimum mean-square-error power; the value of K_1 giving this is then the desired optimum

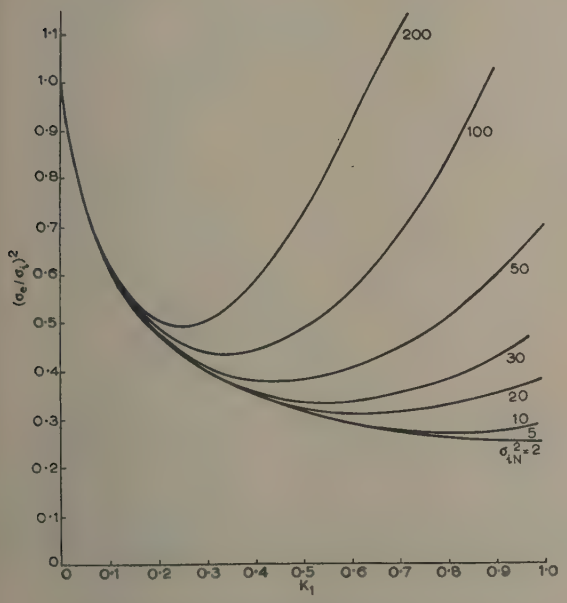

Fig. 4.—Evaluation of optimum gain.
$\mu = 8 \quad \zeta = 0{\cdot}5$

gain and can now be related to the error power from Fig. 4. This relationship is shown in Fig. 5 for three input bandwidths, $\mu = 2$, 4 and 8.

Thus, if a non-linearity is formed so as to give such a variation of equivalent gain, the control system will have minimum mean-square error for all input signals of a given spectrum. It is then said to be optimized.

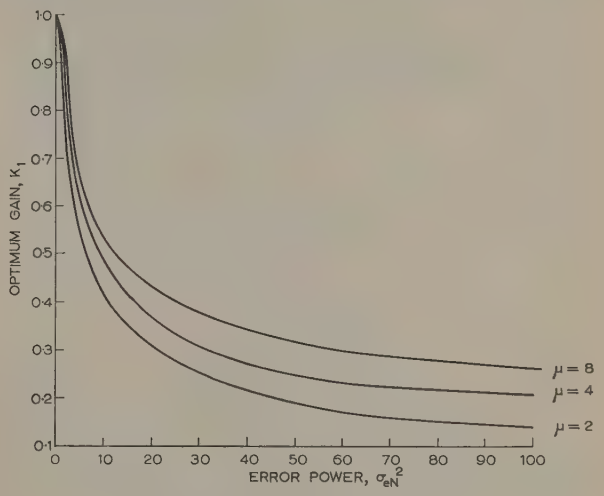

Fig. 5.—Variation of optimum gain with error power for different input spectra.

By plotting log K_1 against log σ_{eN}^2 a straight-line relationship is obtained experimentally. This shows that the desired characteristic is of the form

$$K_1 = B\sigma_{eN}^{2\beta} \quad . \quad . \quad . \quad . \quad . \quad . \quad . \quad (8)$$

where $\beta \leqslant 0$ and B and β are constants for a given input-signal bandwidth.

It is shown in Section 8.1 that a non-linearity of the form $y = a\dfrac{x}{|x|}(|x|)^{\nu}$ has an equivalent gain which varies with input signal in the desired manner. The equivalent gain of such a non-linearity is related to its input power, σ_x^2, by

$$K_1 = a\theta(\nu)\sigma_x^{\nu-1} \quad . \quad . \quad . \quad . \quad . \quad . \quad . \quad (9)$$

Comparing eqns. (8) and (9), the required input-output characteristic of the error-processing device is of the form

$$y = f(x_e)$$

$$= a\frac{x_e}{|x_e|}(|x_e|)^{1+2\beta} \quad . \quad . \quad . \quad . \quad . \quad (10)$$

The desired non-linear characteristics corresponding to the three different input spectra are shown in Fig. 6.

As the bandwidth of the input signal is reduced, i.e. as $\mu \to \infty$, the non-linear characteristic approaches the form $k\dfrac{x}{\sqrt{|x|}}$. This corresponds to the non-linear characteristic required for optimum step response of the system. This relationship may be expected if the signals are considered solely in terms of their respective frequency spectra. The power spectrum of a single step is of the form

$$G(\omega) = \frac{G(0)}{\mu^2 T^2}\frac{1}{\omega^2}$$

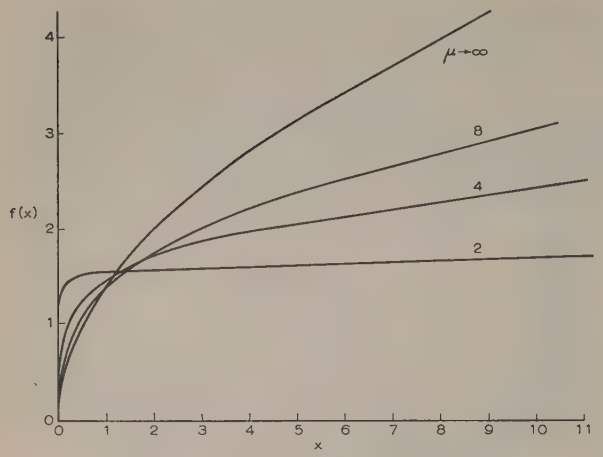

Fig. 6.—Optimum non-linear characteristics.

and that of the random signal considered is of the form

$$G(\omega) = \frac{G(0)}{1 + \mu^2\omega^2T^2}$$

As the cut-off frequency of this signal becomes very low, $\mu \to \infty$, and for frequencies above zero, these two expressions become identical.

(4) COMPARISON OF RESULTS

Experimental results were obtained using an electronic simulator: the natural undamped frequency ω_0 was in the range 200–800 c/s, the input noise spectrum having a half-power frequency of 100 c/s. Mean-square powers were determined experimentally using a thermocouple instrument.

The error powers were measured as functions of input power with and without the error-processing non-linearity. In all cases the power of the processed system was less than that of the initial system, and for the particular case shown in Fig. 7 for $\mu = 8$, the reduction ratio was approximately 3 : 1 for large input powers. This is in good agreement with the theoretical results.

In the practical system the maximum slope of the processing non-linearity was limited to unity. This gives satisfactory performance for small-signal operation, and does not significantly affect the large-signal behaviour of the system.

(5) SPECTRAL RESPONSE OF THE SYSTEM

When the non-linear elements are replaced by their respective equivalent gains the output and error-voltage spectra may be evaluated from

$$|\Phi_o(j\omega, \sigma_i)| = |Y(j\omega, \sigma_i)|\ |\Phi_i(j\omega)|$$

and

$$|\Phi_e(j\omega, \sigma_i)| = |E(j\omega, \sigma_i)|\ |\Phi_i(j\omega)|$$

respectively.

For the particular case considered

$$|\Phi_e(j\omega, \sigma_i)| = \sqrt{\frac{\omega^4T^4 + 4\zeta^2K_2^2\omega^2T^2}{[(K_1K_2 + \omega^2T^2)^2 + \zeta^2K_2^2\omega^2T^2](1 + \mu^2\omega^2T^2)}} \quad . \quad . \quad . \quad . \quad (11)$$

which is plotted in Fig. 8.

For a sinusoidal signal, the effect of the non-linearity is to produce harmonics of the input frequency, and these are heavily attenuated by the inherent low-pass frequency dependence of the linear portion of the control system. When, however, the input

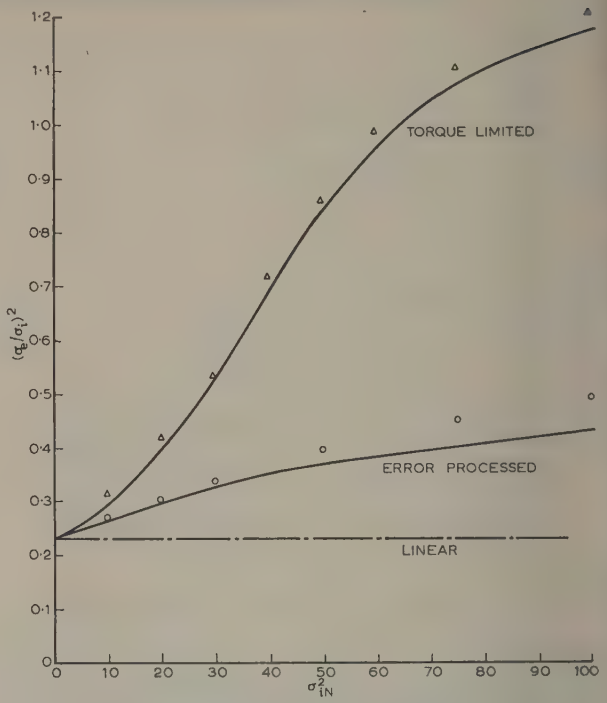

Fig. 7.—Variation of error power with input power.
Δ, ○ Experimental. —— Theoretical.

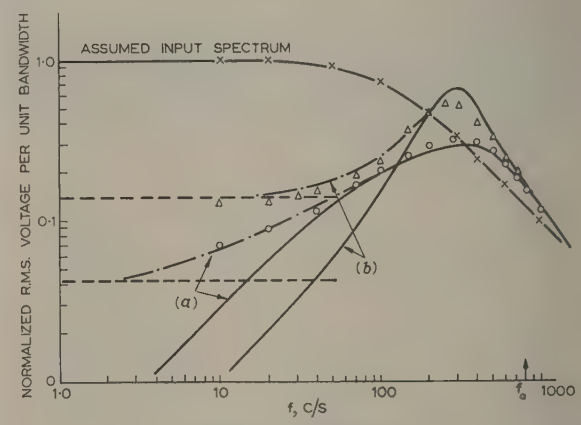

Fig. 8.—Error spectra.
$\sigma^2_{iN} = 50$ $\mu = 8$ $\zeta = 0{\cdot}5$ $f_o = 100$ c/s
×, Δ, ○ Experimental.
—·—·— Including distortion.
———— Neglecting distortion.
(*a*) Theoretical response of error-processed system.
(*b*) Theoretical response of system with limited torque.

to the non-linearity is a random signal, the distortion contains harmonic frequencies of the input spectrum and intermodulation terms, which contain important low-frequency signals, to which the closed-loop system will respond. Hence, when evaluating the error spectrum of a non-linear system subject to a random disturbance this distortion must be taken into account. The total distortion power* and its spectral distribution can be

* The output of a non-linearity may be regarded as

$$y(t) = Kx(t) + D(t)$$

where K is Booton's equivalent gain, $Kx(t)$ is the coherent output and $D(t)$ is the distortion. The mean-square value of $D(t)$ is termed the distortion power.

evaluated for any single-valued non-linearity provided that the form of the input spectrum is known. For complex spectra this can be extremely tedious and thus first-order approximations have been made in the analysis.

For the type of input spectra encountered the distortion has a spectrum which is uniform over the frequency range of the input to the system and the power per unit bandwidth can be evaluated.[11]

When the error-processing device is added to the inherently non-linear system the control-signal power is very much reduced. Hence maximum torque is demanded for a much smaller fraction of the time and negligible distortion terms are now generated by the inherent torque-limiting non-linearity. It is therefore legitimate to consider only the distortion introduced by the error-processing device when this is added to the system.

An approximate evaluation of the distortion spectra of both systems is presented in Section 8.3. Fig. 8 shows theoretical error spectra illustrating the pronounced reduction in error voltage in the system near the resonant frequency and the important effects of distortion at low frequencies.

In the particular example evaluated, the distortion power per unit bandwidth for the error-processed system is shown to be approximately one-third that of the initial torque-limited system for the same input power.

Agreement between theoretical and experimental results provides justification for the approximations made in the theoretical analysis.

(6) CONCLUSION

It has been shown how an intentionally introduced non-linearity can effect considerable improvement to the behaviour of a non-linear control system subjected to a random signal. Two criteria have been used to measure the performance of the servo mechanism, namely the mean-square error and the spectral density of the error signal. The error power is used to design the additional non-linearity, giving reductions of up to 3 : 1 when compared with the initial system for the case considered. Frequency-spectrum analysis shows that the change in error power combines as diminished resonance with a reduction in low-frequency errors due to non-linear distortion.

Whilst the best additional non-linearity depends on the spectrum of the input signal, considerable latitude is permissible for the non-linear characteristic without departing significantly from the optimum behaviour. Fig. 9 shows how a system adjusted for best response when the input signal has a bandwidth of one-quarter the servo bandwidth, ω_0, behaves when subjected to inputs having bandwidths $\frac{1}{8}\omega_0$ and $\frac{1}{2}\omega_0$.

It is appreciated that the type of input considered has not necessarily a typical spectrum. It has been chosen mainly as a first approximation and for its mathematical simplicity.

Further work will investigate the possibility of combining a non-linear error detector with a linear filter, to optimize a non-linear system for input signals having a wide range of powers and spectra.

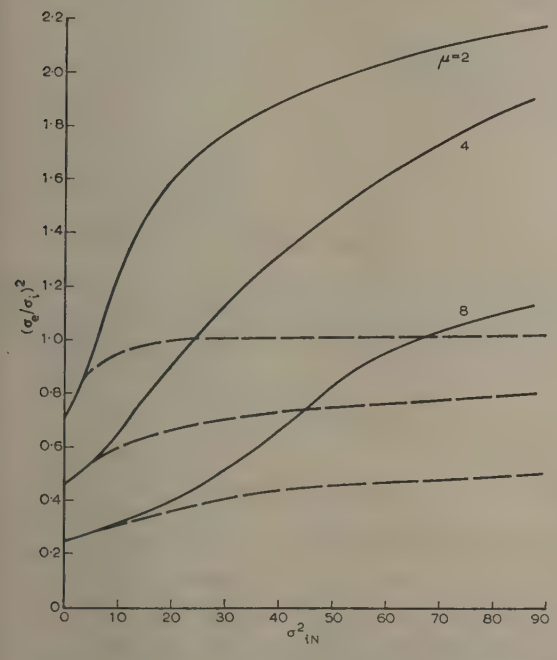

Fig. 9.—Reduction of error power by error processing.
——— Torque limited.
– – – – – Error processed.

(7) REFERENCES

(1) McDonald, D.: 'Non-Linear Techniques for Improving Servo Performance', *Proceedings of the National Electronics Conference*, Chicago, 1950, **6**, p. 400.

(2) West, J. C., Douce, J. L., and Naylor, R.: 'The Effects of the Addition of Some Non-Linear Elements on the Transient Performance of a Simple R.P.C. System Possessing Torque Limitation', *Proceedings I.E.E.*, Paper No. 1549 M, August, 1954 (**101**, Part II, p. 156).

(3) West, J. C., and Nikiforuk, P. N.: 'The Frequency Response of a Servomechanism Designed for Optimum Transient Response', *Transactions of the American I.E.E.*, 1956, **75**, Part II, p. 234.

(4) James, H. M., Nichols, N. B., and Phillips, R. S.: 'Theory of Servomechanisms', M.I.T. Radiation Laboratory Series (McGraw-Hill, 1947).

(5) Truxal, J. G.: 'Control System Synthesis' (McGraw-Hill, 1955).

(6) Davenport, W. B., and Root, W. L.: 'An Introduction to the Theory of Random Signals and Noise', M.I.T. Lincoln Laboratory Publications, 1958.

(7) Newton, G. C., Gould, L. A., and Kaiser, J. F.: 'Analytical Design of Linear Feedback Controls' (John Wiley, 1957).

(8) Shen, D. W. C.: 'Non-Linear Amplitude Sensitive Systems with Stochastic Inputs', Institute of Radio Engineers Wescon Convention IV, p. 196.

(9) Wiener, N.: 'Extrapolation, Interpolation and Smoothing of Stationary Time Series' (Technology Press, Cambridge, 1949).

(10) Booton, R. C.: 'Non-Linear Control Systems with Statistical Inputs', Massachusetts Institute of Technology, Dynamic Analysis and Control Laboratory, Report No. 61.

(11) West, J. C.: 'The Effect of Non-Linearity on the Statistical Behaviour of Feedback Systems', Data Processing and Automatic Computing Machines Proceedings, Weapons Research Establishment, June, 1957.

(12) Barrett, J. F., and Coales, J. F.: 'An Introduction to the Analysis of Non-Linear Control Systems with Random Inputs', *Proceedings I.E.E.*, Monograph No. 154 M, November, 1955 (**103** C, p. 190).

(13) Thomson, W. E.: 'The Response of a Non-Linear System to Random Noise', *ibid.*, Monograph No. 106 R, September, 1954 (**102** C, p. 46).

(14) RICE, S. O.: 'Mathematical Analysis of Random Noise', *Bell System Technical Journal*, 1944, **23**, p. 282; 1945, **24**, p. 46.
(15) WEST, J. C., DOUCE, J. L., and LEARY, B. G.: 'Frequency Spectrum Distortion of Random Signals in Non-Linear Feedback Systems', *Proceedings I.E.E.* (to be published).
(16) JAHNKE, E., and EMDE, F.: 'Tables of Functions' (Dover Publications, New York, 1945).
(17) DOUCE, J. L.: 'A Note on the Evaluation of the Response of a Non-Linear Element to Sinusoidal and Random Signals', *Proceedings I.E.E.*, Monograph No. 257 M, October, 1957 (**105** C, p. 88).

(8) APPENDICES

(8.1) Equivalent Gain of νth Law Error-Processing Device

For a non-linear function described by

$$\begin{aligned} y = f(x) &= ax^{\nu} && x \geqslant 0 \\ &= -a(-x)^{\nu} && x \leqslant 0 \\ &= a\frac{x}{|x|}(|x|)^{\nu} \text{ for all } x \end{aligned}$$

The equivalent gain by Booton's method is, from eqn. (1),

$$K = \frac{2}{\sigma^2}\int_0^{\infty} xf(x)p_1(x)dx$$

Substituting for $f(x)$ and $p_1(x)$, which is assumed Gaussian and of the form

$$p_1(x) = \frac{1}{\sigma\sqrt{(2\pi)}}\varepsilon^{-x^2/2\sigma^2}$$

$$\begin{aligned} K &= \frac{1}{\sigma^3}\sqrt{\frac{2}{\pi}}\int_0^{\infty} ax^{\nu+1}\varepsilon^{-x^2/2\sigma^2}dx \\ &= \theta(\nu)a\sigma^{\nu-1} \quad \ldots\ldots\ldots \quad (12) \end{aligned}$$

where $$\theta(\nu) = \frac{2^{(\nu+1)/2}}{\sqrt{\pi}}\Gamma\left(\frac{2+\nu}{2}\right)$$

where $$\int_0^{\infty} x^q\varepsilon^{-x^2/2\sigma^2}dx = 2^{(q-1)/2}\sigma^{q+1}\Gamma\left(\frac{1+q}{2}\right)$$

is derived from $\Gamma(s) = \int_0^{\infty} z^{s-1}\varepsilon^{-z}dz$ which is tabulated in Reference 16.

(8.2) Evaluation of Distortion Components

The output auto-correlation function of a non-linear function is given by

$$R_y(\tau) = \sum_{n=0}^{\infty} \alpha_n^2\rho_x^n(\tau)$$

In general

$$\alpha_n = \frac{1}{\sqrt{x}}\sqrt{\frac{2}{\pi}}\int_0^{\infty} f(x)\frac{H_n(\xi)}{\sqrt{(n!)}}\varepsilon^{-x^2/2\sigma_x^2}dx$$

where $\xi = x/\sigma_x$, and $H_n(\xi)$ is the nth Hermite polynomial

$$H_n(\xi) = (-1)^n\varepsilon^{-\xi^2/2}\frac{d^n\varepsilon^{-\xi^2/2}}{d\xi^n}$$

For a symmetrical function $\alpha_2, \alpha_4, \alpha_6 \ldots = 0$.

The first term given by $n = 1$ represents the undistorted or correlated component of the output and is related to Booton's equivalent gain by $\alpha_1 = K\sigma_x$. The higher terms in the series for $R_y(\tau)$ tend rapidly to zero and terms above α_3 can be neglected.

For the νth-power error-processing non-linearity the correlated term is given by

$$\begin{aligned} \alpha_1(\nu) &= \frac{1}{\sigma_e}\sqrt{\frac{2}{\pi}}\int_0^{\infty} ax_e^{\nu}H_1(\xi)\varepsilon^{-x^2/2\sigma_e^2}dx \\ &= \frac{a}{\sqrt{\pi}}2^{(\nu+1)/2}\sigma_e^{\nu}\Gamma\left(\frac{\nu+2}{2}\right) \end{aligned}$$

and the main distortion term by

$$\begin{aligned} \alpha_3(\nu) &= \sigma_e\sqrt{\frac{2}{\pi}}\int_0^{\infty} ax_e^{\nu}\frac{H_3(\xi)}{\sqrt{(3!)}}\varepsilon^{-x^2/2\sigma_e^2}dx \\ &= -\frac{a2^{\nu/2}}{\sqrt{(3\pi)}}(1-\nu)\Gamma\left(\frac{\nu+2}{2}\right)\sigma_e^{\nu} \quad . \quad . \quad (13) \end{aligned}$$

Thus $$\left|\frac{\alpha_3(\nu)}{\alpha_1(\nu)}\right| = \frac{1-\nu}{\sqrt{6}}$$

For a saturation characteristic with limits $\pm h$,

$$\alpha_1 = \frac{2\sigma}{\sqrt{\pi}}\int_0^{h/\sigma\sqrt{2}}\varepsilon^{-x^2}dx = \sigma \operatorname{erf}\left(\frac{h}{\sigma\sqrt{2}}\right)$$

and $$\alpha_3 = -\frac{h}{\sqrt{3\pi}}\varepsilon^{-h^2/2\sigma^2}$$

For such a function for large signals, i.e. $\sigma \to \infty$, $\left|\frac{\alpha_3}{\alpha_1}\right| \to \frac{1}{\sqrt{6}}$.

(8.3) Very-Low-Frequency Distortion Spectrum

When the input spectrum to a non-linearity is known, previous work has shown[12–14] how the output spectrum may be determined. This technique enables the non-linearity to be represented by an equivalent gain K, as given by Booton's method, and an additional distortion generator, as shown in Fig. 10.

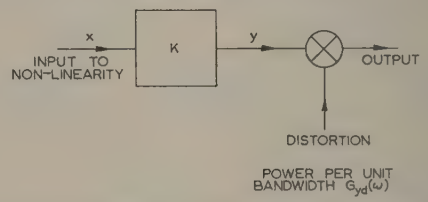

Fig. 10.—Equivalent representation of non-linearity.

In the derivation of the output spectrum of a non-linear element it is necessary to consider the auto-correlation function, $R(\tau)$, of the input and output signals, which is related to the power spectrum $G(\omega)$ by the Wiener–Khinchin relationships

$$R(\tau) = \frac{1}{2\pi}\int_{-\infty}^{+\infty} G(\omega)\varepsilon^{j\omega\tau}d\omega$$

and $$G(\omega) = \int_{-\infty}^{+\infty} R(\tau)\varepsilon^{-j\omega\tau}d\tau$$

The normalized auto-correlation function is given by

$$\rho(\tau) = \frac{R(\tau)}{R(0)} = \frac{R(\tau)}{\sigma^2}$$

$R(\tau)$ may be expressed as a power series in $\rho(\tau)$, i.e.

$$R_y(\tau) = \sum_{n=0}^{\infty} \alpha_n^2\rho_x^n(\tau)$$

The coefficients α_n are functions of the form of the non-linearity, and are evaluated for saturation and the error-shaping function in Section 8.2.

Thus the output-power spectrum of a non-linearity is obtained from the inverse transform

$$G_y(\omega) = \int_{-\infty}^{\infty} \left[\sum_{n=0}^{\infty} \alpha_n^2 \rho_x^n(\tau) \right] \varepsilon^{-j\omega\tau} d\tau \quad . \quad . \quad (14)$$

α_1 gives the undistorted component of the output, and for any symmetrical non-linearity $\alpha_0 = \alpha_2 = \alpha_{2n} = 0$, whence α_3, α_5, α_{2n+1} give contributions to the distortion.

To estimate the power spectrum of the distortion, it is found to be sufficiently accurate to represent the input-power spectrum to the non-linearity by

$$G_x(\omega) = G_x(0) \left[\frac{1}{1 + \left(\frac{\omega}{m\omega_c}\right)^2} - \frac{1}{1 + \left(\frac{\omega}{\omega_c}\right)^2} \right] \quad . \quad (15)$$

This signal has a relatively simple normalized auto-correlation function given by

$$\rho_x(\tau) = \frac{1}{m-1} (m\varepsilon^{-m\omega_c|\tau|} - \varepsilon^{-\omega_c|\tau|})$$

Considering only the first two terms in eqn. (14) the resultant output spectrum is

$$G_y(\omega) = \frac{2\alpha_1^2}{\omega_c(m-1)} \left[\frac{1}{1 + \left(\frac{\omega}{m\omega_c}\right)^2} - \frac{1}{1 + \left(\frac{\omega}{\omega_c}\right)^2} \right] + \frac{2\alpha_3^2}{\omega_c(m-1)^3} \left\{ \frac{m^2/3}{1 + \left(\frac{\omega}{3m\omega_c}\right)^2} - \frac{3m^2/(2m+1)}{1 + \left[\frac{\omega}{(2m+1)\omega_c}\right]^2} + \frac{(3m/m+2)}{1 + \left[\frac{\omega}{(m+2)\omega_c}\right]^2} - \frac{1/3}{1 + \left(\frac{\omega}{3\omega_c}\right)^2} \right\}$$

$$= G_{yf}(\omega) + G_{yd}(\omega)$$

The second term represents the distortion signal and gives a uniform power spectrum from zero frequency to about $\omega = 3\omega_c$.

Thus, at low frequencies, where the servo error and control signals are small, the distortion introduces a signal of uniform power per unit bandwidth. The magnitude of this distortion may be assessed by the ratio of very-low-frequency output distortion power per unit bandwidth to mid-band correlated power per unit bandwidth, given by

$$\left(\frac{\alpha_3}{\alpha_1}\right)^2 \frac{\frac{m^2}{3} - \frac{3m^2}{2m+1} + \frac{3m}{m+2} - \frac{1}{3}}{(m-1)^2} \quad . \quad . \quad . \quad (16)$$

At very low frequencies, the system will respond faithfully to the distortion signal, so that an additional signal will be present at the input to the non-linearity of low-frequency power per unit bandwidth equal to $(1/K^2)G_{yd}(\omega)$ (Fig. 10).

By graphical analysis the error or control-signal spectrum (Fig. 8) of the equivalent linear system is approximated to the form of eqn. (15), giving $m = 10$.

For the two non-linear systems, α_1 and α_3 have been evaluated in Section 8.2. Thus the low-frequency error power may be determined. The particular input corresponding to Fig. 8 gives a normalized low-frequency error power per unit bandwidth with and without error processing of 0·002 and 0·02, respectively.

These results agree well with experimental observations and demonstrate a significant improvement in the response of the system.

621.372.826

The Institution of Electrical Engineers
Monograph No. 362 E
Feb. 1960
©

POWER FLOW AND NEGATIVE WAVE IMPEDANCE IN THE DIELECTRIC-ROD WAVEGUIDE

By E. F. F. GILLESPIE, M.Eng., Graduate.

(*The paper was first received 16th July, and in revised form 6th November*, 1959. *It was published as an* INSTITUTION MONOGRAPH *in February*, 1960.)

SUMMARY

In most waveguides of practical interest the wave impedance in the direction of propagation of the wave is positive and its magnitude does not vary with position. It is shown that, in general, a guiding structure supporting a hybrid mode, i.e. a mode having axial components of both the electric and magnetic fields, can present a negative wave impedance. The case of the EH_{11} mode on a dielectric rod is then considered, and it is shown that for this mode the wave impedance is negative over part of the transverse plane and hence leads to regions of negative power flow if the usual interpretation of the Poynting vector is employed. The total power flow, however, is still positive, since the negative power density and the negative wave impedance occur only in a restricted part of the cross-section.

The orthogonality of the fields is also discussed, and it is shown that for hybrid modes the transverse electric and magnetic fields are not at right angles to each other.

LIST OF PRINCIPAL SYMBOLS

x, y, z = Cartesian co-ordinates.
r, θ, z = Cylindrical polar co-ordinates.
E'_x, E'_y = Electric field components of H mode.
H'_x, H'_y, H'_z = Magnetic field components of H mode.
E''_x, E''_y, E''_z = Electric field components of E mode.
H''_x, H''_y = Magnetic field components of E mode.
E'_t, H'_t = Transverse electric and magnetic components respectively, of H mode.
E''_t, H''_t = Transverse electric and magnetic components, respectively, of E mode.
Z', Z'' = Wave impedances in the z-direction of H and E modes, respectively.
Z_1, Z_2 = Wave impedances in the z-direction of a hybrid mode.
$J_1(u), H_1^{(1)}(v)$ = Bessel and Hankel functions of first kind and first order.
$J'_1(u), H_1^{(1)\prime}(v)$ = First derivatives of the Bessel and Hankel functions of first kind and first order.
μ_0, ϵ_0 = Permeability and permittivity of free space.
μ, ϵ = Permeability and permittivity respectively of medium.
λ_0, λ_g = Free-space and guide wavelength.
$s = \lambda_0/\lambda_g$.
a = Radius of dielectric rod.
ϵ_r = Dielectric constant of rod.
P_r, P_0 = Total power flow and power flow outside the rod, respectively.
A, B = Amplitude constants.

The rationalized M.K.S. system of units is used throughout.

(1) INTRODUCTION

During the course of an investigation on dielectric-rod waveguides it was found necessary to make use of an electronic digital computer to obtain solutions of the characteristic equation which relates the propagation coefficient of a wave travelling down the rod to the parameters of the rod. The mode under consideration was the hybrid EH_{11} mode. At the same time the opportunity was taken to evaluate the power flow inside and outside the dielectric rod, and this led to the surprising result that under certain conditions the power flow outside the dielectric rod is negative. This phenomenon can be interpreted in terms of the wave impedance.

The concept of wave impedance, originally due to Schelkunoff,[1] has now been used for a number of years in electromagnetic field theory, and has been expounded in a clear and interesting manner in a paper by Booker.[2]

In field theory the power flow through the surface of a guiding system is usually derived from the Poynting vector or, when the complex representation of sinusoidally varying quantities is employed, from the complex Poynting vector:

$$\boldsymbol{S} = \tfrac{1}{2}\boldsymbol{E} \times \boldsymbol{H}^* \quad . \quad . \quad . \quad . \quad . \quad (1)$$

where $\boldsymbol{H}^*$ is the complex conjugate of $\boldsymbol{H}$. The time-average power flow, P, through the surface s is then

$$P = \mathscr{R} \int_s \boldsymbol{S} \,.\, \boldsymbol{n} ds \quad . \quad . \quad . \quad . \quad . \quad . \quad (2)$$

where $\boldsymbol{n}$ is the unit vector normal to the surface.

If a right-handed Cartesian set of co-ordinates is used with propagation in the positive z-direction, the Poynting vector reduces to

$$S_z = \tfrac{1}{2}(E_x H_y^* - E_y H_x^*) \quad . \quad . \quad . \quad . \quad . \quad (3)$$

By defining the wave impedances Z_1 and Z_2 as $Z_1 = E_x/H_y$ and $Z_2 = E_y/H_x$, eqn. (3) may be written as

$$S_z = \tfrac{1}{2}(Z_1 H_y H_y^* + Z_2 H_x H_x^*) \quad . \quad . \quad . \quad . \quad (4)$$

The power flow, as given by eqn. (4), can thus become negative only if one or both of the wave impedances Z_1 and Z_2 becomes negative. It has been found that this condition can occur under certain circumstances, but only if the guiding system is capable of supporting a hybrid mode (one which is obtained by combining an H mode and an E mode).

From Maxwell's equations it can be shown that, for an H mode,

$$\left.\begin{aligned} Z' &= \sqrt{\frac{\mu}{\epsilon}}\frac{\lambda_g}{\lambda} \\ \text{and} \qquad Z'\boldsymbol{H}'_t &= \boldsymbol{k} \times \boldsymbol{E}'_t \end{aligned}\right\} \quad . \quad . \quad . \quad . \quad . \quad . \quad (5)$$

Similarly, for an E mode,

$$\left.\begin{aligned} Z'' &= \sqrt{\frac{\mu}{\epsilon}}\frac{\lambda}{\lambda_g} \\ \text{and} \qquad Z''\boldsymbol{H}''_t &= \boldsymbol{k} \times \boldsymbol{E}'_t \end{aligned}\right\} \quad . \quad . \quad . \quad . \quad . \quad . \quad (6)$$

Correspondence on Monographs is invited for consideration with a view to publication.
Mr. Gillespie is in the Department of Electrical Engineering, University of Sheffield.

where k is the unit vector in the z-direction. For the hybrid EH mode, since this can be expressed as the sum of an E and H mode,

$$H_x = H'_x + H''_x$$
$$H_y = H'_y + H''_y$$

and, using eqns. (5) and (6), also

$$E_x = Z'H'_y + Z''H''_y$$
$$E_y = -Z'H'_x - Z''H'_x$$

Hence
$$\frac{E_x}{H_y} = Z'\frac{H'_y}{H_y} + Z''\frac{H''_y}{H_y}$$

so that
$$Z_1 = (1-b)Z' + bZ''$$

and similarly
$$Z_2 = (1-c)Z' + cZ''$$

where $b = H''_y/H_y$ and $c = H''_x/H_x$.

Substituting from eqns. (5) and (6),

$$\left.\begin{aligned} Z_1 &= \sqrt{\frac{\mu}{\epsilon}}\left[\frac{\lambda_g}{\lambda} + b\left(\frac{\lambda}{\lambda_g} - \frac{\lambda_g}{\lambda}\right)\right] \\ \text{and} \quad Z_2 &= \sqrt{\frac{\mu}{\epsilon}}\left[\frac{\lambda_g}{\lambda} + c\left(\frac{\lambda}{\lambda_g} - \frac{\lambda_g}{\lambda}\right)\right] \end{aligned}\right\} \quad . \quad . \quad . \quad . \quad (7)$$

If an air-filled metal waveguide is being considered, then $\lambda = \lambda_0$, the free-space wavelength, and $\lambda_g > \lambda$, so that the impedances Z_1 and Z_2 can become negative if b and c are greater than unity. This is possible if the fields of the E and H modes are in antiphase.

Alternatively, if a dielectric rod is being used as the waveguide, then, for the dielectric region, λ is the wavelength of propagation in an infinite medium having constants ϵ and μ. Hence $\lambda = \lambda_0(\epsilon_r)^{-1/2}$, so that $\lambda_g > \lambda$ and the impedances Z_1 and Z_2 can become negative if b and c are greater than unity as before. For the region outside the dielectric $\lambda = \lambda_0$, so that $\lambda > \lambda_g$ and the impedances Z_1 and Z_2 can become negative if b and c are negative. This is again possible if the fields of the E and H modes are in antiphase.

Although negative power density and negative impedance have been obtained, it should be noted that the power flow in the direction of propagation remains positive, since the negative values occur over a limited fraction of the cross-section. The genuine hybrid mode, such as the EH_{11} mode of the dielectric rod, in which the E and H parts must both be present with a definite phase and amplitude relationship if the boundary conditions are to be satisfied, should not be confused with the 'bogus' hybrid mode, such as the rectangular waveguide one, which is really just the simultaneous passage along the guide of independent E and H modes, both of which individually satisfy the boundary conditions. In the latter case, a small deformation will split the degeneracy, i.e. the phase velocities, of the two modes, whilst in the former case a deformation will not lead to individually travelling E and H modes.

(2) WAVE IMPEDANCE AND FIELD ORTHOGONALITY

It is interesting to note that the relationship

$$\frac{E_x}{H_y} = -\frac{E_y}{H_x}$$
$$\text{i.e. } \boldsymbol{E}_t \,.\, \boldsymbol{H}_t = 0 \quad . \quad . \quad . \quad . \quad . \quad . \quad . \quad (8)$$

which is the condition for the orthogonality of $\boldsymbol{E}_t$ and $\boldsymbol{H}_t$, and which is true for E and H modes, no longer applies for the hybrid EH mode.

From either $\text{curl}\, \boldsymbol{H} = j\omega\epsilon\boldsymbol{E}$ or $\text{curl}\, \boldsymbol{E} = -j\omega\mu\boldsymbol{H}$ it can easily be shown that $\boldsymbol{E}$ and $\boldsymbol{H}$ must always be orthogonal.

Let $\boldsymbol{E} = \boldsymbol{E}_t + k\boldsymbol{E}_z$ and $\boldsymbol{H} = \boldsymbol{H}_t + k\boldsymbol{H}_z$. Then, since $\boldsymbol{E} \,.\, \boldsymbol{H} = 0$,

$$\boldsymbol{E}_t \,.\, \boldsymbol{H}_t + \boldsymbol{E}_z\boldsymbol{H}_z = 0$$

Hence, for either an E mode or an H mode, $\boldsymbol{E}_t \,.\, \boldsymbol{H}_t = 0$, i.e. $\boldsymbol{E}_t$ and $\boldsymbol{H}_t$ are orthogonal.

In a hybrid mode, neither E_z nor H_z is zero, so that $\boldsymbol{E}_t \,.\, \boldsymbol{H}_t \neq 0$. Therefore $\boldsymbol{E}_t$ and $\boldsymbol{H}_t$ are not orthogonal and hence

$$\frac{E_x}{H_y} \neq -\frac{E_y}{H_x} \text{ or } Z_1 \neq Z_2 \quad . \quad . \quad . \quad . \quad (9)$$

(3) THEORY OF WAVES ON CIRCULAR DIELECTRIC RODS

In the investigation carried out on dielectric rods the aim was to develop a method of measuring the dielectric properties of materials at millimetric wavelengths by launching a surface wave along a sample of the material in the form of a long thin rod. Details of this method will not be discussed here as they are given elsewhere.[3]

From field theory and the matching of boundary conditions an equation can be obtained which relates the propagation coefficient in terms of the rod parameters (dielectric constant and diameter). The general form of this equation is given by Stratton.[4] For the present case (EH_{11} mode), for a time dependence of $\exp(+j\omega t)$ and for a z-dependence of $\exp(-j\beta z)$, where z is the direction of propagation, it takes the form:

$$s^2\left(\frac{1}{u^2} - \frac{1}{v^2}\right)^2 = \left[\frac{J'_1(u)}{uJ_1(u)} - \frac{H_1^{(1)\prime}(v)}{vH_1^{(1)}(v)}\right]\left[\frac{\epsilon_r J'_1(u)}{uJ_1(u)} - \frac{H_1^{(1)\prime}(v)}{vH_1^{(1)}(v)}\right] \quad . \quad (10)$$

where
$$u = \frac{2\pi a}{\lambda_0}(\epsilon_r - s^2)^{1/2}$$

$$v = j\frac{2\pi a}{\lambda_0}(s^2 - 1)^{1/2}$$

and
$$s = \frac{\lambda_0}{\lambda_g}$$

Eqn. (10) can thus be solved to give the relationship between the propagation coefficient, the rod diameter and the dielectric constant of the rod. By measuring the first two the third can be determined. To give a wide range of conditions, eqn. (10) was solved a number of times with the aid of a digital computer.

The loss tangent of the dielectric rod is obtained from a measurement of attenuation, since they are related by

$$\alpha = \frac{\pi\epsilon_r R}{\lambda_0}\tan\delta \quad . \quad . \quad . \quad . \quad . \quad (11)$$

The form of the factor R is rather involved[5] and depends on the values obtained from the solution of eqn. (10). To speed up the calculations a computer was again used. Since the calculation of R involved the evaluation of the power density inside and outside the rod, the opportunity was taken to find the fraction of power flowing outside the rod.

The power flow can be obtained from the complex Poynting vector, so that

$$\frac{P_0}{P_r} = \frac{\tfrac{1}{2}\mathscr{R}\int_{\theta=0}^{2\pi}\int_{r=a}^{\infty}(E_r H_\theta^* - E_\theta H_r^*)r\,dr\,d\theta}{\tfrac{1}{2}\mathscr{R}\int_{\theta=0}^{2\pi}\int_{r=0}^{a}(E_r H_\theta^* - E_\theta H_r^*)r\,dr\,d\theta + \tfrac{1}{2}\mathscr{R}\int_{\theta=0}^{2\pi}\int_{r=a}^{\infty}(E_r H_\theta^* - E_\theta H_r^*)r\,dr\,d\theta}$$

which leads to

$$\frac{P_0}{P_r} = \frac{(1+V^2)sY - \frac{2V}{v^4}(1+s^2)}{(\epsilon_r+V^2)sX + \frac{2V}{u^4}(\epsilon_r+s^2) + (1+V^2)sY - \frac{2V}{v^4}(1+s^2)} \quad . \quad . \quad . \quad (12)$$

where $X = f^2 + \frac{2f+1}{u^2} - \frac{1}{u^4}$ $\quad Y = -g^2 - \frac{2g+1}{v^2} + \frac{1}{v^4}$

$$f = \frac{1}{u}\frac{J_1'(u)}{J_1(u)} \quad g = \frac{1}{v}\frac{H_1^{(1)\prime}(v)}{H_1^{(1)}(v)}$$

and $$V = \left[\frac{\epsilon_r f - g}{f - g}\right]^{1/2}$$

In the above terms v is positive imaginary and hence g is positive, whereas u is positive real and f can be either positive or negative.

When measuring dielectric constants, a convenient way of presenting results is to plot the relationship between the dielectric constant ϵ_r and the normalized guide wavelength λ_g/λ_0 for constant values of the normalized diameter $2a/\lambda_0$. In this way, curves of the ratio P_0/P_r of the power outside the rod to the total power have been plotted in Fig. 1 as a function of ϵ_r for

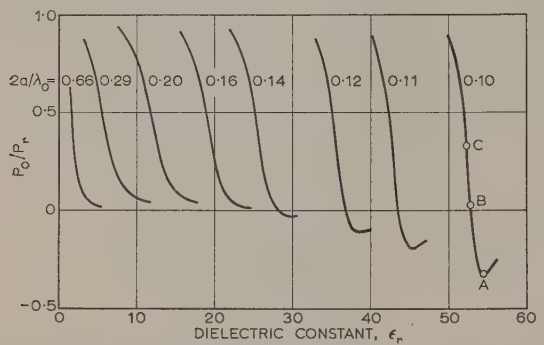

Fig. 1.—Ratio of power outside the rod to total power as a function of dielectric constant.

constant values of $2a/\lambda_0$. This clearly exhibits the phenomenon of negative power flow under certain conditions.

(4) INTERPRETATION OF RESULTS

In order to interpret the curves plotted in Fig. 1 it is necessary to examine the Poynting vector at different points in the cross-section of the guiding system to obtain values of the average power density.

Thus $$S_z = \tfrac{1}{2}E_t \times H^*$$

which after substituting for the field components leads to, for $r < a$,

$$S_z = \frac{1}{2Z_0}\left[A\frac{2\pi r}{\lambda_0}J_1(u_r)\right]^2\left\{\cos^2\theta\left[\frac{V}{u_r^2} + sf(r)\right]\left[\frac{Vs}{u_r^2} + \epsilon_r f(r)\right] + \sin^2\theta\left[Vf(r) + \frac{s}{u_r^2}\right]\left[Vsf(r) + \frac{\epsilon_r}{u_r^2}\right]\right\} \quad . \quad (13)$$

where $Z_0 = \sqrt{\frac{\mu_0}{\epsilon_0}}$, the characteristic impedance of free space,

$$u_r = \frac{2\pi r}{\lambda_0}(\epsilon_r - s^2)^{1/2}$$

and $$f(r) = \frac{1}{u_r}\frac{J_1'(u_r)}{J_1(u_r)}$$

This can be written

$$S_z = C\cos^2\theta + D\sin^2\theta$$

and will be negative for certain values of θ if C or D is negative. The locus of zero power density can be obtained from eqn. (13), which reduces to

$$\tan^2\theta = \frac{-[V + u_r^2 sf(r)][Vs + u_r^2\epsilon_r f(r)]}{[u_r^2 Vf(r) + s][u_r^2 Vsf(r) + \epsilon_r]} \quad . \quad . \quad (14)$$

For each working-point, V, s, ϵ_r and $2a/\lambda_0$ are constant. Since the remaining terms on the right-hand side of eqn. (14), u_r and $f(r)$, are functions of r, θ can be obtained for a range of r. Similarly, for $r \geqslant a$,

$$S_z = \frac{1}{2Z_0}\left[B\frac{2\pi r}{\lambda_0}H_1^{(1)}(v_r)\right]^2\left\{\cos^2\theta\left[\frac{V}{v_r^2} + sg(r)\right]\left[\frac{Vs}{v_r^2} + g(r)\right] + \sin^2\theta\left[Vg(r) + \frac{s}{v_r^2}\right]\left[Vsg(r) + \frac{1}{v_r^2}\right]\right\} \quad . \quad (15)$$

where $$v_r = j\frac{2\pi r}{\lambda_0}(s^2 - 1)^{1/2}$$

and $$g(r) = \frac{1}{v_r}\frac{H_1^{(1)\prime}(v_r)}{H_1^{(1)}(v_r)}$$

and for $$S_z = 0$$

$$\tan^2\theta = \frac{-[V + v_r^2 sg(r)][Vs + v_r^2 g(r)]}{[v_r^2 Vg(r) + s][v_r^2 Vsg(r) + 1]} \quad . \quad (16)$$

In Fig. 2 the loci of zero power density have been plotted for three different working-points. These correspond to a total

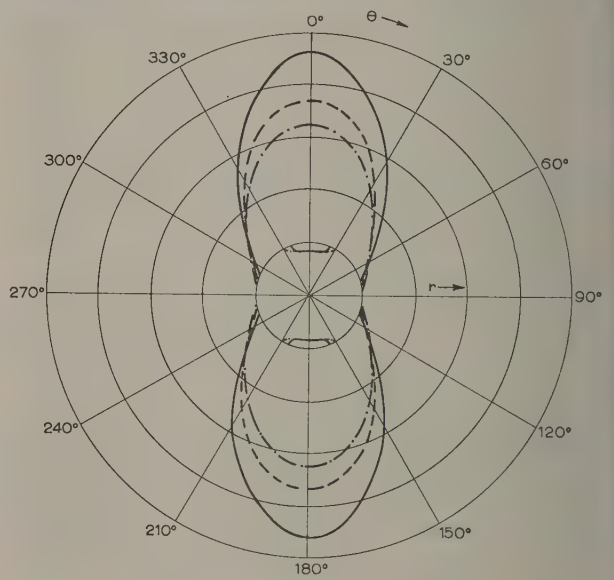

Fig. 2.—Loci of zero power density.
—— Total power outside rod negative.
– – – – Total power outside rod approximately zero.
–·–·– Total power outside rod positive.

energy flow outside the rod which is negative at A, approximately zero at B and positive at C, as shown in Fig. 1 on the curve for $2a/\lambda_0 = 0{\cdot}10$. The power density everywhere inside the loops formed by these loci is negative and conversely is positive outside.

If eqn. (13) is examined, the term which gives rise to the negative power flow inside the rod can be determined. By equating this to zero and solving for r, the limiting radius within which the

power flow can only be positive is obtained. This can be written, in general, as

$$u_r^2 f(r) + p = 0 \quad . \quad . \quad . \quad . \quad . \quad (17)$$

where p is the smallest of the quantities V/s, Vs/ϵ_r, s/V and ϵ_r/Vs. From numerical work this has been found to be Vs/ϵ_r.

The sign of eqn. (17) is determined by the function $f(r)$, which ranges from $+\infty$ at the first zero of $J_1(u_r)$ (i.e. $u_r = 0$) to $-\infty$ at the second zero (i.e. $u_r = 3{\cdot}8317$). Eqn. (17) can thus be written approximately as

$$f(r) \simeq 0 \quad . \quad . \quad . \quad . \quad . \quad . \quad . \quad (18)$$

and leads to an approximate value of u_r of 1·84 from which r can again be evaluated.

Similarly, by examining eqn. (15), the term which gives rise to the negative power flow outside the rod can be determined and when equated to zero will give the limiting value of r outside which the power flow can only be positive. This can be written, in general, as

$$v_r^2 g(r) + q = 0 \quad . \quad . \quad . \quad . \quad . \quad . \quad . \quad (19)$$

where q is the smallest of the quantities V/s, Vs, s/V and $1/Vs$. Numerical work shows this to be Vs. Limiting values calculated from eqns. (17)–(19) are given in Table 1 for the three cases considered.

Table 1

	Point A	Point B	Point C
Upper limit of $2r/\lambda_0$	0·460	0·368	0·325
Lower limit of $2r/\lambda_0$	0·0846	0·0836	0·0835
Approximate lower limit of $2r/\lambda_0$	0·0825	0·0823	0·0824

To obtain some idea of the relative power density inside and outside the rod, eqns. (13) and (15) can be solved for specific values of θ. In Fig. 3, the relative power density has been

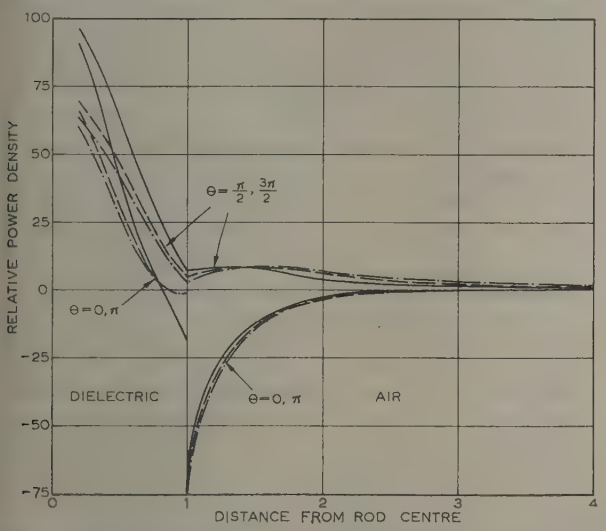

Fig. 3.—Relative power density as a function of distance from the centre of rod for $\theta = 0$, π and $\theta = \pi/2$, $3\pi/2$.

——— Total power outside rod negative.
– – – – Total power outside rod approximately zero.
–·–·– Total power outside rod positive.

plotted as a function of r for the three cases considered for $\theta = 0$ (or π) and $\theta = \pi/2$ (or $3\pi/2$).

For completeness, the power flow density in the transverse directions must be examined.

$$S_r = \tfrac{1}{2}(E_\theta H_z^* - E_z H_\theta^*)$$

$$S_\theta = \tfrac{1}{2}(E_z H_r^* - E_r H_z^*)$$

For $r \leqslant a$,

$$S_r = \frac{j}{2Z_0}\left[A\frac{2\pi r}{\lambda_0}J_1(u_r)\right]^2\left\{\sin^2\theta\frac{\lambda_0 V}{2\pi r}\left[Vf(r) + \frac{s}{u_r^2}\right] + \cos^2\theta\frac{\lambda_0}{2\pi r}\left[\frac{sV}{u_r^2} + \epsilon_r f(r)\right]\right\} \quad . \quad (20)$$

$$S_\theta = \frac{j}{2Z_0}\left[A\frac{2\pi r}{\lambda_0}J_1(u_r)\right]^2\left\{\frac{\lambda_0}{2\pi r}\left[sVf(r) + \frac{\epsilon_r}{u_r^2}\right] + \frac{\lambda_0 V}{2\pi r}\left[\frac{V}{u_r^2} + sf(r)\right]\right\}\tfrac{1}{2}\sin 2\theta \quad . \quad (21)$$

For $r > a$,

$$S_r = \frac{j}{2Z_0}\left[B\frac{2\pi r}{\lambda_0}H_1^{(1)}(v_r)\right]^2\left\{\sin^2\theta\frac{\lambda_0 V}{2\pi r}\left[Vg(r) + \frac{s}{v_r^2}\right] + \cos^2\theta\frac{\lambda_0}{2\pi r}\left[\frac{sV}{v_r^2} + g(r)\right]\right\} \quad . \quad (22)$$

$$S_\theta = \frac{j}{2Z_0}\left[B\frac{2\pi r}{\lambda_0}H_1^{(1)}(v_r)\right]^2\left\{\frac{\lambda_0}{2\pi r}\left[sVg(r) + \frac{1}{v_r^2}\right] \frac{\lambda_0 V}{2\pi r}\left[\frac{V}{v_r^2} + sg(r)\right]\right\}\tfrac{1}{2}\sin 2\theta \quad . \quad (23)$$

The power densities evaluated from eqns. (20)–(23) are purely reactive and therefore denote pulsating energy only in the r and θ directions.

(5) CONCLUSIONS

A general theory of power flow for a hybrid mode has been derived. In the case of the dielectric rod, the theory is of some importance since the easiest mode to propagate in a pure form is the hybrid EH_{11} mode.[3] The curves plotted in Figs. 1–3 for this mode support the theory and demonstrate that an unusual phenomenon does occur.

(6) ACKNOWLEDGMENTS

The author wishes to thank Professor A. L. Cullen for his stimulating discussions, Mr. P. H. Blundell for his guidance in the preparation of the computer programmes, and the United Steel Company for allowing the use of their Pegasus computer. The work described forms part of a programme of research sponsored by the C.V.D. and the author gratefully acknowledges their support of this work.

(7) REFERENCES

(1) SCHELKUNOFF, S. A.: 'The Impedance Concept and its Application to Problems of Reflection, Refraction, Shielding and Power Absorption', *Bell System Technical Journal*, 1938, **17**, p. 17.

(2) BOOKER, H. G.: 'The Elements of Wave Propagation using the Impedance Concept', *Journal I.E.E.*, 1947, **94**, Part III, p. 171.

(3) CULLEN, A. L., and GILLESPIE, E. F. F.: 'A New Method for Dielectric Measurements at Millimetre Wavelengths', Proceedings of the Symposium on Millimetre Waves, Microwave Research Institute Symposia Series, **9**, March–April, 1959 (Polytechnic Press).

(4) STRATTON, J. A.: 'Electromagnetic Theory' (McGraw-Hill, 1941).

(5) ELSASSER, W. M.: 'Attenuation in a Dielectric Circular Rod', *Journal of Applied Physics*, 1949, **20**, p. 1193.

621.396.677 : 621.372.826

The Institution of Electrical Engineers
Monograph No. 363 E
Feb. 1960

©

THE SURFACE-WAVE AERIAL

By W. HERSCH, Ph.D., B.Sc.(Eng.), Associate Member.

(*The paper was first received* 10*th March*, 1958, *and in revised form* 20*th November*, 1959. *It was published as an* INSTITUTION MONOGRAPH *in February*, 1960.)

SUMMARY

The radiation from the open-circuited end of an externally dielectric-coated metallic waveguide can be controlled by varying the size of the guide, the thickness and/or the dielectric constant of the coating. A new type of aerial designed around this principle is given the name 'surface-wave aerial' and radiation-pattern measurements are used to confirm the theory underlying this type of radiator.

According to its mode of operation it belongs to the category of end-fire aerials, which are briefly reviewed to show that surface-wave aerials occupy a place in their own right amongst the many possible arrangements that utilize the end-fire effect to produce a directional radiation pattern.

The theory of the surface-wave aerial is developed in detail, a necessary preliminary step being a full theoretical analysis of the properties of the first-order cylindrical surface wave. It is shown that a dielectric-coated cylinder which is approximately a wavelength in circumference can act as a waveguide for higher-order surface waves, of which the first order is an example.

The 'characteristic equation' is determined for the general case from which the cut-off frequency, propagation coefficient and conditions under which propagation can take place are derived in turn.

Two specific cases are evaluated numerically and the results are used to calculate the polar diagrams of surface-wave aerials operating at 9 Gc/s.

The wavelength constant as well as the continuous radiation loss of a surface waveguide for which $\lambda_g/\lambda_0 \simeq 1$ are measured directly and the results obtained are used to account for the radiation pattern of very long aerials. In conclusion, an outline of future work is given.

LIST OF SYMBOLS

a = Radius of waveguide without dielectric.
a_2, a_3, a_4 = Coefficients.
α = Attenuation coefficient.
b = Radius of waveguide including dielectric.
b_2, b_3, b_4 = Coefficients.
β_0 = Phase-change coefficient of wave in free space.
β_g = Phase-change coefficient of guided wave.
c = Ratio a/b.
∇ = Laplacian operator.
$\Delta_1, \Delta_2 \ldots$ = Ratios of Bessel functions, defined in Section 2.4.
ϵ_0 = Absolute permittivity of vacuum.
$\epsilon_1, \epsilon_2, \epsilon_3$ = Relative permittivity of medium 1, 2, 3.
ϵ = Relative permittivity of a medium.
E = Electric field.
f = Frequency of wave.
γ = Propagation coefficient.
H = Magnetic field.
J_n = Bessel function of order n
H_n = Hankel function of order n
Y_n = Neumann function of order n
} Addition of prime denotes differentiation with respect to argument.
$k_p = (\omega^2\mu_p\epsilon_p - \gamma^2)^{1/2}$.
λ_0 = Free-space wavelength.
λ_g = Guide wavelength.
μ_0 = Absolute permeability of vacuum.
μ_1, μ_2, μ_3 = Relative permeability of medium 1, 2, 3.
μ = Relative permeability of a medium.
$N = k_3 b$.
$\omega = 2\pi f$.
q = Ratio b/λ_0.
$Q = \omega^2\mu_0\epsilon_0/\gamma^2 = (\lambda_g/\lambda_0)^2$.
r, ϕ, z = Cylindrical polar co-ordinates.
$T = (1/V)^2 + (1/W)^2$.
θ = Angle of direction with respect to longitudinal axis of aerial.
$\tan\delta$ = Loss tangent of dielectric medium.
v_g = Velocity of propagation of guided wave.
$V = k_2 b$.
$W = jN$.
x, y, z = Rectangular co-ordinates.

(1) INTRODUCTION

The surface-wave aerial, according to the mode of operation, belongs to the category of end-fire aerials.

In general, end-fire aerials consist of a launching device and a waveguide along which the wave travels with a phase shift approximately equal to 360° per free-space wavelength. Radiation takes place either at points of discontinuity or from the end or as a result of a combination of both.

Many different types of end-fire aerial are known, the simplest being the leaky transmission line consisting, at low frequencies, of a wire suspended above ground and terminated in its characteristic impedance at the far end. An array of separately-excited dipoles, or the Yagi aerial, although consisting of discrete radiators, can be thought of as a guiding structure for a surface wave, the radiation taking place from the end plane.[1]

Helical aerials may radiate in many modes, the two of greatest interest being the normal and the axial modes. The latter type turns the helix into an end-fire aerial, the radiation being practically circularly polarized.[2]

Dielectric rods can support various modes, the so-called dipole mode, HE_{11}, being much preferred because, when a dielectric rod is used as an aerial, the radiation consists of a single main lobe coaxial with the rod. Great bandwidth and freedom from side lobes are the main virtues of this type of radiator.[3] The waveguide properties of a dielectric tube are similar to those of a dielectric rod and provided that a critical wall thickness is maintained, single-lobed radiation patterns can be produced with dielectric tube aerials.[4]

A bare wire can act as a waveguide for a surface wave (zero order) irrespective of diameter[5] although, in practice, such surface-wave guides are coated with a dielectric in order to confine the radial spread of the wave.[6]

By introducing regular controlled discontinuities along the whole length of the wire, an aerial having a radially omni-directional radiation pattern can be constructed.[7]

The paper first deals with an extension of surface-waveguide theory to include higher-order modes, which are hybrid modes,

Correspondence on Monographs is invited for consideration with a view to publication.
The paper is based on a thesis submitted for the degree of Doctor of Philosophy at London University.
Dr. Hersch is with Electric and Musical Industries, Ltd.

nd then describes how such a waveguide, when supporting a irst-order surface wave, can be used to design a high-gain aerial which is physically small compared with a wavelength. In heory very high gains can be obtained from aerials not more han one wavelength long, since the aperture is a function only of the guide diameter, and the thickness and dielectric constant of the coating.

(2) THE FIRST-ORDER SURFACE WAVE

(2.1) Historical Background

The theoretical study of surface waves dates back to the year 1899 when Sommerfeld[8] predicted that a straight cylindrical conductor of finite conductivity and having a smooth surface could act as a guide for electromagnetic waves.

Two of his pupils carried out further theoretical studies into the properties of cylindrical surface waves. Harms[9] calculated the velocity of propagation of Sommerfeld's wave (the zero-order mode using present-day nomenclature) for a dielectric-coated wire. Hondros[10] examined the existence of higher-order modes on metallic wires and concluded that they were possible but could never be observed because they were too heavily damped.

More recently, Stratton[5] considered higher-order surface waves on a cylinder embedded in a dielectric and proved that pure E or H waves die away in the space of a few hundredths of a wavelength.

So far as the author is aware only the zero-order mode has received any attention up to now because it had been demonstrated that it could propagate on a bare wire, small in diameter compared with a wavelength, with very little attenuation. In fact, many papers have appeared in recent years dealing with various aspects of this mode.

The application of the single-wire waveguide to military purposes formed the subject of American reports in which it was referred to as the G-string waveguide. Goubau[6] was the first to show renewed interest in this type of waveguide by pointing out that the addition of a thin dielectric layer to the wire considerably reduces the radial spread of the wave and that losses due to the scattering from nearby objects can thus be made negligibly small. Methods of launching the wave were studied by Dyott[11] and Goubau himself[12] and experimental work carried out by Goubau, and his design data, were critically reviewed by Barlow and Karbowiak.[13]

Higher-order surface waves, which were dismissed as being of no practical significance by the few authors who have made reference to them, have, in fact, a low attenuation provided that they are allowed to propagate along a dielectric-coated metallic cylinder which is approximately a wavelength in circumference. Under those conditions a higher-order surface wave is not a pure E or H mode, but this is only of academic interest, as there are also other types of waveguide, such as the dielectric rod, which support waves of one predominant mode and in addition require a subsidiary mode to enable propagation to take place.

In the following Sections the properties of the first-order surface wave are studied, expressions for the field equations and propagation coefficient are derived and the results are experimentally verified.

(2.2) General Theory

The solution of the general problem of wave propagation along a dielectric-coated metallic cylinder, which includes the case of asymmetric hybrid modes, has not been attempted so far. The first-order surface wave is a specific case of such a mode and the method used to determine the propagation coefficient of this mode as a function of the diameter of the cylinder and the thickness and dielectric constant of the coating follows the method employed by Astrahan[14] for the case of a dielectric tube, as reported by Kiely.[4] Maxwell's equations expressed in vector notation are

$$\left.\begin{aligned} \text{curl } \boldsymbol{E} &= -j\omega\mu H \\ \text{curl } \boldsymbol{H} &= j\omega\epsilon E \\ \text{div } \boldsymbol{E} &= 0 \\ \text{div } \boldsymbol{H} &= 0 \end{aligned}\right\} \quad \ldots \quad (1)$$

provided that the time dependence is of the form $\varepsilon^{j\omega t}$, and that this holds for regions of zero conductivity and no charge. By taking the curl of either of the first two equations and substituting from the others, the well-known wave equations for a region with constant values of μ and ϵ are obtained:

$$\left.\begin{aligned} \nabla E_z &= -\omega^2\mu\epsilon E_z \\ \nabla H_z &= -\omega^2\mu\epsilon H_z \end{aligned}\right\} \quad \ldots \quad (2)$$

Solutions of these wave equations which satisfy Maxwell's equations at all boundary surfaces will satisfy Maxwell's equations everywhere. It is assumed that the field dependence on z is of the form $\varepsilon^{-j\gamma z}$, where γ, the propagation coefficient, is real and positive. This form represents a wave propagating without attenuation in the positive z-direction. From the wave equations (2) the following scalar equations for the z-field components are derived:

$$\left.\begin{aligned} \frac{\partial^2 E_z}{\partial r^2} + \frac{1}{r}\frac{\partial E_z}{\partial r} + \frac{1}{r^2}\frac{\partial^2 E_z}{\partial \phi^2} &= -k^2 E_z \\ \frac{\partial^2 H_z}{\partial r^2} + \frac{1}{r}\frac{\partial H_z}{\partial r} + \frac{1}{r^2}\frac{\partial^2 H_z}{\partial \phi^2} &= -k^2 H_z \end{aligned}\right\} \quad \ldots \quad (3)$$

where

$$k^2 = \omega^2\mu\epsilon - \gamma^2 \quad \ldots \quad (4)$$

The most general solutions of eqns. (3) are linear combinations of

$$\left.\begin{aligned} E_{zn} &= [A_n \mathrm{J}_n(k_p r) + B_n \mathrm{Y}_n(k_p r)]\varepsilon^{j(n\phi - \gamma z)} \\ H_{zn} &= [C_n \mathrm{J}_n(k_p r) + D_n \mathrm{Y}_n(k_p r)]\varepsilon^{j(n\phi - \gamma z)} \end{aligned}\right\} \quad \ldots \quad (5)$$

for different values of n, where a time variation of $\varepsilon^{j\omega t}$ is assumed; A, B, C and D are arbitrary constants and J_n and Y_n are Bessel functions of the first and second kinds respectively and nth order.

In order that the fields are unchanged when ϕ is increased by 2π, n must be restricted to positive and negative integers, including zero. It can be shown that the boundary conditions can be satisfied and therefore each value of n corresponds to a wave mode that can be guided by the system shown in Fig. 1.

In the following derivations only the first-order mode is con-

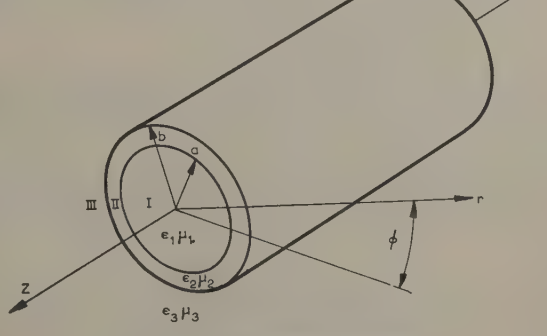

Fig. 1.—Co-ordinate system.

sidered and the subscript $n = 1$ will therefore be omitted, for the Bessel and Hankel functions of the first and zero order. If ∂/∂_z is replaced by $-j\gamma$ and ∂/∂_t by $j\omega$ in the six curl relations of the first two of eqns. (1), the r- and ϕ-components can then be expressed in terms of the z-components, resulting in

$$\left.\begin{aligned} E_\phi &= \frac{1}{k^2}\left(\frac{-j\gamma}{r}\frac{\partial E_z}{\partial \phi} + j\omega\mu\frac{\partial H_z}{\partial r}\right) \\ E_r &= \frac{-1}{k^2}\left(j\gamma\frac{\partial E_z}{\partial r} + \frac{j\omega\mu}{r}\frac{\partial H_z}{\partial \phi}\right) \\ H_\phi &= \frac{-1}{k^2}\left(j\omega\epsilon\frac{\partial E_z}{\partial r} + \frac{j\gamma}{r}\frac{\partial H_z}{\partial \phi}\right) \\ H_r &= \frac{1}{k^2}\left(\frac{j\omega\epsilon}{r}\frac{\partial E_z}{\partial \phi} - j\gamma\frac{\partial H_z}{\partial r}\right) \end{aligned}\right\} \quad . \quad . \quad . \quad (6)$$

The most general form of eqns. (5) is now determined for each of the three regions I, II and III (Fig. 1). The two components of E and H are matched at the boundary surfaces to the corresponding ϕ obtained from eqns. (6) where ϵE_z and μH_z must be continuous. For region I,

$$\left.\begin{aligned} E_{z1} &= a_1 J_1(k_1 r)F \\ H_{z1} &= b_1 J_1(k_1 r)F \end{aligned}\right\} \quad . \quad . \quad . \quad . \quad . \quad (7)$$

where $F = \varepsilon^{j(\phi+\omega t-\gamma z)}$. The Y_1 solution is discarded because the fields must remain finite and $Y(r)$ becomes infinite as r approaches zero. In the case of a dielectric-coated cylinder for which infinite conductivity is assumed, the field components E_{z1} and H_{z1} are zero inside and on the surface of the metallic cylinder. For region II,

$$\left.\begin{aligned} E_{z2} &= [a_2 J_1(k_2 r) + a_3 Y_1(k_2 r)]F \\ H_{z2} &= [b_2 J_1(k_2 r) + b_3 Y_1(k_2 r)]F \end{aligned}\right\} \quad . \quad . \quad . \quad (8)$$

For region III,

$$\left.\begin{aligned} E_{z3} &= a_4 H_1^{(1)}(k_3 r)F \\ H_{z3} &= b_4 H_1^{(1)}(k_3 r)F \end{aligned}\right\} \quad . \quad . \quad . \quad . \quad . \quad (9)$$

where $H^{(1)}(r) = J_1(r) + jY_1(r)$ is the Bessel function of the third kind, or Hankel function. Now from eqn. (4),

$$k_3^2 = \omega\mu_3\epsilon_3 - \gamma^2 = \left(\frac{\omega}{v_3}\right)^2 - \left(\frac{\omega}{v_g}\right)^2 \quad . \quad . \quad (10)$$

where v_3 is the velocity of a uniform plane wave in medium III, i.e. free space, and v_g is the velocity of propagation of the guided wave; γ is the same for all three regions. A guided wave cannot travel faster than a wave propagating in free space and k_3^2 must therefore be less than or equal to zero; consequently k_3 must be either zero or purely imaginary.

Now the field must approach zero at large distances from the axis and the most general combination of Bessel functions which approaches zero for large imaginary arguments is $H_1^{(1)}$, henceforth abbreviated to H_1.

In fact, the boundary conditions can be met by either using $H_n^{(1)}$ or $H_n^{(2)}$. In the following treatment $H_n^{(1)}$ with positive imaginary argument is used throughout.

(2.3) Field Equations

Substituting eqns. (7), (8) and (9) into eqns. (6) to obtain the r- and ϕ-components results in the following set of field equations:

$$\left.\begin{aligned} E_{\phi 1} &= 0 \\ H_{\phi 1} &= 0 \\ E_{\phi 2} &= \frac{1}{k_2^2}\left\{\frac{\gamma}{r}[a_2 J_1(k_2 r) + a_3 Y_1(k_2 r)] + j\omega\mu_2 k_2[b_2 J_1'(k_2 r) + b_3 Y_1'(k_2 r)]\right\}F \\ H_{\phi 2} &= -\frac{1}{k_2^2}\left\{j\omega\epsilon_2 k_2[a_2 J_1'(k_2 r) + a_3 Y_1'(k_2 r)] - \frac{\gamma}{r}[b_2 J_1(k_2 r) + b_3 Y_1(k_2 r)]\right\}F \\ E_{\phi 3} &= \frac{1}{k_3^2}\left[\frac{\gamma a_4}{r}H(k_3 r) + j\omega\mu_3 k_3 b_4 H_1'(k_3 r)\right]F \\ H_{\phi 3} &= -\frac{1}{k_3^2}\left[j\omega\epsilon_3 k_3 a_4 H_1'(k_3 r) - \frac{\gamma b_4}{r}H_1(k_3 r)\right]F \end{aligned}\right\} \quad (11)$$

$$\left.\begin{aligned} E_{r1} &= 0 \\ H_{r1} &= 0 \\ E_{r2} &= -\frac{1}{k_2^2}\left\{j\gamma k_2[a_2 J_1'(k_2 r) + a_3 Y_1'(k_2 r)] - \frac{\omega\mu_2}{r}[b_2 J_1(k_2 r) + b_3 Y_1(k_2 r)]\right\}F \\ H_{r2} &= \frac{1}{k_2^2}\left\{-\frac{\omega\epsilon_2}{r}[a_2 J_1(k_2 r) + a_3 Y_1(k_2 r) - j\gamma k_2[b_2 J_1'(k_2 r) + b_3 Y_1'(k_2 r)]\right\}F \\ E_{r3} &= -\frac{1}{k_3^2}\left[j\gamma k_3 a_4 H_1'(k_3 r) - \frac{\omega\mu_3 b_4}{r}H_1(k_3 r)\right]F \\ H_{r3} &= \frac{1}{k_3^2}\left[-\frac{\omega\epsilon_3 a_4}{r}H_1(k_3 r) - j\gamma k_3 b_4 H_1'(k_3 r)\right]F \end{aligned}\right\} \quad (12)$$

(2.4) The Characteristic Equation

The properties of the first-order surface wave can be determined from the field equations (11) and (12) by equating the ϕ- and z-components at the boundaries $r = a$ and $r = b$ where the fields must be continuous. From the condition that the determinant of the coefficients of the a's and b's must be zero, the characteristic equation is derived. The complete derivation is given in the Appendix, where it is shown that the characteristic equation is

$$\begin{aligned} Q\{&(\Delta_1\Delta_3 - \Delta_4\Delta_6)(\Delta_3 - \Delta_4)\Delta_5^2 - (\Delta_1\Delta_3\Delta_7 - \Delta_2\Delta_4\Delta_6)(\Delta_3 - \Delta_4)\Delta_5 \\ &+ \epsilon[(\Delta_1\Delta_3\Delta_8 - \Delta_2\Delta_4\Delta_6)(\Delta_3\Delta_7 - \Delta_2\Delta_4) \\ &- (\Delta_1\Delta_3 - \Delta_4\Delta_6)(\Delta_3\Delta_7 - \Delta_2\Delta_4)\Delta_5]\} \\ &- T^2(\Delta_1\Delta_3 - \Delta_4\Delta_6)(\Delta_3 - \Delta_4) = 0 \quad . \quad . \quad . \quad (13) \end{aligned}$$

the various symbols being defined as follows:

$$\left.\begin{aligned} \Delta_1 &= \frac{J_1'(cV)}{cVJ_1(cV)} & \Delta_4 &= \frac{J_1(V)}{VJ_1(V)} & \Delta_7 &= \frac{Y_1'(V)}{VY_1(V)} \\ \Delta_2 &= \frac{J_1'(V)}{VJ_1(V)} & \Delta_5 &= \frac{H_1'(N)}{NH_1(N)} & Q &= \frac{\omega^2\mu_0\epsilon_0}{\gamma^2} \\ \Delta_3 &= \frac{J_1(cV)}{VJ_1(cV)} & \Delta_6 &= \frac{Y_1'(cV)}{cVY_1(cV)} & T &= \left(\frac{1}{V}\right)^2 - \left(\frac{1}{N}\right)^2 \end{aligned}\right\} \quad (14)$$

The following abbreviations are introduced to simplify the writing:

$$c = a/b; \quad k_2 a = cV; \quad k_2 b = V; \quad k_3 b = N \text{ or } jW \qquad (15)$$

where W is real and positive, since k_3 must be imaginary.

The significance of the characteristic equation will now be discussed using some of the relationships obtained earlier on. From eqn. (4),

$$\gamma^2 = \omega^2\mu_2\epsilon_2 - \left(\frac{V}{b}\right)^2 = \omega^2\mu_3\epsilon_3 + \left(\frac{W}{b}\right)^2 \qquad (16)$$

Since $\gamma^2 = (2\pi/\lambda_g)^2$ and $\omega^2\mu_0\epsilon_0 = (2\pi/\lambda_0)^2$, where λ_g is the guide wavelength and λ_0 is the free-space wavelength, Q can also be written as $Q = (\lambda_g/\lambda_0)^2$, and eqn. (16) can be written in the forms

$$\left(\frac{2\pi b}{\lambda_0}\right)^2(\epsilon - 1) = V^2 + W^2 \quad . \quad . \quad . \quad . \quad (17)$$

$$\left(\frac{2\pi}{\lambda_g}\right)^2 = \epsilon\left(\frac{2\pi}{\lambda_0}\right)^2 - \left(\frac{V}{b}\right)^2 \quad . \quad . \quad (18)$$

It is thus found that

$$\left(\frac{b}{\lambda_0}\right)^2 = \frac{V^2 + W^2}{(2\pi)^2(\epsilon - 1)} \quad . \quad . \quad . \quad . \quad (19)$$

$$\left(\frac{\lambda_g}{\lambda_0}\right)^2 = \frac{V^2 + W^2}{V^2 + \epsilon W^2} \quad . \quad . \quad . \quad . \quad (20)$$

The characteristic equation expresses a relationship between two parameters $V = k_2 b$ and $N = k_3 b$ which are proportional to the radial and axial propagation coefficients respectively.

The Δ's are dependent either upon V or W; Q and T are both functions of V as well as W. Hence each pair of V and W which satisfies the characteristic equation for given values of ϵ and c determines a dimensionless pair, b/λ_0 and λ_g/λ_0. In a 3-dimensional plot, Fig. 2 shows how the value of the characteristic equation changes as a function of V and W for the case of a polythene-coated cylinder ($\epsilon = 2{\cdot}3$) for which $c = 0{\cdot}9$. The value of the characteristic equation goes to infinity whenever J_1 or Y_1 goes to zero. The Δ's in which J_1 occurs in the denominator are always associated with other Δ's where J_1 occurs in the numerator so that cancellation takes place. The only two Δ's which make the value of the characteristic equation display discontinuities are therefore Δ_3 and Δ_4 and infinities occur when either $Y_1(V)$ or $Y_1(cV)$ is zero.

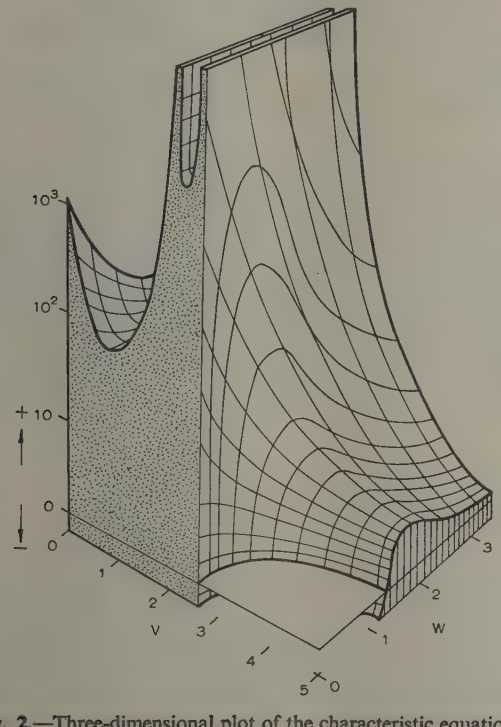

Fig. 2.—Three-dimensional plot of the characteristic equation.
$c = 0{\cdot}9; \epsilon = 2{\cdot}3$

Now $Y_1(V)$ and $Y_1(cV)$ are related by the factor c and whenever there is a value of V for which the function $Y_1(V)$ has a zero there will be a second zero when the function is $1/c$ times greater. Reference to tables of Bessel functions shows that zeros occur at 2·197, 5·430, 8·596, etc.

(2.5) Cut-Off Frequency and Higher-Order Modes

Points for which the characteristic equation is satisfied lie along the intersection of the 3-dimensional plateau and the zero plane. These points are replotted in Fig. 3, as outlined in the previous Section, to show the relationship between λ_g/λ_0 and b/λ_0. Two specific cases with which the experimental work has been concerned were evaluated numerically, namely $c = 0{\cdot}96$, $\epsilon = 23$ (titanium-dioxide-loaded polystyrene) and $c = 0{\cdot}90$, $\epsilon = 2{\cdot}3$ (polythene). It is not easy to prove analytically where the characteristic equation has solutions for V when $W = 0$, although it can be shown that a critical value must exist and that the first-order wave therefore has a cut-off frequency. The graphical solution indicates that the value of V associated with the first intersection of $W = 0$ is 2·197, which is related to the zeros of the Bessel functions of the second kind. Substituting the value found into eqn. (19) one obtains the cut-off condition for the first-order surface wave:

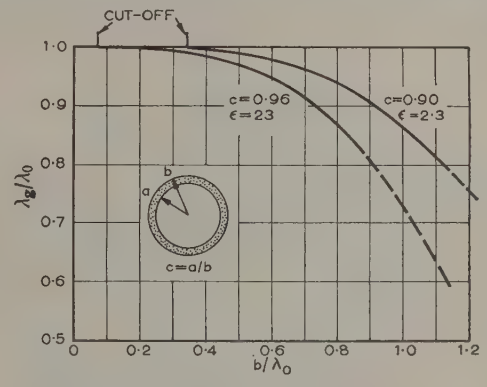

Fig. 3.—Characteristics of the HE_{11} mode.

$$\frac{b}{\lambda_0} = \frac{2{\cdot}197(1/c)}{2\pi\sqrt{(\epsilon - 1)}} \quad . \quad . \quad . \quad . \quad . \quad (21)$$

This relationship holds so long as the characteristic equation has no zeros in the range for which V lies between the limits $2{\cdot}197 < V < 2{\cdot}197/c$. For practical values of c, which are never likely to be as small as 0·5, so that $2{\cdot}197/c < 5{\cdot}430$ (the next zero), eqn. (21) applies to all cases of the HE_{11} mode.

The dependence of the cut-off frequency on the dimensions of the waveguide are better appreciated if eqn. (21) is rearranged thus:

$$2\pi b = \frac{2{\cdot}197(1/c)}{\sqrt{(\epsilon - 1)}}\lambda_0 \quad . \quad . \quad . \quad . \quad . \quad (22)$$

where $2\pi b$ represents the circumference of the guide. Examina-

tion of eqn. (22) clearly shows that the first-order surface wave cannot exist in the absence of a dielectric coating. For the case of air ($\epsilon = 1$) the guide would need to be of infinite circumference. Low-loss solid dielectrics, mixtures and foams excepted, have a dielectric constant greater than 2 so that, in general, the circumference of a surface waveguide supporting the first-order mode will have to be at least twice the free-space wavelength; however, by making ϵ large, the size can be very much reduced.

It was pointed out in Section 2.4 that the characteristic equation can be satisfied by more than one value of V for the same value of W, owing to the behaviour of the Bessel function. The second, third and subsequent zeros of this function determine the onset of higher-order modes of the first-order surface wave, i.e. HE_{21}, HE_{31}, etc., which can be analysed in a similar manner by modifying the numerical constant in eqn. (22).

So far, one set of limiting conditions applicable to Fig. 2 has been found. A second set of limiting conditions can be obtained from eqn. (20). If W is large compared with V, the value of $(\lambda_g/\lambda_0)^2$ will tend to $1/\sqrt{\epsilon}$ and if V is large compared with W, $(\lambda_g/\lambda_0)^2$ will tend to 1. It therefore follows that the ratio of guide wavelength to free-space wavelength is confined to the range $1/\sqrt{\epsilon} < \lambda_g/\lambda_0 < 1$.

(3) THE SURFACE-WAVE AERIAL

(3.1) Theoretical Radiation Pattern

(3.1.1) General Considerations.

In the preceding Section the conditions were derived under which the first-order surface wave can exist. The radiation pattern of an unterminated surface waveguide, i.e. a surface-wave aerial, is the result of a variety of factors, varying in relative importance, depending upon the size and the length of the aerial as well as upon the launching conditions.

Without further experimental work it is not possible to put forward a single unified theory to predict the radiation pattern of surface-wave aerials as a number of assumptions have to be made concerning the mechanisms of radiation and it is therefore possible to account for an observed polar diagram in more than one way, depending upon the nature of those assumptions. The radiation pattern may be due to a combination of

(*a*) Direct radiation from the dipole.
(*b*) Radiation from along the length of the aerial.
(*c*) Radiation from the open end.

The direct radiation from the launching dipole tends to make the pattern omnidirectional in the H-plane, though in general this direct contribution to the field can be kept small. Continuous radiation from the whole length of the aerial was specifically excluded when the characteristic equation was derived, it being assumed that the first-order mode is non-radiating. Radiation from the length of the aerial can nevertheless be present, owing to discontinuities on the surface. It is difficult to treat this case mathematically in a general form since the results depend upon the precise arrangement of the discontinuities.

The contribution of most interest is that from the open end of the guide for aerials that are comparatively short; for long aerials different considerations may apply. A small amount of radiation from discrete points along the length of the aerial gives rise to a polar diagram of decreasing beam width as the length of the aerial is increased; at the same time the power radiated from the end is reduced.

(3.1.2) Radiation from the Open End.

The fields E_{r3} and $E_{\phi 3}$ at the end of a surface waveguide are given by eqns. (11) and (12) and the radiation pattern is obtained from the sum of all the fields in that plane. Using the above equations it is shown elsewhere[15] that the E- and H-plane polar diagrams are given by

$$E_\theta = \text{constant} \times \int_1^\infty \frac{r}{b} H_0\left(jW\frac{r}{b}\right) \times J_0\left(\frac{2\pi}{q}\frac{r}{b}\sin\theta\right) d\left(\frac{r}{b}\right) \quad . \quad (23)$$

where $q = \lambda_0/b$ and the other symbols are defined in Fig. 4. The above integral can readily be evaluated graphically, using the normalized parameter r/b and varying $\sin\theta$ in discrete steps, since it is the product of an oscillating function, $J_0(z)$, and a rapidly decreasing function, $H_0(jz)$, both of which are tabulated.

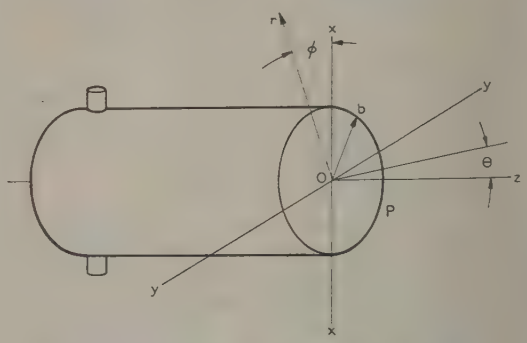

Fig. 4.—Co-ordinate system of surface-wave aerial.

The value of W is known from the particular solution of the characteristic equation from which b/λ_0 was calculated.

(3.1.3) The Long Aerial (Fig. 5, next page).

In a long aerial there is a possibility that radiation may occur from along the length of the aerial owing to regularly spaced discontinuities. The effect can be included by treating it separately and by adding this radiation vectorially to that of the end plane; however, agreement between the measured and the predicted polar diagrams is never entirely satisfactory. Considering the radiation to originate from two line sources in the x–z plane on either side of the surface waveguide, it can be shown[15] that the E- and H-plane polar diagram is given by

$$E_\theta = \varepsilon^{(j\pi l/\lambda_0)\left(\cos\theta - \frac{\lambda_0}{\lambda_g}\right)} \frac{\left[\sin\frac{\pi l}{\lambda_0}\left(\cos\theta - \frac{\lambda_0}{\lambda_g}\right)\cosh\frac{\alpha l}{2} + j\cos\frac{\pi l}{\lambda_0}\left(\cos\theta - \frac{\lambda_0}{\lambda_g}\right)\sinh\frac{\alpha l}{2}\right]}{\alpha - j\frac{2\pi}{\lambda_0}\left(\cos\theta - \frac{\lambda_0}{\lambda_g}\right)} \quad . \quad . \quad . \quad . \quad (24)$$

where α is the radiation loss per unit length in nepers.

When performing the vector addition, the phase reference plane is assumed to be at the centre of the aerial rod for the contribution from the continuous radiation and at the end of the aerial for the contribution from the end plane. Similarly, the contribution from the launching dipole could be added if it was thought to be of sufficient magnitude to warrant its inclusion.

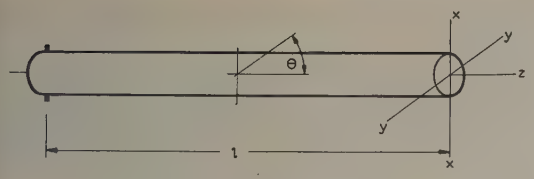

Fig. 5.—Continuous radiation.

(3.2) Methods of Launching First-Order Surface Wave

In order to excite a particular surface wave on a dielectric-coated cylinder it is, in general, necessary to create at the end of the cylinder a field configuration as closely similar to that of the required mode as possible. From Fig. 6 it is seen that the

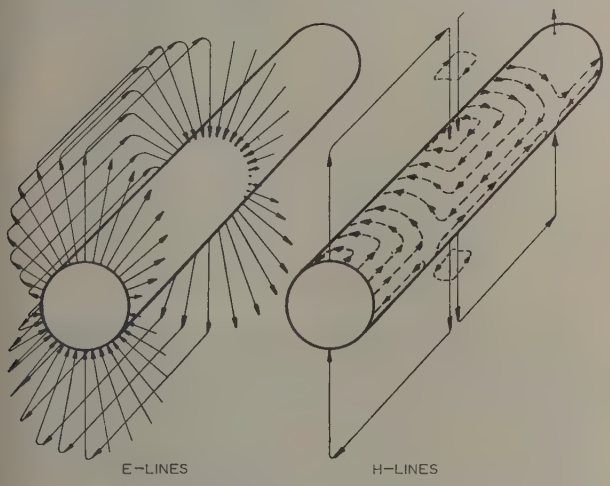

Fig. 6.—Configuration of first-order surface wave.

field distribution of the first-order surface wave along a line perpendicular to the cylinder resembles that of a $\lambda/2$ dipole which can therefore be used to launch the wave.

In order that power may conveniently be fed to the exciting dipole, a surface-wave aerial is best constructed as a dielectric-coated tube.

At microwave frequencies the aerial tube can be used as a waveguide and energy can be converted in several ways. The direction of the electric field of the H_{11} mode at the centre of a circular waveguide is perpendicular to the axis of the guide; two $\lambda/4$ dipoles projecting into the tube through insulating bushes can therefore be used to transfer energy from the inside of the tube to the outside. An adjustable reflecting piston inside the guide can be used to achieve maximum power transfer. Fig. 7(*a*) shows the principle applied to a first-order surface-wave launcher operating at 9 Gc/s.

An altogether different method is shown in Fig. 7(*b*). The H_{11} mode in a circular metal guide is used to excite the H_{11} mode in a dielectric rod. The rod is then continued as a thin dielectric sleeve surrounding the metal rod along which it is desired to propagate the surface wave. Tapered transitions ensure smoother conversion from one mode to another and result in better launching efficiency.

For operation at centimetre wavelengths a surface-wave aerial can easily be constructed from thin metallic tubing which is self-supporting, in the manner shown in Fig. 7(*a*), the outside being coated with the appropriate amount of dielectric. Since the diameter of a surface waveguide can be reduced as the dielectric

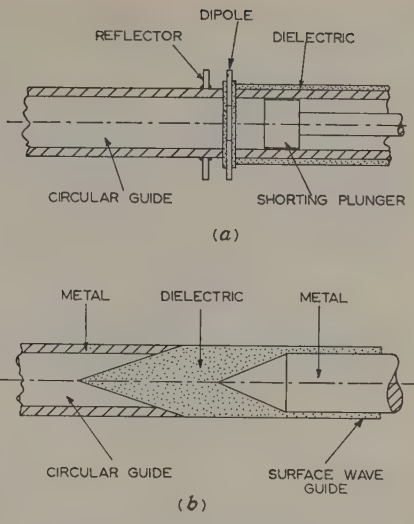

Fig. 7.—Surface-wave launchers.
(*a*) Dipole transition.
(*b*) Waveguide transition.

constant is increased, it is often desirable to make this as large as possible.

In mixtures of titanium dioxide and polystyrene this constant can be readily controlled between the limits 2·3 and 23; for appreciably higher dielectric constants solid ceramic tubes must be used.

(4) EXPERIMENTAL VERIFICATION OF AERIAL AND WAVEGUIDE THEORIES

(4.1) Test Procedure

A schematic of the experimental arrangement is shown in Fig. 8. A klystron, tunable from 8 to 10 Gc/s, was used as

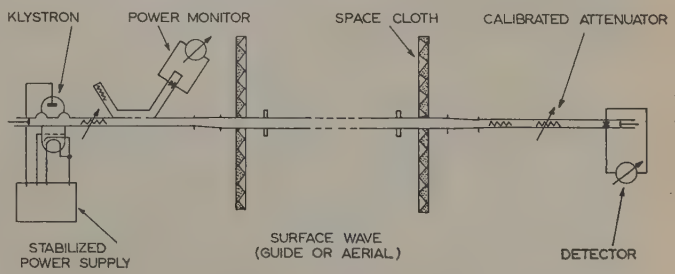

Fig. 8.—Microwave test arrangement.

the source of r.f. power. By inserting a rectangular-to-circular waveguide transition, the HE_{11} surface wave was launched from the end of the internally short-circuited waveguide, as described in Section 3.2.

In order to avoid unwanted reflections from supports, that part of the wave which travelled away from the desired direction of propagation was absorbed by a screen of carbon-loaded rubber ('space cloth') which was placed on one side of the launching dipoles. The receiving termination was constructed in an identical manner, the received energy, after being transformed back from circular to rectangular waveguide, being detected by a probe and crystal diode, the output of which was indicated on a galvanometer. A calibrated attenuator was inserted in the

waveguide and, by keeping the galvanometer deflection constant, gain or loss relative to a standard signal could be measured directly.

Propagation measurements were carried out by applying dielectric coatings of different materials to the outside of the guide. When radiation patterns were measured, the launcher in Fig. 8 was replaced by a horn which was used to illuminate the aerial under observation. In this case the aerial, used as a receiver, resembled the launching arrangement of Fig. 7, suitably extended to the appropriate length.

(4.2) Polar Diagrams

The *E*- and *H*-plane polar diagram for a surface-wave aerial two wavelengths long, for which $b/\lambda_0 = 0{\cdot}375$, is shown in Fig. 9. There are two side lobes on either side of the main

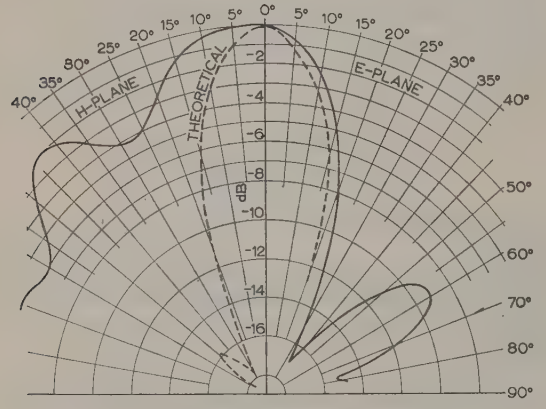

Fig. 9.—Polar diagram of 2λ aerial.
$b/\lambda_0 = 0{\cdot}375$; $c = 0{\cdot}9$; $\epsilon = 2{\cdot}3$

beam in the *E*-plane and the polar diagram in the *H*-plane shows little directivity.

The theoretical radiation pattern, calculated from the results of Section 3.1.2 and shown dotted, contains one small side lobe, but only when b/λ_0 exceeds a critical value.

The departure of the actual radiation pattern from the ideal pattern is due to the direct radiation from the launching dipole. Two sources 2λ apart, i.e. the dipole and the end plane of the aerial, will result in minima at 41·6° and 75·5° and maxima at 0°, 60° and 90°. Examination of Fig. 9 shows that this is, in fact, the case. The polar diagram of the main beam agrees well with the theoretical diagram as calculated with the aid of eqn. (23). The length of the launching dipoles projecting from the aerial was kept to $0{\cdot}1\lambda$, this being a compromise between a reasonable launching efficiency and the desire to keep the effect of direct radiation from the launcher as low as possible.

Fig. 10 shows the polar diagram of a 10λ aerial with $c = 0{\cdot}9$. The reduction in beam width of the major lobe is very noticeable compared with a short aerial. A possible explanation could be the presence of radiation from the length of the aerial, since the pattern due to the end plane has not changed.

Assuming that the phase reference plane of the radiation from the aerial length is at the centre of the aerial, five side lobes on either side of the main lobe can be expected when the radiation from a 10λ aerial is combined with that from the end plane.

The position of the side lobes depends upon the exact length of the aerial in terms of λ_g. Maxima occur whenever $\zeta \pm \frac{2\pi L}{\lambda} \cos\theta = 2n\pi$ and minima are observed whenever it equals $(2n-1)\pi$, ζ being the phase angle between the two equivalent sources.

This phase angle is determined from eqn. (24) and, as can be seen, it is also a function of α, the radiation loss per unit length. The amplitude distribution expressed by eqn. (24) obeys a $(\sin n\theta)/\theta$ law, where n denotes the number of wavelengths, provided that α is small and λ_g/λ_0 does not depart appreciably from unity.

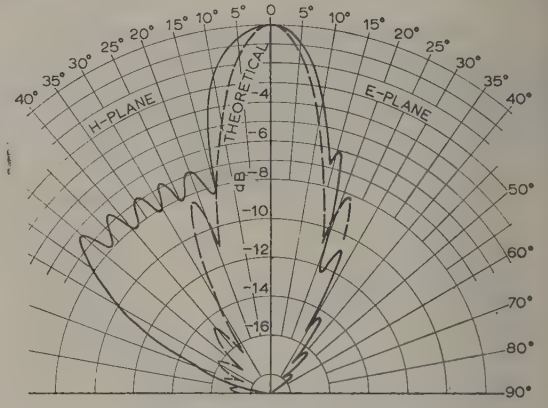

Fig. 10.—Polar diagram of 10λ aerial.
$b/\lambda_0 = 0{\cdot}375$; $c = 0{\cdot}9$; $\epsilon = 2{\cdot}3$

In Fig. 10 the theoretical polar diagram has been superimposed dotted on the measured polar diagram. The radiation from the dipole was neglected and in adding the two fields it was assumed that the power was divided in the ratio 30% : 70%, 30% being the contribution from the radiation along the length of the aerial. This figure is based on measurements described in the next Section, which indicate that power along a surface waveguide of the type used is lost at the rate of approximately 4 dB/m.

The effect of varying the ratio b/λ_0 is demonstrated in Fig. 11 which shows the polar diagrams of two aerials, 10 wavelengths long, one aerial having a dielectric thickness twice that of the

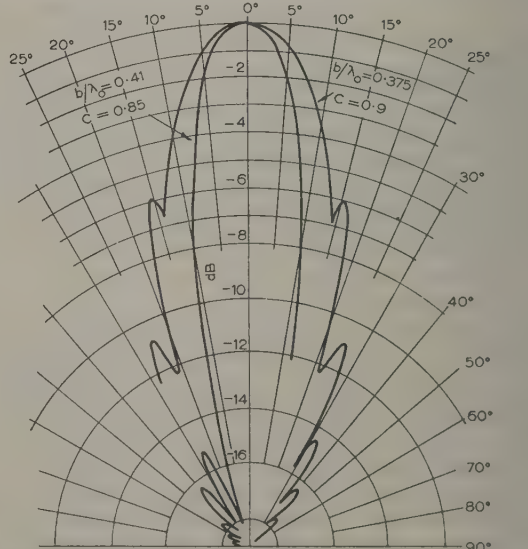

Fig. 11.—*E*-plane polar diagram showing effect of varying thickness of dielectric.

other. The actual values are $b/\lambda_0 = 0{\cdot}375$, $c = 0{\cdot}9$ and $b/\lambda_0 = 0{\cdot}41$, $c = 0{\cdot}85$.

Theoretically the beam width should decrease as the ratio $q = b/\lambda_0$ is increased [see eqn. (23)]. The phase across the aerial aperture then changes more rapidly as one moves away from the centre of the aerial, resulting in a reduced beam width.

The appearance of side lobes is the penalty that has to be paid for exceeding an optimum ratio of b/λ_0. The reduced side lobe level indicates that a greater portion of the total energy reaches the end plane in the second case and that a smaller amount of energy is lost by radiation from the length of the aerial.

Lastly, in Fig. 12 a comparison is shown between two similar

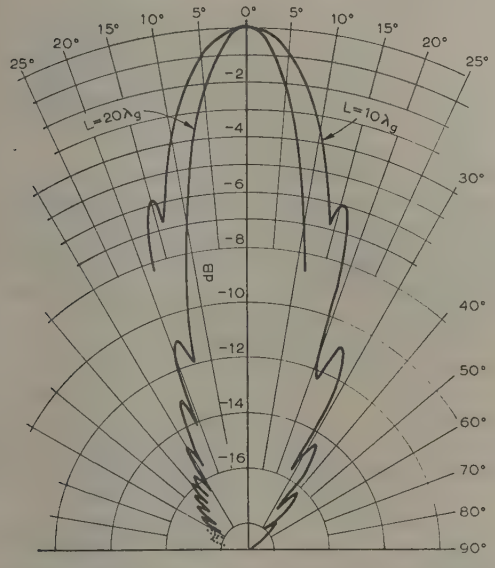

Fig. 12.—*E*-plane polar diagram showing effect of increasing length of aerial.

aerials, of length 10λ and 20λ respectively. A further reduction in the width of the major lobe is apparent as the length of the aerial is increased, with an attendant increase in the number of side lobes. The actual improvement in gain is probably masked by the additional field from the dipole, which cannot be entirely eliminated with this method of launching.

(4.3) Measurement of the Propagation Coefficient

When a dipole is used to launch a surface wave in the manner shown in Fig. 7(*a*), the launching efficiency is not very great and the field propagating outwards consists of a guided surface wave of wavelength λ_g and an unguided free-space wave of wavelength λ_0. The guided wave suffers attenuation as a result of loss in the dielectric, resistive loss in the conductor and, under certain circumstances, radiation loss due to a variety of reasons, the decay being exponential. Along the waveguide the two waves are periodically in and out of phase, and this effect can be used to determine the guide wavelength directly by measuring the resultant field at a point along the guide, either the frequency or the separation between launcher and receiver being varied until a phase change of 2π has occurred.

Experimentally it was found more convenient to choose the second method, as this ensured that the klystron power remained constant, that the conditions at the receiving end did not vary and that the launching efficiency of the transmitting and receiving dipoles remained unaltered.

Sections of waveguide of different lengths, arranged in various combinations, were used to change the guide length in discrete steps. They consisted in one case of thin-walled (telescopic) brass tubing coated with polythene tape making $b/\lambda_0 = 0{\cdot}38$ (at 9 Gc/s) and $c = 0{\cdot}9$.

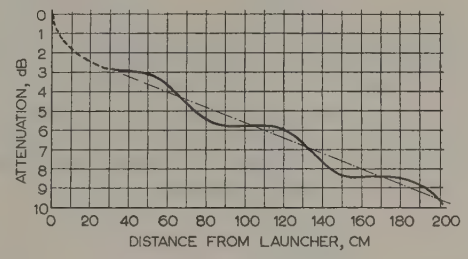

Fig. 13.—Interference pattern between direct and guided waves.

The result is plotted in Fig. 13 and it can be seen that a phase change of 2π between the two waves takes place every 66·6 cm. Since the free-space wavelength at 9 Gc/s is 3·33 cm, this distance corresponds to $20\lambda_g$. The guided wave, travelling at a reduced velocity, occupies one additional cycle in the same space, so that $n\lambda_0 = (n+1)\lambda_g$. Hence the ratio λ_0/λ_g is 20 : 21 or 0·95. Comparing this result with the calculated value of 0·99 (see Fig. 3) for the case $b/\lambda_0 = 0{\cdot}375$, it is found that the difference between the theoretical and measured values is rather large considering the order of magnitude involved. The explanation can be sought in the fact that dielectric and resistive losses as well as radiation losses were neglected in solving the characteristic equation.

Losses along the surface of the guide provide additional retardation of the wave and this would account for λ_0/λ_g being smaller than the calculated value. Since only a very small portion of the wave travels in the dielectric coating, the effect of dielectric loss is negligible, particularly in view of the fact that $\tan\delta$ is small for the material used. Resistive losses can account for some of the retardation, although radiation is believed to be the main cause.

Measurements to determine the attenuation along the guide lent support to this supposition. It can be seen from Fig. 13 that the attenuation corresponds to 4·0 dB/m which cannot all be due to resistive and dielectric losses, particularly since most of the energy travels in the space surrounding the guide. (The contribution of the direct wave in these measurements was small. This was established by measuring the received signal with and without the guide, the free-space signal being approximately 14 dB down on the guided signal except in close proximity to the dipole.)

(5) CONCLUSIONS

The existence of a first-order cylindrical surface wave has been proved and the feasibility of designing end-fire aerials utilizing this mode has been successfully demonstrated.

The properties of this wave, which is a hybrid mode, as well as those of any other higher-order mode can be studied by examining the characteristic equation, which has been derived for the general case. In solving it for specific cases, it was assumed that the wave mode is non-radiating (i.e. the radial propagation coefficient is a purely imaginary quantity) and that the longitudinal propagation is loss-free. These assumptions, although substantially correct, limit the validity of the results.

The range of conditions for which the characteristic equation can be solved, even allowing for the above simplifying assumptions, is at present severely restricted owing to the limitations imposed by available tables. In particular, it is not possible to predict the behaviour of cylindrical surface waveguides which are coated with dielectric materials having a substantially higher dielectric constant than was used by the author, i.e. compounds of titanium dioxide and barium and/or strontium which have been developed in recent years.[16]

The experimental work has been concerned only with basic, straightforward surface-wave aerials and adequate theories have been put forward to predict their radiation patterns. However, different constructions can be envisaged. Since the size of a surface-wave aerial of given gain is proportional to $1/\sqrt{(\epsilon - 1)}$, the arrival of high-dielectric-constant ceramic materials should make it possible to design high-gain surface-wave aerials, particularly for the microwave bands, which are physically much smaller than any conventional type of aerial.

A ceramic sleeve supported by a metal tube is one form of construction which is not only rigid, but is also inherently immune to great heat. Such surface-wave aerials can be built into the noses of supersonic aircraft, or rocket-propelled vehicles equipped with forward-looking radar, where the effect of aerodynamic heating prevents the use of protective covering which is normally required by microwave aerials forming an integral part of airframe structures. An aerial of tapered construction, fed from an internal waveguide by means of hole couplers, would combine desirable electrical properties with great mechanical strength and reduced wind resistance.

Complete freedom from side lobes, which is characteristic of short surface-wave aerials, was never achieved in practice, mainly because the very ineffective but convenient dipole method of launching the wave was used. The waveguide-transition type of launcher described in Section 3.3 is superior, as it is possible by proper design to eliminate direct radiation from the primary source. Further work on launching methods and their efficiency needs to be carried out if it is desired to establish the propagation characteristics of higher-order surface waves more accurately.

Although the work described in the paper had as its primary objective investigation into a new type of aerial, it has prompted research into higher-order surface waves and these have, in turn, given rise to many new problems. Further research into the losses associated with the propagation of the first-order surface wave is needed to determine the effect of regularly-spaced discontinuities on the surface impedance and hence the conditions under which such discontinuities may give rise to radiation.

The radiation loss that has been observed is attributed to a regular pattern of surface irregularities which may have led to radiation of the very loosely guided wave, particularly as λ_g/λ_0 was almost unity.

Other higher-order modes have not yet been investigated and the properties of the complete range of higher-order modes which a dielectric-coated cylinder can support still remain to be explored.

(6) ACKNOWLEDGMENTS

I am indebted to Mr. F. R. Robinson for checking the characteristic equation and the numerical results and to Dr. J. Brown for many valuable discussions during the preparation of the paper.

(7) REFERENCES

(1) Brown, J., and Spector, J. O.: 'The Radiating Properties of End-Fire Aerials', *Proceedings I.E.E.*, Paper No. 2216 R, January, 1957 (**104** B, p. 27).
(2) Kraus, J. D., and Williamson, J. C.: 'Characteristics of Helical Antennas Radiating in the Axial Mode', *Journal of Applied Physics*, 1948, **19**, p. 87.
(3) Halliday, D. F., and Kiely, D. G.: 'Dielectric-Rod Aerials', *Journal I.E.E.*, 1947, **94**, Part IIIA, p. 610.
(4) Kiely, D. G.: 'Dielectric Aerials' (Methuen, 1952).
(5) Stratton, J. A.: 'Electromagnetic Theory' (McGraw-Hill, 1941).
(6) Goubau, G.: 'Surface Waves and Their Application to Transmission Lines', *Journal of Applied Physics*, 1950, **21**, p. 1119.
(7) Goubau, M.: 'An Omni-directional Surface Wave Antenna', Congrès International des Circuits et Antennes Hyperfréquences, Paris, October, 1957, Paper No. 29.
(8) Sommerfeld, A.: 'Über die Fortpflanzung elektrodynamischer Wellen längs eines Drahtes', *Annalen der Physik und Chemie*, 1899, **67**, p. 233.
(9) Harms, D.: 'Elektromagnetische Wellen an einem Draht mit isolierender zylindrischer Hülle', *Annalen der Physik*, 1907, **23**, p. 44.
(10) Hondros, D.: 'Über elektromagnetische Drahtwellen', *ibid.*, 1909, **30**, p. 905.
(11) Dyott, R. B.: 'The Launching of Electromagnetic Waves on a Cylindrical Conductor', *Proceedings I.E.E.*, Paper No. 1374 R, November, 1952 (**99**, Part III, p. 408).
(12) Goubau, G.: 'On the Excitation of Surface Waves', *Proceedings of the Institute of Radio Engineers*, 1952, **40**, p. 865.
(13) Barlow, H. M., and Karbowiak, A. E.: 'An Investigation of the Characteristics of Cylindrical Surface Waves', *Proceedings I.E.E.*, Paper No. 1462 R, April, 1953 (**100**, Part III, p. 321).
(14) Astrahan, M. M.: Ph.D. Thesis, Northwestern University, Illinois, 1949.
(15) Hersch, W.: 'The Surface Wave Aerial', Ph.D. Thesis, London University, 1957.
(16) von Hippel, A. R. (Ed.): 'Dielectric Materials and Applications' (John Wiley, 1954).

(8) APPENDIX: DERIVATION OF THE CHARACTERISTIC EQUATION

In this Section the general characteristic equation of the first-order surface wave is determined and the method of solving it by systematic trial and error is described. Solutions are obtained for specific cases for which tables have been compiled[15] to assist with the numerical computations. These tables can be used for the solution of problems not considered in the paper.

The field equations (11) and (12) in Section 2.3 contain six arbitrary coefficients a_2, a_3, a_4 and b_2, b_3, b_4, which can be found by applying the boundary conditions requiring continuity of the ϕ- and z-components at $r = a$ and $r = b$. To simplify the writing the following notations are adopted:

$$a/b = c;\ k_2a = cV;\ k_2b = V;\ k_3b = N \text{ or } jW$$

A set of six equations in the a's and b's is then obtained as follows:

$$
\left.\begin{aligned}
&\text{At } r=a,\\
&E_{z2}=0 \quad a_2J_1(cV)+a_3Y_1(cV)=0\\
&E_{\phi 2}=0 \quad \frac{1}{c^2V^2}\Big\{\gamma[a_2J_1(cV)+a_3Y_1(cV)]\\
&\qquad\qquad +j\omega\mu_2cV[b_2J_1'(cV)\\
&\qquad\qquad +b_3Y_1'(cV)]\Big\}=0\\
&\text{At } r=b,\\
&E_{z2}=E_{z3} \quad a_2J_1(V)+a_3Y_1(V)=a_4H_1(N)\\
&H_{z2}=H_{z3} \quad b_2J_1(V)+b_3Y_1(V)=b_4H_1(N)\\
&E_{\phi 2}=E_{\phi 3} \quad \frac{1}{V^2}\Big\{\gamma[a_2J_1(V)+a_3Y_1(V)]\\
&\qquad\qquad +j\omega\mu_2V[b_2J_1'(V)+b_3Y_1'(V)]\Big\}\\
&\qquad\qquad =\frac{1}{N^2}[\gamma a_4H_1(N)+j\omega\mu_3Nb_4H_1'(N)]\\
&H_{\phi 2}=H_{\phi 3} \quad \left(\frac{-1}{V}\right)^2\Big\{j\omega\epsilon_2V[a_2J_1'(V)+a_3Y_1'(V)]\\
&\qquad\qquad -\gamma[b_2J_1(V)+b_3Y_1(V)]\Big\}\\
&\qquad\qquad =\left(\frac{-1}{N}\right)^2[j\omega\epsilon_3Na_4H_1'(N)-\gamma b_4H_1(N)]
\end{aligned}\right\} \quad (25)
$$

If eqns. (25) are written in the standard form so that corresponding terms in a's and b's are placed in the same order on the left-hand side of each equation, an array of six equations results in which the right-hand members are zero. As these equations are only consistent if the determinant of the coefficients of the a's and b's is zero. Determinant No. 1 must be solved:

This determinant is simplified in stages, the first being the introduction of a new set of variables to reduce the total number of variables, thus facilitating the numerical evaluation of the resulting expression, which involves a considerable amount of computational effort.

Substituting the symbols defined by eqn. (14) and multiplying or dividing the various rows and columns by suitable factors such as $J_1(V)$, $J_1'(V)$, $-Y_1(cV)$, $J_1'(cV)/cV$, γ/V^2, γ/c^2V^2 where appropriate, so that the new variables are introduced, results in the simplified form, Determinant No. 2.

By a process of pivotal condensation the determinant is reduced from a 6×6 to a 3×3 determinant which can be solved in the usual manner. The 3×3 determinant

$\frac{j\omega}{\gamma}\epsilon_3\Delta_3\Delta_5(\Delta_3-\Delta_4)-$ $\frac{j\omega}{\gamma}\epsilon_2\Delta_3(\Delta_3\Delta_7-\Delta_2\Delta_4)$	0	$\Delta_3(\Delta_3-\Delta_4)T$
T	$\frac{j\omega\mu_2}{\gamma}(\Delta_1\Delta_3\Delta_7-\Delta_2\Delta_4\Delta_6)$	$\frac{-j\omega\mu_3}{\gamma}\Delta_5$
0	$\Delta_1\Delta_3-\Delta_6\Delta_4$	-1

Determinant No. 1

a_2	a_3	a_4	b_2	b_3	b_4
$-J_1(cV)$	$-Y_1(cV)$	0	0	0	0
$-\frac{\gamma}{c^2V^2}J_1(cV)$	$-\frac{\gamma}{c^2V^2}Y_1(cV)$	0	$-\frac{j\omega\mu_2}{cV}J_1'(cV)$	$-\frac{j\omega\mu_2}{cV}Y_1'(cV)$	0
$J_1(V)$	$Y_1(V)$	$-H_1(N)$	0	0	0
0	0	0	$J_1(V)$	$Y_1(V)$	$-H_1(N)$
$\frac{\gamma}{V^2}J_1(V)$	$\frac{\gamma}{V^2}Y_1(V)$	$-\frac{\gamma}{N^2}H_1(N)$	$\frac{j\omega\mu_2}{V}J_1'(V)$	$\frac{j\omega\mu_2}{V}Y_1'(V)$	$-\frac{j\omega\mu_3}{N}H_1'(N)$
$\frac{j\omega\epsilon_2}{V}J_1'(V)$	$\frac{j\omega\epsilon_2}{V}Y_1'(V)$	$-\frac{j\omega\epsilon_3}{N}H_1'(N)$	$-\frac{\gamma}{V^2}J_1'(V)$	$-\frac{\gamma}{V^2}Y_1(V)$	$\frac{\gamma}{N^2}H_1(N)$

Determinant No. 2

a_2	a_3	a_4	b_2	b_3	b_4
Δ_3	1	0	0	0	0
0	0	0	$\Delta_1\Delta_3$	Δ_6	0
Δ_4	1	-1	0	0	0
0	0	0	Δ_4	1	-1
0	0	T	$\frac{j\omega\mu_2}{\gamma}\Delta_2\Delta_4$	$\frac{j\omega\mu_2}{\gamma}\Delta_7$	$\frac{-j\omega\mu_3}{\gamma}\Delta_5$
$\frac{-j\omega\epsilon_2}{\gamma}\Delta_2\Delta_4$	$\frac{-j\omega\epsilon_2}{\gamma}\Delta_7$	$\frac{j\omega\epsilon_3}{\gamma}\Delta_5$	0	0	T

after putting $\mu_3 = \mu_2 = \mu_0$, $\epsilon_3 = \epsilon_0$, $\epsilon_2 = \epsilon\epsilon_0$ and introducing $Q = \omega^2\mu_0\epsilon_0/\gamma^2$, is expanded to

$$[Q(\Delta_3 - \Delta_4)\Delta_3\Delta_5 - \epsilon Q\Delta_3(\Delta_3\Delta_7 - \Delta_2\Delta_4)][\Delta_1\Delta_3\Delta_7 - \Delta_2\Delta_4\Delta_6]$$
$$- Q\Delta_3\Delta_5^2(\Delta_1\Delta_3 - \Delta_4\Delta_6)(\Delta_3 - \Delta_4) + T^2\Delta_3(\Delta_3 - \Delta_4)(\Delta_1\Delta_3 - \Delta_4\Delta_6)$$
$$+ \epsilon Q\Delta_3\Delta_5(\Delta_1\Delta_3 - \Delta_4\Delta_6)(\Delta_3\Delta_7 - \Delta_2\Delta_4) = 0 \quad . \quad . \quad (26)$$

Simplifying and rearranging eqn. (26) yields the characteristic equation from which the properties of the first-order surface wave can be derived for any particular set of conditions.

$$Q\{(\Delta_1\Delta_3 - \Delta_4\Delta_6)(\Delta_3 - \Delta_4)\Delta_5^2 - (\Delta_1\Delta_3\Delta_7 - \Delta_2\Delta_4\Delta_6)(\Delta_3 - \Delta_4)\Delta_5$$
$$+ \epsilon[(\Delta_1\Delta_3\Delta_7 - \Delta_2\Delta_4\Delta_6)(\Delta_3\Delta_7 - \Delta_2\Delta_4)$$
$$- (\Delta_1\Delta_3 - \Delta_4\Delta_6)(\Delta_3\Delta_7 - \Delta_2\Delta_4)\Delta_5]\}$$
$$- T^2(\Delta_1\Delta_3 - \Delta_4\Delta_6)(\Delta_3 - \Delta_4) = 0. \quad . \quad . \quad (27)$$

All the Δ's with the exception of Δ_5 are functions of V and Δ_5 depends only on W;

Using the relationship $Z_1'(x) = Z_0(x) - \frac{1}{x}Z(x)$ reduces the Δ's as defined by eqns. (14) to functions which are tabulated. Thus

$$\left.\begin{aligned} \Delta_1 &= \frac{J_0(cV)}{cVJ_1(cV)} - \frac{1}{(cV)^2} & \Delta_5 &= \frac{H_0(jW)}{jWH_1(jW)} + \frac{1}{W^2} \\ \Delta_2 &= \frac{J_0(V)}{VJ_1(V)} - \frac{1}{V^2} & \Delta_6 &= \frac{Y_0(cV)}{cVY_1(cV)} - \frac{1}{(cV)^2} \\ \Delta_3 &= \frac{J_1(cV)}{Y_1(cV)} & \Delta_7 &= \frac{Y_0(V)}{VY_1(V)} - \frac{1}{V^2} \\ \Delta_4 &= \frac{J_1(V)}{Y_1(V)} \end{aligned}\right\} \quad (28)$$

Since N is a purely imaginary number it is replaced by jW.

For any particular value of c the above Δ's can now determined.

621.316.933.1 : 621.387

The Institution of Electrical Engineers
Monograph No. 364 M
Mar. 1960
©

THE CHARACTERISTICS OF THE TRIGATRON SPARK-GAP AT VERY HIGH VOLTAGES

By T. E. BROADBENT, M.Sc., Ph.D., Associate Member.

(*The paper was first received* 19*th August, and in revised form* 30*th October*, 1959. *It was published as an* INSTITUTION MONOGRAPH *in March*, 1960.)

SUMMARY

Curves are given showing the working range and time-lag characteristics of a trigatron spark-gap working in air at voltages up to 1 MV. It is shown that, for voltages of this magnitude, a single-stage trigatron spark-gap of suitable design provides a simple and convenient method of chopping the voltage at any required instant. Factors which affect the performance of the gap are discussed.

(1) INTRODUCTION

In a recent study of triggered spark-gaps[1–3] the performance of trigatrons[4] working in air at voltages up to 200 kV (d.c. and impulse) was investigated. Similar work using voltages up to 100 kV was carried out independently by Sletten and Lewis,[5] their results agreeing with those of the author. No information, however, has subsequently been published on the performance of single-stage trigatron spark-gaps at voltages in excess of 200 kV. Since the trigatron is of value in engineering applications as a voltage chopping gap the original investigation has been extended to cover voltages up to 1 MV. It is the purpose of the paper to report on the results obtained.

(2) REQUIREMENTS FOR SUCCESSFUL OPERATION

If the maximum direct voltage which a trigatron spark-gap will withstand without the trigger mechanism in operation is V_{DC}, the trigatron gap will break down over a range of voltage V_{DC} down to V_{min} each time the trigger pulse is applied. Thus V_{min} is the minimum voltage at which breakdown is ensured on the application of a trigger pulse. The region of voltage $V_{DC} - V_{min}$ therefore represents the range over which the gap will operate satisfactorily, and is termed the 'working range'. Expressed as a percentage of V_{DC}, the working range is

$$\frac{V_{DC} - V_{min}}{V_{DC}} \times 100 \text{ per cent}$$

Since a trigatron spark-gap is liable to spark over occasionally when held at voltages within a few per cent of V_{DC} (mainly owing to the presence of dust particles) it is desirable to have as high a working range as possible. Further, in order that the trigatron may be made to operate at any required instant (determined by the setting of a low-voltage circuit which delays the production of the trigger pulse) the time delay between the application of the pulse to the trigatron and the breakdown of its main gap should be negligible.

(3) EXPERIMENTAL EQUIPMENT

The trigatrons used in the investigation were constructed as shown in Fig. 1. Throughout the experiments (except where otherwise stated) the diameter of the trigatron spherical electrodes was 75 cm. These electrodes were of aluminium, and the gap

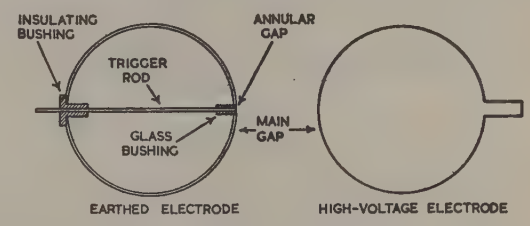

Fig. 1.—The trigatron spark-gap.

was arranged with its axis vertical, the sparking surface of the lower (earthed) sphere being about 6 ft from the ground. The diameter of the hole in the sparking surface was $\frac{5}{16}$ in, and the diameter of the silver-steel trigger rod was $\frac{1}{8}$ in. The main purpose of the glass bushing was to keep the rod central in the hole. A secondary purpose was that any corona produced across the radial face of the glass served to assist breakdown of the main gap.[4] Voltage was supplied from a generator giving up to 1 MV d.c. of either polarity and was measured to within ±5%. The time delay between the application of a voltage pulse to the trigger electrode and the breakdown of the main trigatron gap was measured to within 0·05 microsec, using a cathode-ray oscillograph of a type described previously.[6]

(4) EXPERIMENTAL RESULTS

(4.1) Working-Range Curves

Curves showing the working range as a function of gap spacing and V_{DC} are shown in Fig. 2. With the trigatron high-voltage electrode negative the working range is seen to be greater than 30% for values of V_{DC} up to 850 kV. With this electrode positive the working range is greater than 30% for values of V_{DC} up to 825 kV; the working range falls away more rapidly at values of V_{DC} greater than about 800 kV, but it is still as high as 19% with $V_{DC} = 935$ kV. The results of Fig. 2 thus show that, for a trigatron like that shown in Fig. 1 using 75 cm-diameter electrodes, a relatively high working range is obtained with both polarities for values of V_{DC} up to about 800 kV. With V_{DC} in the range 800–1 000 kV the working range with the high-voltage electrode negative is noticeably better than when this electrode is positive. Experiments show[1] that an increased working range occurs when the applied voltage is positive if the arrangement of the two main electrodes shown in Fig. 1 is reversed. The high-voltage electrode then contains the annular gap and the other main electrode is earthed. It is then necessary, however, to trigger the system through a capacitor capable of withstanding the full charging voltage, or to use a scheme of triggering in which there is no electrical connection between the pushbutton trigger control and the trigatron. In this system the light output from a flash tube actuates a photocell; the resulting electrical pulse is then amplified and used to fire the trigatron. The need for the high-voltage capacitor is thereby eliminated.

Correspondence on Monographs is invited for consideration with a view to publication.
Dr. Broadbent is in the Electrical Engineering Department, University of Manchester.

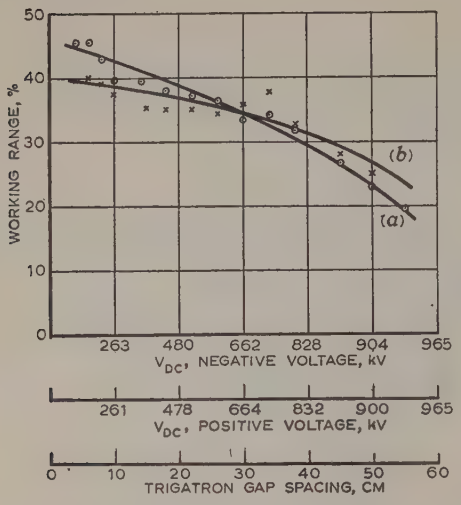

Fig. 2.—Working range curves for the trigatron shown in Fig. 1.

(*a*) –⊙– Positive voltage.
(*b*) –×– Negative voltage.
75 cm-diameter trigatron electrodes.

This triggering scheme has been tried in our laboratories and been found to work successfully. In our equipment the triggering pulse for the trigatron is derived from a hydrogen thyratron pulse-generating circuit. The anode voltage for the thyratron is obtained from an r.f. power supply operated from batteries. Batteries also supply the photocell, amplifier and thyratron filament. The complete triggering equipment, including batteries, is mounted inside the trigatron sphere, which, in this particular case, is 100 cm in diameter.

(4.2) Time-Lag Curves

Curves were obtained relating the time lag (between the application of a voltage pulse to the trigger electrode and the breakdown of the main trigatron gap) with voltage, for a number of trigatron gap spacings. Preliminary experiments were carried out first with 25 measurements per experimental condition and then with only ten measurements. The mean time lag obtained from ten measurements did not differ from that obtained from 25 measurements by more than 8·8% in any single case. This small difference is not significant on a logarithmic time scale, and it was therefore considered sufficient to determine and average ten time lags for each experimental condition. Much saving in time was therefore achieved. The results are shown in Fig. 3, each point on the curves being the arithmetic mean of ten time-lag measurements. The maximum and minimum time lags are represented on the curves by horizontal lines through the points. With the trigatron high-voltage electrode either positive or negative the mean time lag to breakdown is less than 1 microsec over most of the operating range of the trigatron for the whole range of trigatron gap spacings investigated. It is also seen that, for trigatron gap spacings up to about 20 cm (corresponding to $V_{DC} \simeq 480$ kV), the mean time lag is less than 0·1 microsec for a voltage range of 85–100% of V_{DC}. Thus the trigatron shown in Fig. 1, using 75 cm-diameter electrodes, operates rapidly (within 0·1 microsec) over a 15% range of voltage for gap spacings up to about half an electrode radius. It operates less rapidly (within 1 microsec) over a slightly lower voltage range for gap spacings greater than this figure.

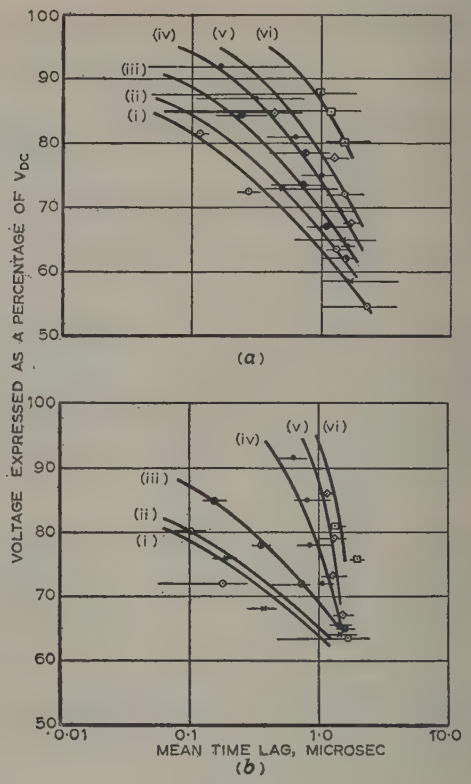

Fig. 3.—Voltage/time-lag curves for the trigatron shown in Fig. 1.

(*a*) Positive voltage.
(*b*) Negative voltage.
(i) –⊙– 4 cm gap spacing.
(ii) –×– 10 cm gap spacing.
(iii) –⊗– 18 cm gap spacing.
(iv) –●– 26 cm gap spacing.
(v) –◊– 38 cm gap spacing.
(vi) –⊡– 50 cm gap spacing.
75 cm-diameter trigatron electrodes.

(4.3) Path of the Trigatron Spark

An interesting effect was found to occur in connection with the path taken by the spark discharge between the spherical electrodes of the trigatron gap. Each spark appeared to consist of two parts. The first was a straight part along the axis of the gap and reaching from one electrode to a distance of 10–30% of the gap length. The remainder was of the familiar tortuous nature of a spark discharge. The straight part of the spark path was always that part adjacent to the anode. The effect was sufficiently pronounced as to enable the experimenter to determine immediately which of the trigatron electrodes was the anode simply by observation of the spark path. Similar observations have previously been made[2] using smaller trigatrons at voltages up to 200 kV.

It has been previously shown[3,5] that a streamer mechanism may be operative in the breakdown of the trigatron gap, and a possible explanation of the effect described above is that breakdown depends on the propagation of a negative streamer. When this streamer approaches the anode a positive streamer is initiated at the anode and proceeds towards the negative streamer. The streamers meet at a point in the mid-gap region, giving a change in direction of the spark path at this point. The theory would explain the straight nature of that part of the spark near the anode, since the negative streamer would con-

stitute a conducting path. At the instant propagation of the positive streamer begins the system would be approximately equivalent to a very high over-voltage on a point-plane gap, and experiments with high over-voltages on point-plane gaps show that straight spark paths do, in fact, occur. Similar theories concerning change in the direction of spark paths have previously been given in connection with lightning discharges, in which it is suggested that positive streamers might grow from the ground to meet the descending negative leader stroke.

(4.4) Effect of Varying the Parameters

Tests were carried out to find whether the results shown in Figs. 2 and 3 were significantly modified by varying the experimental parameters. The results of these experiments are described in the following Sections.

(4.4.1) Diameter of Trigatron Electrodes.

Experiments with trigatrons having electrode diameters of 15, 25 and 75 cm showed that, in general, when the trigatron gap spacing exceeded the electrode radius by more than a few per cent, the working range began to fall away rapidly, particularly with the high-voltage electrode positive. It is therefore necessary to use electrodes sufficiently large to ensure a relatively uniform field in the gap.

Preliminary experiments were carried out using a trigatron in which the earthed electrode was hemispherical instead of spherical, as in Fig. 1. The diameter of the trigatron electrodes used in these experiments was 25 cm. The working range occurring with the trigatron having a hemispherical electrode was up to about 15% less than that obtained for the trigatron having both electrodes spherical. This was due to the low values of V_{DC} which occurred using the hemispherical earthed electrode. Breakdown frequently took place to the edge of the hemisphere instead of to the spherical sparking surface.

Experiments were also carried out to investigate the effect of electrode diameter on the time lag to breakdown. These showed that, for a given voltage, the time lag to breakdown decreased rapidly with increasing electrode diameter. By the use of a trigatron electrode diameter of, say, 100 cm instead of 75 cm, the mean time lags shown in Fig. 3 could be reduced to less than half their original value.

(4.4.2) Trigger-Pulse Magnitude.

The effect of varying the trigger pulse voltage was investigated, for both polarities on the main gap, using a range of steep-fronted long-tailed trigger pulses from 5 to 12 kV peak. Negligible change in working range or in time lag to breakdown occurred. The energy of the trigger pulse was also varied, using a constant voltage pulse of 10 kV peak with a range of discharge capacitances from 1000 pF to 0·15 μF. Again the change in working range and time lag to breakdown was found to be negligible.

(4.4.3) Trigatron Annular Gap Configuration.

The effect of increasing the diameter of the trigatron annular gap was investigated using a trigatron having electrodes 15 cm in diameter operating at voltages up to 200 kV. Little change in working range or time lag was produced by increasing the diameter of the annular gap, provided that the distance from the central rod to the periphery of the hole was kept constant by using a trigger rod of greater diameter.

With a rod of fixed diameter the working range increased by several per cent as the diameter of the hole in the sparking surface of the main electrode was increased, but this effect was offset by the increased trigger pulse required to break down the annular gap.

When the trigger electrode projected through the hole by about $\frac{1}{32}$ in a slightly increased working range occurred, even though V_{DC} decreased slightly.

(4.5) Impulse Operation of Trigatron

Measurements were carried out with impulse voltages up to 200 kV peak applied to the high-voltage electrode of a trigatron, instead of having the normal direct voltage on this electrode. The wavefront time (to peak value) of the impulses was 0·1 microsec, and the wavetail time (to half value) 3 millisec. A trigatron having electrodes 15 cm in diameter was used in this experiment. With both positive and negative impulse voltages applied to the trigatron the working range was about the same as with direct applied voltage. The time lags to breakdown were found to be about the same whether the voltage applied to the trigatron was direct or impulse.

(5) CONCLUSIONS

The experiments described in the paper show that trigatrons working in air may be successfully used with direct voltages up to 1 MV provided that the electrode diameter is adequate. The trigger pulse need not be more than about 10 kV in magnitude. There appears to be no reason why trigatrons should not be used for voltages of several megavolts provided that the electrode spacing does not greatly exceed the sphere radius. Experiments indicate that the trigatron works equally well with direct or impulse applied voltage, and the results shown in Figs. 2 and 3 should therefore give an indication of the performance which would be expected with the trigatron operating as an impulse-voltage chopping gap in transformer testing or other applications. The time lags shown in Fig. 3 could be much reduced by the use of trigatron electrodes of larger diameter. Since the trigatron can be fired at will at any predetermined instant (the firing time measured from the application of the trigger pulse to the breakdown of the main gap being small) it provides an attractive alternative to the conventional rod-gap as a voltage chopping device. The single-stage trigatron may also be used as a surge diverter in fundamental research work at high voltages. This application of the trigatron has been fully investigated and is described elsewhere.[7]

(6) ACKNOWLEDGMENTS

The author wishes to thank Dr. R. Cooper for his interest in this work, which was carried out in the Electrical Engineering Department of Manchester University.

(7) REFERENCES

(1) Broadbent, T. E.: 'The Characteristics and Breakdown Mechanism of Triggered Spark Gaps in Air', Ph.D. Thesis, University of Manchester, 1955.

(2) Broadbent, T. E.: 'Path of the Trigatron Spark', *Nature*, 1956, **178**, p. 872.

(3) Broadbent, T. E.: 'The Breakdown Mechanism of Certain Triggered Spark Gaps', *British Journal of Applied Physics*, 1957, **8**, p. 37.

(4) Craggs, J. D., Haine, M. E., and Meek, J. M.: 'The Development of Triggered Spark-Gaps for High-Power Modulators', *Journal I.E.E.*, 1946, **93**, Part IIIA, p. 963.

(5) Sletten, A. M., and Lewis, T. J.: 'Characteristics of the Trigatron Spark-Gap'. *Proceedings I.E.E.*, Monograph No. 193 M, 1957 (**104** C, p. 54).

(6) Waring, S., and Murphy, B.: 'A Portable High-Speed Cathode-Ray Oscillograph', *Journal of Scientific Instruments*, 1953, **30**, p. 469.

(7) Broadbent, T. E., and Fernandez, A.: 'Surge Diverters using Trigatrons', *ibid.*, 1959, **36**, p. 452.

621.396.677.71

The Institution of Electrical Engineers
Monograph No. 365 E
Mar. 1960
©

AN EXPERIMENTAL STUDY OF THE SLOT AERIAL AND THE THREE-ELEMENT COLLINEAR ARRAY OF SLOT AERIALS

By RONOLD KING, Ph.D., and GILBERT H. OWYANG, Ph.D.

(*The paper was first received 27th June, and in revised form 30th November*, 1959. *It was published as an* INSTITUTION MONOGRAPH *in March*, 1960.)

SUMMARY

The principle of complementarity is reviewed with particular reference to its application to the study of slot transmission lines and slot aerials. The conventional techniques for making measurements on transmission lines are shown to be applicable to a two-slot line that is used to centre-drive a slot aerial. The complementary normalized impedance of such an aerial as a function of its half length, and the distributions of the electric and magnetic field along it, have been measured and are described. The experimental results for the slot aerial are compared with the approximately complementary ones derived theoretically for a centre-driven cylindrical aerial. The effect of the finite thickness of the earth screen in which the slot line and aerial are cut is discussed. A similar study is described for a three-element collinear array of slot aerials.

(1) INTRODUCTION

As pointed out by Booker,[1] the electromagnetic or vector form of Babinet's principle for a plane screen differs from the corresponding principle in optics. The more general principle of complementarity was formulated by Booker,[1] Copson,[2] Meixner[3] and, in a compact vector form, by Huang.[4] Its application to slot aerials are discussed by Booker,[1] Bailey,[5] and Uda and Mushiake.[6] In his description of the resonant slot as the complement of the strip dipole, Booker, in Fig. 3 of Reference 1, pictures the former as a narrow rectangular aperture in a conducting surface excited by a generator connected across the centre of the aperture, and the latter as a rectangular conducting strip that is cut in two and has a similar generator connected in series between the halves. Actually, these generators and their connections are complementary only in a schematic sense. The practical feeding device represented, for example, by Fig. 3 of Reference 5 to be the 'slot equivalents' of a two-strip transmission line that centre drives a strip dipole or folded diple is not complementary at all. It consists of a two-wire line perpendicular to, and with the ends of its two wires connected to, the conducting plane, one on each side of the centre of the slot aerial. Evidently, such a feeder violates the fundamental requirement for complementarity, namely that all metal surfaces must lie in one plane. Significantly, none of the other well-known methods of feeding a slot aerial, such as a waveguide or cavity covering one side, or the inner conductor of a coaxial line connected across its centre, is in any true sense the complement of a flat strip line. Indeed, no study of the circuit properties of a complementary radiating and feeding system appears to have been made. It follows that, from a practical point of view, all discussion of the complementary impedances of complementary aerials is academic so long as the feeding system and the driving connections are not complementary structures.

If a flat strip dipole that is centre-driven by a two-strip transmission line is constructed by cutting from a sheet of metal, the aperture left in the sheet is a slot aerial centre-driven by a two-slot line. The two transmission lines and aerials would be truly complementary systems if the metal sheet could have been infinite in extent, perfectly conducting and of zero thickness.

The purpose of the paper is to report on an investigation of the circuit properties of a slot aerial and its feeding two-slot line that are cut in a sheet of aluminium $\frac{1}{4}$ in thick and approximately 6×12 ft in area. The two-slot line is $7\frac{1}{2}$ ft long with slots $\frac{1}{4}$ in wide and separated $\frac{3}{4}$ in between centres. The operating frequency is 750 Mc/s. The paper is not intended to provide an experimental check of the principle of complementarity. Within its postulates the principle is rigorous and requires no verification. This is fortunate, since the assumed conditions can never be met exactly. However, the degree to which it provides a useful approximation when applied to structures made of metal sheets that are finite in extent and moderately thick is of practical interest. Since a general theoretical analysis is difficult, an experimental approach is indicated. If a two-slot line can be used to measure the circuit properties of slot aerials in flat sheets, it can also be used to study the circuit properties of slots in curved, bent or twisted sheets. To these the principle of complementarity has no application and no theory is available.

(2) THEORETICAL BACKGROUND

In the analytical formulation of the general principle of complementarity for a plane it is convenient (but not necessary) to introduce fictitious densities of magnetic charge and current and equally fictitious perfect magnetic conductors. This is accomplished by the simple artifice of arbitrarily adding such densities at appropriate points in the Maxwell equations and the associated boundary conditions when expressed in terms of the $\boldsymbol{E}$ and $\boldsymbol{H}$ vectors. Consider a group of perfect electric conductors S_1, S_2, . . . and perfect magnetic conductors S_1^*, S_2^*, . . . in the form of infinitely thin strips of any shape lying in a single plane. They are surrounded by a homogeneous medium that is characterized by the permeability μ and complex permittivity $\boldsymbol{\epsilon} = \epsilon - j\sigma/\omega$, where ϵ is the permittivity and σ the conductivity. In this medium the Maxwell equations have their usual form with no volume densities appearing explicitly. The boundary conditions at the surfaces of the conductors are

$$\hat{n} \times \boldsymbol{E} = \hat{n} \cdot \boldsymbol{H} = 0; \ \hat{n} \cdot \boldsymbol{E} = -\eta/\epsilon, \ \hat{n} \times \boldsymbol{H} = -\boldsymbol{J} \text{ on } S_1^*, S_2^*, \ldots \quad (1)$$

$$\hat{n} \times \boldsymbol{H} = \hat{n} \cdot \boldsymbol{E} = 0; \ \hat{n} \cdot \boldsymbol{H} = -\eta^*/\mu, \ \hat{n} \times \boldsymbol{E} = \boldsymbol{J}^* \text{ on } S_1, S_2, \ldots \quad (2)$$

where $\hat{n}$ is a unit outward normal at the surface concerned, η and $\boldsymbol{J}$ are the surface densities of electric charge and current, and η^* and $\boldsymbol{J}^*$ are the corresponding fictitious magnetic densities.

If the electromagnetic field is considered in two parts, one of which is generated by the electric and the other by the magnetic

Correspondence on Monographs is invited for consideration with a view to publication.
Dr. King is, and Dr. Owyang was formerly, at the Gordon McKay Laboratory, Harvard University, Massachusetts, U.S.A.
Dr. Owyang is at the University of Michigan, Ann Arbor, Michigan, U.S.A.

currents and charges, it follows directly that an interchange of the electric and magnetic conductors in a given system, together with a change of the electric and magnetic sources according to

$$J_2 = -\zeta_e^{-1} J_1^*, \quad \eta_2 = -\zeta_e^{-1}\eta_1^* \quad . \quad . \quad . \quad (3a)$$

$$J_2^* = \zeta_e J_1, \qquad \eta_2^* = \zeta_e \eta_1 \quad . \quad . \quad . \quad . \quad (3b)$$

requires the electromagnetic fields to be related as follows:

$$E_2 = -\zeta_e H_1, \; H_2 = \zeta_e^{-1} E_1 \quad . \quad . \quad . \quad (4)$$

where the subscripts 1 and 2 indicate the fields before and after the interchange, respectively, and $\zeta_e = (\mu/\epsilon)^{1/2}$.

If the perfectly conducting strips of electric and magnetic conductor are all in the plane $z = 0$, the Cartesian components of the electromagnetic field may be separated into two mutually independent groups that have opposite symmetry with respect to this plane. The E-symmetrical and H-antisymmetrical part of the total electromagnetic field (E, H) is denoted by (E_s, H_a), and the H-symmetrical and E-antisymmetrical part by (E_a, H_s). The vector $\mathbf{A}_s$ is said to be symmetric with respect to the plane $z = 0$ when A_z is an odd function, and A_x and A_y are even functions of z; the vector A_a is antisymmetrical in z when A_z is even and A_x and A_y odd. It is readily verified that the surface currents J_a^* and J_s maintain an E-symmetrical and H-antisymmetrical field, the surface currents J_s^* and J_a an H-symmetrical and E-antisymmetrical field. At the plane of symmetry the E-symmetrical and H-antisymmetrical field satisfies the boundary conditions of a perfect magnetic conductor; while the H-symmetrical and E-antisymmetrical field satisfies the boundary conditions of a perfect electric conductor. A configuration of conductors in the plane $z = 0$ that is excited so that its electromagnetic field (E_1, H_1), is E-symmetrical and H-antisymmetrical is the *dual* of another configuration of conductors in this plane that is excited so that its field (E_2, H_2) satisfies eqn. (4). Evidently the field (E_2, H_2) is H-symmetrical and E-antisymmetrical.

Since several duals may be constructed for a given structure, distinguishing names are required. The circuit of ordinary conducting strips [Fig. 1(*a*)] is the *electric strip circuit* or simply

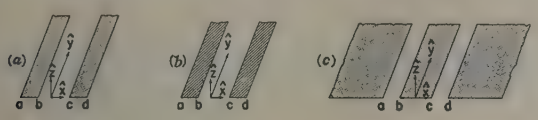

Fig. 1.—Complementarity between strip and slot circuits.

(*a*) Electric circuit or electric strip circuit.
Original (or physical dual).
Field: E symmetry with respect to $z = 0$ plane.
(*b*) Fictitious magnetic or magnetic strip circuit.
Ideal or fictitious dual.
Field: H symmetry with respect to $z = 0$ plane.
(*c*) Slot circuit.
Physical dual (or original).
Field: E symmetry with respect to $z = 0$ plane.

the *electric circuit*. The complementary circuit made of fictitious magnetic strips [Fig. 1(*b*)] is the *fictitious magnetic circuit* or *magnetic strip circuit*. The complementary circuit obtained by cutting slots in a perfectly conducting surface [Fig. 1(*c*)] is the *slot circuit*. The dual obtained by replacing a given original configuration of conductors by its complement is called the *physical dual*. The duality of a system of electric conductors and a similar system of magnetic conductors is termed *ideal* or *fictitious*. The magnetic quantities used for fictitious dual networks are assigned the conventional names preceded by the word 'magnetic', and an asterisk is attached to the symbol. The quantities used for the slot circuit are preceded by the word 'complementary', and their symbols are conventional but primed.

Because the same differential equation applies to complementary quantities in the two-slot line, the two-strip line and the magnetic strip-line, it is clear that the magnetic current and potential difference along the magnetic strip-line, and the complementary current and potential difference along the two-slot line may be described by distribution and resonance curves[7] in a manner similar to that conventionally used for the corresponding quantities along a two-wire line. Such curves may be obtained experimentally for the two-slot line by suitable movable probes, and used to determine the apparent complementary terminal impedance of a complementary load such as a slot aerial.

Since the impedance of a given element is completely determined by its physical configuration and the distribution of current, the complementary normalized admittance of a configuration of slots should be exactly the same as the normalized impedance of the physical dual. Hence the input impedance of a strip antenna driven by a two-strip line must be equal to the normalized input admittance of its physical dual multiplied by the characteristic impedance of the two-strip line.

The instantaneous electromagnetic field of a two-strip line is shown schematically in Fig. 2, and the complementary field of a two-slot line is shown in Fig. 3. The indicated distributions of the field are for resonant lines at the instant $t = 0$ (on the left) when the magnetic and complementary electric fields are at a maximum, and at the instant $t = T/4$ (on the right) when the electric and complementary magnetic fields are at a maximum. It is seen that the H-field encircles each conducting strip of the two-strip line just as the complementary E'-field encircles each slot of the two-slot line, except that the E-field reverses its direction when crossing the plane of symmetry of the two-slot line. The H'-field encircles the central conductor of the two-slot line in the same manner as the E-field encircles the air-gap between the conductors of the two-strip line, except that the E-field reverses its direction when crossing the strips.

The electromagnetic field and the distributions of current and charge along an infinitely thin and very narrow strip aerial when driven by a two-strip line are also shown in Fig. 2. The field and the current are essentially like those along a very thin cylindrical aerial. They are shown at the instants of maximum current ($t = 0$) and maximum charge ($t = T/4$). The complementary electromagnetic field and the distributions of complementary current and charge along a very narrow slot aerial when driven by a two-slot line are shown in Fig. 3. These figures indicate that the H-field encircles the strip antenna while the E'-field encircles the slot. However, the E'-field is oppositely directed on the two sides of the plane of symmetry, and the H-field is not. The lines of the H'-field emerge from one half of the slot and enter the other half; similarly, the lines of the E-field emerge from both sides of one-half of the strip antenna and end on both sides of the other half. It is seen that the distribution of the surface density of current (charge) along the ideal strip aerial is the same as the distribution of the complementary surface density of charge (current) along the physical dual, the slot aerial in an ideal earth-plane.

(3) SLOTS IN SHEETS OF FINITE THICKNESS AND FINITE EXTENT

In Figs. 2 and 3 the electromagnetic field along infinitely thin strips and along slots in earth-planes of zero thickness and infinite size are shown schematically. These are the configurations to which the principle of complementarity applies rigorously, but they are not realizable in practice. It is to be expected that, when strips and sheets have a small thickness and the latter are large but finite in size, the general features of complementarity

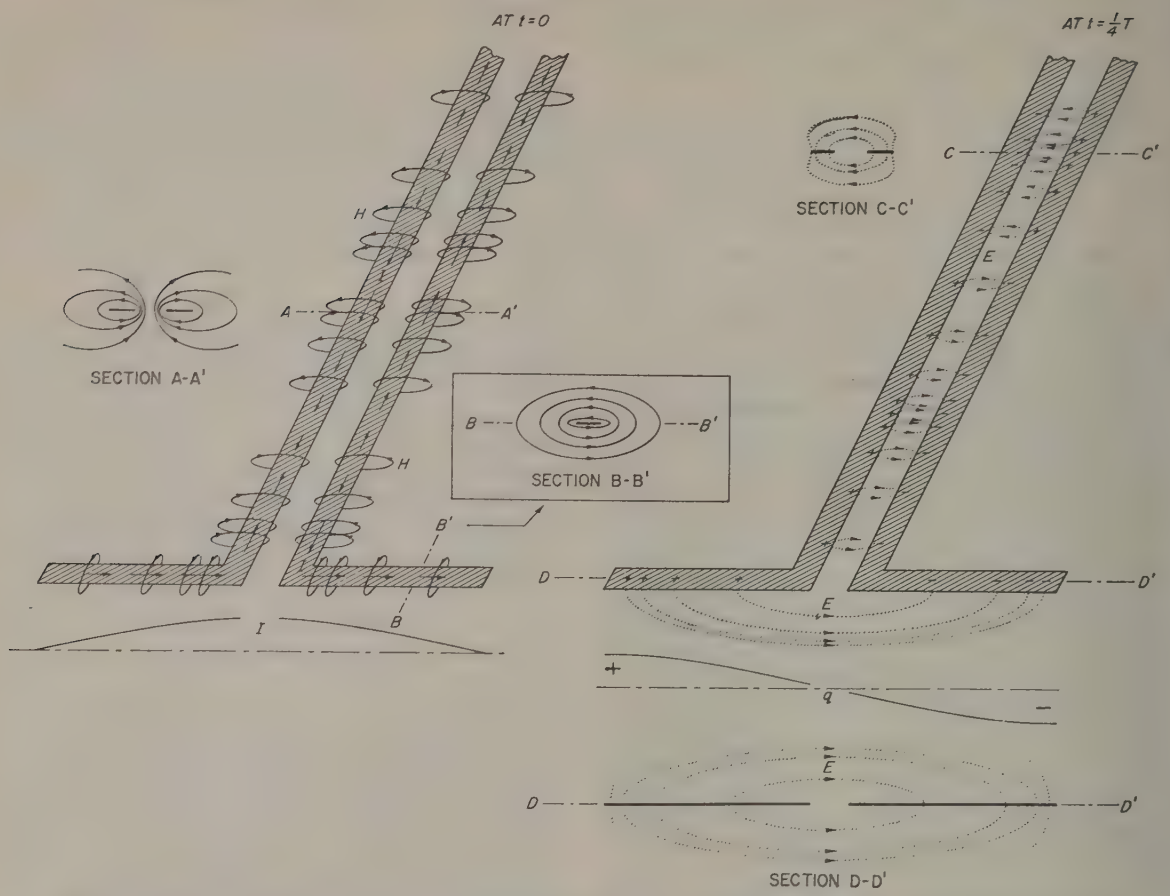

Fig. 2.—Schematic of the instantaneous electromagnetic field of a two-strip line and a narrow strip aerial at two instants of time one-quarter of a period apart.

Some of the field lines in the immediate vicinity of the aerial are shown.

must continue to be valid, but that there will be local differences in the fields and the distributions of current and charge. These may be expected to have an effect on the apparent impedance of both slot and strip aerials.

The effect of the finite thickness of the metal on the properties of a closely spaced and sufficiently long transmission line consisting of either metal strips or slots in a metal sheet may be determined in principle. Since the field in the transverse plane obeys Laplace's equation, it may be studied with the help of methods familiar from electrostatics. Except for wide spacing of strips and slots the rigorous solution of the transverse problem involves very complicated functions such as hyperelliptic integrals. These have not been evaluated. If the thickness is very small compared with the width of the strips or slots and their separation, an approximate solution may be obtained by a first-order perturbation method. This has been applied by Owyang and Wu[8] to determine the resistance per unit length for both the very thin strip line and the two-slot line in a very thin earth screen. When the cross-section of the strips in a two-strip line is square and they are sufficiently widely separated, the width, w, of equivalent infinitely thin strips is $2{\cdot}36s$, where s is the side of the square. From the circuit point of view the only difference between a strip or slot line when the metal has a small thickness and when it has zero thickness is a change in the line constants, and hence in the characteristic impedance. A schematic representation of the transverse electric fields between conductors of zero thickness and those of finite thickness is shown in Fig. 4. In the latter case [see Fig. 4(*b*)] lines of the E-field begin and end on charges on the side surfaces in addition to those that begin and end on the top and bottom. For a given separation, this increases the capacitance per unit length between the two sheets. Alternatively, a slot in a sheet of zero thickness must be narrower in order to have the same capacitance per unit length as a slot in a sheet of finite thickness.

The difference between a two-slot transmission line in an earth-plane that is infinite and one that is very large compared with the distance between the slots is insignificant owing to the very rapid decay of the field along the earth-plane in directions transverse to the slots.[9] A comparison of the transverse magnetic fields in the two cases is shown in Fig. 5. When the earth screen is infinite, the magnetic lines extend to infinity as indicated in Fig. 5(*a*) instead of encircling the finite outer conductors as in Fig. 5(*b*). However, in the vicinity of the slots there is virtually no difference between the field when the earth screen is infinite and when it is very wide compared with the width of the central strip.

The problem of the dependence of the properties of strip and slot aerials on the finite thickness of the metal from which they are cut is much more serious than for the corresponding strip and slot transmission lines. This is also true of the effect of

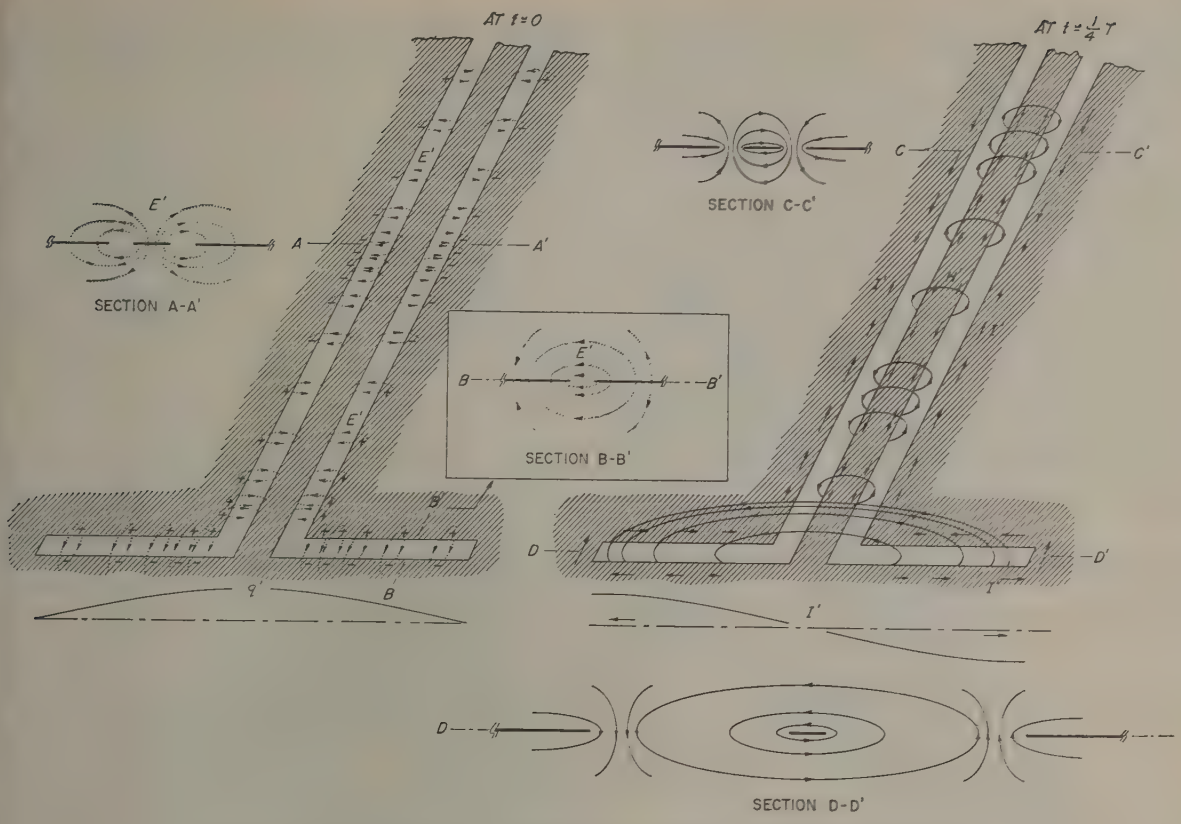

Fig. 3.—As in Fig. 2, but for a complementary two-slot line and a narrow slot aerial.
Some of the field lines in the immediate vicinity of the aerial are shown.

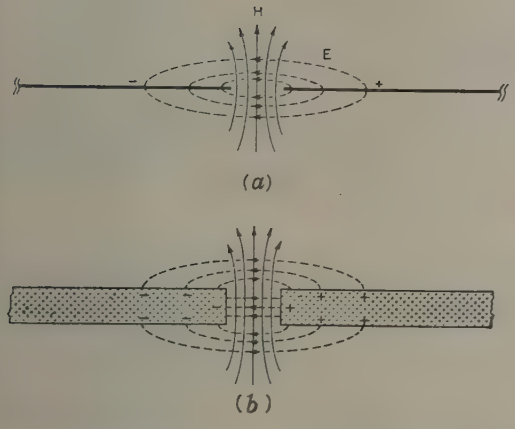

Fig. 4.—Schematic representation of the transverse electromagnetic field between the edges of two conductors.
(*a*) Infinitely thin.
(*b*) Finite thickness.

the finite size of the earth screen surrounding a slot aerial. Actually, there is no accurate solution to the problem of the flat strip aerial driven from a two-strip line for either zero or finite thickness of the conductor. The same is true of the slot aerial driven from a two-slot line in an earth screen of zero or finite thickness and infinite or finite extent. The most closely

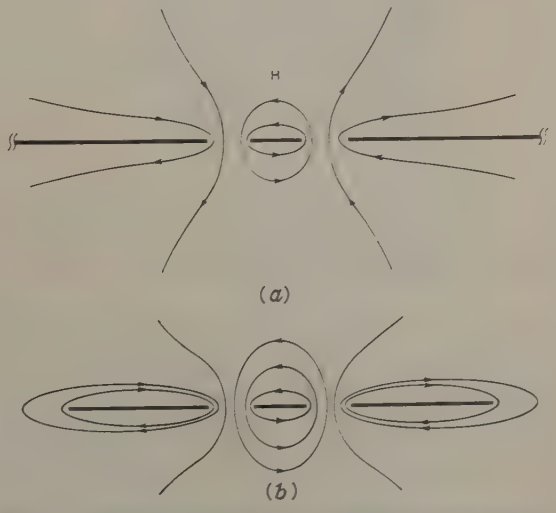

Fig. 5.—Schematic illustrating the transverse magnetic field in a section of a two-slot line.
(*a*) Infinite earth-plane.
(*b*) Finite earth-plane.

related configuration for which a good approximate solution is available is the cylindrical dipole of circular cross-section when driven from a two-wire line[10] or by a δ-function generator.[11] For such a dipole, distributions of current and charge, driving-point impedances and field patterns are available, both theoretically derived and measured (see Reference 10, Chapters II and V and Reference 12). Moreover, it has been shown (see Reference 10, p. 15, and Reference 13) that the theory of the cylindrical aerial with a circular cross-section may be extended approximately to cylinders with non-circular cross-sections if an equivalent radius is introduced. In this manner an approximate solution to the problem of the strip aerial of zero thickness may be obtained, and, by complementarity, of the slot aerial in an earth screen of zero thickness and infinite extent. However, there is no theory that permits the quantitative correlation of the properties of a slot aerial in a physically available earth screen with those of a similar slot in an ideal earth-plane other than the definition of an approximately equivalent width. Except for this purpose, estimates based on electrostatic considerations have no general application, since the wave equation and not Laplace's equation is involved.

(4) COMPLEMENTARY NORMALIZED INPUT IMPEDANCE OF A SLOT AERIAL

The slot aerial to be studied is driven by a two-slot transmission line as shown in Fig. 6. The earth-plane in which the line

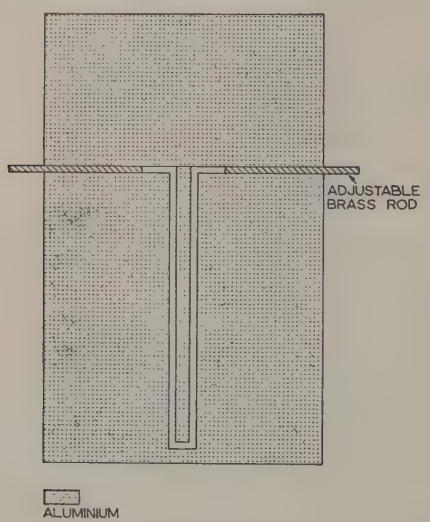

Fig. 6.—Arrangement of the two-slot line and the slot aerial in the ground screen.

Dimensions of the ground screen. 12 ft × 6 ft × ¼ in. The two-slot line is 7½ ft ong with slots ¼ in wide and separated ¼ in between centres.

and aerial are cut is made of three sheets of aluminium ¼ in thick mounted on a wooden frame half way between the third floor of the laboratory and the ceiling 12 ft above it. The adjustable length of the slot aerial is determined by the position of the square brass rods that slide in the slot. Good electrical contact between the rods and the sheets is assured with silver paint and aluminium foil. The edges of the sheets along the slot line and the slot aerial are slotted to permit a very small shielded loop to travel as a probe along the full length (7½ ft) of the two-slot transmission line and a second such probe to travel the length of the aerial. An overhead probe, which may be either a small shielded loop or a short dipole, is also available for exploring the electromagnetic field at all points over the surfaces of the aluminium sheets and over the slots at any desired height. A more detailed description of the apparatus is given in References 9 and 14.

The complementary normalized input impedance of the slot aerial was measured at a frequency of 750 Mc/s by conventional techniques that involve the experimental determination of the width of the distribution curve of the complementary current along the slot line at a certain power level above the minimum[15] and the shift in the position of a minimum in this curve. The half-lengths of the slot aerial were varied from 2·3 cm ($\simeq 0{\cdot}05\lambda$) to 25·3 cm ($\simeq 0{\cdot}625\lambda$). Since the minimum of the distribution curve is usually immersed in noise, its width may be measured at two different convenient power levels.[15] The associated standing-wave ratio, S, has the form[15]

$$S = \left[1 + \frac{4(p^2 - 1)}{\beta_0^2(w_2^2 - p^2 w_1^2)}\right]^{1/2} \quad . \quad . \quad . \quad . \quad (5)$$

where p^2 is the ratio of the power levels, w_1 and w_2 are the widths of the distribution curve corresponding to the two power levels, and $\beta_0 = 2\pi/\lambda$.

The measured complementary normalized input impedance of the slot aerial as a function of its half-length, h, is shown on a Smith chart in Fig. 7. The corresponding normalized resistances and reactances are shown in Fig. 8. For comparison and later discussion the theoretical normalized input admittance, susceptance and conductance of a cylindrical aerial with radius equal to the equivalent radius of a flat strip of width $w = \frac{1}{4}$ in are also shown on these Figures. The normalizing factor used is the characteristic impedance, $Z_c = 298{\cdot}5$ ohms, of an infinitely thin strip-line which would be the physical dual of the two-slot line actually used in the measurements if this had been cut in an earth screen of zero thickness and infinite extent. The corresponding measured curves for the slot aerial and the theoretical curves for the cylindrical aerial are similar but displaced slightly along the $\beta_0 h$ axis, and they differ by a scale factor. The measured impedances of the slot aerial correspond approximately to the theoretical admittances of a cylindrical aerial that has a half-length about 0·64 cm or $0{\cdot}016\lambda$ shorter than the slot and an admittance that is normalized with a characteristic impedance of about 343 ohms instead of the value 298·5 ohms actually used. It must be emphasized that the experimental and theoretical curves in Figs. 7 and 8 apply to physically different and theoretically uncorrelated configurations for which a resemblance may be anticipated but no equivalence has been established. This is discussed later.

(5) DISTRIBUTION OF THE COMPLEMENTARY ELECTRIC FIELD AND CHARGE ALONG THE SLOT AERIAL

The distributions of the E'-field along slot aerials of various lengths were measured by moving a short transversely orientated dipole along the slot at a small distance above it. The probe was connected through a balun to a stiff coaxial line that extended to the movable overhead carriage. A sensitive superheterodyne receiving system was used.

The measured values of the relative amplitude and the relative phase of the distributions of the E'-field along one-half of the slot aerial are shown in Fig. 9. Since the surface density of charge on the edges of the slot is proportional to the normal component of the electric field, the curves in Fig. 9 are also a measure of the distributions of electric charges along the slot. The amplitude of the E'-field varies approximately sinusoidally along the slot, except near the junction of the slot aerial and the slot transmission line and near the end of the slot. In the region near the junction the probe measured the average of a

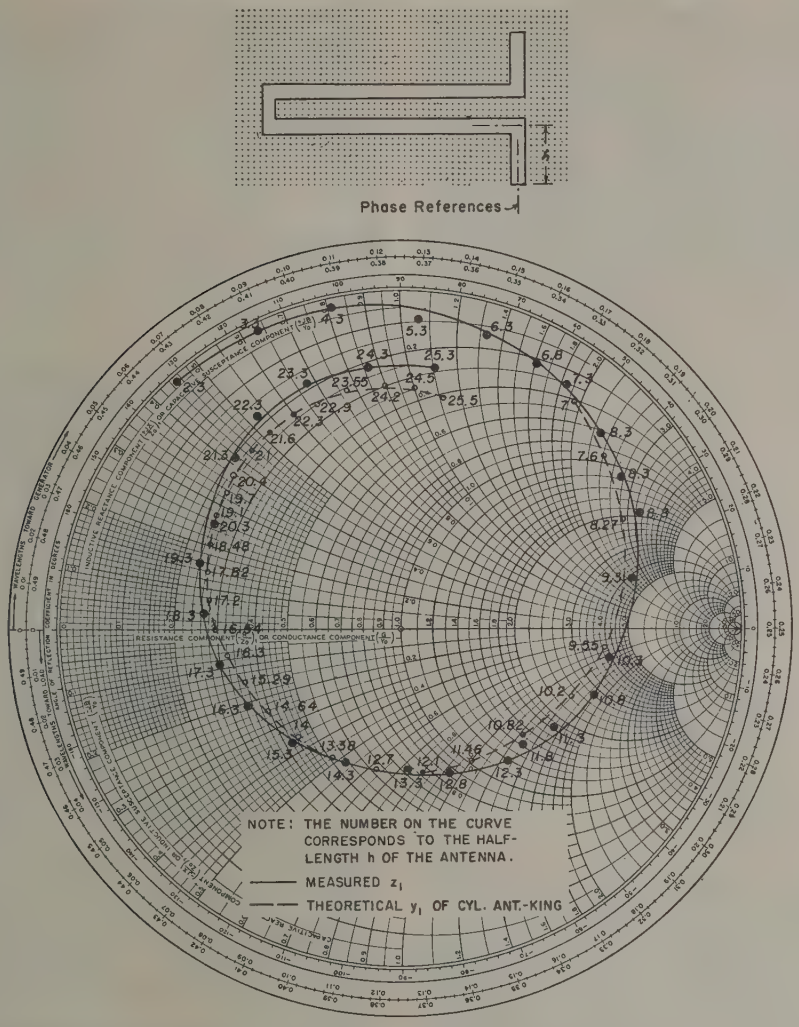

Fig. 7.—Smith chart of the measured complementary normalized input impedance z_1 of a slot aerial and the theoretical normalized input admittance y_1 of a cylindrical aerial.

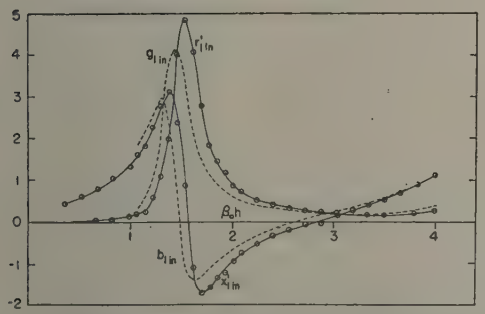

ig. 8.—Real and imaginary parts of the normalized impedance and admittance shown in Fig. 7.

— Measured values of x'_{1in} or r'_{1in}.
--- Theoretical b_{1in} or g_{1in} King second-order theory (cylindrical aerial equivalent to $\frac{1}{4}$ in infinitely thin strip.

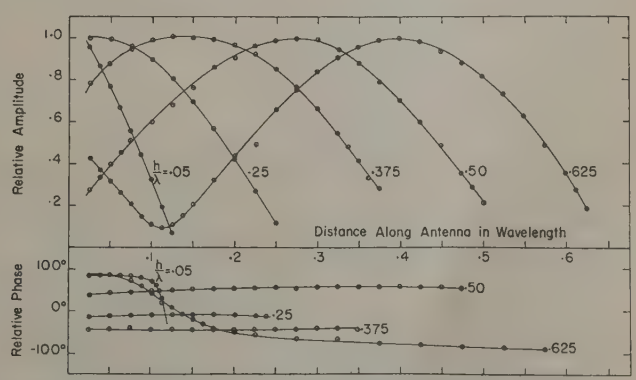

Fig. 9.—Measured distribution of the E' field and complementary charge along slot aerials of different half-lengths h.

complicated field. The measured E'-field does not vanish at the end of the slot aerial since the probe is above the earth-plane.

According to the principle of complementarity, the complementary E'-field of a slot in an ideal earth-plane corresponds to the H-field of the physical dual, a similar ideal strip aerial, i.e. the distribution of the complementary charge along the edges of a slot aerial is analogous to the distribution of the current along a strip aerial. Since the distribution of current along an ideal strip aerial is not available, approximate theoretical curves of the distribution of current along a cylindrical aerial with equivalent radius when centre-driven by a δ-function generator are shown in Fig. 10. A comparison of Figs. 9 and 10

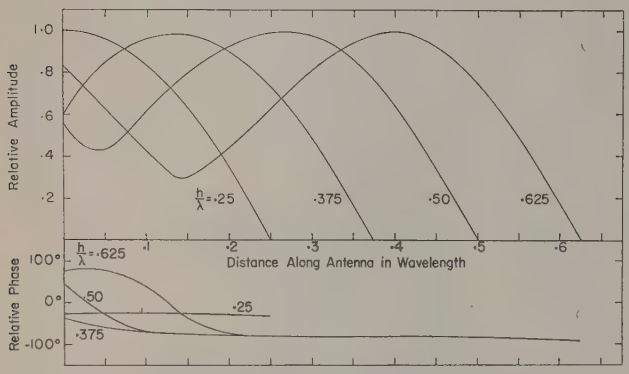

Fig. 10.—Theoretical distribution of the H field and current along a cylindrical aerial (King second-order theory).

shows the expected general similarity but also significant differences. These are discussed later.

(6) DISTRIBUTION OF COMPLEMENTARY MAGNETIC FIELD AND CURRENT ALONG THE SLOT AERIAL

The distribution of the complementary current density along the edges of the slot is proportional to the tangential magnetic field. This was measured with an enclosed-type loop probe with the same receiving system previously employed to measure the E'-field. The measured relative amplitude and relative phase of the tangential H'-field and of the current along the edges of the slot are shown in Fig. 11 for one-half of the slot aerial.

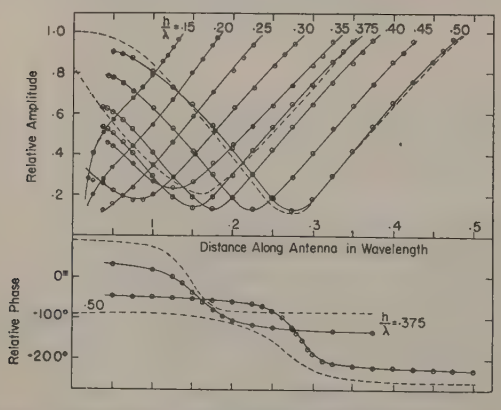

Fig. 11.—Distribution of the H' field and complementary current along the edges of slot aerials.

—— Measured curves for different half-lengths h.
---- Theoretical curves of the distribution of the E field and charge along cylindrical aerial.

Complementarity requires the distribution of the complementary current along a slot aerial in an ideal earth-plane to be like the distribution of charge along an ideal strip aerial. Since no data are available for the ideal strip aerial, comparison may be made with the theoretical distribution of charge per unit length along a cylindrical aerial. This can be provided for only two lengths, for which the distribution curves are shown in Fig. 11 in broken lines together with the measured curves for the slots. It should be noted that the two cases are not strictly comparable but apply to different structures. It is seen that the theoretical distributions of charge along a cylindrical aerial resemble the measured distributions of current along a slot aerial in an earth screen of finite thickness.

(7) DISCUSSION OF THE MEASURED PROPERTIES OF A PRACTICAL SLOT AERIAL AND THE THEORETICAL PROPERTIES OF A CYLINDRICAL AERIAL

When the theoretical normalized admittance and the distributions of current and charge for a cylindrical aerial are compared with the measured normalized impedance and the distributions of charge and current for a slot aerial in an earth screen of finite thickness and extent, the following sequence of steps is implied:

(*a*) The cylindrical aerial is related to an infinitely thin strip aerial by the equivalent radius $a = w/4$, where w is the width of the strip. The equivalence so obtained applies only to the cylindrical surface; there is nothing in the thin strip equivalent to the end surfaces of the cylindrical aerial. If the cylindrical aerial is driven from a two-wire line that is not too closely spaced, the same equivalent radius may be used to relate the circular conductors of the transmission line to the strips of a two-strip line. However, junction effects where the transmission line connects to the aerial are not the same for a line of circular wires as for one made of strips.

(*b*) The principle of complementarity is applied to relate the infinitely thin strip aerial to a slot aerial in an ideal earth-plane. In the same manner the two-strip feeder is related to a two-slot line. No approximations are involved in this step. The correlation of complementary quantities is exact for the aerials, the transmission lines, and for all end and junction effects.

(*c*) The slot aerial and its two-slot feeder in the ideal earth-plane are related to the slot aerial and feeder in a practical earth-plane by determining an equivalent width to take account of the change in cross-sectional shape. As has already been pointed out, such an equivalent width can be determined in principle, but, owing to complicated integrals, it has not, in general, been evaluated. End effects and junction effects are necessarily different in the two structures and are not taken into account by the equivalent width. The finite extent of a practical earth screen has a negligible effect on the two-slot feeder if it is large enough to be useful for the slot aerial. Although no data are available that make it possible to specify a minimum size for an earth screen when the impedance and the distribution of current in a slot aerial are measured, it may be assumed that, in directions other than along an axis through the slot, an earth screen should extend at least five to ten wavelengths, and that some variation in the measured impedance with the size of the screen may be observed even with the larger of these dimensions. This estimate is based on the related problem of a vertical dipole over a finite earth screen. In so far as the field pattern is concerned, no finite earth screen provides an adequate approximation to the ideal field pattern of a slot in an infinite earth-plane.

With these general remarks in mind, it is instructive to reconsider the correlation of the theoretical curves for the normalized admittance and the distributions of current and charge of a cylindrical aerial with the measured curves of the normalized impedance and the distributions of charge and current of a slot aerial in an actual earth screen. It should be noted that the theoretical values apply to a dipole that is centre-driven by a δ-function generator, and the measured values to a slot aerial that is centre-driven by a two-slot line.

Consider first the normalized admittances and impedances in Fig. 8. Here the principal differences between the two pairs of curves are:

(i) A scale factor corresponding to a change in the normalizing characteristic impedance of the theoretical admittances from the 298·5 ohms actually used to 343 ohms.

(ii) A shift in the electrical length $\beta_0 h$ to take account of the fact that the normalized impedance of the slot aerial of half-length h corresponds approximately to the normalized admittance of a cylindrical dipole that is about 0·64 cm or 0·016λ shorter. These differences are readily explained.

With regard to (i), the normalizing characteristic impedance of 298·5 ohms is the characteristic impedance of an infinitely thin two-strip line that would be the physical dual of the two-slot line actually used in the measurements if the earth screen had been infinitely thin. Actually, the ideal equivalent of a two-slot line in an earth screen of finite thickness must have narrower slots, as has already been pointed out. Accordingly, the dual two-strip line must have strips that are narrower than the slots in the earth screen of finite thickness. The characteristic impedance of an ideal two-strip line made of strips about 11% narrower than $\frac{1}{4}$ in is the desired impedance of 343 ohms. In the absence of specific formulae for the equivalent width of the slots in an ideal two-slot line, no quantitative check on the suggested 11% decrease is possible. However, it appears entirely reasonable.

With regard to (ii), the fact that the observed equivalent length of the slot aerial is shorter than its actual length and the length of the cylindrical aerial may be explained as follows: It is well known that, owing to the additional chargeable surfaces at the ends of a cylindrical aerial with flat conducting ends, its equivalent half-length exceeds its actual length by the order of magnitude of its radius. However, the theoretical admittances used in Figs. 7 and 8 are for circular cylinders with hemispherical end caps and axial lengths of $2h$. For these the end-cap correction is negligible, since the total chargeable surface is the same as that of an idealized cylinder without end surfaces. If a circular cylinder with flat metal ends is pressed into a cylinder with an equivalent elliptical cross-section and finally into a flat strip with an equivalent width, the chargeable surfaces at the ends are reduced to zero. The equivalent length of the dipole is thus reduced from $h' \simeq (h + a)$ to $h' = h$. By the principle of complementarity the infinitely thin strip dipole may be replaced by a complementary slot in an ideal earth-plane. For this slot aerial, $h' = h$. If the thickness of the earth screen is now increased to a finite value, additional surfaces for the current are provided on the edges of the conductor bounding the slot. These offer the shortest possible path for the current around the ends of the slot (see Fig. 3, on the right). The thicker the earth screen, the larger is this extra surface and the greater is the fraction of the total current that makes use of this, the shortest path. It follows that the average length of the path of the current around the slot is reduced as the earth screen is made thicker, i.e. the equivalent length of a slot aerial of actual length $2h$ in an earth screen of thickness t is shorter than that of the same slot in an infinitely thin earth screen. A rough estimate of this shortening may be obtained by noting that currents on both sides of the ideal earth screen as far out as $t/2$ from the edges of the slot are, in effect, moved into the side surfaces of the slot when the earth screen has a thickness t. In this way, a path length one-quarter around the slot of width w amounting to $h + t + w/2$ on the ideal earth-plane is reduced to $h + w/2$ on the actual earth-plane. The equivalent half-length of the slot aerial in this latter is $h' \simeq h - t$, where h is the actual half-length. This represents a shortening of 0·64 cm, which is precisely the desired amount. This quantitative agreement has no significance, since the suggested change in path length is reasonable but without analytical foundation. Nevertheless, the differences between the curves in Fig. 8 have been illuminated, at least in a qualitative sense. The preceding discussion is significant primarily for aerials near resonance, where transmission-line end effects and junction effects are negligible. When $\beta_0 h$ is near π, these effects, which depend on the finite spacing of the two-slot line, play a major role in determining the equivalent lengths (see Reference 7, pp. 73 and 407 and Reference 10, Chapter II, Sections 10 and 26).

A comparison of the curves in Fig. 10 for the distributions of current along a cylindrical dipole centre-driven by a δ-function generator with the measured curves in Fig. 9 for the slot aerial shows good agreement except when h/λ is as great as 0·5. The differences when $h/\lambda = 0{\cdot}5$ and 0·625 are presumably a consequence of the end and coupling effects at the junction of the slot aerial and the feeding two-slot line. The impedance measured on the two-slot line is the apparent terminal impedance.[7, 10] With a fairly large separation of the two slots, the apparent impedance differs considerably from the ideal impedance of the aerial when driven by a δ-function generator. This is a consequence of a stretching of the standing-wave patterns along the aerial in the manner shown by the curves for $h/\lambda = 0{\cdot}5$ and 0·625 in Fig. 9 when compared with the corresponding ones in Fig. 10.* However, no explanation can be given for the much deeper minimum in the curve for $h/\lambda = 0{\cdot}625$ in Fig. 9 compared with the corresponding curve in Fig. 10. The apparent admittance of a dipole when centre-driven by an open-wire line is given by the admittance of the same aerial when driven by a δ-function generator in parallel with a negative capacitance.[10] A slot aerial centre-driven by a two-slot line should have an apparent impedance equal to that when driven by a δ-function current generator in series with a negative inductance.

It should be clear from these illustrations that a quantitative correlation of the properties of a cylindrical aerial driven from a two-wire line (or a δ-function generator) with the 'complementary' properties of a slot aerial driven from a two-slot line in an earth screen of finite thickness cannot be made simply by assuming the principle of complementarity to apply. However, a general qualitative correspondence may be expected.

(8) MEASUREMENTS ON A COLLINEAR ARRAY OF SLOT AERIALS

In the collinear array the central slot aerial was driven by a two-slot transmission line, while the two outer units were parasitic. In the experimental arrangement provision was made to vary the lengths of the parasitic slots and the distances between the ends of the driven slot and the two parasitic slots. The half-length of the central slot aerial is denoted by h_1, and the half-lengths of the two identical outer elements by h_2; the distance between adjacent ends of the inner and outer slots is $2s$; the distance between the centre of the array and the centre of each parasitic slot is d.

* Comparable differences are observed with a dipole centre-driven by a two-wire line when the spacing is changed or a stub support is provided (see, for example, Fig. 26.20 of Reference 10).

(8.1) Complementary Normalized Impedance of the Collinear Array

The complementary normalized input impedance of the central unit of the collinear slot array was measured on the two-slot line. In this experiment, the half-length of all three aerials was kept at a quarter wavelength, i.e. $h_1 = h_2 = \lambda/4$, and the distance between them was varied. The measured magnitudes and arguments of the normalized input impedances are shown in Fig. 12, and the real and imaginary parts in Fig. 13. For comparison, the zero-order normalized input admittance of the central unit of a collinear array of cylindrical aerials is also shown in these Figures. Corresponding curves are seen to agree quite well in shape but to be displaced vertically from one another. This displacement may be explained as follows:

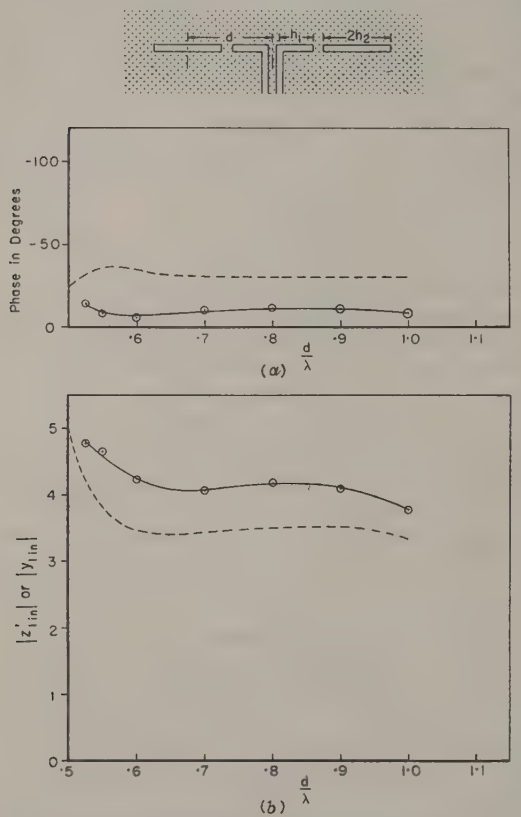

Fig. 12.—Measured complementary normalized input impedance of a collinear array of slot aerials.

(*a*) —— Measured phase of z'_{1in}.
---- Theoretical phase of y_{1in} (King, array of cylindrical aerials).
(*b*) —— Measured $|z'_{1in}|$
---- Theoretical y_{1in} (King, array of cylindrical aerials).
$h_1 = h_2 = \lambda/4 = 10$ cm.

(*a*) The theoretical curves for the cylindrical dipole array are based on zero-order formulae (Reference 10, Table 34.1, p. 441) that are known to lead to results which differ considerably from second-order values at infinite separation of the elements (Reference 10, Fig. 34.7*).

(*b*) As discussed in conjunction with Fig. 8, the equivalent length of a slot aerial in an earth screen of finite thickness is less than its actual length, and the normalizing characteristic impedance for the cylindrical dipole somewhat greater than the 298·5 ohms actually used.

* The relationship $I_2 = 0{\cdot}42I_1$ 186° should replace that given in the Fig. 34.7 o Reference 10.

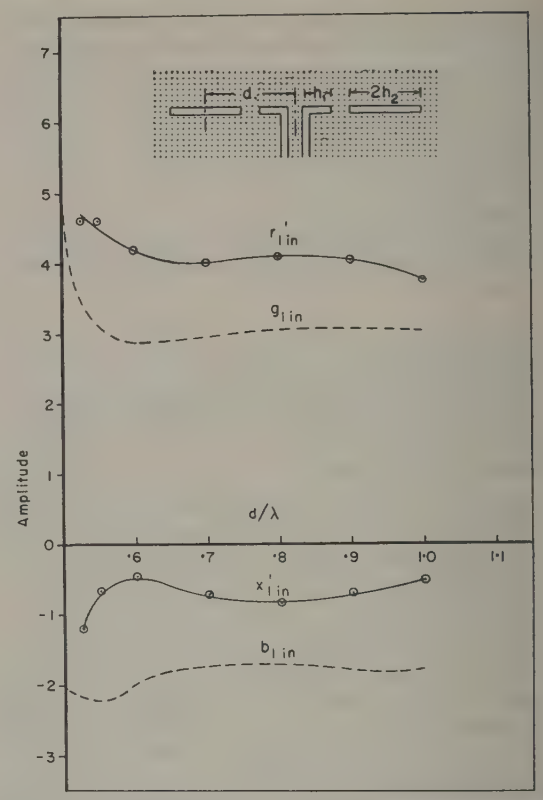

Fig. 13.—Real and imaginary parts of the impedances and admittances in Fig. 12.

—— Measured r'_{1in} or x'_{1in}.
---- Theoretical g_{1in} or b_{1in} (King, array of cylindrical aerials).

It follows that the curves in Figs. 12 and 13 apply to cylindrical dipoles and slot aerials which have somewhat different equivalent lengths and are normalized by different characteristic impedances. The significance of these differences may be determined quantitatively from Fig. 8 for the limiting case when the parasitic elements are at infinite separation. It is readily verified that, when $\beta_0 h = \pi/2$, the differences between g_{1in} and r'_{1in} on the one hand, and between b_{1in} and x'_{1in} on the other, correspond to these same differences in Fig. 13. Thus the differences between the two sets of curves in Figs. 12 and 13 have the same explanation as the differences between the curves in Figs. 7 and 8. If the slots had been cut in an earth screen of zero thickness there would have been no differences.

(8.2) Distribution of the Complementary Electric Field and the Charge along a Collinear Array of Slot Aerials

The distribution of the transverse E'-field along the collinear array was measured for various half-lengths, h_2, of the parasitic elements. The half-length, h_1, of the driven element and the separation, $2s$, between the adjacent ends of the elements were kept constant. A dipole probe was used and its output was fed into the detecting system used in the corresponding measurements for a single-slot aerial. The measured relative amplitude and phase are shown in Fig. 14. These curves may be compared with theoretical values of the distribution of current on a collinear array of cylindrical aerials. They are available in a zero-order approximation with $h_1 = h_2 = \lambda/4$ (Reference 10, Fig. 34.7). For this particular case the measured curve in

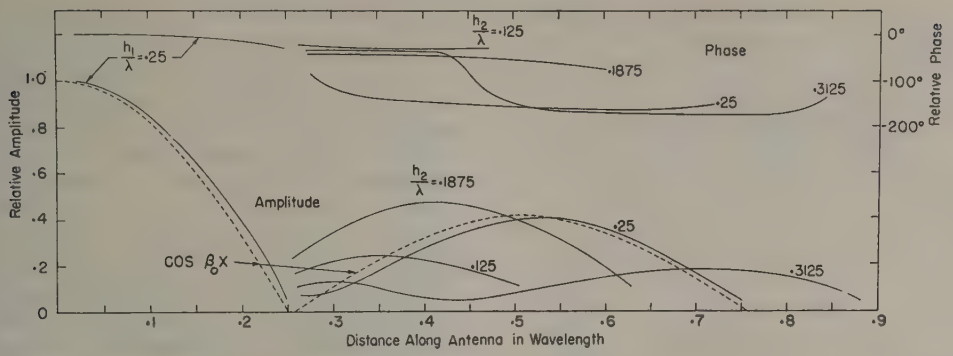

Fig. 14.—Distribution of the E' field and the complementary charge along a collinear array of slot aerials.
$h_1 = \lambda/4 = 10\,\text{cm}$, $2s = 2\,\text{mm}$.

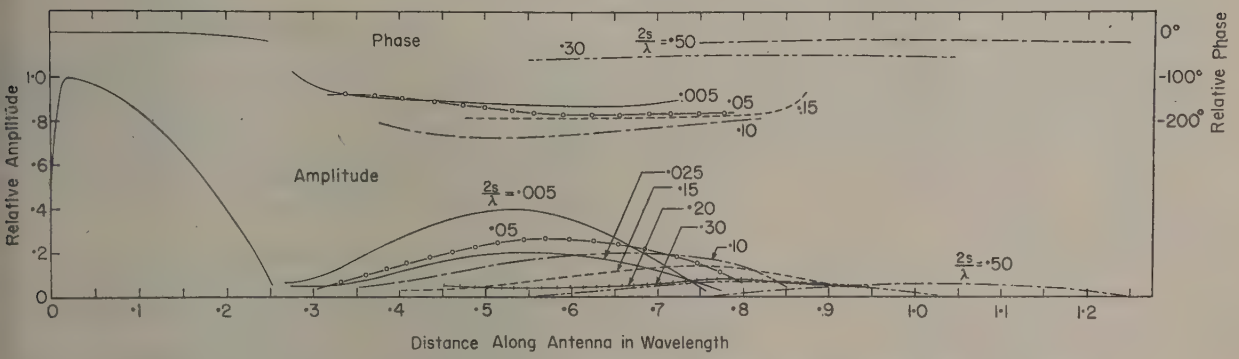

Fig. 15.—Distribution of the E' field and the complementary charge along a collinear array of slot aerials.
$h_1 = h_2 = \lambda/4 = 10\,\text{cm}$.
The distance $2s$ between the adjacent ends is varied.

Fig. 14 agrees well with the theoretical curve except for a slight shift of the experimental curve toward the outer ends of the aerial. The theory of the collinear array of cylindrical aerials indicates that, when $h_1 = h_2 = \lambda/4$, the currents at the centres of the outer units are 186° out of phase with that in the central unit. The measured phase of the E'-field at the centre of the outer slots differs from that in the central unit by approximately this amount.

The distributions of the transverse E'-field along the collinear array of slots were also measured for various separations $2s$ between the adjacent ends of the elements. In this case the half-lengths were kept constant at $h_1 = h_2 = \lambda/4$. The measured fields are shown in Fig. 15. The amplitude of E' along the central slot is practically independent of $2s$, whereas its value along the parasitic elements decreases rapidly as the separation $2s$ increases. (The curves in Figs. 14 and 15 parallel similar ones obtained by Hatch[16] with the central slot driven in a different manner.)

The ratio of the maximum transverse E'-field along the parasitic elements to that near the centre of the driven element, together with the corresponding phase differences, were measured with $h_1 = h_2 = \lambda/4$ as a function of the separation $2s$. The results are shown in Fig. 16. The corresponding zero-order theoretical curves for the current in a collinear array of cylindrical dipoles[26] are also shown. The agreement is quite good.

(8.3) Distribution of the Complementary Magnetic Field and Current along a Collinear Array of Slots

The distribution of the complementary magnetic field H' and the surface density of current (to which the field is proportional) was measured by moving a surface-type loop probe along the edge of the slots with the plane of the loop parallel to the slot. The measured relative amplitudes and phases for various values of h_2, with h_1 and $2s$ fixed, are shown in Fig. 17.

(9) CONCLUSION

An experimental study has been made of the circuit properties of a single-slot aerial and a collinear array of such aerials when centre-driven by a two-slot transmission line All slots were cut in a large earth screen of finite thickness. The usefulness of a two-slot transmission line to feed and study the properties of slot aerials has been demonstrated. Moreover, since the fields and currents associated with the slot line are quite closely confined, it is evident that it may be used to feed and study the properties of slot aerials in curved or twisted surfaces and in fins. In addition to the investigation of the impedances and distributions of current and charge along slot aerials when driven by a two-slot line, a study has been made of the significance of the principle of complementarity when practical slot aerials are involved rather than idealized ones cut in earth screens of zero thickness and infinite extent. In particular, the extensive theoretical results available for the cylindrical dipole antenna, both when driven by a δ-function generator and by practical transmission lines, are compared with the complementary quantities measured on slots cut in an earth screen of finite thickness. It is shown that the exact quantitative equivalence between complementary quantities characteristic of infinitely thin strips and slots in earth-planes of zero thickness and infinite extent becomes a qualitative agreement between 'complementary' quantities when cylindrical dipoles are com-

pared with slot aerials in earth screens of finite thickness. Owing to the existence of additional surfaces that may be charged or may carry currents, the equivalent length of a cylindrical dipole is greater than that of an infinitely thin strip of the same physical length, and the equivalent length of a slot in a ground screen of finite thickness is shorter than that of the same slot cut in an ideal earth-plane of zero thickness. As the half-length of a centre-driven aerial approaches a half-wavelength, transmission-line end and coupling effects become increasingly significant. These depend on the transverse geometry of the transmission line at the junction between aerial and feeder. Except for infinitely thin strips and earth screens, complementarity applies only in a qualitative sense. It may be concluded that the general behaviour of slot aerials driven by slot feeders in practical ground screens may be anticipated from the behaviour of dipole aerials driven by open-wire lines by replacing the dipoles with equivalent strips and ignoring the finite thickness of the earth screen so that the principle of complementarity applies. Quantitative information, however, depends on direct measurement until a more complete theory is developed.

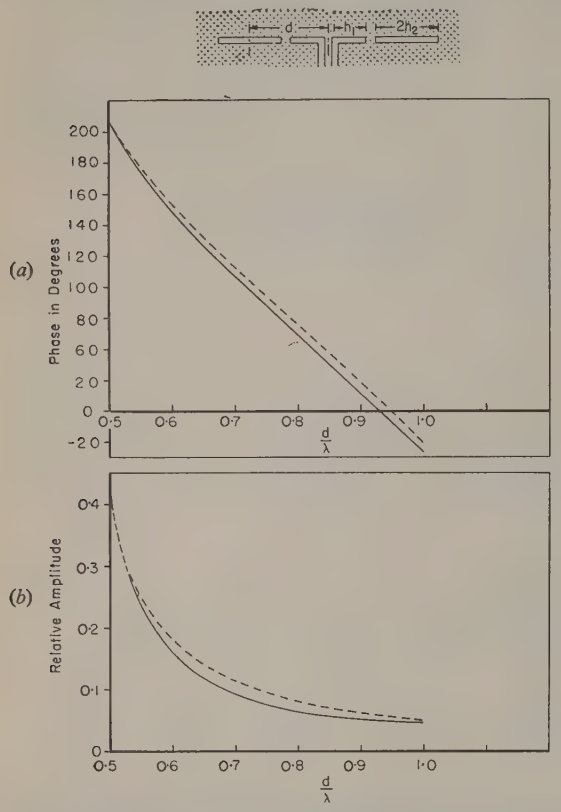

Fig. 16.—Measured ratio of the maximum value of the E_2' field on one of the parasitic slots to the maximum value of the E_1' field on the driven slot.
(*a*) —— Measured phase of E_2'/E_1'.
---- Theoretical phase of I_2/I_1 on cylindrical aerial array (King).
(*b*) —— Measured $|E_2'/E_1'|$.
---- Theoretical $|I_2/I_1|$ on cylindrical aerial array (King).
$h_1 = h_2 = \lambda/4 = 10$ cm.

(10) ACKNOWLEDGMENTS

The research described in the paper was made possible through support extended to the Cruft Laboratory, Harvard University, jointly by the Navy Department (Office of Naval Research), the Signal Corps of the U.S. Army, and the U.S. Air Force, under ONR Contract Nonr—1866(32). The authors are grateful to Dr. T. T. Wu for illuminating discussions and to Mrs. Barbara Hayes for assistance with the illustrations.

(11) REFERENCES

(1) Booker, H. G.: 'Slot Aerials and their Relation to Complementary Wire Aerials—Babinet's Principle', *Journal I.E.E.*, 1946, **93**, Part IIIA, p. 620.
(2) Copson, E. T.: 'An Integral-Equation Method of Solving Plane Diffraction Problems', *Proceedings of the Royal Society*, A, 1946, **186**, p. 100.
(3) Meixner, J.: 'Strenge Theorie der Beugung Elektromagnetischer Wellen and der vollkommen leitenden Kreisscheibe', *Naturforschung*, 1948, **3A**, p. 506.
(4) Huang, C.: 'Babinet's Principle for Plane Obstacles', Technical Memorandum No. 8, Cruft Laboratory, Harvard University, 1953.
(5) Bailey, C. E. G.: 'Slot Feeders and Slot Aerials', *Journal I.E.E.*, 1946, **93**, Part IIIA, p. 615.

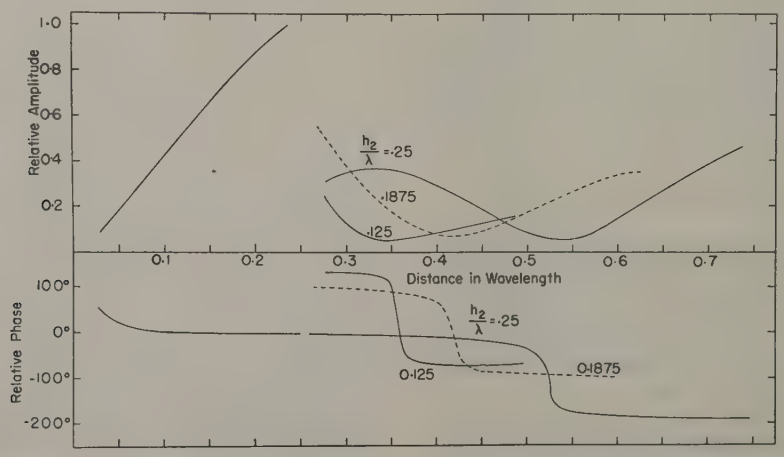

Fig. 17.—Distribution of the H' field and the complementary current along the edges of a collinear array of slot aerials.
$h_1 = \lambda/4 = 10$ cm.
$2s = 0{\cdot}005\lambda = 2$ mm.

(6) UDA, S., and MUSHIAKE, Y.: 'The Input Impedances of Slot Antennas', *Technology Reports of the Tohoku University*, 1949, **14**, p. 46.

(7) KING, R. W. P.: 'Transmission-Line Theory' (McGraw-Hill, 1955), Chapter 4, Sections 7–13.

(8) OWYANG, G. H., and WU, T. T.: 'Approximate Parameters of Slot Lines and their Complements', *Transactions of the Institute of Radio Engineers*, 1958, **AP–6**, p. 49.

(9) OWYANG, G. H., and KING, R.: 'Complementarity in the Study of Transmission Lines', *ibid.*, 1960, **MTT–8**.

(10) KING, R. W. P.: 'Theory of Linear Antennas' (Harvard University Press, 1956), Chapter II, Sections 34–35.

(11) WU, T. T., and KING, R. W. P.: 'Driving Point and Input Admittance of Linear Antennas', *Journal of Applied Physics*, 1959, **30**, 74.

(12) KING, R.: 'Linear Arrays—Currents, Impedances, and Fields, I', *Transactions of the Institute of Radio Engineers* (to be published).

(13) HALLÉN, E.: 'Theoretical Investigations into the Transmitting and Receiving Qualities of Antennae', *Nova Acta Regiae Soc. Sci. Upsaliensis*, 1938, **11**, p. 1.

(14) OWYANG, G. H.: 'Experimental Study of a Two-Slot Transmission Line', Technical Report No. 289, Cruft Laboratory, Harvard University, 1959.

(15) KING, D. D.: 'Measurements at Centimeter Wavelengths' (Van Nostrand, 1952), p. 194.

(16) HATCH, R. M.: 'An Investigation of the Distribution of Current on Colinear Parasitic Antenna Elements', Technical Report No. 28, S.R.I. Project No. 591, Stanford Research Institute, 1952. (See also Reference 10, p. 447.)

621.732.6: 621.317.7.78

The Institution of Electrical Engineers
Monograph No. 366 M
Mar. 1960
©

A THEORY OF STEADY FORCES IN VARIABLE-PARAMETER NETWORKS

Applicable to a Class of Square-Law Measuring Instruments

By W. E. SMITH, B.Sc., A.Inst.P.

(*The paper was first received* 17*th August, and in revised form* 28*th October*, 1959. *It was published as an* INSTITUTION MONOGRAPH *in March*, 1960.)

SUMMARY

Passive linear reciprocal networks with elements dependent upon a generalized co-ordinate x are investigated in order to evaluate the steady component of the corresponding generalized force $(F_x)_{av}$. Methods are found for expressing this force in terms of parameters measurable at the input terminals of the network.

The analysis is particularly relevant to the absolute calibration of a class of square-law electrical measuring instruments, but the formalism is also applicable to other network systems where impedance is a useful concept.

LIST OF SYMBOLS

B = 2-terminal susceptance.
B_{kl}, B_{KL} = Imaginary parts of mesh or terminal admittance matrices.
c = Velocity of light in vacuo.
C_α = Capacitance.
F_x = Instantaneous generalized force.
$(F_x)_{av}$, $(F_x')_{av}$, $(F_l)_{av}$ = Average generalized forces.
$\mathscr{F}_x$, $\mathscr{F}_x'$ = Intermediary quantities for evaluating $(F_x)_{av}$, $(F_x')_{av}$.
G = 2-terminal conductance.
G_{kl}, G_{KL} = Real parts of mesh or terminal admittance matrices.
i_α = Instantaneous current in element α.
I_α = R.M.S. current in element α.
I_k, I_K = R.M.S. current in kth mesh or at Kth terminal pair.
I, I' = R.M.S. 2-terminal network currents.
$L_{\alpha\alpha}$, $L_{\alpha\beta}$ = Element self or mutual inductances.
L_s = Line series inductance per unit length.
l = Transmission line or waveguide length.
P = Complex power.
R_s = Line series resistance per unit length.
R = 2-terminal resistance.
R_{kl}, R_{KL} = Mesh or terminal resistance matrix elements.
v_α = Instantaneous voltage applied to element α.
V = 2-terminal r.m.s. voltage.
V_α = R.M.S. voltage applied to element α.
V_k, V_K = kth mesh or Kth terminal pair voltage.
x = Generalized co-ordinate.
X, X' = 2-terminal reactances.
X_α = Reactance of element α.
$X_{\alpha\beta}$ = Mutual reactance.
X_{kl}, X_{KL} = Mesh or terminal reactance matrix elements.
Y = 2-terminal admittance.
Y_{kl}, Y_{KL} = Mesh or terminal admittance matrix elements.
Z = 2-terminal impedance.
Z_0 = Characteristic impedance.
Z_{kl}, Z_{KL} = Mesh or terminal impedance matrix elements.
γ = Propagation coefficient.
δ_{ln}, δ_{LN} = Kronecker delta.
λ = Free-space wavelength.
λ_g = Guide wavelength.
ω = Angular frequency.

Correspondence on Monographs is invited for consideration with a view to publication.

Mr. Smith was formerly in the Division of Electrotechnology, National Standards Laboratory, Commonwealth Scientific and Industrial Research Organization, Australia, and is now in the Department of Applied Mathematics, University of New South Wales.

(1) INTRODUCTION

In electrical measurements and standards the average electric or magnetic force exerted between current-carrying or charged conductors is made the basis of a number of important measuring instruments. Of prime importance is the current balance or dynamometer used for the absolute determination of the electromagnetic unit of direct current. An electrostatic instrument whose field configuration is calculable would give rise, in a similar manner, to an absolute determination of the electrostatic unit of potential difference. In addition, there are numerous indicating instruments for both alternating and direct voltages or currents, such as the electrostatic voltmeter, dynamometer and moving-iron ammeter, based upon the production of a steady force by charges or currents in the instruments. The distinguishing features of instruments in this class are:

(*a*) The force involved is a quadratic function of the applied voltages or currents.
(*b*) The instruments are not dependent for their operation upon the application of a steady electric or magnetic field.
(*c*) The electrical part of the instrument is in principle loss free or energy conservative.

As a consequence of (*a*), the instruments are square-law or r.m.s. reading and are widely used as d.c./a.c. transfer instruments.

In instruments where the field configuration is calculable, a measurement of force will define absolutely an alternating or direct current or voltage. However, for many practical instruments, particularly at high frequencies, the details of the field configurations are of such complexity as to be beyond practical calculation, and some other means of voltage or current standardization may be required.

In the paper an analysis relevant to a.c. instruments is presented which enables the force to be obtained in terms of parameters measurable at the input terminals.

An instrument of the class above is considered as an electrical network in which some of the circuit-elements are dependent upon a generalized co-ordinate x (e.g. linear displacement or rotation), and the steady component of the corresponding generalized force $(F_x)_{av}$ is evaluated. To preserve linearity it is assumed that in practical instruments x is suitably constrained (e.g. by inertia) such that it is time independent. Accordingly, a theory of steady forces arising from linear passive reciprocal networks in which some circuit-elements are dependent upon x is developed. To preserve generality no restriction is placed upon the number of terminal pairs in the network. The theory yields expressions for the average force $(F_x)_{av}$ in terms of voltages or currents at the input terminals, together with derivatives with respect to x of the impedance or admittance parameters measurable at the input terminals. The results for

certain special cases are exact. However, the most general result is not exact, but will usually give adequate accuracy, and a means of estimating the error is suggested.

The expression of $(F_x)_{av}$ in terms of voltages or currents and derivatives of accessible impedance or admittance parameters allows an absolute calibration of an instrument to be performed by measuring the force together with these derivatives. This absolute calibration is possible even though the internal details of the instrument may be very complicated. For an absolute calibration an impedance standard is required, but the establishment of this standard presents a separate problem. Impedance standards may be derived either by d.c./a.c. transfer or by calculation of a field configuration (e.g. a transmission line or waveguide of calculable characteristic impedance, a calculable capacitance or inductance). It is assumed that a suitable impedance standard is available in every frequency range of interest.

The theory is developed initially for lumped circuit-elements and is later extended to continuous systems. The further extension to microwave circuits is postulated. With these extensions an absolute voltage, current or power may be established at any frequency right up to and including the microwave range.* Moreover, the formalism would be expected to apply for the evaluation of average forces in other fields (e.g. radiation pressure in acoustic ducts).

The practical measurement of the required derivatives of input-terminal parameters is not discussed.

(2) FUNDAMENTAL CIRCUIT EQUATIONS

(2.1) Basic Force Equations for Lumped-Element Circuits

Elementary energy considerations† show that the generalized force F_x corresponding to a generalized co-ordinate x upon which a lumped inductance (self-inductance $L_{\alpha\alpha}$ or mutual inductance $L_{\alpha\beta}$) or lumped capacitance C_α depend is given by

$$F_x = \frac{1}{2} v_\alpha^2 \frac{\partial C_\alpha}{\partial x} \quad . \quad . \quad . \quad . \quad . \quad . \quad (1)$$

$$F_x = \frac{1}{2} i_\alpha^2 \frac{\partial L_{\alpha\alpha}}{\partial x} \quad . \quad . \quad . \quad . \quad . \quad . \quad (2)$$

$$F_x = i_\alpha i_\beta \frac{\partial L_{\alpha\beta}}{\partial x} \quad . \quad . \quad . \quad . \quad . \quad . \quad (3)$$

In a network where a number of elements may depend upon x the individual contributions to the total force are additive, i.e.

$$F_x = \frac{1}{2} \Sigma\, i_\alpha i_\beta \frac{\partial L_{\alpha\beta}}{\partial x} + \frac{1}{2} \Sigma\, v_\alpha^2 \frac{\partial C_\alpha}{\partial x} \quad . \quad . \quad . \quad . \quad (4)$$

where $L_{\alpha\beta} = L_{\beta\alpha}$.

In the summations of eqn. (4) and in the rest of the paper, the convention of summing over repeated suffixes has been adopted, e.g. Σ in eqn. (4) is to be interpreted as $\sum_\alpha \sum_\beta$. Eqn. (4) actually gives the instantaneous force, but it may be suitably averaged to give the required steady force. It is assumed that x is suitably constrained to be independent of time, so that all circuit-elements together with their derivatives are constants. Eqn. (4) then becomes

$$(F_x)_{av} = \frac{1}{2} \Sigma\, (i_\alpha i_\beta)_{av} \frac{\partial L_{\alpha\beta}}{\partial x} + \frac{1}{2} \Sigma\, (v_\alpha^2)_{av} \frac{\partial C_\alpha}{\partial x} \quad . \quad . \quad (5)$$

In view of the quadratic dependence between the average force $(F_x)_{av}$ and the currents or voltages, a Fourier resolution of v_α and i_α may be performed, and each Fourier component will then contribute independently to the total average force. Even in the case of irregular voltages or currents such as noise this approach is still possible provided that the assumptions concerning the constancy of x are valid. Consequently it is adequate to consider only sinusoidal voltages and currents. Eqn. (5) may now be written in terms of the usual complex r.m.s. voltages and currents V_α and I_α:

$$(F_x)_{av} = \frac{1}{2} \Sigma\, I_\alpha I_\beta^* \frac{\partial L_{\alpha\beta}}{\partial x} + \frac{1}{2} \Sigma\, V_\alpha V_\alpha^* \frac{\partial C_\alpha}{\partial x} \quad . \quad . \quad (6)$$

Ordinary a.c. circuit theory then gives the following results:

$$\frac{1}{2} \Sigma\, V_\alpha V_\alpha^* \frac{\partial C_\alpha}{\partial x} = \frac{1}{2\omega} \Sigma\, I_\alpha I_\alpha^* \frac{\partial X_\alpha}{\partial x} \quad . \quad . \quad . \quad . \quad (7)$$

where $$X_\alpha = -1/\omega C_\alpha \quad . \quad . \quad . \quad . \quad . \quad . \quad (8)$$

Also $$\frac{1}{2} \Sigma\, I_\alpha I_\beta^* \frac{\partial L_{\alpha\beta}}{\partial x} = \frac{1}{2\omega} \Sigma\, I_\alpha I_\beta^* \frac{\partial X_{\alpha\beta}}{\partial x} \quad . \quad . \quad . \quad . \quad (9)$$

where $X_{\alpha\beta} = \omega L_{\alpha\beta}$.

After substituting eqns. (7) and (9) in eqn. (6) and considering[6] the element currents I_α to be appropriate sums or differences of mesh currents I_k, the resulting equation may be written in terms of mesh currents and total mesh reactances X_{kl}:

$$(F_x)_{av} = \frac{1}{2\omega} \Sigma\, I_k \frac{\partial X_{kl}}{\partial x} I_l^* \quad . \quad . \quad . \quad . \quad (11)$$

Eqn. (11) is the basic force equation and expresses the average force in terms of derivatives of the total mesh reactances with respect to x and the corresponding mesh currents. The form of eqn. (11) is, of course, unchanged by the actual choice of independent meshes.

(2.2) Mesh Equations and Variation of Mesh Impedances

The circuit equations for a general linear passive reciprocal network may be written[6] in terms of V_k and I_k:

$$V_k = \Sigma\, Z_{kl} I_l \quad . \quad . \quad . \quad . \quad . \quad . \quad (12)$$

with $$Z_{kl} = Z_{lk} \quad . \quad . \quad . \quad . \quad . \quad . \quad . \quad (13)$$

$$= R_{kl} + jX_{kl} \quad . \quad . \quad . \quad . \quad . \quad (14)$$

Alternatively, the equations may be written in inverted form:

$$I_k = \Sigma\, Y_{kl} V_l \quad . \quad . \quad . \quad . \quad . \quad . \quad (15)$$

with $$Y_{kl} = Y_{lk} \quad . \quad . \quad . \quad . \quad . \quad . \quad . \quad (16)$$

$$= G_{kl} + jB_{kl} \quad . \quad . \quad . \quad . \quad . \quad (17)$$

The reciprocity relations (13) and (16) will be used extensively throughout the paper.

The admittance and impedance matrices are inverses of each other, satisfying

$$\Sigma\, Y_{lk} Z_{kn} = \delta_{ln} \quad . \quad . \quad . \quad . \quad . \quad (18)$$

where $\delta_{ln} = 1 \quad l = n$

$= 0$ otherwise.

Using eqns. (14) and (15), the basic force equation (11) becomes

$$(F_x)_{av} = \frac{1}{2\omega} \Sigma\, V_l Y_{kl} \frac{\partial X_{km}}{\partial x} Y_{mn}^* V_n^* \quad . \quad . \quad . \quad (19)$$

$$= \mathscr{R}(\mathscr{F}_x) \quad . \quad . \quad . \quad . \quad . \quad . \quad . \quad . \quad (20)$$

* Absolute torque-operated wattmeters for microwave circuits have been developed using another, though related, approach by Cullen and his collaborators.[1–5]

† When polarizable material is present, eqns. (1)–(3) are best established by thermodynamic methods. In practical circumstances no distinction need be made between isothermal and adiabatic polarization processes.

where
$$\mathscr{F}_x = \frac{1}{2j\omega} \Sigma V_l Y_{kl} \frac{\partial Z_{km}}{\partial x} Y^*_{mn} V^*_n \quad . \quad . \quad . \quad (21)$$

$$= \frac{1}{2j\omega} \Sigma I_k \frac{\partial Z_{kl}}{\partial x} I^*_l \quad . \quad . \quad . \quad . \quad . \quad . \quad . \quad (22)$$

The complex power, P, which is invariant with respect to phase reference angle, is defined by

$$P = \Sigma V_k I^*_k \quad . \quad . \quad . \quad . \quad . \quad . \quad . \quad (23)$$

The real part of P represents power consumed by the network while the imaginary part represents the net energy exchange between the sources and the network. Consider small changes δZ_{lk}, δY_{lk} in the network, keeping all voltages V_k constant.

$$\delta P = \delta(\Sigma V_k I^*_k) \quad . \quad . \quad . \quad . \quad . \quad . \quad . \quad (24)$$

$$= \Sigma V_k \delta I^*_k \quad . \quad . \quad . \quad . \quad . \quad . \quad . \quad . \quad (25)$$

$$= \Sigma V_k \delta Y^*_{kl} V^*_l \text{ from eqn. (15)} \quad . \quad . \quad (26)$$

But from eqn. (18),

$$\Sigma \delta Y_{kl} Z_{ln} + \Sigma Y_{kl} \delta Z_{ln} = 0 \quad . \quad . \quad . \quad (27)$$

and therefors,

$$\Sigma \delta Y_{kl} Z_{ln} Y_{nm} + \Sigma Y_{kl} \delta Z_{ln} Y_{nm} = 0 \quad . \quad . \quad (28)$$

and, by using eqn. (18),

$$\delta Y_{km} = - \Sigma Y_{kl} \delta Z_{ln} Y_{nm} \quad . \quad . \quad . \quad . \quad (29)$$

Substitution of eqn. (29) in eqn. (26) yields

$$\delta P = - \Sigma V_k Y^*_{kl} \delta Z^*_{ln} Y^*_{nm} V^*_m \quad . \quad . \quad . \quad (30)$$

or
$$\left(\frac{\partial P}{\partial x}\right)_V = - \Sigma V_k Y^*_{kl} \frac{\partial Z^*_{ln}}{\partial x} Y^*_{nm} V^*_m \quad . \quad . \quad (31)$$

$$= - \Sigma V_k Y^*_{kl} \frac{\partial Z^*_{ln}}{\partial x} I^*_n \quad . \quad . \quad . \quad . \quad (32)$$

where $(\partial P/\partial x)_V$ indicates that the differentiation has been performed with all V_k held constant.

Eqn. (31) is seen to be very similar to eqn. (21) for finding the force $(F_x)_{av}$, and it will be shown later under what conditions a correspondence may be established. For the present it should be noted that, since the network is passive, P may be expressed simply as a sum over input terminal voltages and currents V_K, I_K, i.e.

$$P = \Sigma V_K I^*_K \quad . \quad . \quad . \quad . \quad . \quad . \quad (33)$$

and the V_K, I_K are related by impedance and admittance matrices whose elements may be measured externally at the input terminals. The following equations (34)–(40) referring to the input terminals are analogous to the mesh equations (12)–(18).

$$V_K = \Sigma Z_{KL} I_L \quad . \quad . \quad . \quad . \quad . \quad . \quad (34)$$

$$Z_{KL} = Z_{LK} \quad . \quad . \quad . \quad . \quad . \quad . \quad . \quad (35)$$

$$= R_{KL} + jX_{KL} \quad . \quad . \quad . \quad . \quad . \quad (36)$$

$$I_K = \Sigma Y_{KL} V_L \quad . \quad . \quad . \quad . \quad . \quad . \quad (37)$$

$$Y_{KL} = Y_{LK} \quad . \quad . \quad . \quad . \quad . \quad . \quad . \quad (38)$$

$$= G_{KL} + jB_{KL} \quad . \quad . \quad . \quad . \quad . \quad (39)$$

$$\Sigma Y_{LK} Z_{KN} = \delta_{LN} \quad . \quad . \quad . \quad . \quad . \quad . \quad (40)$$

Thus
$$P = \Sigma V_K Y^*_{KL} V^*_L \quad . \quad . \quad . \quad . \quad . \quad (41)$$

and
$$\left(\frac{\partial P}{\partial x}\right)_V = \Sigma V_K \frac{\partial Y^*_{KL}}{\partial x} V^*_L \quad . \quad . \quad . \quad . \quad . \quad (42)$$

However, analogously to eqn. (29),

$$\frac{\partial Y_{KM}}{\partial x} = - \Sigma Y_{KL} \frac{\partial Z_{LN}}{\partial x} Y_{NM} \quad . \quad . \quad . \quad (43)$$

and, as with eqn. (32),

$$\left(\frac{\partial P}{\partial x}\right)_V = - \Sigma V_K Y^*_{KL} \frac{\partial Z^*_{LN}}{\partial x} I^*_N \quad . \quad . \quad . \quad (44)$$

(3) EVALUATION OF THE AVERAGE FORCE

(3.1) Force in Purely Reactive Networks

For the case of purely reactive networks a correspondence between eqns. (32) and (22) follows directly from the fact that all Z_{lk} and Y_{lk} are purely imaginary, so that

$$Y^*_{lk} = - Y_{lk} \quad Z^*_{lk} = - Z_{lk} \quad . \quad . \quad . \quad . \quad (45)$$

and
$$\frac{\partial Z_{lk}}{\partial x} = j \frac{\partial X_{lk}}{\partial x} \quad . \quad . \quad . \quad . \quad . \quad . \quad (46)$$

Thus eqn. (32) becomes

$$\left(\frac{\partial P}{\partial x}\right)_V = - j \Sigma V_k Y_{kl} \frac{\partial X_{ln}}{\partial x} I^*_n \quad . \quad . \quad . \quad (47)$$

$$= - j \Sigma I_l \frac{\partial X_{ln}}{\partial x} I^*_n \quad . \quad . \quad . \quad . \quad . \quad (48)$$

from eqns. (15) and (16).

When compared directly with eqn. (11), this gives

$$(F_x)_{av} = - \frac{1}{2j\omega} \left(\frac{\partial P}{\partial x}\right)_V \quad . \quad . \quad . \quad . \quad . \quad (49)$$

Y_{LK} and Z_{LK} are also purely imaginary, i.e.

$$Y^*_{LK} = - Y_{LK} \quad . \quad . \quad . \quad . \quad . \quad . \quad (50)$$

$$Z^*_{LK} = - Z_{LK} \quad . \quad . \quad . \quad . \quad . \quad . \quad (51)$$

and we obtain from eqns. (49) and (42),

$$(F_x)_{av} = \frac{1}{2j\omega} \Sigma V_K \frac{\partial Y_{KL}}{\partial x} V^*_L \quad . \quad . \quad . \quad . \quad (52)$$

or from eqns. (49) and (44),

$$(F_x)_{av} = \frac{1}{2j\omega} \Sigma I_K \frac{\partial Z_{KL}}{\partial x} I^*_L \quad . \quad . \quad . \quad . \quad (53)$$

Thus, in eqns. (52) and (53) the force $(F_x)_{av}$ has been expressed completely in terms of quantities available at the input terminals. A measurement of the derivatives of impedance or admittance together with a force measurement then gives an absolute calibration of the instrument. Simple instruments whose ideal behaviour may be described by eqns. (52) and (53) are the quadrant electrometer and the dynamometer. These equations are particularly simple for 2-terminal networks (electrostatic voltmeter, moving-iron ammeter), being

$$(F_x)_{av} = \frac{1}{2j\omega} VV^* \frac{\partial Y}{\partial x} \quad . \quad . \quad . \quad . \quad . \quad (54)$$

$$= \frac{1}{2j\omega} II^* \frac{\partial Z}{\partial x} \quad . \quad . \quad . \quad . \quad . \quad (55)$$

which reduce to the original forms [eqns. (1) and (2)] for a single reactive element. The 2-terminal network may have any number of individual elements, provided that it remains loss free.

(3.2) Force in Arbitrary Networks with One Variable Reactive Element

A general network in which only one pure reactance X' is dependent upon x is considered. The 2-terminal reactance, X', may consist of an arbitrary number of loss-free elements any number of which may depend on x. The force $(F_x)_{av}$ may then be found as in the previous Section, i.e.

$$(F_x)_{av} = \frac{1}{2\omega} I' I'^* \frac{\partial X'}{\partial x} \quad . \quad . \quad . \quad . \quad (56)$$

Consider now the derivative of a quantity $\Sigma V_k I_k$ which has no obvious physical interpretation and is not invariant with respect to phase reference angle.

Using eqn. (15),

$$\left(\frac{\partial}{\partial x}\right)_V (\Sigma V_k I_k) = \Sigma V_k \frac{\partial Y_{kl}}{\partial x} V_l \quad . \quad . \quad . \quad . \quad . \quad . \quad . \quad . \quad (57)$$

$$= -\Sigma V_k Y_{kl} \frac{\partial Z_{ln}}{\partial x} Y_{nm} V_m \quad . \quad . \quad . \quad . \quad . \quad (58)$$

$$= -\Sigma I_l \frac{\partial Z_{ln}}{\partial x} I_m \text{ from eqns. (15) and (16)} \quad . \quad (59)$$

Suppose that X' is common to a number of meshes $r, s, t, \ldots$; then

$$\left(\frac{\partial}{\partial x}\right)_V (\Sigma V_k I_k) = -j\left(I_r^2 \frac{\partial X'}{\partial x} + I_s^2 \frac{\partial X'}{\partial x} + \ldots \pm 2I_r I_s \frac{\partial X'}{\partial x} \pm 2I_r I_t \frac{\partial X'}{\partial x} \pm \ldots\right) \quad . \quad (60)$$

$$= -j(I_r \pm I_s \pm I_t \ldots)^2 \frac{\partial X'}{\partial x} \quad . \quad . \quad . \quad . \quad (61)$$

$$= -jI'^2 \frac{\partial X'}{\partial x} \quad . \quad . \quad . \quad . \quad . \quad . \quad . \quad . \quad . \quad (62)$$

The signs of the coupling terms $2I_r I_s(\partial X'/\partial x)$ in eqn. (60) depend upon the senses of the mesh currents $I_r, I_s, I_t, \ldots$, but the result, eqn. (62), follows regardless. This result is essentially a generalization of a theorem recently propounded by Vratsanos.[7-10]

Using eqns. (62) and (56), the average force may be obtained:

$$|(F_x)_{av}| = \frac{1}{2\omega}\left|\left(\frac{\partial}{\partial x}\right)_V (\Sigma V_k I_k)\right| \quad . \quad . \quad . \quad (63)$$

$$= \frac{1}{2\omega}\left|\left(\frac{\partial}{\partial x}\right)_V (\Sigma V_K I_K)\right| \quad . \quad . \quad . \quad (64)$$

$$= \frac{1}{2\omega}\left|\Sigma V_K \left(\frac{\partial I_K}{\partial x}\right)_V\right| \quad . \quad . \quad . \quad . \quad (65)$$

The transition from mesh voltages and currents in eqn. (63) to terminal voltages in eqn. (64) follows by an interchange of order of summation, since the mesh voltages V_k are composed of sums of terminal voltages V_K and the terminal currents I_K are sums of mesh currents I_k.

Eqns. (64) and (65) thus achieve the desired aim of expressing the force in terms of quantities available at the input terminals of the network, although the sign of $(F_x)_{av}$ has been lost. Eqn. (65) may be written in useful impedance or admittance form by the use of eqns. (37), (38) and (43):

$$|(F_x)_{av}| = \frac{1}{2\omega}\left|\Sigma V_K \frac{\partial Y_{KL}}{\partial x} V_L\right| \quad . \quad . \quad . \quad . \quad (66)$$

$$= \frac{1}{2\omega}\left|\Sigma I_K \frac{\partial Z_{KL}}{\partial x} I_L\right| \quad . \quad . \quad . \quad . \quad (67)$$

Specialization to a 2-terminal network gives

$$|(F_x)_{av}| = \frac{1}{2\omega}|V^2|\left|\frac{\partial Y}{\partial x}\right| \quad . \quad . \quad . \quad . \quad . \quad (68)$$

$$= \frac{1}{2\omega}|I^2|\left|\frac{\partial Z}{\partial x}\right| \quad . \quad . \quad . \quad . \quad . \quad (69)$$

(3.3) Force in General Slightly Lossy Networks

Exact expressions for the force have been found for special cases. Unfortunately, the methods make use of some special properties of the networks considered and are consequently incapable of extension to general parameter dependence in arbitrary networks. In this Section an approximate formula appropriate to the general case is derived for networks which conform to a rather special definition of being slightly lossy. Initially the parameter dependence will be general, i.e.

$$\frac{\partial Z_{lk}}{\partial x} = \frac{\partial R_{lk}}{\partial x} + j\frac{\partial X_{lk}}{\partial x} \quad . \quad . \quad . \quad . \quad . \quad (70)$$

However, later discussion will show that in practical instrument design the $\partial R_{lk}/\partial x$ are essentially zero and may usually be neglected. For convenient reference eqns. (20), (21) and (31) are rewritten as

$$(F_x)_{av} = \mathscr{R}(\mathscr{F}_x) \quad . \quad . \quad . \quad . \quad . \quad (71)$$

$$\mathscr{F}_x = \frac{1}{2j\omega} \Sigma V_l Y_{kl} \frac{\partial Z_{km}}{\partial x} Y^*_{mn} V^*_n \quad . \quad . \quad . \quad (72)$$

$$\left(\frac{\partial P}{\partial x}\right)_V = -\Sigma V_l Y^*_{lk} \frac{\partial Z^*_{km}}{\partial x} Y^*_{mn} V^*_n \quad . \quad . \quad . \quad (73)$$

Now consider the effect of replacing all voltages V_k by their complex conjugates V^*_k. From eqn. (73) and the reciprocity relation (16) it is seen that $(\partial P/\partial x)_V$ is unchanged but $\mathscr{F}_x$, and as a result $(F_x)_{av}$, will, in general, be different—$\mathscr{F}'_x$ and $(F'_x)_{av}$, say. Hence

$$2j\omega\mathscr{F}'_x = \Sigma V^*_l Y_{kl} \frac{\partial Z_{km}}{\partial x} Y^*_{mn} V_n \quad . \quad . \quad . \quad (74)$$

$$2j\omega(\mathscr{F}_x - \mathscr{F}'_x) = \Sigma (V_l V^*_n - V^*_l V_n) Y_{kl} \frac{\partial Z_{km}}{\partial x} Y^*_{mn} \quad . \quad (75)$$

By taking the imaginary parts of both sides of eqn. (75) and simplifying somewhat using the reciprocity relation (13), the following result is obtained:

$$(F_x)_{av} - (F'_x)_{av} = \frac{1}{j\omega} \Sigma (V_l V^*_n - V^*_l V_n) G_{kl} \frac{\partial X_{km}}{\partial x} B_{mn} \quad . \quad (76)$$

If all terminal voltages are of equal or opposite phase the right-hand side of eqn. (76) vanishes, giving

$$(F_x)_{av} = (F'_x)_{av} \quad . \quad . \quad . \quad . \quad . \quad . \quad . \quad (77)$$

This, of course, always applies for 2-terminal instruments. Otherwise $(F_x)_{av}$ and $(F'_x)_{av}$ are not necessarily exactly equal, the difference being given by eqn. (76).

$$\text{Also} \quad 2j\omega(\mathscr{F}_x + \mathscr{F}'_x) = \Sigma V_l Y_{kl} \frac{\partial Z_{km}}{\partial x} Y^*_{mn} V^*_n + \Sigma V^*_l Y_{kl} \frac{\partial Z_{km}}{\partial x} Y^*_{mn} V_n \quad . \quad (78)$$

which after some rearrangement together with the reciprocity relations (13) and (16) and eqn. (73) may be written

$$2j\omega(\mathscr{F}_x + \mathscr{F}'_x) = \left(\frac{\partial P^*}{\partial x}\right)_V - \left(\frac{\partial P}{\partial x}\right)_V - 4\Sigma V_l G_{kl} \frac{\partial Z_{km}}{\partial x} G_{mn} V^*_n - 2\Sigma V_l Y^*_{kl} \frac{\partial R_{km}}{\partial x} Y^*_{mn} V^*_n \quad . \quad (79)$$

Taking the imaginary parts of both sides of eqn. (79), and after some further algebra involving the reciprocity relations (13) and (16), the force $(F_x)_{av} + (F_x')_{av}$ is obtained:

$$\omega[(F_x)_{av} + (F_x')_{av}] + \mathscr{I}\left[\left(\frac{\partial P}{\partial x}\right)_V\right] = 2\Sigma V_l G_{kl} \frac{\partial X_{km}}{\partial x} G_{mn} V_n^* + \Sigma (V_l^* V_n + V_n V_l^*) G_{kl} \frac{\partial R_{km}}{\partial x} B_{mn} \quad . \quad (80)$$

The right-hand side of eqn. (80) is of second order in lossy terms. Therefore, we may write to first order in G_{kl}, i.e. for slightly lossy networks,

$$(F_x)_{av} + (F_x')_{av} = -\frac{1}{\omega}\mathscr{I}\left[\left(\frac{\partial P}{\partial x}\right)_V\right] \quad . \quad . \quad . \quad (81)$$

As before, $(\partial P/\partial x)_V$ may, with the help of eqns. (42) and (44), be written in terms of terminal parameters; thus

$$(F_x)_{av} + (F_x')_{av} = -\frac{1}{\omega}\mathscr{I}\left(\Sigma V_K \frac{\partial Y_{KL}^*}{\partial x} V_L^*\right) \quad . \quad (82)$$

$$= \frac{1}{\omega}\mathscr{I}\left(\Sigma V_K Y_{KL}^* \frac{\partial Z_{LN}^*}{\partial x} I_N^*\right) \quad . \quad (83)$$

These are the required forms for expressing $(F_x)_{av}$ in terms of quantities measurable at the input terminals to provide an absolute calibration. For 2-terminal networks (instruments) or for networks (instruments) with all applied voltages in phase, $(F_x)_{av}$ and $(F_x')_{av}$ are equal and eqns. (82) and (83) may be used directly; otherwise $(F_x)_{av} - (F_x')_{av}$ may be found from experiment and used in conjunction with eqns. (82) and (83). It must be noted that in instrument design every endeavour would be made to minimize $(F_x)_{av} - (F_x')_{av}$, usually to good effect, but eqn. (76) shows that it is still a quantity of first order in the losses.

The replacement of voltages by their complex conjugates may be made with any convenient phase reference, since eqn. (76) is invariant with respect to phase reference angle. The transformation to complex conjugate voltages has the effect of reversing the relative angles between terminal voltages.

For an indicating instrument containing no sliding contacts it will be seen that the variations in circuit-elements are essentially reactive, e.g. capacitances, self or mutual inductances are variable. It should be noted that the plate of a capacitor which may move in a lossy dielectric must be classed under the category of sliding contacts, although this is of no concern in practical instruments having a plate in a vacuum, air or some other gas of negligible power factor. Even eddy-current losses are changed not by any direct resistance variation but by changes of mutual inductance between current-carrying circuits and eddy-current meshes. A similar situation applies to lossy dielectrics where a capacitance change influences the dielectric loss. Thus, for most practical purposes,

$$\frac{\partial R_{lk}}{\partial x} \equiv 0 \quad . \quad . \quad . \quad . \quad . \quad . \quad . \quad (84)$$

leaving only one residual term in eqn. (80).

The requirement that the right-hand side of eqn. (80) should be small may be fulfilled by having all $G_{lk} \ll B_{lk}$. Such a condition (considered here as slightly lossy) is rather restrictive. However, eqns. (82) and (83) may still be useful approximations when some of the G_{lk} are not small, provided that the appropriate $\partial X_{lm}/\partial x$ are sufficiently small. The exact conditions under which eqns. (82) and (83) are applicable may not be stated simply in terms of quantities directly measurable at the input terminals. It is necessary to examine a reasonable model of an instrument before using them with confidence.

(4) EXTENSION OF VALIDITY OF THE THEORY

The work of the previous Sections has implicitly dealt with finite lumped-element networks. The extension to networks containing continuously distributed elements (e.g. transmission lines) presents no difficulty except for Section 3.3. The results of Sections 3.1 and 3.2 are expressible exactly in terms of parameters measurable at the input terminals independently of the number of terms present in the various summations. These results are thus integral results, which are unchanged by approximating a continuous network by a larger and larger number of finally infinitesimal elements. It is then concluded that the results of Sections 3.1 and 3.2 are valid for distributed parameter circuits. Furthermore, without formal proof this validity may be expected to extend to microwave networks or continuous systems in other fields where impedance is a useful concept, e.g. acoustics and mechanically vibrating systems. For microwave circuits each mode coupled to a generator would be considered as a separate pair of input terminals.

The results of Section 3.3 are not capable of immediate extension to continuous systems since they are approximate results and the error may be estimated only from an examination of the internal structure of the network, i.e. the error is not expressible in terms of parameters measurable at the input terminals. Even in the case of lumped-element networks some examination has to be made of the internal structure of the network before applying eqns. (82) and (83) of Section 3.3. For continuous-element networks such an examination becomes more complex and it may not always be possible to estimate the size of the error incurred. In a 2-terminal instrument having a Q-factor Q it amounts to ensuring that the error is of order $1/Q^2$.

(5) APPLICATIONS

The theory is applicable in principle to a wide variety of practical electrical instruments, ranging from power-frequency dynamometers and electrostatic voltmeters to microwave field or power meters, used to determine experimentally both absolute sensitivities and variations of sensitivity with frequency. A determination of the variation of sensitivity with frequency provides an absolute calibration if a standardization has been performed at some reference frequency.

The theory is of greatest utility as the basis of an experimental calibration when applied to systems where the force is not simply calculable because of complications caused by secondary effects or by unknown internal circuit parameters. However, to provide a simple illustration involving results from Section 3 the force along the line on a short-circuit of a transmission line or waveguide will be considered. To justify the use of the theory here it may be supposed that the line constants are not accurately known.

Consider a length l of lossless transmission line or waveguide in vacuum having characteristic impedance Z_0 (real) with a source of voltage V applied at one end and short-circuited by a perfectly conducting plane at the other end. Let I be the source current. The force $(F_l)_{av}$ on the short-circuiting plane may then be calculated from Section 3.1. The impedance presented to the generator is

$$Z = jZ_0 \tan \frac{2\pi l}{\lambda_g} \quad . \quad . \quad . \quad . \quad . \quad (85)$$

Eqn. (55) then gives

$$(F_l)_{av} = \frac{1}{2j\omega} II^* \frac{\partial Z}{\partial l} \quad . \quad . \quad . \quad . \quad . \quad (86)$$

$$= II^* \frac{Z_0 \lambda}{2c\lambda_g} \sec^2 \frac{2\pi l}{\lambda_g} \quad . \quad . \quad . \quad . \quad (87)$$

The force $(F_l)_{av}$ is always directed in the sense of increasing l and arises from the change in electromagnetic momentum required to reverse a travelling wave to give rise to the actual standing wave on the line.

If another section of line or waveguide (lossy or not) or an arbitrary reciprocal 2-terminal-pair network is interposed between the short-circuited loss-free line and the generator, the force $|(F_x)_{av}|$ may be calculated from eqns. (68) and (69).

If the short-circuited length of line considered is lossy, the results of Section 3.3 may be applicable. Let γ be the propagation coefficient of the line.

Eqn. (81) may be used to find $(F_l)_{av}$ provided that the right-hand side of eqn. (80) is suitably small. In considering a lumped-circuit approximation to the line the meshes may be chosen such that the source V is contained in one mesh only (mesh 1). Likewise the short-circuit may be confined to only one mesh (mesh s). The remainder in eqn. (80) becomes

$$2VV^*\left(G_{s1}^2 \frac{\partial X_{ss}}{\partial l} + G_{s1}B_{s1}\frac{\partial R_{ss}}{\partial l}\right) \quad . \quad . \quad . \quad (88)$$

But $\partial X_{ss}/\partial l$ and $\partial R_{ss}/\partial l$ are simply $j\omega L_s$ and R_s, respectively. Also, from transmission-line theory,

$$Y_{s1} = G_{s1} + jB_{s1} = -\frac{j}{Z_0}\operatorname{cosec}\gamma l \quad . \quad . \quad . \quad (89)$$

Sufficient conditions for applicability of eqn. (81) are

$$\mathscr{I}\left(\frac{1}{Z_0}\operatorname{cosec}\gamma l\right) \ll \mathscr{R}\left(\frac{1}{Z_0}\operatorname{cosec}\gamma l\right) \quad . \quad . \quad . \quad (90)$$

and

$$R_s \ll \omega L_s \quad . \quad . \quad . \quad . \quad . \quad . \quad (91)$$

giving finally

$$(F_l)_{av} = \frac{VV^*}{2\omega}\frac{\partial B}{\partial l} \quad . \quad . \quad . \quad . \quad . \quad (92)$$

In this example the force is directly expressible as $\frac{1}{2}I_sI_s^*L_s$, but eqn. (92) involves only quantities accessible at the input terminals. The theory of Section 3.2 may be used to give a result of wider applicability. Using Vratsanos's theorem[7] as obtained in eqn. (36),

$$\left(\frac{\partial}{\partial l}\right)_V (VI) = -I_s^2\frac{\partial Z_{ss}}{\partial l} \quad . \quad . \quad . \quad . \quad (93)$$

$$= -I_s^2 j\omega L_s \quad . \quad . \quad . \quad . \quad (94)$$

if

$$R_s \ll \omega L_s$$

But

$$|(F_l)_{av}| = \tfrac{1}{2}|I_s|^2 L_s \quad . \quad . \quad . \quad . \quad . \quad (95)$$

Hence

$$|(F_l)_{av}| \leqslant \frac{1}{2\omega}\left|\left(\frac{\partial}{\partial l}\right)_V (VI)\right| \quad . \quad . \quad . \quad . \quad . \quad (96)$$

$$= \frac{VV^*}{2\omega}\left[\left(\frac{\partial G}{\partial l}\right)^2 + \left(\frac{\partial B}{\partial l}\right)^2\right]^{1/2} \quad . \quad . \quad . \quad (97)$$

This result is correct to second order in $R_s/\omega L_s$ without the qualifying condition (90) required for the use of eqn. (92).

(6) CONCLUSIONS

The average generalized force $(F_x)_{av}$ corresponding to a generalized co-ordinate x upon which a number of circuit-elements in a passive linear reciprocal network may depend has been expressed in terms of quantities accessible at the input terminals. For loss-free networks or networks in which a single loss-free 2-terminal subnetwork is variable, exact results are obtained. For a general network with general parameter dependence an approximation applicable to slightly lossy networks has been derived. However, in this case some examination of the detailed network structure may be necessary to assess the error incurred in using the approximation. The results have been generalized from lumped-element networks to continuous systems and are found to have applicability in other fields where impedance is a useful concept.

Of particular immediate interest is the application of the theory to electrical measuring instruments. It has been shown that the theory gives, in principle, a method for establishing absolute standards of voltage, current and power over the range of the whole radio-frequency spectrum. However, practical problems concerning the accuracy with which the required derivatives of impedance or admittance parameters may be measured have not been discussed and need to be considered for each individual situation.

(7) REFERENCES

(1) CULLEN, A. L.: 'A General Method for the Absolute Measurement of Microwave Power', *Proceedings I.E.E.*, Monograph No. 24, April, 1952 (**99**, Part IV, p. 112).

(2) CULLEN, A. L., and STEPHENSON, I. M.: 'A Torque-Operated Wattmeter for 3 cm Microwaves', *ibid.*, Monograph No. 42, December, 1952 (**99**, Part IV, p. 294).

(3) CULLEN, A. L., ROGAL, B., and OKAMURA, S.: 'A Wide-Band Double-Vane Torque-Operated Wattmeter for 3 cm Microwaves', *Transactions of the Institute of Radio Engineers*, April, 1958, **MTT-6**, p. 133.

(4) CULLEN, A. L., and FRENCH, H. A.: 'An Instrument for the Absolute Measurement of Low-Level Microwave Power in the 3 cm Band', *Proceedings I.E.E.*, Monograph No. 237 R, May, 1957 (**104** C, p. 456).

(5) OKAMURA, S., KANZAKI, S., KUROKAWA, S., and KONDO, G.: 'A Double-Vane Torque-Operated Wattmeter for 7,000 Mc', *Journal of the Radio Research Laboratories, Tokyo*, 1958, **5**, p. 157.

(6) GUILLEMIN, E. A.: 'Introductory Circuit Theory' (Wiley, 1953).

(7) VRATSANOS, J.: 'Zur Berechnung der Stromverteilung in einem linearen Netzwerk', *Archiv der elektrischen Übertragung*, 1957, **11**, p. 76.

(8) ANSELL, H. G.: 'Vratsanos's Theorem', *Transactions of the Institute of Radio Engineers*, June, 1958, **CT-5**, p. 143.

(9) DEARDS, S. R.: 'Vratsanos's Theorem', *ibid.*, June, 1958, **CT-5**, p. 143.

(10) HOWE, C. M.: 'Extension of a Theorem of Vratsanos', *ibid.*, September, 1958, **CT-5**, p. 229.

621.376.6 : 517.524

The Institution of Electrical Engineers
Monograph No. 367 M
Mar. 1960
©

FURTHER THEORY OF A CERTAIN CONTINUED FRACTION

By O. P. D. CUTTERIDGE, M.Sc.(Eng.), Ph.D., Associate Member.

(*The paper was first received* 12*th October, and in revised form* 14*th December*, 1959. *It was published as an* INSTITUTION MONOGRAPH *in March*, 1960.)

SUMMARY

The paper develops further theory of a certain type of continued fraction relevant to the problem of determining the character of the zeros of a polynomial. Two theorems provide tests for the number of positive zeros, real zeros and pairs of conjugate complex zeros of a real polynomial. Two numerical examples are included, one of which shows the application of the method to a problem in linear-network theory.

(1) INTRODUCTION

In a previous paper[1] the author introduced a type of continued fraction which, it was suggested, was less laborious to form from two suitable polynomials than either a Stieltjes fraction or a J-fraction.[2] Sufficient theory was given to deal with the question of linear system stability and related problems, and it is the purpose of this paper to develop further theory relevant to the problem of determining the character of the zeros of a polynomial.

(2) CONTINUED-FRACTION EXPANSION AND TWO THEOREMS

Let $f(p)$ be a polynomial in p with real coefficients and $f'(p)$ its derivative with respect to p. Now form the continued-fraction expansion

$$\frac{f'(p)}{f(p)} = \cfrac{1}{a_1p + b_1 + \cfrac{1}{\cfrac{a_2}{p} + b_2 + \cfrac{1}{a_3p + b_3 + \cfrac{1}{\cfrac{a_4}{p} + b_4 + \ddots}}}} \quad . \quad (1)$$

The final quotient takes the form $a_k/p + b_k$ or $a_kp + b_k$ according as k, the number of distinct zeros of $f(p)$, is even or odd. If the polynomial $f(p)$ has no multiple zeros then $k = n$, the degree of the polynomial. It is supposed that

$$a_i \neq 0 \quad b_i \neq 0 \quad i = 1, 2, 3, \ldots k \quad . \quad . \quad . \quad (2)$$

We now have the following theorems, proofs of which will be given in Section 3.

Theorem 1.

The number of positive zeros of $f(p)$ is equal to the number of negative b_i minus the number of negative a_i.

Theorem 2.

The number of real zeros of $f(p)$ is equal to $(k - 2N)$ and the number of pairs of conjugate-complex zeros is equal to N, where N is equal to the number of negative a_i.

Both theorems yield the numbers of distinct zeros in each case, the multiplicity of zeros not being counted.

(3) PROOFS OF THEOREMS

Eqn. (1) can be rewritten as

$$\frac{f'(p)}{f(p)} = \cfrac{1}{a_1p + b_1 - \cfrac{1}{\cfrac{-a_2}{p} - b_2 - \cfrac{1}{a_3p + b_3 - \cfrac{1}{\cfrac{-a_4}{p} - b_4}}}} \quad . \quad (3)$$

$$= \cfrac{1}{q_1 - \cfrac{1}{q_2 - \cfrac{1}{q_3 - \cfrac{1}{q_4}}}} \quad . \quad . \quad . \quad . \quad . \quad . \quad . \quad . \quad . \quad . \quad (4)$$

$$\ddots \; - \frac{1}{q_k}$$

where

$$q_i = a_ip + b_i \qquad i \text{ odd} \quad . \quad . \quad . \quad (5)$$

$$= -\left(\frac{a_i}{p} + b_i\right) \qquad i \text{ even} \quad . \quad . \quad . \quad (6)$$

Now define a sequence of rational functions $f_0, f_1, f_2, \ldots f_k$ by the relations

$$\left.\begin{aligned} f_0 &= 1 \\ f_1 &= q_k \\ f_{i+1} &= q_{k-i}f_i - f_{i-1} \quad i = 1, 2, 3, \ldots k-1 \end{aligned}\right\} \quad . \quad . \quad (7)$$

These functions, f_i, would occur in the evaluation of the continued fraction in eqn. (4) from first principles, i.e. from the bottom, and in these terms the value of this continued fraction would be f_{k-1}/f_k. When the q_i have the values given in eqns. (5) and (6), if $f(p)$ has no multiple zeros,

$$p^{k/2}f_k = f(p) \quad \text{and} \quad p^{k/2}f_{k-1} = f'(p) \quad . \quad . \quad . \quad (8)$$

for k even

$$p^{(k-1)/2}f_k = f(p) \quad \text{and} \quad p^{(k-1)/2}f_k = f'(p) \quad . \quad . \quad (9)$$

for k odd

The zeros of f_k and f_{k-1} can therefore be identified with the distinct zeros of $f(p)$ and $f'(p)$, respectively, and f_{k-1} is positive

---

Correspondence on Monographs is invited for consideration with a view to publication.

Dr. Cutteridge is in the Electrical Engineering Department, Faculty of Technology, University of Manchester.

The main results of this paper were given in a paper 'On Some Uses of a Certain Continued Fraction', contributed to the Conference on Modern Network Theory held at the University of Birmingham, September, 1959.

f f_k is increasing through a zero and negative if f_k is decreasing hrough a zero.

The sequence of functions

$$f_0, f_1, f_2, \ldots f_k \quad . \quad . \quad . \quad . \quad . \quad . \quad (10)$$

s similar to the sequence of Sturm functions, and a similar type of argument to that used in the proof of Sturm's theorem[3] is applicable. The functions f_i have the following properties, easily derived from eqns. (7):

(*a*) No two consecutive functions of the sequence can vanish for the same value of p.

(*b*) At a value of p that makes f_i vanish, f_{i-1} and f_{i+1} have opposite signs.

The number of changes of sign along the sequence $f_0, f_1, f_2, \ldots f_k$ can therefore change in only one of two ways, either by p passing through a zero of f_k or by p passing through the origin. This last possibility follows from the presence of poles at the origin in the functions f_i owing to the inverse powers of p. Any difficulties caused by the presence of these poles are easily overcome by excluding the origin itself from the discussion. We therefore have the following results:

(*c*) The number of negative zeros of f_k is equal to the number of changes of sign along sequence (10) at $p = -\infty$ minus the number of changes of sign along sequence (10) at $p = -0$.

(*d*) The number of positive zeros of f_k is equal to the number of changes of sign along sequence (10) at $p = +0$ minus the number of changes of sign along sequence (10) at $p = +\infty$.

We shall now associate the numbers of changes of sign at the origin and infinity with the signs of the coefficients a_i and b_i. First, it should be noted that it is the product terms $q_k, q_kq_{k-1}, q_kq_{k-1}q_{k-2}, \ldots$ which contain the highest and the lowest powers of p in $f_1, f_2, f_3, \ldots$ respectively, and therefore the behaviour of these functions at zero and infinity is easily obtained. As the argument is somewhat different in detail accordingly to whether k is even or odd, we shall consider the cases separately.

(3.1) Case of k Even

The behaviour of sequence (10) at infinity for k even becomes

$$1, -b_k, -a_{k-1}b_kp, b_{k-2}a_{k-1}b_kp, a_{k-3}b_{k-2}a_{k-1}b_kp^2, \ldots \quad (11)$$

and at the origin

$$1, \frac{-a_k}{p}, \frac{-b_{k-1}a_k}{p}, \frac{a_{k-2}b_{k-1}a_k}{p^2}, \frac{b_{k-3}a_{k-2}b_{k-1}a_k}{p^2}, \ldots \quad (12)$$

Thus,

number of sign changes in sequence (12) when $p = +0$
= number of terms $a_k, a_{k-2}, \ldots a_2$ that are positive
+ number of terms $b_{k-1}, b_{k-3}, \ldots b_1$ that are negative
. . . . (13)

and

number of sign changes in sequence (11) when $p = +\infty$
= number of terms $b_k, b_{k-2}, \ldots b_2$ that are positive
+ number of terms $a_{k-1}, a_{k-3}, \ldots a_1$ that are negative
. . . . (14)

Therefore,

number of positive zeros of f_k
= (number of terms $a_k, a_{k-2}, \ldots a_2$ that are positive
+ number of terms $b_{k-1}, b_{k-3}, \ldots b_1$ that are negative)
− (number of terms $b_k, b_{k-2}, \ldots b_2$ that are positive
+ number of terms $a_{k-1}, a_{k-3}, \ldots a_1$ that are negative)
. . . . (15)

Similarly,

number of sign changes in sequence (11) when $p = -\infty$
= number of terms $b_k, b_{k-2}, \ldots b_2$ that are positive
+ number of terms $a_{k-1}, a_{k-3}, \ldots a_1$ that are positive
. . . . (16)

and

number of sign changes in sequence (12) when $p = -0$
= number of terms $a_k, a_{k-2}, \ldots a_2$ that are negative
+ number of terms $b_{k-1}, b_{k-3}, \ldots b_1$ that are negative
. . . . (17)

and therefore,

number of negative zeros of f_k
= (number of terms $b_k, b_{k-2}, \ldots b_2$ that are positive
+ number of terms $a_{k-1}, a_{k-3}, \ldots a_1$ that are positive)
− (number of terms $a_k, a_{k-2}, \ldots a_2$ that are negative
+number of terms $b_{k-1}, b_{k-3}, \ldots b_1$ that are negative)
. . . . (18)

Adding eqns. (15) and (18),

number of real zeros of f_k
= number of terms $a_k, a_{k-1}, a_{k-2}, \ldots a_1$ that are positive,
− number of terms $a_k, a_{k-1}, a_{k-2}, \ldots a_1$ that are negative
. . . (19)

(3.2) Case of k Odd

The behaviour of sequence (10) at infinity for k odd becomes

$$1, a_kp, -b_{k-1}a_kp, -a_{k-2}b_{k-1}a_kp^2, b_{k-3}a_{k-2}b_{k-1}a_kp^2, \ldots \quad . \quad . \quad . \quad . \quad (20)$$

and at the origin

$$1, b_k, \frac{-a_{k-1}b_k}{p}, \frac{-b_{k-2}a_{k-1}b_k}{p}, \frac{a_{k-3}b_{k-2}a_{k-1}b_k}{p^2}, \ldots \quad (21)$$

Thus

number of sign changes in sequence (21) when $p = +0$
= number of terms $b_k, b_{k-2}, \ldots b_1$ that are negative
+ number of terms $a_{k-1}, a_{k-3}, \ldots a_2$ that are positive
. . . . (22)

and

number of sign changes in sequence (20) when $p = +\infty$
= number of terms $a_k, a_{k-2}, \ldots a_1$ that are negative
+ number of terms $b_{k-1}, b_{k-3}, \ldots b_2$ that are positive
. . . . (23)

Therefore,

number of positive zeros of f_k
= (number of terms $b_k, b_{k-2}, \ldots b_1$ that are negative
+ number of terms $a_{k-1}, a_{k-3}, \ldots a_2$ that are positive)
− (number of terms $a_k, a_{k-2}, \ldots a_1$ that are negative
+ number of terms $b_{k-1}, b_{k-3}, \ldots b_2$ that are positive)
. . . . (24)

which is exactly the same result as eqn. (15) for k even.

Similarly,

number of sign changes in sequence (20) when $p = -\infty$
= number of terms $a_k, a_{k-2}, \ldots a_1$ that are positive
+ number of terms $b_{k-1}, b_{k-3}, \ldots b_2$ that are positive
. . . . (25)

and

number of sign changes in sequence (21) when $p = -0$
= number of terms $a_{k-1}, a_{k-3}, \ldots a_2$ that are negative
+ number of terms $b_k, b_{k-2}, \ldots b_1$ that are negative
. . . . (26)

and therefore,

number of negative zeros of f_k
= (number of terms $a_k, a_{k-2}, \ldots a_1$ that are positive
+ number of terms $b_{k-1}, b_{k-3}, \ldots b_2$ that are positive)
− (number of terms $a_{k-1}, a_{k-3}, \ldots a_2$ that are negative
+ number of terms $b_k, b_{k-2}, \ldots b_1$ that are negative)
. . . . (27)

Adding eqns. (24) and (27),

number of real zeros of f_k
= number of terms $a_k, a_{k-1}, a_{k-2}, \ldots a_1$ that are positive
− number of terms $a_k, a_{k-1}, a_{k-2}, \ldots a_1$ that are negative
. . . . (28)

which is exactly the same result as eqn. (19) for k even.

(3.3) Completion of Proof

The results of Sections 3.1 and 3.2 can be rearranged as follows:

Let $N =$ Number of negative a_i . . . (29)

then $k - N =$ Number of positive a_i . . . (30)

and eqns. (19) and (28) both yield

number of real zeros of $f_k = k - 2N$ . . . (31)

and

number of pairs of conjugate complex zeros of $f_k = N$ (32)

which completes the proof of Theorem 2.

As eqns. (15) and (24) correspond to the following result:

number of positive zeros of f_k =
number of negative b_i − number of negative a_i . (33)

the proof of Theorem 1 is also complete.

(4) NUMERICAL EXAMPLES

(4.1) Example 1

If $f(p) = p^4 + 2p^3 + 3p^2 + 2p + 1$ . . (34)

then $f'(p) = 4p^3 + 6p^2 + 6p + 2$ . . . . (35)

and
$$\frac{f'(p)}{f(p)} = \cfrac{1}{\cfrac{p}{4} + \cfrac{1}{\cfrac{1}{2} + \cfrac{1}{\cfrac{-4}{3p} - \cfrac{8}{3}}}} \quad . . . . (36)$$

which indicates no positive zeros and one pair of conjugate complex zeros each member of which must be of the order 2 owing to the premature termination of the continued fraction. Since

$$f(p) = (p^2 + p + 1)^2 = (p + 1/2 + j\sqrt{3}/2)^2(p + 1/2 - j\sqrt{3}/2)^2 \quad . . . . (37)$$

this result is seen to be correct.

(4.2) Example 2

This example illustrates the application of the continued fraction in testing for positive real functions in network theory. According to Bode,[4] a driving-point impedance function of a passive network can have no poles or zeros in the right half-plane and its real part cannot be negative at real frequencies. Consider now the examination of the function $Z(p)$, where

$$Z(p) = \frac{p^3 + 4p^2 + 2p + 1}{2p^3 + 2p^2 + 5p + 3} \quad . . . (38)$$

i.e.
$$\mathcal{R}[Z(j\omega)] = \frac{2\omega^6 - \omega^4 - 4\omega^2 + 3}{\text{sum of squares}} \quad . . . (39)$$

It is required to verify that

$$F_1(p) = p^3 + 4p^2 + 2p + 1 \quad . . . (40)$$

and
$$F_2(p) = 2p^3 + 2p^2 + 5p + 3 \quad . . . (41)$$

have their zeros confined to the left half p-plane, which is evident by inspection (see, for example, Reference 5), and that

$$f(x) = 2x^3 - x^2 - 4x + 3 \quad . . . . (42)$$

has no positive real zero of odd multiplicity.

From eqn. (42),

$$f'(x) = 6x^2 - 2x - 4$$

and the working for the appropriate continued-fraction test is

$$\begin{array}{l}
6x^2-2x-4\,\big)\,2x^3 - x^2 - 4x + 3\,\big(\frac{x}{3} - \frac{3}{4} \\
\qquad 2x^3 - \frac{2}{3}x^2 - \frac{4}{3}x \\
\qquad\quad -\frac{9}{2}x^2 + \frac{3}{2}x + 3 \\
\qquad\quad \underline{\qquad\qquad\qquad\qquad} \\
\qquad\quad \frac{25}{6}x^2 - \frac{25}{6}x \quad\big)\,6x^2 - 2x - 4\,\big(\frac{36}{25} + \frac{24}{25x} \\
\qquad\qquad\qquad 6x^2 - 6x \\
\qquad\qquad\qquad \underline{\qquad\qquad} \\
\qquad\qquad\qquad\quad 4x - 4
\end{array}$$

Using Theorems 1 and 2, therefore, $f(x)$ has one positive and one negative zero, one of which must be of order 2 owing to the premature termination of the continued fraction. However, since $f(0)$ and $f(+\infty)$ are both positive it is the positive zero of $f(x)$ which is of order 2 and hence the original function $Z(p)$ corresponds to the driving-point impedance of a passive network.

(5) CONCLUSIONS

The theory of a continued fraction, begun in a previous paper, has been extended here to provide a test for the character of the zeros of a polynomial and, in particular, for the number of positive zeros of a polynomial. The results are given in the form of two theorems which are illustrated by numerical examples in Section 4, the second example being an application to linear network theory. The methods can also be used to investigate other types of continued fraction that may arise, for example from degenerate cases.

By using the determinantal expressions for the continued fraction coefficients in terms of the coefficients of the divisor and dividend polynomials given in Reference 1, the tests for the character of the zeros of a polynomial can be put into determinantal form giving results alternative to those given in Reference 6.

In the author's opinion the type of continued-fraction expansion given here is quicker to compute than either a Stieltjes fraction or a J-fraction.[2] For most rapid computation a scheme of detached coefficients should be used or, better still, an easily constructed numerical algorithm.

(6) REFERENCES

(1) CUTTERIDGE, O. P. D.: 'Two-Terminal *RC* Networks and Theoretically Related Topics' (see p. 275).
(2) WALL, H. S.: 'Analytic Theory of Continued Fractions' (Van Nostrand, 1948).
(3) TURNBULL, H. W.: 'Theory of Equations' (Oliver and Boyd, 1947), 4th Edition, p. 103.
(4) BODE, H. W.: 'Network Analysis and Feedback Amplifier Design' (Van Nostrand, 1945), p. 120.
(5) CUTTERIDGE, O. P. D.: 'The Stability Criteria for Linear Systems', *Proceedings I.E.E.*, Monograph No. 328 M, February, 1959 (**106** C, p. 125).
(6) CUTTERIDGE, O. P. D.: 'Some Tests for the Number of Positive Zeros and for the Numbers of Real and Complex Zeros of a Real Polynomial', *ibid.*, Monograph No. 350 M, December, 1959 (**107** C, p. 105).

621.3.013.2

The Institution of Electrical Engineers
Monograph No. 368 M
Mar. 1960
©

FLUX DISTRIBUTION IN A PERMEABLE SHEET WITH A HOLE NEAR AN EDGE

By B. V. JAYAWANT, Ph.D., B.Eng., Graduate.

(*The paper was first received* 28*th October, and in revised form* 29*th December*, 1959. *It was published as an* INSTITUTION MONOGRAPH *in March*, 1960.)

SUMMARY

In the measurement of the distribution of magnetic flux in the cores of electrical machines by locating search coils in them, the presence of a search-coil will alter the flux in that region. It is therefore necessary to make a correction to the measured flux. The problem is the solution of Laplace's equation in two dimensions in a material assumed to be of constant permeability, and it has an analogy in hydrodynamics. The solution is obtained by a conformal transformation; it is found that the correction is quite significant when the distance of the centre of the hole from the edge is equal to its diameter.

(1) INTRODUCTION

The distribution of magnetic flux in a sheet of constant finite permeability with a hole near an edge is similar in nature to the flow of a frictionless incompressible fluid past a circular cylinder parallel to a plane in hydrodynamics, or any other analogous problem obeying Laplace's equation in two dimensions. In electrostatics the equivalent is a conducting cylinder held insulated near a plate at some potential and where the electric field is initially perpendicular to the plate, which would be the case if there is another plate at a great distance from it. In electrodynamics the equivalent is current flow in a conducting medium round an embedded insulator. The problem of magnetic flux distribution mentioned above has arisen in the determination of the penetration of flux in the cores of electrical machines, built up of laminations, by locating search coils in them.[1] In the presence of a search-coil hole sufficiently close to the edge of the laminations the flux distribution will clearly no longer remain the same as it would be in the absence of the hole. The measured flux, therefore, as deduced from the e.m.f. induced in the search coil when the machine is excited, will be less than the flux which exists in the region enclosed by the search coil in the absence of the hole. An attempt has been made here to determine analytically the correction necessary to the measured flux. Alternatively, an allowance may be made in the location of the hole.

(2) GENERAL SOLUTION

In the hydrodynamic problem of the flow past a cylinder, as with the other analogous problems, the streamlines and velocity potentials can be determined by means of a conformal transformation. This conformal transformation, in the form of an infinite series, is derived from the fact that the disturbance of a cylindrical obstacle to the flow in an unbounded, initially uniform, stream can be represented by means of a doublet source placed at the centre of the cylinder in the stream. The effect of another cylinder of a different radius, and in the limit of a plane surface, i.e. a cylinder of infinite radius, is accounted for by the method of images. The successive approximations then give an infinite series, the terms of which involve the radius and the displacement of the cylinder from the plane surface. Assuming that the plane surface and the cylinder extend to and from infinity, i.e. a purely two-dimensional problem, if the radius of the cylinder is R and the distance of its centre from the plane surface is b, the series for the complex potential for the region can be written as (see Section 7)

$$w = \phi + j\psi = -jUz + 2jUR^2z\left[\frac{1}{x^2 - b^2} + \sum_{n=1}^{\infty} \frac{R^{2n}}{\prod_{r=0}^{n-1}(b + x_r)^2 . (z^2 - x_n^2)}\right] \quad (1)$$

where $z = x + jy$; $x_0 = b$ and $x_n = b - \dfrac{R^2}{b + x_{n-1}}$

(3) MAGNETIC CASE

In any of the problems stated, to determine completely the field in the region it is necessary to evaluate the complex potential W, i.e. the values ϕ and ψ of the real and imaginary parts of the series at different points in the z-plane. In the magnetic case 'constant ψ' lines represent the flux lines and 'constant ϕ' lines

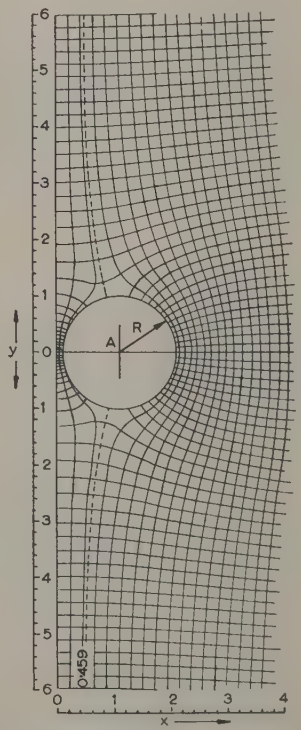

Fig. 1.—Field plot in the region of a hole near an edge.
OA = $b = 1 \cdot 1R$.

Correspondence on Monographs is invited for consideration with a view to publication.

Dr. Jayawant was formerly with the Metropolitan-Vickers Electrical Co., Ltd., and is now in the Department of Electrical Engineering, Queen's University, Belfast.

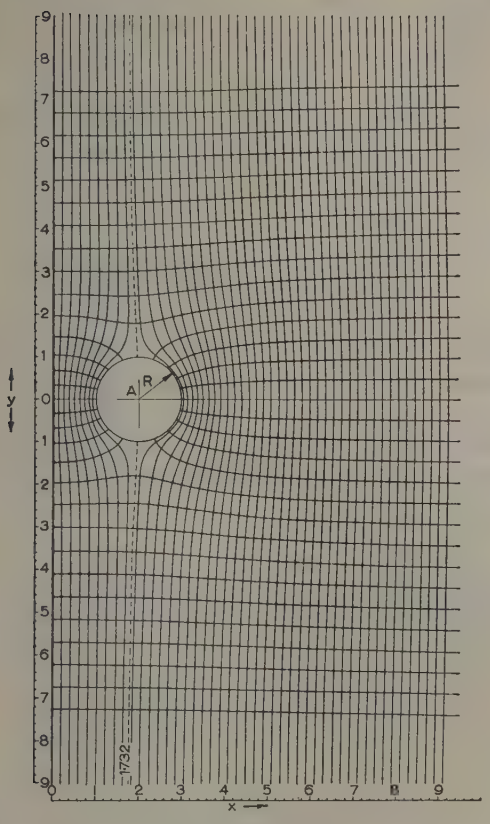

Fig. 2.—Field plot in the region of a hole near an edge.
OA = $b = 2R$.

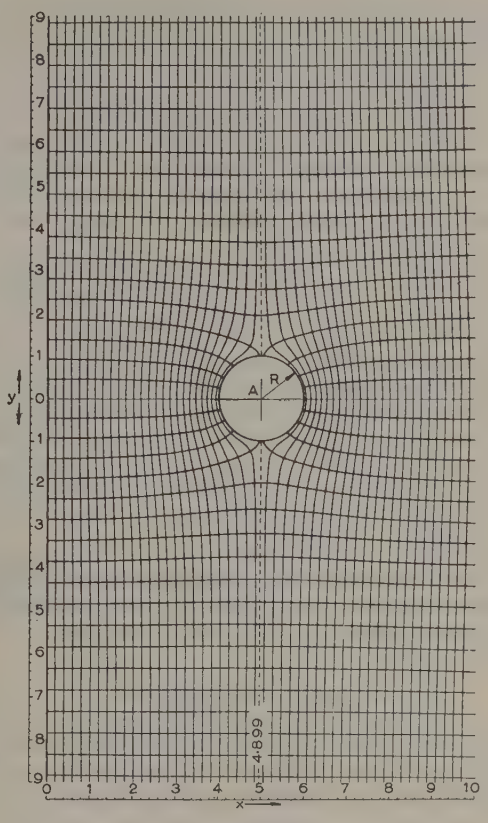

Fig. 3.—Field plot in the region of a hole near an edge.
OA = $b = 5R$.

the scalar magnetic equipotentials. It would be virtually impossible, however, without the use of a high-speed digital computer to evaluate these quantities from the series, at the number of points in the z-plane, to give the field plots (Figs. 1–3) each for a different location of the hole. In these Figures the edge of the laminations is assumed to be the imaginary axis and the hole is located a distance b along the real axis in the z-plane. The series is rapidly convergent and it is sufficient to evaluate the first five terms only.

The flux in these Figures as measured by a search coil is the value of the stream function ψ_c on the circumference of the hole, or the value of the dividing streamline (which is shown dotted in each field plot of Figs. 1–3). The flux in the absence of the hole would be the x-co-ordinate of the centre of the hole, b. The correction is therefore the difference of these two quantities, i.e. $b - \psi_c$, and as a percentage it may be expressed as

$$\text{Percentage correction} = 100(1 - \psi_c/b) \quad . \quad . \quad (2)$$

(4) RESULTS AND CONCLUSIONS

The calculated corrections for a range of positions of the hole are given in Table 1.

For the purposes of calculating only the correction factor of Table 1 it is not necessary to obtain the field plot of the whole region. Since the stream function anywhere on the circumference of the hole is the same, ψ_c may be calculated with greatest ease at the point where the circle cuts the x-axis, i.e. $y = 0$, from

Table 1

Distance of the centre of the hole from the edge	Percentage correction
$1{\cdot}1R$	58·27
$1{\cdot}5R$	25·47
$2R$	13·40
$3R$	5·73
$4R$	3·20
$5R$	2·02
$6R$	1·40

The distance of the *circumference* of the hole in these cases above will be $0{\cdot}1R$, $0{\cdot}5R$, R, $2R$, $3R$, etc.

the imaginary part of the series conformal transformation [eqn. (1)]. This value may also be approximately calculated as

$$\psi_c = \sqrt{(b^2 - R^2)} \quad . \quad . \quad . \quad . \quad . \quad (3)$$

It has since been brought to the notice of the author that the correction factors may be calculated by the following formula:

$$\text{Percentage correction} = 100 \times \left[1 - \sqrt{\left(1 - \frac{1}{n^2}\right)}\right] \quad . \quad (4)$$

where $n = \dfrac{\text{Distance of the centre of hole}}{\text{Radius of the hole}}$

This result is obtained by substituting the value of ψ_c from eqn. (3) in eqn. (2).

An assumption besides that of a constant permeability for the material, implicit in drawing the field plots, is that of zero

permeability of the hole. At high flux densities, where the permeability of the material is no longer constant and may itself become comparable to that of the region of the hole, no rigid analytical treatment would seem to be valid. Another problem where the hole has a different but definite permeability is that of bolts in poles.[2] An analytical treatment of this problem along the lines indicated here, but with a good deal more complexity, is thought possible and is contemplated. However, it seems that in this problem only a combination of experiment and analytically obtained field plots would give results consistent with practice.

The formula given shows that the correction diminishes approximately as the square of the distance of the centre of the hole from the edge, except when very near.

The results of the analytical solution are now being used for the flux-penetration measurements in rotating electrical machines with search coils located in the cores, especially for the tooth-ripple flux measurements. In the case of the tooth-ripple flux penetration, owing to the high ripple frequencies it is of extreme importance to locate the search coils as close to the inside edge of the core as possible. The corrections are therefore of considerable value in determining with greater accuracy the flux that penetrates the core laminated or otherwise.

The field plots have also been used to check the accuracy of an electrolytic tank with a new type of probe under development by setting up a model of the electrostatic case and by comparing the tank measurements with the analytical field plots.

(5) ACKNOWLEDGMENTS

The author wishes to thank Sir Willis Jackson, Director of Research and Education, Metropolitan-Vickers Electrical Co., Ltd., for constant encouragement during the course of this investigation and for permission to publish the paper.

(6) REFERENCES

(1) GREIG, J., and MUKHERJI, K. C.: 'An Experimental Investigation of the Tooth Ripple Flux Pulsations in Smooth Laminated Pole-Shoes', *Proceedings I.E.E.*, Monograph No. 223 S, February, 1957 (**104** C, p. 332).

(2) HAGUE, B.: 'The Effect produced on the Permeance of a Laminated Pole-Core by the Insertion of a Solid Steel Fixing-Piece', *Journal I.E.E.*, 1926, **64**, p. 476.

(7) APPENDIX

The disturbance of a circular cylinder in an unbounded, initially uniform flow can be represented by a doublet at the centre of the cylinder. Thus the complex potential for a circular cylinder of radius R in an unbounded stream of velocity U along the imaginary axis [Fig. 4(*a*)] is

$$w = -jU\left(z + \frac{R^2}{z}\right)$$

where UR^2/z is the complex potential due to the doublet.

We can then take into account the presence of the plane surface by the method of images using the following well-known theorem:

A doublet of strength μ at a point $(-\xi, 0)$ has an image in the circle $(x-b)^2 + y^2 = R^2$ of strength $\mu\left(\frac{R}{b+\xi}\right)^2$ and at the inverse point $\left(b - \frac{R^2}{b+\xi}, 0\right)$ [see Fig. 4(*b*)].

A doublet of strength UR^2 at the point $(b, 0)$ has an image in the plane $x = 0$ of strength UR^2 at the point $(-b, 0)$. This

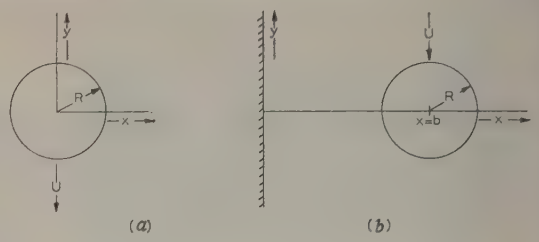

Fig. 4.—(*a*) Cylinder in an unbounded region.
(*b*) Cylinder near a plane boundary.

doublet has an image in the cylinder of strength $UR^2\left(\frac{R}{2b}\right)^2$ at the point $\left(b - \frac{R^2}{2b}, 0\right)$, which, in turn, has an image in $x = 0$ of strength $UR^2\left(\frac{R}{2b}\right)^2$ at the point $\left[-\left(b - \frac{R^2}{2b}\right), 0\right]$; this latter doublet has an image in the circle at the inverse point of strength $UR^2\left(\frac{R}{2b}\right)^2\left(\frac{R}{2b - \frac{R^2}{2b}}\right)^2$, etc.

Accordingly the flow is built up of a doubly infinite set of doublets arranged symmetrically with respect to the plane $x = 0$. The location of the doublets in the region $x > 0$ are given by

$$x = b,\ x = b - \frac{R^2}{2b},\ x = b - \frac{R^2}{b + \left(b - \frac{R^2}{2b}\right)}$$

$$x = b - \frac{R^2}{b + \left(b - \frac{R^2}{2b - \frac{R^2}{2b}}\right)}, \text{ etc.}$$

or as indicated in Fig. 5,

$$x = x_0,\ x = x_1,\ x = x_2 \ldots x = x_n$$

where $$x_0 = b;\ x_n = b - \frac{R^2}{b + x_{n-1}}$$

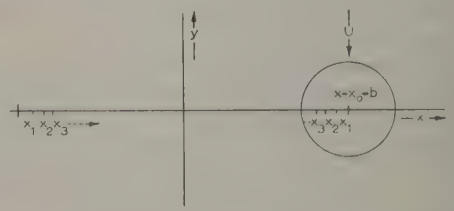

Fig. 5.—Successive images of a doublet representing a cylinder near a plane.

The strengths of these doublets for the indicated direction of flow are

$$\mu = UR^2,\ UR^2\left(\frac{R}{b+x_0}\right)^2,\ UR^2\left(\frac{R}{b+x_0}\right)^2\left(\frac{R}{b+x_1}\right)^2,$$

$$\ldots \frac{UR^{2n}}{\prod_{r=0}^{n-1}(b+x_r)^2}$$

The complex potential from the double set (one set lying in
ne region $x > 0$ and the other in the region $x < 0$) is therefore

$$= \phi + j\psi$$

$$= -jUz + jUR^2\left[\frac{1}{z-b} + \sum_{n=1}^{\infty} \frac{1}{z-x_n} \frac{R^{2n}}{\prod_{r=0}^{n-1}(b+x_r)^2}\right]$$

$$+ jUR^2\left[\frac{1}{z+b} + \sum_{n=1}^{\infty} \frac{1}{z+x_n} \frac{R^{2n}}{\prod_{r=0}^{n-1}(b+x_r)^2}\right]$$

$$= -jUz + 2jUR^2 z\left[\frac{1}{z^2-b^2} + \sum_{n=1}^{\infty} \frac{R^{2n}}{\prod_{r=0}^{n-1}(b+x_r)^2.(z^2-x_n^2)}\right]$$

621.391

The Institution of Electrical Engineers
Monograph No. 369 E
Mar. 1960
©

ORTHOGONAL CODES

By H. F. HARMUTH, Dipl.Ing., Dr.tech.

(*The paper was first received* 21*st April, and in revised form* 28*th September*, 1959. *It was published as an* INSTITUTION MONOGRAPH *in March* 1960.)

SUMMARY

Code alphabets whose characters can be represented by a finite sequence of digits of value +1 or −1 have been extensively investigated. The characters of these binary codes may be considered to be superpositions of orthogonal functions, one for each digit, which are multiplied by +1 or −1. A character of an orthogonal code consists of one function of a set of orthogonal functions multiplied by +1 or −1.

(1) INTRODUCTION

Since Hamming's early work on error-detecting and error-correcting codes[1] considerable effort has been devoted to the study of binary codes,[2,3] the main drawback of which is the difficulty usually involved in producing the characters of a code.[4] Among possible non-binary code alphabets, those consisting of sets of orthogonal time functions will be investigated in the paper.

The term 'distance' is used for the comparison of binary codes. The distance between two characters of a binary code is the number of binary digits by which the two characters differ. For instance, the character 1 in Fig. 1 has the distance

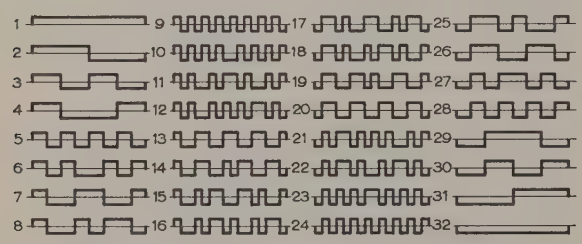

Fig. 1.—Orthogonal code consisting of step functions.

16 from the character 32 and the distance 8 from any other character. A closer inspection of this Figure shows that each character i ($i = 1, 2, \ldots 32$) has the distance 16 from the character $32 - i + 1$ and the distance 8 from any other character.

To generalize the concept of distance for non-binary codes one may proceed in the following fashion: Consider the 32 characters in Fig. 1 as time functions $F_1(t)$ to $F_{32}(t)$ with amplitudes $\pm A$ and with duration τ. The purpose for the introduction of the concept of distance is to provide a simple measure of the ease with which one character can be distorted into another by additive noise. Since such a distortion requires a certain noise energy, we determine the energy, W_{ik}, of the time function $F_k(t)$–$F_i(t)$ which, superimposed on the character $F_i(t)$, transforms it into $F_k(t)$, $i, k = 1, 2, \ldots$, i.e.

$$W_{ik} = \int_0^\tau [F_i(t) - F_k(t)]^2 dt \quad . \quad . \quad . \quad . \quad (1)$$

The distance, d, between $F_i(t)$ and $F_k(t)$ will be defined as W_{ik} normalized by the average energy, W, of all characters of the code alphabet:

$$2d = \frac{1}{W}\int_0^\tau [F_i(t) - F_k(t)]^2 dt \quad . \quad . \quad . \quad (2)$$

$$W = \frac{1}{m}\sum_{i=1}^{m} W_i$$

$$W_i = \int_0^\tau F_i^2(t) dt$$

where m = Number of characters in the code alphabet.

If all characters have the same energy, $W_i = W$, eqn. (2) yields

$$d = 1 - \frac{1}{W}\int_0^\tau F_i(t)F_k(t) dt \quad . \quad . \quad . \quad . \quad (3)$$

The definition (3) yields the values 2 and 1 for the distances between the characters in Fig. 1. If W_{ik} had not been normalized by W but by $W/8$, the energy required to change a negative digit into a positive one or vice versa, we would have obtained the distances 16 and 8. Although this latter normalization has merits in the investigation of binary codes, it cannot be applied to codes whose characters do not consist of a superposition of readily distinguishable functions, such as the 16 block pulses with positive or negative amplitude, of which the characters in Fig. 1 may be considered to consist.

The first 16 characters in Fig. 1 satisfy the relation

$$A^2 \tau^{-1} \int_0^\tau F_i(t)F_k(t) dt = \begin{cases} 1 \text{ for } i = k \\ 0 \text{ for } i \neq k \end{cases}$$

and form a set of orthogonal time functions. The characters 17–32 equal the characters 1–16 with reversed amplitude; they also form a set of orthogonal time functions. Together the sets form an 'extended set of orthogonal functions' or an 'orthogonal code'.

A set of m time functions is called an orthogonal code if the following relation holds for any two functions $F_i(t)$, $F_k(t)$ of the set.

$$W^{-1}\int_{-\infty}^{+\infty} F_i(t)F_k(t) dt = \left\{ \begin{array}{c} 1 \text{ for } i = k \\ -1 \text{ for } i = m + 1 - k \\ 0 \text{ for } i \neq k, m + 1 - k \end{array} \right\} \quad (4)$$

The extension of the integral from $-\infty$ to $+\infty$ makes the definition sufficiently general to include band-limited functions but is of no consequence if $F_i(t)$ and/or $F_k(t)$ are zero outside the interval $-\frac{1}{2}\tau \leqslant t \leqslant +\frac{1}{2}\tau$.

It will be assumed that the characters are always listed in such a sequence that the relation

$$F_i(t) = -F_{m+1-i}(t) \quad . \quad . \quad . \quad . \quad . \quad (5)$$

holds.

The following property of the characters of an orthogonal code is seen to exist from eqns. (3) and (4): character i has the distance $d = 2$ from character $m + 1 - i$ and the distance $d = 1$ from all other characters, $i = 1, 2, \ldots m$.

Correspondence on Monographs is invited for consideration with a view to publication.

Dr. Harmuth is in the Research Division, Stromberg-Carlson Co., a subsidiary of the General Dynamics Corporation, Rochester, N.Y.

According to the definition (4), the characters of an orthogonal code may be represented by m orthogonal vectors with positive or negative sign in an m-dimensional signal space.

(2) TRIGONOMETRIC CODES

Orthogonal codes of practical interest may be obtained from sine and cosine functions. The characters of the code shown

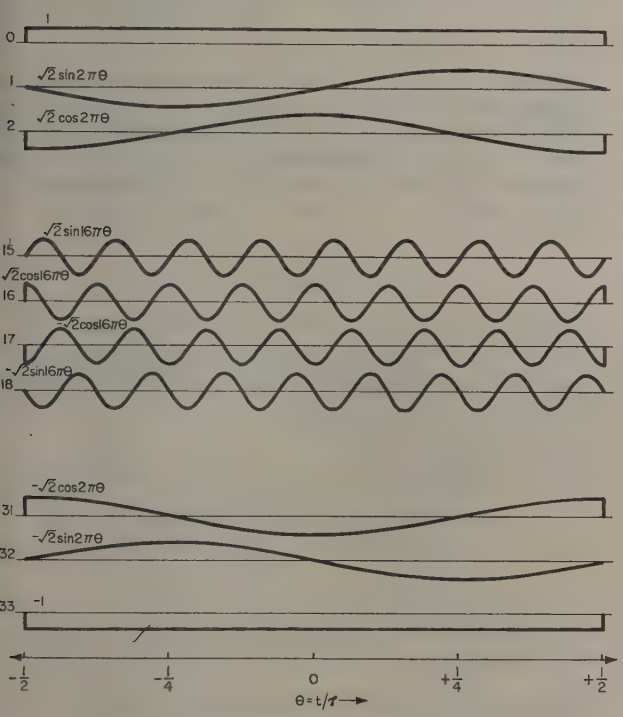

Fig. 2.—Orthogonal trigonometric code.

in Fig. 2 may be written in the following form ($\theta = t/\tau$, $-\frac{1}{2} \leqslant \theta \leqslant +\frac{1}{2}$):

$$\left.\begin{aligned} F_i(t) &= -F_{33-i}(t) = A(\sqrt{2})\sin(i+1)\pi\theta \\ &\qquad i = 1, 3, \ldots 15 \\ F_i(t) &= -F_{33-i}(t) = A(\sqrt{2})\cos i\pi\theta \\ &\qquad i = 2, 4, \ldots 16 \\ F_0(t) &= -F_{33}(t) = 1 \end{aligned}\right\} \quad . \quad (6)$$

The energy of any one of these characters is

$$W = A^2\tau \quad . \quad . \quad . \quad . \quad . \quad . \quad . \quad (7)$$

and relation (4) is obviously satisfied. The distance, d, between the characters in Fig. 2 is the same as that between the characters in Fig. 1. The code in Fig. 1 is a 4-error-detecting 3-error-correcting code in Hamming's terminology, since any two characters differ by either 8 or 16 digits, but these terms cannot be applied to the code in Fig. 2. However, the 'error correcting' features of the code in Fig. 2 may be stated in the following form: the minimum energy ($d = 1$) required to change any character into another character is $2dW = 2A^2\tau$; hence no noise sample with energy smaller than $A^2\tau$ superimposed on a character can change this character so much that it could not be distinguished from the other characters.

The information contained in each character in Figs. 1 or 2 equals 5 bits, since each code consists of 32 characters. In binary coding theory it is possible to define the 'redundancy' of the characters. Originally, the redundancy of a character was defined as the number of redundant digits added to the information digits. No distinction between information digits and redundant digits can be made for the code in Fig. 1. However, one may still apply the concept of redundancy to this particular orthogonal code, since each character may be considered to consist of a superposition of 16 block pulses with amplitude $+1$ or -1 which form an orthogonal set of 16 functions. Since only 5 block pulses are required to produce 32 characters, one may say that this code contains 5 bits of information and 11 bits of redundancy, but the term 'bits' rather than 'digits' must be used now. No such statement can be made without ambiguity about the code in Fig. 2. One may, of course, represent the characters in Fig. 2 by a superposition of functions of an orthogonal set, but it is not obvious which set should be used. Since we will not need the concept of redundancy we will not attempt to elaborate a new definition for it that is sufficiently general to be applicable to orthogonal codes.

The frequency band required for the transmission of the characters defined by eqn. (6) is readily obtained by a Fourier transformation. With the definitions

$$\left.\begin{aligned} a(c, 0, \nu) &= \frac{\sin \pi\nu}{\pi\nu} \\ a(c, k, \nu) &= \frac{1}{2}\left[\frac{\sin\pi(\nu-k)}{\pi(\nu-k)} + \frac{\sin\pi(\nu+k)}{\pi(\nu+k)}\right] \\ a(s, k, \nu) &= \frac{1}{2}\left[\frac{\sin\pi(\nu-k)}{\pi(\nu-k)} - \frac{\sin\pi(\nu+k)}{\pi(\nu+k)}\right] \end{aligned}\right\} \quad . \quad (9)$$

the frequency spectra for the sine, cosine and constant terms of eqn. (6) become

$$\left.\begin{aligned} a_{s,i+1}(\nu) &= A(\sqrt{2})a\left(s, \frac{i+1}{2}, \nu\right) \\ a_{c,i}(\nu) &= A(\sqrt{2})a(c, \tfrac{1}{2}i, \nu) \\ a_0(\nu) &= Aa(c, 0, \nu) \end{aligned}\right\} \quad . \quad . \quad (10)$$

where $\nu = \tau f$, f = frequency and τ = length of the characters.

The frequency spectra, eqns. (10), are plotted in Fig. 3; this shows that almost all the energy of the characters is concentrated at frequencies $\nu < 9$.

An orthogonal code with frequency components only in the

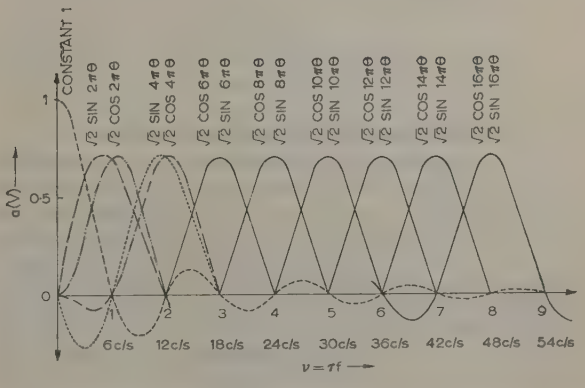

Fig. 3.—Frequency spectra of the characters of a trigonometric code.

interval $-\frac{1}{2} \leqslant \nu \leqslant +\frac{1}{2}$ is obtained by substituting f for t and ν for θ in the functions (6), giving

$$\left.\begin{aligned} F_i(f) &= -F_{33-i}(f) = A(\sqrt{2}) \sin (i+1)\pi\nu \\ &\qquad \text{where } i = 1, 3, \ldots 15 \\ F_i(f) &= -F_{33-i}(f) = A(\sqrt{2}) \cos i\pi\nu \\ &\qquad \text{where } i = 2, 4, \ldots 16 \\ -\tfrac{1}{2} &\leqslant \nu \leqslant +\tfrac{1}{2} \end{aligned}\right\} \quad (11)$$

The functions shown in Fig. 2 now represent frequency spectra rather than time functions. The time functions belonging to these spectra are obtained by applying an inverse Fourier transformation to the functions (11). This transformation yields

$$\left.\begin{aligned} F_i(t) &= -F_{33-i}(t) = A(\sqrt{2})\mathrm{a}\left(s, \frac{i+1}{2}, \theta\right) \\ &\qquad \text{where } i = 1, 3, \ldots 15 \\ F_i(t) &= -F_{33-i}(t) = A(\sqrt{2})\mathrm{a}(c, \tfrac{1}{2}i, \theta) \\ &\qquad \text{where } i = 2, 4, \ldots 16 \\ F_0(t) &= -F_{33}(t) = A\mathrm{a}(c, 0, \theta) \end{aligned}\right\} \quad (12)$$

$\mathrm{a}(c, 0, \theta)$, $\mathrm{a}(c, \frac{1}{2}i, \theta)$, and $\mathrm{a}(s, \frac{1}{2}i + \frac{1}{2}, \theta)$ are defined by eqns. (9), ν being replaced by θ.

The functions (9) are orthogonal in the interval $-\infty < \nu < +\infty$; in addition, the symmetric and the skew-symmetric functions for themselves are orthogonal in the interval $0 \leqslant \nu < +\infty$. Fig. 3 shows that the frequency spectra for sine and cosine functions differ little for $\nu > 0$ but these functions may be distinguished by their symmetry and skew-symmetry for $\nu < 0$. The continuation of the functions in Fig. 3 to negative values of ν and the substitution of θ for ν yields a graph of the functions (12).

The functions (6) as well as their Fourier transforms (12) form extended orthogonal sets. This preservation of orthogonality under a Fourier transformation is true for all functions which have a Fourier transform. Let $f_i(\omega)$ and $f_k(\omega)$ denote the Fourier transforms of $F_i(t)$ and $F_k(t)$, where $F_i(t)$ and $F_k(t)$ satisfy eqn. (4), and let the conjugate complex be denoted by an asterisk.[5] Then

$$\begin{aligned} \int_{-\infty}^{\infty} f_i^*(\omega) f_k(\omega) d\omega &= \int_{-\infty}^{\infty} f_i^*(\omega)\left[\int_{-\infty}^{\infty} F_k(t)\varepsilon^{-j\omega t} dt\right] d\omega \\ &= \int_{-\infty}^{\infty} F_k(t)\left[\int_{-\infty}^{\infty} f_i^*(\omega)\varepsilon^{-j\omega t} d\omega\right] dt \\ &= \int_{-\infty}^{\infty} F_k(t)\left[\int_{-\infty}^{\infty} f_i(\omega)\varepsilon^{j\omega t} d\omega\right]^* dt \\ &= \int_{-\infty}^{\infty} F_k(t) F_i^*(t) dt = \left\{\begin{array}{l} W \text{ for } i = k \\ -W \text{ for } i = m + 1 - k \\ 0 \text{ for } i \neq k, m + 1 - k \end{array}\right\} \end{aligned} \quad (13)$$

(3) ORTHOGONAL CODES AND NOISE

Let the character $F_i(t)$ of an orthogonal code be represented by a Fourier series. The functions of this series equal zero outside the interval $-\frac{1}{2}\tau \leqslant t \leqslant +\frac{1}{2}\tau$. This means that the functions $F_i(t)$ are represented by a superposition of the functions in Fig. 2—if the real Fourier series is used—and not by a superposition of sine and cosine functions of infinite extension. Although this representation of a time-limited function is conceptually different from the representation of a periodic function by a Fourier series, there is no difference in the mathematical sense since any function defined in a finite interval only may be extended as periodic function outside this interval to infinity.

$$\left.\begin{aligned} F_i(t) &= \sum_{k=-\infty}^{\infty} A_{ik}\varepsilon^{j2k\pi\theta} \\ A_{ik} &= \int_{-\tau/2}^{\tau/2} F_i(t)\varepsilon^{-j2k\pi\theta} dt \\ W &= \int_{-\tau/2}^{\tau/2} F_i^2(t) dt = \tau \sum_{k=-\infty}^{\infty} A_{ik} A_{ik}^* \\ \text{where} \qquad \theta &= t/\tau,\ i = 1, 2, \ldots s, \ldots m \end{aligned}\right\} \quad \ldots \quad (14)$$

Consider white noise in the frequency domain and let the frequency band be divided into intervals $\Delta f = f_l - f_{l-1}$. The probability that a sample of noise has a frequency component between f_l and f_{l-1} is independent of l. The amplitudes of the frequency components in any interval Δf have a normal distribution. A sample of noise can be represented by a Fourier series,[6] i.e.

$$g(t) = \sum_{l=-\infty}^{\infty} A_l \varepsilon^{j2l\pi\Delta f t} \quad \ldots \quad (15)$$

If the character $F_s(t)$ is transmitted through a channel with additive noise the signal arriving at the receiver has the form $F_s(t) + g(t)$. The correlation of this signal with the m characters $F_i(t)$ yields the values W, 0, or $-W$ according to eqn. (4) plus the contribution $P_{ni}\tau$ of $g(t)$, where

$$\left.\begin{aligned} P_{ni}\tau &= \int_{-\tau/2}^{\tau/2} g(t) F_i(t) dt \\ &= \int_{-\tau/2}^{\tau/2}\left[\sum_{k=-\infty}^{\infty} A_{ik}\varepsilon^{j2k\pi t/\tau} \sum_{l=-\infty}^{\infty} A_l \varepsilon^{j2l\pi\Delta f t}\right] dt \\ &= \tau \sum_{k=-\infty}^{\infty} \sum_{l=-\infty}^{\infty} A_{ik} A_l \sin \pi(k+\nu)/\pi(k+\nu) \\ \nu &= l\Delta f\tau = f\tau \end{aligned}\right\} \quad (16)$$

ν becomes a continuous variable for $\Delta f \to 0$ and the sum over l becomes an integral.

For computation of the error probability the distribution of $N_{ni}\tau$ normalized by W is required. Since A_l has a normal distribution with the average equal to zero, the joint distribution of $P_{ni}\tau/W$ has the form

$$W(P_{ni}\tau/W) = (2\pi)^{-1/2}\sigma^{-1} \exp\left[-(P_{ni}\tau/W)^2/2\sigma^2\right] \quad (17)$$

A component of $g(t)$ with amplitude A_λ and frequency $\nu = \lambda\Delta f\tau$ correlated with $F_i(t)$ produces the term for $l = \lambda$ in eqn. (16). The square of this term divided by W is the square deviation $\sigma_{A\nu}^2$ from the average $\langle P_{ni}\tau/E\rangle = 0$.

$$\sigma_{A\nu}^2 = \left(\frac{\tau}{W}\right)^2 A_\lambda A_\lambda^* \sum_{l=-\infty}^{\infty} A_{lk} \frac{\sin \pi(k+\nu)}{\pi(k+\nu)} \sum_{k=-\infty}^{\infty} A_{ik}^* \frac{\sin \pi(k+\nu)}{\pi(k+\nu)} \quad \ldots \quad (18)$$

σ^2 is the average of R deviations $\sigma_{A\nu}^2$ for large values of R. The averaging may be performed first for the frequencies and then for the amplitudes.

$$\begin{aligned} \sigma_A^2 &= \lim_{\Delta f \to 0,\ R \to \infty} R^{-1} \sum_{r=1}^{R} (\sigma_{A\nu}^2)_r \\ &= \int_{-\infty}^{\infty} \sigma_{A\nu}^2 d\nu = (\tau/W)^2 A_\lambda A_\lambda^* \sum_{k=-\infty}^{\infty} A_{ik} A_{ik}^* \\ &= \tau W^{-1} A_\lambda A_\lambda^* \end{aligned} \quad \ldots \quad (19)$$

$A_\lambda A^*$ is the power dissipated in a unit resistance by the noise

components with an amplitude in the interval $\Delta A_\lambda = |A_\lambda| - |A_{\lambda-1}|$. Hence it follows from eqn. (19) that the average power of all noise components with amplitudes $|A_\lambda|$ in the frequency interval $-\infty < \nu < +\infty$ equals after the correlation (16) the average power of all noise components with amplitudes $|A_\lambda|$ in the frequency band $-\frac{1}{2} \leqslant \nu \leqslant +\frac{1}{2}$ before correlation. Averaging eqn. (19) over all amplitudes A_λ yields the average noise power P_n in the band $-\frac{1}{2} \leqslant \nu \leqslant +\frac{1}{2}$ or $0 \leqslant f \leqslant 1/2\tau$ in real notation.

$$\sigma^2 = \tau W^{-1} P_n = P_n/P_s = P/nP_s \quad . \quad . \quad . \quad (20)$$

where P_s designates the average signal power, W/τ. P is the average noise power in the band $0 \leqslant f \leqslant n/2\tau$, which is the theoretical minimum of the bandwidth required for a transmission rate of n binary digits per time interval τ.

In the presence of noise the correlation integral (4) becomes

$$W^{-1} \int_{-\infty}^{\infty} F_i(t)[F_k(t) + g(t)]dt = \left\{ \begin{array}{ll} 1 + \alpha_k & \text{for } i = k \\ -(1 + \alpha_k) & \text{for } i = m + 1 - k \\ \alpha_i = -\alpha_{m+1-i} & \text{for } i \neq k,\ m + 1 - k \end{array} \right\} \quad (21)$$

The probability of $P_{ni}\tau/W$ equalling α_i is obtained from eqns. (17) and (20):

$$W(\alpha_i) = (2\pi)^{-1/2}(nP_s/P)^{1/2} \exp(-\tfrac{1}{2}\alpha_i^2 nP_s/P) \quad (22)$$

The probability of $|P_{ni}\tau/W|$ exceeding $|\alpha_i|$ becomes

$$\left. \begin{array}{l} p(|\alpha_i|) = 1 - \Theta[2^{-1/2}|\alpha_i|(nP_s/P)^{1/2}] \\ \Theta(x) = 2\pi^{-1/2} \int_0^x \varepsilon^{-y^2} dy \end{array} \right\} \quad . \quad . \quad (23)$$

Assume for any $F_k(t)$ that it is equally probable to have been transmitted. An error occurs if either one of the following conditions holds:

(*a*) $1 + \alpha_k \leqslant 0$; character k will be interpreted as character $m + 1 - k$.

(*b*) $\alpha_i \geqslant 1 + \alpha_k \geqslant 0$; character k will be interpreted as one of the characters i.

The probability of the first case occurring follows from eqn. (22).

$$p_1 = \tfrac{1}{2}\{1 - \Theta[(nP_s/2P)^{1/2}]\} \quad . \quad . \quad . \quad (24)$$

The factor $\frac{1}{2}$ takes into account the fact that only negative values of α_k can cause an error.

The probability $W(\alpha_k)$ that $1 + \alpha_k$ will occur is obtained from eqn. (22) by substituting α_k for $\alpha_i (-1 \leqslant \alpha_k < +\infty)$. The probability $p(1 + \alpha_k)$ that α_l will be larger than $1 + \alpha_k$ follows from eqn. (23).

$$p(1 + \alpha_k) = 1 - \Theta[(1 + \alpha_k)(nP_s/2P)^{1/2}] \quad . \quad (25)$$

If $W(\alpha_k)$ and $p(1 + \alpha_k)$ are statistically independent, the probability p_2 that α_l will be larger or equal to $1 + \alpha_k$ becomes

$$p_2 = \int_{-1}^{\infty} W(\alpha_k) p(1 + \alpha_k) d\alpha_k \quad . \quad . \quad . \quad (26)$$

It is shown in Section 7 that $W(\alpha_k)$ and $p(1 + \alpha_k)$ are statistically independent if the bandwidth of the transmission channel is sufficiently large. p_1 may be obtained from a table of the error integral, but p_2 must be computed by numerical methods.

There are 15 characters $F_i(t)$ into which the correct character $F_k(t)$ may be decoded erroneously by the process with probability p_2, because of the relation $\alpha_l = -\alpha_{33-l}$. Since this relation shows that for any negative α_l there is an equally large positive α_{33-l}, the probability p_2 is not multiplied by $\frac{1}{2}$. The probability $p_{2,15}$ for $F_k(t)$ to be decoded into $F_i(t) (1 \neq k, 33 - k)$ becomes $p_{2,15} = 1 - (1 - p_2)^{15}$.

Fig. 4 shows a graph of $p_{2,15}$; for comparison the error

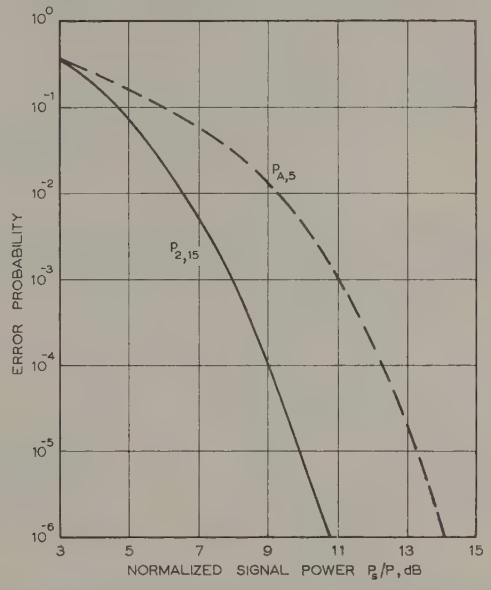

Fig. 4.—Variation of error probability with normalized signal power for an orthogonal code with five bits of information ($p_{2,15}$) and a 5-digit binary code with five bits of information ($p_{A,5}$).

probability $p_{A,5}$ for a balanced system transmitting binary pulse characters with five digits, using amplitude sampling, $\sin 2\pi f_0 t/2\pi f_0 t$ pulses and an ideal low-pass filter of bandwidth f_0 is also shown.

$$p_{A,5} = 1 - (1 - p_A)^5$$
$$p_A = \tfrac{1}{2}\{1 - \Theta[2^{1/2}(P_s/P)^{1/2}]\}$$

P is the average noise power in the band $0 \leqslant f \leqslant f_0$. f_0 equals $5/2\tau$ for a transmission rate of 5 binary digits per time interval τ. Comparison of p_A and p_1 shows that n times less signal power is required to obtain the same value for p_1 as for p_A. In Fig. 4 the graph of p_1 will thus be more than 7 dB to the left of $p_{A,5}$, and p_1 can be neglected in comparison with $p_{2,15}$ for the range of values shown.

$p_{A,5}$ is the theoretical limit of the error probability for amplitude sampling if a binary code alphabet with five digits is used. This limit also holds if correlation schemes are used, e.g. pulse by pulse integration of teletype signals.

It follows from Fig. 4 that orthogonal codes with 5 bits of information require about 3 dB less signal power than a 5-digit binary code with 5 bits of information for error rates between 1 % and 0·01 % if the data rate is the same. This gain is obtained at the cost of increased bandwidth. A teletype system transmitting six letters per second with the code in Fig. 2 requires a bandwidth of about 60 c/s according to Fig. 3, but only some 24 c/s are needed if each teletype character is transmitted by a superposition of five orthogonal sine and cosine functions.

For large values of n one may compute the error probability analytically. Since p_1 decreases with n it may be neglected for large values of n, and the error probability, p, for orthogonal codes with n bits of information becomes

$$\lim_{n \to \infty} p = \lim_{n \to \infty} [1 - (1 - p_2)^{2^{n-1}} - 1] \quad . \quad . \quad (27)$$

Using the asymptotic expansion

$$\Theta(x) \simeq 1 - \frac{1}{\sqrt{\pi}} \frac{1}{x} \varepsilon^{-x^2} \quad . \quad . \quad . \quad . \quad (28)$$

for the error function one obtains, from eqns. (25)–(27),

$$\lim_{n\to\infty} p = \lim_{n\to\infty} \left\{ 1 - \left[1 - \frac{1}{\pi} \exp\left(-nP_s/4P\right) \int_{-1+\delta}^{\infty} \frac{1}{1+\alpha_k} \exp\left[-n(\alpha_k + \tfrac{1}{2})^2 P_s/2P\right] \right]^{2n-1} \right\}$$

δ is an arbitrarily small constant whose purpose is to keep the pole at $\alpha_k = -1$ outside the integration interval. $(1+\alpha_k)^{-1}$ may be expanded into a geometric series. We obtain

$$\lim_{n\to\infty} p = \lim_{n\to\infty} \left[1 - \exp\left(-\eta\varepsilon^{n\xi}\right)\right] - \eta\varepsilon^{n\xi} \quad . \quad . \quad . \quad (29)$$

where $$\eta = \frac{2}{\sqrt{\pi}} \sqrt{\frac{P}{nP_s}} \text{ and } \xi = \log_\varepsilon 2 - \frac{P_s}{4P}$$

The function defined by eqn. (29) equals zero for $\xi < 0$ and unity for $\xi > 0$. It follows that the error probability for orthogonal codes approaches zero with increasing information content, n, per character for $P_s/P > 4 \log_\varepsilon 2$ and unity for $P_s/P < 4 \log_\varepsilon 2$.

The ratio $4 \log_\varepsilon 2$ expressed in decibels yields 4·43. It follows from Fig. 4 that one cannot decrease the required signal power by more than about 6·4–4·4 = 2 dB for an error probability of 0·01 if one replaces the 5-bit orthogonal code ($p_{2,15}$) by one which contains more information per character. For an error probability of 10^{-6}, however, the possible gain increases to about 10·6–4·4 = 6 dB.

(4) PRINCIPLES OF A COMMUNICATION SYSTEM USING A TRIGONOMETRIC CODE

Fig. 5 shows the block diagram of a communication system using the characters in Fig. 2. Eight oscillators deliver the required sine and cosine functions, and synchronous closing of any one of the switches 1–32 for the period τ produces the respective character. Note that none of the characters has a d.c. component. Sine and cosine oscillations with stable phase difference may be obtained by integrating a sine wave by a *RC* integrator.

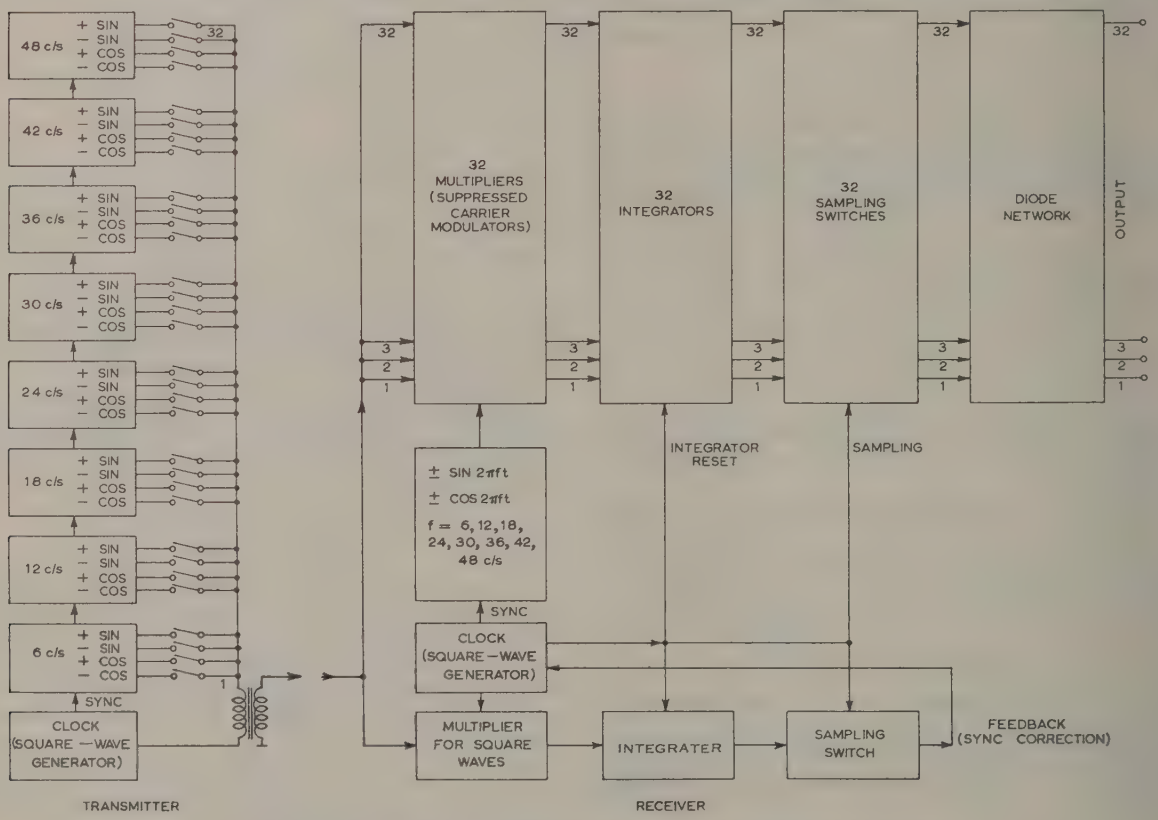

Fig. 5.—Block diagrams of a communication system using orthogonal functions.

A transmitted character is fed in the receiver to 32 multipliers. Eight oscillators of the type used in the transmitter continuously feed sine and cosine functions to these multipliers. The products of the received character with the sine and cosine functions are integrated over the period τ. The output voltages of the integrators at the end of the period τ represent the values $\pm(1+\alpha_k)$ and $\pm\alpha_l$ of eqn. (21). By feeding these voltages via sampling switches to a diode network one may determine the largest voltage and obtain the character which has most likely been transmitted.

For the synchronization of the communication system one

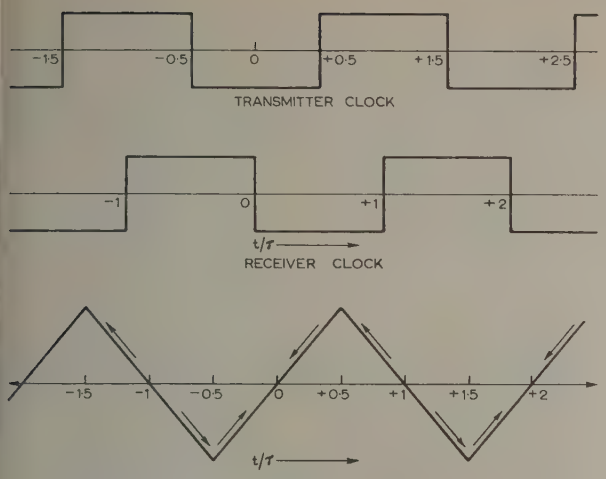

Fig. 6.—Synchronization by orthogonal functions.

may alternatingly transmit characters 0 and 33 of Fig. 2. The resulting square wave of period 2τ is shown in Fig. 5. A similar square wave, delayed by $\frac{1}{2}\tau$, is produced in the receiver. Multiplication of the two square waves and integration of the product over the period τ yields zero if transmitter and receiver are in phase. A phase difference of $\pm T$ between the two square waves makes the output of the integrator vary like the sawtooth function in Fig. 5. Transmitter and receiver are in phase at the points $T/\tau = 0, \pm 1, \pm 2, \ldots$ The deviation of the integrator voltage from zero may be used to correct the phase of the receiver. The points $T/\tau = 0, \pm 2, \pm 4, \ldots$ of the sawtooth function are stable if the receiver is retarded by a positive integrator voltage and advanced by a negative one.

If the communication system transmits six characters per second (U.S. teletype standard), the oscillators must provide the frequencies shown in Table 1. This Table also lists the tolerable synchronization error which is obtained by considering that a sine wave advanced by one-eighth of its period cannot be distinguished from a cosine wave of the same frequency retarded by one-eighth of its period.

Table 1

CHARACTERS OF A TELETYPE ALPHABET

Number	Character	Fundamental frequency	Limit for tolerable synchronization error
		c/s	±millisec
1	$\sin 2\pi\theta$	6	20·8
2	$\cos 2\pi\theta$	6	20·8
3	$\sin 4\pi\theta$	12	10·4
4	$\cos 4\pi\theta$	12	10·4
5	$\sin 6\pi\theta$	18	6·94
6	$\cos 6\pi\theta$	18	6·94
7	$\sin 8\pi\theta$	24	5·21
8	$\cos 8\pi\theta$	24	5·21
9	$\sin 10\pi\theta$	30	4·17
10	$\cos 10\pi\theta$	30	4·17
11	$\sin 12\pi\theta$	36	3·47
12	$\cos 12\pi\theta$	36	3·47
13	$\sin 14\pi\theta$	42	2·97
14	$\cos 14\pi\theta$	42	2·97
15	$\sin 16\pi\theta$	48	2·60
16	$\cos 16\pi\theta$	48	2·60
17	$-\cos 16\pi\theta$	48	2·60
18	$-\sin 16\pi\theta$	48	2·60
19	$-\cos 14\pi\theta$	42	2·97
20	$-\sin 14\pi\theta$	42	2·97
21	$-\cos 12\pi\theta$	36	3·47
22	$-\sin 12\pi\theta$	36	3·47
23	$-\cos 10\pi\theta$	30	4·17
24	$-\sin 10\pi\theta$	30	4·17
25	$-\cos 8\pi\theta$	24	5·21
26	$-\sin 8\pi\theta$	24	5·21
27	$-\cos 6\pi\theta$	18	6·94
28	$-\sin 6\pi\theta$	18	6·94
29	$-\cos 4\pi\theta$	12	10·4
30	$-\sin 4\pi\theta$	12	10·4
31	$-\cos 2\pi\theta$	6	20·8
32	$-\sin 2\pi\theta$	6	20·8

(5) ACKNOWLEDGMENT

The author wishes to express his appreciation to Messrs. R. Schwartz, J. Navarro, and A. Konheim of the Advanced Electronics Center of the General Electric Company, and to Messrs. G. Franco and G. Lachs of the Stromberg-Carlson Company for several helpful discussions.

(6) REFERENCES

(1) HAMMING, R. W.: 'Error-Detecting and Error-Correcting Codes', *Bell System Technical Journal*, 1950, **29**, p. 147.
(2) SLEPIAN, P.: 'A Class of Binary Signalling Alphabets', *ibid.*, 1956, **35**, p. 203.
(3) REED, I. S.: 'A Class of Multiple-Error-Correcting Codes and the Decoding Scheme', *Transactions of the Institute of Radio Engineers*, 1954, **IT–4**, p. 38.
(4) GREEN, J. H., and SAN SOUCIE, R. L.: 'An Error-Correcting Encoder and Decoder of High Efficiency', *Proceedings of the Institute of Radio Engineers*, 1958, **46**, p. 1741.
(5) TITCHMARSCH, E. C.: 'Theory of Fourier Integrals' (Oxford University Press, London).
(6) RICE, S. O.: 'Mathematical Analysis of Random Noise', *Bell System Technical Journal*, 1944, **23**, p. 282 and 1945, **24**, p. 46.
(7) HAYTON, T., HUGHES, C. J., and SANDERS, R. L.: 'Telegraph Codes and Code Convertors', *Proceedings I.E.E.*, Paper No. 1585 R, November, 1953 (**101**, Part III, p. 137).
(8) FLOOD, J. E.: 'Noise-Reducing Codes for Pulse-Code Modulation', *ibid.*, Monograph No. 291 R, February, 1958 (**105** C, p. 391).

(7) APPENDIX

The statistical independence of $W(\alpha_i)$ and $p(1 + \alpha_k)$ follows from that of α_k and α_i; $i \neq k$, $m + 1 - k$. To prove the statistical independence of α_k and α_l it is sufficient to prove that the relation $\langle(1 + \alpha_k)\alpha_l\rangle = 0$ holds, since α_k and α_l have a normal distribution according to eqn. (21).

$$\langle(1 + \alpha_k)\alpha_i\rangle = W^{-2}\Big\langle \int_{-\infty}^{+\infty} F_k(t)[F_k(t) + g(t)]dt \int_{-\infty}^{+\infty} F_l(t')[F_k(t') + g(t')]dt' \Big\rangle$$

$$= W^{-2}\Big\langle \Big[1 + \int_{-\infty}^{+\infty} F_k(t)g(t)dt\Big] \int_{-\infty}^{+\infty} F_l(t')g(t')dt' \Big\rangle$$

$$= W^{-2}\Big[\Big\langle \int_{-\infty}^{+\infty} F_k(t')g(t')dt' \Big\rangle + \Big\langle \int_{-\infty}^{+\infty}\int_{-\infty}^{+\infty} F_k(t)F_l(t')g(t)g(t')dtdt' \Big\rangle\Big]$$

$$= W^{-2}\Big[\langle\alpha_l\rangle + \int_{-\infty}^{+\infty}\int_{-\infty}^{+\infty} F_k(t)F_l(t')\langle g(t)g(t')\rangle dtdt'\Big]$$

From eqn. (21) follows $\langle \alpha_i \rangle = 0$. The average of the noise samples $\langle g(t)g(t') \rangle$ equals zero for $t \neq t'$. For $t = t'$ the integral over $F_k(t)F_i(t)$ vanishes, owing to the orthogonality of these functions. However, $\langle g^2(t) \rangle$ is infinite, since the noise energy received during a time interval $\tau \neq 0$ from an infinite frequency band is infinite and the integral is indetermined. By limiting the bandwidth with an ideal low-pass filter one may limit the noise energy to a finite value and may then make the transition to arbitrarily large bandwidths.

$\langle g(t)g(t') \rangle$ is the auto-correlation function of the noise which depends on $t - t'$ only, since the statistics are assumed to be stationary. Writing $R(t - t')$ for $\langle g(t)g(t') \rangle$ and substituting $t - t' = T$ one obtains

$$\langle (1 + \alpha_k)\alpha_i \rangle = \int_{-\infty}^{+\infty} \left[R(T) \int_{-\infty}^{+\infty} F_k(t + T)F_i(t)dt \right] dT$$

$R(T)$ is a symmetric function. If the integral over $F_k(t + T)F_i(t)$ yields a function skew-symmetric in T, one obtains $\langle (1 + \alpha_k)\alpha_i \rangle = 0$, and this result remains unchanged for arbitrarily increasing bandwidth.

For more general functions, $F_i(t)$ and $F_k(t)$, the argument is as follows: Let $\int F_k(t + T)F_i(t)dt$ be in a certain small region around $T = 0$, either symmetric or skew-symmetric. If the integral is skew-symmetric the relation $\langle (1 + \alpha_k)\alpha_i \rangle = 0$ will be satisfied in the limit for arbitrarily large bandwidth, since $R(T)$ becomes an arbitrarily narrow peak, symmetric in T. If $\int F_k(t + T)F_i(t)dt$ is symmetric in T the relation $\langle (1 + \alpha_k)\alpha_i \rangle = 0$ can be satisfied if this integral is zero not only for $T = 0$ but also in a certain region $\pm\Delta t$ around $T = 0$, since $R(T)$ will differ arbitrarily little from zero outside the interval $-\Delta t \leqslant T \leqslant +\Delta t$ for a sufficiently large bandwidth. For $\Delta t \to dt$ it follows that $\int F_k(t + T)F_i(t)dt$ and at least its first derivative must vanish at $T = 0$. The statistical independence of α_k and α_i is thus assured for all orthogonal functions $F_k(t)$, $F_i(t)$ which are continuous in the region of definition if the bandwidth approaches infinity. The statistical independence is not assured for discontinuous functions, e.g. those in Fig. 1 whose cross-correlation behaves like $|T|$ around $T = 0$ for some characters.

521—526

The Institution of Electrical Engineers
Monograph No. 370 M
Apr. 1960
©

A CALCULATION OF SWITCHING FUNCTIONS AS A MEANS OF MINIMIZING ERROR IN AN ON-OFF CONTROL SYSTEM

By R. F. BROWN, B.Eng., Associate Member.

(*The paper was first received* 31*st August*, 1959, *and in revised form* 22*nd January*, 1960. *It was published as an* INSTITUTION MONOGRAPH *in April*, 1960.)

SUMMARY

Self-optimization of control systems is becoming a practical proposition through new developments in the electronics field, notably in digital-computer techniques. To this end, the paper, after discussion of some essential basic concepts, proposes an adaptive switching function as an on–off controller. Results are given for repeated application of step and ramp inputs to a mathematical model of an ideal servo mechanism, set up on a Deuce digital computer. The results neglect relay imperfections, they are preliminary in nature, and intended to provoke further research.

(1) INTRODUCTION

The term 'on–off control' usually implies that the servomechanism input has two possible states, equal in magnitude but opposite in sign. An example is the use of a relay to reverse the d.c. connections to the field winding of a d.c. motor in order to control the shaft position. In the present context the relay position (on or off) is given by the sign of a switching function, which, in general, will be dependent upon the reference input, the controlled output, and the parameters of the controlled system. On–off control elements were originally used in automatic control systems because of their simple construction. In recent years it has been found that they can be designed to give performance superior to linear servo mechanisms. However, the potentialities of on–off control have not been explored to the full because of the impracticability of the switching function as a relay controller except for the simplest of systems.

In the paper an elementary self-optimizing control is described whereby the switching function may, to a limited extent, adapt itself to the nature of the input and to a slow variation in the characteristics of the controlled system. This manner of approach reflects a growing trend in automatic control, evidence of which was given by the large number of participants in the Symposium[1] on the Mechanization of Thought Processes held at the National Physical Laboratory in November, 1958. A classification of adaptive systems in general has been attempted by Aseltine, Mancini and Sarture.[2]

In Section 2 some basic ideas are introduced to provide a foundation for the treatment of adaptive switching functions given in Section 3. In Section 4 the principles outlined in Section 3 are demonstrated on a mathematical model of an ideal servo mechanism.

(2) BASIC THEORY OF ON–OFF PREDICTION

(2.1) Techniques for the Synthesis of On–Off Servo Mechanisms

The published methods for the synthesis of on–off servo mechanisms may be classified into two broad divisions which Flügge-Lotz and Lindberg[3] have described as the phase-space method and the frequency-response method.

Correspondence on Monographs is invited for consideration with a view to publication.
Mr. Brown is in the Electrical Engineering Department, University of New South Wales, Australia.

(2.1.1) Phase-Space Method.

Consider a system whose controlled output position, $c(t)$, is given by the Nth order linear differential equation

$$\sum_{n=1}^{N} a_n \frac{d^n}{dt^n} c(t) = F \quad . \quad . \quad . \quad . \quad . \quad (1)$$

where F, the relay input function, has two possible states, equal in magnitude but opposite in sign. For convenience, the states will be given normalized values $F = \pm 1$.

Suppose, for the present, that the reference input, $r(t)$, can be represented as a Maclaurin series expansion to the Mth term, namely

$$r(t) = \sum_{n=0}^{M} r^{(n)}(0) \frac{t^n}{n!} \quad . \quad . \quad . \quad . \quad . \quad (2)$$

where $$r^{(n)}(0) = \frac{d^n}{dt^n} r(t)\Big|_{t=0}$$

Provided that M is less than N, the system error and all its time derivatives may be reduced simultaneously to zero by appropriate switching of the relay input function. If M equals N, the relay input function must be sufficiently large to reduce the Nth derivative of the error to zero. A manner of switching such as to reduce the error and all its time derivatives to zero in minimum time has been defined by previous workers[4, 5, 6] as 'optimum' switching.

In the phase-space method, the instantaneous polarity of the relay control is given by the sign of some function of the error and its time derivatives, the function being referred to as the switching function. In a phase space whose dimensions are the error and its time derivatives, the transient response of the system becomes a trajectory, the switching function becomes a switching line, and the switching instants are marked off as discontinuous changes in trajectory occurring at the intersections of the trajectory with the switching line. Since eqn. (1) is unaltered by replacing $c(t)$ by $c(t) +$ constant, the optimum switching line is uniquely given by the error and time derivatives of error for steps of reference input. For arbitrary reference input, dimensions of time derivatives of the reference input must be added to the phase space if the optimum switching line is to remain unique.

(2.1.2) Frequency-Response Method.

Flügge-Lotz and Lindberg[3] give a good summary of the frequency-response method originally presented by Kochenburger.[7] In the method the action of the relay is expressed by a describing function, thereby enabling the Nyquist stability criterion to be applied to the design of a series-compensation network. The application of root-locus techniques in such a design are given by Embler and Weaver.[8]

This topic is not pursued further since the phase-space method is the one followed in the ensuing treatment.

(2.2) Linear and Quadratic Switching Functions

Let us consider an ideal system consisting of a frictionless motor, capable of instantaneous torque reversal, coupled to a pure inertia load. Such a system has been treated by a number of workers[4, 5, 6] in order to illustrate optimum switching.

The torque equation is

$$J\ddot{c} = T_m \quad . \quad . \quad . \quad . \quad . \quad . \quad . \quad (3)$$

where J = Moment of inertia.

T_m = Motor torque.

$\ddot{c} = \dfrac{d^2}{dt^2}c(t)$ = Angular acceleration of controlled variable.

In torque-normalized form eqn. (3) assumes the form of eqn. (1), i.e.

$$\ddot{c} = F \quad . \quad . \quad . \quad . \quad . \quad . \quad . \quad (4)$$

For reference input

$$r(t) = r(0) + \dot{r}(0)t$$

to be written as

$$r = r_0 + \dot{r}_0 t \quad . \quad . \quad . \quad . \quad . \quad . \quad (5)$$

the optimum switching function is easily shown[4, 5, 6] to be

$$F = \text{sgn}\,(2e + |\dot{e}|\dot{e}) \quad . \quad . \quad . \quad . \quad . \quad (6)$$

where $e = r - c$ is the error of the controlled system.

If the system is initially at rest, eqn. (6) may be expressed in the form

$$F = \text{sgn}\,(2e + T_0\dot{e}) \quad . \quad . \quad . \quad . \quad . \quad (7)$$

where $$T_0 = |\dot{e}| = \sqrt{[|r_0| + \tfrac{1}{2}(\dot{r}_0)^2]} \quad . \quad . \quad . \quad (8)$$

The linear switching function is defined as

$$F = \text{sgn}\,(2e + T\dot{e}) \quad . \quad . \quad . \quad . \quad . \quad (9)$$

where T is an arbitrary constant chosen as a compromise to the variable T_0.

For linear switching it follows from eqns. (4), (5) and (9) that the error torque equation is

$$\begin{aligned}\ddot{e} &= -F \\ &= -\text{sgn}\,(2e + T\dot{e}) \quad . \quad . \quad . \quad . \quad . \quad (10)\end{aligned}$$

Let us consider the effect of scaling the variables in eqn. (10). Thus if $e = \lambda e_n$ and $t = \mu t_n$, eqn. (10) becomes

$$\frac{\lambda}{\mu^2}\frac{d^2e_n}{dt_n^2} = -\text{sgn}\left(2\lambda e_n + T\frac{\lambda}{\mu}\frac{de_n}{dt_n}\right)$$

If $\lambda = \mu^2$,

$$\frac{d^2e_n}{dt_n^2} = -\text{sgn}\left(2e_n + \frac{T}{\mu}\frac{de_n}{dt_n}\right)\mu^2 \quad . \quad . \quad . \quad (11)$$

Eqn. (11) has the same form as eqn. (10). Therefore the error response is independent of the initial values of r_0 and $\dot{r}_0$ provided that the variables are scaled according to the relations

$$\left.\begin{aligned} e &= \mu^2 e_n \\ t &= \mu t_n \\ T &= \mu T_n \end{aligned}\right\} \quad . \quad . \quad . \quad . \quad . \quad . \quad (12)$$

Eqn. (10) was solved (using a Deuce digital computer) for a step and ramp input, respectively. The scaling factors of eqn. (12) were chosen such that the values of the step, $r_0 = 64$, and the ramp, $\dot{r}_0 = 8\sqrt{2}$, gave a convenient time scale for programming purposes, and such that T_0 would be the same in each case, namely $T_0 = 8$. The results are plotted in Fig. 1 for a range of values of T. It will be seen that T, normalized with respect to T_0, becomes analogous to the damping coefficient ζ in a second-order linear servo mechanism. Thus the waveforms of Fig. 1, for the analogy of $T/T_0 = \zeta$, exhibit the phenomena of critical damping ($\zeta = 1$), under-damping ($\zeta < 1$), over-damping ($\zeta > 1$), and zero damping ($\zeta = 0$). The case of zero damping, for which $T = 0$, represents simple on–off control, i.e. switching of the input as the error reverses sign. For $T = 0$, the magnitudes of successive peaks should be the same, whereas they differ slightly. This is attributed to the use in the Deuce programme of a finite sub-interval of time, $h = 1/32$, for evaluation of the switching function, thus allowing a maximum time error in switching of 1/32 of a unit.

Let us now consider the effect of viscous and Coulomb friction upon on–off control of a second-order linear servo mechanism. As illustrative of typical values, the differential equation characterizing the experimental system of Coales and Noton[4] has been chosen. In eqn. (21), their torque equation in normalized form is shown to be

$$\ddot{c} + 0{\cdot}2c + 0{\cdot}144\ \text{sgn}\,\dot{c} = F \quad . \quad . \quad . \quad . \quad (13)$$

The results of Coales and Noton for a step input (upper curve of Fig. 11 of Reference 4) and for a ramp input (upper curve of Fig. 12 of Reference 4) are shown as dotted curves in Fig. 2; the curves represent an attempt at optimum switching by the use of an analogue computer operating in faster than real time. The full-line curves in Fig. 2 give the solution to the respective error-torque equations [eqns. (22) and (23) of Section 8.1] for the linear switching function of eqn. (9); the results are plotted for a range of values of T and were obtained using a Deuce digital computer. Results were also obtained when the Coulomb friction term, $0{\cdot}144\ \text{sgn}\,\dot{c}$, was omitted from eqn. (13), but they were not significantly different and are not included. The lack of difference is understandable, since Coulomb friction, being the constant component of the dynamic friction, will not become the dominant cause of damping until the output shaft velocity is small. For the curves $T = 0$ in Fig. 2, the full decelerating torque is being applied as far as the zero-error cross-over point; it should not therefore be possible for the experimental curves of Coales and Noton to lie below the curves $T = 0$. The discrepancy probably arises from non-constancy in calibration of the system parameters and from eqn. (13) being an ideal not attained by their experimental apparatus.

In Section 8.2 it is shown that the switching function to minimize the integral of the absolute error over advanced time T is

$$F = \text{sgn}\,(2e + T\dot{e} + \tfrac{1}{2}T^2\ddot{e}) \quad . \quad . \quad . \quad . \quad (14)$$

if the assumption is made that the error acceleration $\ddot{e}$ is constant. Eqn. (14) is a quadratic switching function and reduces to eqn. (9) for the physically trivial case of constant error velocity $\dot{e}$. At the instant when the function of eqn. (14) changes sign, the parameter T may be interpreted as the advanced time over which the integral of the absolute error is minimum. Quadratic switching functions are mentioned by Flügge-Lotz and Lindberg,[3] who give no indication that a unique relation exists between the coefficients of $\dot{e}$ and $\ddot{e}$. The interpretation given in Section 8.2 is believed to be novel.

Most of the previous workers stress the importance of noise at the input and the difficulties of measuring time derivatives of the input and output higher than the first derivative. For example, Bognor and Kazda[5] develop a switching theory for nth order on–off servo mechanisms. But in the discussion on the paper it was pointed out that noise, inherently present in all physical systems, makes the development of the theory to higher-

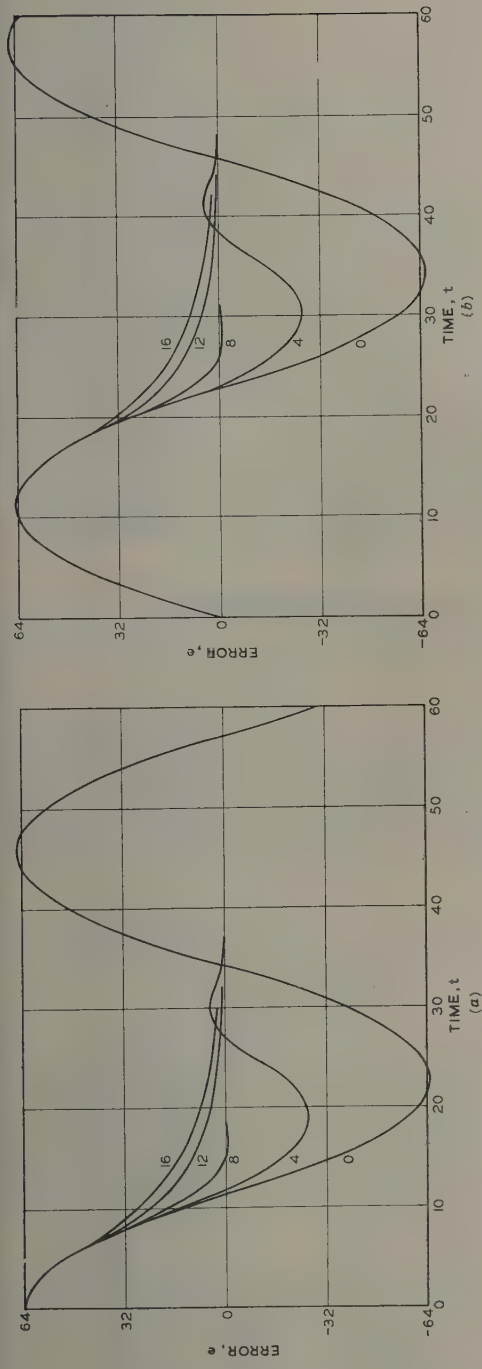

Fig. 1.—Error response of system $\ddot{c} = \text{sgn}\,(2e + T\dot{e})$ where, T is a constant.

a) Step input, $r = 64$. (*b*) Ramp input, $\dot{r} = 8\sqrt{2}$.
Numbers denote values of T.

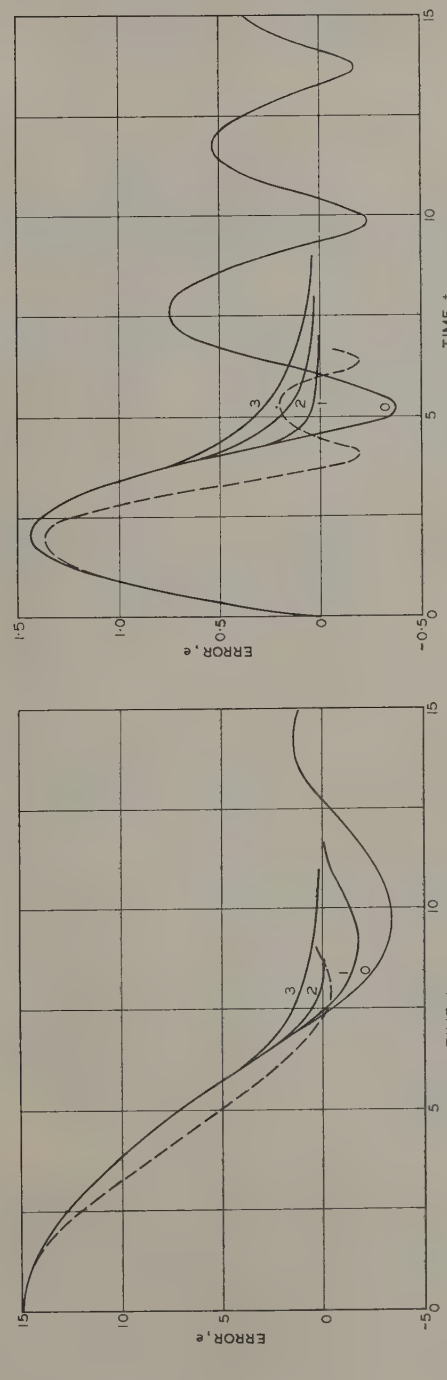

Fig. 2.—Error response of system $\ddot{c} + 0{\cdot}2\dot{c} + 0{\cdot}144\ \text{sgn}\ \dot{c} = \text{sgn}\,(2e + T\dot{e})$, where T is a constant.

(*a*) Step input, $r = 15$. (*b*) Ramp input, $r = 1{\cdot}45$.
Experimental curve of Coales and Noton.[4]
Numbers denote values of T.

order systems of little or no practical importance. Such comment is admittedly debatable, but none the less there seems need to investigate the effect of noise on any switching criterion which has been established. This is not attempted in the present paper, but bearing in mind the problem of noise, the ensuing treatment has been restricted to consideration of linear switching functions.

(3) ADAPTIVE SWITCHING FUNCTIONS

(3.1) General

Physical realization of the optimum switching function as an electrical network has been found difficult, even for a second-order linear system. Thus Smith and Leondes[6] propose approximation to the function by straight-line segments since these may be realized by biased diodes. Coales and Noton[4] regard the use of switching functions as impracticable except for the simplest of systems and propose an analogue of the system, operating on a fast time scale compared with real time, in order to predict the required switching instants. In Section 3.2 and 3.3 a self-optimizing control technique is advanced, its merit being that the switching criterion is not explicitly dependent upon the characteristics of the controlled system.

(3.2) Concept of Adaptive Switching

For the ideal system of eqn. (4) and an input given by eqn. (5), it was shown that the optimum switching function could assume the form of a linear switching function [eqn. (7)], where the parameter T_0 is a function of the input [eqn. (8)]. In general T_0 will also be a function of the output. The remainder of the paper is devoted to consideration of the linear switching function of eqn. (9), where the parameter T is continually adjusted according to some criterion in order to approximate to the optimum value T_0. The restriction is imposed that the switching function should not involve explicitly the parameters of the controlled system; i.e. the information to be used in adjustment of T may be derived only from the reference input and the response of the controlled system to the input. This allows the switching function to become adjusted to slow variation in the parameters of the controlled system and in the nature of the input. It is in this sense that the switching function is to be described as 'adaptive'. The discussion on the paper by Drenick and Shahbender,[9] is informative as to the appropriateness of the term 'adaptive'. For a system to exhibit adaptive properties it must have a 'memory'. In the present context this means that previous values of T, computed for particular input and output conditions according to some criterion, must be stored in order to be used as a basis for the computation of fresh values of T for other input and output conditions. A criterion for computation of T is propounded in Section 3.3.

(3.3) A Simple Adaptive Switching Function

Let us consider the ideal system given by eqn. (1). At some time $t = t_0$, the error velocity will become zero; let the error at this instant be e_0. At a later time $t = t_s$, F, as given by eqn. (10), will change sign; let the error velocity at this instant be $\dot{e}_s$, and the error be e_s. Then T must satisfy the equation

$$2e_s + T\dot{e}_s = 0$$

Assuming that F does not reverse sign again, the error velocity will eventually become zero at some time $t = t_1$; let the error at this instant be e_1.

Since the left-hand side of eqn. (1) is unaltered by replacing e by $e +$ constant, the final error e_1 may be chosen as reference zero without changing time-instants t_s and t_1, provided that T now satisfies the equation

$$2(e_s - e_1) + T\dot{e}_s = 0$$

i.e.
$$T = \frac{2(e_1 - e_s)}{\dot{e}_s} \quad . \quad . \quad . \quad (15)$$

The value of T given by eqn. (15) causes switching at time t_s to reduce the error velocity $\dot{e}_s$ and error $e_s - e_1$ simultaneously to zero, and hence gives optimum switching for these values. Let us assume that this value of T is stored in a memory unit in compartment m where $m \leqslant |e_1 - e_s| < m + 1$. In other words, T is tabulated at unit intervals of the numerical error $|e_1 - e_s|$. Initially the memory unit is empty, i.e. the value of T in each compartment is zero. As the simplest means of filling the table quickly, 'stepped' approximations to T may be made by causing a newly inserted value to fill also all previous compartments up to an occupied one. Since, from eqn. (15), $T = 0$ when $e_1 - e_s = 0$, an alternative is 'tapered' approximations to T. By this is meant that a newly inserted value, in filling all previous compartments up to an occupied one, is scaled linearly toward zero at zero error. A better approximation still would be to fit some curve, say a parabola, to the computed points to give minimum deviation. For the ideal system so far considered the latter method would be able to give an exact solution, since the optimum curve, as may easily be shown, is parabolic.

Let us consider now the effect of viscous damping, i.e. eqn. (4) becomes

$$\ddot{c} + D\dot{c} = F \quad . \quad . \quad . \quad . \quad . \quad (16)$$

where D is the viscous damping coefficient.

Then eqn. (10) becomes

$$\ddot{e} + D(\dot{e} - \dot{r}_0) = -F$$
$$= -\operatorname{sgn}(2e + T\dot{e}) \quad . \quad . \quad (17)$$

For viscous damping the reasoning leading to eqn. (15) is still valid. However, eqn. (17) is a function not only of the error and its time derivatives, but also of the reference input velocity $\dot{r}_0$. Therefore the value of T obtained from eqn. (15) will be dependent upon $\dot{r}_0$. Thus, for optimum switching, the memory unit must be a two-dimensional table of T values, with co-ordinates $(e, \dot{r}_0)$.

(4) MATHEMATICAL MODEL OF ADAPTIVE ON–OFF SERVO MECHANISM

(4.1) General

A convenient engineering realization of the memory unit propounded in Section 3.3. follows if the values of T, e and $\dot{r}_0$ are expressed in binary units. The adaptive control system then contains a special-purpose digital computer. Analogue-to-digital conversion will be required at the reference input and controlled output terminals, but no digital-to-analogue conversion will be required for on–off control. Useful background information on the engineering problems involved is given in Chapter 1 of Reference 10.

In the present investigation a high-speed general-purpose computer (Deuce) has been used as the control element for the servo mechanism. The investigation being of a preliminary nature, the servo mechanism itself has been simulated within the computer by a differential equation. The ideal system of eqn. (10) has been chosen rather than the damped system of eqn. (17) in order that the switching condition of eqn. (15) might not be dependent upon $\dot{r}_0$. But this consideration apart, the lack of intrinsic damping (damping for $T = 0$) in the ideal

system enables the corrective action of the adaptive switching function to be demonstrated clearly without being obscured by the natural damping of the system.

Fig. 3 is a block schematic of the manner in which the adaptive switching function given in Section 3.3 was programmed for the Deuce digital computer. Broadly speaking, the blocks above mid-level refer to storage and punch-out of computed data; the blocks below mid-level refer to computation of the relay input function F according to eqn. (9), and of the switching parameter T according to eqn. (15). The value of the input (a step r_0 or a ramp $\dot{r}_0$) is read in by a parameter card. The differential equation of the controlled system [eqn. (10)] is solved by the finite-difference method, using a counter n_1, for the sub-intervals of time $h = 1/32$. Counters n_2 and n_3 control storage and punch-out of the error e over a length of time $32N_3$, after which the values of T are punched out and another parameter card is read in. In operation, storage of successive values of error (in consecutive minor cycles of delay line 12) were found to occur at about half-second intervals and could be watched on the console display tube.

It may be noted that the layout of Fig. 3 was chosen to simplify programming and is not intended to be optimum. For example, the punch-out process could be improved if the contents of delay lines 9, 10 and 12 (containing T and e) were transferred to the magnetic drum store. Results could then be punched out in one operation and grouped better for subsequent tabulation.

(4.2) Stepped and Tapered Approximations to the Adaptive Switching Function

The results given in Fig. 1 were repeated using the computer system of Fig. 3 and are plotted in Figs 4 and 5. The significant difference between the two sets of results is in the switching parameter T, which for Fig. 1 was a constant, but which for Figs. 4 and 5 depended upon the stepped and tapered approximations referred to in Section 3.3.

Let us consider curve (i) in Figs. 4 and 5, namely the first application of the step or ramp input. Since the memory unit is empty until the error velocity reverses sign, the waveform until the time of the first overshoot peak will be identical with that given in Fig. 1 for $T = 0$. However, at the instant of error-velocity reversal a value of T will be computed according to eqn. (15) and be stored in the memory unit. Let us consider the manner of storage. For a step input, the contents of the memory unit at the end of each application (after 64 intervals) are given in Fig. 6. (For a ramp input the contents were almost identical and are not given.) It will be seen that the computed values of T become levels in the stepped approximation and become varying inclines in the tapered approximation. Furthermore, it will be seen that the stepped approximations always lie above the optimum curve [given by eqn. (8)], whereas the tapered approximations always lie below the curve. Therefore, from the discussion given in Section 2.2 on the results of Fig. 1, it is to be expected that the stepped approximations will give rise to an 'over-damped' response [curve (i) of Fig. 4] and the tapered approximations to an 'under-damped' response [curve (i) of Fig. 5].

The results of Figs. 4 and 5 exhibit a number of remarkable features. Most noteworthy is that, after a very limited number of applications (two for the step input, four for the ramp input), there ceases to be any improvement in performance. A qualitative explanation is readily forthcoming in terms of the 'over-damped' and 'under-damped' effects mentioned earlier. Thus, for the stepped approximation, 'over-damping' caused the changes in error between error-velocity reversals to be small. Therefore newly computed values of T were written into the small-error end of the table (Fig. 6), with no further improvement at the

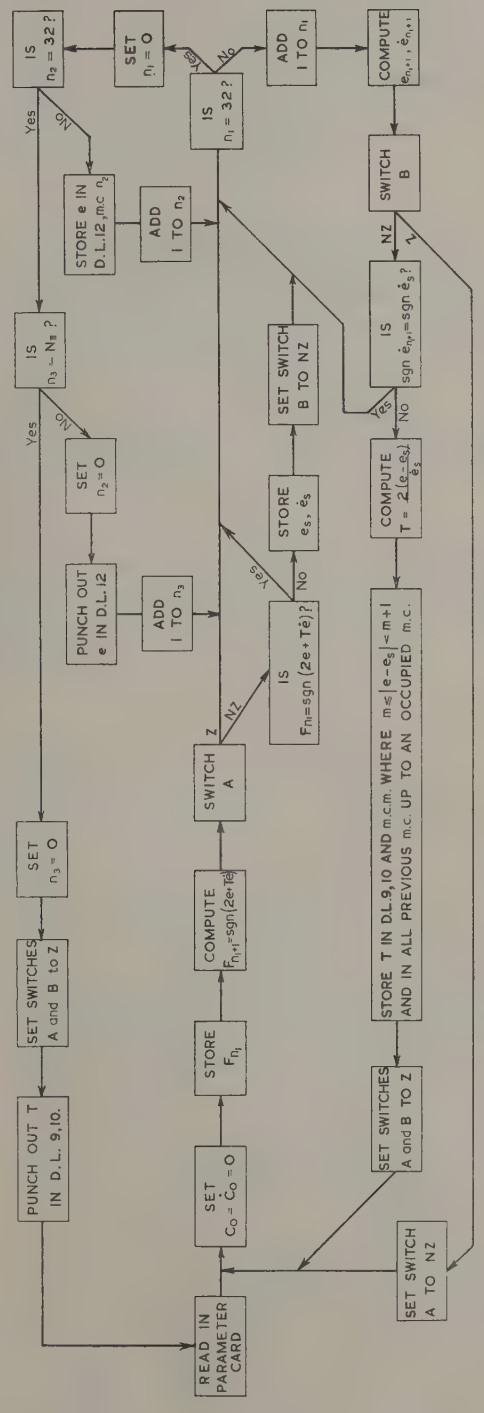

Fig. 3.—Block schematic of adaptive on–off servo mechanism for T a 'stepped' function of error.

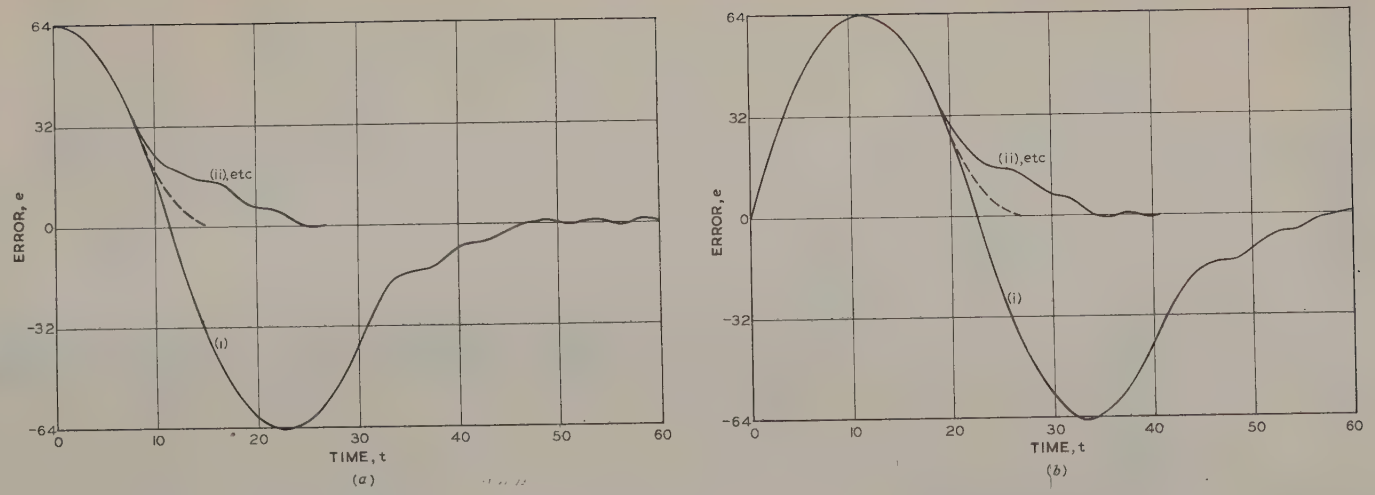

Fig. 4.—Error response of system $\ddot{c} = \text{sgn}\,(2e + T\dot{e})$, where T is a 'stepped' function of error.

(*a*) Step input, $r = 64$. (*b*) Ramp input, $\dot{r} = 8\sqrt{2}$.

——— Response of system to repetition of input, in each case from rest.
– – – – 'Optimum' response.
Numbers denote repetition sequence.

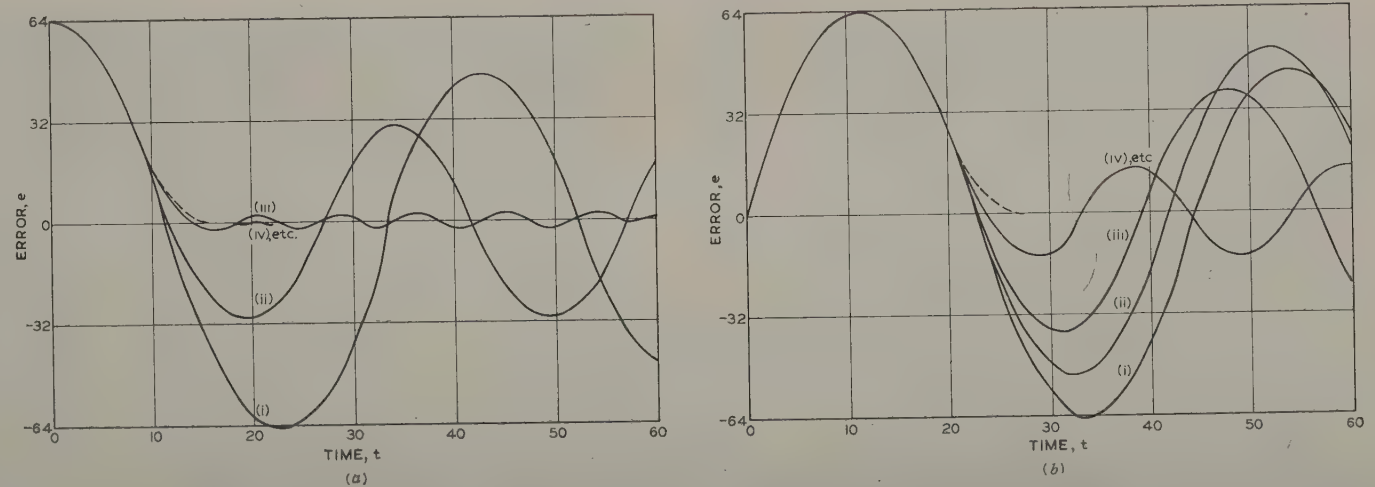

Fig. 5.—Error response of system $\dddot{c} = \text{sgn}\,(2e + T\dot{e})$, where T is a 'tapered' function of error.

(*a*) Step input, $r = 64$. (*b*) Ramp input, $\dot{r} = 8\sqrt{2}$.

——— Response of system to repetition of input, in each case from rest.
– – – – 'Optimum' response.
Numbers denote repetition sequence.

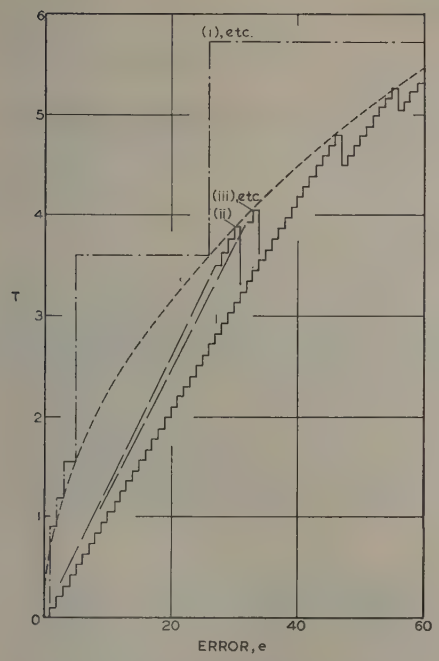

Fig. 6.—T as a function of error.
—·—·— 'Stepped' T for results of Fig. 4.
——— 'Tapered' T for results of Fig. 5.
– – – – 'Optimum' T.
Numbers denote repetition sequence.

large-error end. (The second application of step input caused two extra levels to be inserted at the small-error end of the table; these are not shown in Fig. 6 because the changes were too small to be clearly depicted.) For the tapered approximation 'under-damping' caused the response to settle down to a steady oscillation, as shown in Fig. 5. An ultimate steady oscillation would be expected from the switching condition of eqn. (15), which, for T varying directly as the error (tapered approximation), becomes

$$T = \text{constant} \times (e_1 - e_s) = \frac{2(e_1 - e_s)}{\dot{e}_s} \quad . \quad . \quad (18)$$

Eqn. (18) can be satisfied only at zero error for which T is zero, and this is the condition for steady oscillation (see curve $T = 0$ in Fig. 1). That the oscillatory state is unstable is shown by curve (iii) of Fig. 5(*a*), where, at $t = 55$ units, the oscillation jumped to a smaller value. The jump occurred because the amplitude of the oscillation was increasing slowly, and is indicated in Fig. 6 by a jump from curve (ii) to curve (iii). [Note that curve (ii) is curve (i) in which is inserted incline (ii), and that curve (iii) is curve (i) in which is inserted incline (iii).]

(4.3) Further Considerations

For many practical systems the spectral-energy distribution of the reference input does not differ markedly from that of 'white noise', when integrated over an indefinitely long period. Therefore, repeated application of random values of step and ramp input, rather than the constant values so far considered, would be nearer to reality. It follows from the adaptive procedure of Section 3.3 that, for an infinite sequence of random values, the optimum curve for T will be obtained ultimately regardless of whether or not some quick method, such as stepped or tapered approximations, is used to fill the table. However, the particular curve-fitting technique will determine the rate of approach to the optimum curve, this being expressed in some statistical measure. The rate provides an indirect performance criterion for comparison of different curve-fitting techniques; a more direct criterion would be given by the minimization of some function of the error, e.g. the absolute or the mean-square error.

Detailed investigation of the effect of random input to the mathematical model of Fig. 3 has not been attempted. Instead, present efforts are being directed toward a model which simulates more closely a practical servo mechanism.

(5) CONCLUSIONS

The use of adaptive switching functions to self-optimize on–off control systems appears to have engineering possibilities. In the case of an ideal servo mechanism, a learning process has been shown to take place. However, no account has been taken of relay imperfections, in particular inertial time delay and hysteresis effects. Also only step and ramp inputs have been considered.

Further theoretical work is being undertaken prior to an experimental investigation. In the meantime it is hoped that the paper may be of some value even in an imperfect state.

(6) ACKNOWLEDGMENTS

The work described was carried out in the Electrical Engineering Department of the University of New South Wales in partial fulfilment of the requirements for the Degree of Doctor of Philosophy. The author is grateful to Professor R. E. Vowels for supervision during the course of the work.

(7) REFERENCES

(1) 'Mechanization of Thought Processes', *Journal I.E.E.*, 1959, **5**, p. 31.

(2) Aseltine, J. A., Mancini, A. R., and Sarture, C. W.: 'A Survey of Adaptive Control Systems', *Transactions of the Institute of Radio Engineers*, 1958, **PGAC–6**, p. 102.

(3) Flügge-Lotz, I., and Lindberg, H. E.: 'On the Design and Comparison of Contactor Control Systems', *I.R.E. Wescon Convention Record*, 1957, **1**, Part 4, p. 3.

(4) Coales, J. F., and Noton, A. R. M.: 'An On–Off Servo Mechanism with Predicted Change-over', *Proceedings I.E.E.*, Paper No. 1895 M, August, 1955 (**103** B, p. 449).

(5) Bognor, I., and Kazda, L. F.: 'An Investigation of the Switching Criteria for Higher-Order Contactor Servomechanisms', *Transactions of the American I.E.E.*, 1954, **73**, Part II, p. 118.

(6) Smith, C. L., and Leondes, C. T.: 'An Analysis of the Effects of Certain Non-Linearities on Servomechanism Performance', *I.R.E. Wescon Convention Record*, 1957, **1**, Part 4, p. 24.

(7) Kochenburger, R. J.: 'A Frequency Response Method for Analysing and Synthesising Contactor Servomechanisms', *Transactions of the American I.E.E.*, 1950, **69**, Part I, p. 270.

(8) Embler, J. N., and Weaver, C. H.: 'A New Method for Compensating Contactor Servomechanisms', *ibid.*, 1957, **76**, Part II, p. 165.

(9) Drenick, R. F., and Shahbender, R. A.: 'Adaptive Servomechanisms', *ibid.*, 1957, **76**, Part 2, p. 286.

(10) Susskind, A. K., *et al.*: 'Notes on Analog-Digital Conversion Techniques' (John Wiley, 1958).

(8) APPENDICES

(8.1) Differential Equation of On–Off Predictor Servo Mechanism of Coales and Noton (Reference 4)

The differential equation of Coales and Noton, defining the angular position X of their output shaft, is given in eqn. (21) of their paper as

$$J\ddot{X} + F(\dot{X}) + \lambda\dot{X} = L \quad . \quad . \quad . \quad . \quad (19)$$

where the moment of inertia, $J = 29 \times 10^3$ g-cm^2
$= 29 \cdot 56$ g-cm per unit $\ddot{X}$

Applied torque, $L = \pm 660$ g-cm

Coulomb torque, $F(\dot{X}) = 95 \operatorname{sgn} \dot{X}$ g-cm

$J/\lambda = 5 \cdot 0$ sec

For convenience, the controlled output variable X will be replaced by a normalized variable $c = (J/L)X$ to give

$$\ddot{c} + \frac{1}{L}F(\dot{c}) + \frac{\lambda}{J}\dot{c} = F \quad . \quad . \quad . \quad . \quad (20)$$

where $F = \pm 1$.

Substituting numerical values in eqn. (20),

$$\ddot{c} + 0 \cdot 2\dot{c} + 0 \cdot 144 \operatorname{sgn} \dot{c} = F \quad . \quad . \quad . \quad . \quad (21)$$

In Fig. 11 of their paper the upper curve corresponds to a normalized step input

$$r = \frac{J}{L}(0 \cdot 8\pi \times 133) = 15 \cdot 0$$

i.e. the error torque equation is

$$\ddot{e} + 0 \cdot 2\dot{e} - 0 \cdot 144 \operatorname{sgn} \dot{c} = -F \quad . \quad . \quad . \quad (22)$$

In Fig. 12 of their paper the upper curve corresponds to a normalized ramp input

$$r = \frac{J}{L}\left(0 \cdot 34 \times 2\pi \times \frac{910}{60}\right) = 1 \cdot 45$$

i.e. the error torque equation is

$$\ddot{e} + 0 \cdot 2(\dot{e} - 1 \cdot 45) - 0 \cdot 144 \operatorname{sgn} \dot{c} = -F \quad . \quad . \quad (23)$$

(8.2) Switching Function to Minimize the Integral of the Absolute Error

Let us assume that the error acceleration $\ddot{e}$ is constant. Then the error at time t may be expressed in terms of the error and its time derivatives at time $t = 0$ by the relation

$$e = e_0 + \dot{e}_0 t + \tfrac{1}{2}\ddot{e}_0 t^2 \quad . \quad . \quad . \quad . \quad (24)$$

Suppose that the initial error e_0 is positive and that the error reverses sign at some time $t_1 < T$. Then the integral of the absolute error over a range of time $0 \leqslant t \leqslant T$ is

$$I = \int_0^{t_1} (e_0 + \dot{e}_0 t + \tfrac{1}{2}\ddot{e}_0 t^2)dt - \int_{t_1}^{T} (e_0 + \dot{e}_0 t + \tfrac{1}{2}\ddot{e}_0 t^2)dt \quad (25)$$

where t_1 satisfies the equation

$$e_0 + \dot{e}_0 t_1 + \tfrac{1}{2}\ddot{e}_0 t_1^2 = 0$$

Integrating eqn. (23),

$$I = 2\left(e_0 t_1 + \frac{1}{2}\dot{e}_0 t_1^2 + \frac{1}{6}\ddot{e}_0 t_1^3\right) - \left(e_0 T + \frac{1}{2}\dot{e}_0 T^2 + \frac{1}{6}\ddot{e}_0 T^3\right)$$

$$= 2T_1\left[\frac{2}{3}e_0 + \frac{1}{6}\dot{e}_0 t_1 + \frac{1}{3}\left(e_0 + \dot{e}_0 t_1 + \frac{1}{2}\ddot{e}_0 t_1^2\right)\right] - \left(e_0 T + \frac{1}{2}\dot{e}_0 T^2 + \frac{1}{6}\ddot{e}_0 T^3\right)$$

Substituting from eqn. (26),

$$I = 2t_1\left(\frac{2}{3}e_0 + \frac{1}{6}\dot{e}_0 t_1\right) - \left(e_0 T + \frac{1}{2}\dot{e}_0 T^2 + \frac{1}{6}\ddot{e}_0 T^3\right) \quad (27)$$

It is required to find a switching function which involves e, $\dot{e}$ and $\ddot{e}$, and which reverses sign when the integral I is minimum. The necessary condition is that

$$\frac{dI}{dt} = \frac{\partial I}{\partial e_0}\dot{e}_0 + \frac{\partial I}{\partial \dot{e}_0}\ddot{e}_0 + \frac{\partial I}{\partial \ddot{e}_0}\dddot{e}_0 = 0$$

But eqn. (24) implies that $\dddot{e}_0$ is constant.

Therefore $$\frac{\partial I}{\partial e_0}\dot{e}_0 + \frac{\partial I}{\partial \dot{e}_0}\ddot{e}_0 = 0 \quad . \quad . \quad . \quad . \quad . \quad (28)$$

Eqn. (28) defines the switching function.

From eqn. (27),

$$\frac{\partial I}{\partial e_0} = \frac{4}{3}\frac{\partial}{\partial e_0}(t_1 e_0) + \frac{1}{3}\dot{e}_0\frac{\partial}{\partial e_0}(t_1^2) - T$$

$$= \frac{4}{3}t_1 - T + \frac{2}{3}(2e_0 + \dot{e}_0 t_1)\frac{\partial t_1}{\partial e_0} \quad (29)$$

and $$\frac{\partial I}{\partial \dot{e}_0} = \frac{4}{3}e_0\frac{\partial t_1}{\partial \dot{e}_0} + \frac{1}{3}\frac{\partial}{\partial \dot{e}_0}(t_1^2\dot{e}_0) - \frac{1}{2}T^2$$

$$= \frac{1}{3}t_1^2 - \frac{1}{2}T^2 + \frac{2}{3}(2e_0 + \dot{e}_0 t_1)\frac{\partial t_1}{\partial \dot{e}_0} \quad (30)$$

Substituting eqns. (29) and (30) into eqn. (28), the switching function is

$$\dot{e}_0\left(\frac{4}{3}t_1 - T\right) + \ddot{e}_0\left(\frac{1}{3}t_1^2 - \frac{1}{2}T^2\right) + \frac{2}{3}(2e_0 + \dot{e}_0 t_1)\left(\dot{e}_0\frac{\partial t_1}{\partial e_0} + \ddot{e}_0\frac{\partial t_1}{\partial \dot{e}_0}\right) = 0 \quad (31)$$

From eqn. (26) it follows that

$$\dot{e}_0\frac{\partial t_1}{\partial e_0} + \ddot{e}_0\frac{\partial t_1}{\partial \dot{e}_0} = -1$$

Therefore eqn. (31) becomes

$$-\frac{4}{3}e_0 + \frac{2}{3}\dot{e}_0 t_1 + \frac{1}{3}\ddot{e}_0 t_1^2 - \dot{e}_0 T - \frac{1}{2}\ddot{e}_0 T^2 = 0 \quad . \quad (32)$$

Substituting for t_1^2 from eqn. (26), eqn. (32) becomes

$$2e_0 + \dot{e}_0 T + \tfrac{1}{2}\ddot{e}_0 T^2 = 0$$

i.e. the switching function is

$$F = \operatorname{sgn}(2e_0 + \dot{e}_0 T + \tfrac{1}{2}\ddot{e}_0 T^2) \quad . \quad . \quad . \quad (33)$$

621.318.132.017.31

The Institution of Electrical Engineers
Monograph No. 371 M
Apr. 1960
©

EDDY-CURRENT EFFECTS IN RECTANGULAR FERROMAGNETIC RODS

By E. W. LEE, B.Sc., Ph.D.

(*The paper was first received* 12*th May*, 1958, *and in revised form* 20*th October*, 1959. *It was published as an* INSTITUTION MONOGRAPH *in April*, 1960.)

SUMMARY

Expressions are obtained for the eddy-current distribution and the resulting loss angle for an infinitely long ferromagnetic rod of rectangular cross-section containing a number of domains magnetized parallel and anti-parallel to the axis of the rod and separated by domain walls running perpendicular to the long edge of the cross-section. Results are expressed in terms of the ratio of the lengths of the sides of the rod and the number of walls. Two cases are considered—the low-frequency limit in which the domain walls remain plane and the more general case in which the wall becomes bowed because of eddy-current screening effects.

LIST OF PRINCIPAL SYMBOLS

a = Half-thickness of ferromagnetic domain in a multi-domain sheet, cm.
d = Thickness of ferromagnetic sheet or bar, cm.
l = Half-width of ferromagnetic bar, cm.
m' = Effective oscillating mass of domain wall, g.
n = Odd integer.
q = Number of domain walls in a multi-domain sheet of finite width.
t = Time, sec.
v = Velocity of propagation of a ferromagnetic domain boundary, cm/sec.
α = Restoring force per unit area of domain wall, dynes/cm^2.
β_e = Domain-wall viscous damping constant due to eddy-currents.
β_r = Domain-wall viscous damping constant due to spin relaxation.
γ = Magnetomechanical ratio equal to $ge/2m$, where g is the Landé splitting factor (2 for electron spin) and e/m is the charge/mass ratio of the electron ($\gamma = 1{\cdot}76 \times 10^7$ if $g = 2$).
δ = Loss angle due to eddy-currents, rad.
δr = Loss angle due to spin relaxation, rad.
η = Loss ratio defined in Section 2.3.
ϕ = Scalar magnetic potential.
λ = Spin relaxation damping constant, sec.$^{-1}$
μ = Magnetic permeability at zero frequency.
ρ = Electrical resistivity, e.m.u.
ω = Angular frequency of magnetic field and magnetization, rad/sec.
A = Exchange energy per unit volume, ergs/cm^3.
B = Magnetic induction, gauss.
B_s = Magnetic induction at saturation, gauss.
H = Magnetic field, oersteds.
K = Magnetocrystalline anisotropy constant, ergs/cm^3.
M_s = Intensity of magnetization at saturation, gauss.
P = Instantaneous power loss, ergs/sec.

Correspondence on Monographs is invited for consideration with a view to publication.
Dr. Lee is in the Department of Physics, University of Sheffield, and was formerly in the Department of Physics, University of Nottingham.

(1) INTRODUCTION

There is at the present time considerable interest attached to the behaviour of ferromagnetic substances possessing a simple domain structure. There are several reasons for this. First, if the domain structure is simple the mechanism of magnetization is also likely to be simple, and by studying the behaviour of such materials one may reasonably hope to gain further insight into the behaviour of materials which are magnetically more complex. Secondly, materials possessing a simple domain structure usually exhibit rectangular B/H loop characteristics; the rectangular hysteresis loop is, in fact, one of the most elementary types and is a direct consequence of a simple magnetization mechanism. Nowadays rectangular-loop materials are much in demand for use as storage elements in magnetic memory arrays, and for such an application it is desirable to have some knowledge of, and—ideally—some degree of control over, the switching time of a magnetic core. If the domain structure is simple and the mechanism of the magnetization-reversal correspondingly simple, it is quite an easy matter to investigate theoretically the factors which limit the switching time and steps can then be taken to reduce it. Finally, it is known widely that simplicity of domain structure is invariably accompanied by eddy-current losses which are greater—often by a large factor—than those to be expected if the material could be characterized by a uniform scalar permeability.[1] A study of losses in these simple materials should go some way towards an explanation of the well-known eddy-current anomaly such as is observed, for example, in electrical transformer sheet.

These points may be illustrated with reference to Perminvar (43% nickel, 34% iron and 23% cobalt); when annealed in a magnetic field it develops a characteristic uniaxial magnetic anisotropy and the B/H loop becomes markedly rectangular. Powder-pattern and other observations[2] indicate quite clearly that in a Perminvar specimen in the form of a punched ring the magnetic structure is often simply that of two anti-parallel domains running tangentially round the ring and separated by a circular 180° wall, as shown in Fig. 1. When a magnetic field

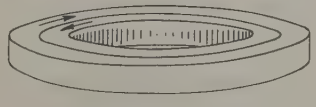

Fig. 1.—Domain structure in Perminvar after being annealed in a circular magnetic field.

Sometimes more than one domain wall is observed but the structure shown is quite usual.

is applied the wall moves to the left or right in such a way as to reduce the field energy, $-M_sH$. The B/H loop is rectangular with a remanent induction which often approaches 0·95 of the saturation induction, and experiments[1] have shown that the velocity of propagation of the domain wall is limited almost entirely by the eddy-current system set up by the moving wall. The eddy-currents and the associated losses in a material con-

taining a single domain wall are considerably greater than those which would exist if the permeability were uniform. The reason for this is quite simple. In a domain-and-wall structure one must associate a very high permeability with the wall, since the permeability is unity outside it. Now a given flux change gives rise to a definite e.m.f., V, and $\int V dl$ is the same whatever mechanism is responsible for the change in flux. However, the power dissipation is proportional to V^2 and will be large if the current lines are close together, owing to the production of a highly localized e.m.f. such as would be produced by a moving domain wall.

So far as is known, all magnetic materials possess a domain-and-wall structure; consequently, calculations of eddy-current losses based on the assumption of a uniform scalar permeability can never give any more than approximate results. The fact that the eddy-current loss in sheet steel is always greater than the calculated loss is well known, and it has been suggested[3] that a good deal of the discrepancy may be due to domain-wall effects. More recently it has been shown[4] that eddy-current losses measured in fields so low that hysteresis and other non-linear effects are absent are always greater than the calculated values. The reason for this may be found in the inhomogeneity of magnetic permeability produced by the domain structure.[5] It thus appears that these so-called anomalies are not anomalies at all, but arise from the fact that the expected eddy-current losses have been calculated using assumptions which cannot be justified for any real ferromagnetic material.

Calculations of the eddy-current losses to be expected in a domain-and-wall structure must depend upon the shape and size of the individual domains. It is necessary to postulate some fairly simple geometrical form as a model upon which to base calculations. The first thing, however, is to be absolutely certain that the model used is relevant to the case to which the calculations are intended to apply. In the paper, calculations are presented for a model in which a rod of rectangular cross-section is split up by domain walls running as shown in Fig. 2. This is certainly the situation in Perminvar and similar materials, and reasons have been given elsewhere[5] for believing that this model is a good approximation to the situation in magnetic materials with normal B/H characteristics. The calculations given below are intended for the initial permeability region, in which such a small field is applied to the material that the walls move reversibly and only by an infinitesimal amount. They do not apply at high fields to the extent that the induction is not then linearly dependent upon the applied field strength.

Calculations relevant for a rectangular bar containing a single wall at the centre have been made by Williams, Shockley and Kittel,[1] and for an infinite sheet containing a regular distribution of walls by Polivanov.[6] Although the former calculations are fairly well known, this does not seem to be true of Polivanov's work in spite of the fact that his calculations are much more general. Thus Brouwer[7] constructed an electrical analogue of domains, apparently unaware that explicit mathematical solutions appropriate to the model considered had been given by Polivanov, whilst Pry and Bean[8] analysed mathematically the same model as that used by Polivanov. In the present paper these calculations are generalized and extended. In presenting the results it was felt desirable to develop equations *ab initio*, although some repetition of results already in existence is thus unavoidable. However, this seems to be no bad thing in view of the fact that most of these calculations are so little known.

(2) DERIVATION OF BASIC EQUATIONS FOR THE CASE IN WHICH EDDY-CURRENT SCREENING IS NEGLIGIBLE

Consider a rectangular bar divided into two anti-parallel domains as shown in Fig. 2(*b*). If the wall moves from left to right the eddy-current lines are roughly as sketched in the diagram—the situation treated by Williams, Shockley and Kittel. If there is more than one domain wall the eddy-currents due to the moving domain walls interact, so that the y-component of the current is zero for all points midway between the domain walls. The form of the eddy-current lines is then as shown in Fig. 2(*c*)—the case investigated by Polivanov. The only differences between the two cases come from the differences in boundary conditions, and the general method of solution is the same. This is illustrated below with references to the case shown in Fig. 2(*b*).

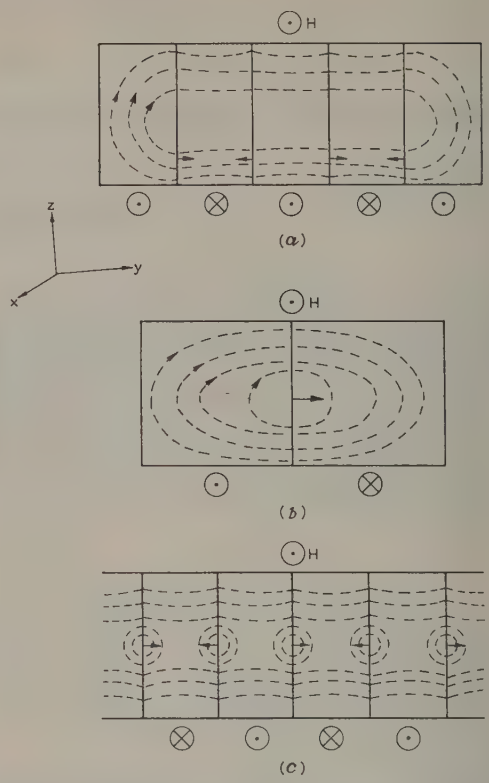

Fig. 2.—Rectangular bar divided into domains by transverse boundaries.

(*a*) Showing boundaries and fields. The arrows indicate the direction of movement of the domain boundaries and the symbols below show the directions of magnetization within the domains.
(*b*) Rectangular bar containing a single domain wall.
(*c*) Part of an infinite sheet divided by transverse domain boundaries.

(2.1) Systems containing One Wall

(2.1.1) Single Wall at the Centre.

With the centre of co-ordinates at the centre of the cross-section the wall position is in the plane $y = 0$. Outside the wall, curl $E = 0$ and the electric field can be derived from a scalar potential, ϕ, which satisfies Laplace's equation, $\nabla^2\phi = 0$. The boundary conditions are obtained in the following manner, which considers only the region to the right of the wall:

(*a*) The line $z = 0$ must be an equipotential, since E is always at right angles to it. Since only the current strength is of interest, ϕ may be equated to zero, i.e.

$$\phi = 0 \text{ at } z = 0 \text{ for all } y \quad . \quad . \quad . \quad . \quad (1)$$

(*b*) The boundaries of the bar are current lines and hence

$$\frac{\partial\phi}{\partial y} = 0 \text{ at } y = l \text{ for all } z \quad . \quad . \quad . \quad . \quad (2)$$

$$\frac{\partial\phi}{\partial z} = 0 \text{ at } z = \pm d/2 \text{ for all } y \quad . \quad . \quad . \quad (3)$$

From these equations it may readily be shown that

$$\phi = \Sigma' A_n \sin\frac{n\pi z}{d} \cosh\frac{n\pi(l-y)}{d} \quad . \quad . \quad . \quad (4)$$

in which the prime denotes summation over odd values of n only. The boundary condition at the wall may be obtained from the law of electromagnetic induction, namely

$$\text{curl } \boldsymbol{E} = \frac{\partial \boldsymbol{B}}{\partial t}$$

in integral form this becomes

$$\int_s \text{curl } \boldsymbol{E}.\boldsymbol{n}da = \int \boldsymbol{E}dl = \int_s \frac{\partial \boldsymbol{B}}{\partial t}.\boldsymbol{n}da$$

where $\boldsymbol{n}$ is a unit normal perpendicular to the element of order da. Since the wall is assumed to be infinitely thin the contribution of E_y to the line integral is zero. It follows that

$$E_z = B_s v$$

and so at the wall position

$$\phi = B_s v z \quad . \quad . \quad . \quad . \quad . \quad . \quad . \quad . \quad (5)$$

Expressing eqn. (5) as a Fourier series and equating coefficients with the right-hand side of eqn. (4) at $y = 0$, one obtains

$$A_n = \pm\frac{4B_s v d}{n^2\pi^2} \text{ sech}\frac{n\pi l}{d} \quad . \quad . \quad . \quad . \quad (4a)$$

the positive sign being operative for $n = 1, 5, 9, \ldots$ and the negative sign for $n = 3, 7, 11, \ldots$. The currents are therefore

$$i_y = +\Sigma' A_n' \sin\frac{n\pi z}{d} \sinh\frac{n\pi(l-y)}{d}$$

$$i_z = -\Sigma' A_n' \cos\frac{n\pi z}{d} \cosh\frac{n\pi(l-y)}{d}$$

with $$A_n' = \pm\frac{4B_s v}{n\pi\rho} \text{ sech}\frac{n\pi l}{d}$$

(2.1.2) Power Loss and Loss Angle.

The power loss per unit length in the x-direction is given by

$$P = 4\rho\int_0^l\int_0^{d/2}(i_y^2 + i_z^2)dydz$$

$$= \frac{16B_s^2v^2d^2}{\pi^3\rho}\Sigma' n^{-3}\tanh\frac{n\pi l}{d} \quad . \quad . \quad . \quad . \quad (6)$$

During alternating magnetizations v will be a sinusoidal function of time. If $\hat{P}$ is the maximum value of the instantaneous power loss the energy per cubic centimetre per cycle is

$$W = \pi\hat{P}/2ld\omega \quad . \quad . \quad . \quad . \quad . \quad . \quad . \quad (7)$$

Now the equation of motion of the wall is

$$m'\ddot{y} + \beta_e\dot{y} + \alpha y = 2HM_s\varepsilon^{j\omega t} \quad . \quad . \quad . \quad (8)$$

m', the effective mass of the moving domain wall, is usually so small as to be negligible at frequencies below about 10 Mc/s and so eqn. (8) becomes

$$\beta_e\dot{y} + \alpha y = 2HM_s\varepsilon^{j\omega t}$$

which has as its solution

$$y = \frac{2M_sH}{\alpha}\frac{1}{1 + j\omega\beta_e/\alpha}\varepsilon^{j\omega t} \quad . \quad . \quad . \quad . \quad (9)$$

The change in magnetization is $M = M_s y/l$ and the permeability $\mu = 4\pi M/H$, assuming $\mu \gg 1$. Therefore, from eqn. (9),

$$\mu(\omega) = \frac{8\pi M_s^2}{\alpha l}\frac{1}{1 + j\omega\beta_e/\alpha} \quad . \quad . \quad . \quad . \quad (10)$$

If μ denotes the permeability at very low frequencies then, from eqn. (10),

$$\mu = 8\pi M_s^2/\alpha l \quad . \quad . \quad . \quad . \quad . \quad . \quad (11)$$

From eqn. (9) the maximum velocity of the wall is

$$\hat{v} = 2j\omega M_s H/\alpha$$

Elimination of α through eqn. (11) gives

$$\hat{v} = \omega\dot{y}_{max} = \omega l\frac{M}{M_s} \quad . \quad . \quad . \quad . \quad . \quad (12)$$

Now $$W = \tfrac{1}{4}\mu H^2 \tan\delta \quad . \quad . \quad . \quad . \quad . \quad (13)$$

and so from eqns. (6), (7), (12) and (13) one finds

$$\tan\delta = \frac{32\omega\mu l d}{\pi^2\rho}\Sigma' n^{-3}\tanh\frac{n\pi l}{d} \quad . \quad . \quad . \quad (14)$$

(2.1.3) Single Wall, Arbitrary Position.

The more general case of a single wall situated in any arbitrary position can now be easily obtained. If the wall position is at $y = a$ then at the wall position

$$\phi = \Sigma' B_n \sin\frac{n\pi z}{d}\cosh\frac{n\pi(l-a)}{d}$$

In this case it is easily shown that, to the right of the wall,

$$\phi = \Sigma' B_n^r \sin\frac{n\pi z}{d}\cosh\frac{n\pi(l-y)}{d}$$

with $$B_n^r = \pm\frac{4B_s v d}{n^2\pi^2}\text{ sech}\frac{n\pi(l-a)}{d}$$

and for points to the left

$$\phi = \Sigma' B_n^l \sin\frac{n\pi z}{d}\cosh\frac{n\pi(l+y)}{d}$$

with $$B_n^l = \pm\frac{4B_s v d}{n^2\pi^2}\text{ sech}\frac{n\pi(l+a)}{d}$$

In this case the instantaneous power loss is

$$P = \frac{8B_s^2v^2d^2}{\pi^3\rho}\Sigma' n^{-3}\left[\tanh\frac{n\pi(l-a)}{d} + \tanh\frac{n\pi(l+a)}{d}\right]$$

which reduces to eqn. (6) when $a = 0$. Inspection of this shows that the power loss is a maximum when the wall is at the centre and is reduced by half when the wall is very near one edge. The maximum is so broad, however, that the power loss is virtually independent of wall position unless this happens to be very close to one edge.

(2.1.4) **Single Wall in the Plane of a Sheet.**

The case in which a single wall lies in the plane of a sheet has been considered by Aspden[3] in connection with a study of losses in transformer sheet at high inductions. This situation may be covered by the present equations by taking the limiting case in which $l/d \to 0$. If the wall is at the centre of the sheet,

$$\tan \delta' = \lim_{l/d \to 0} \tan \delta = \lim_{d \to \infty} \tan \delta$$

where $\tan \delta$ is obtained from eqn. (14).

Now
$$\lim_{d \to \infty} d \Sigma' n^{-3} \tanh \frac{n\pi l}{d}$$
$$= \tfrac{1}{8}\pi^3 l$$

Hence
$$\lim_{d \to \infty} \tan \delta = 4l^2 \omega \mu \pi / \rho$$
$$= \pi \omega \mu d^2 / \rho$$

since in this case $2l$ is now the sheet thickness d. This is just three times the classical value of the loss tangent calculated assuming uniform permeability, in agreement with Aspden's result.[3]

(2.2) Systems containing More than One Wall

It is extremely difficult to extend the preceding analysis to a system containing a finite number of domain walls. At first sight it would seem sufficient to calculate the potential for each wall as in Section 2.1.3 and sum the potentials, there being as many terms as there are walls. The currents could then be obtained by differentiation of the total potential thereby obtained. Unfortunately the summation involved cannot be put in a manageable form and the resulting equations are hopelessly cumbersome. In any case, such a procedure is unsound, because every domain wall is subject not only to its own eddy-current field but to the resultant z-component of the currents produced by all the other walls and so the boundary condition, eqn. (5), is no longer valid. This difficulty does not arise in the case of an infinite array of regularly spaced walls, because each wall is then situated with the same number of walls to its right as to its left. The z-components of the eddy-current at any wall due to all the other walls thus cancel completely and so the only z-component of the current is that produced by the wall itself. This case was first treated by Polivanov. If the origin of co-ordinates is taken to be the mid-point of a domain and the wall is situated at $y = \pm a$, the potential to the left of the wall, i.e. for $0 \leqslant y \leqslant +a$, is

$$\left.\begin{aligned} \phi &= \Sigma' C_n \sin \frac{n\pi z}{d} \sinh \frac{n\pi y}{d} \\ \text{in which} \quad C_n &= \pm \frac{4B_s v d}{n^2\pi^2} \operatorname{cosech} \frac{n\pi a}{d} \end{aligned}\right\} \quad . \quad . \quad . \quad (15)$$

and with the same restrictions on the sign of C_n as for the coefficient A_n.

In Sections 2.2.1 and 2.2.2 it is assumed that a situation in which there is a finite number of domain walls may be approximated by using, for the potential, Polivanov terms [eqn. (16)] for points between the domain walls, and terms of the form given in Section 2.1.3 for the two areas between the edge of the specimen and the first and last domain wall. This approximation may be expected to be a good one for wide sheets in which L/d is large, irrespective of the number of domain walls, and for rectangular bars containing only a few domain walls. Further brief discussion is given at the end of Section 2.2.2.

(2.2.1) **System containing Two Walls.**

To the right of the wall the potential is given by eqns. (4) and (4a). To the left of the wall the potential is that obtained by Polivanov [eqn. (15)]. The current components in this case are

$$i_z = \Sigma' C_n' \cos \frac{n\pi z}{d} \sinh \frac{n\pi y}{d}$$

with
$$C_n' = \pm \frac{4B_s v}{n\pi\rho} \operatorname{cosech} \frac{n\pi a}{d}$$

The power loss to the left of the wall is thus

$$P = 2\rho \int_0^{d/2} \int_0^a (i_y^2 + i_z^2) dy dz$$
$$= \frac{8B_s^2 v^2 d^2}{\pi^3 \rho} \Sigma' n^{-3} \coth \frac{n\pi a}{d} \quad . \quad . \quad . \quad . \quad (16)$$

after carrying out the indicated integrations. The power loss per wall is obtained by adding eqns. (6) and (16). The total power loss is twice this, since there are two walls, and so

$$P = \frac{16B_s^2 v^2 d^2}{\pi^3 \rho} \Sigma' n^{-3} \left[\tanh \frac{n\pi(l-a)}{d} + \coth \frac{n\pi a}{d} \right]$$

From this it is a simple matter, using the same procedure as that adopted in Section 2.1.2 and bearing in mind that μ is in this case twice the value given by eqn. (10), to show that the loss angle, δ, is given by

$$\tan \delta = \frac{8\omega\mu l d}{\pi^2 \rho} \Sigma' n^{-3} \left[\tanh \frac{n\pi(l-1)}{d} + \coth \frac{n\pi a}{d} \right]$$

In the symmetrical case in which $a = l/2$ this reduces to

$$\tan \delta = \frac{16\omega\mu l d}{\pi^2 \rho} \Sigma' n^{-3} \coth \frac{n\pi l}{d}$$

or approximately half that given by eqn. (14) for a single wall.

(2.2.1) **System Containing n Walls.**

If the walls are symmetrically distributed with the distance between successive walls equal to $2a$, then $a = l/q$, where q is the total number of walls (q being even and greater than 0). The total power loss is obtained from eqn. (16) by substituting l/q for a in the summation. There will now be two terms corresponding to the eddy-current distribution at the edges, which is of the type shown in Fig. 2(b), and $2q - 2$ terms corresponding to the distribution shown in Fig. 2(c). One thus obtains

$$P = 2\frac{8B_s^2 v^2 d^2}{\pi^3 \rho} \Sigma' n^{-3} \tanh \frac{n\pi l}{qd} + (2q-2)\frac{8B_s^2 v^2 d^2}{\pi^3 \rho} \Sigma' n^{-3} \coth \frac{n\pi}{q}$$

The corresponding loss angle, δ, is obtained by putting $v = a\omega M/M_s$ and setting

$$\tan \delta = \frac{4}{\mu H^2} \frac{\pi P}{2ld\omega}$$

from which one obtains

$$\tan \delta = \frac{32\omega\mu l d}{\pi^2 q^2 \rho} \left[\Sigma' n^{-3} \tanh \frac{n\pi(q-1)l}{qd} + (q-1) \Sigma' n^{-3} \coth \frac{n\pi l}{qd} \right] \quad . \quad (17)$$

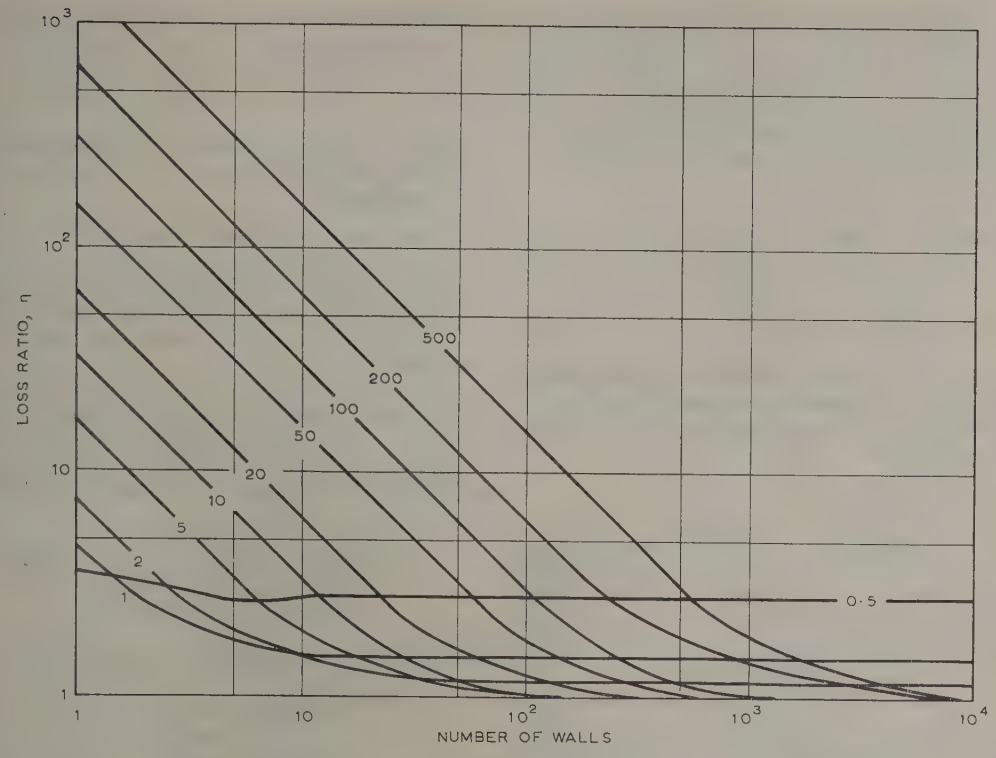

Fig. 3.—Loss ratio η as a function of the number of domain walls for rectangular bars of various dimensional ratios ($= 2l/d$).

It is quite usual to find experimentally that losses in thin ferromagnetic sheets are greater than the calculated losses.[4] In such cases it has become customary to express the results as the ratio of the observed to calculated loss, denoted here by η. This procedure is legitimate, since it is found that the observed losses, although greater than expected, vary with frequency like an eddy-current loss, at least over a restricted frequency range. Reasons have been given[5] for believing that this discrepancy arises because the classical calculation of eddy-current losses, which assumes the existence of a uniform isotropic permeability, is an approximation which always underestimates their true value. This is because magnetization takes place by movement of domain walls, and the resulting inhomogeneous permeability gives rise to an eddy-current system with which are associated losses which are always greater than those to be expected if the permeability were uniform. On this view the loss ratio, η, is the ratio of the tan δ calculated in the present paper to the classical value assuming uniform permeability. For bars of rectangular cross-section the classical losses are[9]

$$\tan\delta_c = \frac{\pi}{3}\xi\left[1 - 0{\cdot}630\frac{d}{2l} - \frac{256}{\pi^2}\xi^2\left(0{\cdot}985 - 1{\cdot}178\frac{d}{2l}\right) + \ldots\right] \quad . \quad . \quad . \quad . \quad (18)$$

in which $\xi = \omega\mu d^2/\rho$ is the usual skin-depth parameter. In the low-frequency limit considered here the third term in the parentheses may be ignored. Then $\eta = \tan\delta/\tan\delta_c$ which, from eqns. (17) and (18), is

$$\eta = \frac{96\left(1 - 0{\cdot}630\frac{d}{2l}\right)^{-1}}{\pi^3 q^2}\,\frac{l}{d}\left[\Sigma' n^{-3}\tanh\frac{n\pi(q-1)l}{qd} + (q-1)\,\Sigma' n^{-3}\coth\frac{n\pi l}{qd}\right] \quad . \quad (19)$$

This relation is shown graphically in Fig. 3. For sheets in which $l \gg d$ and in which the domain structure is so coarse that the distance between successive domain walls is not less than the sheet thickness ($2a \not< d$), eqn. (19) reduces to $\eta \simeq 3l/qd$. As a result of the approximation used to derive it eqn. (17) always tends in the limit of infinite subdivision by domains ($q \to \infty$) to the classical eddy-current losses for an infinite thin sheet. Consequently although the uniform permeability and the domain model give the same results (i.e. $\eta = 1$) for wide sheets, for which $l/d \to \infty$ in the limiting case, $q \to \infty$, this is not true for rectangular bars. Indeed, denoting the loss ratio for infinite subdivision by domains, by η_∞, it follows from eqn. (19) that

$$\eta_\infty = \left(1 - 0{\cdot}315\frac{d}{l}\right)^{-1}$$

$$\simeq 1 + 0{\cdot}315\frac{d}{l} \text{ if } d < l$$

This is, in fact, a measure of the error incurred in calculating the eddy-currents by the approximate method described in Section 2.2. If $l > 10d$ this error is not greater than 3%.

(3) EDDY-CURRENT SOLUTIONS AT HIGH FREQUENCIES

In the previous Sections eddy-current relationships have been derived on the understanding that the domain walls remained plane. This is the limiting situation at low frequencies, and it is obvious that this can be no more than an approximation, since at any finite frequency the moving walls give rise to an eddy-current system which screens the interior of the cross-section from the external field. There is nothing inherent in the walls themselves that requires them to remain plane; indeed Néel has shown that domain-wall stiffness effects are very small and that

they may be regarded as infinitely flexible. It is therefore of interest to investigate the situation in which the displacement of any point on the wall is proportional to field at that point, this field being made up of the applied field and the screening field due to the eddy-currents. The calculations have already been carried out by Polivanov for the case shown in Fig. 1(*c*) and his method is used here to cover the case in Fig. 2(*b*).

(3.1) Single Walls

(3.1.1) Single Wall at the Centre.

As already stated, the potential outside the wall must be of the form

$$\phi = \Sigma' D_n \sin\frac{n\pi z}{d} \cosh\frac{n\pi(l-y)}{d} \quad . \quad . \quad . \quad (20)$$

However, the coefficients D_n will now be different, since they are determined by boundary conditions at the wall. If the wall is imagined to be divided into a series of segments, each of which moves parallel to itself, then

$$E_z = -\left(\frac{\partial\phi}{\partial z}\right)_{y=\text{wall position}}$$

$$= B_s dy/dt \quad . \quad . \quad . \quad . \quad . \quad . \quad . \quad . \quad . \quad (21)$$

where the displacement y is now a function of z. If α is the restoring force per unit area of wall,

$$B_s\frac{dy}{dt} = B_s\frac{2M_s}{\alpha}\frac{dH}{dt}$$

If the field is $H = H_0 e^{j\omega t}$,

$$B_s\frac{dy}{dt} = j\omega\mu l H \quad . \quad . \quad . \quad . \quad . \quad (22)$$

in which μ is the permeability at zero frequency and H is a function of t and z. From eqns. (20) and (21) it follows that

$$\phi_{\text{wall position}} = j\omega\mu l\int_0^z H dz \quad . \quad . \quad . \quad . \quad (23)$$

from Ampère's law, $\quad \text{curl } H_e = 4\pi i$

from which $\quad H_e = 4\pi\int_z^{d/2} i_y dz$

If $H(d/2)$ is the field at the surface, the field inside the specimen is

$$H(z) = H(d/2) - H_e$$

$$= H(d/2) - 4\pi\int_z^{d/2} i_y dz \quad . \quad . \quad . \quad . \quad (24)$$

in which i_y is to be obtained from eqn. (20). Eqns. (20), (23) and (24) lead readily to the following result, obtained exactly as in Section 2.1.1:

$$D_n = \pm\frac{j\omega\mu l d}{\cosh\frac{n\pi l}{d} + \frac{j\omega\mu l d}{\rho}\frac{4}{n}\sinh\frac{n\pi l}{d}}\frac{4H(d/2)}{n^2\pi^2} \quad . \quad (25)$$

The currents are

$$i_y = -\Sigma' D_n' \sin\frac{n\pi z}{d}\sinh\frac{n\pi(l-y)}{d}$$

$$i_z = \Sigma' D_n' \cos\frac{n\pi z}{d}\cosh\frac{n\pi(l-y)}{d}$$

with $\quad D_n' = \frac{n\pi}{\rho d}D_n$

The instantaneous power loss is obtained exactly as before, and

$$P = \frac{16\rho\xi^2 H^2 l^2}{\pi^3 d^2}\Sigma'\frac{1}{n^3\coth\frac{n\pi l}{d} + 16n\xi^2\frac{l^2}{d^2}\tanh\frac{n\pi l}{d}} \quad . \quad (26)$$

in which $\xi = \omega\mu d^2/\rho$ as before. This reduces to eqn. (6) in the low-frequency limit in which $\xi \to 0$, if it is remembered that ωl is then equal to v.

(3.1.2) Single Wall in Arbitrary Position.

It is easy to show that, if the wall is at $y = a$ instead of at the origin, the only effect is to change l to $l - a$ in the cosh and sinh terms in eqn. (25). This has the effect of changing l to $l - a$ everywhere in eqn. (36), which then reduces to eqn. (15) in the limit $\xi \to 0$.

(3.2) Infinite Sheet with Uniform Distribution of Domain Walls

The situation shown in Fig. 2(*c*) has already been treated by Polivanov, who finds that for the coefficients in eqn. (20)

$$D_n = \frac{j\xi\frac{a}{d}}{\sinh\frac{n\pi a}{d} + \frac{4j\xi a}{nd}\cosh\frac{n\pi a}{d}}\frac{4H(d/2)}{n^2\pi^2}$$

In this case the instantaneous power loss per wall is

$$P = \frac{16\rho\xi^2 H^2 a^2}{\pi^3 d^2}\Sigma'\frac{1}{n^3\tanh\frac{n\pi a}{d} + 16n\xi^2\frac{l^2}{a^2}\coth\frac{n\pi a}{d}} \quad (27)$$

which reduces to eqn. (16) in the low-frequency limit. It may be noted that for large values of l/d and a/d both eqns. (26) and (27) give identical results for the instantaneous power loss, since both $\tanh n\pi a/d$ and $\coth n\pi l/d$ are unity. For very small values of l/d the two equations give quite different results.

(3.3) Domain-Wall Profile

As mentioned earlier, on account of the screening effect of the eddy-currents the field experienced by the wall at the centre of the sheet is less than that at the surface. If the displacement of the wall is elastic and if the restoring force per unit area of wall is everywhere the same, it follows that the wall cannot remain plane but must be distorted as it moves about its position of equilibrium. It is possible to calculate the shapes of the profile of the wall at any state of its motion on the basis of the equations already obtained. If the restoring force per unit area of wall is the same everywhere and equal to α, the displacement of the wall at any point z is

$$y(z) = 2H(z)M_s/\alpha$$

where $H(z)$ is the magnetic field strength at that point. The ratio of this field to that existing at the surface, $H(d/2)$, is

$$\frac{H(z)}{H(d/2)} = 1 - 4\pi\int_z^{d/2} i_y dz$$

Hence the ratio of the displacement of the wall at any point to its displacement at the surface is the same as this, i.e.

$$\frac{y(z)}{y(d/2)} = 1 - 4\pi\int_z^{d/2} i_y dz \quad . \quad . \quad . \quad . \quad . \quad . \quad . \quad (28)$$

$$= 1 - \frac{4\pi}{\rho}\Sigma' D_n \cos\frac{n\pi z}{d}\sinh\frac{n\pi(l-y)}{d} \quad . \quad (29)$$

or the situation shown in Fig. 1(*b*), by direct integration of qn. (28). Substituting for D_n and taking the wall position to e at $y = 0$, one finds from eqn. (29)

$$\frac{y(z)}{y(d/2)} = 1 - \frac{16j\xi l/d}{\pi}\Sigma' \pm \frac{\cos\frac{n\pi z}{d}}{n^2\coth\frac{n\pi l}{d} + 4j\xi\frac{l}{d}n} \quad . \quad (30)$$

For Polivanov's model [Fig. 1(*c*)] one finds

$$\frac{y(z)}{y(d/2)} = 1 - \frac{16j\xi a/d}{\pi}\Sigma' \pm \frac{\cos\frac{n\pi z}{d}}{n^2\tanh\frac{n\pi a}{d} + 4j\xi\frac{a}{d}n} \quad . \quad (31)$$

The difference between these two expressions is negligible for arge values of l/d or a/d since in this case both hyperbolic unctions are unity. The utility of both equations is limited n practice, since the rate of convergence is rather low, particularly or the interesting cases in which $\xi > 1$. Fig. 4 shows the wall

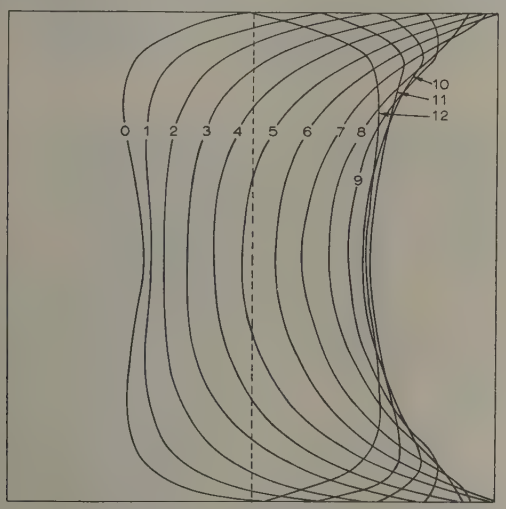

Fig. 4.—Profile of single domain wall in a bar of rectangular cross-section at various phases of the applied field.

The profile is shown at intervals of ωt of $\pi/12$ for $\xi = 1{\cdot}0$. For convenience n drawing the wall is shown moving over the entire width of the cross-section, but the ctual displacements are meant to be infinitely small.

rofiles calculated by taking the first sixteen terms of eqn. (30) or a square rod ($l/d = \frac{1}{2}$) with $\xi = 1$, for various phases of the pplied magnetizing field.

(3.4) Effective Permeability and Loss Angle

It is not easy to calculate the loss angle directly from eqns. (26) nd (27), since the effective permeability is not yet known (μ is the ermeability at zero frequency). It is simpler to calculate the omplex effective permeability from equations already obtained, ince the result will contain the loss angle implicitly. The best ay to do this is to use Polivanov's method, which uses the fact hat the mean complex permeability $\boldsymbol{\mu}$ is related to μ by the elation

$$\frac{\boldsymbol{\mu}}{\mu} = \frac{\Phi_{eff}}{\Phi}$$

his is therefore equal to the average (in the z-direction) maxi- num displacement of the wall in the y-direction divided by the maximum displacement of the wall at the surface. Taking the wall position to be at $y = 0$, eqn. (30) gives, for the case shown in Fig. 1(*b*),

$$\frac{\bar{y}}{y(d/2)} = 1 - \frac{16j\xi\frac{l}{d}}{\pi}\frac{2}{d}\int_0^{d/2}\Sigma'\frac{\cos\frac{n\pi z}{d}}{n^2\coth\frac{n\pi l}{d} + 4j\xi\frac{l}{d}n}dz$$

Thus

$$\frac{\boldsymbol{\mu}}{\mu} = 1 - \frac{32j\xi\frac{l}{d}}{\pi^2}\Sigma'\frac{1}{n^3\coth\frac{n\pi l}{d} + 4j\xi\frac{l}{d}n^2} \quad . \quad (32)$$

For the model shown in Fig. 2(*c*) Polivanov finds

$$\frac{\boldsymbol{\mu}}{\mu} = 1 - \frac{32j\xi\frac{a}{d}}{\pi^2}\Sigma'\frac{1}{n^3\tanh\frac{n\pi a}{d} + 4j\xi\frac{a}{d}n^2} \quad . \quad (33)$$

The effective loss angle may be obtained for any value of the parameters ξ and l/d by expressing eqns. (32) and (33) in the form

$$\boldsymbol{\mu} = \mu' - j\mu''$$

whence the loss angle, δ, is given by $\tan\delta = \mu''/\mu'$. However, since the formulae giving $\boldsymbol{\mu}$ as a function of frequency are no longer of the simple relaxation type, $\tan\delta/\omega$ is not a constant independent of frequency.

When measuring permeability by bridge methods it is quite usual to choose a measuring frequency (often 1–2 kc/s) at which the out-of-balance signal may conveniently be amplified and detected. If the skin depth at this frequency is such that eddy-current screening effects occur it is customary to correct for the incomplete penetration of the flux by means of correction formulae derived from standard eddy-current theory. This procedure is justifiable only if a/d is sufficiently low to ensure the validity of the standard eddy-current theory. If this is not so the actual losses will be greater than those calculated on a uniform-permeability model. It is usual to describe these losses as anomalous, although this is misleading since they arise merely from incorrect eddy-current calculations. Hence if eddy-current screening effects occur in this case it is not permissible to correct for them using the standard eddy-current calculations, since these are invalid. For sheets in which the domain size is comparable with the sheet thickness it is therefore impossible to determine the true value of the permeability at a high frequency by measuring $\boldsymbol{\mu}$ and applying a screening correction based on standard eddy-current theory assuming a uniform permeability, and one must instead use eqn. (33). This requires knowledge of a/d, which must be obtained by experiment, for example by measuring the loss angle at very low frequencies, and using eqn. (17) in the limiting case of an infinite sheet, namely

$$\tan\delta = \frac{32\omega\mu ad}{\pi^2\rho}\Sigma' n^{-3}\coth\frac{n\pi a}{d}$$

(4) SPIN-RELAXATION EFFECTS

It was first shown by Landau and Lifshitz[10] that the motion of the individual electron spins responsible for ferromagnetism is subject to a viscous damping which exists quite apart from the usual eddy-current damping. The origin and mechanism of this spin relaxation is still not completely understood, but it is believed to arise from a pseudo-dipolar interaction which also

gives rise to the linear magnetostriction. As a result, the motion of a domain wall is damped, since in a moving domain wall the spin system is essentially rotating about an axis parallel to the direction of propagation of the wall. This rotation of the spins associated with a moving domain wall is quite similar to the mass rotation of spins in a ferromagnetic resonance experiment, and one can in principle obtain the domain-wall damping factor from the width of the ferromagnetic resonance line.

To include spin-relaxation effects use is made of the fact that since the damping is viscous the equation of motion of the wall is exactly the same as before [eqn. (8)] except that the damping constant is now different and denoted by β_r, i.e.

$$m'\ddot{y} + \beta_r\dot{y} + \alpha y = 2HM_s\varepsilon^{j\omega t}$$

One then obtains expressions similar to those found previously, namely

$$y = \frac{2M_sH}{\alpha}\,\frac{1}{1 + j\omega\beta_r/\alpha}\varepsilon^{j\omega t}$$

and

$$\mu(\omega) = \frac{\mu}{1 + j\omega\beta_r/\alpha}$$

in which μ is the zero-frequency permeability as before. From these equations one finds that all the equations obtained in the preceding Sections retain their validity if μ is replaced by the complex permeability $\mu(\omega)$ throughout. Whether spin relaxation is important or not in comparison with eddy-current damping can be decided only by inserting numerical values for β_r. The expression given by Galt *et al.*[11] is

$$\beta_r = \frac{\lambda|K|^{1/2}}{2\gamma^2A^{1/2}}$$

for a 180° wall. The (angular) relaxation frequency for relaxation process alone is α/β_r or $B_s^2/2\pi\mu l\beta_r$ and the loss angle is given by

$$\tan\delta_R = \frac{\omega\beta_r}{\alpha} = \frac{2\pi\mu l\omega\beta_r}{B_s^2}$$

so that such effects may be of some importance in connection with alloys of very high permeability. Moreover $\tan\delta_R$ is independent of the sheet thickness, unlike the eddy-current loss angle, which decreases with decreasing sheet thickness; it thus follows that spin-relaxation effects in metals become more important as the sheet thickness decreases. The author has shown[5] that, for high permeability nickel-iron alloys, spin relaxation should make a significant contribution to the low-field magnetic losses when the thickness of the sheet is reduced below about 3 μ. In thinner sheets and evaporated films spin-relaxation effects are likely to provide the dominant loss mechanism. This should also be the case in all high-resistivity ferrites.

(5) MAGNETO-MECHANICAL DAMPING

Ferromagnetic materials are known to exhibit severe internal friction which, moreover, is found to be a function of their magnetization. It has been established that most of this internal friction arises from eddy-current damping. The domain boundaries in a ferromagnetic material may be displaced by the application of an external stress in a manner similar to their displacement by an external field. However, a stress is uniaxial whereas a magnetic field is unidirectional, and consequently stress cannot change the bulk magnetization of a ferromagnet substance unless it is already magnetized.

If an alternating stress is applied to a ferromagnetic materi in the demagnetized state the domain walls will be set int alternating motion, but the motion of adjacent walls will diff in phase by 180° in order to preserve zero bulk magnetizatio Consequently the eddy-current lines around a single moving wa are like those shown in Fig. 2(*b*), and all equations based on th situation are valid for the magneto-mechanical damping of a infinite sheet in the demagnetized state if $2l$ is now taken to be th distance between successive domain walls. If the material polarized, or in the presence of an external field, the bul magnetization may be altered by stress, and in this case th equations based on Fig. 1(*c*) apply.

(6) ACKNOWLEDGMENTS

The author would like to express his thanks to Professor L. Bates for his interest in this work. It was begun in collaboratio with Dr. A. G. H. Troughton, whose assistance is grateful acknowledged. The revision of the paper was carried out o the basis of a close scrutiny by Mr. J. E. L. Bishop, who has bee responsible for correcting certain errors in the original.

(7) REFERENCES

(1) Williams, H. J., Shockley, W., and Kittel, C.: 'Studies the Propagation Velocity of a Ferromagnetic Doma Boundary', *Physical Review*, 1950, **80**, p. 1090.

(2) Williams, H. J., and Goertz, M.: 'Domain Structure Perminvar having a Rectangular Hysteresis Loo *Journal of Applied Physics*, 1952, **23**, p. 316.

(3) Aspden, H.: 'The Eddy-Current Anomaly in Electric Sheet Steel', *Proceedings I.E.E.*, Monograph No. 164 M January, 1956 (**103** C, p. 272).

(4) Richards, C. E., Walker, E. V., and Lynch, A. C.: 'A Experimental Study of High-Permeability Nickel-Iro Alloys', *ibid.*, Paper No. 2136 M, August, 1956 (**104** p. 343).

(5) Lee, E. W.: 'Eddy-Current Losses in Thin Ferromagnet Sheets', *ibid.*, Monograph No. 284 M, February, 19 (**105** C, p. 337).

(6) Polivanov, K. M.: 'Dynamic Characteristics of Ferr magnetic Materials', *Izvestia Akademii Nauk, S.S.S.R Seria Fiziki*, 1952, **16**, p. 449.

(7) Brouwer, G.: 'Electrical Analog of the Eddy-Curren Limited Domain-Boundary Motion in Ferromagnetic *Journal of Applied Physics*, 1955, **26**, p. 1297.

(8) Pry, R. H., and Bean, C. P.: 'Calculation of the Energy Lo in Magnetic Sheet Materials using a Domain Mode *ibid.*, 1958, **29**, p. 532.

(9) Debye, P.: 'Wirbelströme in Stäben von rechteckige Querschnitt', *Zeitschrift für Mathematik und Physi* 1907, **54**, p. 418.

(10) Landau, L., and Lifshitz, E.: 'On the Theory of the D persion of Magnetic Permeability in Ferromagnet Bodies', *Physikalische Zeitschrift der Sowjetunion*, 193 **8**, p. 153.

(11) Galt, J. K., Andrus, J., and Hopper, H. G.: 'Motion Domain Walls in Ferrite Crystals', *Reviews of Mode Physics*, 1953, **25**, p. 93.

20.179.14: 669.18

The Institution of Electrical Engineers
Monograph No. 372 M
Apr. 1960
©

INVESTIGATION OF AN ELECTRICAL NON-DESTRUCTIVE METHOD OF MEASURING THE DEPTH OF SURFACE HARDNESS IN FLAME-HARDENED STEELS

By J. A. BETTS, B.Sc., Ph.D., and J. P. NEWSOME, M.Sc., Associate Member.

(*The paper was first received* 28*th August, and in revised form* 17*th November*, 1959. *It was published as an* INSTITUTION MONOGRAPH *in April*, 1960.)

SUMMARY

At the present time there exist no established, non-destructive methods for the measurement of depth of hardness in surface-hardened steels which are independent of the effects of chemical composition and quench procedure. Electrical non-destructive methods are dependent upon changes in the electrical and magnetic properties of steel which occur when it is hardened.

The electrical method investigated by the authors was an a.c. one, based upon the measurement of the complex impedance of a search coil magnetically coupled to the test surface. Distinctly favourable results were obtained, and the paper is concerned with the theoretical and practical aspects of the procedure.

LIST OF SYMBOLS

A, C, D = Ferrite core dimensions.
$B, \hat{B}$ = Magnetic flux density and maximum value.
b = Probe unit factor.
e = Eddy-current loss coefficient.
f, ω = Frequency and angular frequency.
G_m = Conductance representing total power loss in steel test specimen.
h = Hysteresis loss coefficient.
$H, \hat{H}$ = Magnetizing force and maximum value.
$J, \hat{J}$ = Current density and maximum value.
L = Effective series inductance of probe-coil impedance.
L_p = Effective shunt inductance component of the probe-coil impedance.
N = Number of turns on probe-coil winding.
P_e, P_h = Eddy-current and hysteresis power loss.
R_e, R_h = Shunt resistive components of the probe-coil impedance due to eddy-current and hysteresis loss in the steel test specimen.
R_c = A.C. resistance of probe-coil winding.
R_m = Effective series resistance of probe-coil impedance representing total power loss in test steel specimen.
R = Total effective series resistance of probe-coil impedance.
r_1, r_2 = Effective radii of inner and outer limbs of ferrite core.
α = Rayleigh's hysteresis loop constant.
σ, ρ = Conductivity and resistivity.
$\mu, \hat{\mu}, \mu_r$ = Permeability, maximum value and relative value.
$\Phi, \hat{\Phi}$ = Magnetic flux and maximum value.

(1) INTRODUCTION

The accepted mechanical methods of measuring depth of surface hardness frequently require destruction of all or part of the test specimen. Such a procedure is usually costly and wasteful, and, perhaps more important, a hardened component which is to be put into service cannot be proved to be adequately hardened except by inference.

There is thus a definite need for a reliable non-destructive method of measuring the depth of surface hardness. There is evidence of research in this field in America using ultrasonics[1] and in Russia using an a.c. electromagnetic method.[2] The latter is used in industry for testing or sorting ferrous materials by comparison, but there is some doubt whether the existing technique permits separate detection of a variable when more than one variable is involved.

The paper is concerned with the electromagnetic method, in which a coil is closely coupled to the steel test surface by a ferrite cup-core and carries alternating current. Flat flame-hardened steel surfaces were used throughout. Two techniques were examined, one using low frequencies (approximately 5–500 c/s) such that the magnetic-flux penetration was significantly greater than the depth of the hardened layer, the other using higher frequencies (approximately 8–15 kc/s) such that significant magnetic-flux penetration was very much less than the depth of the hardened layer. In an entirely experimental approach the first technique did not show successful results; a theoretical examination of the problem, if it were possible, would require a knowledge of the variation of resistivity and permeability within the hardened layer. Encouraging results were, however, obtained with the second technique. A relationship has been found to exist between the probe-coil electrical parameters and the depth of hardness, and this relationship has been studied theoretically and experimentally.

(2) ELECTRICAL AND MAGNETIC PROPERTIES OF HARDENED STEELS

The electrical and magnetic properties of a hardened steel are a function of the pre-quenching temperature and the type (or severity) of quench employed. Fig. 1, taken from a paper by Estulin,[3] shows the relation between the saturation value of the intensity of magnetization and the pre-quenching temperature for a chrome-nickel and a chrome-manganese steel. Fig. 2, due to Edwards and Norbury,[4] shows the relation between resistivity and pre-quenching temperature for various chrome steels subjected to a rapid air or water quench; Powell,[5] in a more recent paper, gives further data on this subject.

Webb, in the discussion following a paper by Hadfield,[6] shows a graph of electrical resistivity against mechanical degree of hardness for four steels; the heat treatment is not quoted, but it is assumed that the steels are heated, quenched and then tempered to obtain variation in the degree of hardness.

Fig. 3 is a graph of the degree of hardness against depth below the steel surface for a flame-hardened steel; the sharp transition between the unhardened and hardened regions is pronounced and noteworthy.

Correspondence on Monographs is invited for consideration with a view to publication.
The authors are in the Department of Electrical Engineering, University of Nottingham.

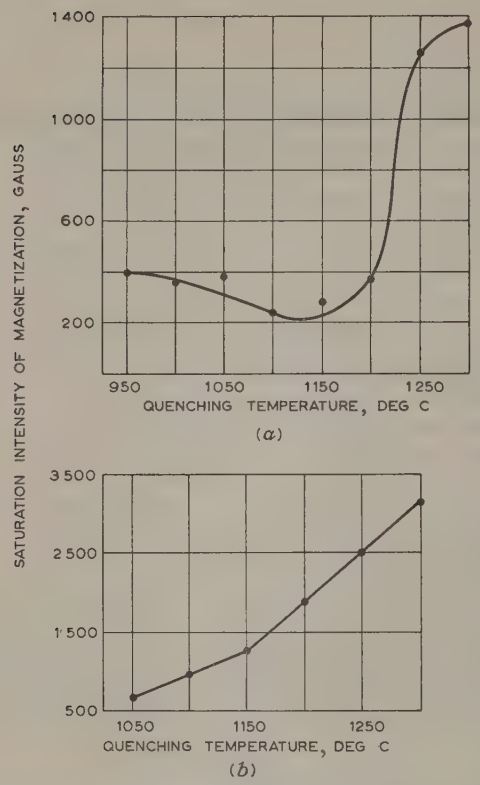

Fig. 1.—Variation of saturation intensity of magnetization with quenching temperature.
(*a*) A chrome-nickel steel.
(*b*) A chrome-manganese steel.

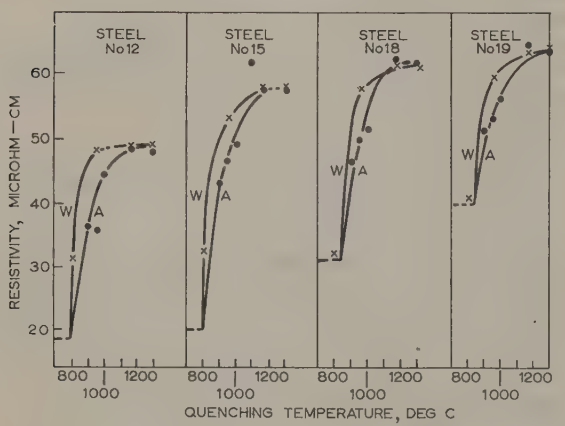

[Iron and Steel Institute

Fig. 2.—Resistivity versus quenching temperature for a number of chrome steels.

(3) THE HIGH-FREQUENCY A.C. METHOD

(3.1) Basic Principles

For a given gas-burner configuration and quench procedure, the resulting depth of surface hardness in a given process will depend upon the speed of traverse of the burners over the surface; the slower the speed of the burners, the higher the pre-quenching surface temperature and the greater the depth of surface hardness.

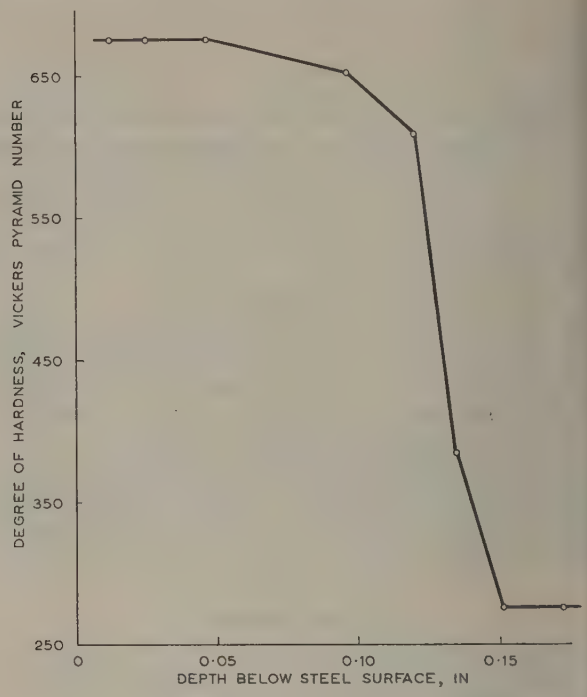

[Crown copyright

Fig. 3.—Variation of degree of hardness with depth below steel surface.
Steel type V9D; nominal depth of hardness, 0·15 in.

It has been stated in Section 2 that the electrical and magnetic properties of a hardened steel are functions of the pre-quenching temperature. Thus, a method of measuring the electrical and magnetic surface properties of a flame-hardened steel would give a measure of the depth of surface hardness. Such a method would be comparative for a given shape and composition of test specimen and would assume a consistent quenching procedure and a fixed gas-burner configuration.

The product of resistivity and permeability of the test steel surface (termed the electrical surface factor) can be measured in terms of the complex impedance of a coil magnetically coupled to the test steel surface. The form of coil and its associated ferrite core, collectively termed a probe unit, is shown in Fig. 4.

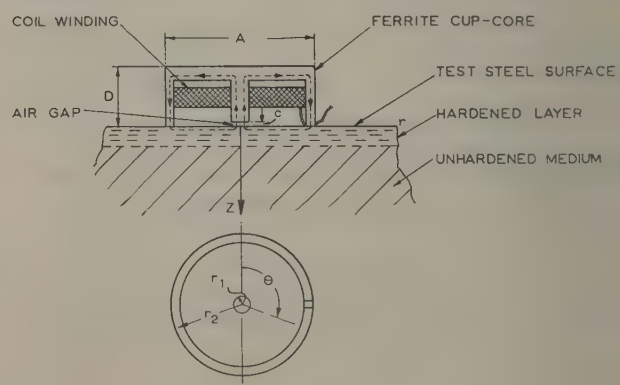

Fig. 4.—Details of probe unit.
---- Magnetic flux path.

An equation is developed in the Appendices which relates the electrical surface factor, $\mu\rho$, with G_m, the conductance representing the power loss in the test steel with which the ferrite core is in contact. This is eqn. (20), which is repeated here for convenience:

$$G_m = \frac{b}{\sqrt{(\mu\rho)}} \frac{1}{\sqrt{f}} + h$$

where b and h are constants. Thus, if G_m is measured over a range of frequencies and plotted against $1/\sqrt{f}$ the electrical surface factor is obtained from the slope of the curve. This relation is sufficiently accurate for experimental purposes provided that the following conditions are met:

(*a*) The flux density in the steel must be kept low to ensure that Rayleigh's relation for the hysteresis loop is valid (see Section 7.3).
(*b*) The total flux in the steel must be maintained constant and independent of frequency.
(*c*) The test frequency must be high enough for the significant depth of flux penetration to be very much less than the length of the radial flux path in the steel.

(3.2) Evaluation of Test Frequency

From eqn. (16) of Section 7.3, it is seen that the attenuation of flux within the steel may be expressed as

$$\frac{[\hat{B}_r]_{z=0}}{[\hat{B}_r]_z} = \exp\left(\frac{kz}{\sqrt{2}}\right) \text{ or } \log_e \frac{[\hat{B}_r]_{z=0}}{[\hat{B}_r]_z} = \sqrt{(\mu\sigma\pi f)}z$$

The depth at which this ratio has the value ε is known as the skin depth. Thus

$$\text{Skin depth} = \frac{1}{\sqrt{(\mu\sigma\pi f)}}$$

The nominal depths of hardness used in this work vary between 0·05 and 0·2 in. It is a requirement of the method that significant flux penetration in the steel should be very much less than the depth of hardness. To evaluate a suitable test frequency, a skin depth of 0·01 in is assumed; if typical values of μ and σ for a steel are taken, say $\mu = 75 \times 4\pi \times 10^{-7}$ and $\sigma = 4 \times 10^6$ mhos/m, then a test frequency of 13 kc/s is obtained. This figure is for guidance only.

If a skin depth less than 0·01 in is used the results obtained might well become erratic owing to surface irregularities and impurities and also to the effect of surface preparation for testing (e.g. grinding and polishing) upon the values of μ and ρ close to the surface.

(3.3) Details of Probe Units

Two probe units were employed, both of the form shown in Fig. 4. Details of the probes are given in Table 1, in which the probe factor has been calculated from eqn. (21).

The initial relative permeability of the ferrite material used in the probe units was about 800.

Table 1

Probe unit	Ferrite* type	Coil winding		Probe factor	Dimensions		
					A	D	C
		s.w.g.	turns		mm	mm	mm
1	FX1922	32	210	$1{\cdot}6 \times 10^{-6}$	25	8	0·1
2	FX1824	40	270	$0{\cdot}756 \times 10^{-6}$	17·5	6	0·1

* Ferroxcube material.

(3.4) Method of Measuring Probe-Coil Parameters

Probe-coil impedance measurements were carried out using a Maxwell bridge with a Wagner earthing system and tuned detector over the frequency range 5–10 kc/s. The overall sensitivity was such that the measured quantities could be determined with a precision of 1 part in 5000.

The peak flux density in the centre section of the probe was maintained at 1 mWb/m^2. This necessitated control of the voltage across the probe at each test frequency, which was effected by means of an amplifier and voltmeter.

(3.5) Experimental Examination of the Relation between Probe-Coil Parameters and Electrical Surface Factor

To verify the correctness of eqn. (20) the electrical surface factor was measured and compared with a value of $\mu\rho$ obtained by steady flux measurements for four different steels, all unhardened.

Bars 6 × 1 × ¼ in were cut from each type of steel, and one 6 × 1 in surface was ground so that the undulation over the area seating a probe was significantly less than 0·001 in; the grinding process was carried out slowly and with much coolant so that the surface layer would not be unduly heated or worked. Impedance measurements were carried out on these surfaces using the spring-loaded jig shown in Fig. 5, with probe unit 2,

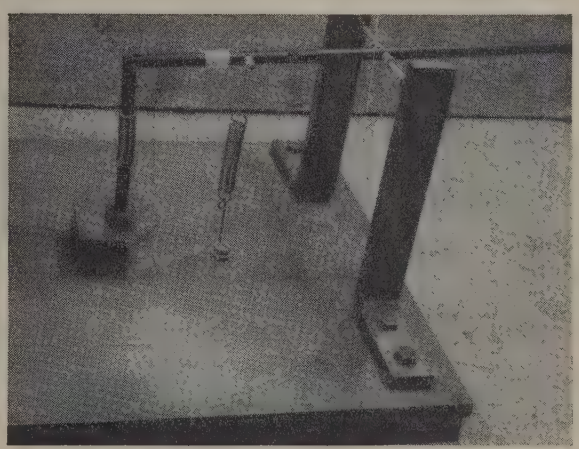

[Crown copyright

Fig. 5.—The spring-loaded probe on a steel test surface.

over the frequency range 5–10 kc/s. With this arrangement, and by first cleaning the probe and test surfaces with a cleaning fluid to remove small particles, the impedance measurements were repeatable with a precision of 1 part in 10^3.

It was found to be very important to maintain the most intimate contact between the ferrite core and the test surface; the air-gap (dimension C in Fig. 4) was purposely introduced to diminish the effects of any accidental air-gap between ferrite and steel caused by small particles of dirt.

The equivalent circuit for the probe-coil impedance is shown in Fig. 6 and is discussed in Section 7.4. G_m was determined from the measured values of L and R using the following procedure. Reference to Fig. 6(*a*) shows that $R_m = R - R_c$, and from Fig. 6(*b*), $G_m = R_m/(R_m^2 + \omega^2 L^2)$. It was found necessary to make a small correction for the loss in the ferrite core and also to use a value of R_c appropriate to the ambient temperature. Graphs of G_m against $1/\sqrt{f}$ are shown in Fig. 7 for the four test steel bars.

A rod 6 × ¼ × ¼ in was then cut out of the centre of each

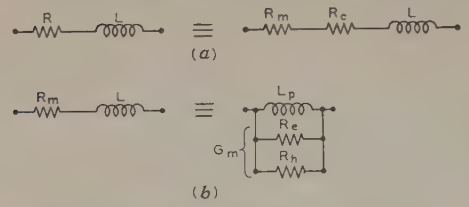

Fig. 6.—Equivalent circuits of the probe coil.

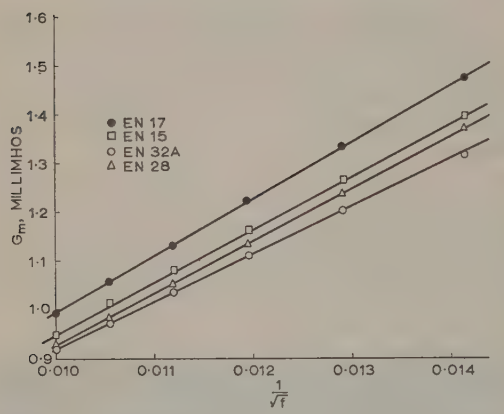

Fig. 7.—G_m plotted against $1/\sqrt{f}$ for four types of steel.

bar and used for determination of resistivity by the Kelvin double-bridge method, and of permeability by the solenoid and ballistic-galvanometer method; this permitted an evaluation of $\mu\rho$ for steady-flux conditions. These results, together with electrical surface factors determined from the slopes of the graphs of Fig. 7, are given in Table 2.

Table 2

Steel type	Steady flux measurements			Probe measurement	$\frac{(\mu\rho)_{probe}}{(\mu\rho)_{steady}}$
	ρ	μ_r	$(\mu\rho)_{steady}$	$(\mu\rho)_{probe}$	
	microhm-m		$\times 10^{-12}$	$\times 10^{-12}$	
EN17	0·268	52·7	17·8	42·7	2·40
EN15	0·241	62·4	18·9	50·9	2·69
EN28	0·273	58·5	20·0	49·5	2·48
EN32A	0·168	122	25·8	60·8	2·36

It can be seen from Fig. 7 that the relation between G_m and $1/\sqrt{f}$ is linear, thus verifying the form of eqn. (20). Table 2 shows that the same value of $\mu\rho$ is not obtained in the steady-flux and probe measurements, but that there is a fixed ratio between the two values. This may be accounted for as follows:

(*a*) Eqn. (20) is based on a flux distribution which is never exactly achieved in practice; it is not an exact equation.

(*b*) The steady-flux measurement of $\mu\rho$ gives an average for the whole material, whereas the probe measurement of $\mu\rho$ gives a value for the surface layer of the material; these values may differ.

(*c*) In the steady-flux measurement of μ the direction of flux is along the bar, but in the probe measurement the flux extends radially outwards in all directions from the centre of the bar; the value of μ may differ with direction.

It is concluded that the electrical surface factor calculated from probe measurements by means of eqn. (20) is an effective value which is a function of the electrical and magnetic surface properties of the test steel and can therefore be related to the depth of surface hardness, as discussed in Section 3.1.

(3.6) Electrical Surface Factors of Surface-Hardened Steels

The specimens tested were of two types:

(*a*) Type V9D* in billets 9 in diameter, 4 in thick (tested with probe 1).

(*b*) Types EN17,† EN19,† V10* and V13 in blocks 2 × 2 × 1 in (tested with probe 2).

Three specimens of each type were flame-hardened to depths of 0·05, 0·1 and 0·15 in; in the case of the EN19 steel, three sets of test blocks were obtained from three different forgings.

The depth of hardness was verified by means of Vickers diamond hardness readings taken below the hardened surface some distance within the specimen; this necessitated cutting off a section of the block. Probe-type measurements were then made on the hardened and unhardened faces of each specimen

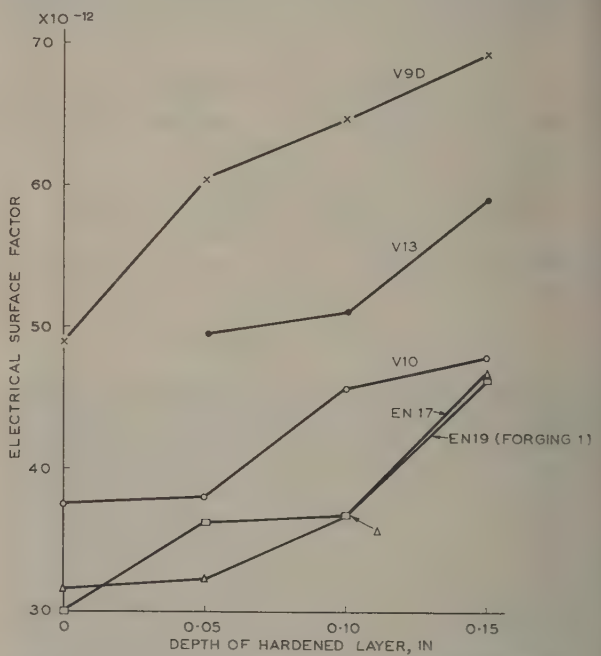

Fig. 8.—Variation of electrical surface factor with depth of hardened layer for several types of steel.

Table 3

Depth of hardened layer	Electrical surface factor		
	Forging 1	Forging 2	Forging 3
in	$\times 10^{-12}$	$\times 10^{-12}$	$\times 10^{-12}$
Unhardened	29·8	30·1	29·2
0·05	36·1	36·4	34·9
0·1	36·7	37·9	—
0·15	46·1	—	47·0

at frequencies of 8 and 10 kc/s; from these measurements the electrical surface factor was calculated. The overall results obtained are shown in Fig. 8 and the variation of electrical surface factor for the three forgings of EN19 steel are shown in Table 3.

* For identification see Ministry of Supply steel specifications.
† For identification see B.S. 970.

The results confirm the variation of the electrical surface ctor with depth of hardness and thus form the basis of a ɔssible comparative method of measuring this quantity. It ould be necessary for a given probe to have a calibration curve the form shown in Fig. 8 for each type of steel; such a curve ould hold good for a given process, as stated in Section 3.1.

(4) CONCLUSIONS

Many non-destructive testing techniques of the eddy-current ɣpe are empirical; an attempt has been made here to avoid this ɛature.

The work covered by the paper is exploratory, and if the high-ɛequency a.c. method is to be developed it is necessary for the ɔllowing factors to be examined:

(*a*) The variation of resistivity and permeability of steels with uenching temperature and severity of quench, and with depth ɛlow the surface of a surface-hardened material; the possibility f ambiguity in the method may arise through $\mu\rho$ having the ɑme value for different depths of hardness.

(*b*) The behaviour of the relation between G_m and $1/\sqrt{f}$ with robes of differing dimensions.

(*c*) The development of probes of different shapes (e.g. J-shaped), possibly to deal with curved hardened surfaces.

(5) ACKNOWLEDGMENT

The authors wish to thank Professor J. E. Parton for facilities ranted in connection with this work at the University of Nottingham.

(6) REFERENCES

1) 'Ultrasonic Non-Destructive Measurement of Case Depth and Case Hardness', Sperry Products Engineering Report TRO61.

2) UNTERWEISER, P. M.: 'Electromagnetic Test Measures Effects of Shot Peening', *Iron Age*, 5th June, 1958, p. 121.

3) ESTULIN, G. V.: 'The Study of Transformations in Austenitic Alloys by the Magnetic Method', *Zavodskaya Laboratoriya*, 1949, **15**, p. 1262.

4) EDWARDS, C. A., and NORBURY, A. L.: 'Effect of Heat Treatment on the Electrical Resistivity of Chromium Steels', *Journal of the Iron and Steel Institute*, 1920, **101**, No. 1, p. 447.

5) POWELL, R. W.: 'The Effect of Quenching on the Thermal Conductivities and Electrical Resistivities of Steels', *ibid.*, 1956, **184**, p. 6.

6) HADFIELD, D.: 'Magnetic Measurement of Mechanical Hardness', *Proceedings I.E.E.*, Paper No. 1956 M, January, 1954 (**101**, Part II, p. 529).

7) LORD RAYLEIGH: 'Investigation of Hysteresis Effects in Magnetic Materials', *Philosophical Magazine*, 1887, **23**, p. 113.

8) LEGG, V. E.: 'Magnetic Measurements at Low Flux Densities', *Bell System Technical Journal*, 1936, **15**, p. 39.

9) BETTS, J. A.: 'Investigation of Electrical Non-Destructive Methods of Measuring the Depth of Surface Hardness of Flame-Hardened Steel', Ph.D. Thesis, University of Nottingham, 1958.

(7) APPENDICES

(7.1) Magnetic Flux Distribution in the Test Material

Maxwell's equations for a conducting medium where displacement current can be ignored take the form

$$\text{div } \boldsymbol{B} = 0, \text{ curl } \boldsymbol{H} = \boldsymbol{J}, \text{ curl } \boldsymbol{E} = -\frac{d\boldsymbol{B}}{dt}$$

Also $$\boldsymbol{B} = \mu\boldsymbol{H}, \boldsymbol{J} = \sigma\boldsymbol{E}$$

Now curl curl $\boldsymbol{H}$ = grad div $\boldsymbol{H} - \nabla^2\boldsymbol{H} = \sigma$ curl $\boldsymbol{E}$

giving $$\nabla^2\boldsymbol{H} = \sigma\frac{d\boldsymbol{B}}{dt}$$

or $$\nabla^2\boldsymbol{B} = \mu\sigma\frac{d\boldsymbol{B}}{dt} \quad . \quad . \quad . \quad . \quad . \quad . \quad (1)$$

Fig. 4 shows the probe unit located on a flat steel surface. Owing to the relatively high permeability of the ferrite and steel materials, leakage flux is ignored. The flux is considered to leave the outer annulus of the cup-core, pass through the test steel and re-enter the centre limb of the cup-core. The flux in the steel is considered to be radial and tangential to the surface; the component of flux normal to the steel surface is assumed to be negligible by making the radial length of the flux path, $r_2 - r_1$, very much greater than the depth of flux penetration.

Using cylindrical co-ordinates in the manner shown,

$$B_\theta = B_z = 0, B_r = \mathrm{F}_1(r)\mathrm{F}_2(z)$$

These conditions cannot be exactly achieved but may be approached adequately for experimental purposes.

Assuming a sinusoidal variation of flux with time, $\boldsymbol{B} = \hat{\boldsymbol{B}}\varepsilon^{j\omega t}$, which defines a flux density $\hat{\boldsymbol{B}}\cos\omega t$, and $\dot{\boldsymbol{B}} = j\omega\boldsymbol{B}$, which defines a quantity $-\omega\hat{\boldsymbol{B}}\sin\omega t$.

Thus,

$$\nabla^2\boldsymbol{B} = j\mu\sigma\omega\boldsymbol{B} = jk^2\boldsymbol{B} \quad . \quad . \quad . \quad . \quad . \quad (2)$$

where $$k^2 = \mu\sigma\omega$$

Now $\nabla^2\boldsymbol{B}$ can be expanded thus:

$$\nabla^2\boldsymbol{B} = \frac{1}{r}\frac{\partial}{\partial r}\left(r\frac{\partial\boldsymbol{B}}{\partial r}\right) + \frac{1}{r^2}\frac{\partial^2\boldsymbol{B}}{\partial\theta^2} + \frac{\partial^2\boldsymbol{B}}{\partial z^2}$$

which reduces to

$$\nabla^2\boldsymbol{B} = \boldsymbol{l}_r\left(\frac{\partial^2 B_r}{\partial r^2} + \frac{1}{r}\frac{\partial B_r}{\partial r} + \frac{\partial^2 B_r}{\partial z^2}\right) \quad . \quad . \quad . \quad (3)$$

where $\boldsymbol{l}_r$ is a unit vector in the r-direction. Substituting for B_r in terms of eqn. (2) gives

$$\ddot{F}_1F_2 + \frac{1}{r}\dot{F}_1F_2 + F_2\ddot{F}_2 = jk^2F_1F_2$$

or $$\frac{1}{r}\frac{\dot{F}_1}{F_1} + \frac{\ddot{F}_1}{F_1} = jk^2 - \frac{\ddot{F}_2}{F_2} \quad . \quad . \quad . \quad . \quad . \quad . \quad (4)$$

The left-hand side of this equation is a function of r only, and the right-hand side is a function of z only; for this equality to hold for all values of r and z both sides must equal a constant, m^2.

Thus, $$\ddot{F}_1 + \frac{1}{r}\dot{F}_1 - m^2F_1 = 0 \quad . \quad . \quad . \quad . \quad (5)$$

and $$\ddot{F}_2 + (m^2 - jk^2)F_2 = 0 \quad . \quad . \quad . \quad . \quad (6)$$

The solutions to eqns. (5) and (6) are

$$F_1 = A'\mathrm{I}_0(mr) + C'\mathrm{K}_0(mr). \quad . \quad . \quad . \quad . \quad (7)$$

and

$$F_2 = A''\exp\left[-\sqrt{(jk^2 - m^2)}z\right] + C''\exp\left[\sqrt{(jk^2 - m^2)}z\right] \quad (8)$$

Since B_r decreases with an increase in either z or r, $A' = C'' = 0$. For a given value of z, it is evident from the idealized flux distribution assumed that B_r must vary inversely with r; further, if m is then unity, $m^2 \ll k^2$ for the frequencies used in this work.

The approximate forms of eqns. (7) and (8) to be used are therefore

$$F_1 = \frac{1}{r_1},\ F_2 = A'' \exp(-\sqrt{jkz})$$

The expression for B_r is finally

$$B_r = \frac{A''}{r} \exp(-\sqrt{jkz}) \quad . \quad . \quad . \quad . \quad (9)$$

The flux, $\delta\phi'$, passing through an elemental cylindrical surface of radius r', width $\delta z'$ at a depth z' below the test steel surface is

$$\delta\phi' = 2\pi r'\delta z' \frac{A''}{r'} \exp(-\sqrt{jkz}) = 2\pi A'' \exp(-\sqrt{jkz'})\delta z'$$

The total flux is then given by

$$\Phi = 2\pi A'' \int_0^\infty \exp(-\sqrt{jkz'})dz' = \frac{2\pi A''}{\sqrt{jk}}$$

Substituting for A'' in terms of Φ, eqn. (9) becomes

$$B_r = \frac{\Phi\sqrt{jk} \exp(-\sqrt{jkz})}{2\pi r} \quad . \quad . \quad . \quad . \quad (10)$$

(7.2) Derivation of Expression for Eddy Current Loss in Test Material

Reintroducing the time variable into eqn. (10),

$$B_r = \frac{\hat{\Phi}}{2\pi r}\sqrt{jk} \exp(j\omega t - \sqrt{jkz}) \quad . \quad . \quad . \quad (11)$$

Now $J = \frac{1}{\mu}$ curl B, where curl $B = \begin{vmatrix} \frac{l_r}{r} & l_\theta & \frac{k}{r} \\ \frac{\partial}{\partial r} & \frac{\partial}{\partial\theta} & \frac{\partial}{\partial z} \\ B_r & rB_\theta & B_z \end{vmatrix}$

Since it is considered that $B_\theta = B_z = 0$, the expression for curl B reduces to curl $B = l_\theta \partial B_r/\partial z$, whence the induced eddy currents, which are in the θ-direction, are given by

$$J_\theta = \frac{\hat{\Phi}}{\mu}\frac{(1+j)}{\sqrt{2}}\frac{k}{2\pi r}\exp(j\omega t)\frac{d}{dz}\exp\left[\frac{-(1+j)kz}{\sqrt{2}}\right]$$

$$= -\frac{1}{\mu}\frac{\hat{\Phi}jk^2}{2\pi r}\exp(-kz/\sqrt{2})\left[\cos\left(\omega t - \frac{kz}{\sqrt{2}}\right) + j\sin\left(\omega t - \frac{kz}{\sqrt{2}}\right)\right]$$

The magnitude of J_θ is the maximum value of the real part of this expression:

$$\hat{J}_\theta = \frac{\hat{\Phi}k^2}{\mu}\frac{\exp(-kz/\sqrt{2})}{2\pi r} \quad . \quad . \quad . \quad . \quad (12)$$

Consider now an elemental disc of width δr at a radius r and thickness δz at a depth z:

Resistance of elemental disc $= \dfrac{\rho 2\pi r}{\delta r\delta z}$

R.M.S. current in elemental disc $= \dfrac{\hat{J}_\theta}{\sqrt{2}}\delta r\delta z$

The average power loss in the elemental disc due to eddy currents is

$$\delta P_e = \left(\frac{\hat{J}_\theta}{\sqrt{2}}\delta r\delta z\right)^2 \frac{\rho 2\pi r}{\delta r\delta z} = \pi r\rho\hat{J}_\theta^2\delta r\delta z$$

$$= \frac{\hat{\Phi}^2}{\mu^2}\frac{k^4}{4\pi r}\frac{\exp(-\sqrt{2}kz)}{\rho\delta r\delta z}$$

The total power loss due to eddy currents is

$$P_e = \int_{r_1}^{r_2}\int_0^\infty \frac{\hat{\Phi}^2}{\mu^2}\frac{k^4\rho\exp(-\sqrt{2}kz)}{4\pi r}drdz$$

$$= \hat{\Phi}^2\frac{\sqrt{\pi}}{2}\log_e\left(\frac{r_2}{r_1}\right)f^{3/2}\frac{1}{(\sqrt{\mu\rho})} \quad . \quad . \quad . \quad (13)$$

(7.3) Derivation of Expression for Hysteresis Loss in Test Material

Rayleigh's relation[7, 8] for the hysteresis loop at low flux levels is

$$B = (\mu + \alpha\hat{H})H \pm \alpha/2(\hat{H}^2 - H^2) \quad . \quad . \quad (14)$$

and the area of the loop is given by

$$\oint HdB = \frac{4\alpha\hat{H}^3}{3} = \frac{4\alpha\hat{B}^3}{3\hat{\mu}^3} \quad . \quad . \quad . \quad . \quad (15)$$

Eqn. (11) may be written in the form

$$B_r = \frac{\hat{\Phi}(1+j)k}{2\sqrt{(2)}\pi r}\exp\left(\frac{-kz}{\sqrt{2}}\right)\left[\cos\left(\omega t - \frac{kz}{\sqrt{2}}\right) + j\sin\left(\omega t - \frac{kz}{\sqrt{2}}\right)\right]$$

The flux density at any time t is given by the real part of the expression

$$B_{r(t)} = \frac{\hat{\Phi}k\exp\left(\frac{-kz}{\sqrt{2}}\right)}{2\pi r}\cos\left(\omega t - \frac{kz}{\sqrt{2}} + \pi/4\right)$$

The amplitude of B_r is then

$$\hat{B}_r = \frac{\hat{\Phi}k\exp\left(\frac{-kz}{\sqrt{2}}\right)}{2\pi r} \quad . \quad . \quad . \quad . \quad (16)$$

The hysteresis loss in an elemental disc of width δr at a radius r and thickness δz at a depth z is

$$\delta P_h = 2\pi r\delta r\delta z f\oint HdB$$

$$= \frac{\hat{\Phi}^3\alpha k^3\exp\left(\frac{-3kz}{\sqrt{2}}\right)f}{3\hat{\mu}^3\pi^2r^2}\delta r\delta z$$

The total power loss due to hysteresis is then

$$P_h = \int_{r_1}^{r_2}\int_0^\infty \frac{\hat{\Phi}^3\alpha k^3\exp\left(\frac{-3kz}{\sqrt{2}}\right)f}{3\hat{\mu}^3\pi^2r^2}drdz$$

$$= \hat{\Phi}^3\frac{2\sqrt{2}}{9\pi}\frac{\alpha\mu\sigma}{\hat{\mu}^3}\left(\frac{1}{r_1} - \frac{1}{r_2}\right)f^2 \quad . \quad . \quad . \quad . \quad (17)$$

.4) Relation between Probe-Coil Parameters and the Electrical and Magnetic Properties of the Steel Test Piece

The equivalent circuit of the probe coil shown in Fig. 6(*a*) is ade up of a series resistance R and inductance L. Assuming e power loss in the ferrite to be negligible, R may be split to R_m, a resistance representing the loss in the steel test aterial, and R_c the a.c. resistance of the coil winding. R_m and may be converted to an equivalent shunt form, shown in ig. 6(*b*), the loss resistance being split into R_e and R_h repre-nting the eddy-current and hysteresis loss respectively. If the oltage across this circuit is V,

$$V = 4{\cdot}44fN\hat{\Phi} \quad . \quad . \quad . \quad . \quad . \quad (18)$$

nd
$$P_e + P_h = V^2 G_m \quad . \quad . \quad . \quad . \quad (19)$$

here
$$G_m = 1/R_e + 1/R_h$$

ubstitution for P_e, P_h and V in eqn. (19), using eqns. (13), 17) and (18), yields

$$\hat{\Phi}^2 \frac{\sqrt{\pi}}{2} \log_e \left(\frac{r_2}{r_1}\right) f^{3/2} \frac{1}{\sqrt{(\mu\rho)}} + \hat{\Phi}^3 \frac{2\sqrt{2}}{9\pi} \frac{\alpha\sigma\mu}{\hat{\mu}^3} \left(\frac{1}{r_1} - \frac{1}{r_2}\right) f^2 = (4{\cdot}44fN\hat{\Phi})^2 G_m$$

or
$$G_m = \frac{b}{\sqrt{(\mu\rho)}} \frac{1}{\sqrt{f}} + h \quad . \quad . \quad . \quad . \quad (20)$$

The probe factor is

$$b = \frac{\sqrt{\pi}}{2 \times 4{\cdot}44^2 N^2} \log_e (r_2/r_1) \quad . \quad . \quad . \quad (21)$$

and
$$h = \frac{\hat{\Phi}}{4{\cdot}44^2 N^2} \frac{2\sqrt{2}}{9\pi} \frac{\alpha\sigma\mu}{\hat{\mu}^3} \left(\frac{1}{r_1} - \frac{1}{r_2}\right) \quad . \quad . \quad (22)$$

Thus, an experimental determination of G_m over a range of frequencies at constant value of $\hat{\Phi}$ leads to a knowledge of the quantity $\mu\rho$ if b is known.

621.372.413:621.317.41

The Institution of Electrical Engineers
Monograph No. 373 E
Apr. 1960
©

PERTURBATION THEORY OF RESONANT CAVITIES

By R. A. WALDRON, M.A., A.Inst.P.

(*The paper was first received* 22*nd July, and in revised form* 11*th December*, 1959. *It was published as an* INSTITUTION MONOGRAPH *in April*, 1960.)

SUMMARY

A detailed derivation is given of the perturbation formula for the frequency shift on introducing a sample of ferrite or dielectric material into a resonant cavity. The purpose of this is to make clear what assumptions are involved in the derivation; it is necessary to appreciate what these assumptions are in order to design accurate experiments.

(1) INTRODUCTION

When a small piece of ferrite or dielectric material is introduced into a resonant cavity the frequency of resonance is changed by a small amount and the selectivity of the cavity is lowered. These effects are commonly used in the measurement of the properties of the sample; the relation between the changes in frequency and selectivity and the properties can be derived by perturbation theory and the derivation has been given by several authors. The earliest treatments were given by Bethe and Schwinger,[1] Kahan[2] and Slater,[3] the perturbation considered being a small deformation of the boundary surface of the cavity. Casimir[4] has applied the theory to this case and also to the case of a small body introduced into the cavity. The latter case is applicable to the measurement of dielectric constants of small samples of material at microwave frequencies. The present author[5] has modified Casimir's treatment to allow of its application to anisotropic magnetic samples, namely ferrites. In all these treatments the aim has been to obtain a formula relating the frequency shift to the magnitude of the deformation, e.g. to the dielectric constant of a test sample. It is implicit in References 1 to 4 and explicit in Reference 5 that, by taking the frequency shift to be complex, the imaginary part as well as the real part of the property of the sample under test can be measured.

The relation between frequency shift and deformation obtained in the above treatments is now well known, but none of the treatments mentioned above, nor any other known to the author, gives the derivation in great detail, so that the assumptions on which it depends are not so well known. It is, in fact, more accurate than is sometimes thought, but to make full use of this accuracy in measurements on a specimen it is necessary to choose the specimen shape with some care. The purpose of this paper is to give the derivation of the perturbation formula in detail so as to demonstrate the approximations made, and the absence of others that are sometimes thought to have been made. The circumstances under which the formula may be applied will then be discussed.

(2) DERIVATION OF THE PERTURBATION FORMULA

In the unperturbed state, i.e. in the empty cavity, oscillating in one only of its normal modes, let the electric and magnetic fields in the cavity be

$$\left.\begin{aligned} E &= E_0\varepsilon^{j\omega t} \\ H &= H_0\varepsilon^{j\omega t} \end{aligned}\right\} \quad . \quad . \quad . \quad . \quad . \quad . \quad . \quad (1)$$

where E_0 and H_0 are functions of position. The field configurations are independent of the field magnitudes, always supposing that in normal working these will not be so large as to cause dielectric breakdown in the cavity or appreciable heating of the walls by induced currents. On introducing a small ferrite or dielectric sample into the cavity, the fields and resonance frequency are modified so that we now have

$$\left.\begin{aligned} E' &= (E_0 + E_1)\varepsilon^{j(\omega+\delta\omega)t} \\ H' &= (H_0 + H_1)\varepsilon^{j(\omega+\delta\omega)t} \end{aligned}\right\} \quad . \quad . \quad . \quad . \quad (2)$$

where it is supposed that the fields in the perturbed case can be represented as the sums of the unperturbed fields, E_0, H_0, and additional fields, E_1, H_1, with a frequency change $\delta\omega$. It will later be necessary to stipulate that $\delta\omega \ll \omega$ and that over most of the cavity volume E_1 and H_1 are small compared with E_0 and H_0. It is convenient to make these assumptions at the present stage. It should be noted that it is not required that E_1 and H_1 should be small compared with E_0 and H_0 in the neighbourhood of the sample. (In this paper, the neighbourhood of the sample will be taken to include the region occupied by the sample itself.)

E_0 and H_0 in eqn. (2) will, in practice, not necessarily be identical with E_0 and H_0 in eqn. (1). The significance of E_0 and H_0 in eqn. (2) is that they have the same configuration as in eqn. (1) and that they comprise all fields that are expressible as the empty-cavity mode in question. E_1 and H_1 may be regarded as a Fourier sum over all modes except this one, to give the actual field in the cavity. The quantity that is to be measured is the complex frequency shift; this is independent of the amplitudes of oscillation in the perturbed and unperturbed cases, so that, for theoretical purposes, E_0 and H_0 of eqn. (1) may be regarded as multiplied by some scale factor to make them equal to E_0 and H_0 of eqn. (2). The requirement that E_1 and H_1 are small compared with E_0 and H_0 may then be expressed as the requirement that the field configurations are only slightly distorted, except in the neighbourhood of the sample. This is equivalent to requiring $\delta\omega$ to be small compared with ω. It is not necessary to stipulate that the energy stored in the sample is small compared with that in the empty cavity, as is sometimes thought. It is sufficient to stipulate that it is a small fraction of the total energy in the cavity in the perturbed condition. This point was first made by Spencer, LeCraw, and Ault.[6]

Substituting from eqns. (1) and (2), in turn, into the Maxwell equation

$$\operatorname{curl} E = -\frac{\partial B}{\partial t} \quad . \quad . \quad . \quad . \quad . \quad . \quad (3)$$

we obtain $$\operatorname{curl} E_0 = -\frac{\partial B_0}{\partial t} = -j\omega B_0$$

and $$\operatorname{curl}(E_0 + E_1) = -j(\omega + \delta\omega)(B_0 + B_1)$$

Subtracting,

$$\operatorname{curl} E_1 = -j[\omega B_1 + \delta\omega(B_0 + B_1)] \quad . \quad . \quad . \quad (4)$$

Correspondence on Monographs is invited for consideration with a view to publication.

Mr. Waldron is with Marconi's Wireless Telegraph Co., Ltd.

imilarly, using the Maxwell equation

$$\text{curl } H = \frac{\partial D}{\partial t} \quad . \quad . \quad . \quad . \quad . \quad . \quad . \quad (5)$$

ve find that $\text{curl } H_1 = j[\omega D_1 + \delta\omega(D_0 + D_1)]$ . . . (6)

orming the scalar product of H_0 with eqn. (4) and of E_0 with qn. (6) and adding, we obtain

$$E_0 \cdot \text{curl } H_1 + H_0 \cdot \text{curl } E_1 = j\omega[E_0 \cdot D_1 - H_0 \cdot B_1] + j\delta\omega[(E_0 \cdot D_0 - H_0 \cdot B_0) + (E_0 \cdot D_1 - H_0 \cdot B_1)] \quad . \quad (7)$$

Here,

$$\left.\begin{aligned} B_0 &= \mu_0 H_0 \qquad D_0 = \epsilon_0 E_0 \\ B_1 &= \mu_0 H_1 \qquad D_1 = \epsilon_0 E_1 \end{aligned}\right\} \quad . \quad . \quad . \quad . \quad (8)$$

outside the sample and

$$D_1 = \epsilon_0[\epsilon_r(E_0 + E_1) - E_0] \quad . \quad . \quad . \quad . \quad (9)$$

nside the sample. If the sample is of a magnetically isotropic material,

$$B_1 = \mu_0[\mu_r(H_0 + H_1) - H_0] \quad . \quad . \quad . \quad (10)$$

while if it is a gyromagnetic material,

$$B_1 = \mu_0\{[\mu_r](H_0 + H_1) - H_0\} \quad . \quad . \quad . \quad (11)$$

nside the sample. ϵ_r is the relative permittivity or dielectric constant of the sample; μ_r is the relative permeability of an sotropic magnetic sample, while $[\mu_r]$ is the well-known tensor elative permeability of a ferrite. ϵ_0 and μ_0 are the permittivity nd permeability of free space.

We now use the vector identity

$$\text{div}\,[(H_0 \times E_1) + (E_0 \times H_1)] \equiv E_1 \cdot \text{curl } H_0 - H_0 \cdot \text{curl } E_1 + H_1 \cdot \text{curl } E_0 - E_0 \cdot \text{curl } H_1$$

which, by virtue of eqns. (3) and (5), may be written

$$H_0 \cdot \text{curl } E_1 + E_0 \cdot \text{curl } H_1 = j\omega(E_1 \cdot D_0 - H_1 \cdot B_0) - \text{div}\,[(H_0 \times E_1) + (E_0 \times H_1)]$$

Substituting this into the left-hand side of eqn. (7), we obtain

$$\omega(E_1 \cdot D_0 - H_1 \cdot B_0) - \text{div}\,[(H_0 \times E_1) + (E_0 \times H_1)] = j\omega(E_0 \cdot D_1 - H_0 \cdot B_1) + j\delta\omega[(E_0 \cdot D_0 - H_0 \cdot B_0) + (E_0 \cdot D_1 - H_0 \cdot B_1)] \quad . \quad . \quad . \quad . \quad . \quad . \quad . \quad (12)$$

Let V_0 be the volume of the cavity and V_1 the volume of the ample. Thus $V_0 - V_1$ is the part of the cavity not occupied by the sample. Integrate eqn. (12) over the volume V_0:

$$j\omega \iiint_{V_0} (E_1 \cdot D_0 - H_1 \cdot B_0)dV - \iiint_{V_0} \text{div}\,[(H_0 \times E_1) + (E_0 \times H_1)]dV = j\omega \iiint_{V_0} (E_0 \cdot D_1 - H_0 \cdot B_1)dV + j\delta\omega \iiint_{V_0} [(E_0 \cdot D_0 - H_0 \cdot B_0) + (E_0 \cdot D_1 - H_0 \cdot B_1)]dV \quad . \quad . \quad . \quad . \quad . \quad (13)$$

In the region $V_0 - V_1$, eqns. (8) apply, and the contribution rom this region to the first integral on the left-hand side of qn. (13) is identical with that to the first integral on the right-and side. Thus we only require the contributions to these integrals from the region V_1. For the divergence integral we have, by Green's theorem,

$$\iiint_{V_0} \text{div}\,(H_0 \times E_1 + E_0 \times H_1)dV = \iint_{S_0} (H_0 \times E_1 + E_0 \times H_1) \cdot n\,dS$$

where S_0 is the surface of the cavity and n is a unit vector normal to the element dS of S_0. To the extent to which the cavity walls may be regarded as perfectly conducting, $H_0 \times E_1$ and $E_0 \times H_1$ are tangential to the walls, and their scalar product with n is zero. Thus the divergence integral vanishes.

So far, to the extent to which the cavity may be regarded as having perfectly conducting walls (infinite selectivity), the treatment is exact. The assumption that $\delta\omega$ is much smaller than ω has been pointed out, but no step has been taken which depends on this assumption. We now make our first approximation, which depends on the smallness of $\delta\omega$, namely to neglect D_1 and B_1 in comparison with D_0 and B_0 in the second integral on the right-hand side of eqn. (13). This is justified, except in the neighbourhood of the sample, by the fact that, when $\delta\omega \ll \omega$, E_1 and H_1 are small compared with E_0 and D_0, bearing in mind also eqn. (8). In the neighbourhood of the sample, the contribution to the integral will be small, provided that the perturbed fields do not depart by more than, say, an order of magnitude from their unperturbed values. This approximation becomes the more accurate the smaller V_1, and as V_1 is made smaller the amount by which the perturbed fields may depart from their unperturbed values, without reducing accuracy, increases. Eqn. (13) now becomes

$$j\omega \iiint_{V_1} (E_1 \cdot D_0 - H_1 \cdot B_0)dV = j\omega \iiint_{V_1} (E_0 \cdot D_1 - H_0 \cdot B_1)dV + j\delta\omega \iiint_{V_0} (E_0 \cdot D_0 - H_0 \cdot B_0)dV$$

$$\text{i.e. } \frac{\delta\omega}{\omega} = \frac{\iiint_{V_1} [(E_1 \cdot D_0 - E_0 \cdot D_1) - (H_1 \cdot B_0 - H_0 \cdot B_1)]dV}{\iiint_{V_0} (E_0 \cdot D_0 - H_0 \cdot B_0)dV} \quad . \quad . \quad . \quad . \quad (14)$$

which is the required formula for the frequency shift. An analogous formula is frequently quoted with a plus sign in the denominator. This is because, with the definitions of E_0 and H_0 given by eqn. (1), E_0 and D_0 both contain a phase factor j if the cavity is oscillating in an H mode, or H_0 and B_0 both contain a factor j in the case of an E mode. Thus $E_0 \cdot D_0$ and $-H_0 \cdot B_0$ both have the same sign. Where a plus sign appears in the denominator, the factors j have been rendered explicitly.

(3) DISCUSSION

It is clear from the derivation given in Section 2 that the only condition necessary for eqn. (14) to hold is that $\delta\omega/\omega$ be small. If the equation is to be of any value, however, it must be possible to evaluate the right-hand side. By virtue of eqns. (8), (9), (10) and (11), only the fields need be considered; the inductions are readily obtained from the fields if these are known. E_0 and H_0 present no difficulty, since they are well known for cavities of simple shape.

E_1 and H_1 can be calculated under certain circumstances. If the sample is in the form of a special case of the general triaxial ellipsoid and if the microwave field in the cavity at the position

of the sample is, in the absence of the sample, sensibly uniform over a volume large compared with that of the sample, the calculation can be made with an accuracy approaching exactness as the volume of the sample approaches zero. This situation usually obtains in practice; sample shapes commonly used are the sphere and the rod of circular section. The former is an ellipsoid with all three axes equal; the latter appears as an ellipsoid with two equal finite axes and one infinite axis, if the ends of the rod fit flush with the cavity, by virtue of the reflections in the end-faces. The sample is placed at a position of zero electric field for a measurement of permeability, or of zero magnetic field for a measurement of permittivity. When one field is zero, the other is a maximum and so may be taken as uniform over a limited range.

The calculation of E_1 and H_1 requires that the sample be placed in such a position in the cavity that the modifications it produces in the fields are not influenced by reflection effects in the cavity walls. Attention has been drawn to this point by Spencer, LeCraw, and Reggia.[7] This source of error is avoided if the specimen is kept well away from curved walls, or if curved specimen surfaces are only allowed to come near a plane cavity wall if they intersect orthogonally. Thus a spherical specimen must always be placed well away from cavity walls, while a rod-shaped specimen may be placed with its axis normal to plane walls, the ends fitting flush against the walls. If the rod is shorter than the cavity, it must be much shorter, so that the ends of the rod are not near the walls. A hemispherical specimen could be placed with its plane surface in contact with a plane wall, although this case is not likely to be of practical interest.

Sometimes a specimen is used in the form of a disc,[8] but in this case it is not possible to evaluate E_1 and H_1 accurately. The approximation is made that the internal field in the disc is the same as the field, parallel to the plane surfaces of the disc, which exists in the cavity in the absence of the disc. This is true if the disc is a special case of an ellipsoid, i.e. if the ratio of thickness to diameter is zero, but this case is of no practical interest. Discs used in practice have values of this ratio of the order of 0·2 or more, and the approximation under these conditions is not very close.

It is not possible to discuss errors quantitatively in a general treatment, although, if necessary, they could be assessed in a particular case. However, provided that the precautions are taken that are described in the paper, eqn. (14) will hold to a greater degree of accuracy than is likely to be attainable practically. In this respect it should be noted that the fact that the field in the neighbourhood of the specimen is considerably different from the unperturbed field does not detract from the accuracy of eqn. (14), provided that the sample shape is suitably chosen and that the sample is suitably positioned in the cavity. Seidel and Boyet[9] have stated:

> In any particular geometrical and modal situation . . . the assumption in the perturbation theory is that electric and magnetic fields just outside the sample are their (known) empty cavity values.

If this were true, the accuracy of the perturbation formula would not be high, and it would be justifiable to work to a low standard of accuracy. The assumption has not been made, however, in deriving eqn. (14), and if ellipsoidal samples are used, it need not be made. The assumption *is* made for disc samples, and renders results of measurements on such samples of doubtful accuracy.

A final point bearing on accuracy is the value of the quantity being measured. Usually this will not depart greatly from the value of that property for free space. This may not be the case for a ferrite at ferromagnetic resonance, when the fraction of the cavity energy stored in the specimen may become quite large.[10] Care is needed, therefore, in dealing with this case; however, as long as the sample is sufficiently small, so that $\delta\omega/\omega$ remains small, eqn. (14) is still applicable.

(4) CONCLUSION

The frequency-shift formula, eqn. (14), is valid to a high degree of accuracy and the limitations on accuracy obtained in an experiment will be imposed by the apparatus used. Thus, an improvement in technique can be expected to give an improvement in the accuracy of results. The high accuracy of the perturbation formula will only be realized if the specimen shape is suitably chosen and if the specimen is suitably placed in this cavity.

(5) ACKNOWLEDGMENT

The author wishes to thank the Engineer-in-Chief of Marconi's Wireless Telegraph Co., Ltd., for permission to publish the paper.

(6) REFERENCES

(1) Bethe, H. A., and Schwinger, J.: 'Perturbation Theory for Cavities', N.R.D.C. Report D1—117, Cornell University, March, 1943.

(2) Kahan, T.: 'Méthode de perturbation appliquée a l'étude des cavités électromagnétiques', *Comptes Rendus*, 1945, **221**, p. 536.

(3) Slater, J. C.: 'Microwave Electronics' (Van Nostrand, 1950), p. 80.

(4) Casimir, H. B. G.: 'On the Theory of Electromagnetic Waves in Resonant Cavities', *Philips Research Reports*, 1951, **6**, p. 162.

(5) Waldron, R. A.: 'Theory of the Measurement of the Elements of the Permeability Tensor of a Ferrite by Means of a Resonant Cavity', *Proceedings I.E.E.*, Paper No. 2225 R, October, 1956 (**104** B, Suppl. 6, p. 307).

(6) Spencer, E. G., LeCraw, R. C., and Ault, L. A.: 'Note on Cavity Perturbation Theory', *Journal of Applied Physics*, 1957, **28**, p. 130.

(7) Spencer, E. G., LeCraw, R. C., and Reggia, F.: 'Measurement of Microwave Dielectric Constants and Tensor Permeabilities of Ferrite Spheres', *Proceedings of the Institute of Radio Engineers*, 1956, **44**, p. 790.

(8) Von Aulock, W., and Rowen, J. H.: 'Measurement of Dielectric and Magnetic Properties of Ferromagnetic Materials at Microwave Frequencies,' *Bell System Technical Journal*, 1957, **36**, p. 427.

(9) Seidel, H., and Boyet, H.: 'Frequency Shifts in Cavities with Longitudinally Magnetized Small Ferrite Discs', *ibid.*, 1958, **37**, p. 637.

(10) Waldron, R. A.: 'What is Ferromagnetic Resonance?', *British Journal of Applied Physics*, 1960, **11**, p. 69.

21.372.45

The Institution of Electrical Engineers
Monograph No. 374 M
Apr. 1960
©

TWO-TERMINAL *RC* NETWORKS AND THEORETICALLY RELATED TOPICS

By O. P. D. CUTTERIDGE, M.Sc.(Eng.), Ph.D., Associate Member.

(*The paper was first received 28th May, and in revised form 14th December*, 1959. *It was published as an* INSTITUTION MONOGRAPH *in April*, 1960.)

SUMMARY

A derivation is given of the properties of the principal minors of successive orders of the nodal determinant of a lumped linear *RC* network, with particular reference to the question of multiple zeros of the various minors. The remainder of the paper is devoted to the study of a certain continued-fraction expansion which is shown to be of particular use in connection with 2-terminal *RC* networks, stability and related problems; new canonical forms for a Hurwitz polynomial are derived with its aid. Determinantal expressions for the continued-fraction coefficients are used to obtain some new forms of the stability criteria.

(1) INTRODUCTION

The basic properties of a 2-terminal *RC* network were first demonstrated by Cauer[1] in 1926 by means of an analysis based on the energy functions of the network. Cauer showed, by investigating certain continued-fraction expansions, that two ladder realizations with the minimum number of elements were always possible, and further showed how these results for 2-terminal *RC* networks could be applied to 2-terminal *LC* and *RL* networks. Earlier, in 1924, Foster[2] had given two realizations for 2-terminal reactance networks using partial-fraction methods, which were applied by Cauer for the realization of the corresponding *RC* and *RL* cases.

Foster did not give a proof from first principles but based his argument on the solution of the analogous dynamical problem of small oscillations given by Routh.[4] (Routh had earlier included these results in his Adams Prize Essay[5] of 1877.) It is interesting to note that a basic method, somewhat different from Routh's, by which the properties of 2-element-kind 2-terminal networks can be obtained, was given by Sylvester[6] in 1853. In the language of *RC* networks and nodal determinants Sylvester showed that the zeros of Δ_{11} were real and interlaced the real zeros of Δ provided that a series of determinants of the network capacitances were all positive. It requires to be shown that if, in addition, a series of determinants of the network conductances are all positive, and both series of determinants are positive for positive network elements, then the zeros of Δ_{11} are real and negative and interlace the real and negative zeros of Δ. This is shown in Section 2 of the present paper.

The remainder of the paper is concerned with the theory of a certain continued fraction which is shown always to provide a realization of a 2-terminal *RC* network with the minimum number of elements. Some of the numerical examples given by Vowels[3] can be thought of as examples of the continued-fraction expansion considered here and the present paper as providing the relevant theory. A number of other applications of this continued-fraction expansion are also given in Sections 3 and 4.

Correspondence on Monographs is invited for consideration with a view to publication.

Dr. Cutteridge is in the Electrical Engineering Department, Manchester College of Science and Technology (Faculty of Technology, University of Manchester).

(2) NODAL DETERMINANTS OF *RC* NETWORKS

(2.1) Preliminary Discussion

The usual method of deriving the basic properties of *RC* networks falls into two sections. First, a consideration of the energy functions associated with the network leads to the conclusion that two quadratic forms must be positive definite and thence, the relevant algebra of quadratic forms being assumed known, to the conclusion that certain sequences of determinants of the network capacitances and conductances must be positive. Secondly, use is made of this to derive the basic properties of *RC* networks by analogy with the corresponding case in dynamics given by Routh.[4, 5]

The purpose of this Section is to provide an alternative and, it is thought, simpler derivation of these results, which again falls into two parts. First, the positiveness of the above-mentioned determinants is shown to be obtained easily by considering driving-point admittances of two networks, in one of which all the original network capacitances have been removed and in the other all the network conductances; the argument is also extended to the case corresponding to the above-mentioned quadratic forms being positive semidefinite rather than positive definite. Secondly, the properties of the zeros of the nodal determinant and of its minors are obtained by making use of a mathematical method given by Sylvester[6] in 1853. With this method the properties of a third-order nodal determinant are obtained from evident properties of second- and first-order nodal determinants, then the properties of a fourth-order nodal determinant are obtained from those of third and second orders and so on. This method differs somewhat from Routh's,[4, 5] which was based on a consideration of sign changes along the set of determinants considered as a whole, as in the argument used in the proof of Sturm's theorem.[7] It is interesting to note that the converse form of Sylvester's argument was used by Cauer[1] in 1926 in connection with the theory of the continued-fraction expansion of the driving-point impedance functions of *RC* networks.

(2.2) Derivation of Properties of Nodal Determinants of *RC* Networks

The general expression for the nodal determinant, Δ, of an *RC* network is

$$\Delta = \begin{vmatrix} G_{11}+pC_{11} & -G_{12}-pC_{12} & \cdots & -G_{1n}-pC_{1n} \\ -G_{12}-pC_{12} & G_{22}+pC_{22} & \cdots & -G_{2n}-pC_{2n} \\ \cdots & \cdots & \cdots & \cdots \\ -G_{1n}-pC_{1n} & -G_{2n}-pC_{2n} & \cdots & G_{nn}+pC_{nn} \end{vmatrix} \quad (1)$$

where p $(=j\omega)$ is the complex frequency; only real values of p will be involved in the arguments to follow. All the network elements are either positive or zero.

Now write

$$\Delta' = \begin{vmatrix} G_{11}-G_{12}-G_{13} & \cdots & -G_{1n} \\ -G_{12} & G_{22}-G_{23} & \cdots & -G_{2n} \\ \cdots & \cdots & \cdots & \cdots \\ -G_{1n} & -G_{2n} & -G_{3n} & \cdots & G_{nn} \end{vmatrix} \quad \ldots (2)$$

and

$$\Delta'' = \begin{vmatrix} pC_{11} & -pC_{12} & -pC_{13} & \cdots & -pC_{1n} \\ -pC_{12} & pC_{22} & -pC_{23} & \cdots & -pC_{2n} \\ \cdots & \cdots & \cdots & \cdots & \cdots \\ -pC_{1n} & -pC_{2n} & -pC_{3n} & \cdots & pC_{nn} \end{vmatrix} \quad \ldots (3)$$

Δ' would be the network nodal determinant if all the capacitances were removed, and Δ'' would be the network nodal determinant if all the conductances were removed. Further, let Δ_i be written for the determinant of order i obtained from Δ by striking out the $(i+1)$th to nth rows and columns, and let Δ_n equal Δ. Let Δ_i' and Δ_i'' be defined similarly.

Consider the possible range of values for Δ_i'. The ratio Δ_i'/Δ_{i-1}' is the conductance seen looking into the network, with all the capacitances removed, between the ith node and earth when nodes $i+1$, $i+2$, . . . n are short-circuited to earth.* It is evident physically, since the network contains only non-negative resistances, that Δ_i'/Δ_{i-1}' must be non-negative for all i. Thus, if Δ_i'/Δ_{i-1}' is positive for all i, Δ_n', Δ_{n-1}', . . . Δ_2', Δ_1' must all have the same sign. But as Δ_1' $(=G_{11})$ cannot be negative, Δ_1', Δ_2', . . . Δ_{n-1}', Δ_n' must all be positive. Suppose now that a certain ratio Δ_i'/Δ_{i-1}' is zero. Then Δ_i' must be zero since Δ_{i-1}' cannot be infinite. But as none of the ratios Δ_{i+1}'/Δ_i', $\Delta_{i+2}'/\Delta_{i+1}'$, . . . Δ_n'/Δ_{n-1}' can be infinite Δ_{i+1}', Δ_{i+2}', . . . Δ_{n-1}', Δ_n' must all be zero. Thus the determinants

$$\Delta_1', \Delta_2', \ldots \Delta_{i-1}' \quad \ldots (4)$$

must all be positive and the determinants

$$\Delta_i', \Delta_{i+1}', \ldots \Delta_n' \quad \ldots (5)$$

must all be zero, where i can here have any value from 1 to $n+1$. [Of course, if $i=1$ there are no terms in sequence (4) and if $i=n+1$ there are no terms in sequence (5).]

Corresponding results are obtained in the same way for the sign of Δ_i'' for positive p. Thus† Δ_i, a polynomial in p of degree i, having the values Δ_i' at $p=0$ and Δ_i'' at $p=+\infty$, is positive at the origin, positive at $p=+\infty$ and either positive or negative at $p=-\infty$ according as i is even or odd, respectively. In particular, Δ_1, Δ_2, Δ_3, . . . are linear, quadratic, cubic, . . . polynomials that are all positive at the origin and having signs $-$, $+$, $-$, . . . at $p=-\infty$, respectively.

Since Δ is symmetrical, we can write[8]

$$\Delta\Delta_{1122} = \Delta_{11}\Delta_{22} - \Delta_{12}^2 \quad \ldots (6)$$

and, therefore, at a zero of Δ_{11} the product $\Delta\Delta_{1122}$ will be negative, unless the zero of Δ_{11} is also a zero of Δ_{12}, in which case the product $\Delta\Delta_{1122}$ will vanish. Assuming that Δ_{11} and Δ_{12} have no common zeros, Δ and Δ_{1122} have opposite signs at zeros of Δ_{11}. Similarly, and subject to corresponding assumptions regarding common zeros, Δ_n and Δ_{n-2} have opposite signs at zeros of Δ_{n-1}, and Δ_{i+1} and Δ_{i-1} have opposite signs at zeros of Δ_i for $i=2, 3, \ldots n-1$.

* This follows by letting $G_{i+1,i+1}, G_{i+2,i+2}, \ldots G_{nn}$ tend to infinity in the complete expression for the conductance between the ith node and earth.

† It is assumed here that Δ_i' is not zero and that Δ_i'' is zero only when $p=0$.

The general form of the functions Δ_i can now be obtained by the following argument; it will be assumed initially that no Δ_i' is zero, and no Δ_i'' is zero except when $p=0$.

$$\Delta_1 = G_{11} + pC_{11} \quad \ldots (7)$$

and

$$\Delta_2 = \begin{vmatrix} G_{11}+pC_{11} & -G_{12}-pC_{12} \\ -G_{12}-pC_{12} & G_{22}+pC_{22} \end{vmatrix}$$

$$= (G_{11}+pC_{11})(G_{22}+pC_{22}) - (G_{12}+pC_{12})^2 \quad \ldots (8)$$

Therefore Δ_1 has one negative real zero at $p=-G_{11}/C_{11}$, is positive at $p=0$ and negative at $p=-\infty$, and Δ_2 is positive at $p=-\infty$ and $p=0$ but negative at the zero of Δ_1. Hence, the two zeros of Δ_2 are real and negative and lie either side of the zero of Δ_1. Since Δ_3 and Δ_1 have opposite signs at zeros of Δ_2 it follows that Δ_3, which is negative at $p=-\infty$, is positive at the more negative zero of Δ_2, negative at the more positive zero of Δ_2 and positive at $p=0$. Therefore, the three zeros of Δ_3 are real and negative and are interlaced by the zeros of Δ_2.* By continually repeating the argument (or, more formally, by induction) it is evident that the zeros of Δ_i are real and negative and are interlaced by the zeros of Δ_{i-1}, and finally that the zeros of Δ and Δ_{11} are real and negative with the zeros of Δ_{11} interlacing those of Δ.

Suppose now that Δ_{i-1}'' is not zero for $p \neq 0$ but that Δ_i'' vanishes. Then Δ_{i+1} will be a polynomial of order i, not $i+1$. However, the argument that Δ_{i+1} and Δ_{i-1} have opposite signs at zeros of Δ_i may still be invoked, leading again to the conclusion that the zeros of Δ_{i+1} are real and interlace the zeros of Δ_i, but with the proviso that it is a zero of Δ_{i+1} that is the most positive. If Δ_j' vanishes but Δ_{j-1}' does not then again the interlacing property will be maintained with Δ_j (and also Δ_{j+1}, Δ_{j+2}, . . . Δ_n) passing through the origin.

The above argument, based on the fact that the product $\Delta_{i-1}\Delta_{i+1}$ is negative at zeros of Δ_i, inevitably leads to the result that the zeros of Δ (and similarly Δ_{11}, Δ_{1122}, etc.) are all simple, since the number of distinct zeros of each Δ_i was in each case equal to the order of the polynomial, and no common zeros can exist between any two consecutive polynomials Δ_i and Δ_{i+1}. Multiple zeros in the various polynomials Δ_i and common zeros between two consecutive polynomials Δ_i and Δ_{i+1} can occur only if, for some values of i, the product $\Delta_{i-1}\Delta_{i+1}$ vanishes at one or more zeros of Δ_i. From eqn. (6) it is seen that the condition for the product $\Delta\Delta_{1122}$ to vanish at a zero of Δ_{11} is that the zero in question should also be a zero of Δ_{12}. In general, the product $\Delta_{i-1}\Delta_{i+1}$ will be zero at one or more zeros of Δ_i if the principal minor Δ_i and the appropriate non-principal minor have common zeros. Permissible zero patterns for Δ, Δ_{11}, Δ_{1122}, etc., with multiple zeros can be derived by coalescing the appropriate number of adjacent zeros in the allowable patterns for simple zeros obtained above. Thus, for example, at the value of p at which Δ has a third-order zero, Δ_{11} must also have a multiple-order zero. Since three adjacent first-order zeros of Δ must enclose at least two first-order zeros of Δ_{11} it must be at least a zero of the second order; but its order cannot be greater than four, since four adjacent zeros of Δ_{11} must enclose three zeros of Δ. Thus the ratio Δ/Δ_{11} can have only simple poles and zeros even when Δ and/or Δ_{11} have zeros of multiple order. Hence, after dividing out any common factors, the function Δ/Δ_{11} is of exactly the same general type as was the function Δ/Δ_{11} when all the zeros of both Δ and Δ_{11} were simple. With reference to the sequence of polynomials Δ_i, it is interesting to note that it is possible for a multiple-order zero to occur at a certain

* The argument is easier to follow with the aid of rough graphs of possible linear, quadratic and cubic curves for Δ_1, Δ_2 and Δ_3, respectively.

value of i, the order of the zero at first to increase with i and then to decrease and the zero eventually becoming eliminated with increasing i.

Summarizing: the driving-point-impedance function of a 2-terminal *RC* network must be positive at infinity and must have simple real poles and zeros that alternate along the negative real axis of the complex-frequency plane, the most positive critical frequency being a pole. This pole can occur at the origin, as a limiting case, and the number of poles must be equal to or one greater than the number of zeros.

(3) A CONTINUED-FRACTION EXPANSION AND SOME APPLICATIONS

(3.1) Continued-Fraction Expansion

Theorem 1.

If P and Q are polynomials in p of degree $n-1$ and n, respectively, and if the zeros of P and Q are all simple and negative, with the zeros of P interlacing those of Q and the polynomials P and Q have the same sign at either zero or infinity, then, in the continued-fraction expansion

$$\frac{P}{Q} = \cfrac{1}{a_1 p + b_1 + \cfrac{1}{b_2 + \cfrac{a_2}{p} + \cfrac{1}{a_3 p + b_3 + \ddots}}} \qquad (9)$$

$$\left.\begin{aligned} a_i &> 0 \quad i = 1, 2, \ldots n \\ b_i &> 0 \quad i = 1, 2, \ldots n \end{aligned}\right\} \qquad (10)$$

In the continued-fraction expansion of eqn. (9) $a_1 p$ is the quotient of the highest powers in Q and P and b_1 is the quotient of the lowest powers. Similarly for b_2 and a_2/p, etc. For n even the final quotient takes the form $b_n + a_n/p$ and for n odd the form $a_n p + b_n$.

A proof of the theorem follows immediately by considering the process of deriving the continued fraction of eqn. (9) as equivalent to the alternate expansion, to the extent of one term only, by first one and then the other Cauer-type continued fraction.[1]

(3.2) Application to Realization of 2-Terminal *RC* Networks

If the ratio P/Q is regarded as a driving-point impedance, eqn. (9) immediately provides a realization in the form of a ladder structure, as shown in Fig. 1 for the case $n = 4$.

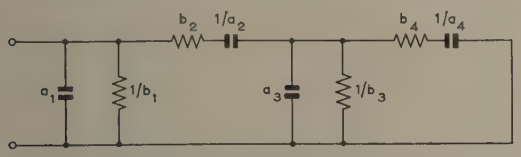

Fig. 1.—Realization of 2-terminal *RC* network by the continued-fraction expansion.
Element values in ohms and farads.

Comparison of the above conditions regarding the continued-fraction expansion with the necessary conditions for the driving-point impedance of an *RC* network derived in Section 2 shows that the normal form of such a driving-point function (i.e. there is no pole at the origin and the number of poles is one greater than the number of zeros) always has the expansion given by eqns. (9) and (10) and therefore always has the realization of the type shown in Fig. 1. If the most positive pole of the impedance is at the origin, the coefficient b_1 in eqn. (9) is zero and the first shunt resistance in Fig. 1 is omitted. If there are equal numbers of poles and zeros, the coefficient a_1 in eqn. (9) is zero and the first shunt capacitance in Fig. 1 is omitted; and if, in addition, the most positive pole of the impedance is at the origin then once again b_1 is zero and the first shunt resistance in Fig. 1 also is omitted.

The process of obtaining the continued-fraction expansion in eqn. (9) eliminates any algebraic factor common to P and Q and results in a realization containing the minimum number of elements.

(3.3) Application as a Criterion for Stability

By virtue of the well-known connection[9] between the criteria for the stability of linear systems and the criteria for the realizability of 2-terminal *RC* networks,* the former follows immediately from the results of Section 3.2.

Writing p^2 for p in eqn. (9),

$$\frac{P(p^2)}{Q(p^2)} = \cfrac{1}{a_1 p^2 + b_1 + \cfrac{1}{b_2 + \cfrac{a_2}{p^2} + \cfrac{1}{a_3 p^2 + b_3 + \ddots}}} \qquad (11)$$

or

$$\frac{Q(p^2)}{pP(p^2)} = a_1 p + \frac{b_1}{p} + \cfrac{1}{b_2 p + \cfrac{a_2}{p} + \cfrac{1}{a_3 p + \cfrac{b_3}{p} + \ddots}} \qquad (12)$$

The condition that $P(p)$ and $Q(p)$ shall have simple zeros interlacing on the negative real p-axis is equivalent to the zeros in p of $P(p^2)$ and $Q(p^2)$ interlacing on the positive imaginary and negative imaginary p-axes† and therefore to $Q(p^2)$ and $pP(p^2)$ being the even and odd parts respectively of a Hurwitz polynomial of degree $2n$, where the final coefficients in the continued fraction are a_n and b_n.

Similarly, the corresponding continued-fraction test for a polynomial of odd degree can be obtained from the result with a_1 in eqn. (9) equal to zero. An alternative form can be obtained in the following manner. If X/Y is a 2-terminal *RC* impedance having equal numbers of poles and zeros, we can write

$$\frac{X}{Y} = b_0 + \cfrac{1}{a_1 p + b_1 + \cfrac{1}{b_2 + \cfrac{a_2}{p} + \cfrac{1}{a_3 p + b_3 + \ddots}}} \qquad (13)$$

with all the coefficients in the continued fraction positive; b_0 is the quotient of the two highest powers in X and Y.

* The basis of this connection is that the poles and zeros of a 2-terminal *RC* network interlace on the negative real axis and the zeros of the odd and even parts of a Hurwitz polynomial interlace on the imaginary axis.

† This is easily seen by noting that a factor $(p + c^2)$ in $P(p)$, for example, becomes $(p^2 + c^2)$, i.e. $(p + jc)(p - jc)$, in $P(p^2)$.

Writing p^2 for p in eqn. (13), we have finally

$$\frac{pX(p^2)}{Y(p^2)} = pb_0 + \cfrac{1}{a_1p + \cfrac{b_1}{p} + \cfrac{1}{b_2p + \cfrac{a_2}{p} + \cfrac{1}{a_3p + \cfrac{b_3}{p} + \ddots}}} \quad (14)$$

and the condition that $X(p)$ and $Y(p)$ shall have simple zeros interlacing on the negative real p-axis, with the most positive zero belonging to $Y(p)$, is equivalent to $pX(p^2)$ and $Y(p^2)$ being the odd and even parts respectively of a Hurwitz polynomial of degree $2n + 1$, where the final coefficients in the continued fraction are a_n and b_n.

The continued-fraction expansions (12) and (14) thus provide tests for the Hurwitz character of polynomials of even and odd degree respectively. In each case all coefficients in the continued fraction must be positive and the continued fraction must not terminate prematurely.

(3.4) Derivation of a Canonical Form for a Hurwitz Polynomial

The continued-fraction tests (12) and (14) for a Hurwitz polynomial can be used to derive a canonical form for a Hurwitz polynomial as a determinant whose order is about half that of Bückner's[10] form.

Consider first a polynomial of even degree. Write the continued fraction (12) as the ratio of two continuants;[11] when multiplied by the appropriate power of p one of these can be considered as the even part and the other as the odd part of a certain polynomial. The new canonical form now follows on writing the sum of these two continuants as a single determinant. Thus, for the sixth-degree case,

$$a_1p + \frac{b_1}{p} + \cfrac{1}{b_2p + \cfrac{a_2}{p} + \cfrac{1}{a_3p + \cfrac{b_3}{p}}} = \frac{p^3\begin{vmatrix} a_1p + \frac{b_1}{p} & -1 & 0 \\ 1 & b_2p + \frac{a_2}{p} & -1 \\ 0 & 1 & a_3p + \frac{b_3}{p} \end{vmatrix}}{p_3\begin{vmatrix} b_2p + \frac{a_2}{p} & -1 \\ 1 & a_3p + \frac{b_3}{p} \end{vmatrix}} \quad . \quad . \quad . \quad . \quad . \quad . \quad (15)$$

and

$$p^3\begin{vmatrix} a_1p + \frac{b_1}{p} & -1 & 0 \\ 1 & b_2p + \frac{a_2}{p} & -1 \\ 0 & 1 & a_3p + \frac{b_3}{p} \end{vmatrix} + p^3\begin{vmatrix} b_2p + \frac{a_2}{p} & -1 \\ 1 & a_3p + \frac{b_3}{p} \end{vmatrix} = p^3\begin{vmatrix} 1 + a_1p + \frac{b_1}{p} & -1 & 0 \\ 1 & b_2p + \frac{a_2}{p} & -1 \\ 0 & 1 & a_3p + \frac{b_3}{p} \end{vmatrix} \quad . \quad . \quad (16)$$

The expression on the right-hand side of eqn. (16) will be a Hurwitz polynomial for all positive values of the coefficients a_1, a_2, a_3, b_1, b_2, b_3; and conversely any 6th-degree Hurwitz polynomial can be expressed in this form.

By similar reasoning the corresponding result for Hurwitz polynomials of odd degree can be derived. The expression for a 5th-degree Hurwitz polynomial is

$$p^2\begin{vmatrix} 1 + pb_0 & -1 & 0 \\ 1 & a_1p + \frac{b_1}{p} & -1 \\ 0 & 1 & b_2p + \frac{a_2}{p} \end{vmatrix} \quad . \quad . \quad . \quad (17)$$

with $a_1, a_2, b_0, b_1, b_2 > 0$.

The new canonical form for a Hurwitz polynomial can also be written as the product of continued fractions of the types shown in eqns. (12) and (14), the derivation being exactly analogous to that used in connection with another type of continued fraction in a previous paper.[12]

Canonical forms for positive polynomials (polynomials which are positive for positive values of the variable) can also be derived corresponding to each of the canonical forms for a Hurwitz polynomial.

(3.5) Determinantal Expressions for the Continued-Fraction Coefficients

If, in eqn. (9), the polynomials P and Q are given by

$$P = c_{n-1}p^{n-1} + c_{n-2}p^{n-2} + \ldots + c_1p + c_0 \quad . \quad (18)$$

$$Q = d_np^n + d_{n-1}p^{n-1} + \ldots + d_1p + d_0 \quad . \quad . \quad (19)$$

the coefficients a_i and b_i of the continued fraction can be written in terms of determinants whose elements are the c_i and d_i above. The expressions are more complicated than the corresponding ones for the Stieltjes-type continued fraction given by Bader,[13] and it is not proposed to give a complete derivation here. Instead, results are given for $n = 5$, from which the general pattern of the results is apparent and from which the results for other values of n can be easily inferred. The highest-order determinant involved is always of order $2n - 1$ and the remaining determinants can be regarded as minors of this one.

Writing Δ for the highest-order determinant when $n = 5$, we have

$$\Delta = \begin{vmatrix} c_4 & c_3 & c_2 & c_1 & c_0 & 0 & 0 & 0 & 0 \\ d_5 & d_4 & d_3 & d_2 & d_1 & d_0 & 0 & 0 & 0 \\ 0 & c_4 & c_3 & c_2 & c_1 & c_0 & 0 & 0 & 0 \\ 0 & d_5 & d_4 & d_3 & d_2 & d_1 & d_0 & 0 & 0 \\ 0 & 0 & c_4 & c_3 & c_2 & c_1 & c_0 & 0 & 0 \\ 0 & 0 & d_5 & d_4 & d_3 & d_2 & d_1 & d_0 & 0 \\ 0 & 0 & 0 & c_4 & c_3 & c_2 & c_1 & c_0 & 0 \\ 0 & 0 & 0 & d_5 & d_4 & d_3 & d_2 & d_1 & d_0 \\ 0 & 0 & 0 & 0 & c_4 & c_3 & c_2 & c_1 & c_0 \end{vmatrix} \quad . \quad (20)$$

$$a_1 = \frac{d_5}{c_4} \quad . \quad (21)$$

$$b_1 = \frac{d_0}{c_0} \quad . \quad (22)$$

$$b_2 = \frac{c_4^2 c_0}{\begin{vmatrix} c_4 & c_3 & 0 \\ d_5 & d_4 & d_0 \\ 0 & c_4 & c_0 \end{vmatrix}} = \frac{c_4^2 c_0}{\Delta_{456789,\,345789}} \quad . \quad (23)$$

$$a_2 = \frac{c_0^2 c_4}{\begin{vmatrix} c_4 & c_0 & 0 \\ d_5 & d_1 & d_0 \\ 0 & c_1 & c_0 \end{vmatrix}} = \frac{c_0^2 c_4}{\Delta_{456789,\,234789}} \quad . \quad (24)$$

$$a_3 = \frac{\begin{vmatrix} c_4 & c_3 & 0 \\ d_5 & d_4 & d_0 \\ 0 & c_4 & c_0 \end{vmatrix}^2 \begin{vmatrix} c_4 & c_0 & 0 \\ d_5 & d_1 & d_0 \\ 0 & c_1 & c_0 \end{vmatrix}}{c_4^2 c_0^2 \Delta_{6789,\,4589}} \quad . \quad (25)$$

$$b_3 = \frac{\begin{vmatrix} c_4 & c_3 & 0 \\ d_5 & d_4 & d_0 \\ 0 & c_4 & c_0 \end{vmatrix} \begin{vmatrix} c_4 & c_0 & 0 \\ d_5 & d_1 & d_0 \\ 0 & c_1 & c_0 \end{vmatrix}^2}{c_4^2 c_0^2 \Delta_{6789,\,3489}} \quad . \quad (26)$$

$$b_4 = \frac{c_4^2 c_0^2 \Delta_{6789,\,4589}^2 \Delta_{6789,\,3489}}{\begin{vmatrix} c_4 & c_3 & 0 \\ d_5 & d_4 & d_0 \\ 0 & c_4 & c_0 \end{vmatrix}^2 \begin{vmatrix} c_4 & c_0 & 0 \\ d_5 & d_1 & d_0 \\ 0 & c_1 & c_0 \end{vmatrix}^2 \Delta_{89,\,59}} \quad . \quad (27)$$

$$a_4 = \frac{c_4^2 c_0^2 \Delta_{6789,\,4589} \Delta_{6789,\,3489}^2}{\begin{vmatrix} c_4 & c_3 & 0 \\ d_5 & d_4 & d_0 \\ 0 & c_4 & c_0 \end{vmatrix}^2 \begin{vmatrix} c_4 & c_0 & 0 \\ d_5 & d_1 & d_0 \\ 0 & c_1 & c_0 \end{vmatrix}^2 \Delta_{89,\,49}} \quad . \quad (28)$$

$$a_5 = \frac{\begin{vmatrix} c_4 & c_3 & 0 \\ d_5 & d_4 & d_0 \\ 0 & c_4 & c_0 \end{vmatrix}^2 \begin{vmatrix} c_4 & c_0 & 0 \\ d_5 & d_1 & d_0 \\ 0 & c_1 & c_0 \end{vmatrix}^2 \Delta_{89,\,59}^2 \Delta_{89,\,49}}{c_4^2 c_0^2 \Delta_{6789,\,4589}^2 \Delta_{6789,\,3489}^2 \Delta} \quad . \quad (29)$$

$$b_5 = \frac{\begin{vmatrix} c_4 & c_3 & 0 \\ d_5 & d_4 & d_0 \\ 0 & c_4 & c_0 \end{vmatrix}^2 \begin{vmatrix} c_4 & c_0 & 0 \\ d_5 & d_1 & d_0 \\ 0 & c_1 & c_0 \end{vmatrix}^2 \Delta_{89,\,59}\ \Delta_{89,\,49}^2}{c_4^2 c_0^2 \Delta_{6789,\,4589}^2 \Delta_{6789,\,3489}^2 \Delta} \quad . \quad (30)$$

where $\Delta_{89,59}$, for example, is the minor formed from Δ by omitting the 8th and 9th rows and 5th and 9th columns.

(3.6) Determinantal Forms of Criteria for Stability and Criteria for Realizability of 2-Terminal *RC* Networks

The determinantal forms of both criteria follow by comparing the determinantal form of the continued-fraction coefficients, given in Section 3.5, with the continued-fraction form of the relevant criterion given in Section 3.2 for 2-terminal *RC* networks and Section 3.3 for stability. In each case the result so derived differs somewhat from results that have been given previously.

Consider, for example, the derivation of a determinantal form of the stability criteria for the following polynomial of the 10th degree:

$$\alpha_0 + \alpha_1 p + \alpha_2 p^2 + \ldots + \alpha_8 p^8 + \alpha_9 p^9 + \alpha_{10} p^{10} \quad (31)$$

$$\text{Odd part of polynomial} \equiv pP(p^2) = \alpha_9 p^9 + \alpha_7 p^7 + \alpha_5 p^5 + \alpha_3 p^3 + \alpha_1 p \quad (32)$$

$$\text{Even part of polynomial} \equiv Q(p^2) = \alpha_{10} p^{10} + \alpha_8 p^8 + \alpha_6 p^6 + \alpha_4 p^4 + \alpha_2 p^2 + \alpha_0 \quad (33)$$

The criterion for stability is that the coefficients a_i and b_i in the continued-fraction expansion of $Q(p^2)/pP(p^2)$ [as in eqn. (12)] shall all be positive. Thus, comparing with eqns. (21)–(30),

$$\left.\begin{array}{l} D,\ D_{89,\,49},\ D_{89,\,59},\ D_{6789,\,3489},\ D_{6789,\,4589}, \\ \begin{vmatrix} \alpha_9 & \alpha_7 & 0 \\ \alpha_{10} & \alpha_8 & \alpha_6 \\ 0 & \alpha_9 & \alpha_7 \end{vmatrix},\ \begin{vmatrix} \alpha_9 & \alpha_1 & 0 \\ \alpha_{10} & \alpha_2 & \alpha_0 \\ 0 & \alpha_3 & \alpha_1 \end{vmatrix},\ \alpha_1,\ \alpha_0,\ \alpha_9,\ \alpha_{10} \end{array}\right\} \text{must all have the same sign} \quad (34)$$

$$\text{where } D = \begin{vmatrix} \alpha_9 & \alpha_7 & \alpha_5 & \alpha_3 & \alpha_1 & 0 & 0 & 0 & 0 \\ \alpha_{10} & \alpha_8 & \alpha_6 & \alpha_4 & \alpha_2 & \alpha_0 & 0 & 0 & 0 \\ 0 & \alpha_9 & \alpha_7 & \alpha_5 & \alpha_3 & \alpha_1 & 0 & 0 & 0 \\ 0 & \alpha_{10} & \alpha_8 & \alpha_6 & \alpha_4 & \alpha_2 & \alpha_0 & 0 & 0 \\ 0 & 0 & \alpha_9 & \alpha_7 & \alpha_5 & \alpha_3 & \alpha_1 & 0 & 0 \\ 0 & 0 & \alpha_{10} & \alpha_8 & \alpha_6 & \alpha_4 & \alpha_2 & \alpha_0 & 0 \\ 0 & 0 & 0 & \alpha_9 & \alpha_7 & \alpha_5 & \alpha_3 & \alpha_1 & 0 \\ 0 & 0 & 0 & \alpha_{10} & \alpha_8 & \alpha_6 & \alpha_4 & \alpha_2 & \alpha_0 \\ 0 & 0 & 0 & 0 & \alpha_9 & \alpha_7 & \alpha_5 & \alpha_3 & \alpha_1 \end{vmatrix} \quad . \quad (35)$$

Eqns. (35) and (34) give necessary and sufficient conditions for the polynomial of eqn. (31) to have all its zeros confined to the left-half p-plane. D will be recognized as the penultimate Hurwitz determinant. The remaining determinants of (34) occur in pairs whose orders differ from that of D by successive multiples of two. These pairs of determinants are non-principal minors of D, unlike the remaining determinants of the Hurwitz set which are principal minors of the highest-order determinant in the set. Similar results follow for polynomials of other degrees.

(4) FURTHER THEORY OF CONTINUED-FRACTION EXPANSION AND APPLICATIONS

It is possible to extend the theory of the continued fraction of eqn. (9) beyond that given in Section 3.1. Thus, if P is a polynomial in p of degree $n - 1$ and Q is a polynomial in p of degree n, the necessary and sufficient conditions for P and Q to have the same sign at infinity and to have only simple real zeros with the zeros of P interlacing those of Q are that

$$a_i > 0 \quad i = 1, 2, 3, \ldots n \quad . \quad (36)$$

Further, if all the zeros of Q are negative, then $b_i > 0$; every negative b coefficient indicates a positive zero of Q. Evidently, if $a_i > 0$, the condition $b_i > 0$ can be replaced by the condition

that all the coefficients of the polynomial Q must have the same sign. [The notation is that used in eqn. (9).] Details of the derivation of these results are given in Section 7.1.

Exactly as in Reference 12, this result can be used to replace half the determinants used in the determinantal formulation of the various criteria given in Section 3.6 by algebraically simpler conditions. Consider the stability criteria for a 10th-degree polynomial given in Section 3.6. For the coefficients a_i of the continued-fraction expansion of $Q(p^2)/pP(p^2)$ to be positive,

$$D, D_{89,49}, D_{6789,4589}, \left|\begin{matrix}\alpha_9 & \alpha_1 & 0\\ \alpha_{10} & \alpha_2 & \alpha_0\\ 0 & \alpha_3 & \alpha_1\end{matrix}\right|, \alpha_9, \alpha_{10} \left.\begin{matrix}\\ \\ \\ \\ \end{matrix}\right\} \begin{matrix}\text{must all}\\ \text{have the}\\ \text{same sign}\end{matrix} \quad (37)$$

Combining this with the condition that all the coefficients of the polynomial $Q(p^2)$ must have the same sign, we have

$$D, D_{89,49}, D_{6789,4589}, \left|\begin{matrix}\alpha_9 & \alpha_1 & 0\\ \alpha_{10} & \alpha_2 & \alpha_0\\ 0 & \alpha_3 & \alpha_1\end{matrix}\right|, \alpha_{10}, \alpha_9, \alpha_8, \alpha_6, \alpha_4, \alpha_2, \alpha_0 \left.\begin{matrix}\\ \\ \\ \\ \\ \\ \\ \\ \end{matrix}\right\} \begin{matrix}\text{must all}\\ \text{have the}\\ \text{same sign}\end{matrix} \quad (38)$$

as a form of the stability criteria simpler than that given in conditions (34). Conditions (38) are similar to those given by Fuller[9] and Gantmacher,[14, 15] the main point of difference being that here non-principal minors of the highest-order Hurwitz determinant are used.

(5) CONCLUSIONS

The derivation of the properties, as functions of the complex frequency, of principal minors of successive orders of the nodal determinant of a lumped linear *RC* network given in Section 2 of the paper was based essentially on a mathematical method given by Sylvester in 1853. Particular attention has been given here to the question of multiple zeros of the various minors. These results give immediately the well-known properties of a driving-point impedance of a 2-terminal *RC* network, and similar results can be deduced for any 2-element-kind network.

The remaining Sections give an account of the theory of a certain continued fraction and its relationship to these, and to the related problems of stability, etc., is shown. The use of this type of continued fraction as a test for stability or realizability gives, in the author's opinion, a considerable reduction in the numerical working as compared with the use of a Stieltjes-type continued fraction.

Expressions for the coefficients of the continued fraction are obtained in determinant form and are used to derive some new determinantal formulations of the stability criteria. New canonical forms for a Hurwitz polynomial are also given.

(6) REFERENCES

(1) CAUER, W.: 'Die Verwirklichung von Wechselstrom-widerständen vorgeschriebener Frequenzabhängigkeit', *Archiv für Elektrotechnik*, 1926, **17**, p. 355.

(2) FOSTER, R. M.: 'A Reactance Theorem', *Bell System Technical Journal*, 1924, **3**, p. 259.

(3) VOWELS, R. E.: 'Synthesis of Driving-Point and Transfer Functions by Continued Fraction Expansion', *Australian Journal of Applied Science*, 1957, **8**, p. 151.

(4) ROUTH, E. J.: 'Dynamics of a System of Rigid Bodies', 6th edition (Macmillan, 1905), Part II.

(5) ROUTH, E. J.: 'A Treatise on the Stability of a Given State of Motion' (Macmillan, 1877).

(6) SYLVESTER, J. J.: 'The Algebraical Theory of the Secular-Inequality Determinantive Equation Generalized', *Philosophical Magazine*, 4th Series, 1853, **6**, p. 214.
SYLVESTER, J. J.: 'Mathematical Papers' (Cambridge University Press, 1904), Vol. 1, p. 634.

(7) TURNBULL, H. W.: 'Theory of Equations', 4th edition (Oliver and Boyd, 1947), p. 103.

(8) AITKEN, A. C.: 'Determinants and Matrices', 3rd edition (Oliver and Boyd, 1944), p. 97.

(9) FULLER, A. T.: 'Stability Criteria for Linear Systems and Realizability Criteria for *RC* Networks', *Proceedings of the Cambridge Philosophical Society*, 1957, **53**, p. 878.

(10) BÜCKNER, H.: 'A Formula for an Integral occurring in the Theory of Linear Servomechanisms and Control-Systems', *Quarterly of Applied Mathematics*, 1952–53, **10**, p. 205.

(11) Reference 8, p. 126.

(12) CUTTERIDGE, O. P. D.: 'The Stability Criteria for Linear Systems', *Proceedings I.E.E.*, Monograph No. 328 M, February, 1959 (**106** C, p. 125).

(13) BADER, W : 'Beitrag zur Verwirklichung von Wechselstrom-widerständen vorgeschriebener Frequenzabhängigkeit', *Archiv für Elektrotechnik*, 1940, **34**, p 293.

(14) GANTMACHER, F. R.: 'Theory of Matrices' (Moscow, 1954), p. 457.

(15) GANTMACHER, F. R.: 'Applications of the Theory of Matrices' (Interscience Publishers, 1959), p. 263. (English translation of second part of Reference 14.)

(16) CUTTERIDGE, O. P. D.: 'Further Theory of a Certain Continued Fraction' (see p. 234).

(7) APPENDICES

(7.1) Further Theorems on a Continued Fraction

Theorem 2.

If P is a polynomial in p of degree $n-1$ and Q is a polynomial in p of degree n, the necessary and sufficient conditions for P and Q to have the same sign at infinity and to have only simple real zeros with the zeros of P interlacing those of Q are that, in the continued-fraction expansion of eqn. (9),

$$a_i > 0 \quad i = 1, 2, 3, \ldots n \quad (39)$$

A proof of this theorem can be obtained in a manner analogous to that of Theorem 1. Of the two basic results required one has been given in a previous paper,[12] and the other can be developed either from this or otherwise. Alternatively, there is the following derivation, from first principles, which is quite instructive.*

The necessity of these conditions will first be shown. The first steps in the formation of the continued fraction of eqn. (9) can be written

$$\frac{P}{Q} = \frac{1}{a_1 p + \dfrac{Q_1}{P}} \quad (40)$$

$$\frac{Q_1}{P} = b_1 + \frac{Q_2}{P} \quad (41)$$

$$\frac{Q_2}{P} = \frac{1}{\dfrac{a_2}{p} + \dfrac{P_1}{Q_2}} \quad (42)$$

$$\frac{P_1}{Q_2} = b_2 + \frac{P_2}{Q_2} \quad (43)$$

* Yet a further derivation is by the methods used in Reference 16.

hus,

$$Q = a_1 pP + Q_1 \quad . \quad . \quad . \quad . \quad . \quad (44)$$

$$Q_1 = b_1 P + Q_2 \quad . \quad . \quad . \quad . \quad . \quad (45)$$

$$P = \frac{a_2 Q_2}{p} + P_1 \quad . \quad . \quad . \quad . \quad . \quad (46)$$

$$P_1 = b_2 Q_2 + P_2 \quad . \quad . \quad . \quad . \quad . \quad (47)$$

lere Q is of degree n, Q_1 and P are of degree $n-1$, Q_2 and P_1 f degree $n-1$ each with a zero at the origin, and P_2 is of egree $n-2$ with a zero at the origin.

Since P and Q have the same sign at infinity, $a_1 > 0$ in eqn. (44). ' now P and Q have the same numbers of positive zeros, they ave the same sign at the origin and $b_1 > 0$ in eqn. (45); other- ise Q has one more positive zero than P and $b_1 < 0$. Consider ie latter case first. With the appropriate values for a_1 and b_1 i eqns. (44) and (45), we have

$$Q = Q_1 = Q_2 \text{ at zeros of P} \quad . \quad . \quad . \quad . \quad . \quad . \quad . \quad . \quad (48)$$

$$\left.\begin{array}{l} Q_1 \text{ has the opposite sign to P at positive zeros of Q} \\ \text{and } Q_1 \text{ has the same sign as P at negative zeros of Q} \end{array}\right\} \quad (49)$$

$$Q_2 \text{ has the same sign as P at all zeros of } Q_1 \quad . \quad . \quad . \quad (50)$$

rom these, by the same arguments as were given in the previous aper, the following results are obtained:

(*a*) The zeros of Q_1 are all real and alternate with those of P along the real p-axis. If a zero of Q_1 is the most positive, case (i), P and Q_1 have the same sign at infinity and Q_1 and Q have the same number of positive zeros. If, on the other hand, a zero of P is the most positive, case (ii), P and Q_1 have opposite signs at infinity and Q_1 has one less positive zero than Q.

(*b*) The zeros of Q_2 are all real and alternate with the zeros of P along the real p-axis. For case (i), a zero of Q_2 is the most positive, P and Q_2 have the same sign at infinity, the slope of Q_2 has the same sign as P at the origin and Q_2 has one less positive zero than Q_1 and Q; thus a_2 and b_2 in eqns. (46) and (47) are both positive. For case (ii) there are two possibilities: either a zero of Q_2 is the most positive, case (iii), P and Q_2 have the same sign at infinity, the slope of Q_2 has the same sign as P at the origin and the number of positive zeros of Q_2 and Q_1 are equal and one less than the number of positive zeros of Q; or a zero of P is the most positive, case (iv), P and Q_2 have opposite signs at infinity, the slope of Q_2 has the same sign as P at the origin and the number of positive zeros of Q_2 is one less than the corresponding number for Q_1 and two less than the number for Q. For case (iii), a_2 and b_2 in eqns. (46) and (47) are both positive, whereas for case (iv), a_2 is positive and b_2 is negative.

Thus, as the final results for cases (i) and (iii) are the same, nly two cases need to be considered in the next portion of the nalysis, namely (i) and (iv). In each case, a_2 in eqn. (46) will e positive, and if Q_2 has two less positive zeros than Q, then oth b_1 of eqn. (45) and b_2 of eqn. (47) will be negative, whereas f Q_2 has one less positive zero than Q only b_1 is negative and $_2$ is positive.

From eqn. (46), since $a_2 > 0$,

$$P = P_1 \text{ at zeros of } Q_2, \text{ excluding that at the origin} \quad . \quad (51)$$

$$\left.\begin{array}{l} P_1 \text{ has the opposite sign to } Q_2 \text{ at positive zeros of P} \\ P_1 \text{ has the same sign as } Q_2 \text{ at negative zeros of P} \end{array}\right\} \quad (52)$$

From eqn. (47),

$$P_2 = P_1 \text{ at zeros of } Q_2 \quad . \quad . \quad . \quad . \quad . \quad . \quad . \quad . \quad (53)$$

$$\left.\begin{array}{l} P_2 \text{ has the opposite sign to } Q_2 \text{ at zeros of } P_1 \text{ if } b_2 > 0 \\ P_2 \text{ has the same sign as } Q_2 \text{ at zeros of } P_1 \text{ if } b_2 < 0 \end{array}\right\} \quad (54)$$

Application of these equations yields the following results:

(*c*) The zeros of P_1 are all real and, if the zeros at the origin are excluded, alternate with the zeros of Q_2 along the real p-axis. For case (i) there are two possibilities: either, case (v), P_1 has one less positive zero than has Q_2 or P and P_1 and Q_2 have slopes of opposite signs at the origin or, case (vi), P_1 and Q_2 have the same numbers of positive zeros and P_1 and Q_2 have slopes of the same sign at the origin. In both cases, P_1 and Q_2 have the same sign at infinity and a zero of Q_2 is the most positive. For case (iv) also there are two possibilities: either, case (vii), P_1 has one less positive zero than P and P_1 and Q_2 have slopes of opposite signs at the origin or, case (viii), P_1 has the same number of positive zeros as P and P_1 and Q_2 have slopes of the same sign at the origin. In both cases, P_1 and Q_2 have opposite signs at infinity and a zero of P_1 is the most positive.

(*d*) For all the above cases the zeros of P_2 are real and, if the zeros at the origin are excluded, interlace the real zeros of Q_2 along the real p-axis; P_2 and Q_2 always have the same signs at infinity. For case (v), P_2 has one less positive zero than Q_2 and each has one less positive zero than the original P and Q; P_2 and Q_2 have slopes of opposite signs at the origin. For case (vi) there are two possibilities one of which has just been covered. For the other, P_2 and Q_2 have the same number of positive zeros equal to one less than the number of positive zeros of Q; P_2 and Q_2 have slopes of the same sign at the origin. Cases (vii) and (viii) yield the same result, namely that P_2 and Q_2 have slopes of the same sign at the origin and have the same number of positive zeros, being two less than the number of positive zeros of Q.

All these results apply for the case in which Q has one more positive zero than P and hence $b_1 < 0$, but exactly similar reasoning applies to the case in which P and Q have the same number of positive zeros and $b_1 > 0$. The results for both these cases can be summarized as follows:

Let P_2^* and Q_2^* be polynomials formed by deleting the zero at the origin from P_2 and Q_2 respectively. The ratio P_2^*/Q_2^* has the same properties as the original ratio P/Q, but the degrees of both numerator and denominator have been reduced by two. Hence continual repetition of the argument is possible with the conclusion that all coefficients $a_i > 0$, thus demonstrating the necessity of the conditions of Theorem 2. The sufficiency of these conditions can be shown by a converse form of the above argument.

In the course of the proof of Theorem 2 the following theorem has also been established.

Theorem 3.

If in the continued-fraction expansion of eqn. (9) all the coefficients a_i are positive, the total number of the coefficients b_i that are negative is equal to the number of positive zeros of Q.

(7.2) Numerical Example

The following simple numerical example both illustrates Theorems 2 and 3 and shows the economy of working relative to the formation of a Cauer-type continued-fraction expansion.

If
$$\frac{P}{Q} = \frac{(p+1)(p-2)}{(p+2)(p-1)(p-3)} \quad . \quad . \quad . \quad (55)$$

$$= \frac{p^2 - p - 2}{p^3 - 2p^2 - 5p + 6} \quad . \quad . \quad . \quad . \quad (56)$$

Then
$$\frac{P}{Q} = \cfrac{1}{p - 3 + \cfrac{1}{\cfrac{1}{2} + \cfrac{1}{3p} + \cfrac{1}{\cfrac{3p}{2} - \cfrac{9}{2}}}} \quad . \quad . \quad . \quad (57)$$

the detailed working being as follows:

$$
\begin{array}{l}
p^2-p-2\big)p^3-2p^2-5p+6\big(p-3\\
\quad p^3-p^2-2p\\
\quad\overline{\quad -3p^2+3p+6}\\
\quad 2p^2-6p\quad\big)p^2-\ p-2\big(\frac{1}{2}+\frac{1}{3p}\\
\qquad\qquad p^2-3p\\
\qquad\qquad\overline{\qquad\qquad\frac{2}{3}p-2}\\
\qquad\qquad\frac{4}{3}p\quad\big)2p^2-6p\big(\frac{3p}{2}-\frac{9}{2}
\end{array}
$$

The positive p coefficients in the continued-fraction expansion of eqn. (57) correspond to all the zeros of P and Q being real, with the zeros of P interlacing those of Q, and the two negative numerical coefficients correspond to the two positive zeros of Q.

For contrast, the detailed working to obtain a Cauer-type expansion is as follows:

$$
\begin{array}{l}
-2-p+p^2\big)6-5p-2p^2+p^3\big(-3\\
\quad\overline{\quad 6+3p-3p^2}\\
\quad -8p+p^2+p^3\big)-2-p+p^2\big(\frac{1}{4p}\\
\qquad\qquad\overline{\qquad -2+\frac{p}{4}+\frac{p^2}{4}}\\
\qquad\qquad\frac{-5p}{4}+\frac{3p^2}{4}\big)-8p+p^2+p^3\big(\frac{32}{5}\\
\qquad\qquad\qquad\overline{\qquad\qquad -8p+\frac{24}{5}p^2}\\
\qquad\qquad\qquad -\frac{19}{5}p^2+p^3\big)-\frac{5p}{4}+\frac{3p^2}{4}\big(\frac{25}{76p}\\
\qquad\qquad\qquad\qquad\overline{\qquad\qquad -\frac{5p}{4}+\frac{25p^2}{76}}\\
\qquad\qquad\qquad\qquad\frac{8p^2}{19}\big)\frac{-19p^2}{5}+p^3\big(\frac{-361}{40}\\
\qquad\qquad\qquad\qquad\qquad\overline{\qquad\frac{-19p^2}{5}}\\
\qquad\qquad\qquad\qquad\qquad\qquad p^3\big)\frac{8p^2}{19}\big(\frac{8}{19p}
\end{array}
$$

It will be noted that all the p coefficients are positive and there are two negative numerical coefficients, exactly the same result as with the continued fraction of eqn. (57).

21.313.36.017.42: 621.371.384

The Institution of Electrical Engineers
Monograph No. 375 U
Apr. 1960
©

BRUSH CONTACT LOSSES DUE TO LOAD AND PARASITIC CURRENTS IN POLYPHASE COMMUTATOR MOTORS

By O. E. MAINER, M.Sc.(Tech.), Associate Member.

(*The paper was first received* 14*th October*, 1959, *and in revised form* 13*th January*, 1960. *It was published as an* INSTITUTION MONOGRAPH *in April*, 1960.)

SUMMARY

After brief reference to present methods of measurement, the interpendence of the brush losses due to load and parasitic currents is scussed and the need for measuring them simultaneously is argued. wing to the impossibility of doing this satisfactorily on a motor, an pparatus for simulating brush parasitic currents is described and test ata obtained with this apparatus are used to establish the argument. he effects of rotor power factor and speed on the losses are also dis-ussed and established experimentally. Finally, a new test is described y means of which the total rotor I^2R losses of a polyphase com-utator motor can be measured with reasonable accuracy. Curves btained by this method of test using plain and sandwich brushes how the dependence of these losses on the coil e.m.f. between egments.

(1) INTRODUCTION

The brush parasitic-current loss is normally measured, in the bsence of load current, by an open-circuit method, an improved ersion of which has recently been described.[1]

The brush contact loss due to load current comprises the major art of the load-current I^2R loss in the rotor circuit which is sually measured by a short-circuit test at standstill. During the hort-circuit test the e.m.f. in a coil short-circuited by the brush ace is too small to set up an appreciable parasitic current. Thus he brush contact loss due to load current is measured in the bsence of brush parasitic currents.

Under normal load conditions both load and parasitic currents re present simultaneously, and it is necessary to consider how his will modify their respective brush contact losses.

The brush contact resistance comprises the major part of the mpedance opposing the circulation of parasitic current through coil and across the brush. It follows that the parasitic current oss for a given coil voltage is nearly inversely proportional to he contact resistance. It is well known that brush contact esistance decreases as current density increases. Accordingly, hen full-load current is passing through the brushes, the brush ontact resistance opposing the circulation of parasitic currents an be expected to be less than during the open-circuit test, and o it is reasonable to expect that the brush parasitic current loss or a given coil voltage will be higher on load than when measured y the open-circuit method. Confirmation of this has already een obtained by Richter.[2]

On the other hand, the brush contact-resistance loss for a given oad current is directly proportional to the contact resistance and may be expected that this loss will decrease if the current ensity is increased by the flow of parasitic currents. There are, owever, no published data on this matter.

Unless the increase in the brush parasitic-current loss balances he decrease in the loss due to load current, the total loss at the rush contact cannot be equal to the sum of these losses determined independently by open-circuit and short-circuit tests. Again, there are no published data on this matter.

It needs to be emphasized that the maximum current density under the brush, as well as the average current density, plays an important part in determining the overall contact resistance. If the current density is periodically high under one part of the brush all segments will sooner or later experience this high current density. It is not necessary to maintain this high current density on a segment, for, once a segment has experienced a high current density, it will retain a lower contact resistance for an appreciable period.[3]

In view of the fact that the brush contact-resistance losses are only a small percentage of the total input to a polyphase commutator motor, it is considered impossible to make reliable measurements of these losses under load conditions. It is true that Richter[2] managed to measure the brush parasitic-current loss under load conditions, but his test depends on the difference between large quantities and is subject to appreciable error unless the brushes are set very accurately in the neutral zone. Moreover, Richter's test does not enable the brush losses due to load current to be evaluated. In order, therefore, to obtain reliable information on the mutual effect of parasitic and load currents an apparatus was devised for simulating brush parasitic currents and enabling the simultaneous measurement of brush losses due to both load and parasitic currents.

(2) DESCRIPTION OF PARASITIC-CURRENT SIMULATOR

The apparatus used consisted of a commutator having 62 segments and no commutator winding. Numbering the segments 1 to 62 around the periphery, the risers of all odd segments were soldered together and a connection taken along the shaft to a brass slip-ring. Similarly all the even segments were connected to a second ring. A number of brushes with high copper content and correspondingly low contact resistance made sliding contact between the rings and a low-voltage 50 c/s supply through the instruments shown in Fig. 1.

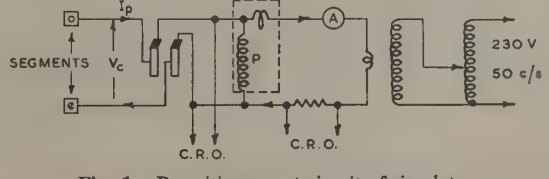

Fig. 1.—Parasitic-current circuit of simulator.
e: even. o: odd.

Brushes having a thickness equal to the pitch of two commutator segments rested on the commutator at diametrically opposite positions. There were two brushes placed axially side by side in each position. The odd and even segments were short-circuited at the brushes, so that a current circulated across each brush, as shown in Fig. 2, in which V_c represents the

Correspondence on Monographs is invited for consideration with a view to ublication.

Mr. Mainer is Principal Lecturer in Electrical Engineering at the Royal Military ollege of Science, Shrivenham.

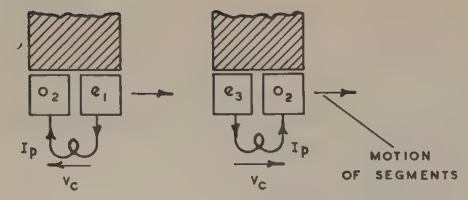

Fig. 2.—Circulation of parasitic currents.

equivalent coil voltage between segments obtained from the a.c. source and I_p the equivalent brush parasitic current.

The flow of current is similar to the brush parasitic current in a polyphase commutator motor except that a reversal takes place in its direction as the commutator moves through one segment pitch. If the segments had been connected to a polyphase armature winding, the coil voltage, V_c, would have remained in the direction right to left during the short interval required for segments 1, 2 and 3 to pass under the brush. However, it is considered that this will not affect the qualitative information obtainable from the parasitic-current simulating circuit.

(3) LOAD-CURRENT CIRCUIT

The arrangements made for passing load current through the brushes are shown in Fig. 3. The load current, I, flowed

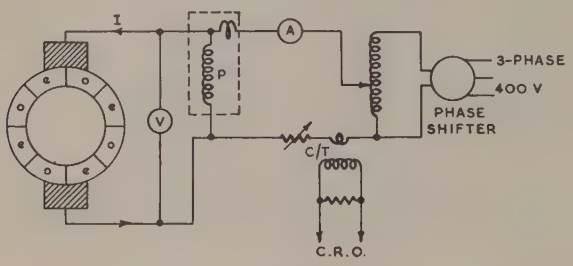

Fig. 3.—Load-current circuit.

through the brushes and the wires which connect diametrically opposite odd and even segments under the brushes. The flow of parasitic currents did not produce any deflection on the ammeter or wattmeter in the load circuit.

(4) MEASUREMENT OF EQUIVALENT COIL VOLTAGE

No part of the load current was detectable on the ammeter or wattmeter in the equivalent parastic-current circuit of Fig. 1. Nevertheless an h.f. voltage appeared across the slip-ring brushes owing to the load current and was discernible on the cathode-ray oscillograph. The frequency of this voltage depended on the speed of rotation, and its magnitude was sufficient to make it impossible to use a voltmeter for accurate measurement of the equivalent coil voltage, V_c. The latter was therefore calculated from the wattmeter and ammeter readings in the following manner.

The power P_1 represents the total I^2R losses registered on the wattmeter in Fig. 1 for some parasitic current I_p. The odd and even segments where then short-circuited together by two links screwed into the ends of the commutator segments. These links were placed diametrically opposite, so that on supplying a voltage to the slip-ring brushes the current follows along exactly the same paths in the circuit, with the exception that the brushes are by-passed. For the same current, I_p, and the same speed of rotation the power input is P_2, so that $P_1 - P_2$ is the power dissipated by I_p in the brushes and at the brush contact. The equivalent coil voltage is then $(P_1 - P_2)/I_p$.

The value of P_2 is almost entirely dependent on the current density at the slip-ring brushes. The area of brush contact at the slip-rings used in these tests was sufficient to make P_2 less than 10% of P_1.

(5) EFFECT OF PHASE RELATIONSHIPS OF PARASITIC AND LOAD CURRENTS ON CONTACT RESISTANCE

If the rotor of a polyphase commutator motor operates at unity power factor the load and parasitic currents are in quadrature under both leaving and entering edges of the brush, and for given load and parasitic currents the brush current density is a minimum. If the rotor power factor is zero these currents are in phase either under the leaving edge or under the entering edge of the brush, and for given load and parasitic currents the brush current density attains a maximum under one edge. Corresponding to this higher maximum current density the contact resistance at zero power factor is less than at unity power factor.

In the above argument it is assumed that the reactance voltage has a negligible effect, so that the current distribution is determined solely by contact resistance, in which case maximum current density and minimum contact resistance will occur equally with rotors operating at either zero lagging or zero leading power factor.

The introduction of a phase shifter in the load-current circuit of Fig. 3 together with observations on a double-beam cathode-ray oscillograph enabled the relative phase of the load and equivalent parasitic currents to be adjusted on the simulator. Owing to the reversal of the equivalent coil voltage illustrated by Fig. 2 the simulator operated at zero power factor with currents in phase alternately at the leaving and entering edges. The simulator was therefore equivalent to a rotor with negligible reactance voltage operating at either zero lagging or zero leading power factor.

(6) SKIN FORMATION

The commutator was turned true with a hard tool and polished with progressively finer glass papers. The brushes were bedded in with very fine glass paper and the skin formed by increasing gradually the load current supplied from the circuit illustrated in Fig. 3 over a period of 4 hours until the brush current density attained 40 A/in^2. This current density was then maintained for a further period of 36 hours. During the entire bedding-in period the commutator was driven at 1 500 r.p.m. The brushes were examined periodically during this period and the bedding-in process was repeated where necessary, so that at the end of the skin-forming period nearly perfect contact was made from edge to edge of each brush.

(7) DETAILS OF BRUSHES AND COMMUTATOR

The commutator had a diameter of 5 in with 62 segments and undercut mica. The segment pitch was therefore almost exactly $\frac{1}{4}$ in. Half-inch-square brushes were arranged radially, so that each brush covered two segment pitches. The brush positions were diametrically opposite with two axially-placed brushes in each position. Tests were carried out with high-resistance brushes, type A, at a brush pressure of 4 lb/in^2 and speeds of 500 and 2 500 r.p.m. After carrying out tests with these brushes the commutator was cleaned with emery paper, repolished with fine glass paper and a new skin formed with type B brushes. The tests were then repeated with type B brushes. The brush pressures recommended by the makers are 2·5 lb/in^2 for type B and 3 lb/in^2 for type A. Pressures of 5 or 6 lb/in^2 are quite usual for high-speed fractional horse-power motors and for large

motors subject to vibration. Increasing the pressure stabilizes the contact and prevents sparking. It was to prevent sparking at 2 500 r.p.m. that a pressure of 4 lb/in^2 was chosen. As the contact resistance decreases with brush pressure the effect of operating at 4 lb/in^2 rather than the recommended brush pressure will reduce the load-current losses and increase the parasitic-current losses.

(8) TEST SCHEDULE

After forming the skin the commutator was driven for 2 hours at 2 500 r.p.m. and the same load current density of 40 A/in^2. The parasitic-current loss was then increased in steps from zero to a maximum whilst maintaining the load current density constant. At each step, readings of both wattmeters (Figs. 1 and 2) and of the parasitic current were taken at intervals of about half a minute. The parasitic-current loss was then reduced in the same steps down to zero, and the readings were repeated. Three such cycles were carried out at unity power factor, i.e. with the load and parasitic currents in quadrature, a fourth was carried out at zero power factor and a fifth with the load current switched off so as to give open-circuit conditions. Finally, the short-circuiting links were placed in position and the slip-ring losses evaluated as described in Section 4.

The above test schedule was repeated at 500 r.p.m.

(9) DISCUSSION OF TEST CURVES

Except in one respect, which is discussed subsequently, the results for type B brushes were similar to those for type A. Consequently, only the curves for type A brushes are depicted. These curves represent the mean values of the 3rd, 4th and 5th cycles, the equivalent coil voltage between segments being calculated as explained in Section 4.

(9.1) Parasitic-Current Brush Loss

The brush loss due to parasitic currents is shown plotted against coil voltage in Fig. 4. It is apparent that the loss on open-circuit

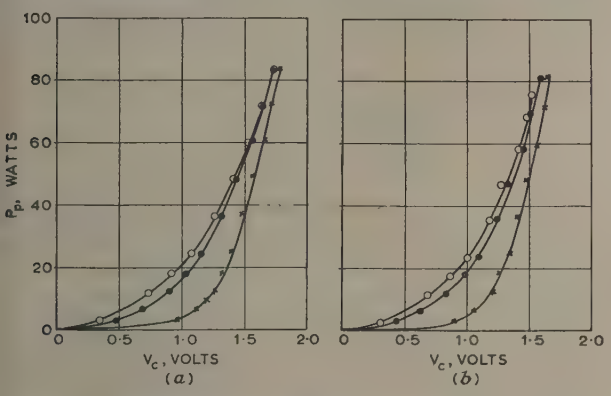

Fig. 4.—Dependence of parasitic-current brush loss, P_p, on coil voltage, V_c.
(*a*) 2 500 r.p.m. (*b*) 500 r.p.m.
○ Zero power factor. Load, 40 A/in^2.
● Unity power factor. Load, 40 A/in^2.
× Open-circuit.

is appreciably less than that when load current is flowing for small coil voltages. This is due to the load current opening relatively low-resistance paths through the skin and confirms Richter's[2] findings. The difference is less marked at higher coil voltages, because at these the load current plays a decreasing part in contributing to the total brush current density.

The curves also show that the higher current densities occurring with zero-power-factor rotors lower the contact resistance and result in an increase in the parasitic-current loss.

(9.2) Open-Circuit Parasitic-Current Loss

The open-circuit losses for speeds of 500 and 2 500 r.p.m. may be compared from Fig. 4. It will be seen that for a given coil voltage the loss is somewhat higher at 500 r.p.m. than at 2 500 r.p.m. This is to be expected, as it is well known that brush contact resistance increases somewhat with speed. However, for reasons not understood, there was a marked reduction in the open-circuit parasitic-current loss at 2 500 r.p.m. when employing type B brushes. This marked difference had already been observed from open-circuit tests on a small polyphase commutator motor equipped with type B brushes.

(9.3) Load-Current Brush Loss

It is apparent that the load-current brush loss, shown in Fig. 5, diminishes with decrease in brush contact resistance resulting

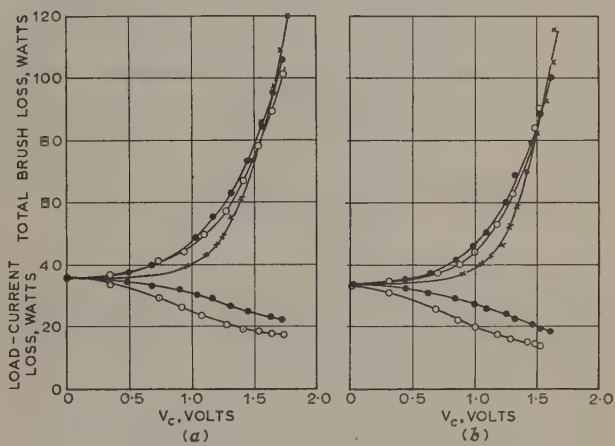

Fig. 5.—Load-current loss and total brush loss.
(*a*) 2 500 r.p.m. (*b*) 500 r.p.m.
○ Zero power factor. Load, 40 A/in^2.
● Unity power factor. Load, 40 A/in^2.
× Composite curve.

from the higher current densities accompanying the flow of parasitic currents set up by the equivalent coil voltage between segments. The fall is particularly marked in the case of zero-power-factor load current. In itself this reduction in the loss is an advantage; however, it is due to a fall in the brush contact resistance, and polyphase commutator motors rely on high-resistance brushes for forcing commutation. Coil voltages of 2 volts are by no means abnormal and it is clear that they cause the brush to change from a high- to a medium-resistance brush. It follows that the reactance voltage becomes more capable of setting up injurious sparking.

(9.4) Total Brush Contact Loss

The total loss, obtained by adding the individual losses due to parasitic and load currents, is shown in Fig. 5 for both unity- and zero-power-factor rotors, together with a composite curve obtained by adding to the open-circuit parasitic-current loss the value of load-current loss occurring in the absence of parasitic currents. This latter curve is equivalent to that obtained by adding the open-circuit parasitic-current loss of a normal machine to the brush contact loss determined from a short-circuit test.

The total losses obtained at zero power factor are rather less than those at unity power factor, because the lowering of the contact resistance by higher current densities at zero power factor results in a fall in the load current loss which is greater than the rise in the parasitic loss.

The composite curve gives total losses somewhat lower than those measured, but, with the exception of type B brushes at 2 500 r.p.m., the agreement was quite reasonable. This would appear to justify the existing method of measuring the brush parasitic-current loss by the open-circuit method and of including the load-current brush loss as part of the loss evaluated by a short-circuit test. However, there appears to be no scientific justification for this agreement and it is possible that it may not exist for other grades of brushes or even for the same grades under other conditions. For this reason it seems desirable to employ a simple test which will enable both losses to be measured simultaneously.

Before describing such a test attention is drawn to the total loss curves in Fig. 5. It will be seen that, at coil voltages too small to set up an appreciable parasitic-current loss, the brush loss is somewhat higher at 2 500 r.p.m. than at 500 r.p.m. This is due to the somewhat higher brush contact resistance occurring at the higher speed. However, as the coil voltage increases and the parasitic-current loss preponderates, the lower contact resistance associated with the lower speed causes the total loss at 500 r.p.m. to rise above that at 2 500 r.p.m.

(10) TOTAL ROTOR I^2R LOSS OF A POLYPHASE COMMUTATOR MOTOR

(10.1) Measurement

For the measurement of the total I^2R loss the stator is open-circuited and the rotor is fed with a variable voltage from a 3-phase supply and driven by a prime mover, which is preferably a d.c. shunt motor arranged for wide speed variation by Ward Leonard control.

The theory of testing from the rotor side has been given previously,[4] and it has been shown that the line wattmeters measure $P_R + sP_S$, where P_R and P_S are the powers dissipated in the rotor and stator, respectively. P_R is the rotor core loss at slip s plus the total rotor I^2R losses due to load and parasitic brush currents. P_S is the stator core loss corresponding to an internal stator e.m.f. V_1 measured by a voltmeter connected to the open-circuited stator terminals.

It is necessary to evaluate the stator and rotor core losses in terms of V_1 and s and to deduct these losses from the power registered on the wattmeters. The difference gives the total brush electrical losses due to load and parasitic currents together with the I^2R loss in the rotor winding.

The active component of the current is largely dependent on the brush parasitic-current loss and increases rapidly for a given flux at high slips. It follows that a test carried out at different slips with full-load rotor current results in some variation in the magnetizing current and stator e.m.f., V_1. As the motor is highly saturated slight changes in V_1 are accompanied by large changes in core losses, which must be carefully measured for each value of V_1.

The work involved in this evaluation is not justified and the following approximate method has been used.

The rotor current was adjusted to full load at synchronous speed and the stator e.m.f. V_1 carefully noted and then kept constant at subsequent values of slip. Core losses were determined for this e.m.f. by the normal method giving P_S as the stator core loss, and P_{Rh} and P_{Re} as the hysteresis and eddy-current components of the rotor core loss at standstill.

The total rotor I^2R losses were obtained by deducting from the wattmeter power the loss*

$$sP_S + |s|P_{Rh} + s^2P_{Re}$$

As the slip varies the current changes somewhat owing to changes in its active component. During tests carried out on a small motor the maximum increase in rotor current was about 7·5% and took place at a positive slip of $\frac{1}{3}$. At this slip the load-current losses are so small compared with the brush parasitic-current loss that the error in the total losses caused by this variation in load current is at most likely to be 3 or 4%.

The coil e.m.f. behind the parasitic current is given by $V_c = KsV_1$, where K is a constant relating the coil e.m.f. to the stator line e.m.f. at standstill.

(10.2) Discussion of Test Curves

Curves of the total I^2R losses at 75 and 100% full-load current were determined for both plain and sandwich brushes of types A and B. The sandwich brushes are designated types A_1 and B_1. All the curves were similar and only those for type A brushes are shown in Fig. 6.

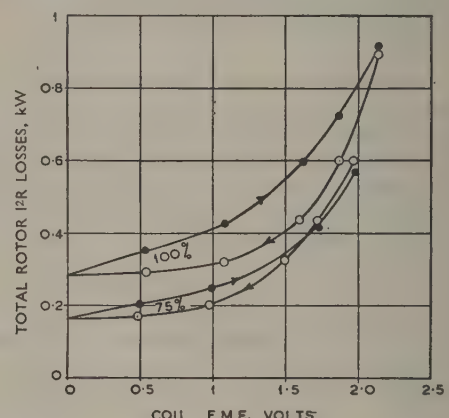

Fig. 6.—Total rotor I^2R losses at 100% and 75% full load.

● Super-synchronous speeds.
○ Sub-synchronous speeds.
→← Speed increasing.
Brush pressure, 3·65 lb/in² } at full load.
Current density, 38·5 A/in² }

For reasons explained in Section 9 the total I^2R losses of the simulator at low and high speeds cross. To a certain extent the same behaviour is apparent in Fig. 6. However, at full load the divergence between super- and sub-synchronous curves is much more marked in Fig. 6, and tends to delay the cross-over.

The effect of rotor power factor on the contact resistance for the case of a rotor with negligible reactance voltage has been discussed in Section 5. If, now, the reactance voltage is not negligible there will be a tendency for the load current density to increase towards the leaving edge of the brush.

The major part of the rotor current in the test described in Section 10.1 is the magnetizing component, so that the power factor approaches zero lagging at sub-synchronous speeds and zero leading at super-synchronous speeds. The parasitic and

* It is widely accepted that the rotor core losses are divisible into a hysteresis component proportional to the slip speed and an eddy-current component proportional to the square of the slip speed. Experimental work undertaken after the results in the paper had been completed suggests that the above formula is inaccurate, and that rotor core losses may be determined more accurately by the empirical formula

$$(P_{Rh} + P_{Re})s^x$$

where the index x is chosen to agree with the measured rotor loss at half synchronous speed.[5]

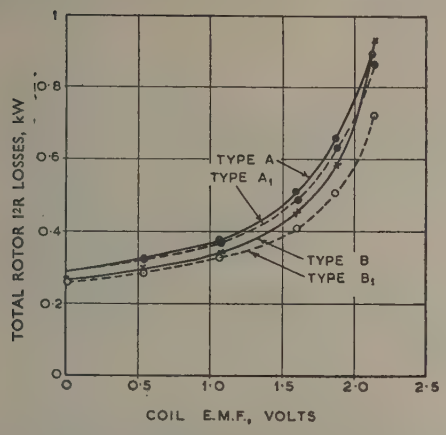

Fig. 7.—Mean full-load total rotor I^2R losses for plain and sandwich brushes.

load currents are in phase under the leaving edge of the brush when the rotor power factor is zero leading and under the entering edge when the power factor is zero lagging. It follows that the reactance voltage and parasitic currents combine at zero leading power factor to raise the current density under the leaving edge of the brush. At zero lagging power factor their actions are opposing. Thus at zero leading power factor a higher current density and a lower contact resistance will occur than at zero lagging. It seems highly probable that the reactance voltage is responsible for the major part of the divergence between the curves of total I^2R loss depicted in Fig. 6.

Under normal operating conditions the rotor power factor of a polyphase commutator motor will be nearer unity than either zero leading or zero lagging. Therefore, it is recommended that the total I^2R losses be taken as the mean of the values on the sub- and super-synchronous curves shown in Fig. 6. Then, for tests carried out at equal positive and negative slips, the stator core loss need not be evaluated, the total I^2R losses being given by one-half the total wattmeter powers at $\pm s$ minus $|s|P_{Rh} + s^2P_{Re}$.

Curves of this kind plotted for full-load rotor current are shown in Fig. 7. It is apparent that there is little advantage in using sandwich brushes, which confirms deductions already reached by open-circuit tests.[1]

(11) CONCLUSION

The tests carried out with the parasitic current simulator show that the electrical brush losses due to load and parasitic currents are interdependent and ought therefore to be measured simultaneously. A new test is described by which the total rotor I^2R losses may be evaluated.

(12) ACKNOWLEDGMENT

The types A and B brushes used in the experiments are Morgan Crucible grade IM3 and EG8101 brushes, respectively.

The author wishes to thank the Morgan Crucible Co. Ltd. for supplying the brushes, and the authorities of the Royal Military College of Science, Shrivenham, for the facilities made available and for permission to publish the paper.

(13) REFERENCES

(1) MAINER, O. E.: 'Reducing Brush Losses', *Electrical Journal*, 1959, **163**, p. 598.

(2) RICHTER, R.: 'Experimentelle Ermittelung des susaetzlichen Drehmomentes der mehrphasiges staendergespeisten Maschine mit Stromwender', *Elektrotechnik und Maschinenbau*, 1943, p. 333.

(3) MAINER, O. E.: 'Brush Drop when Several Brushes rub on the same Track on a Commutator', *Bulletin of Electrical Engineering Education*, December, 1955, No. 15, p. 13.

(4) MAINER, O. E.: 'Measurement of Effective Stator and Rotor Resistances of Stator Fed Polyphase Commutator Motors', *ibid.*, December, 1959, No. 23, p. 21.

(5) MAINER, O. E., and EDWARDS, J. R.: 'Induction Motor Losses', *Electrical Review*, 1960, **166**, p. 100.

621.319.33:621.317.333.8

The Institution of Electrical Engineers
Monograph No. 376 S
Apr. 1960
©

CALCULATION OF THE CURRENT IN NON-LINEAR SURGE-CURRENT-GENERATOR CIRCUITS

By T. F. MONAHAN, B.Sc., Member.

(*The paper was first received* 15*th August*, 1959, *and in revised form* 18*th January*, 1960. *It was published as an* INSTITUTION MONOGRAPH *in April*, 1960.)

SUMMARY

Surge-current generators are used to test non-linear resistors and surge diverters. Although the circuit is basically very simple, it is possible to calculate the surge current only by numerical solutions of the differential equation for particular values of the parameters. The paper gives the results of such calculations made at Manchester University on the differential analyser and the electronic computer. The application of the results to certain practical problems is discussed.

LIST OF SYMBOLS

C, L = Equivalent capacitance and inductance of surge-current generator.
R = Resistance of surge-current generator.
R_c = Critical resistance.
V = Charging voltage of surge-current generator.
i, i' = Instantaneous current in circuit and its generalized value.
t, t' = Time, and its generalized value.
v = Instantaneous voltage across non-linear resistor.
K, β = Constants defining the non-linear resistor according to the relation $v = Ki^{\beta}$.
i_p, i'_p = Peak current and its generalized value.
v_p = Peak voltage across non-linear resistor.
t_f, t'_f = Nominal wavefront and its generalized value.
t_t, t'_t = Nominal wavetail and its generalized value.
B = Generalized constant defining the non-linear resistor by the relation $B = KV^{(\beta-1)}(C/L)^{\beta/2}$.

(1) INTRODUCTION

A surge-current generator designed to test non-linear resistors and surge diverters can usually be considered to have the simple equivalent circuit shown in Fig. 1. In order to determine the capacitance, inductance and charging voltage required to produce a specified current and waveshape in a given non-linear resistor, it is necessary to solve a non-linear differential equation. This cannot be done analytically, but numerical or graphical solutions can be obtained for particular values of the circuit parameters. This has been done on the differential analyser and the electronic computer at Manchester University. The results cover the range of circuit parameters likely to be met when carrying out tests (other than the rectangular wave test) on surge diverters to B.S. 2914: 1957 and when doing development work on non-linear resistors and surge diverters.

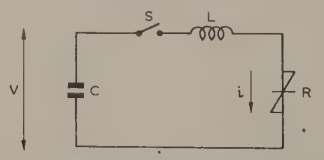

Fig. 1.—Equivalent circuit of surge-current generator.

(2) METHOD OF CALCULATION

The equivalent circuit of a surge-current generator and its load is shown in Fig. 1; it consists of a capacitor, C, an inductance, L, a switch, S, and a non-linear resistance, R. The initial voltage on the capacitor is V, and when the switch is closed the differential equation of the circuit is

$$L\frac{di}{dt} + \int \frac{i}{C}dt + Ki^{\beta} = V \quad . \quad . \quad . \quad . \quad (1)$$

This can be put in more general form by writing

$$i = V\sqrt{\frac{C}{L}}i' \quad . \quad . \quad . \quad . \quad . \quad . \quad . \quad (2)$$

and

$$t = \sqrt{(LC)}t' \quad . \quad . \quad . \quad . \quad . \quad . \quad . \quad (3)$$

giving

$$\frac{di'}{dt'} + \int i'dt' + Bi'^{\beta} = 1 \quad . \quad . \quad . \quad . \quad (4)$$

where

$$B = KV^{(\beta-1)}\left(\frac{C}{L}\right)^{\beta/2} \quad . \quad . \quad . \quad . \quad . \quad (5)$$

When numerical values of B and β are inserted in eqn. (4) it can be solved in graphical or numerical form. This was originally done on the differential analyser at Manchester University for $\beta = 0{\cdot}2$, $0{\cdot}25$ and $0{\cdot}3$ and for values of B up to $1{\cdot}5$. Later the range of solutions was extended, using the electronic computer at Manchester University, to cover $\beta = 0{\cdot}15$ and $0{\cdot}35$ and values of B up to 2.

It should be noted that the representation of the non-linear resistance by the equation $v = Ki^{\beta}$ is not sufficient when the sign of i changes. In order to comply with the physical properties of the material it is necessary to specify that the sign of i^{β} shall always be taken as the same as the sign of i. Correspondingly, the signs of i'^{β} and i' must always be taken as the same.

(3) RESULTS

The results for $\beta = 0{\cdot}2$ are plotted as curves of i'/t' in Fig. 2, and the other results are given in Table 1.

The curve for $B = 0$ is an undamped sine wave and has been plotted from trigonometrical tables.

For most purposes it is unnecessary to know the detailed shape of the curves, only the crest values of i' and the values of t' corresponding to the wavefront and wavetail. Crest values of i' are plotted against B, for each value of β, in Fig. 3. Nominal wavefronts and wavetails (measured as shown in Fig. 4) are plotted against B in Fig. 5. Except for the larger values of B, the influence of β on the wavefronts and wavetails is small and mean curves have been drawn which apply, within about $\pm 3\%$, to all values of β from $0{\cdot}15$ to $0{\cdot}35$.

Correspondence on Monographs is invited for consideration with a view to publication.
Mr. Monahan is with A.E.I. Pty., Ltd., Melbourne, Australia, and was formerly with the Metropolitan-Vickers Electrical Co., Ltd.

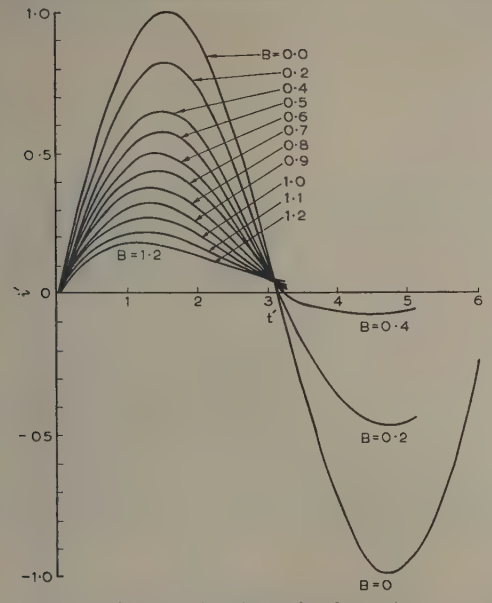

Fig. 2.—Waveshapes for $\beta = 0{\cdot}2$.

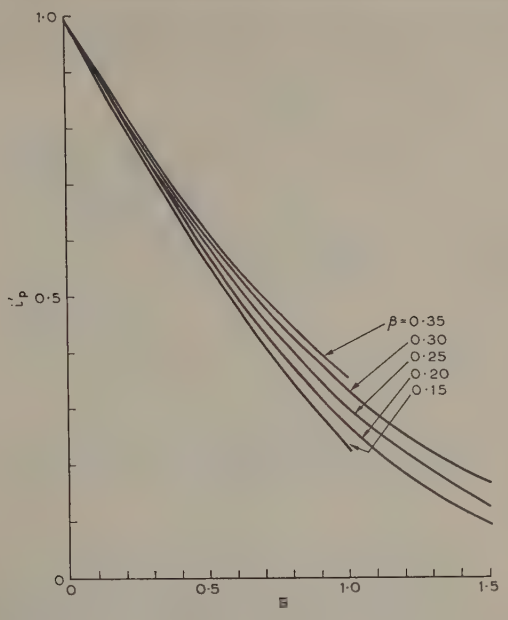

Fig. 3.—First positive peak values of i'.

Table 1

WAVESHAPE PARAMETERS FOR VARIATIONS IN B AND β

B	i'_p	Wavefront		Nominal wavetail	Nominal ratio of tail to front
		Actual	Nominal		
		microsec	microsec	microsec	
		$\beta = 0{\cdot}15$			
0·2	0·817	1·54	1·26	2·64	2·09
0·6	0·484	1·48	1·15	2·57	2·24
1·0	0·228	1·28	0·99	2·50	2·53
2·0	0·009 67	0·35	0·137	—	—
		$\beta = 0{\cdot}25$			
0·25	0·793	1·53	1·22	2·61	2·13
0·3	0·740	1·52	1·21	2·60	2·15
0·4	0·664	1·50	1·17	2·58	2·20
0·5	0·588	1·46	1·15	2·57	2·25
0·6	0·525	1·43	1·11	2·55	2·29
0·7	0·458	1·39	1·09	2·54	2·33
0·8	0·407	1·33	1·04	2·52	2·43
0·9	0·348	1·29	0·99	2·50	2·52
1·0	0·300	1·24	0·95	2·48	2·62
1·1	0·259	1·19	0·91	2·46	2·72
1·2	0·223	1·14	0·86	2·45	2·84
1·3	0·187	1·08	0·80	2·48	3·10
1·4	0·160	1·02	0·73	2·54	3·49
1·5	0·129	0·97	0·65	2·60	4·00
		$\beta = 0{\cdot}30$			
0·5	0·600	1·42	1·13	2·55	2·26
0·6	0·540	1·40	1·10	2·53	2·30
0·7	0·487	1·37	1·06	2·53	2·38
0·8	0·428	1·34	1·01	2·52	2·49
0·9	0·379	1·29	0·97	2·51	2·58
1·0	0·336	1·24	0·94	2·50	2·67
1·1	0·280	1·20	0·90	2·49	2·77
1·2	0·258	1·15	0·87	2·47	2·82
1·3	0·222	1·10	0·81	2·49	3·07
1·4	0·194	1·04	0·75	2·55	3·40
1·5	0·170	1·00	0·70	2·66	3·80
		$\beta = 0{\cdot}35$			
0·2	0·830	1·54	1·23	2·61	2·12
0·6	0·553	1·38	1·07	2·58	2·41
1·0	0·354	1·24	0·94	2·49	2·67
2·0	0·112 3	0·80	0·532	3·426	6·44

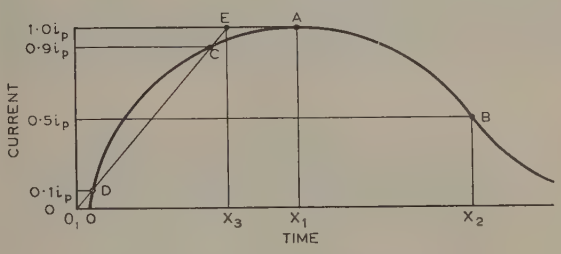

Fig. 4.—Measurement of surge-current wave.

OX_1 = Actual wavefront.
O_1X_3 = Nominal wavefront.
OX_2 = Actual wavetail.
O_1X_2 = Nominal wavetail.

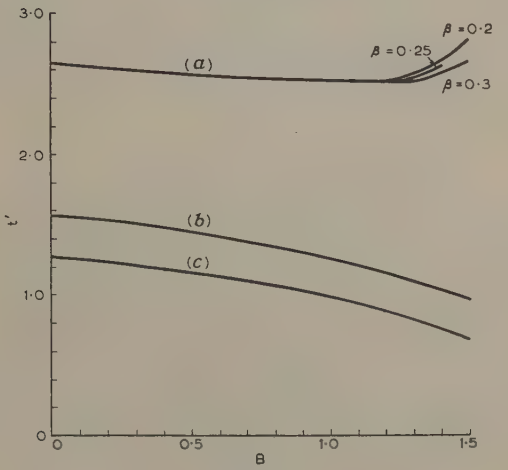

Fig. 5.—Wavefronts and wavetails.

(*a*) Nominal wavetails ($\beta = 0{\cdot}15$ to $0{\cdot}35$).
(*b*) Actual wavefronts ($\beta = 0{\cdot}15$ to $0{\cdot}35$).
(*c*) Nominal wavefronts ($\beta = 0{\cdot}15$ to $0{\cdot}35$).

Fig. 6 shows the ratios of nominal wavetail to nominal wavefront plotted against B. This ratio must usually be kept within specified limits, and the range over which B can be varied for a specified test is therefore limited.

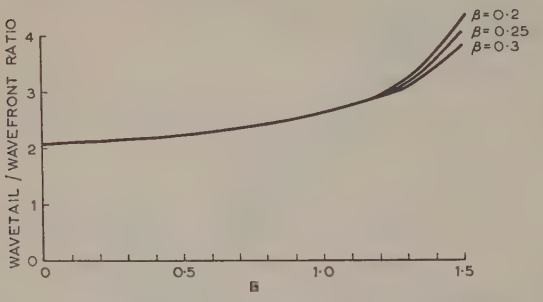

Fig. 6.—Ratio of nominal wavetail to nominal wavefront.
($\beta = 0{\cdot}15$ to $0{\cdot}35$)

(4) COMMENTS ON THE RESULTS

β is a measure of the non-linearity of the resistance material, and for a typical material is approximately $0{\cdot}2$. For a linear resistance $\beta = 1$, and the smaller the value of β the greater is the departure from linearity.

B is a measure of the damping in the circuit; when B is zero the circuit is undamped and the current is sinusoidal. The form of B in a linear circuit can be derived by putting $K = R$ and $\beta = 1$. Then

$$B = R\sqrt{\frac{C}{L}} \quad . \quad . \quad . \quad . \quad . \quad . \quad . \quad (6)$$

But the critical resistance, R_c, is given by $2\sqrt{(L/C)}$, so that

$$B = \frac{2R}{R_c} \quad . \quad . \quad . \quad . \quad . \quad . \quad . \quad (7)$$

Curves such as those of Fig. 2 show clearly the way in which increasing B changes the waveshape from an undamped sine wave to a critically damped wave and then to an overdamped wave. It will be noticed that there is a discontinuity in the slope of the current/time curve at zero current. The physical explanation of this is that the resistance in the circuit is $Ki^{\beta-1}$ and this approaches infinity as i approaches zero, so that the damping near to zero currents is very large.

(5) APPLICATION OF THE RESULTS

(5.1) Variation of Charging Voltage

Suppose that a single-stage surge-current generator has a fixed capacitance C and a fixed inductance L, and suppose that it is discharged through a particular non-linear resistor, so that K and β are fixed. Thus the only variable which can be controlled is the charging voltage, V. For each value of V a value of B can be calculated from eqn. (5). When V is small B will be large and the circuit will be heavily damped. When V is larger B will be smaller and the damping will be less.

For each value of V, and therefore of B, the peak current can be determined from Fig. 3 and eqn. (2), which can be written as a relation between peak values

$$i_p = V\sqrt{\frac{C}{L}}i'_p \quad . \quad . \quad . \quad . \quad . \quad . \quad . \quad (8)$$

Similarly, the nominal wavefront and wavetail can be obtained from Fig. 5 and the equations

$$t_f = \sqrt{(LC)}t'_f \quad . \quad . \quad . \quad . \quad . \quad . \quad . \quad (9)$$

and

$$t_t = \sqrt{(LC)}t'_t \quad . \quad . \quad . \quad . \quad . \quad . \quad . \quad (10)$$

It is not usually permissible to allow the output of a surge-current generator to depart far from a specified waveshape. It is therefore not usually sufficient to control the output current by varying V alone (except over a narrow range) and at least two parameters must be capable of adjustment.

(5.2) Variation of V and K

It is often convenient to choose a value of the charging voltage, V, which would produce an insufficiently damped wave and then to add non-linear resistance in series with that which is being tested until K has been increased to a value which gives the required degree of damping.

The appropriate values of V and K can most easily be found from a family of curves such as those of Fig. 7. These have

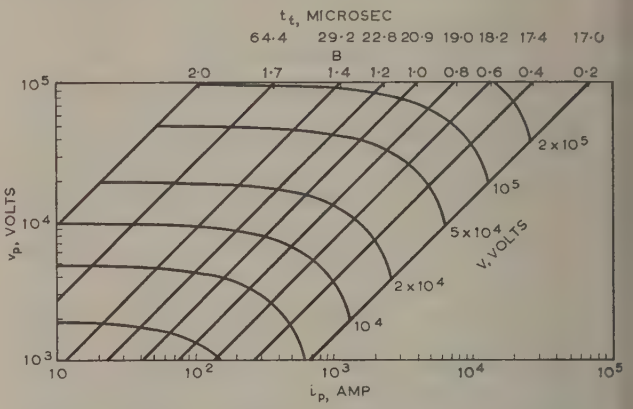

Fig. 7.—Curves for calculation of surge-current-generator output.
$C = 1\,\mu$F, $t_f = 8$ microsec, $\beta = 0{\cdot}2$.

been plotted for a $1\,\mu$F capacitor, a wavefront of 8 microsec (as specified in B.S. 2914: 1957) and $\beta = 0{\cdot}2$.

The peak voltage across the non-linear resistor (including test object and any series resistance) is plotted against the peak current for values of B from $0{\cdot}2$ to $2{\cdot}0$. A scale of charging voltage has been added and also a scale of wavetails.

From these curves it is easy to see whether the required peak current can be obtained from the capacitor without charging it above its rated voltage, and whether the waveshape will be acceptable. If the value of v_p read from the curves exceeds the peak voltage expected across the test object at the peak current, a suitable non-linear series resistance can be added to the circuit. If v_p is less than that expected across the test object the circuit is unsuitable and C must be modified by suitable series-parallel connections of capacitors as described later.

The curves in Fig. 7 are calculated from

$$v_p = Ki_p^{\beta} \quad . \quad . \quad . \quad . \quad . \quad . \quad . \quad (11)$$

Eliminating V, L and K from eqns. (5), (8), (9) and (11) gives

$$v_p = \frac{Bi_p t_f}{Ci_p'^{(1-\beta)}t'} \quad . \quad . \quad . \quad . \quad . \quad . \quad (12)$$

This gives the lines of constant B. Eqns. (5), (8) and (11) give

$$v_p = Bi_p'^{\beta}V \quad . \quad . \quad . \quad . \quad . \quad . \quad (13)$$

This gives the lines of constant V. The values of t_t are obtained from Fig. 6.

(5.3) Series-Parallel Connections of Capacitors

From eqn. (12) it can be seen that the effect of connecting m capacitors in parallel is to multiply the current determined from Fig. 7 by m.

Similarly, the effect of connecting n capacitors in series in a multi-stage generator, without altering the charging voltage, is to multiply by n the value of v_p determined from Fig. 7.

The curves in Fig. 7 can therefore be readily used to find the series-parallel capacitors appropriate in those cases where a single capacitor is inadequate.

(5.4) Variation of Capacitance

If a capacitance differing from that for which Fig. 7 was drawn is used, there is no need to draw a new set of curves. If the capacitance is m times as large, the current corresponding to any particular values of B and v_p will be m times that shown in Fig. 7.

On the other hand, if the new value of capacitance is to be regularly used a new set of curves can be drawn. They will differ from those of Fig. 7 only in being shifted to right or left along the current axis.

(5.5) Variation of Wavefront

Fig. 7 can also be used if a wavefront other than 8 microsec is required, since for given values of B and β the wavefront is inversely proportional to the peak current. For example, the current from a 1 μF capacitor would be double that shown in Fig. 7 if the wavefront were reduced to 4 microsec.

(5.6) Calculation of Inductance

It is usually possible to adjust the inductance of a surge-current generator, although it may not always be possible to reduce it sufficiently to allow the generation of waves having fronts very much shorter than 8 microsec. The appropriate value can be calculated from eqn. (9) using data from Fig. 5.

(5.7) Approximations

The values of v_p, K and β for the non-linear material which is to be tested are often unknown because it is often the purpose of the test to measure them. Moreover, it may be convenient to use a series resistance which has a different β from the test object. Figs. 5 and 6 show that, so long as B is less than unity, the waveshape will not be much affected by departures of β from the assumed value. The peak current is more dependent on β and depends very much on B.

It has been found that a rough calculation based on assumed values of v_p and β is normally sufficient to set up a circuit. If the circuit is adjusted to give $B \simeq 0{\cdot}6$ the current can be brought to the required value by varying the charging voltage, and the waveshape will stay within permitted limits. A number of impulses may be needed before the correct charging voltage is found. On the rare occasions when a sample whose characteristics are not accurately known beforehand must pass the correct current on the first impulse, it is useful to increase the number of stages in the generator to allow the use of a series resistance large enough to swamp the uncertainties in the characteristics of the test object.

Although it has been assumed that any series resistor will be non-linear and have a value of β not greatly different from that of the test object, it has sometimes been found convenient to use a linear series resistor. Even in this case curves such as those in Fig. 7 have been found to be a useful guide to the performance of the circuit.

(6) ACKNOWLEDGMENTS

The differential-analyser solutions were obtained at Manchester University by the late Professor D. R. Hartree. The electronic-computer solutions were obtained on the Manchester University Mark I computer by the Computation Section of the Metropolitan-Vickers Research Department. The author wishes to thank Sir Willis Jackson, Director of Research and Education, A.E.I. (Manchester), Ltd., for permission to publish.

621.396.677.015.34

The Institution of Electrical Engineers
Monograph No. 377 E
Apr. 1960
©

TRANSIENTS IN CYLINDRICAL ANTENNAE

By HANS J. SCHMITT.

(*The paper was first received* 17*th August, and in revised form* 25*th January*, 1960. *It was published as an* INSTITUTION MONOGRAPH *in April*, 1960.)

SUMMARY

The transient response of the radiation field of a driven cylindrical antenna is investigated for the particular case of a step-function excitation. The theoretical analysis makes use of Fourier's theorem to express the response as an integral over the response to all individual frequency components. The response as a function of time shows damped oscillations with a frequency determined by the first resonance frequency of the antenna. The response of the same antenna used as a receiver in a transient plane wave field is shown to be related to the radiation response by a simple integration process. By proper loading of the dipole, transient times of the order of the time needed for a wave to travel along the dipole axis can be obtained. An experimental investigation is described in which the reception of a transient field due to a shock-excited distant transmitter is observed.

LIST OF SYMBOLS

a = Radius of cylindrical antenna.
c = Velocity of light.
h = Half-length of cylindrical antenna.
h_e = Effective half-length of cylindrical antenna.
r, θ, ψ = Co-ordinates of spherical co-ordinate system.
r_1, r_2 = Distances from centre of antenna to reference points.
x, y, z = Co-ordinates of rectangular co-ordinate system.
E = Electric field strength.
E_0 = Amplitude of incident electric field.
$E_y^{rad}, E_\theta^{rad}$ = Components of radiated electric field.
$F\left(\theta, \beta h, \frac{a}{h}\right)$ = Field factor of antenna.
I = Current at centre point of driven antenna.
I_L = Current at centre point of receiving antenna.
R_c = Characteristic resistance of connecting cable.
R_g = Internal generator resistance.
R_L = Load resistance of receiving antenna.
V = E.M.F. of driving generator.
V_0 = Amplitude of generator e.m.f.
V_{oc} = E.M.F. at centre point of receiving antenna.
V_L = Voltage across load of receiving antenna.
T = Transient time.
Z_g = Internal impedance of generator.
Z_{in} = Input impedance of cylindrical antenna.
Z_L = Load impedance of receiving antenna.
$\alpha = c\tau/h$ = Relative time scale.
$\beta = 2\pi/\lambda$ = Phase-change coefficient.
ϵ = Permittivity.
ψ' = Expansion parameter.
λ = Wavelength.
μ = Permeability.
ω = Angular frequency.
$r = 2 \log 2h/a$ = Logarithmic measure for relative antenna thickness.
$\tau_1 = t - r_1/c$, $\tau_2 = t - r_2/c$ = Shifted-time-scale co-ordinates.

Correspondence on Monographs is invited for consideration with a view to publication.
Mr. Schmitt is in the Gordon McKay Laboratory, Harvard University, Massachusetts.

(1) INTRODUCTION

For a harmonic time dependence of the excitation the radiation properties and circuit properties of linear antennae are found by solving the time-independent Maxwell equations with the appropriate boundary conditions at the driving point or load point and on the surface of the antenna.[1,2] Important applications of antennae, however, involve the situation where, at a certain time t_0, one or more of the boundary conditions (usually the exciting voltage or field) are rapidly changed. Whenever such a change is made, transient oscillations occur in the antenna due to the finite bandwidth of the system. These transient currents provide the continuous transition from the stationary distribution of charges and currents in the state I for $t < t_0$ to the final distribution of charges and currents in the state II long after the change in conditions is effected.

Practical cases involving transients in antennae include sudden changes in the driving voltage, such as in the transmission of short pulses, and rapid non-periodic changes of the exciting field at a receiving antenna such as are encountered in lightning or similar electromagnetic disturbances. Another application where use is made of transient oscillations in antennae is the generation of millimetre waves by spark-excited small particles in the so-called 'mass generator'.

(2) RECIPROCITY RELATION BETWEEN TRANSMITTING AND RECEIVING ANTENNAE

In the steady state the radiation field of a centre-driven electric dipole of length $2h$ and wire radius a [Fig. 1(*a*)] is given by[3]

$$E_\theta^{rad} = \frac{jI\sqrt{\frac{\mu}{\epsilon}}}{2\pi r_1} F\left(\theta, \beta h, \frac{a}{h}\right) \varepsilon^{-j\beta r_1} \quad . \quad . \quad . \quad (1)$$

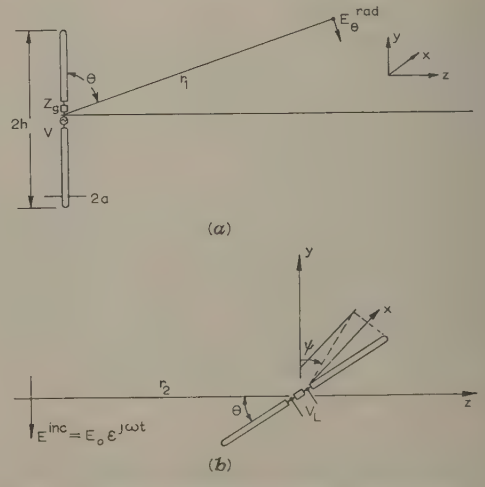

Fig. 1.—Geometrical configuration of the antennae.
(*a*) Driven antenna.
(*b*) Receiving antenna.

n terms of the e.m.f. of the driving generator $V = V_0\varepsilon^{j\omega t}$ and ith $\sqrt{(\mu/\epsilon)} = 120\pi$ ohms the radiation field becomes

$$E_\theta^{rad} = \frac{jV_0 60}{Z_{in}+Z_g}\mathrm{F}\left(\theta, \beta h, \frac{a}{h}\right)\frac{\varepsilon^{j\omega[t-(r_1/c)]}}{r_1} \quad . \quad . \quad (2)$$

If the same antenna, used as a receiver, is placed at the origin f the co-ordinate system, inclined against the direction of the lectric vector of an incident linearly polarized plane wave by ngles θ and ψ [Fig. 1(*b*)] the induced open-circuit voltage V_{oc} t the terminals of the antenna is, by definition of the 'effective alf-length' h_e (see Reference 3, p. 467),

$$V_{oc} = -2h_e\left(\theta, \beta h, \frac{a}{h}\right)E_0\varepsilon^{j\omega[t-(r_2/c)]}\cos\psi \quad . \quad . \quad (3)$$

he term $\varepsilon^{-j\omega r_2/c}$ gives the phase measured against a point in pace at a distance r_2 from the centre of the dipole. By the pplication of Thévenin's theorem the induced current through ne load and the voltage V_L across the load impedance becomes

$$_L = \frac{V_L}{Z_L} = \frac{V_{oc}}{Z_{in}+Z_L} = \frac{-2h_e\left(\theta, \beta h, \frac{a}{h}\right)}{Z_{in}+Z_L}E_0\varepsilon^{j\omega[t-(r_2/c)]}\cos\psi \quad (4)$$

Applying the Rayleigh–Carson reciprocity theorem it can be roved (see Reference 3, p. 570) that it always holds that

$$\mathrm{F}\left(\theta, \beta h, \frac{a}{h}\right) = \beta h_e\left(\theta, \beta h, \frac{a}{h}\right) \quad . \quad . \quad . \quad (5)$$

e. the receiving pattern and the transmitting pattern are the ame for a given antenna.

Upon differentiating eqn. (4) with respect to time and using qn. (5) it is seen that, in the special case when $Z_L = Z_g$,

$$\frac{\partial I_L}{\partial t} = -2jE_0 c\frac{\beta h_e\left(\theta, \beta h, \frac{a}{h}\right)}{Z_{in}+Z_g}\varepsilon^{j\omega\tau_2}\cos\psi$$

$$= \frac{-2E_0 c r_1\cos\psi}{V_0 60}\varepsilon^{j\omega(\tau_2-\tau_1)}E_\theta^{rad} \quad (6)$$

hus the response of a receiving antenna differentiated with espect to time is proportional to the time dependence of the adiated electric field at a fixed point in space given by θ and ψ. he constant of proportionality depends neither on the particular ntenna size nor on the frequency. If the excitation is of non-nusoidal time dependence, the signal may be represented by s Fourier spectrum, and since eqn. (6) holds for any single omponent, it also holds for the composite signal. Hence, with knowledge of the induced current I_L on a receiving antenna ue to an incident wave of arbitrary time dependence, the adiated field of an identical transmitting antenna excited by a oltage of the same time dependence can be computed directly y differentiation. If the radiated transient field of a driven ntenna is known, the transient current in a receiving antenna an be computed by integration.

(3) TRANSIENT RESPONSE

As a particular case, the broadside ($\theta = 90°$, $\psi = 0°$) radia-on from a dipole excited by a voltage that is a step function i its time dependence is considered. The Fourier representation f the voltage step is

$$V(t) = \frac{V_0}{2} + \frac{V_0}{\pi}\int_0^\infty \frac{\sin\omega t}{\omega}d\omega \quad . \quad . \quad . \quad . \quad (7)$$

where the sudden rise in the signal occurs at $t = 0$ at the dipole centre. The field due to transient currents is defined by

$$E(t) = E_{trans}(t) + E_{II}(t) \quad . \quad . \quad . \quad . \quad . \quad (8)$$

where $E(t)$ is the actual field under investigation at any time $t > 0$ and $E_{II}(t)$ is the final field in the new steady state II after the transient part has died out. Since it is known that the radiation field is zero for static excitation, $E_{II}(t)$ vanishes and the total field is due to transient currents only.

For a driving voltage of time dependence sin ωt, the response is given by the imaginary part of eqn. (2). Thus, owing to the linearity of all components, the application of eqn. (7) to eqn. (2) yields for the broadside radiation field of a dipole excited at the time $t = 0$ by a voltage step

$$E_\theta^{rad}(t) = E_y^{rad}(t) = \frac{60V_0}{\pi r_1}\mathscr{I}\left[\int_0^\infty \frac{j\beta h_e\left(90°, \beta h, \frac{a}{h}\right)\varepsilon^{j\omega\tau_1}}{(Z_{in}+Z_g)\omega}d\omega\right] \quad (9)$$

Let the variable of integration be changed from ω to $\beta h = \omega h/c$.

$$E_\theta^{rad}(t) = \frac{V_0 60}{r_1\pi}\left[\int_0^\infty A(\beta h)\cos\beta h\left(\frac{c}{h}\tau_1\right)d\beta h + \int_0^\infty B(\beta h)\sin\beta h\left(\frac{c}{h}\tau_1\right)d\beta h\right] \quad (10)$$

$$\begin{matrix}A(\beta h)\\ [B(\beta h)]\end{matrix} = \mathscr{I}\left[\mathscr{R}\right]\left[\frac{j\beta h_e\left(90°, \beta h, \frac{a}{h}\right)}{(Z_{in}+Z_g)\beta h}\right]$$

The retardation of the total response at the point of observation is contained in $\tau_1 = t - \frac{r_1}{c}$.

Since the spectrum of the applied step-function signal extends to infinite frequencies, the integrations in eqn. (10) have to be extended to infinity. However, numerical values of the input impedance and the complex effective length from the second-order expansion (Reference 3, pp. 154 and 488) or the variational solution[2,4] are known only up to $\beta h \simeq 5$, thus just including the second resonance frequency of a centre-driven dipole of length $2h$. For a particular ratio of thickness to length of the antenna $a/h = 1/904$ [$\Omega = 2\log(2h/a) = 15$] and zero generator impedance, the quantities $A(\beta h)$ and $B(\beta h)$ are plotted as a function of βh in Fig. 2. It is seen that the values decrease sufficiently with increasing βh (increasing frequency for fixed antenna length) so that the integration may be discontinued at $\beta h \simeq 5$ without introducing a large error.

In order to obtain some quantitative results for the transient response due to a step-function input signal, the integrations (10) have been carried out graphically by means of a planimeter for different values of τ_1. The computed response of the far-zone field, assuming a generator with negligible internal impedance ($Z_g = 0$), is plotted in Fig. 3. The abscissa is the dimensionless quantity

$$\alpha = \frac{c\tau_1}{h} = \frac{c}{h}\left(t - \frac{r_1}{c}\right)$$

The quantity α measures the time in terms of the time required by an electromagnetic wave to travel a distance h, i.e. from the dipole centre to the tips of the dipole. It is seen that the main part of the signal starts at an instant $\alpha = 0$, and thus with a retardation r_1/c. For positive values of α the response jumps rather rapidly from positive to negative values, resembling a pulse-shaped curve. It can be seen from Fig. 2 that the main

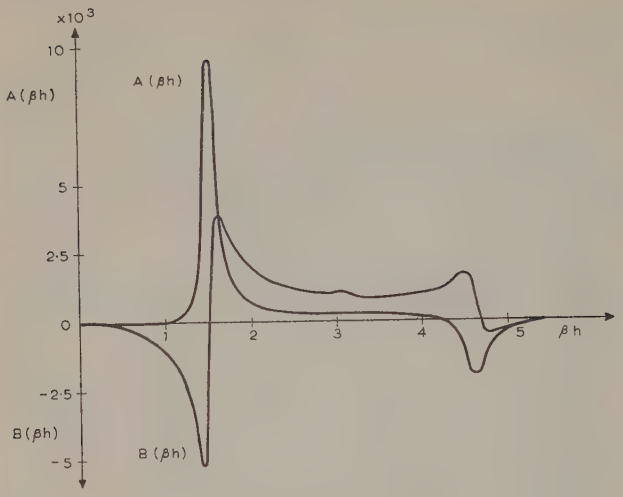

Fig. 2.—$A(\beta h)$ and $B(\beta h)$ for $\Omega = 15$.
Numerical values from King–Middleton expansion, $Z_g = 0$.

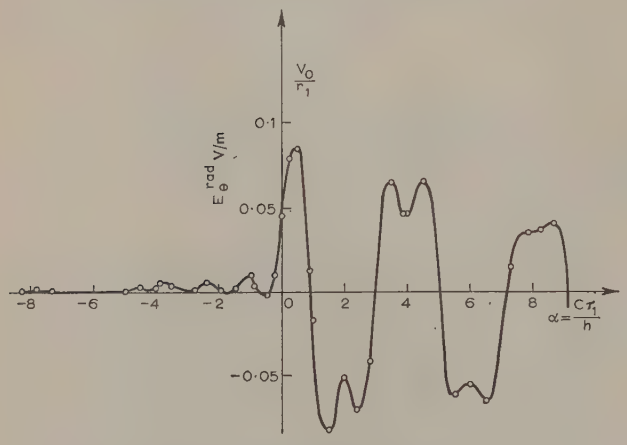

Fig. 3.—Far-zone field response of a cylindrical antenna to step-function driving signal ($\Omega = 15$, $Z_g = 0$).

contributions to the response come from the first and second resonance peaks at $\beta h = \pi/2$ and $3\pi/2$, corresponding to a fundamental frequency and its second harmonic. These are also the leading terms in the spectrum of a simple pulse function. It should be noted that the response plotted over α is independent of the particular length of the antenna and should be identical for a very short antenna (Hertzian dipole) or a very long antenna. Physically, the response can be explained by making use of the close analogy between the electric dipole antenna and an open-ended 2-wire transmission line. In the first moment after the switching operation, $0 < \alpha < 1$, positive charges travel in one arm of the dipole towards the antenna tip and negative charges in the other arm (Fig. 4). The associated currents set up a strong electric field in the far zone. At $\alpha = 1$ a reflection of the electromagnetic field associated with the moving charges takes place at the antenna tips, which, by analogy with the open-ended transmission line have a positive reflection factor. Hence, for $1 < \alpha < 2$, charges of the same sign as before travel in the opposite sense and the associated currents are reversed. For $\alpha = 2$ a reflection at the centre of the dipole takes place, where, by analogy with the transmission line, the

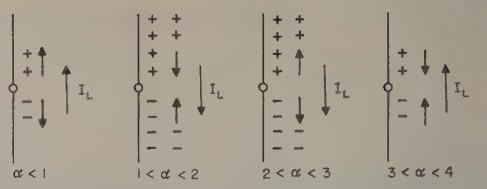

Fig. 4.—Total charges and currents in a step-function-excited transmitting antenna.

lossless generator gives a reflection factor of -1. Hence, for $2 < \alpha < 3$, discharge waves travel from the dipole centre outward, and thus the field remains negative until, at $\alpha = 3$, the direction of the discharge waves is reversed and the whole process starts repeating itself at $\alpha = 4$. The radiation field will have the largest amplitude when the moving discontinuity of charges is close to the antenna tips. It will be weaker if the discontinuity is close to the gap. This explains the marked dip in the response for $\alpha = 2$, and in the succeeding peaks. Owing to the radiation of energy the transient signal at any point of observation dies out after a number of successive maxima and minima.

Owing to the finite velocity of electromagnetic waves no signal should occur for $\alpha < 0$. Strictly, in eqn. (10) the condition

$$\int_0^\infty A(\beta h) \cos \beta h \left(\frac{c}{h}\tau_1\right) d\beta h = \int_0^\infty B(\beta h) \sin \beta h \left(\frac{c}{h}|\tau_1|\right) d\beta h \quad (11)$$

should hold. Since the numerical values of input impedance and effective length of the antenna are derived from non-physical solutions (second-order expansion or variational solution), condition (11) is only approximately fulfilled, giving rise to a small (~10% of the main peak) signal for negative times. This error also includes the effect of the discontinued integration.

From the simplified explanation of the transient process in terms of charges and currents on a transmission line it is evident that the decay of the transient signal can be greatly influenced by the internal impedance of the generator. Investigations have been made for various generator resistances and antenna thicknesses. It is found that the transient time T in terms of a decay of $1/\varepsilon$ of the power decreases first with increasing generator resistance, reaches a minimum at around $R_g = 600$ ohms for $\Omega = 15$ and slowly rises again thereafter. The computed transient response of the far-zone field due to a step-function excitation for the critical value of $R_g = 600$ ohms is plotted in Fig. 5. Apparently the electromagnetic wave, reflected at the

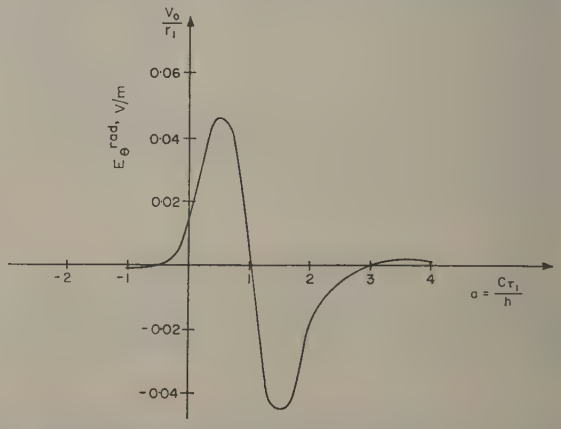

Fig. 5.—Far-zone field response of a cylindrical antenna to step-function driving voltage ($\Omega = 15$, $Z_0 = R_0 = 600$ ohms).

ipole tips and travelling back to the dipole centre is reflection-ree absorbed in the generator resistance. The total transient eld lasts just the time needed for a wave to travel from dipole entre to the tip and back, in complete analogy to the transient ehaviour of an open-ended section of transmission line excited y a generator with an impedance equal to the characteristic esistance of the line. In the zeroth-order antenna theory Reference 3, p. 144) the input impedance of cylindrical antennae s given by the impedance of such an open-ended section of transmission line with a characteristic resistance

$$R_c = \sqrt{\frac{\mu}{\epsilon}} \Big/ 2\pi\psi' = 60\psi' = 60(\Omega - 2)$$

Hence, for $\Omega = 15$, the value of R_c is 780 ohms. This is the ame order of magnitude as deduced from the investigation of the transient process. This simple relation also shows orrectly that, for thicker antennae (smaller values of Ω), the ritical resistance is smaller. Recalling the relation between ransient time T and the bandwidth of any resonant system Δf measured at half-energy points on the resonance curve),

$$T \sim \frac{1}{\Delta f} \quad . \quad . \quad . \quad . \quad . \quad . \quad (12)$$

t is apparent that a driving source with this internal resistance also maximizes the useful bandwidth of the antenna.*

Using the reciprocity relation (6), the response of a centre-loaded receiving antenna to a transient plane-wave field of step-function time dependence (broadside incidence) is easily found by integrating the radiation field response in time. The received transient signal at the centre terminals for $Z_L = 0$ and for a load resistance $R_L = 600$ ohms are plotted in Figs. 6 and 7,

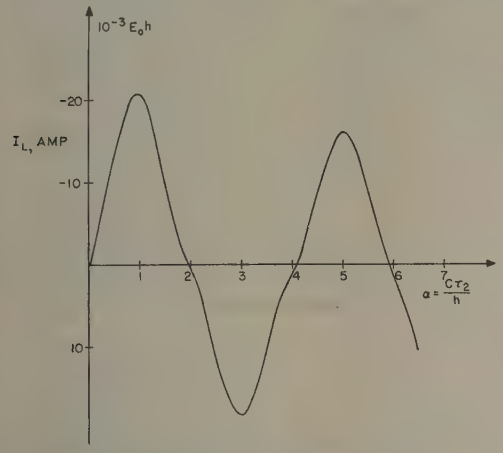

Fig. 6.—Transient response of the current at the dipole centre due to step-function rise in field strength.
Broadside incidence, $Z_L = 0$, $\Omega = 15$, obtained from Fig. 3.

respectively. For the unloaded antenna the response again has the shape of a weakly-damped oscillation with a fundamental frequency determined by the first resonance of the antenna. The decay of the transient signal is entirely due to re-radiation. A physical interpretation of the transient process in terms of charges and currents can be given as follows. Initially, before the arrival of the signal, the antenna is uncharged so that positive and negative charges are equally distributed. In the final steady state for t sufficiently long after the arrival of the step signal, the

* For an antenna loaded at the tips (travelling-wave antenna) the transient time may be less.

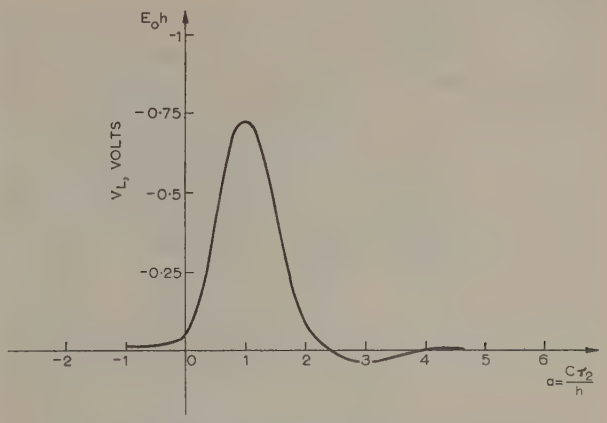

Fig. 7.—Transient response of voltage across load resistor ($R_L = 600$ ohms) due to step-function rise in field strength.
Broadside incidence, $\Omega = 15$.

antenna is in a static field. Thus charges will be induced on the surface of the dipole, concentrated close to the antenna ends and with opposite signs at the lower and the upper end. Analogous to eqn. (8) the distribution of total charges is described for any time $\tau > 0$ by a superposition of the steady-state distribution for t very large and the transient part. Since the total charge is zero for $\tau = 0$, the distribution of charges that give rise to the transient currents in the antenna initially has to be similar to that in the final steady state, but with charges of the opposite signs (see Fig. 8). The relaxation of

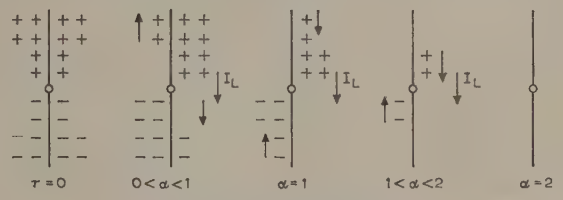

Fig. 8.—Transient currents at the dipole centre, and charges in a loaded receiving antenna.

these charges for $\tau > 0$ corresponds closely to the discharge of a charged section of transmission line.[5]

Particularly interesting is the case when the load impedance corresponds to the characteristic impedance of the equivalent transmission line (Fig. 7). The transient response then shows a single peak with a total transient time exactly twice that needed for a wave to travel from dipole centre to the dipole tips. The instantaneous distribution of charges connected with the transient process* and the current through the dipole terminals are indicated in Fig. 8. The current in the peak at $\alpha = 1$ is very nearly one-half the peak current for the unloaded antenna.

(4) EXPERIMENTS

Since no ideally broad-band field probes or transmitters are available, the radiated electric field of a shock-excited dipole antenna and the received voltage of an incident wave that is a step function cannot easily be investigated experimentally. However, the combined reception of a transient signal due to a transient-excited transmitter forms a complete system that can

* In order to obtain the total charges the distribution in the steady state II has to be superimposed.

be realized experimentally and may serve as a check on the accuracy of the computations.

For one particular case, $R_L = 120$ ohms and $Z_g = 0$ (impedanceless generator), the transient voltage across the load of the receiving antenna due to a step-function excitation at $t = 0$ of the distant transmitting antenna has been computed by combining eqns. (2) and (4) and subsequent graphical integration. Again $\Omega = 15$ is chosen and both dipoles are equal in length and parallel to each other. The total response, as calculated from numerical values of the variational solution, is plotted in Fig. 9. The electric field radiated from the distant transmitter is the one represented in Fig. 3. It arrives at the time $\tau_1 = (t - r_1/c) = 0$ at the loaded receiving antenna and induces the transient voltage V_L, which shows almost a sinusoidal character. The total attenuation of the transient signal is due to the overall decrease in the incident field, to re-radiation, and to losses in the load resistance. Since the antennae are assumed to be in the far zone with respect to each other, no mutual coupling is included. The response shown in Fig. 9 is independent of the antenna length, since an ideal step-function input signal is assumed. Only the amplitude of the transient response is linearly proportional to the antenna length.

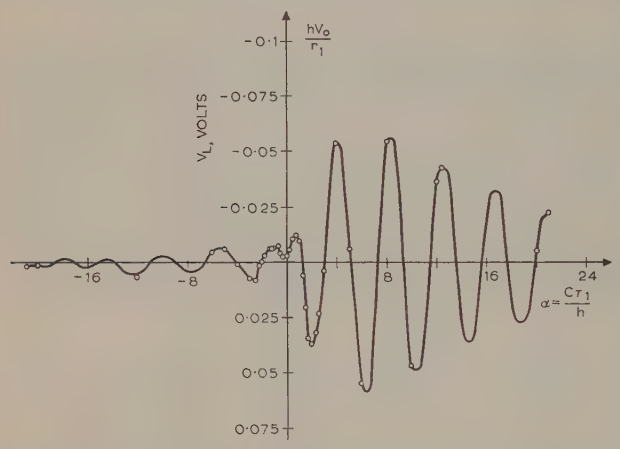

Fig. 9.—Transient voltage across load resistance of receiving antenna in far-zone field of identical antenna excited by step-function voltage.
$\Omega = 15$, $R_L = 120$ ohms, $Z_g = 0$.

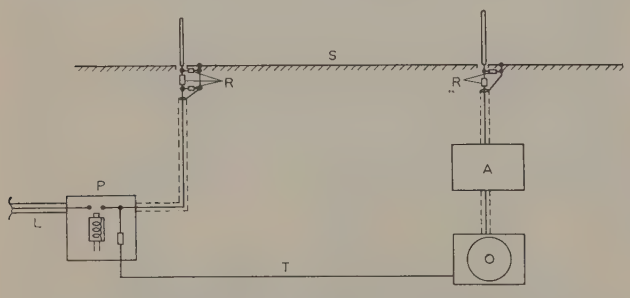

Fig. 10.—Experimental arrangement for measuring transient responses from cylindrical antennae.
S = Ground screen.
R = Resistive networks.
P = Fast-rise pulse generator.
L = Pulse-forming line.
A = Wide-band chain amplifiers.
O = Oscillograph.
T = Trigger line.

For the experiment, the arrangement shown schematically in Fig. 10 was used. The main parts consist of a large 24 × 48 ft metallic earth screen on top of the laboratory building, and two metallic rods of variable length as cylindrical antennae. The transmitting antenna is fed by a Spencer Kennedy fast-rise pulse generator. The rectangular d.c. pulse output is generated by connecting a previously charged coaxial line through a mercury switch to a load resistance equal to the characteristic resistance of the charged line. In the experiment a very long pulse-forming coaxial line has been used so that the negative step occurs at a time when the primary transient process due to the sudden rise in the signal has long decayed. The voltage step with a rise time of less than 1 millimicrosec is about 150 volts, and the repetition rate is 130 pulses/sec. It is fed through a long coaxial cable of matched characteristic resistance ($R_c = 50$ ohms) to the driven antenna above the earth screen. Between antenna and coaxial line a resistive network is used to match the coaxial line* and to represent different generator resistances for the antenna. Account is taken of the fact that antenna and resistance have an image in the earth screen, so that load and generator resistances are actually twice the value represented by the network. Since the voltage step has a finite rise time, care has to be taken to make this fact unimportant for a comparison with the theoretical response. The criterion here is that the rise time should be short compared with the time a wave needs to travel along the antenna. With an antenna length of 121 cm (travel time from centre to top of about 4 millimicrosec) this condition is reasonably well fulfilled.

The receiving dipole is located at a distance of about 4 m from the driven antenna with its axis parallel to it. The received signal is fed through a resistive network to represent different loads into a long coaxial cable with $R_c = 120$ ohms. The signal is amplified in several wide-band chain amplifiers with a cut-off frequency of 300 Mc/s, and finally fed directly to the vertical deflection plates of a high-speed oscillograph. The sweep of the instrument has a minimum deflection time of 10 millimicrosec/cm and is externally triggered by a small fraction of the pulse output from the pulse generator.

To test the total equipment the two coaxial lines leading to and from the antennae were connected directly, and the pulse obtained was photographed. The rise time was about 1 millimicrosec, with some small oscillations on the top, which were found to be due to transients in the resonant circuit formed by the capacitance of the deflection plates and the lead inductances of the oscillograph. Several images of this pulse due to reflections could be seen on the oscillograph; all of these images, however, arrive at a much later time.

In the first experiments all conditions assumed for the theoretical curve (Fig. 9) were realized. The impedance looking from driven antenna into the generator was adjusted to 10 ohms, which is negligible compared with the real part of Z_{in} at almost any frequency. The load resistance at the receiver side was 120 ohms. With a brass rod of radius $a = \frac{1}{16}$ in (1·52 mm), $\Omega = 14{\cdot}7 - 15$. The photographed response with different sweep times is shown in Fig. 11. It is apparent that it shows the same overall character as the theoretically computed response in Fig. 9. The time for one complete transient oscillation can best be read from the picture with a sweep speed of 20 millimicrosec to be about 16·5 millimicrosec, which compares with the theoretical value of 16·7 millimicrosec. Also, the typical shape of the build-up of the transient oscillations is clearly indicated. The first peak (owing to phase reversal it appears in the positive direction) is much smaller than the ensuing peaks. An evaluation of T for a decrease to $\varepsilon^{-1/2}$ of the largest amplitude gives

* Actually, this would not be necessary since a sufficiently long cable is used so that eventual reflections occur after the primary transient has died out.

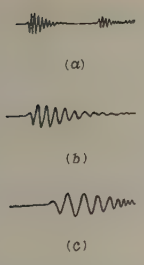

ig. 11.—Transient voltage across load of receiving antenna in far-zone field of an identical antenna excited by step-function voltage.

$\Omega = 14{\cdot}7$.
$R_L = 120$ ohms.
$R_g = 10$ ohms.
$h = 121$ cm.

(*a*) 50 millimicrosec/cm sweep.
(*b*) 20 millimicrosec/cm sweep.
(*c*) 10 millimicrosec/cm sweep.

0·5 and 68 millimicrosec from theory and experiment, respectively. The amplitude of the received signal has been measured nd agrees to within 1 dB with the theoretical value.*

In order to investigate whether the antenna length is already ufficient, in view of the finite rise time of the pulse, the response as been measured for different antenna lengths. It was found hat, with decreased antenna length, differences between theory

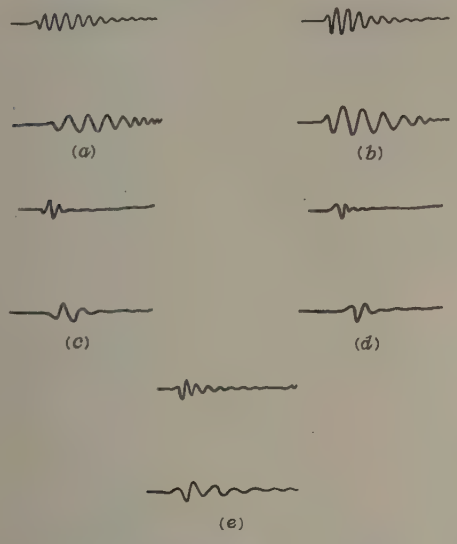

Fig. 12.—Transient voltage across load of receiving antenna in the far-zone field of an identical antenna excited by step-function voltage.

$\Omega = 14{\cdot}7$.
$h = 121$ cm.

Sweep rate 20 and 10 millimicrosec/cm.

(*a*) $R_L = R_g = 30$ ohms.
(*b*) $R_L = R_g = 120$ ohms.
(*c*) $R_L = R_g = 400$ ohms.
(*d*) $R_L = R_g = 800$ ohms.
(*e*) $R_L = R_g = 3\,000$ ohms.

and experiment occur only if antenna length and the product of rise time of the pulse and phase velocities become comparable.

* On the 10 millimicrosec/cm sweep position, the sweep was found to be not exactly linear, showing the correct deflection rate only very close to the starting-point, as can be seen from the photographed response. In the picture taken with 50 millimicrosec/cm deflection, the transient due to the negative step of the rectangular pulse enters the picture. This step is not quite so sharp and gives a somewhat smaller response signal.

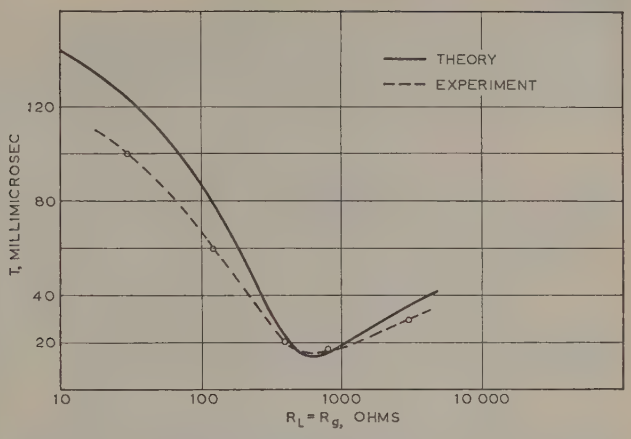

Fig. 13.—Transient time of voltage across load induced by distant transmitter excited with voltage step.

$\Omega = 15$.
$h = 121$ cm.

In the next series of measurements the dependence of T on the generator and load resistances is investigated for antennae with $h = 121$ cm and $\Omega \simeq 15$. The resistive networks are adjusted in each case to give the same resistances, presented from the antennae to the networks ($R_L = R_g$). The photographed responses are shown in Fig. 12. The period of transient oscillations is in all cases about equal. The total transient time is seen to be critically dependent on the load impedances. The transient times measured from these photographs are plotted in Fig. 13, and, for comparison, the transient times obtained theoretically are included. Because of the inaccuracy in reading the $\varepsilon^{-1/2}$ amplitude decrease from the photographs, the agreement cannot be expected to be more than qualitative. However, the expected minimum of the transient time is clearly indicated in the measured results, and the position of the minimum at about 600 ohms agrees well with the approximate theory.

(5) CONCLUSIONS

From a comparison of the experimental results and the theoretically computed curve for the response in the combined transmission-reception case the conclusion can be drawn that the theory adequately describes the transient process in a cylindrical antenna. Because of the close agreement between the values obtained from the variational method and those from the second-order King–Middleton expansion, this applies to both theoretical formulations.

It is found that, in order to minimize the transient time of cylindrical antennae, they should be loaded with a resistance of about 600 ohms for practical antennae ($\Omega = 15$). This will be important in all cases where a correct transmission of wide-band signals is desired. It is, however, at the cost of sensitivity, particularly in the case of a driven antenna.

If interest lies rather in the generation of long sustained transient oscillations, impedanceless generators should be used, such as would be approximated by a spark between the narrow terminals in a driven antenna. Thin wires should also be used.

For the analysis of general transient processes it could be shown that only the receiving or transmitting case has to be investigated, since each case is connected to the other one by a differentiation or integration process.

(6) ACKNOWLEDGMENT

The author is indebted to Professor R. W. P. King for his support of this work and stimulating discussions. Thanks are due to Mrs. B. Hayes for carrying out part of the numerical work.

(7) REFERENCES

(1) KING, R. W. P., and MIDDLETON, D.: 'The Cylindrical Antennas; Current and Impedance', *Quarterly of Applied Mathematics*, 1946, **3**, p. 302.

(2) STORER, J. E.: 'Variational Solution to the Problem of the Symmetrical Cylindrical Antenna', Technical Report 101, Cruft Laboratory, Harvard University, February, 1950.

(3) KING, R. W. P.: 'The Theory of Linear Antennas' (Harvard University Press, 1956), p. 529.

(4) SCHMITT, H. J.: 'Transients in Cylindrical Antennas', Technical Report 296, Cruft Laboratory, Harvard University, January, 1959.

(5) WAGNER, K. W.: 'Elektromagnetische Ausgleichsvorgaenge in Freileitungen und Kabeln' (B. G. Teubner Verläg, 1908).

621.313.1.011.1

The Institution of Electrical Engineers
Monograph No. 378 S
May 1960
©

A NEW FORM OF THE TENSOR EQUATIONS OF ELECTRICAL MACHINES

By G. S. BROSAN, Ph.D., B.Sc.(Eng.), Member.

(*The paper was first received* 23*rd March*, 1959, *and in revised form* 22*nd January*, 1960. *It was published as an* INSTITUTION MONOGRAPH *in May*, 1960.)

SUMMARY

Previous tensor methods applied to electrical engineering systems have been based on Lagrange's equations, which are not always suitable for non-holonomic systems. As a consequence, the defining equations lose much of their simplicity and the component terms in the equations may no longer be tensors.

The paper presents a new set of equations based on the principle of least curvature. These equations are suitable for both holonomic and non-holonomic systems, and their application is shown by examples.

(1) INTRODUCTION

Recent papers[1, 2] have set out very concisely the classical equations of electrical machinery expressed in tensor form, these equations having been first propounded by Kron in 1936. Kron showed that it was possible to set up, using tensor notation, equations that correctly represented the performance of a large variety of networks or rotating machines. Once such tensor equations have been set up, it is possible to find the equations of any machine or any group of machines by a largely routine method, i.e. by inserting into the general equations the particular constants applicable to the machine it is desired to analyse. Examples of this method are abundant in current literature. If the method of analysis and the physical phenomena involved have been appreciated, it is not necessary to deal with each case *ab initio*; the same tensor equations, which may be set up for the simplest possible machine, are valid for several types of connections.

Electrical machine analysis consists essentially in the derivation of equations of performance for the purpose of predicting as accurately as possible the characteristics of the various types of machine. Comprehensive analysis of an ideal machine is difficult to achieve, both because of the segregation of the problems involved and also because of a more fundamental difficulty which is dealt with in Section 2.1. In all cases, the electrical elements of the machines under study are considered as constituting a number of linear electrical networks in relative motion, the networks having lumped constants. This assumption is widely made and is justified by comparison of the predicted and experimental results.

(2) DESCRIPTION OF KRON'S METHOD

(2.1) Principles

For convenience and easy extension of tensor methods to complicated problems Kron makes a detailed analysis of the simplest machine, known as the primitive machine. The equations of the primitive machine are first developed from the fundamental laws of electrodynamics; then, by setting up a connection tensor between the primitive machine and the machine under study, the equations of the latter can be established in a routine manner. The study of all rotating machines in Kron's method thus consists of three fundamental steps:

(*a*) The establishment of equations of the primitive machine.
(*b*) The establishment of the connection tensor showing how the given machine differs from the primitive machine.
(*c*) The determination of the equations of performance of the machine under study.

Step (*a*) presents no difficulty; in any case, it has been done once and for all. (*b*), on the face of it, also presents no difficulty; connection tensors for various types of machine and windings are given in Reference 3. On approaching step (*c*), however, a complication becomes apparent, namely that the equation to be used will depend on the type of axes (or reference frames in general) which have been adopted. The equations of performance, as well as the transformation formulae, are considerably different for the different frames of reference and it is also disconcerting to realize that, of the terms in the equation, some may not even be tensors. With such a situation, it is not surprising that the limitations of the method should be investigated. This has been done extensively in Reference 6.

(2.2) Dynamical Basis of Kron's Method

It is well known that the standard theory of classical dynamical systems is applicable to the analysis of stationary networks, and that the form of the equations is invariant under a change of co-ordinates. Section 8 gives the equations in tensor form. On identifying charge with displacement and current with velocity, for a system without electrostatic charges Lagrange's function is

$$\mathscr{L} = T = \tfrac{1}{2}L_{\alpha\beta}i^{\alpha}i^{\beta} \quad . \quad . \quad . \quad . \quad . \quad (1)$$

The Rayleigh dissipation function is

$$\mathscr{R} = \tfrac{1}{2}R_{\alpha\beta}i^{\alpha}i^{\beta} \quad . \quad . \quad . \quad . \quad . \quad . \quad (2)$$

and the generalized force may be identified with the voltage in this case.

Consequently, Lagrange's equation

$$\frac{d}{dt}\left(\frac{\partial\mathscr{L}}{\partial\dot{x}^{\gamma}}\right) - \frac{\partial\mathscr{L}}{\partial x^{\gamma}} + \frac{\partial\mathscr{R}}{\partial\dot{x}^{\gamma}} = F_{\gamma} \quad . \quad . \quad . \quad . \quad (3)$$

becomes

$$\frac{d}{dt}(L_{\alpha\beta}i^{\alpha}) + R_{\alpha\beta}i^{\alpha} = V_{\beta} \quad . \quad . \quad . \quad . \quad (4)$$

which is the equation of voltage in circuits containing resistances and inductances.

The invariant form of these equations is preserved under transformation of the co-ordinates of the form

$$i^{a} = C^{a}_{\alpha}i^{\alpha} \quad . \quad . \quad . \quad . \quad . \quad . \quad . \quad (5)$$

where the connection tensors, C^{a}_{α}, are not functions of either the currents, i^{a}, i^{α}, or of the time, t.

In this case the components of the connection tensor are often determinable from mere inspection of the circuit, and this is an important advantage of the tensor method. But more general transformations are possible, which, in theory at least, could

Correspondence on Monographs is invited for consideration with a view to publication.
Dr. Brosan is Senior Assistant Education Officer, County Council of Middlesex.

depend on both the currents i^a and i^α and the time t. For example, in rotating machines, the slip-ring connections of rotor conductors to the external circuits are such that the connection tensor has constant components; on the other hand, a commutator introduces relations

$$i^a = A^a_\alpha i^\alpha \quad . \quad . \quad . \quad . \quad . \quad . \quad . \quad (6)$$

which are not integrable. Here, i^α are the rotor currents and i^a are the currents in the external windings. The tensor A^a_α is an explicit function of the rotor angle, and in general, therefore, an implicit function of the currents.

It is not possible to use Lagrange's equations in such a circumstance. To overcome the difficulty, Kron resorted to the use of quasi-co-ordinates which are fully discussed in Reference 7, and this led him to electrical equations which were the counterpart of the Boltzmann–Hamel equations of motion in dynamics. But an important restriction remained; the tensor A^a_α was still limited to a function of a geometrical variable only, e.g. in the above case a function of the rotor angle only. Further, the form of the equation was by now somewhat complicated, and this led to its criticism on various grounds.

(3) MORE INVOLVED DYNAMICAL SYSTEMS

(3.1) Classification of Systems

A dynamical system may be classified as (*a*) holonomic or non-holonomic, and (*b*) scleronomic or rheonomic. In (*a*) the kinematical constraints may be relations between the co-ordinates themselves (holonomic) or a non-integrable relation between the differentials of the co-ordinates (non-holonomic), while in (*b*) the kinematical constraints may be explicitly independent of the time (scleronomic) or explicitly dependent on the time (rheonomic).

One fundamental problem in dynamics is the formulation of the equations of motion in the various cases. For holonomic systems, the equations of Lagrange provide the solution. However, when non-holonomic systems are encountered, the Lagrangian equations may only be used in conjunction with the λ-operator methods.

As regards time-dependence, scleronomic systems are covered by the above, but with rheonomic systems another modified form of the Lagrangian equations must be used. Both the kinetic energy and the potential energy in the rheonomic case are dependent on the time, as a result of the time-variation of the kinematic constraints. The total energy of the system is not a constant but changes according to the equation

$$\delta W = \int_{t_2}^{t_1} \frac{\partial \mathscr{L}}{\partial t} dt \quad . \quad . \quad . \quad . \quad . \quad . \quad . \quad (7)$$

where $\mathscr{L}$ is the Lagrangian function depending on the generalized co-ordinates, their time derivatives and the time t. In this case the law of conservation of energy is no longer valid. As may be imagined, non-holonomic auxiliary conditions which are also rheonomic present a problem in which the modification to the simple form of the Lagrangian equations is extensive.

In the tensor theory of electrical machines, the auxiliary conditions are, in general, non-holonomic. This produces extra terms in the differential equations corresponding to the equations of motion which are not tensors, and a great deal of homogeneity and simplicity is lost thereby. For example, in the tensor equation of motion[7]

$$g_{mp}\ddot{x}^m + \left(\frac{\partial g_{pn}}{\partial x^m} - \frac{1}{2}\frac{\partial g_{mn}}{\partial x_p} + 2\Lambda_{pn,m}\right)\dot{x}^m\dot{x}^n = f_p$$

the bracketed expression is not a tensor and the equation is not well suited for general study. Similar remarks apply to time-dependence. However, it should be remembered that the combination of terms on the left-hand side of this equation is a tensor, derived by covariant differentiation of the x^m, and that this procedure is basic in tensor analysis.

The fault, of course, does not lie with the tensor theory, but with the lack of generality implied in the dynamical equations to which the theory was applied. In endeavouring to produce some simplification one is naturally led to consider the principle from which Lagrange's equations may be derived, namely the principle of stationary action. This, however, is not the only variational method which is used in dynamics, and the question arises, whether some other principle would yield the desired alternative approach. The form of this principle would preferably allow for both holonomic and non-holonomic systems, as well as time dependence.

The principle which most nearly parallels that of least action was first formulated by Gauss, using a special form of variation to transform d'Alembert's principle into an actual minimum condition. It is the principle of least curvature, sometimes called the principle of least constraint, and, as will be shown, it yields equations which allow for generalized auxiliary conditions.

(3.2) The Principle of Least Curvature

Consider a general dynamical system, either holonomic or non-holonomic, subject to a number of constraints which may, if necessary, be supposed to depend on the time explicitly. The impressed forces on the system may also be completely arbitrary:

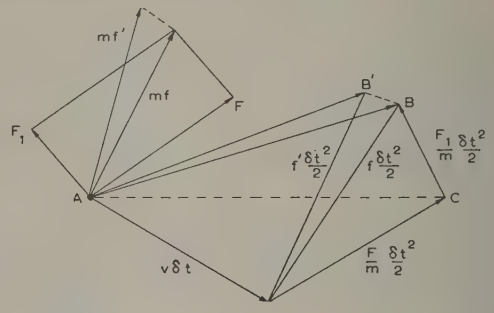

Fig. 1.—Dynamic displacement of a particle.

the constraints are frictionless. Then, with reference to Fig. 1, the displacement of a mass m in an interval of time δt may be expressed as

$$\mathrm{AB} = v\delta t + f\frac{\delta t^2}{2} \quad . \quad . \quad . \quad . \quad . \quad (8)$$

where v and f are the velocity and acceleration vectors respectively.

Let F = resultant of the impressed forces and F_1 = resultant of the constraint forces. Then $F + F_1 = mf$. With the constraint forces removed, the displacement of m would be from point A to a point C such that

$$\mathrm{AC} = v\delta t + \frac{F}{m}\frac{\delta t^2}{2} \quad . \quad . \quad . \quad . \quad . \quad (9)$$

so that $$\mathrm{CB} = \mathrm{AB} - \mathrm{AC} = \left(f - \frac{F}{m}\right)\frac{\delta t^2}{2} = \frac{F_1}{m}\frac{\delta t^2}{2} \quad . \quad (10)$$

The constraint K in the time-interval δt was defined by Gauss according to the equation

$$K = \tfrac{1}{2}\Sigma m(\mathrm{CB})^2 = \tfrac{1}{2}\Sigma (mf - F)^2\frac{\delta t^4}{4} \quad . \quad . \quad (11)$$

and it will now be shown that this quantity is less for the actual trajectory than for any neighbouring trajectory. For, consider a hypothetical displacement AB′ subject to the given constraints and satisfying the given initial conditions. If f' is the acceleration vector in this displacement,

$$\mathrm{AB}' = v\delta t + \tfrac{1}{2}f'\frac{\delta t^2}{2}$$

and consequently $$\mathrm{BB}' = (f' - f)\frac{\delta t^2}{2}$$

Hence $$m(\mathrm{CB})(\mathrm{BB}') = F_1(f' - f)\frac{\delta t^4}{4}$$

Now the velocity v may be expressed in terms of a number of components

$$v_i = a_{ij}\dot{q}^j + b_i \qquad \left.\begin{matrix} i = 1, 2 \ldots n \\ j = 1, 2 \ldots m \end{matrix}\right\} \quad . \quad . \quad (12)$$

where the q^j are general co-ordinates equal in number to the degrees of freedom of the system. Consequently the acceleration may be expressed as

$$f_i = a_{ij}\ddot{q}^j + \theta_i(\dot{q}, q, t) \quad . \quad . \quad . \quad . \quad (13)$$

where θ_i is some function of $\dot{q}$, q and the time t. Since the accelerations f and f' are both compatible with the constraints, corresponding to the same set of values of $\dot{q}$, q and time t, they only differ in the values of $\ddot{q}$. Therefore f' is given by the components $\ddot{q}^j = \Delta\ddot{q}^j$ and it follows that

$$f' - f = a_{ij}\Delta\ddot{q}^j \quad . \quad . \quad . \quad . \quad . \quad (14)$$

Again, the work done by the constraint forces in a virtual displacement $\delta q^K = \Delta q^K\frac{\delta t^2}{2}$ is $\Sigma F_{1K}\delta q^K$, and since the constraints are by hypothesis frictionless, the work is zero.

Therefore $\frac{1}{4}\Sigma F_1(f' - f)\delta t^4 = 0$ or $\Sigma m(\mathrm{CB})(\mathrm{BB}') = 0$.

Finally, $$\mathrm{CB}' = \mathrm{CB} + \mathrm{BB}'$$

i.e. $$\tfrac{1}{2}\Sigma m(\mathrm{CB}')^2 = \tfrac{1}{2}\Sigma m(\mathrm{CB})^2 + \tfrac{1}{2}\Sigma m(\mathrm{BB}')^2 + \Sigma m(\mathrm{CB})(\mathrm{BB}')$$

or $$K' = K + \tfrac{1}{2}\Sigma m(\mathrm{BB}')^2$$

Therefore $$K' > K \quad . \quad . \quad . \quad . \quad . \quad . \quad . \quad (15)$$

as was to be proved.

It should be noted that the number of components of v_i was not assumed to be the same as the number of co-ordinates q^j; in general, $n > m$ owing to the equations of constraint

$$C_{kj}\delta q^j = 0 \quad k = 1, 2 \ldots (n - m) \quad . \quad . \quad . \quad (16)$$

These equations of constraint are not necessarily integrable, or time-independent.

(3.3) Appell's Equations

From the foregoing principle, it is possible to derive a set of equations first formulated by Appel.[8]

Putting $v = \dot{x}$ and $f = \ddot{x}$, the constraint is

$$K = \Sigma m\left(\ddot{x}_i - \frac{F_i}{m}\right)^2 \qquad i = 1, 2 \ldots n \quad . \quad . \quad (17)$$

and the components of velocity and acceleration are

$$\dot{x}_i = a_{ij}\dot{q}^j + b_i \quad . \quad . \quad . \quad . \quad . \quad . \quad . \quad (18)$$

$$\ddot{x}_i = a_{ij}\ddot{q}^j + \theta_i(\dot{q}, q, t) \quad . \quad . \quad . \quad . \quad . \quad (19)$$

Consequently K is also a function of $\ddot{q}$, $\dot{q}$, q and t. For a minimum of K, one of the conditions is

$$\frac{\partial K}{\partial \ddot{q}^j} = 0 \quad . \quad . \quad . \quad . \quad . \quad . \quad . \quad (20)$$

which yields $$2\Sigma m\left(\ddot{x}_i - \frac{F_i}{m}\right)\frac{\partial \ddot{x}_i}{\partial q^j} = 0 \quad . \quad . \quad . \quad . \quad (21)$$

Since $\frac{\partial F_i}{\partial \ddot{q}^j} = 0$ on account of the arbitrary nature of the impressed forces, on transposition there results

$$\Sigma m\ddot{x}_i\frac{\partial \ddot{x}_i}{\partial \ddot{q}^j} = F_i\frac{\partial \ddot{x}_i}{\partial q_j}$$

or $$\frac{\partial}{\partial \ddot{q}^j}(\Sigma \tfrac{1}{2}m\ddot{x}_i^2) = F_i\frac{\partial \ddot{x}_i}{\partial \ddot{q}^j} \quad . \quad . \quad . \quad . \quad . \quad (22)$$

The term inside the brackets is Appell's function, S, i.e. the sum of the squares of the acceleration terms.

Also, $$\frac{\partial \ddot{x}_i}{\partial \ddot{q}^j} = a_{ij} \quad . \quad . \quad . \quad . \quad . \quad . \quad . \quad (23)$$

and it is usual to put $a_{ij}F_i = Q_j$, the generalized impressed force. In terms of this, the equation may be written

$$\frac{\partial S}{\partial \ddot{q}^j} = Q_j \quad . \quad . \quad . \quad . \quad . \quad . \quad . \quad (24)$$

(3.4) The Equations in Tensor Notation

The preceding equations may also be established as follows, using tensor notation. Consider any two sets of co-ordinates, x and y, which are related by the equations

$$\dot{x}^m = a_n^m\dot{y}^n + b^m \quad . \quad . \quad . \quad . \quad . \quad . \quad (26)$$

where no restrictive assumption is made regarding the ranges of the indices m and n. In general, the transformation tensor a_n^m will be a function of the y's and the time t. From this there follows

$$\ddot{x}^m = a_n^m\ddot{y}^n + \phi(\dot{y}, y, t) \quad . \quad . \quad . \quad . \quad (27)$$

where ϕ is some function of the variables indicated.

The virtual work in a small displacement is

$$\delta W = g_{mp}\ddot{x}^p\delta x^m \quad . \quad . \quad . \quad . \quad . \quad (28)$$

where g_{mp} is the metric tensor of the system. Therefore

$$\delta W = g_{mp}\ddot{x}^p \times a_n^m\delta y^n$$

This may be written

$$\delta W = \frac{\partial}{\partial \ddot{y}^n}(\tfrac{1}{2}g_{mp}\ddot{x}^p\ddot{x}^m)\delta y^n \quad . \quad . \quad . \quad . \quad (29)$$

If the substitution $S = \frac{1}{2}g_{mp}\ddot{x}^m\ddot{x}^p$ is made, and if the generalized force corresponding to the co-ordinate y^n is F_n, then

$$\frac{\partial S}{\partial \ddot{y}^n}\delta y^n = F_n\delta y^n \quad . \quad . \quad . \quad . \quad . \quad (30)$$

or $$\frac{\partial S}{\partial \ddot{y}^n} = F_n \quad . \quad . \quad . \quad . \quad . \quad . \quad . \quad (31)$$

which is the required equation.

In general, with curvilinear co-ordinates, the acceleration is given by

$$f^n = \ddot{x}^n + \left\{ \begin{matrix} n \\ m\ p \end{matrix} \right\} \dot{x}^m \dot{x}^p \quad . \quad . \quad . \quad . \quad (32)$$

where the Christoffel symbol is formed in conjunction with the metric tensor g_{mn}. Appell's function is

$$S = \tfrac{1}{2} g_{mn} f^m f^n \quad . \quad . \quad . \quad . \quad . \quad . \quad (33)$$

and Appell's equations yield

$$\frac{1}{2} \frac{\partial g_{mn}}{\partial \ddot{y}^\beta} f^m f^n + g_{mn} f^n \frac{\partial f^m}{\partial \ddot{y}^\beta} = F_\beta \quad . \quad . \quad . \quad (34)$$

Now f^m is a function of $\ddot{x}^m$ and $\dot{x}^n$ so that

$$\frac{\partial f^m}{\partial \ddot{y}^\beta} = \frac{\partial f^m}{\partial \ddot{x}^r} \frac{\partial \ddot{x}^r}{\partial \ddot{y}^\beta} + \frac{\partial f^m}{\partial \dot{x}^r} \frac{\partial \dot{x}^r}{\partial \ddot{y}^\beta} \quad . \quad . \quad . \quad . \quad (35)$$

Again, $\dot{x}^r = a^r_\beta \dot{y}^\beta + b^r$ [eqn. (26)], therefore $\ddot{x}^r = a^r_\beta \ddot{y}^\beta + \phi(\dot{y}, y, t)$ [eqn. (27)], i.e. $\partial \ddot{x}^r / \partial \ddot{y}^\beta = a^r_\beta$. Further, $\partial \dot{x}^r / \partial \ddot{y}^\beta = 0$ and $\partial f^m / \partial \ddot{x}^r = \delta^m_r$.

Hence,

$$\frac{\partial f^m}{\partial \ddot{y}^\beta} = \delta^m_r a^r_\beta + 0 = a^m_\beta \quad . \quad . \quad . \quad . \quad (36)$$

Substituting this in Appell's equation, there results

$$\frac{1}{2} \frac{\partial g_{mn}}{\partial \ddot{y}^\beta} f^m f^n + g_{mn} a^m_\beta f^n = F_\beta \quad . \quad . \quad . \quad (37)$$

That this equation is true, irrespective of the nature of the constraints, is due to two factors:

(*a*) The inclusion of the term b^r in the expression for x^r allows for rheonomic constraints.

(*b*) It is not necessary at any stage to assume that $a^m_\beta = \partial x^m / \partial x^\beta$ since the components of a^β_m may still be exhibited without this assumption. As is well known, it is this restriction which makes the holonomic constraints necessary in Lagrange's equations.

If $\partial g_{mn} / \partial \ddot{y}^\beta = 0$, the above equation may be reduced to the simple form

$$g_{mn} a^m_\beta f^n = F_\beta \quad . \quad . \quad . \quad . \quad . \quad (38)$$

and on expansion will give the equation of motion in explicit terms. On substituting for f^n,

$$g_{mn} a^m_\beta \left[\ddot{x}^n + \left\{ \begin{matrix} n \\ m\ p \end{matrix} \right\} \dot{x}^m \dot{x}^p \right] = F_\beta \quad . \quad . \quad . \quad (39)$$

or

$$g_{mn} a^m_\beta \left[a^n_\alpha \ddot{y}^\alpha + \frac{\partial a^n_\alpha}{\partial y^\gamma} \dot{y}^\alpha \dot{y}^\gamma + \left\{ \begin{matrix} n \\ m\ p \end{matrix} \right\} \dot{x}^m \dot{x}^p \right] = F_\beta \quad . \quad (40)$$

Therefore

$$g_{mn} a^m_\beta a^n_\alpha \ddot{y}^\alpha + g_{mn} a^m_\beta \frac{\partial a^n_\alpha}{\partial y^\gamma} \dot{y}^\alpha \dot{y}^\gamma + [mp, n] a^n_\beta \dot{x}^m \dot{x}^p = F_\beta \quad . \quad (41)$$

The first term on the left-hand side is

$$g_{mn} a^m_\beta a^n_\alpha \ddot{y}^\alpha = g_{\alpha\beta} \ddot{y}^\alpha \quad . \quad . \quad . \quad . \quad . \quad (42)$$

The second term is

$$g_{mn} a^m_\beta \frac{\partial a^n_\alpha}{\partial y^\gamma} a^n_\alpha a^\alpha_\eta \dot{y}^\alpha \dot{y}^\gamma = - g_{mn} a^m_\beta a^n_\alpha \frac{\partial a^n_\alpha}{\partial x^p} a^n_\alpha a^p_\gamma \dot{y}^\alpha \dot{y}^\gamma$$

$$= - g_{\beta\delta} \frac{\partial a^\delta_n}{\partial x^p} a^n_\alpha a^p_\gamma \dot{y}^\alpha \dot{y}^\gamma \quad . \quad . \quad . \quad (43)$$

For the third term,

$$[mp, n] a^n_\beta \dot{x}^m \dot{x}^p = \left\{ [\beta\gamma, \alpha] a^\beta_m a^\gamma_p a^\alpha_n + g_{\beta\gamma} a^\beta_m \frac{\partial a^\gamma_p}{\partial x_n} \right\} a^n_\beta \dot{x}^m \dot{x}^p$$

$$= [\beta\gamma, \alpha] \dot{y}^\alpha \dot{y}^\gamma + g_{\beta\delta} \frac{\partial a^\delta_p}{\partial x^n} a^n_\alpha a^p_\gamma \dot{y}^\alpha \dot{y}^\gamma \quad . \quad . \quad (44)$$

Therefore

$$g_{\alpha\beta} \ddot{y}^\alpha + \left\{ [\beta\gamma, \alpha] + g_{\beta\delta} \left(\frac{\partial a^\delta_p}{\partial x^n} - \frac{\partial a^\delta_n}{\partial x^p} \right) a^n_\alpha a^p_\gamma \right\} \dot{y}^\alpha \dot{y}^\gamma = F_\beta \quad . \quad (45)$$

which is the equation required.

(4) THE NEW EQUATIONS IN ELECTRICAL NOTATION

(4.1) General

To utilize the equations previously given, one can identify the electrical charge q with the displacement x; the current I is then represented by a velocity $\dot{x}$. With two sets of co-ordinates, x and y, related according to

$$\dot{x}^m = a^m_n \dot{y}^n + b^m \quad . \quad . \quad . \quad . \quad . \quad (46)$$

no restriction being placed on the ranges of m and n, the corresponding electrical equations are

$$I^m = C^m_\alpha I^\alpha \quad . \quad . \quad . \quad . \quad . \quad . \quad (47)$$

where C^m_α is some function of q^α and t. This simplification is due to the fact that, in general, no electrostatic charges are present in rotating electromagnetic machinery. It follows that

$$\dot{I}^m = \dot{C}^m_\alpha I^\alpha + C^m_\alpha \dot{I}^\alpha \quad . \quad . \quad . \quad . \quad . \quad (48)$$

It is not necessary, however, to assume that $C^m_\alpha = \partial q^m / \partial q^\alpha$; i.e. the system may properly be considered as non-holonomic. It follows that

$$\frac{\partial \dot{I}^m}{\partial \dot{I}^\alpha} = C^m_\alpha \quad . \quad . \quad . \quad . \quad . \quad . \quad (49)$$

Appell's equations in this notation are, with inductance tensor L_{mn},

$$\frac{\partial}{\partial \dot{I}^\alpha} (\tfrac{1}{2} L_{mn} \dot{I}^m \dot{I}^n) = Q_\alpha \quad . \quad . \quad . \quad . \quad . \quad (50)$$

where Q_α is the term corresponding to the generalized force and will be evaluated later. This gives

$$L_{mn} \dot{I}^n \frac{\partial \dot{I}^m}{\partial \dot{I}^\alpha} = Q_\alpha \quad . \quad . \quad . \quad . \quad . \quad (51)$$

if L_{mn} is assumed non-varying. On substituting for $\partial \dot{I}^m / \partial \dot{I}^\alpha$ and $\dot{I}^n$ there results

$$(L_{mn} C^n_\beta \dot{I}^\beta + L_{mn} \dot{C}^n_\beta I^\beta) C^m_\alpha = Q_\alpha \quad . \quad . \quad . \quad (52)$$

and therefore

$$L_{\alpha\beta} \dot{I}^\beta + L_{\alpha\beta} C^\beta_n \dot{C}^n_\beta I^\beta = Q_\alpha \quad . \quad . \quad . \quad (53)$$

where

$$L_{\alpha\beta} = L_{mn} C^m_\alpha C^n_\beta \quad . \quad . \quad . \quad . \quad . \quad (54)$$

Now

$$\dot{C}^n_\beta I^\beta = \frac{d}{dt} C^n_\beta I^\beta = \frac{dC^n_\beta}{d\theta} \frac{d\theta}{dt} I^\beta = \frac{dC^n_\beta}{d\theta} p\theta I^\beta \quad . \quad . \quad (55)$$

so that

$$L_{\alpha\beta} \dot{I}^\beta + L_{\alpha\beta} C^\beta_n \frac{dC^n_\beta}{d\theta} p\theta I^\beta = Q_\alpha \quad . \quad . \quad . \quad (56)$$

(4.2) Evaluation of Q_α and Final Form of the Equation

It now remains to evaluate Q_α and this may be done as follows. Consider a small change in the system in which q^m is increased

by δq^m so that the current I^m flows for a time given by $I^m \delta t = \delta q^m$. If the impressed voltage is V_m, the work done by the supply $V_m \delta q^m$ and the work done by reaction with the conductor material, being equal and opposite to the heat generated, is $-R_{mn} I^m I^n \delta t$. Thus, if the generalized force corresponding to q^m is Q_m, we have

$$Q_m \delta q^m = V_m \delta q^m - R_{mn} I^m I^n \delta t \quad . \quad . \quad . \quad (57)$$

so that

$$Q_m = V_m - R_{mn} I^n \quad . \quad . \quad . \quad . \quad . \quad (58)$$

Multiplying by C_α^m gives the transformed value of Q_m, for

$$Q_m C_\alpha^m = V_m C_\alpha^m - R_{mn} C_\alpha^m C_\beta^n I^\beta$$

$$= V_\alpha - R_{\alpha\beta} I^\beta \quad . \quad . \quad . \quad . \quad . \quad . \quad (59)$$

The left-hand side of this equation is clearly Q_α, which is thus known. Therefore there finally results

$$V_\alpha = R_{\alpha\beta} I^\beta + L_{\alpha\beta} \dot{I}^\beta + L_{\alpha\beta} C_n^\beta \frac{dC_\beta^n}{d\theta} p\theta I^\beta \quad . \quad . \quad (60)$$

which is the voltage equation for general rotating axes.[5]

(4.3) Equations in Direct Notation

In direct notation[6] eqn. (60) may be written

$$V' = \left(R' + L'p + L'C^{-1}\frac{dC}{d\theta} p\theta\right) I' \quad . \quad . \quad (61)$$

or

$$V' = Z'I' \quad . \quad . \quad . \quad . \quad . \quad . \quad (62)$$

where

$$Z' = R' + L'p + L'C^{-1}\frac{dC}{d\theta} p\theta \quad . \quad . \quad . \quad (63)$$

Since

$$L' = C_t L C \quad . \quad . \quad . \quad . \quad . \quad . \quad (64)$$

$$L'C^{-1} = C_t L \quad . \quad . \quad . \quad . \quad . \quad . \quad (65)$$

and

$$Z' = R' + L'p + C_t L \frac{dC}{d\theta} p\theta$$

or

$$Z' = R' + L'p + C_t L \frac{dC}{dt} \quad . \quad . \quad . \quad (66)$$

These equations are in the same form as in Kron's papers.[5]

(4.4) Reduction of the Equation in Simple Cases

When the connection tensors are not variable, i.e. when

$$\frac{\partial C}{dt} = 0 \text{ or } \frac{\partial C}{\partial \theta} = 0 \quad . \quad . \quad . \quad . \quad . \quad (67)$$

the equation reduces to $C_t L C p I' = V' - R'I'$ or, since $R' = C_t R C$, to

$$C_t(R + Lp)CI' = V' \quad . \quad . \quad . \quad . \quad (68)$$

which is the usual form. In an even simpler case, say with constant inductance and without any sort of transformation, the equation gives

$$\frac{\partial}{\partial \dot{I}}(\tfrac{1}{2} L \dot{I}^2) = V - IR$$

or

$$L\dot{I} = V - IR$$

which is the simple equation of voltage in a series RL circuit.

(5) USE OF THE EQUATIONS IN MACHINE ANALYSIS

By use of the method given above, the equations of systems can be obtained in some cases with considerable ease. For example, the inductance tensor of the simplest generalized machine is[5]

$L_{\alpha\beta} =$

	d_s	d_r	q_r	q_s
d_s	L_{ds}	M_d	0	0
d_r	M_d	L_{dr}	0	0
q_r	0	0	L_{qr}	M_q
q_s	0	0	M_q	L_{qs}

. (69)

For a machine with moving reference axes, say a 2-phase salient-pole synchronous motor, the connection equation is

$$I = CI' \quad . \quad . \quad . \quad . \quad . \quad . \quad . \quad (70)$$

where $C =$

	d_s	a	b	q_s
d_s	1	0	0	0
d_r	0	$\cos\theta$	$-\sin\theta$	0
q_r	0	$\sin\theta$	$\cos\theta$	0
q_s	0	0	0	1

. (71)

and therefore

$\frac{\partial C}{\partial \theta} =$

	d_s	a	b	q_s
d_s	0	0	0	0
d_r	0	$-\sin\theta$	$-\cos\theta$	0
q_r	0	$\cos\theta$	$-\sin\theta$	0
q_s	0	0	0	0

. (72)

Now

$$pI = p(CI') = pCI' + CpI' \quad . \quad . \quad . \quad . \quad (73)$$

$$= (pC + Cp)I' \quad . \quad . \quad . \quad . \quad . \quad . \quad (74)$$

$$= KI'$$

where

$$K = (pC + Cp) \quad . \quad . \quad . \quad . \quad . \quad (75)$$

Since

$$pC = \frac{\partial C}{\partial \theta} p\theta$$

$$K = \frac{\partial C}{\partial \theta} p\theta + Cp \quad . \quad . \quad . \quad . \quad (76)$$

Hence

$K =$

	d_s	a	b	q_s
d_s	p			
d_r		A	$-B$	
q_r		B	A	
q_s				p

. (77)

in which
$$\left.\begin{aligned} A &= \cos\theta p - \sin\theta p\theta \\ B &= \sin\theta p + \cos\theta p\theta \end{aligned}\right\} \quad . \quad . \quad . \quad . \quad (78)$$

With these values, $\frac{\partial S}{\partial \dot{I}'}$ becomes $\frac{\partial}{\partial(pI')}(\frac{1}{2}\dot{I}_t L\dot{I})$

or
$$\frac{\partial S}{\partial \dot{I}'} = \frac{\partial}{\partial(pI')}\tfrac{1}{2}(pI_t LpI) \quad . \quad . \quad . \quad . \quad (79)$$

$$= \frac{\partial}{\partial(pI')} I_t'(K_t LK)I' \quad . \quad . \quad . \quad . \quad (80)$$

Now

$K_t LK =$

	d_s	a	b	q_s
d_s	p^2L_{ds}	pAM_d	$-pBM_d$	0
a	pAM_d	$A^2L_{dr} + B^2L_{qr}$	$(L_{qr} - L_{dr})AB$	pBM_q
d	$-pBM_d$	$(L_{qr} - L_{dr})AB$	$A^2L_{qr} + B^2L_{dr}$	pAM_q
q_s	0	pBM_q	pAM_q	p^2L_{qs}

. . . . (81)

This result must be multiplied by I_t' and I' and differentiated partially with respect to pI'. It follows that terms which do not contain a 'free' p to operate on I' will, when differentiated, be zero. For example, the differentiation of $A^2L_{dr} + B^2L_{qr}$ results in

$$\frac{\partial}{\partial(pI')} I_t'(A^2L_{dr} + B^2L_{qr})I'$$
$$= \frac{\partial}{\partial(pI')} I_t'[L_{dr}\cos^2\theta p^2 + L_{qr}\sin^2\theta p^2 + 2\sin\theta\cos\theta pp(L_{dr} - L_{dr}) + L_{dr}\sin^2\theta(p\theta)^2 + L_{qr}\cos^2\theta(p\theta)^2]I' \quad . \quad . \quad . \quad (82)$$
$$= I_t'[L_{dr}\cos^2\theta p + L_{qr}\sin^2\theta p + 2\sin\theta\cos\theta p\theta(L_{qr} - L_{dr})] \quad . \quad . \quad . \quad . \quad (83)$$

That is, it results in the disappearance of the terms in $(p\theta)^2$ and there is apparent 'cancelling' of one p in the remaining terms. If this is done throughout, there results

	d_s	a	b	q_s
d_s	pL_{ds}	$(\cos\theta p - \sin\theta p\theta)M_d$	$-(\sin\theta p + \cos\theta p\theta)M_d$	0
a	$(\cos\theta p - \sin\theta p\theta)M_d$	$L_{dr}\cos^2\theta p + L_{qr}\sin^2\theta p + 2\sin\theta\cos\theta p\theta(L_{qr} - L_{dr})$	$(L_{qr} - L_{dr})[(\sin\theta\cos\theta)p + (\cos^2\theta - \sin^2\theta)p\theta]$	$(\sin\theta p + \cos\theta p\theta)M_q$
b	$-(\sin\theta p + \cos\theta p\theta)M_d$	$(L_{qr} - L_{dr})[\sin\theta\cos\theta p + (\cos^2\theta - \sin^2\theta)p\theta]$	$L_{dr}\sin^2\theta p + L_{qr}\cos^2\theta p + 2\sin\theta\cos\theta p\theta(L_{qr} - L_{dr})$	$(\cos\theta p - \sin\theta p\theta)M_q$
q_s	0	$(\sin\theta p + \cos\theta p\theta)M_q$	$(\cos\theta p - \sin\theta p\theta)M_q$	pL_{qs}

. . . . (84)

It has been shown elsewhere[5] that this is the sum of the conventional inductance and torque tensors when multiplied by p and $p\theta$ respectively.

(6) CONCLUSION

The use of eqn. (60) has been somewhat restricted and it is not possible to give an assurance of its wide application to electrical problems. However, the use of the equations certainly simplifies both proofs and procedures in the more complicated cases of machine analysis. The equation will also apply to circuits in which the parameters are functions of the time. This is possible since, as stated, there are no restrictive assumptions necessary in the proof of its validity. Similarly, it applies to systems in which the transformation tensors, C_α^a, are functions of the currents as well as of the interconnections. The analysis of Section 3 has added some generality to certain steps in the derivation of the covariant form of the dynamical equation (45); in particular, it is now possible to utilize the equations in time-varying situations.

(7) REFERENCES

(1) LYNN, J. W.: 'The Tensor Equations of Electrical Machines', *Proceedings I.E.E.*, Monograph No. 117 S, January, 1955 (**102** C, p. 149).

(2) LYNN, J. W.: 'Tensor Analysis of Electrical Machine Hunting', *ibid.*, Monograph No. 295 S, March, 1958 (**105** C, p. 420).

(3) GIBBS, W. J.: 'Tensors in Electrical Machine Theory (Chapman and Hall, 1952).

(4) BEWLEY, L. V.: 'Application of Tensors to Electrical Circuits and Machines' (Lehigh University Press, 1958).

(5) KELLER, E. G.: 'Mathematics of Modern Engineering', Vol. II (John Wiley, 1942).

(6) GIBBS, W. J.: 'Limitations of Lagrangian Methods in Electrical Machine Theory', *Beama Journal*, 1950, **57**, p. 342 and 382.

(7) HOFFMANN, B.: 'Kron's Non-Riemannian Electrodynamics', *Reviews of Modern Physics*, 1949, **21**, p. 535.

(8) WHITTAKER, E. T.: 'A Treatise on the Analytical Dynamics of Particles and Rigid Bodies' (Cambridge University Press, 1937).

(8) APPENDIX: LAGRANGE'S EQUATIONS

In textbooks on dynamics[8] it is shown that Lagrange's equation for a dissipative system having n degrees of freedom is

$$\frac{d}{dt}\left(\frac{\partial \mathscr{L}}{\partial \dot{x}}\right) - \frac{\partial \mathscr{L}}{\partial x} + \frac{\partial \mathscr{R}}{\partial \dot{x}} = F \quad . \quad . \quad . \quad . \quad (85)$$

One such equation applies to each of the degrees of freedom.

When the equation is written in this way, it is assumed that the system has no moving constraints, i.e. that it is 'holonomic'. In tensor notation the equation may be written

$$\frac{d}{dt}\left(\frac{\partial \mathscr{L}}{\partial \dot{x}^\gamma}\right) - \frac{\partial \mathscr{L}}{\partial x^\gamma} + \frac{\partial \mathscr{R}}{\partial \dot{x}^\gamma} = F_\gamma \quad . \quad . \quad . \quad (86)$$

Further, in electrical systems the potential energy, i.e. the energy of the electrostatic charges, is usually assumed to be zero so that

$$\mathscr{L} = T = \tfrac{1}{2} g_{\alpha\beta}\dot{x}^\alpha \dot{x}^\beta \quad . \quad . \quad . \quad . \quad . \quad (87)$$

and

$$\mathscr{R} = \tfrac{1}{2} r_{\alpha\beta}\dot{x}^\alpha \dot{x}^\beta \quad . \quad . \quad . \quad . \quad . \quad . \quad (88)$$

where the metric tensor, $g_{\alpha\beta}$, and the dissipation tensor, $r_{\alpha\beta}$, are some functions of x^α only.

Now
$$\frac{\partial T}{\partial \dot{x}^\gamma} = \frac{1}{2}\frac{\partial}{\partial \dot{x}^\gamma}(g_{\alpha\beta}\dot{x}^\alpha \dot{x}^\beta) = \tfrac{1}{2} g_{\alpha\beta}\delta^\alpha_\gamma \dot{x}^\beta + \tfrac{1}{2} g_{\alpha\beta}\delta^\beta_\gamma \dot{x}^\alpha$$

$$= \tfrac{1}{2} g_{\gamma\beta}\dot{x}^\beta + \tfrac{1}{2} g_{\gamma\alpha}\dot{x}^\alpha \quad . \quad . \quad . \quad . \quad . \quad . \quad . \quad . \quad (89)$$

Hence,

$$\frac{d}{dt}\left(\frac{\partial T}{\partial \dot{x}^\gamma}\right) = \frac{1}{2}\left(\frac{dg_{\gamma\beta}}{dt}\dot{x}^\beta + g_{\beta\gamma}\ddot{x}^\beta + \frac{dg_{\gamma\alpha}}{dt}\dot{x}^\alpha + g_{\gamma\alpha}\ddot{x}^\alpha\right) \quad . \quad (90)$$

Now $\tfrac{1}{2} g_{\gamma\beta}\ddot{x}^\beta + \tfrac{1}{2} g_{\gamma\alpha}\ddot{x}^\alpha = g_{\gamma\beta}\ddot{x}^\beta$ since α is a free index. Hence,

$$\frac{d}{dt}\left(\frac{\partial T}{\partial \dot{x}^\gamma}\right) = \frac{1}{2}\left(\frac{\partial g_{\gamma\beta}}{\partial x^\alpha}\frac{\partial x^\alpha}{\partial t}\dot{x}^\beta + \frac{\partial g_{\gamma\alpha}}{\partial x^\beta}\frac{\partial x^\beta}{\partial t}\dot{x}^\alpha\right) + g_{\gamma\beta}\ddot{x}^\beta \quad . \quad (91)$$

$$= \frac{1}{2}\left(\frac{\partial g_{\gamma\beta}}{\partial x^\alpha} + \frac{\partial g_{\gamma\alpha}}{\partial x^\beta}\right)\dot{x}^\alpha \dot{x}^\beta + g_{\gamma\beta}\ddot{x}^\beta \quad . \quad . \quad . \quad . \quad (92)$$

Again,
$$\frac{\partial T}{\partial x^\gamma} = \frac{1}{2}\frac{\partial (g_{\alpha\beta}\dot{x}^\alpha \dot{x}^\beta)}{\partial x^\gamma} = \frac{1}{2}\frac{\partial g_{\alpha\beta}}{\partial x^\gamma}\dot{x}^\alpha \dot{x}^\beta \quad . \quad . \quad . \quad (93)$$

and
$$\frac{\partial \mathscr{R}}{\partial \dot{x}^\gamma} = \frac{1}{2}\frac{\partial (r_{\alpha\beta}\dot{x}^\alpha \dot{x}^\beta)}{\partial \dot{x}^\gamma} = r_{\alpha\beta}\dot{x}^\beta \quad . \quad . \quad . \quad . \quad (94)$$

The final form of Lagrange's equations of motion is therefore

$$g_{\gamma\beta}\ddot{x}^\beta + \frac{1}{2}\left(\frac{\partial g_{\gamma\beta}}{\partial x^\alpha} + \frac{\partial g_{\alpha\gamma}}{\partial x^\beta} - \frac{\partial g_{\alpha\beta}}{\partial x^\gamma}\right)\dot{x}^\alpha \dot{x}^\beta + r_{\gamma\beta}\dot{x}^\beta = F_\gamma \quad . \quad (95)$$

or
$$g_{\gamma\beta}\ddot{x}^\beta + [\alpha\beta,\gamma]\dot{x}^\alpha \dot{x}^\beta + r_{\gamma\beta}\dot{x}^\beta = F_\gamma \quad . \quad . \quad . \quad (96)$$

where
$$[\alpha\beta,\gamma] = \frac{1}{2}\left(\frac{\partial g_{\gamma\beta}}{\partial x^\alpha} + \frac{\partial g_{\alpha\gamma}}{\partial x^\beta} - \frac{\partial g_{\alpha\beta}}{\partial x^\gamma}\right)$$

is the Christoffel symbol of the first kind.

621.3.013:621.319.7

The Institution of Electrical Engineers
Monograph No. 379
May 1960
©

ELECTRIC AND MAGNETIC IMAGES

By P. HAMMOND, M.A., Member.

(*The paper was first received* 17*th November*, 1959, *and in revised form* 12*th February*, 1960. *It was published as an* INSTITUTION MONOGRAPH *in May*, 1960.)

SUMMARY

The method of images as applied to electrostatic, magnetostatic and electromagnetic fields is investigated. By considering the uniqueness of the field it is shown within what limits the method can safely be used, and rules are given for its use. The application of the method is illustrated by a discussion of the electric field near a cylindrical cathode and the magnetic fields near the end-windings of electrical machines.

LIST OF PRINCIPAL SYMBOLS

A, C = Vector potential functions.
B = Magnetic flux density.
c = Velocity of light.
D = Electric flux density.
E = Electric field strength.
H = Magnetic field strength.
I = Current.
i = Surface current.
J = Current density.
$k = \omega/c$.
n = Unit vector normal to a surface.
P, Q = Vector functions.
q, q' = Electric charges.
R = Radius.
r = Polar co-ordinate.
S = Surface area.
v = Volume.
x, y, z = Cartesian co-ordinates.
α, β = Angles.
ε = Base of natural logarithms.
ϵ_0 = Primary electric constant.
ϵ = Permittivity.
$\zeta = \varepsilon^{jkr}/r$.
μ_0 = Primary magnetic constant.
μ = Permeability.
ρ = Volume density of electric charge.
σ = Surface density of electric charge or magnetic pole strength.
ϕ, χ, ψ = Scalar potential functions.
ω = Angular frequency.
∇ = Hamilton's vector operator.

(1) INTRODUCTION

The method of images is of great use to electrical engineers in the determination of electric and magnetic fields in cases where there are reflecting boundaries. A typical example is the calculation of the forces on electrons emitted from a cathode: these forces can be easily calculated by a consideration of the images of the electrons in the cathode surface. In magnetostatics, too, it is customary to calculate the attraction between a current and a parallel iron boundary by considering the image of the current in the iron. Again, in high-frequency problems it is usual to consider the effect of the earth on the field pattern of an aerial to be the same as that of the image of the aerial.

Because of the wide field of application and great practical interest of the method of images it would seem reasonable to conclude that the method is well understood and can be safely applied to new problems. Various factors have, however, convinced the author that this conclusion is mistaken; among these might be listed the denial by a writer recently that there is any image force on electrons around a cylindrical cathode.[1] Even more seriously, there was in the author's mind the doubt whether the method of images is applicable to magnetic boundaries of finite permeability, since the original proof of the image theory apparently depends on the provision of boundaries at constant potential. This doubt was reinforced by the observation that writers on images in electromagnetic theory confined their attention to problems of infinitely conducting boundaries.

The paper is the outcome of a close examination of the method of images and has been written with two aims in view: the first is to examine the magnetic field of current distributions near iron boundaries with special reference to the fields of the end-windings of rotating machines; the second is the more general aim of arriving at a clearer understanding of the method of images in order to determine the conditions under which this method can be safely applied.

(2) HISTORICAL BACKGROUND

The method of images is due to Lord Kelvin,[2] who in 1848 published a paper in which he showed that the field of an electric charge in front of a conducting sheet could be correctly represented as the field of the charge alone plus the field of its mirror image in the conducting sheet. Lord Kelvin used the term 'image' in order to point out the close similarity of electrical with optical images. In optics an image is defined as a point or system of points which, if it existed, would emit the system of rays which are actually due to reflected light from a mirror or lens. Two kinds of images are distinguished in optics: *virtual* images are located on the far side of the mirror or lens and *real* images are located on the near side. Lord Kelvin's electrical images were all virtual ones.

Lord Kelvin confined his attention to electrostatic problems. He was followed by Maxwell,[3] who greatly enlarged the treatment. Maxwell was mainly concerned with problems concerning spheres, and he lists all the combinations of spheres and planes which in the presence of electric charges give a finite number of images. Maxwell, like Lord Kelvin, was chiefly interested in the image treatment of electrostatic problems. There are, however, in his treatise passing references to the method of images applied to the electric potential of steady current conduction, to magnetostatics[4] and to the magnetic images of slowly varying current sheets.[5] Searle[6] successfully applied the method of images to magnetic problems of finite permeability, and Hague,[7] in an excellent presentation of the subject, pays great attention to Searle's method. Both Searle and Hague, however, present the method of images as a ready-made solution to certain problems. It is clear that the method

Correspondence on Monographs is invited for consideration with a view to publication.
Mr. Hammond is in the Department of Engineering, University of Cambridge.

is correct, but the reader is left wondering how the solution was obtained. Other writers follow Maxwell's treatment and restrict their attention to electrostatic problems involving conducting boundaries. Among these, Jeans[8] bases his proof, like Maxwell, on the provision of equipotential boundaries,* but then paradoxically shows that the method is also applicable to problems involving dielectric boundaries, in which there is an electric field along the boundary.

(3) GENERAL CONSIDERATIONS

The basic requirement of the method of images is that the effect of the boundaries shall be correctly represented by the images. In electrostatic problems, for example, there will generally be induced charges on the boundaries of the region considered. The field of the image charges within this region must be identical with that of the induced charges. We are thus led to examine how the field within a bounded region of space depends on the charges at the boundary. When we have discovered how the field within a volume depends on the field at the boundaries, we can then postulate an image distribution of sources which will give the same boundary field and therefore the same field within the volume considered. This image distribution will then correctly simulate the effect of the boundaries.

(3.1) Electrostatic Fields

An electrostatic field can be described by a scalar potential ϕ. In seeking a relationship between surface and volume effects we can make use of Gauss's identity

$$\iint_S \boldsymbol{P}.\boldsymbol{n}dS = \iiint_v \nabla.\boldsymbol{P}dv \quad . \quad . \quad . \quad . \quad (1)$$

where $\boldsymbol{P}$ is an arbitrary vector, $\boldsymbol{n}$ is a unit vector drawn from within v normal to S and the mathematical surface S completely encloses the volume v. If we choose $\boldsymbol{P} = \psi\nabla\phi$, where ψ and ϕ are two scalar functions, then

$$\iint_S \psi\frac{\partial\phi}{\partial n}dS = \iiint_v [\psi\nabla^2\phi + (\nabla\psi.\nabla\phi)]dv \quad . \quad . \quad (2)$$

and this is known as Green's theorem.[9]

If $\psi = \phi$

$$\iint_S \phi\frac{\partial\phi}{\partial n}dS = \iiint_v [\phi\nabla^2\phi + (\nabla\phi)^2]dv \quad . \quad . \quad . \quad (3)$$

We seek for a unique relationship between the surface field and the volume field. Consider then the possibility of two scalar potentials ϕ_1 and ϕ_2 to satisfy eqn. (3). Then $\nabla^2\phi_1 = -\rho/\epsilon_0$, where ρ is the charge density within v and $\nabla^2\phi_2 = -\rho/\epsilon_0$. If $\chi = \phi_1 - \phi_2$, then $\nabla^2\chi = 0$.

Applying eqn. (3) to the function χ gives

$$\iint_S \chi\frac{\partial\chi}{\partial n}dS = \iiint_v (\nabla\chi)^2dv \quad . \quad . \quad . \quad . \quad (4)$$

If the left-hand side of this equation is zero, the integrand of the right-hand side must be zero. In such a case $\nabla\chi = 0$ and both χ and $\phi_1 - \phi_2$ are constants. Thus the field derivable from ϕ_1 is identical with that derivable from ϕ_2. The field is therefore unique.

Reference to eqn. (4) shows that the field will be unique if $\partial\chi/\partial n$ is zero everywhere on the surface. If χ is zero on the surface uniqueness is again achieved, but this condition is not necessary. All that is necessary is that χ shall be constant on S, since we have then

$$\iint_S \chi\frac{\partial\chi}{\partial n}dS = \chi\iint_S \frac{\partial\chi}{\partial n}dS = \chi\iiint_v \nabla^2\chi dv = 0$$

The criterion of uniqueness is therefore that either χ shall be constant or $\partial\chi/\partial n$ shall be zero everywhere on S. This means that either the tangential or the normal components of the electric field must be specified everywhere on S. A particular case of great importance arises when S is an equipotential surface, and it is this case which has occupied the attention of writers on image methods. Almost invariably their discussion starts with the consideration of a surface S at earth potential. In such a case

$$\iint_S \phi\frac{\partial\phi}{\partial n}dS = \phi\iint_S \frac{\partial\phi}{\partial n}dS$$

and if ϕ is zero (or some other known constant value), it is clear that the field is unique. Such a method starts with the consideration of charges near perfect conductors, or of currents near surfaces of infinite permeability. Of course, such discussion is perfectly valid, but it obscures the issue. The condition that S shall be a conducting surface is sufficient to determine the uniqueness of the field within v, but this condition is by no means a necessary one. All that is necessary is that the value of the tangential or normal electric field shall be specified at every point on the surface. Thus there can be fields tangential to the surface S. It is therefore not at all surprising that image methods can be applied to dielectric boundaries. From a consideration of eqn. (4) we arrive at the following formulation of the image problem in electrostatics:

> Consider a surface S which totally encloses a volume v. Determine the tangential electric field (or the normal field) on S due to the induced charges on the boundaries. Find a distribution of charges outside S to give on S the same tangential field (or the same normal field). Then this distribution of charges will give within v the same field as is given by the induced charges on the boundaries. Thus it is the image distribution required.

It should be noted that the image distribution is to be placed outside S. In the language of optics, we require a virtual image. Real images, i.e. charges within v, are inadmissible, because they do violence to the physical conditions of the problem. The only sources of an electrostatic field are electric charges and it is incorrect to insert charges unless these are made inaccessible. The image charges must always lie outside the region under consideration, because we require the field of these charges but not the charges themselves. Furthermore, although the field of the image distribution is unique, no such uniqueness is required of the image distribution itself. It is not uniqueness but convenience that is the criterion of the image distribution.

(3.1.1) An Example: Line Charge Parallel to the Face of a Semi-Infinite Dielectric Slab.

Fig. 1 shows an infinite line charge q at a distance d from the face of a semi-infinite dielectric slab of permittivity ϵ. Let the density of induced charge at P be σ; then E normal to the slab at P due to the charge q is given by

$$E_n = \frac{qd}{\epsilon_0(d^2 + x^2)}$$

and σ is derived from

$$\frac{\sigma}{2\epsilon_0} - E_n = -\epsilon\left(\frac{\sigma}{2\epsilon_0} + E_n\right) \quad . \quad . \quad . \quad . \quad (5)$$

$$\sigma = -\left(\frac{\epsilon - 1}{\epsilon + 1}\right)2\epsilon_0 E_n$$

* He writes in article 209: The principle underlying this method (of images) is that of finding a system of electric charges such that a certain surface, ultimately to be made into a conductor, is caused to coincide with the equipotential $V = 0$.

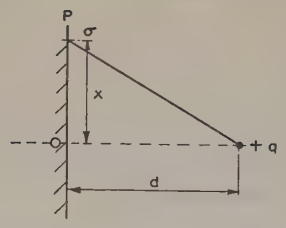

Fig. 1.—Line charge parallel to the face of a semi-infinite dielectric slab.

Then the normal field of the distribution σ is given by

$$-\frac{\sigma}{2\epsilon_0} = \left(\frac{\epsilon - 1}{\epsilon + 1}\right) E_n = \frac{\epsilon - 1}{\epsilon + 1} \frac{qd}{\epsilon_0(d^2 + x^2)}$$

Comparing this with the normal field due to q we note that it is a field which would be produced by a charge of line density $-q[(\epsilon - 1)/(\epsilon + 1)]$ placed at distance d from O within the dielectric. This is the required image charge.

(3.1.2) The Physical Meaning of the Boundary Conditions.

It is of great interest to examine the physical meaning of the surface conditions, which are sufficient to guarantee the uniqueness of an electrostatic field. On first looking at the problem it would seem essential to specify all three components of electric field on S.* Green's theorem, however, teaches that it is sufficient to specify either the normal or the tangential field components. Thus in the example in Section 3.1.1 it was sufficient to consider the normal component of field only.

The physical basis of this is as follows. An arbitrary value of normal field can be introduced at any part of S by placing close to S a surface distribution of electric charge. Green's theorem states that it is possible to produce any arbitrary field within a closed volume solely by a layer of surface charge. A special case is that of zero electric field. It is clear that zero electric field can always be produced by surface charge on conductors of any arbitrary shape. Green's theorem shows that not only zero field but any other field can be produced in this manner.

Just as a step in the normal field is due to a charge layer, so a step in the tangential field can be produced by a layer of electric doublets.[10] This is of great interest in magnetostatic problems and is mentioned in Section 3.2.2.

The fact that we can specify either tangential or normal field seems to imply a possibility of choice of surface distributions. This, however, is only a mathematical possibility, since layers of electric doublets do not occur in nature.† If they did exist, they would correspond to a surface distribution of steady magnetic current.

(3.2) Magnetostatic Fields

Magnetostatic fields can be regarded as being due either to a distribution of steady electric currents or to a distribution of magnetic poles (or dipoles). We shall consider each point of view in turn.

If the sources of the magnetostatic field are electric currents, it is convenient to describe the field by a vector potential $\boldsymbol{A}$, where $\boldsymbol{B}$, the magnetic flux density, is related to $\boldsymbol{A}$ by $\boldsymbol{B} = \nabla \times \boldsymbol{A}$. Stratton[11] gives a vector form of Green's theorem, which he obtains as follows:

In Gauss's identity [eqn. (1)] let the vector be $\boldsymbol{P} \times \nabla \times \boldsymbol{Q}$. Then

$$\iint_S (\boldsymbol{P} \times \nabla \times \boldsymbol{Q}) \,.\, n dS = \iiint_v \nabla \,.\, (\boldsymbol{P} \times \nabla \times \boldsymbol{Q}) dv \qquad (6)$$

Therefore

$$\iint_S (\boldsymbol{P} \times \nabla \times \boldsymbol{Q}) \,.\, n dS = \iiint_v [(\nabla \times \boldsymbol{P}) \,.\, (\nabla \times \boldsymbol{Q}) - \boldsymbol{P} \,.\, (\nabla \times \nabla \times \boldsymbol{Q}) dv] \qquad (7)$$

It will be seen that eqn. (7) is closely analogous to eqn. (2): it is, in fact, Green's theorem in vector form. We proceed as in Section 3.1. Let $\boldsymbol{P} = \boldsymbol{Q} = \boldsymbol{A}$. Then

$$\iint_S (\boldsymbol{A} \times \nabla \times \boldsymbol{A}) \,.\, n dS = \iiint_v [(\nabla \times \boldsymbol{A})^2 - \boldsymbol{A} \,.\, (\nabla \times \nabla \times \boldsymbol{A})] dv \qquad (8)$$

Let $\boldsymbol{A}$ be the vector potential. Then $\nabla \times \boldsymbol{A} = \boldsymbol{B}$ and $\nabla \times \nabla \times \boldsymbol{A} = \nabla \times \boldsymbol{B} = \mu_0 \boldsymbol{J}$, where $\boldsymbol{J}$ is the electric current density. To find the criterion for uniqueness we examine the possibility of two solutions, $\boldsymbol{A}_1$ and $\boldsymbol{A}_2$, to satisfy eqn. (8). Then $\nabla \times \nabla \times \boldsymbol{A}_1 = \mu_0 \boldsymbol{J}$ and $\nabla \times \nabla \times \boldsymbol{A}_2 = \mu_0 \boldsymbol{J}$. Let $\boldsymbol{C} = \boldsymbol{A}_1 - \boldsymbol{A}_2$ and apply eqn. (8) to this difference field. Then $\nabla \times \nabla \times \boldsymbol{C} = 0$ and

$$\iint_S (\boldsymbol{C} \times \nabla \times \boldsymbol{C}) \,.\, n dS = \iiint_v (\nabla \times \boldsymbol{C})^2 dv \qquad (9)$$

If the left-hand side of this equation is zero, the integrand of the right-hand side must be zero. In such a case $\nabla \times \boldsymbol{C} = 0$, i.e. $\nabla \times \boldsymbol{A}_1 = \nabla \times \boldsymbol{A}_2$ and $\boldsymbol{B}_1 = \boldsymbol{B}_2$. The magnetic field is then unique. The left-hand side of eqn. (9) can be written

$$\iint_S (\boldsymbol{C} \times \nabla \times \boldsymbol{C}) \,.\, n dS = \iint_S (\nabla \times \boldsymbol{C}) \times \boldsymbol{n} \,.\, \boldsymbol{C} dS = \iint_S (\boldsymbol{n} \times \boldsymbol{C}) \,.\, (\nabla \times \boldsymbol{C}) dS$$

Now if $\boldsymbol{n} \times \boldsymbol{C}$ is constant on S we have

$$\iint_S (\boldsymbol{n} \times \boldsymbol{C}) \,.\, (\nabla \times \boldsymbol{C}) dS = (\boldsymbol{n} \times \boldsymbol{C}) \iint_S (\nabla \times \boldsymbol{C}) \times n dS = \boldsymbol{n} \times \boldsymbol{C} \iiint_v (\nabla \times \nabla \times \boldsymbol{C}) dv = 0$$

Thus the criterion for uniqueness is that either the tangential components of $\boldsymbol{C}$ shall be constant or the tangential components of $\nabla \times \boldsymbol{C}$ shall be zero everywhere on S. This means that either normal B or tangential B must be specified everywhere on S. The formulation of the image problem in the magnetostatic case is therefore as follows:

> Consider a surface S which totally encloses a volume v. Determine the normal magnetic field (or the tangential magnetic field) on S due to the induced currents on the boundaries. Find a distribution of current outside S to give on S the same normal or tangential B. Then this distribution of currents will give within v the same field as is given by the induced currents on the boundaries. Thus it is the image distribution required.

As in the electrostatic case the images must be virtual, i.e. they must lie outside v.

* It should be noted that the surface S considered here is not the actual boundary but an adjacent surface just to the right of the boundary. The reason for this is that $\partial\phi/\partial n$ is discontinuous at the boundary and Green's theorem [eqn. (3)] applies only if $\partial\phi/\partial n$ is continuous throughout v.

† It should be pointed out that we are here dealing with movable surface distributions like electric charges and currents which can be induced on a boundary. It is, of course, true that fixed layers of electric doublets occur very commonly, if not universally, on the surfaces of solids and are necessary for an explanation of the existence of the 'potential barrier' which is observed as an electron passes into or out of a solid.

The alternative view of the magnetostatic field is to regard its sources as magnetic dipoles. All currents must be replaced by equivalent magnetic shells. The magnetic field can then be derived from a scalar potential and the treatment in Section 3.1 applies throughout. The formulation of the image problem is therefore identical whether one proceeds from consideration of currents or dipoles.

(3.2.1) An Example: Line Current Parallel to the Face of a Semi-Infinite Magnetic Slab.

Fig. 2 shows an infinite line current I at a distance d from the face of a semi-infinite magnetic slab of permeability μ.

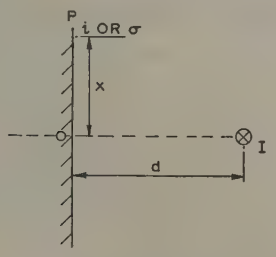

Fig. 2.—Line current parallel to the face of a semi-infinite magnetic slab.

First, let all sources of the magnetic field be electric currents. Let i be the induced current density at P, and let B_t be the tangential magnetic field due to I at P. Then

$$\mu_0 \frac{i}{2} - B_t = -\mu\left(\frac{\mu_0 i}{2} + B_t\right) \quad . \quad . \quad . \quad (10)$$

Therefore

$$i = -\left(\frac{\mu - 1}{\mu + 1}\right) 2\frac{B_t}{\mu_0}$$

The tangential field due to i just to the right of the boundary is

$$\frac{\mu_0 i}{2} = -\left(\frac{\mu - 1}{\mu + 1}\right) B_t$$

Thus the image current is $I[(\mu - 1)/(\mu + 1)]$ at a distance d to the left of O.

Alternatively, let all sources of the magnetic field be magnetic poles. Let σ be the induced pole strength at P, and B_n be the normal magnetic field due to the magnetic shell bounded at I.

Then

$$\frac{\sigma}{2} + B_n = -\mu\left(\frac{\sigma}{2} - B_n\right) \quad . \quad . \quad . \quad . \quad (11)$$

$$\frac{\sigma}{2} = \frac{\mu - 1}{\mu + 1} B_n$$

Thus the image magnetic shell can be represented by a current $I[(\mu - 1)/(\mu + 1)]$ as before.

(3.2.2) The Physical Meaning of the Magnetostatic Boundary Conditions.

There are some unsatisfactory features in the discussion of the example in Section 3.2.1 which throw a great deal of light on the physical nature of the magnetostatic field. If we consider that all sources of this field are electric currents, we must postulate a surface current i in a magnetic material. Physically, however, no such current will flow. This current i would have to be greatest at O, but if the magnetic material is iron, having a domain structure, there will be no effect at all at O. Thus i describes the magnetic effect mathematically but not physically. A better physical description is given by the surface polarity σ, which gives the average magnetic effect of domains which have been rotated by the current I.

If, on the other hand, all sources of the magnetic field are to be poles, I must be replaced by a magnetic shell, and this is a mathematical device without physical content.

We are thus led to the conclusion that there are two types of source—electric currents and magnetic poles. These poles may, in turn, be due to the orbital and spin motions of electrons. In this case we should have to talk about two types of current—normal electric current and atomic electric current. But because of the difficulties of a fully relativistic treatment, engineers who use magnetic materials find the notion of magnetic pole-strength very convenient.

Eqns. (3) and (8) now assume a new significance. Tangential B is a double layer of pole strength and normal B is a single layer. Thus tangential B represents a current loop and normal B a magnetized surface. Similarly A is a single layer of pole strength and B an electric current layer.[12] In other words, the field can be uniquely specified either by electric currents or by magnets or by a combination of both. This is, of course, reasonable. We can use air-cored coils, permanent magnets or iron-cored coils to produce a magnetostatic field.

In the method of images we can therefore use either current images or magnetic images or a combination of both types. This greatly enlarges the scope of the method.

(3.3) Electromagnetic Fields

Consideration of the uniqueness of electromagnetic fields is complicated by the fact that the sources of the electric field are not only electric charges but also changing magnetic fields. In other words, the electric field has both divergence and curl, and for its definition requires both a scalar and a vector potential. At first sight the magnetic field offers a simpler approach, because it has no divergence and can still be derived solely from a vector potential. But this potential is now a 'delayed' potential and the sources of the magnetic field include displacement current as well as conduction current. Some writers, including Stratton,[13] discuss the uniqueness of the electromagnetic field by using Poynting's theorem, but this discussion seems to the author to be inconclusive.[15] We shall therefore approach the question in a different manner: we shall consider only steady-state variation in time, and since any such variation can be expressed by a Fourier series, we need only consider a single frequency.

In the method of images we are concerned with the field of the induced currents and charges on the boundaries. Discussion can therefore be limited to the case where there are no currents or charges within v. Then it is shown by Stratton[14] that the electric field within v at any point x, y, z is given by

$$\boldsymbol{E} = -\frac{1}{4\pi}\iint_S [j\omega(\boldsymbol{n} \times \boldsymbol{B})\zeta + (\boldsymbol{n} \times \boldsymbol{E}) \times \nabla\zeta + (\boldsymbol{n} \,.\, \boldsymbol{E})\nabla\zeta] dS$$
$$. \quad . \quad . \quad . \quad (12)$$

where $\zeta = \varepsilon^{jkr}/r$ and r is the distance measured from an element of surface dS to the point of observation x, y, z. The frequency is given by ω, and $k = \omega/c$ where c is the velocity of light.

Now $\boldsymbol{n} \times \boldsymbol{B}$, the tangential components of $\boldsymbol{B}$, are defined by a surface electric current. Similarly $\boldsymbol{n} \times \boldsymbol{E}$ is a surface 'magnetic current' and $\boldsymbol{n} \,.\, \boldsymbol{E}$ a surface charge. It therefore appears that we need to specify tangential $\boldsymbol{B}$ and normal and tangential $\boldsymbol{E}$ everywhere on S. But tangential $\boldsymbol{B}$ and normal $\boldsymbol{E}$ are related by Maxwell's equation $\nabla \times \boldsymbol{H} = \partial \boldsymbol{D}/\partial t$. In the same manner the surface current and charge distributions are related by the equation of continuity of charge. Thus a knowledge of

tangential E and H on S is sufficient to make the field unique within v.

The formulation of the image problem is therefore as follows:

> Consider a surface S which totally encloses a volume v. Determine on S the tangential components of the electric and magnetic field due to the induced currents and charges on the boundaries. Find a distribution of current and charge outside S to give on S the same tangential components of electric and magnetic field. Then this distribution will give within v the same field as is given by the induced currents and charges. Thus it is the image distribution required.

Unfortunately it is in general impossible to follow this procedure. For a simple image we should need both the tangential and normal electric field of the image to have a constant ratio to the tangential and normal electric field of the source. Now the induced currents and charges will modify the normal electric field in some definite ratio; but the tangential field will not vary in the same manner, because it depends, not only on the currents and charges, but also on the conductivity of the boundaries. If the boundary could adjust the tangential electric field independently of the normal electric field, an image might be found; but a step in tangential E implies a surface 'magnetic current' and this does not occur in nature. To adjust the two types of electric field we need two types of surface current. Since only one type occurs in nature, the double adjustment is impossible.

There is, however, one important case in which the method of images can be applied. If the boundaries have infinite conductivity, the tangential electric field of the boundary currents and charges will be equal and opposite to the tangential electric field of the source. Furthermore the normal electric fields and the tangential magnetic fields will be equal and of the same sign.* Then an image can be found. It should be noted that the boundaries must be plane in order that there shall be no path difference between the source and the image. In electromagnetic problems the method of images can therefore be used only when the boundaries are flat sheets of very large conductivity.[16, 17]

It should be noted that attention has again been confined to virtual images in spite of the fact that we are dealing with electromagnetism and that light is an electromagnetic phenomenon. The real images of optics are points of intense electric field and are caused by changing magnetic fields. But in the method of electromagnetic images we require an image source of the same characteristics as the actual source. Thus the image source must have currents and charges and we cannot insert such a source into the volume under consideration without doing violence to the physical system. It must be concluded that the real images of optics are approximations only and do not accurately reproduce the characteristics of the true source of light.

(3.3.1) An Example: Aerial near the Face of an Infinite Plane Conducting Sheet of Zero Resistivity.

In Fig. 3 let the surface current density be i and the surface charge density be σ; let the suffix 1 refer to the field of the source and the suffix 2 to the field of i and σ. Then the tangential electric field must obey the relationships

$$\left.\begin{aligned} E_{x1} &= -E_{x2} \\ E_{z1} &= -E_{z2} \end{aligned}\right\} \quad \text{and} \quad \ldots\ldots \quad (13)$$

* It might be asked how it comes about that an image which ensures that tangential E is zero over the boundary also ensures that tangential H is correctly adjusted, i.e. that tangential H is doubled just inside the boundary. The physical reason for this double adjustment lies in the fact that electromagnetic energy cannot be transferred across a surface of infinite conductivity. Consider this with reference to the Poynting vector $E \times H$. Since there is no energy flow across the boundary, it is necessary that the surface integral of the Poynting vector of the image must be equal and opposite to that of the source. But tangential E is already equal and opposite, which demands that tangential H must be equal and of the same sign. Thus the tangential H is doubled.

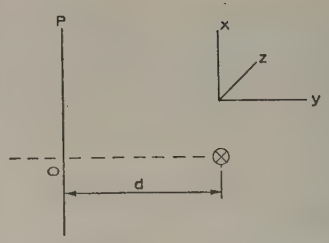

Fig. 3.—Aerial near to the face of an infinite plane conducting sheet.

Moreover, the tangential magnetic field must obey the relationships

$$\left.\begin{aligned} H_{x1} = H_{x2} &= -\frac{i_z}{2} \\ H_{z1} = H_{z2} &= \frac{i_x}{2} \end{aligned}\right\} \quad \ldots\ldots \quad (14)$$

The normal electric field can be derived from Maxwell's equations

$$\left.\begin{aligned} \frac{\partial H_{x1}}{\partial z} - \frac{\partial H_{z1}}{\partial x} &= \frac{\partial E_{y1}}{\partial t} \\ \frac{\partial H_{x2}}{\partial z} - \frac{\partial H_{z2}}{\partial x} &= \frac{\partial E_{y2}}{\partial t} \end{aligned}\right\} \quad \ldots\ldots \quad (15)$$

Therefore $E_{y1} = E_{y2}$. In terms of charge density σ, $E_{y2} = \sigma/2\varepsilon_0$ and therefore $E_{y1} = \sigma/2\varepsilon_0$. Hence the normal electric force within the conducting sheet is given by $E_{y1} + E_{y2} - \sigma/\varepsilon_0 = 0$, and this is the required value. Thus the specification of tangential H has included the specification of normal E.

The image aerial is therefore required to give at the surface S (just to the right of the conducting sheet) $-E_{x1}$, $+E_{y1}$, $-E_{z1}$. This is the field of an equal and opposite aerial at a distance d to the left of O.

(4) APPLICATIONS OF THE METHOD OF IMAGES

(4.1) Image Forces on a Cylindrical Cathode

Refer to Fig. 4 and consider a line charge of strength $+q$ parallel to a conducting cylinder. Let the charge be placed at B.

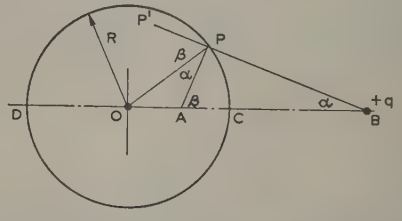

Fig. 4.—Line charge parallel to an infinitely long conducting cylinder.

If there is an image charge it must, by symmetry, lie on the diameter through B. Assume that its position is at A and its strength is $-q'$. In order that this image may correctly specify the field outside the cylinder, it is required that its normal field just outside the cylinder shall be equal to the normal field of the charge $+q$. Consider a typical point P on the cylinder as shown in Fig. 4.

If we choose $\angle OPA = \angle PBA = \alpha$, the angles will be as shown in the Figure and A and B will be inverse points with respect to the circle.

The normal force of $-q'$ will be $\frac{q'}{2\pi\epsilon_0}\frac{\cos\alpha}{PA}$

and of $+q$ $\frac{q}{2\pi\epsilon_0}\frac{\cos\beta}{PB}$

If we choose $q = q'$ the difference of the normal forces will be

$$\frac{q}{2\pi\epsilon_0}\left[\frac{\cos\alpha}{PA} - \frac{\cos\beta}{PB}\right] = \frac{q}{2\pi\epsilon_0}\frac{1}{OP} = \frac{q}{2\pi\epsilon_0}\frac{1}{R}$$

where R is the radius of the cylinder.

Thus the charge $-q$ at A is not sufficient by itself to give the correct normal field at P. If, however, an additional charge $+q$ is placed on the axis of the cylinder, the normal field will be correct. Thus the required image distribution consists of a charge $-q$ at A and a charge $+q$ at O.* If the single line charge $+q$ outside the cylinder is replaced by a tube of charge, it is clear that the image system will be a tube of opposite sign passing through the inverse points inside the cylinder plus a line charge of the same sign at the centre of the cylinder. This system is shown in Fig. 5. There will then be no electric field

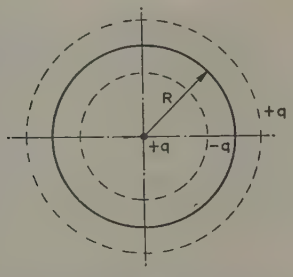

Fig. 5.—Image charges on a long cylindrical cathode surrounded by a tubular charge distribution.

between the cylinder and the tube outside it. The two images entirely cancel and it could justly be said that there is no image at all. There is certainly no image force. If then the outside tube represents a uniform cloud of electrons around a cathode, there will be no image forces on these electrons.

This conclusion appears very paradoxical to engineers familiar with the behaviour of valves. The paradox is, however, explained if we consider the potential of the cathode. In our discussion the cathode has so far been represented by an isolated uncharged metal cylinder. If now this cylinder is kept at earth potential by an external connection, the potential of the external charge plus the image charges must be zero at the surface of the cylinder.

Consider then the sum of the potentials of a charge $+q$ at B and its image charge $-q$ at A. At any point P on the surface of the cylinder the potential is

$$\phi = \frac{q}{2\pi\epsilon_0}\log\frac{PB}{AP} = \frac{q}{2\pi\epsilon_0}\log\frac{OB}{OP} = \frac{q}{2\pi\epsilon_0}\log\frac{OB}{OC}$$

If B is very near the surface of the cylinder OB $\simeq$ OC and ϕ tends to zero. It follows that, if the potential of the cylinder is to be kept constant, it will be necessary to remove the second image charge $+q$ at O. The cylinder then has a net charge of $-q$. Because of this charge there will be a field outside the cylinder even when the external charge $+q$ is arranged in the form of a tube around the cylinder. Thus there will be a force on a distribution of electrons around an earthed cathode, and the paradox is resolved.

* It should be noted that the matching of the normal field automatically ensures that the charge is conserved, i.e. that there is no net charge within the cylinder. If we had made use of the tangential force, the additional charge on the axis of the cylinder would have had to be inserted by invoking the conservation of charge explicitly. In dealing with a field of divergence sources it is thus always safer to match the normal field components. Similarly, in dealing with a field of curl sources it is safer to match the tangential field components.

(4.2) Images of the Current Distributions found in Electrical Machines

In electrical machines such as motors and generators it is of great importance to determine the magnetic field of those parts of the winding which are known as the end-connections. Unlike the slot portion of the windings, the end-connections do not contribute to the useful torque or electromotive force. Their importance lies in the fact that they cause eddy-current losses, which it is the designer's object to reduce. Moreover, these end-windings are particularly vulnerable to forces which may occur on short-circuit and they have to be carefully braced.

The end-windings are not embedded in iron, but they are close to the iron masses of the machine. The method of images offers a useful approach to the problem because it should be possible to estimate the contribution to the magnetic field made by the iron surfaces in terms of an image of the end-winding. Because the end-windings are of complicated shape, it is helpful to examine briefly the effect of small current loops and current elements before considering a complete winding.

(4.2.1) Images of Current Loops and Current Elements.

Consider first a loop of constant current I opposite an iron boundary of permeability μ. The images are shown in Fig. 6. It therefore appears that currents parallel to the iron are reflected with equal sign and perpendicular currents with opposite sign.

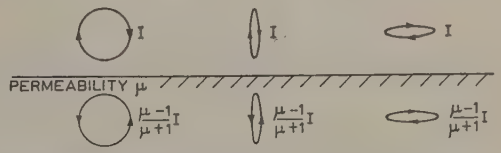

Fig. 6.—Images of current loops in a plane magnetic surface.

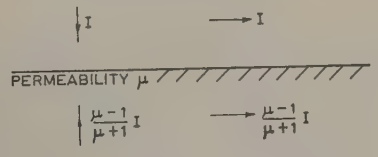

Fig. 7.—Supposed images of current elements in a plane magnetic surface.

It would, in fact, be tempting to formulate a rule for current elements as shown in Fig. 7.

A rule like this is given by Schelkunoff[18] for images in conducting sheets. Consideration will show, however, that Fig. 7 is not justified. Consider the vertical current element: if we use Biot and Savart's expression for the magnetic field of a current element,

$$H = I\frac{dl \times r}{4\pi r^3}$$

we note that the vertical current element has no component of magnetic force perpendicular to the surface of the iron. Hence no polarity is induced and the field outside the iron is not affected by the presence of the iron. Thus it could justly be

said that the vertical current element has no image; but this is not conclusive, because the Biot–Savart law is not unique[19] unless it is applied to a Heaviside rational current element.[20] Moreover, the Heaviside element requires to be immersed in an infinite conducting medium, and the iron surface would interfere with this medium. The plain fact is that a current element is not a physical entity and no amount of theory can make it so. It is impossible to apply the method of images to isolated current elements.

Although steady current elements are a physical impossibility, it is possible to have electric doublets, i.e. alternating current elements with charges at their ends. The images of these in iron are not easy to determine, because currents will flow in the iron by virtue of the alternating fields. Let us approach this problem by a consideration of images in a sheet of infinite conductivity. Fig. 8 shows the images of electric doublets and of small loops of alternating current. Comparison of Fig. 6 with Fig. 8 reveals the fact that the image of an alternating current loop in a conducting surface is opposite in sign to the image of a steady current loop in a magnetic surface. Fig. 9 shows the images of electric doublets in a perfect magnetic conductor (if such a substance existed). If will be noted that the images are of opposite sign to the images in a perfect electrical conductor.

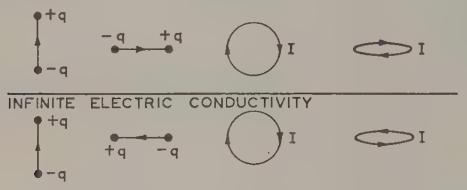

Fig. 8.—Images of electric doublets and current loops in a plane perfect electric conductor.

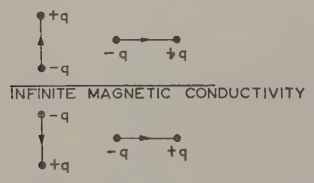

Fig. 9.—Images of electric doublets in a plane perfect magnetic conductor.

The images of the current loops, current elements and electric doublets described in Figs. 6, 7 and 9 arise when the current is outside the magnetic material. In electrical machines, however, parts of the conductors are embedded in iron. We must therefore consider the image distribution of currents inside a magnetic material. This image distribution is easily derived, by the method of this paper, for the fields both within and outside the iron.

Fig. 10 shows the image effect outside the iron of current loops embedded in the iron. It is seen that the iron has the effect of adding a current loop of strength $I[(\mu-1)/(\mu+1)]$ in the same place as the current loop I. The effect of current and iron combined is therefore the same as if the iron were removed and the current strength were increased to $2\mu I/(\mu+1)$. For large values of μ this means doubling the current.

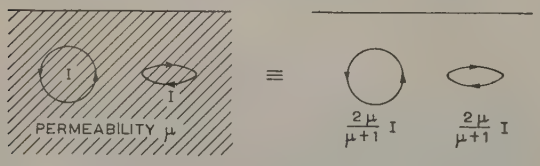

Fig. 10.—Images of current loops embedded in a magnetic material.

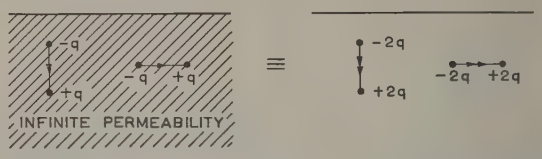

Fig. 11.—Images of electric doublets embedded in an infinitely permeable material.

Fig. 11 shows image effects outside a region of infinite permeability. It will be seen that the strength of the electric doublets has been increased twofold.

(4.2.2) The Method of Images applied to the End-Windings of Electrical Machines.

The discussion in the previous Section shows that a distinction must be made between direct and alternating currents. With alternating currents the conductors can be broken up into electric doublets terminated by finite charges. Direct-current elements are a physical impossibility, but they can be regarded as the limiting case of an electric doublet as the frequency tends to zero.

A further distinction must be made between images in magnetic surfaces and conducting surfaces. The two types of image are of opposite sign, as shown in Figs. 8 and 9. In treating the field of a machine end-winding it has therefore to be decided whether the eddy-currents in the core end-plates make the surface of these plates into a conducting sheet, or whether they are sufficiently inhibited to allow the end-plate to act as a magnetic sheet.

Coils of any arbitrary shape can be treated as a succession of electric doublets, and the method is therefore completely general. Fig. 12 shows the image of a typical coil-end in a perfectly conducting sheet; Fig. 13 shows the image effect outside the iron of a coil emerging from the iron; and Fig. 14 shows the image effect inside the iron for the same coil.

In considering the field outside the iron it is likely that Fig. 13

Fig. 12.—Images of a coil-end near an infinitely conducting sheet.

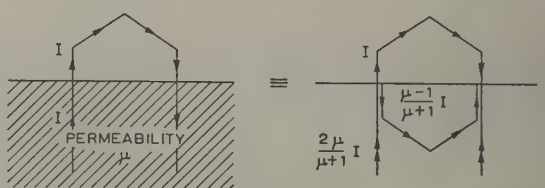

Fig. 13.—Image effect in air of a coil-end emerging from a block of magnetic material.

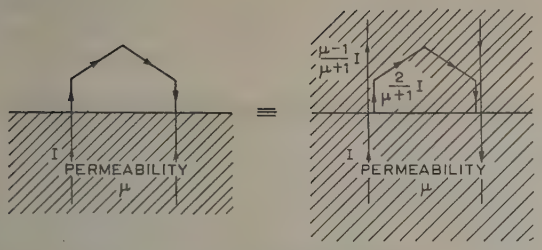

Fig. 14.—Image effect in magnetic material of a coil-end emerging from a block of magnetic material.

is nearer the truth than Fig. 12. Nevertheless, the eddy-currents will reduce the image effect shown in Fig. 13. Recourse must be had to measurement rather than calculation, but the method of images has pointed the way to fruitful experimental investigation.

(5) CONCLUSIONS

The method of images has a very wide field of application. In electrostatics and magnetostatics the method is not confined to problems involving equipotential boundaries. If the problem is expressed in terms of a scalar potential, an image source is adequately specified if the normal component of the field is specified everywhere on a closed surface. If the problem is expressed in terms of a vector potential, it is necessary and sufficient to specify the tangential components of the field everywhere on a closed surface.

In electromagnetic problems the tangential components of both the electric and magnetic field have to be specified on a closed surface. In general this is impossible, and the image method must be confined to problems involving infinitely conducting boundaries.

All electric and magnetic images are virtual, and the analogy with optical images must not be pressed too far.

The application of image methods to problems involving low-frequency currents near iron boundaries is difficult. For certain frequencies there are likely to be very small image effects. Experimental work is required to investigate this tentative conclusion.

(6) REFERENCES

(1) Moullin, E. B.: 'On the Amplification Factor of the Triode', *Proceedings I.E.E.*, Monograph No. 211 R, November, 1956 (**104** C, p. 222).
(2) Lord Kelvin: 'Reprint of Papers on Electrostatics and Magnetism' (Macmillan, 1872), pp. 52 and 144.
(3) Maxwell, J. C.: 'Electricity and Magnetism' (Clarendon Press, 1892), Chapter XI.
(4) *Ibid.*, Article 318.
(5) *Ibid.*, Article 662.
(6) Searle, G. F. C.: 'On the Magnetic Field due to a Current in a Wire Placed Parallel to the Axis of a Cylinder of Iron', *The Electrician*, 28th January, 1898, pp. 453 and 510.
(7) Hague, B.: 'Electromagnetic Problems in Electrical Engineering' (Oxford University Press, 1929), Chapter IV.
(8) Jeans, Sir James: 'Electricity and Magnetism' (Cambridge University Press, 1925), Articles 208–225.
(9) Green, G.: 'An Essay on the Application of Mathematical Analysis to the Theories of Electricity and Magnetism' (Printed privately at Nottingham, 1828), p. 11.
(10) Abraham, M., and Becker, R.: 'Electricity and Magnetism' (Blackie, 1950), Chapter II, Section 8.
(11) Stratton, J. A.: 'Electromagnetic Theory' (McGraw-Hill, 1941), p. 250.
(12) *Ibid.*, pp. 247 and 243.
(13) *Ibid.*, pp. 486–488.
(14) *Ibid.*, pp. 464– 468.
(15) Hammond, P.: 'Electromagnetic Energy Transfer', *Proceedings I.E.E.*, Monograph No. 286, February, 1958 (**105** C, p. 352).
(16) Moullin, E. B.: 'Radio Aerials' (Clarendon Press, 1949), p. 121.
(17) Aharoni, J.: 'Antennae' (Clarendon Press, 1946), pp. 212 and 216.
(18) Schelkunoff, S. A.: 'Electromagnetic Waves' (Van Nostrand, 1943), p. 171.
(19) Whittaker, Sir Edmund: 'A History of the Theories of Aether and Electricity' (Nelson, 1951), Vol. 1, p. 82.
(20) Heaviside, O.: 'Electrical Papers' (Macmillan, 1892), Vol. 2, Article 48.

621.376.3

The Institution of Electrical Engineers
Monograph No. 380 E
May 1960
©

R.F. SPECTRA OF WAVES FREQUENCY MODULATED WITH WHITE NOISE

By R. G. MEDHURST, B.Sc.

(*The paper was first received 28th August, 1959, and in revised form 28th January, 1960. It was published as an* INSTITUTION MONOGRAPH *in May, 1960.*)

SUMMARY

Although comprehensive sets of curves are available giving the radio-frequency spectra of waves phase modulated with band-limited white noise (simulating f.d.m. telephony signals), the corresponding problem for frequency modulation turns out to be much more intractable. In the present paper the frequency-modulation problem is attacked using a method employed in an earlier paper, in conjunction with numerical devices for improving the convergence rate of very slowly converging series. The results are presented as a set of curves covering the range of modulation parameters likely to be encountered in trunk radio systems. This information is necessary for the evaluation of system bandwidth and interference due to unwanted carriers.

To bring the analysis within reasonable bounds, the minimum modulating frequency has been taken as zero. It is known that unless the ratio between r.m.s. frequency deviation and maximum modulating frequency is large, the shape of the central portion of the spectrum changes substantially as the minimum modulating frequency departs from zero. However, for practical ranges of parameters there is evidence indicating that the shape of the spectrum tails (which is of particular importance in connection with distortion problems) is not greatly sensitive to variations in the minimum modulating frequency.

LIST OF PRINCIPAL SYMBOLS

ω_c = Carrier frequency, radians/sec.
ω_M = Frequency modulation, radians/sec.
ω_Δ = R.M.S. frequency deviation, radians/sec.
μ_t = Phase modulation, radians.
$\hat{\omega}_m$ = Maximum modulating frequency, radians/sec.
$\check{\omega}_m$ = Minimum modulating frequency, radians/sec.
ω_m = A representative frequency of the noise-band modulation, radians/sec.
$\phi_{\omega m}$ = A random phase angle associated with the tone of frequency ω_m, radians.
ω = Difference between a general angular frequency and ω_c, radians/sec.
ω_b = Width of a narrow frequency band centred on a frequency $\omega_c \pm \omega$, radians/sec.

$$\mathrm{Si}(x) = \int_0^x \frac{\sin z}{z} dz.$$

$\beta = \omega/\hat{\omega}_m$.

(1) INTRODUCTION

The evaluation of the spectra of waves frequency- or phase-modulated by random noise has been discussed in a number of papers.[1, 3, 6–11] The present position is that adequate numerical results are available for the r.f. spectrum when the spectrum of the noise-band modulation is of Gaussian shape (with either frequency or phase modulation),[7] and for phase modulation when the modulation consists of band-limited white noise.[1] No complete solution is available for frequency modulation by band-limited white noise. Attempts to derive approximate solutions valid for various limiting conditions have not been completely successful; a discussion of the analytical reasons for this is given in Reference 2.

This problem continues to be of interest in connection with f.m. trunk radio systems, carrying multi-channel telephony in frequency-division-multiplex.[22] In these systems the modulating signal is made up of telephony speech channels translated in frequency so as to occupy 4 kc/s bands spaced one above another. For test purposes it is assumed[12, 13] that the signal can be adequately represented by a band of random noise, of suitable level, having a uniform spectrum extending between frequency limits defined by the upper and lower telephony channels (i.e. band-limited 'white' noise). The shape of the r.f. spectrum when a carrier is frequency-modulated by such a signal constitutes essential system design data required in order to calculate system bandwidth[6] and interference due to unwanted carriers;[3] in absence of numerical information it has, in the past, been necessary to resort to guess-work.[26] In both problems, spectral levels in the tail regions (i.e. the regions of low spectral power, well removed from the carrier frequency) are of particular interest.

Whatever the spectral distribution of the random noise modulation, it is found[6, 7, 11] that for sufficiently large deviation ratios (i.e. ratios of r.m.s. frequency deviation to maximum modulating frequency) the r.f. spectrum approaches a Gaussian shape. When the deviation ratio is not large, analytical difficulties enter at two levels. Direct numerical evaluation of the integral defining the r.f. spectrum is found to be impracticable, and proposed approximations break down in the tail region,[2] even on the simplifying assumption that the minimum modulating frequency is zero (a limiting case discussed by Stewart).[11] When the minimum modulating frequency is increased from zero to a finite value, the disturbance—at least to the central part of the r.f. spectrum—is known[2, 6] to be considerable, but the corresponding integral now becomes even more intractable.

Most of the published analytical work[1–3, 7, 9, 11] is based on the Wiener–Khintchine relation between the autocorrelation function and the power spectrum of the modulated wave. This approach always enables one to write down an integral defining the power spectrum of any analytical function of a band of random noise, although the cases in which the integral can be easily evaluated are in a minority. Quite a different approximate method which does not seem subject to the same limitations was used in Reference 8. The method was not, however, applied to systems having low deviation ratio, and in addition it appears not to be easy to assess the accuracy of the results.

In the present paper the integral defining the r.f. spectrum is attacked by a method previously used in Reference 3. In this approach the integral (or rather the sum of an infinite number of such integrals) is replaced by an infinite series. In the examples considered in Reference 3 all the series thus produced converged sufficiently quickly to be summed directly. For smaller deviation ratios it is found that the convergence rate is very slow indeed. Consequently, it has proved necessary to use numerical devices[4, 5] to improve the convergence rate. The theory of these techniques is still in course of development, and during the

Correspondence on Monographs is invited for consideration with a view to publication.
The paper is a communication from the Staff of the Research Laboratories of The General Electric Company Limited, Wembley, England.

present work certain unexpected limitations came to light. However, it appears that if adequate precautions are taken such methods can be made to yield reliable answers.

(2) PRACTICAL MODULATION PARAMETER VALUES

In the absence of pre-emphasis, three parameters define the shape of the r.f. spectrum with white-noise frequency modulation, namely the maximum and minimum modulating frequencies and the r.m.s. frequency deviation. Before commencing the analysis it has to be decided which ranges of these parameters need consideration. Table 1 gives likely modulating conditions characterized by a discrete spike of power at the carrier frequency and abrupt discontinuities in the power distribution away from carrier. With likely values of $\check{\omega}_m/\hat{\omega}_m$ this condition occurs only for small values of $\omega_\Delta/\hat{\omega}_m$.

(3) GENERAL EXPRESSION FOR THE R.F. SPECTRUM

The modulated carrier will be taken as having unit power. It is thus written as

$$\sqrt{2}\cos(\omega_c t + \mu_t) \quad . \quad . \quad . \quad . \quad . \quad . \quad (1)$$

It is shown in Section 7.1 of Reference 3 (in a slightly different context) that the r.f. spectral power in a narrow band of width ω_b, centred on a frequency $\omega_c \pm \omega$, is given by

$$\frac{1}{2}\frac{\omega_b}{\hat{\omega}_m}\mathrm{F}(\omega) \quad . \quad . \quad . \quad . \quad . \quad . \quad (2)$$

where

$$\mathrm{F}(\omega) = \frac{2}{\pi}\exp(-\psi_0)\int_0^\infty \left\{\exp\left[\psi_u(y)\right] - 1\right\}\cos\left(\frac{\omega}{\hat{\omega}_m}y\right)dy \quad . \quad (3)$$

$$\psi_u(y) = \frac{\omega_\Delta^2}{\hat{\omega}_m - \check{\omega}_m}\left\{\frac{1}{\check{\omega}_m}\cos\left(\frac{\check{\omega}_m}{\hat{\omega}_m}y\right) - \frac{1}{\hat{\omega}_m}\cos y + \frac{y}{\hat{\omega}_m}\left[\mathrm{Si}\left(\frac{\omega_m}{\hat{\omega}_m}y\right) - \mathrm{Si}(y)\right]\right\} \quad . \quad (4)$$

and

$$\psi_0 = \omega_\Delta^2/(\hat{\omega}_m\check{\omega}_m) \quad . \quad . \quad . \quad . \quad . \quad (5)$$

It is known on both theoretical and experimental grounds[2, 6, 10]

Table 1

MODULATION CONDITIONS FOR VARIOUS NUMBERS OF TELEPHONY CHANNELS

Number of channels	Base-band range $\left(\frac{1}{2\pi}\check{\omega}_m \text{ to } \frac{1}{2\pi}\hat{\omega}_m\right)$	R.M.S. deviation per channel	Formula for equivalent noise-band r.m.s. level	Equivalent noise-band r.m.s. deviation $\left(\frac{1}{2\pi}\omega_\Delta\right)$	$\frac{\omega_\Delta}{\hat{\omega}_m}$	$\frac{\check{\omega}_m}{\hat{\omega}_m}$	$\frac{\omega_\Delta^2}{\check{\omega}_m\hat{\omega}_m}$
	kc/s	kc/s		kc/s			
6	12–36	20	A	26	0·71	0·33	1·5
6	12–36	50	A	64	1·77	0·33	9·4
12	12–60	20	A	30	0·50	0·20	1·3
12	12–60	50	A	75	1·25	0·20	7·8
12	6–54	20	A	30	0·56	0·11	2·8
12	6–54	50	A	75	1·39	0·11	17·4
24	12–108	35	A	59	0·55	0·11	2·7
24	12–108	50	A	84	0·78	0·11	5·5
36	12–156	35	A	64	0·41	0·08	2·2
36	12–156	50	A	91	0·59	0·08	4·5
36	12–156	100	A	183	1·17	0·08	17·8
60	60–300	50	A	101	0·34	0·20	0·6
60	60–300	100	A	202	0·67	0·20	2·3
60	60–300	200	A	404	1·35	0·20	9·1
120	60–552	50	A	116	0·21	0·11	0·4
120	60–552	100	A	232	0·42	0·11	1·6
120	60–552	200	A	464	0·84	0·11	6·5
240	60–1 052	200	B	551	0·52	0·06	4·8
300	60–1 300	200	B	616	0·47	0·05	4·9
600	60–2 540	200	B	871	0·34	0·02	5·0
960	60–4 028	200	B	1 102	0·27	0·01	5·0
960	316–4 188	200	B	1 102	0·26	0·01	0·9
1 800	316–8 204	140	B	1 056	0·13	0·04	0·4
2 700	316–12 388	140*	B	1 292	0·10	0·03	0·4

Formulae for r.m.s. equivalent noise band level:
A.—$(-1 + 4\log_{10} N)$ dBm0
B.—$(-15 + 10\log_{10} N)$ dBm0
where N = number of channels.

This is a tentative value, not approved by the IXth Plenary Assembly, C.C.I.R.

for numbers of channels ranging from 6 to 2 700. Two formulae for the r.m.s. equivalent noise-band level have been specified,[21] one covering numbers of channels from 12 to 240 and the other from 240 upwards. These are respectively formulae A and B, appended to the Table. The total r.m.s. frequency deviation is obtained by multiplying the r.m.s. deviation per channel by the voltage ratio corresponding to the noise-band level obtained from the appropriate formula. The values for the 6-channel system are tentative, since no noise loading recommendation is available. With 2 700 channels a lower r.m.s. deviation per channel may be used in practice.

It is seen from the Table that the ratio between the minimum and maximum modulating frequencies does not exceed 1/3. The ratio between the r.m.s. frequency deviation and the maximum modulating frequency falls in the range 0·1–2. The expression $\omega_\Delta^2/(\check{\omega}_m\hat{\omega}_m)$ is of interest, since it has been shown experimentally[6] that when this function falls below unity the spectrum takes on a 'low deviation' form (see also Reference 2)

that when $\omega_\Delta/\hat{\omega}_m$ is not large the spectrum in the frequency region between $\omega_c - \hat{\omega}_m$ and $\omega_c + \hat{\omega}_m$ is very sensitive to the value of $\breve{\omega}_m/\hat{\omega}_m$. There is a suggestion in Reference 2 that this sensitivity will not extend to the tail regions of the spectrum. If this can be shown to be so, much useful information will be obtained by evaluating spectrum shapes for various deviation ratios when $\breve{\omega}_m$ is zero. The result of putting $\breve{\omega}_m = 0$ in expression 2 can, of course, be regarded as the first term of an expansion of this expression in powers of $\breve{\omega}_m$. In an attempt not only to carry out the programme just suggested but also to gain more insight into the influence of the value of $\breve{\omega}_m$ on the form of the spectrum, it was decided to try to evaluate terms up to second order of the expansion in $\breve{\omega}_m$ representing expression (2). To this order, $F(\omega)$ is found to be given by

$$F(\omega) = \frac{2}{\pi}\int_0^\infty \exp\left\{\frac{\omega_\Delta^2}{\hat{\omega}_m^2}[1 - \cos y - y\,\mathrm{Si}\,(y)]\right\}\cos\left(\frac{\omega}{\hat{\omega}_m}y\right)dy$$
$$+ \frac{2}{\pi}\frac{\breve{\omega}_m}{\hat{\omega}_m}\int_0^\infty \frac{\omega_\Delta^2}{\hat{\omega}_m^2}\left[1 - \cos y - y\,\mathrm{Si}\,(y) + \frac{y^2}{2}\right]$$
$$\exp\left\{\frac{\omega_\Delta^2}{\hat{\omega}_m^2}[1 - \cos y - y\,\mathrm{Si}\,(y)]\right\}\cos\left(\frac{\omega}{\hat{\omega}_m}y\right)dy$$
$$+ \frac{2}{\pi}\frac{\breve{\omega}_m^2}{\hat{\omega}_m^2}\int_0^\infty \left\{\frac{\omega_\Delta^2}{\hat{\omega}_m^2}\left[1 - \cos y - y\,\mathrm{Si}\,(y) + \frac{y^2}{2}\right]^4\right.$$
$$\left. + \frac{1}{2}\frac{\omega_\Delta^4}{\hat{\omega}_m^4}\left[1 - \cos y - y\,\mathrm{Si}\,(y) + \frac{y^2}{2}\right]^2\right\}$$
$$\exp\left\{\frac{\omega_\Delta^2}{\hat{\omega}_m^2}[1 - \cos y - y\,\mathrm{Si}\,(y)]\right\}\cos\left(\frac{\omega}{\hat{\omega}_m}y\right)dy \quad . \quad . \quad (6)$$

The first term is the one considered by Stewart.[11]

These integrals are somewhat better behaved than the integral in expression (3), in so far as the non-oscillating parts of the integrands go fairly smoothly to zero, whereas a plot of the corresponding term in expression (3) exhibits a protracted series of peaks for large values of y.[3] However, as will appear in the following Section, the problem of numerical evaluation is still formidable.

(4) TECHNIQUE OF NUMERICAL EVALUATION OF THE SPECTRUM TERMS

The evaluation of the slowly converging integrals appearing in expression (6) was based on a formula due to Poisson, which may be written in the form

$$\sum_{n=1}^{\infty}\int_0^\infty \mathrm{f}(y)\cos(n\beta y)dy = \frac{\pi}{\beta}\left[\tfrac{1}{2}\mathrm{f}(0) + \sum_{n=1}^{\infty}\mathrm{f}\left(\frac{2\pi n}{\beta}\right)\right] - \tfrac{1}{2}\int_0^\infty \mathrm{f}(y)dy$$
. . . . . (7)

This is proved rigorously and at some length in Reference 14. A simple alternative derivation based on engineering concepts is given in Section 11.1.

Considering, for example, the first integral of expression (6), write

$$\mathrm{f}(y) = \exp\left\{\frac{\omega_\Delta^2}{\hat{\omega}_m^2}[1 - \cos y - y\,\mathrm{Si}\,(y)]\right\}$$

and
$$\mathrm{S}(A) = \int_0^\infty \mathrm{f}(y)\cos(\beta y)dy \quad . \quad . \quad . \quad . \quad (8)$$

where
$$A = 2\pi/\beta \quad . \quad . \quad . \quad . \quad . \quad . \quad (9)$$

The first term in $F(\omega)$ is then given by

$$\frac{2}{\pi}\mathrm{S}(A) \quad . \quad . \quad . \quad . \quad . \quad . \quad . \quad (10)$$

The method of evaluation to be described applies equally well to the other terms of $F(\omega)$, $f(y)$ in each case representing the whole of the integrand except for the final cosine term. From eqn. (7),

$$\sum_{n=1}^{\infty}\mathrm{S}\left(\frac{A}{n}\right) = \frac{A}{2}\left[\tfrac{1}{2}\mathrm{f}(0) + \sum_{n=1}^{\infty}\mathrm{f}(nA)\right] - \tfrac{1}{2}\int_0^\infty \mathrm{f}(y)dy \quad . \quad (11)$$

Using expression (11), the integrals in expression (6) which have rapidly oscillating integrands of slowly diminishing amplitude are replaced by series of discrete terms. Penalties for this improvement are that the wanted expression, $S(A)$, is replaced by a sum of an infinite number of similar expressions having argument A/n, and, in addition, an integral of the non-oscillating term in the original integrand makes its appearance. The first point is not too serious, particularly in the tail region of the spectrum. Terms of the form $S(A/n)$, for $n \geqslant 2$, represent spectral levels at frequency departures from carrier equal to n times the wanted frequency. Thus, in the tail region $S(A/2)$, etc., will be negligible compared with $S(A)$. In the spectrum region nearer to the carrier frequency the higher-order terms in S have to be allowed for (Section 11.2). The presence of the integral in eqn. (11) is undesirable, and it is removed by introducing the value of S for another argument α, where $\alpha < A$. Thus,

$$\sum_{n=1}^{\infty}\mathrm{S}\left(\frac{A}{n}\right) = \frac{A}{2}\left[\tfrac{1}{2}\mathrm{f}(0) + \sum_{n=1}^{\infty}\mathrm{f}(nA)\right]$$
$$- \frac{\alpha}{2}\left[\tfrac{1}{2}\mathrm{f}(0) + \sum_{n=1}^{\infty}\mathrm{f}(n\alpha)\right] + \sum_{n=1}^{\infty}\mathrm{S}\left(\frac{\alpha}{n}\right) \quad . \quad (12)$$

Proper choice of α yields series which, because of the regularity of the terms, are particularly amenable to the transformations discussed in Section 11.3. For example, putting $\alpha = A/2$ gives

$$\sum_{n=1}^{\infty}\mathrm{S}\left(\frac{A}{n}\right) = \frac{A}{4}\left[\tfrac{1}{2}\mathrm{f}(0) - \mathrm{f}\left(\frac{A}{2}\right) + \mathrm{f}(A) - \mathrm{f}\left(\frac{3A}{2}\right) + \ldots\right]$$
$$+ \sum_{n=1}^{\infty}\mathrm{S}\left(\frac{A}{2n}\right) \quad . \quad (13)$$

while $\alpha = A/3$ gives

$$\sum_{n=1}^{\infty}\mathrm{S}\left(\frac{A}{n}\right) = \frac{A}{3}\left[\tfrac{1}{2}\mathrm{f}(0) - \tfrac{1}{2}\mathrm{f}\left(\frac{A}{3}\right) - \tfrac{1}{2}\mathrm{f}\left(\frac{2A}{3}\right) + \mathrm{f}(A) - \ldots\right]$$
$$+ \sum_{n=1}^{\infty}\mathrm{S}\left(\frac{A}{3n}\right) \quad . \quad (14)$$

Numerical treatment of expressions of the form set out on the right-hand side of eqn. (12) requires evaluation at suitable intervals of the non-oscillatory portions of the integrands appearing in expression (6). The interval chosen will determine the frequencies at which spectral values can be obtained; decreasing the interval increases the maximum deviation from carrier frequency accessible for the computation of spectra values. Thus the interval must be as small as possible compatible with economy considerations. Furthermore, it will be found that, to give the best chance of success in the application of devices to speed convergence of the resulting series (Section 11.3), the interval should be a sub-multiple of the natural periods of any oscillating terms contained in the integrands. These are $\cos y$ and $\mathrm{Si}(y)$, both of which oscillate with period

2π. From these considerations it was decided to evaluate the integrands at intervals of $\pi/8$. The expression

$$\exp\left\{\frac{\omega_\Delta^2}{\hat{\omega}_m^2}[1 - \cos y - y\,\mathrm{Si}(y)]\right\}$$

was evaluated by hand to ten decimal places in the range $0(\pi/8)27\pi$ for $\omega_\Delta/\hat{\omega}_m = 0{\cdot}1$. Integrand values for $\omega_\Delta/\hat{\omega}_m = 0{\cdot}2$, $0{\cdot}3$, $0{\cdot}4$, $0{\cdot}5$, $0{\cdot}7$, $1{\cdot}0$, $2{\cdot}0$ were then obtained from a digital computer by raising the basic hand-computed data to suitable powers and, for the second and third integrals of expression (6), multiplying by appropriate factors.

For the larger values of $\omega_\Delta/\hat{\omega}_m$ the problem of spectral evaluation is now essentially solved, since the series on the right-hand side of expression (12) may be summed directly to a sufficient order of accuracy. For the smaller $\omega_\Delta/\hat{\omega}_m$ values, however, straightforward summation is out of the question because of the very slow convergence of the series. Thus, when $\omega_\Delta/\hat{\omega}_m = 0{\cdot}1$, the 217th term, corresponding to $y = 27\pi$, of the series derived from the first integral of expression (6) is still about 27% of the first term (i.e. unity), whereas for adequate convergence the last term considered should vanish to at least eight decimal places. Thus in this case the least accessible term is too large by a factor of order 10^8.

It is evident that rather drastic measures are required. What has been done here is to make use of numerical methods of improving convergence rate. The application of these techniques is to some extent empirical, in so far as, in a particular case, some or all of the various available transformations[4, 5, 15–19] may not have the desired effect. In all cases, it is necessary to take adequate precautions (Section 11.3). However, considerations of internal consistency and of agreement with the limited available experimental data indicate that good reliance can be placed on the present results.

(5) NUMERICAL RESULTS

It was found possible, using the methods discussed in Section 11.3, to obtain values of the first integral in expression (6) (i.e. the spectral term when the white-noise modulation band extends down to zero frequency) over the full range of $\omega_\Delta/\hat{\omega}_m$ from $0{\cdot}1$ to 2. Results are shown in Fig. 1. For the smaller $\omega_\Delta/\hat{\omega}_m$ values, however, the procedure breaks down when applied to the second and third integrals; when attempts are made to sum the associated very slowly converging series by suitable transformations, it is found that there is insufficient accuracy in the initial numerical data. In the present approach this accuracy is limited by the accuracy of available tables for cosine, sine integral and exponential functions. The minimum value of ω_Δ/ω_m for which both the second and third integrals could be evaluated was $0{\cdot}5$. Fig. 2 shows plots of the three integrals for this case and for $\omega_\Delta/\hat{\omega}_m = 2$.

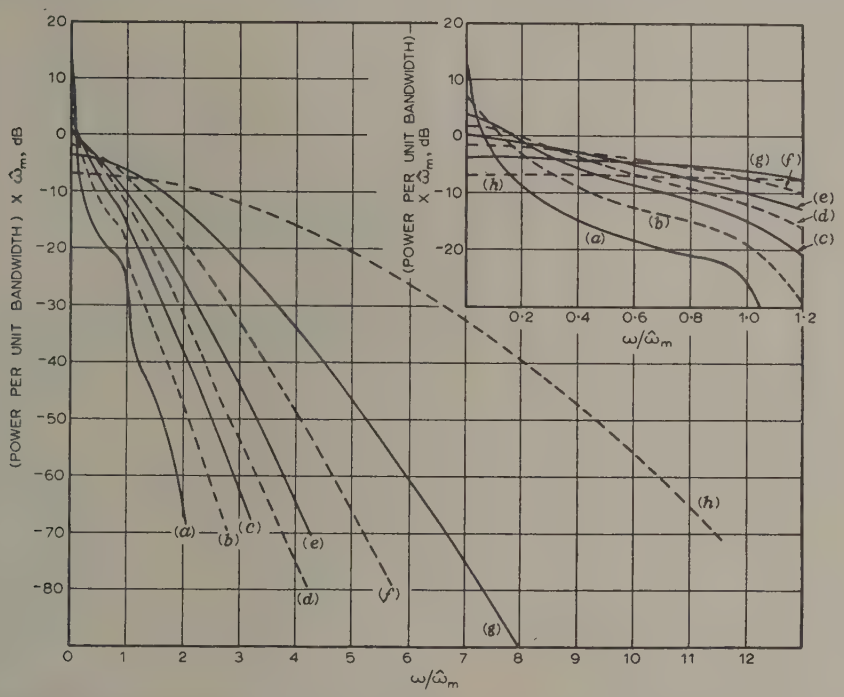

Fig. 1.—Spectral distribution of a carrier frequency-modulated with white noise having zero minimum modulating frequency (power in modulated carrier = 1).

(*a*) $\omega_\Delta/\hat{\omega}_m = 0{\cdot}1$.
(*b*) $\omega_\Delta/\hat{\omega}_m = 0{\cdot}2$.
(*c*) $\omega_\Delta/\hat{\omega}_m = 0{\cdot}3$.
(*d*) $\omega_\Delta/\hat{\omega}_m = 0{\cdot}4$.
(*e*) $\omega_\Delta/\hat{\omega}_m = 0{\cdot}5$.
(*f*) $\omega_\Delta/\hat{\omega}_m = 0{\cdot}7$.
(*g*) $\omega_\Delta/\hat{\omega}_m = 1{\cdot}0$.
(*h*) $\omega_\Delta/\hat{\omega}_m = 2{\cdot}0$.

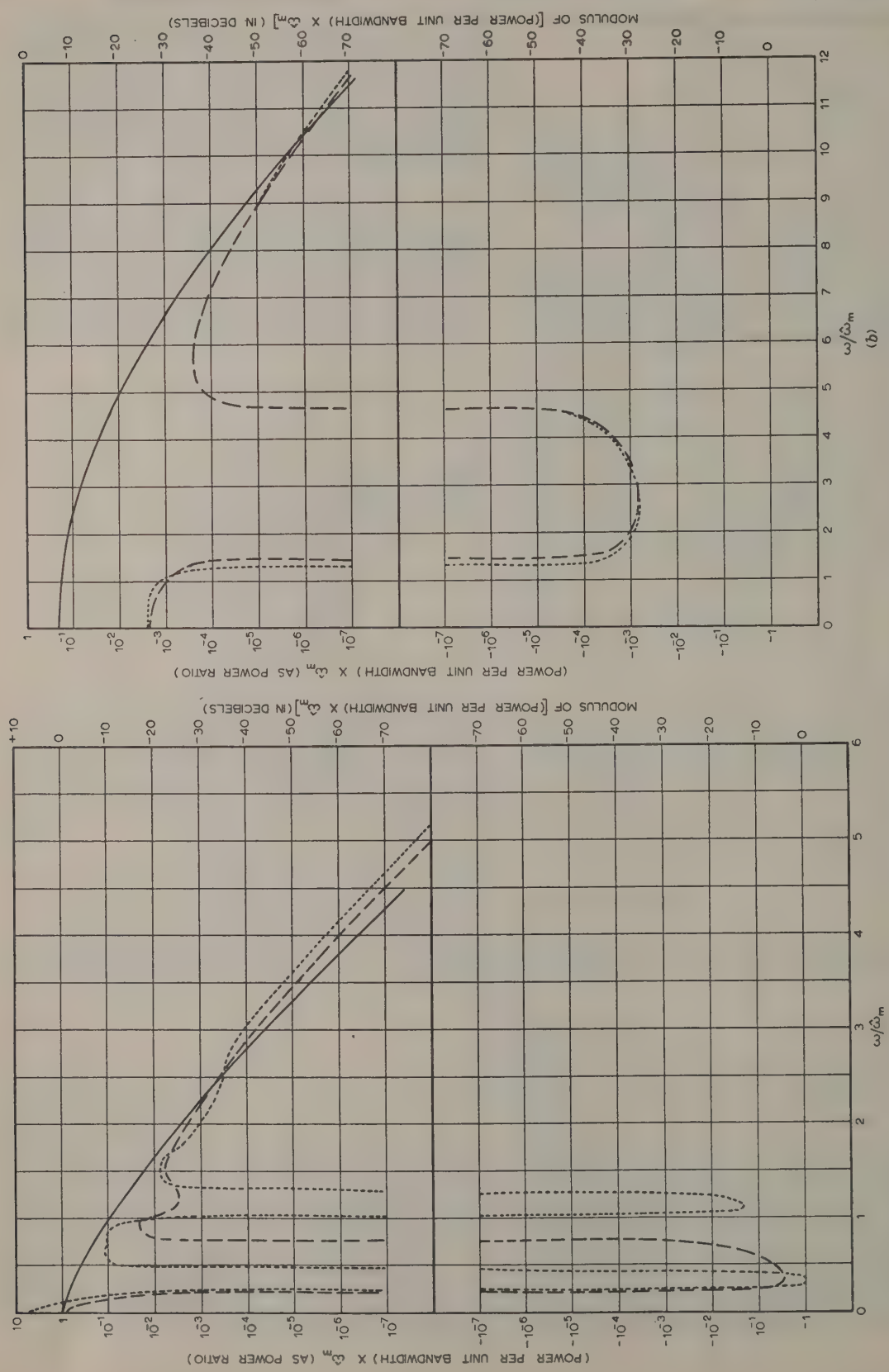

Fig. 2.—Zeroth, first- and second-order terms of the spectral distribution of a carrier frequency-modulated with white noise, when the spectral power is expanded as a power series in the minimum modulating frequency (power in modulated carrier = 1).

—— Zeroth-order term.
– – – First-order term.
····· Second-order term.

(a) $\omega_1/\hat{\omega}_m = 0{\cdot}5$

(6) DISCUSSION OF RESULTS

The numerical results confirm the theoretical expectation that when ω_Δ/ω_m is large enough the spectral distribution follows a Gaussian law. When $\omega_\Delta/\hat{\omega}_m$ is small and the lowest frequency of the white-noise modulation band is taken as zero, it is seen from Fig. 1 that there is a rather abrupt change of slope at $\omega/\hat{\omega}_m = 1$. The portion of the spectrum to the left of this point follows fairly closely the small deviation formula developed in Reference 11. However, for $\omega > \hat{\omega}_m$ this formula breaks down completely, the tails falling off much more rapidly than predicted by the formula. That such a result might be anticipated was suggested in Reference 2.

(7) COMPARISON WITH MEASURED SPECTRA

The only available spectrum measurements applying to white-noise frequency modulation appear to be those of References 6 and 10. The former can be compared with the present theoretical results only over a limited range of parameters, since they were intended to throw light on the variation of spectrum shape with minimum and maximum modulating frequencies and with r.m.s. frequency deviation in the region around carrier. However, Hamer and Acton[10] carried their measurements well down into the tail region, so that comparison with the theory is possible over a satisfactory range of frequency departures from carrier.

Fig. 3 shows measured and theoretical values for deviation ratios of 0·2 and 2, with zero minimum modulating frequency. The agreement for the lower deviation ratio is quite satisfactory. With a deviation ratio of 2 the experimental points fall somewhat below the theoretical curve in the tail region. This could be accounted for by a small error, about 6%, in the measured value of the r.m.s. frequency deviation. The deviation is probably the quantity which is most difficult to measure accurately, and an error of this magnitude seems not at all unlikely.

(8) EFFECT ON THE SPECTRUM TAILS OF NON-ZERO $\check{\omega}_m$

It is of particular practical interest to know how the curves in Fig. 1 must be modified when $\check{\omega}_m$ is not zero. It has been shown both theoretically and experimentally[6] that in the 'small deviation' case corresponding to values of $\omega_\Delta^2/\check{\omega}_m\hat{\omega}_m < 1$ the spectrum is much less smooth than in the 'small deviation' case defined by zero $\check{\omega}_m$ and small $\omega_\Delta/\hat{\omega}_m$. Consider, for example, the left-hand curve of Fig. 1, corresponding to $\omega_\Delta/\hat{\omega}_m = 0{\cdot}1$; if $\check{\omega}_m$ is increased until $\check{\omega}_m/\hat{\omega}_m > 0{\cdot}01$ it will be found that an infinitely narrow spike of energy (a single tone) will appear at the carrier frequency, and that in the central portion of the spectrum discontinuous jumps will occur at frequency deviations $\check{\omega}_m$, $\hat{\omega}_m - \check{\omega}_m$ and $\hat{\omega}_m + \omega_m$. In connection with distortion problems one is mostly concerned with the spectrum tails, so that it becomes important to know whether increase of $\check{\omega}_m$ has as drastic an effect in the tail region as in the central region. No complete answer can yet be given, but there are indications that over the range of $\check{\omega}_m$ of practical interest the spectrum tails will not depart considerably from the shapes calculated for $\check{\omega}_m = 0$.

The problem can be approached from two directions. For the larger $\omega_\Delta/\hat{\omega}_m$ values, computed values of the second and third integrals in expression (6) are available, and these can be used for an estimate of the effect on the spectrum tails of giving $\check{\omega}_m/\hat{\omega}_m$ a non-zero value (provided $\check{\omega}_m/\hat{\omega}_m$ does not approach unity). On the other hand, when $\omega_\Delta/\hat{\omega}_m$ is 0·1 (the lowest value considered) the spectrum is largely confined within a frequency region $\pm 2\hat{\omega}_m$, centred on the carrier frequency. Within this region, when $\omega_\Delta^2/(\check{\omega}_m\hat{\omega}_m)$ is small the spectral distribution is substantially defined by first- and second-order expressions in the phase modulation,[6] so that a good approximation to the tails for finite ω_m/ω_m is available for comparison with the limiting result for zero $\check{\omega}_m$.

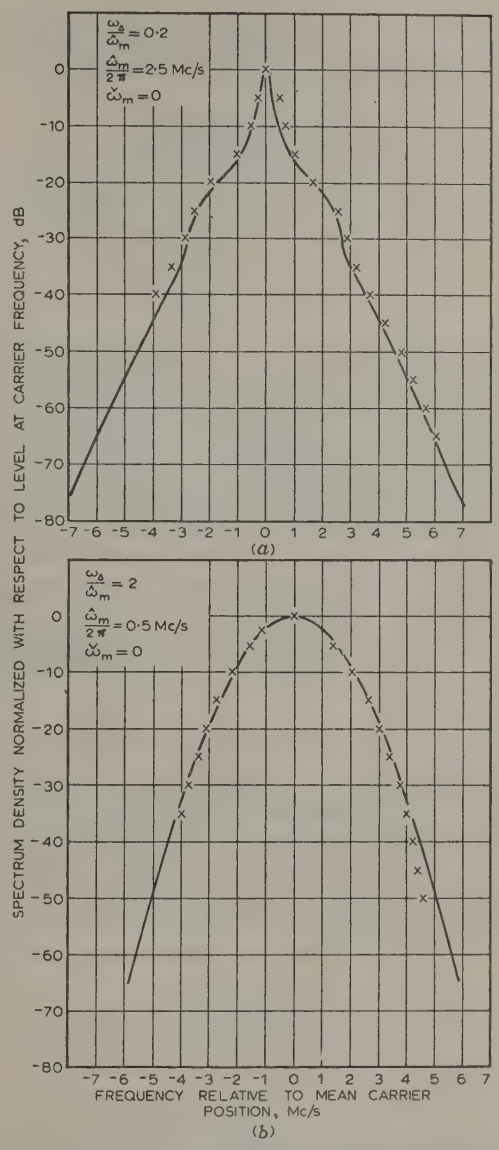

Fig. 3.—Comparison of theoretical spectra with experimental values given in Reference 10.

The smallest $\omega_\Delta/\hat{\omega}_m$ for which first- and second-order spectral terms in ω_m have been computed is 0·5. Table 2 shows the spectrum level at $\omega/\omega_m = 4$ for various values of $\check{\omega}_m/\hat{\omega}_m$, using coefficients read off from Fig. 2. It appears from Table 1 that the highest $\check{\omega}_m/\hat{\omega}_m$ likely to be used in the lower-capacity systems is 1/3.

It is seen that in this case the greatest change to be expected in the tail region due to variation in $\check{\omega}_m$ is about 4 dB. This corresponds to an expansion of the spectrum curve by a little less than 0·2 Mc/s at the 4 Mc/s position which, in view of uncertainties inherent in the noise-band representation of a multiplex signal, is an unimportant change.

When $\omega_\Delta^2/(\check{\omega}_m\hat{\omega}_m)$ is sufficiently small it is permissible to

Table 2

VARIATION WITH $\breve{\omega}_m/\hat{\omega}_m$ OF THE SPECTRUM LEVEL IN THE TAIL REGION ($\omega/\hat{\omega}_m = 4$) WHEN $\omega_\Delta/\hat{\omega}_m = 0{\cdot}5$

$\breve{\omega}_m/\hat{\omega}_m$	Spectrum level (power per unit bandwidth × $\hat{\omega}_m$)
	dB
0	−64·2
0·1	−63·1
0·2	−62·0
1/3	−60·5

expand[6] expression (1) in powers of μ_t. The spectrum in the frequency-deviation range $\breve{\omega}_m$–$\hat{\omega}_m$ then derives substantially from the first-order term in μ_t, that in the range $\hat{\omega}_m$–$2\hat{\omega}_m$ from the second-order term in μ_t, and so on. The second-order term has been evaluated explicitly,[6] but the third- and higher-order terms become excessively complicated. However, when $\omega_\Delta/\hat{\omega}_m$ is as low as 0·1 it is seen from Fig. 1 that the r.f. spectrum is largely confined within the deviation range 0–$2\hat{\omega}_m$. Consequently, for this deviation ratio and for sufficiently large $\breve{\omega}_m\left(\frac{\breve{\omega}_m}{\hat{\omega}_m} > 0{\cdot}01\right)$, the second-order term will be adequate to define the spectrum shape in the tail region down to a low level. The second-order spectrum has been previously evaluated. It is given by

$$\frac{1}{4}\frac{\omega_\Delta^4\hat{\omega}_m}{(\hat{\omega}_m-\breve{\omega}_m)^2}\exp\left(-\frac{\omega_\Delta^2}{\hat{\omega}_m\breve{\omega}_m}\right)\mathrm{F}(\omega, \breve{\omega}_m, \hat{\omega}_m) \quad . \quad . \quad (15)$$

where $\mathrm{F}(\omega, \breve{\omega}_m, \hat{\omega}_m)$ is the square of expression (12) of Reference 6. Expression (15) represents the power per unit bandwidth multiplied by $\hat{\omega}_m$. The exponential factor, which did not appear in the earlier paper, is required to take account of coherent contributions to μ_t^2 from higher-order even terms (Section 11.4). In the frequency region $\hat{\omega}_m + \breve{\omega}_m \leqslant \omega \leqslant 2\hat{\omega}_m$, expression (15) becomes

$$\left\{\frac{1}{\left(1-\frac{\breve{\omega}_m}{\hat{\omega}_m}\right)^2}\exp\left(-\frac{\omega_\Delta^2}{\hat{\omega}_m\breve{\omega}_m}\right)\right\}\frac{1}{4}\left(\frac{\omega_\Delta}{\hat{\omega}_m}\right)^4$$

$$\left[\frac{2-\frac{\omega}{\hat{\omega}_m}}{\left(\frac{\omega}{\hat{\omega}_m}\right)^2\left(\frac{\omega}{\hat{\omega}_m}-1\right)}-\frac{2}{\left(\frac{\omega}{\hat{\omega}_m}\right)^3}\log_\varepsilon\left(\frac{\omega}{\hat{\omega}_m}-1\right)\right] \quad . \quad (16)$$

In this expression, only the term in curly brackets involves $\breve{\omega}_m$. This is a slowly varying term over a wide range of $\breve{\omega}_m/\hat{\omega}_m$. The term independent of $\breve{\omega}_m$ follows very closely the shape of the tail spectrum when $\breve{\omega}_m$ is identically zero, as will be seen by comparing Table 3 with the appropriate curve of Fig. 1.

Over the frequency deviation range $\hat{\omega}_m + \omega_m \leqslant \omega \leqslant 2\hat{\omega}_m$ a change in ω_m, according to expression (16), changes the levels shown in Table 3 by an amount independent of the particular spectral frequency. For comparison with Table 2, Table 4 shows spectrum levels evaluated from expression (16) at a frequency departure from carrier such that the spectrum level for zero $\breve{\omega}_m$ is −64·2 dB.

The agreement between Tables 2 and 4 is striking.

When comparing these Tables it must be remembered that whereas in Table 2 the underlying formulae are such that values can be computed in the whole range $0 \leqslant \breve{\omega}_m/\hat{\omega}_m \leqslant 1/3$, the formulae leading to Table 4 break down in the region 0–0·1.

Table 3

VARIATION WITH ω/ω_m OF THE TERM IN EXPRESSION (16) INDEPENDENT OF $\breve{\omega}_m$

$\omega/\hat{\omega}_m$	Portion of second-order spectrum term independent of $\breve{\omega}_m$
	dB
1·05	−32·5
1·2	−39·4
1·4	−44·5
1·6	−48·9
1·8	−54·2
1·95	−61·6

Table 4

VARIATION WITH $\breve{\omega}_m/\omega_m$ OF THE SPECTRUM LEVEL IN THE TAIL REGION ($\omega/\hat{\omega}_m \simeq 1{\cdot}99$) WHEN $\omega_\Delta/\hat{\omega}_m = 0{\cdot}1$

$\breve{\omega}_m/\hat{\omega}_m$	Spectrum level (power per unit bandwidth × $\hat{\omega}_m$)
	dB
0	−64·2
0·1	−63·5
0·2	−62·5
1/3	−60·8

It is also unfortunately true that there seems to be no obvious analytical way of investigating directly the effect of non-zero $\breve{\omega}_m$ on the tail shape in the deviation region between $\omega_\Delta/\hat{\omega}_m = 0{\cdot}1$ and $\omega_\Delta/\hat{\omega}_m = 0{\cdot}5$. However, what has been derived in the present Section seems to establish a good presumption that, over the whole deviation range of practical interest, variation of $\breve{\omega}_m/\hat{\omega}_m$ between the limits 0–1/3 will not cause variation of the spectrum tails by more than 3 or 4 dB.

(9) CONCLUSIONS

The result of the investigation is a set of curves, spaced sufficiently closely for interpolation, giving r.f. spectra over the full expected range of deviation ratios for the frequency modulation case when the minimum modulating frequency is taken as zero. These curves are considered to be accurate to a small fraction of a decibel. A complete picture of the effect of non-zero minimum modulating frequency has not been obtained; however, evidence is presented suggesting that, unless the ratio between the minimum and maximum modulating frequencies is a sizeable fraction, the change in the spectrum shape when the minimum modulating frequency rises above zero will be largely confined to the central portion of the spectrum, the tail shape being substantially unaltered.

(10) REFERENCES

(1) BOSSE, G.: 'Die Berechnung des Spektrums bei Vielkanal-Richtfunkverbindungen mit Frequenzmodulation', *Frequenz*, 1953, **7**, p. 239.

(2) MULLEN, J. A., and MIDDLETON, D.: 'Limiting Forms of F.M. Noise Spectra', *Proceedings of the Institute of Radio Engineers*, 1957, **45**, p. 874.

(3) MEDHURST, R. G., HICKS, E. M., and GROSSETT, W.: 'Distortion in Frequency-Division-Multiplex F.M. Systems due to an Interfering Carrier', *Proceedings I.E.E.*, Paper No. 2565 R, May, 1958 (**105** B, p. 282).

(4) LUBKIN, S.: 'A Method of Summing Infinite Series', *Journal of Research of the National Bureau of Standards*, 1952, **48**, p. 228.
(5) HARTREE, D. R.: 'Numerical Analysis' (Oxford University Press, 1958), Second Edition, p. 265.
(6) MEDHURST, R. G.: 'R.F. Bandwidth of Frequency-Division Multiplex Systems using Frequency Modulation', *Proceedings of the Institute of Radio Engineers*, 1956, **44**, p. 189.
(7) MIDDLETON, D.: 'The Distribution of Energy in Randomly Modulated Waves', *Philosophical Magazine*, 1951, **42**, p. 689.
(8) SMITH, J. R. W., and SLOW, J. L.: 'Energy Distribution in a Wave Frequency modulated by a Multichannel Telephone Signal', *ATE Journal*, 1956, **12**, p. 182.
(9) BLACHMAN, N. M.: 'Limiting Frequency-Modulation Spectra', *Information and Control*, 1957, **1**, p. 26.
(10) HAMER, R., and ACTON, R. A.: 'Power Spectrum of a Carrier modulated in Phase or Frequency by White Noise', *Electronic and Radio Engineer*, 1957, **34**, p. 246.
(11) STEWART, J. L.: 'The Power Spectrum of a Carrier Frequency modulated by Gaussian Noise'. *Proceedings of the Institute of Radio Engineers*, 1954, **42**, p. 1539.
(12) HOLBROOK, B. D., and DIXON, J. T.: 'Load Rating Theory for Multichannel Amplifiers', *Bell System Technical Journal*, 1939, **18**, p. 624.
(13) BENNETT, W. R.: 'Methods of Solving Noise Problems', *Proceedings of the Institute of Radio Engineers*, 1956, **44**, p. 609.
(14) TITCHMARSH, E. C.: 'Introduction to the Theory of Fourier Integrals' (Oxford University Press, 1937), p. 60.
(15) SZASZ, O.: 'Summation of Slowly Convergent Series', *Journal of Mathematics and Physics*, 1949, **28**, p. 272.
(16) VAN WIJNGAADEN, A.: 'A Transformation of Formal Series', *Proceedings of the Koninklijke Nederlandse Akademie van Wetenschappen*, 1953, **56** (A), Part I, p. 522; Part II, p. 534.
(17) SALZER, H. E.: 'A Simple Method for Summing Certain Slowly Convergent Series', *Journal of Mathematics and Physics*, 1955, **33**, p. 356.
(18) SHANKS, D.: 'Nonlinear Transformations of Divergent and Slowly Convergent Sequences', *ibid.*, 1955, **34**, p. 1.
(19) JONES, C. V.: 'A Method of Series Summation and its application to the Electric Force in Sphere-Gaps', *Proceedings I.E.E.*, Monograph No. 330, March, 1959 (**106** C, p. 140).
(20) THOMSON, W. E.: 'The Response of a Non-Linear System to Random Noise', *ibid.*, Monograph No. 106, September, 1954 (**102** C, p. 46).
(21) C.C.I.R. Documents of the IXth Plenary Assembly, Los Angeles, 1959, Volume 1, Recommendations (International Telecommunications Union, Geneva, 1959), p. 268.
(22) STARR, A. T., and WALKER, T. H.: 'Microwave Radio Links', *Proceedings I.E.E.*, Paper No. 1290, April, 1952 (**99**, p. 241).
(23) ALBERSHEIM, W. J., and SCHAFER, J. P.: 'Echo Distortion in the F.M. Transmission of Frequency-Division Multiplex', *Proceedings of the Institute of Radio Engineers*, 1952, **40**, p. 316.
(24) LEWIN, L.: 'Interference in Multi-Channel Circuits: Dependence on Harmonic Generation', *Wireless Engineer*, 1950, **27**, p. 294.
(25) HARDY, G. H.: 'Divergent Series' (Oxford University Press, 1949).
(26) JACOBSEN, B. B.: 'Frequency Patterns for Multiple-Radio-Channel Routes', *Proceedings I.E.E.*, Paper No. 3033 E, November, 1959 (**107** B, p. 241).

(11) APPENDICES

(11.1) Simplified Derivation of Poisson's Formula

Consider a train of infinitely narrow unit pulses (Dirac delta functions) spaced 2π apart (Fig. 4). These may be represented by the Fourier expansion

$$y = \frac{1}{2\pi} + \frac{1}{\pi}\sum_{n=1}^{\infty}\cos(nx)$$

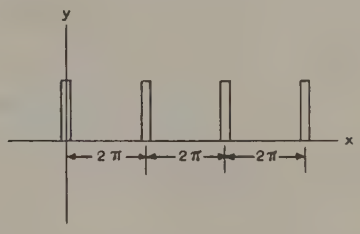

Fig. 4.—Train of narrow unit pulses at $x = 2n\pi$.

Multiplying both sides of this equation by $f(x/\beta)$ and integrating from 0 to ∞ with respect to x, we have

$$\int_0^{\infty} f\left(\frac{x}{\beta}\right)\left[\frac{1}{2\pi} + \frac{1}{\pi}\sum_{n=1}^{\infty}\cos(nx)\right]dx = \tfrac{1}{2}f(0) + \sum_{n=1}^{\infty} f\left(\frac{2\pi n}{\beta}\right)$$

The right-hand side follows since each of the infinitely narrow pulses has unit area. Now, writing $x/\beta = y$ and changing the order of the summation and the integration, the above equation becomes

$$\sum_{n=1}^{\infty}\int_0^{\infty} f(y)\cos(n\beta y)dy = \frac{\pi}{\beta}\left[\tfrac{1}{2}f(0) + \sum_{n=1}^{\infty} f\left(\frac{2\pi n}{\beta}\right)\right] - \tfrac{1}{2}\int_0^{\infty} f(y)dy$$

which is eqn. (7).

(11.2) Correction Formula for the Effect of the Higher-Order Terms in the Poisson Series

Eqn. (11) or (12) when evaluated gives $\sum_{n=1}^{\infty} S\left(\frac{A}{n}\right)$. What is actually required is $S(A)$. In the outer regions of the spectrum $S(A)$ is closely approximated by $\sum_{n=1}^{\infty} S\left(\frac{A}{n}\right)$. Nearer the centre of the spectrum the higher-order terms must be corrected for, and perhaps the most economical device is to express $S(A)$ in terms of

$$\sum_{n=1}^{\infty} S\left(\frac{A}{n}\right),\quad \sum_{n=1}^{\infty} S\left(\frac{A}{2n}\right),\quad \sum_{n=1}^{\infty} S\left(\frac{A}{3n}\right), \text{ etc.}$$

Write $S\left(\frac{A}{n}\right) = x_n$, and assume that

$$\sum_{n=1}^{\infty} x_n = x_1 + \left(C_2\sum_{n=1}^{\infty} x_{2n} + C_3\sum_{n=1}^{\infty} x_{3n} + \ldots\right)$$

Comparing coefficients, C_n will be expressed in terms of all C_m, where m is any factor of n (prime or composite) except n and 1, so that, proceeding stepwise, successive C_n's can be evaluated.

The first twenty are as follows: $C_2 = 1$, $C_3 = 1$, $C_4 = 0$, $C_5 = 1$, $C_6 = -1$, $C_7 = 1$, $C_8 = 0$, $C_9 = 0$, $C_{10} = -1$, $C_{11} = 1$, $C_{12} = 0$, $C_{13} = 1$, $C_{14} = -1$, $C_{15} = -1$, $C_{16} = 0$, $C_{17} = 1$, $C_{18} = 0$, $C_{19} = 1$, $C_{20} = 0$. Certain general rules can be deduced. For example, when m is prime, $C_m = 1$; when m is a product of two primes, $C_m = -1$; when m is a product of three primes, $C_m = 1$.

(11.3) Note on the Use of Transformations to Improve the Convergence Rate of Slowly-Converging Series

The first recorded transformation of this kind is that due to Euler; it involves successive differences formed from the original series. The transformed series is obtained[5] by taking a sequence of entries, one from each of the difference columns, according to a certain selection rule, and attaching to them an alternating sign and a weighting factor. If the original series is convergent and has terms of alternating sign, and if the transformed series converges, it can be shown that both series converge to the same sum. It will frequently happen that, if the original series converges very slowly, the transformed series will converge much more rapidly. In practice, however, the transformed series may be irregular, or even asymptotically divergent. In the latter case a meaningful result can often be obtained by stopping the summation of the transformed series at its least term. Whatever the form of the transformed series, the process of taking successive differences will magnify rounding errors in the original series, and the resulting 'noise' sets one limit to the accuracy of the results obtainable.

Alternative transformations have been proposed,[4, 15–19] some of which are applicable when the Euler transformation gives no useful information. In particular, some may be used on series of non-alternating sign. One of the simplest and most generally useful is due to Lubkin;[4] this transformation has been used extensively in the present work, in conjunction with the Euler transformation. It has the merit that it may be applied repeatedly, first to the original series and then to the transformed series, and so on.

All these transformations are best regarded as experimental, in the sense that in a particular numerical case it will not usually be possible to show by rigorous analysis that the transformed series are convergent or asymptotically divergent. The reliability of the result must be investigated numerically, by, for example, comparing the results of various transformations, or of the same transformation applied in various ways. One condition apparently necessary for success is that the original series must not be too 'irregular'. This became apparent when an initial attempt was made to evaluate the first integral of expression (6) using an associated series evaluated at intervals of $0{\cdot}2\pi$, rather than the $\pi/8$ subsequently used. While the resulting series had the appearance of descending smoothly, application of the Lubkin transformation immediately generated a transformed series showing violent and irregular oscillations. The reason for this appears to be the incompatibility between the interval separating adjacent terms and the natural periodicity associated with the cosine and sine-integal functions in the integrand.

One method often suggested for obtaining a check on the accuracy of a transformation to improve convergence is to carry out the process twice, starting with two successive terms of the original series. It is customary in textbook examples of Euler's transformation, in particular, to demonstrate close agreement between two such 'sums', this being offered as evidence of reliability of the transformation. Such a satisfactory conclusion is, of course, to be expected when the transformed series converges. However, in practice, the terms of the transformed series are liable, after an initial period of convergence, to settle down to a roughly constant value or even to diverge. In such a case useful information can be extracted from the transformed series only if it is, in fact, behaving like an asymptotic expansion.[25] This, as already remarked, can usually be verified only numerically. Under these circumstances it will not be safe to use as a check 'sums' obtained by starting the transformation at successive terms of the original series. What has been done in the present work is to plot out the Euler or Lubkin 'sum' against the sequence number of the first term of the original series used in the transformation. In all cases a smooth curve was thereby generated. This either trended monotonically towards a limit or took the form of a damped oscillation. It was usually possible to establish a limit of sufficient accuracy (i.e. to within a small fraction of a decibel). In a few cases, owing to shortage of initial data, the curve could not be extended far enough to define a limit sufficiently closely; the attempt to determine a spectral level for the particular deviation frequency had then to be abandoned.

(11.4) Effect of Coherence between Terms of the Same Order obtained from Various Powers, in the Taylor Expansion of sin μ_t + cos μ_t

When attempting to evaluate distortion from terms of the power series expansion of sin μ_t + cos μ_t, i.e.

$$1 + \mu_t - \frac{1}{2!}\mu_t^2 - \frac{1}{3!}\mu_t^3 + \frac{1}{4!}\mu_t^4 + \ldots \quad . \quad . \quad (17)$$

one must consider coherence between terms of a particular order which derive from various powers in the series.[24] Thus, coherent second-order terms arise not only from the second-power term but from all higher even-order terms. It will be shown in this Section that, to allow for this, the nth-order power evaluated from the nth-power term has merely to be multiplied by a constant factor. For white-noise frequency modulation this factor is $\exp[-\omega_\Delta^2/(\omega_m\hat{\omega}_m)]$. The method used to arrive at this result involves expanding cos μ_t + sin μ_t in Hermite polynomials and making use of a theorem due to Thomson.[20]

μ_t is normalized by writing it as $V_0x(t)$, where V_0 is the r.m.s. value of μ_t. Writing sin μ_t + cos μ_t in the form

$$\sin\mu_t + \cos\mu_t = c_0\mathrm{H}_0(x) + c_1\mathrm{H}_1(x) + c_2\mathrm{H}_2(x) + \ldots$$

where $\mathrm{H}_n(x)$ is the Hermite polynomial of nth order with argument $x(t)$, we have, from the orthogonality property of Hermite polynomials,

$$c_n = \frac{1}{n!\sqrt{2\pi}}\int_{-\infty}^{\infty}[\sin(V_0x) + \cos(V_0x)]\varepsilon^{-x^2/2}\mathrm{H}_n(x)dx$$

$$= \frac{1}{n!\sqrt{2\pi}}\int_{-\infty}^{\infty}[\sin(V_0x) + \cos(V_0x)](-1)^n\frac{d^n}{d_x^n}\varepsilon^{-x^2/2}dx$$

$$= \frac{1}{n!\sqrt{2\pi}}\int_{-\infty}^{\infty}[\sin(V_0x) + \cos(V_0x)](-1)^n d\left(\frac{d^{n-1}}{dx^{n-1}}\varepsilon^{-x^2/2}\right)$$

Integrating twice by parts, it becomes apparent that

$$c_n = \frac{-V_0^2}{n(n-1)}c_{n-2} \quad . \quad . \quad . \quad . \quad . \quad . \quad (18)$$

By direct integration it is found that

$$c_0 = \varepsilon^{-V_0^2/2}$$

and

$$c_1 = \frac{V_0}{1!}\varepsilon^{-V_0^2/2}$$

Thus, using the recurrence relation (18) it follows that

$$\sin \mu_t + \cos \mu_t = \varepsilon^{-V_0^2/2}$$

$$\left[H_0(x) + \frac{V_0}{1!}H_1(x) - \frac{V_0^2}{2!}H_2(x) - \frac{V_0^3}{3!}H_3(x) + \frac{V_0^4}{4!}H_4(x) + \ldots \right]$$

and hence, from eqn. (7) of Reference 20, the autocorrelation function of $\sin \mu_t + \cos \mu_t$, i.e. $\Psi(\tau)$, is given in terms of the autocorrelation function of $x(t)$, i.e. $\psi(\tau)$, by the relation

$$\Psi(\tau) = \varepsilon^{-V_0^2}\left\{1 + \frac{V_0^2}{1!}\psi(\tau) + \frac{V_0^4}{2!}[\psi(\tau)]^2 + \frac{V_0^6}{3!}[\psi(\tau)]^3 + \ldots\right\}$$

The expression in the curly brackets is that which would be obtained if $\Psi(\tau)$ were evaluated from the Taylor expansion (17), ignoring contributions to a particular order from higher-power terms. Thus the effect of such contributions is given by the factor $\varepsilon^{-V_0^2}$.

To evaluate V_0, write ω_M in the form[23]

$$\omega_M = \sum_{\omega_m=\check{\omega}_m}^{\hat{\omega}_m} a \cos(\omega_m t + \phi_{\omega m})$$

where ω_m increases in unit steps and $\phi_{\omega m}$ is a random phase angle. The stipulation that ω_m should increase in unit steps, which simplifies the formulae by avoiding the introduction of a further frequency symbol, requires that a shall have the dimensions of (frequency)$^{1/2}$. The r.m.s. frequency deviation is then given by

$$\omega_\Delta = \frac{a}{\sqrt{2}}\sqrt{(\hat{\omega}_m - \check{\omega}_m)} \quad . \quad . \quad . \quad . \quad (19)$$

The corresponding phase modulation is

$$\mu_t = \sum_{\omega_m=\check{\omega}_m}^{\hat{\omega}_m} \frac{a}{\omega_m} \sin(\omega_m t + \phi_{\omega m})$$

so the r.m.s. value of μ_t, i.e. V_0, is given by

$$V_0 = \left[\int_{\check{\omega}_m}^{\hat{\omega}_m} \frac{1}{2}\frac{a^2}{\omega_m^2} d\omega_m\right]^{1/2} = \frac{a}{\sqrt{2}}\frac{\sqrt{(\hat{\omega}_m - \hat{\omega}_m)}}{\sqrt{(\hat{\omega}_m\check{\omega}_m)}}$$

$$= \frac{\omega_\Delta}{\sqrt{\hat{\omega}_m\check{\omega}_m}} \text{ from eqn. (19)}$$

Using this value of V_0, the exponential factor in expression (15) follows.

621.372.831.012.8

The Institution of Electrical Engineers
Monograph No. 381 E
May 1960
©

A METHOD FOR THE EVALUATION OF EQUIVALENT CIRCUIT PARAMETERS OF AN ASYMMETRIC WAVEGUIDE JUNCTION

By J. K. SINHA, M.Sc., Ph.D., Graduate.

(*The paper was first received* 16*th September*, 1959, *and in revised form* 1*st February*, 1960. *It was published as an* INSTITUTION MONOGRAPH *in May*, 1960.)

SUMMARY

As an alternative to the variational method of obtaining the equivalent circuit parameters of an asymmetric waveguide junction, the system is solved by considering that only the first few evanescent modes are excited at the junction. The circuit parameters thus obtained agree very well with those obtained experimentally. The limitations of such a procedure are discussed.

LIST OF SYMBOLS

ω = Angular frequency of electromagnetic waves.
r, θ, z = Cylindrical co-ordinates.
E_θ = θ-component of electric field.
H_r = r-component of magnetic field.
a, b = Dimensions of the cross-section of cavity system.
$\beta_0, \beta_1, \beta_2$ = Phase-change coefficients in free space, in the empty portion of the cavity, and in the partially filled portion for H_{01} mode.
Y_0, Y_{0n}, Y_n = Wave admittances in free space, and in the empty and partially filled portion of the cavity, respectively, for H_{0n} mode.
λ_1, λ_2 = Wavelength in the empty and partially filled portions of the cavity.
α_{0n}, α_n = Attenuation coefficients in the empty and partially filled portions of the cavity for H_{0n} mode, $n \geqslant 2$.
K_{0n} = Cut-off constant in the empty portion of the cavity for H_{0n} mode.
K_{1n}, K_{2n} = Cut-off constants in the partially filled portion of the cavity for H_{0n} mode.
γ_n = Propagation coefficient in the partially filled portion for H_{0n} mode.
Z_1, Z_2 = Wave impedances of the principal modes in the empty and partially filled portions of the cavity.
D_0, L_0 = Additional lengths of the transmission lines in the equivalent circuit.
k = Transformer turns ratio.

(1) INTRODUCTION

One of the most general ways of evaluating the equivalent circuit parameters of a waveguide junction is by using the variational method developed by Schwinger.[1] This technique has been used by Miles[2] and Lewin[3] for calculating the parameters of axially asymmetric waveguide junctions. Basically, the method consists of expressing the input impedance at the junction, looking into a matched termination along the direction of incidence, in terms of the required circuit parameters and the unknown field functions at the junction. It is arranged that the expression for the input impedance is stationary with respect to the variations of the assumed field functions about the correct functions. The circuit parameters are calculated from the stationary expressions thus obtained by using approximations for the field functions at the junction. However, as the field functions are complex, the necessary calculations are very tedious and no indication of the errors is given by this approach.

Collin and Brown,[4] however, have developed a modification of the variational technique which minimizes the computational labour and removes the disadvantages mentioned above. They obtain the stationary expression for the input impedance at the junction, looking along the direction of incidence, for a short-circuited termination. As the input impedance for this termination is purely imaginary, only real quantities are required in the calculations. From this approach an indication of the maximum errors in the results may also be obtained.

In place of using the variational method, the equivalent circuit parameters may also be evaluated by solving the field equations obtained by considering the continuity of the electromagnetic fields at the junction. However, as the fields on the two sides of the junction are different, the continuity conditions are not satisfied by the principal modes alone and consequently an infinite number of evanescent modes are excited to satisfy the boundary conditions at the discontinuity. The linear equations, with an infinite number of unknowns, thus obtained may be solved only in certain special cases by using analytic methods as shown by Berz[5] and Whitehead.[6] However, on making the assumption that only the first few modes are excited at the junction, the system may be solved quite simply and the required circuit parameters calculated. Once again, using the short-circuited termination as used by Collin and Brown, only real functions are needed in the computations.

(2) EQUIVALENT CIRCUIT PARAMETERS OF A LOSS-FREE JUNCTION IN A CYLINDRICAL WAVEGUIDE SUPPORTING H_{01} MODE

Consider the cavity system shown in Fig. 1. It is partially filled to the left of the plane OA by a coaxial dielectric rod of permittivity ϵ_1 and permeability μ_0 and is empty to the right of plane OA. The radii a and b of the rod and the waveguide are such that only the H_{01} mode can propagate in the system, the higher H_0 modes being cut-off.

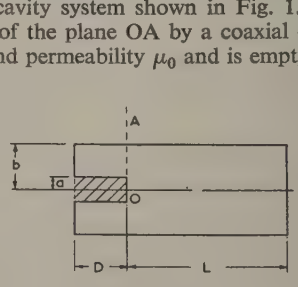

Fig. 1.—Cavity system partially filled with a coaxial dielectric rod.

The cavity system shown in Fig. 1, being the basic system of a new method of dielectric measurement,[7] was chosen for the present investigations because of its ready availability.

The junction plane OA is essentially a junction of two dis-

Correspondence on Monographs is invited for consideration with a view to publication.
Dr. Sinha is with Marconi's Wireless and Telegraph Co., Ltd.

similar waveguides and may be considered to be loss-free. Any loss-free junction between two waveguides may be represented by an equivalent circuit involving at most three parameters, provided that each waveguide can support only one mode.[8] Each waveguide may be represented by a transmission line, provided that the phase-change coefficient in the transmission line is the same as that in the corresponding waveguide. The system, therefore, is basically equivalent to two dissimilar transmission lines connected by an equivalent circuit having three parameters to represent the discontinuity.

It can be shown,[9] however, that any loss-free discontinuity may be represented as an ideal transformer of turns ratio k at certain characteristic planes. Let these terminals T_1 and T_2 be at distances D_0 and L_0 from the actual junction plane. Hence the system of Fig. 1 is equivalent to the transmission-line circuit shown in Fig. 2.

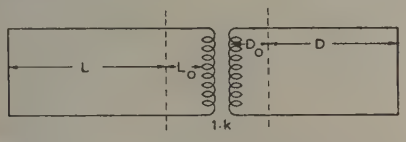

Fig. 2.—Equivalent transmission-line circuit of the cavity system.

The two transmission lines are short-circuited at the ends away from the junction, since the system of Fig. 1, considered at resonance, gives electrical nodes at the two end walls. The discontinuity is characterized by three parameters, namely D_0, L_0 and k. The characteristic impedances of the transmission lines are not uniquely defined. A convenient choice is to take the line impedances equal to those of the principal waveguide modes.

The three parameters may be evaluated from the curve of $(D + L)$ plotted against either L or D, keeping the cavity at resonance for the various values of D and L. The extraction of the parameters from the curve is explained below.

In the circuit of Fig. 2 the impedance presented at the terminal T_1 is equal to $jk^2Z_2 \tan \beta_2(L + L_0)$. Hence the circuit of Fig. 2 is simplified to that shown in Fig. 3, consisting of a lumped

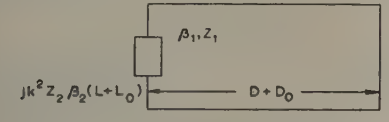

Fig. 3.—The simplified equivalent circuit of the cavity system.

impedance $jk^2Z_2 \tan \beta_2(L + L_0)$ at one end and short-circuited at a distance $D + D_0$ from that end.

As this circuit represents a cavity system at resonance, the total reactive impedance of the circuit is zero.

Hence
$$\tan \beta_1(D + D_0) = -\gamma' \tan \beta_2(L + L_0) \quad . \quad . \quad (1)$$

where $\gamma' = k^2Z_2/Z_1$.

It can be seen from eqn. (1) that a plot of D against L is repetitive in a period of half a wavelength and is symmetrical about the line of slope $-\beta_2/\beta_1$. The curve intersects this line at the points of its maximum and minimum slope. It may be shown[10] that at the point of maximum slope

$$D + D_0 = \tfrac{1}{4}n\lambda_1 \text{ and } L + L_0 = \tfrac{1}{4}m\lambda_2$$

where m and n are odd integers. The value of the maximum slope is either $\lambda_1/\gamma'\lambda_2$ or $\gamma'\lambda_1/\lambda_2$ according as γ' is greater or less than 1.

For a small discontinuity, however, $\gamma' \simeq 1$, and it is very difficult to locate the points of maximum and minimum slopes. In this case, the curves of $(D + L)$ against either D or L are plotted, when the maxima and minima are better defined. These curves are also repetitive in periods of half wavelengths and the equivalent circuit parameters of the waveguide junction can be evaluated from them. The $(D + L)/L$ curve is symmetrical about the line of slope $(\lambda_1 - \lambda_2)/\lambda_2$. At the point of intersection of the curve with its line of symmetry, and corresponding to its maximum slope,

$$D + L + D_0 + L_0 = \tfrac{1}{4}p\lambda_1 + \tfrac{1}{4}q\lambda_2 \quad . \quad . \quad . \quad (2)$$

and
$$L + L_0 = \tfrac{1}{4}q\lambda_2 \quad . \quad . \quad . \quad . \quad . \quad . \quad (3)$$

where $p, q = 1, 3, 5 \ldots$

Hence, the parameters D_0 and L_0 may be evaluated from eqns. (2) and (3) as p and q are known.

The remaining parameters, k, may be obtained from the maximum slope of the $(D + L)/L$ curve, which is given by $1 + \lambda_1/\gamma'\lambda_2$ for $\gamma' < 1$ and $1 + \gamma'\lambda_1/\lambda_2$ for $\gamma' > 1$.

The $(D + L)/L$ curve, required for the evaluation of the equivalent circuit parameters of the junction, may be obtained both experimentally and theoretically. The theoretical curve can be evaluated either by using the modified form of variational method as shown by Collin and Brown, or by solving the system on the assumption that only the first few evanescent modes are excited at the junction.

(3) THEORETICAL EVALUATION

Consider the fields existing within the cavity system shown in Fig. 1. As already mentioned, the parameters of the system are chosen so as to enable only the H_{01} mode to propagate in the system. The co-ordinates are chosen so that the distances to the right of the plane OA are considered positive and the distances to its left negative.

The fields for the H_{0n} mode in circular waveguide are characterized by E_θ, H_r and H_z, which are all independent of θ, and the nature of the discontinuity at the plane $z = 0$ is such that only the circularly symmetrical H_{0n} modes are excited anywhere in the structure. Although the higher H modes are excited at the junction, as explained later, these are evanescent and effectively zero at the positions of the two short-circuits. The propagated H_{01} mode is reflected by the short-circuits, the plane of the reflected waves being such that E_θ must vanish for $z = D$ and $z = -L$, since the cavity is at resonance. Therefore, for incidence from the right of the plane OY to its left, the fields for the H_{01} mode in the partially filled waveguide may be shown to have the form

$$E_\theta = C_1\phi_1(r) \sin \beta_2(L + z) \quad . \quad . \quad . \quad . \quad (4)$$

and
$$H_r = -jC_1Y_1\phi_1(r) \cos \beta_2(L + z) \quad . \quad . \quad (5)$$

where C_1 is the amplitude constant and $\phi_1(r)$ is the function specifying the variation of electric field in a plane at right angles to the direction of propagation.

Similarly, the fields for the principal mode in the empty portion for $z \geqslant 0$ are given by

$$E_\theta = B_1J_1CK_{01}r) \sin \beta_1(D - z) \quad . \quad . \quad . \quad (6)$$

$$H_r = jB_1Y_{01}J_1(K_{01}r) \cos \beta_1(D - z) \quad . \quad . \quad (7)$$

where B_1 is the amplitude constant and

$$\beta_1^2 = \omega^2\mu_0\epsilon_0 - K_{01}^2 \quad . \quad . \quad . \quad . \quad . \quad (8)$$

and
$$Y_{01} = \beta_1 Y_0/\beta_0 \quad . \quad . \quad . \quad . \quad . \quad . \quad (9)$$

The fields existing within the complete waveguide structure must be such that the tangential components of electric and magnetic fields are continuous over the interface plane $z = 0$. As the function $\phi_1(r)$ is not equal to the function $J_1(K_{01}r)$, additional fields in the form of evanescent modes must exist within the regions $z \leqslant 0$ and $z \geqslant 0$. As already mentioned, these fields are of the H_{0n} type and are effectively zero at the two short-circuited ends. Therefore, for $z \leqslant 0$, these fields are given by

$$E_\theta = C_n\phi_n(r)\varepsilon^{\alpha_n z} \quad . \quad . \quad . \quad . \quad . \quad (10)$$

$$H_r = C_n Y_n \phi_n(r)\varepsilon^{\alpha_n z} \quad . \quad . \quad . \quad . \quad . \quad (11)$$

where n takes all the values from 2 to ∞. α_n, $\phi_n(r)$ and Y_n for the nth mode are derived in Section 8.1.

The functions $\phi_n(r)$ are orthogonal, i.e.

$$\int_0^b r\phi_n(r)\phi_m(r)dr = 0 \text{ for } n \neq m \quad . \quad . \quad . \quad (12)$$

and have been normalized to satisfy

$$\int_0^b r\phi_n^2(r)dr = 1 \quad . \quad . \quad . \quad . \quad . \quad (13)$$

Similarly, for $z \geqslant 0$, the fields for the higher H modes are given by

$$E_\theta = B_n J_1(K_{0n}r)\varepsilon^{-\alpha_{0n}z} \quad . \quad . \quad . \quad . \quad . \quad (14)$$

$$H_r = -B_n Y_{0n} J_1(K_{0n}r)\varepsilon^{-\alpha_{0n}z} \quad . \quad . \quad . \quad (15)$$

and

$$\alpha_{0n}^2 = K_{0n}^2 - \omega^2\mu_0\epsilon_0 \quad . \quad . \quad . \quad . \quad . \quad (16)$$

$$Y_{0n} = -j\alpha_{0n}Y_0/\beta_0 \quad . \quad . \quad . \quad . \quad . \quad . \quad (17)$$

α_{0n} being real if $K_{0n}^2 > \omega^2\mu_0\epsilon_0$.

General expressions for the fields throughout the cavity system may now be written down:

For $z \leqslant 0$,

$$E_\theta = C_1\phi_1(r)\sin\beta_2(L+z) + \sum_{n=2}^{\infty} C_n\phi_n(r)\varepsilon^{\alpha_n z} \quad . \quad . \quad (18)$$

$$H_r = -jC_1Y_1\phi_1(r)\cos\beta_2(L+z) + \sum_{n=2}^{\infty} C_nY_n\phi_n(r)\varepsilon^{\alpha_n z} \quad (19)$$

and for $z \geqslant 0$,

$$E_\theta = B_1J_1(K_{01}r)\sin\beta_1(D-z) + \sum_{n=2}^{\infty} B_nJ_1(K_{0n}r)\varepsilon^{-\alpha_{0n}z} \quad . \quad (20)$$

$$H_r = jB_1Y_{01}J_1(K_{01}r)\cos\beta_1(D-z) - \sum_{n=2}^{\infty} B_nY_{0n}J_1(K_{0n}r)\varepsilon^{-\alpha_{0n}z} \quad . \quad . \quad . \quad . \quad (21)$$

As already mentioned, an infinite number of evanescent modes are excited to satisfy the continuity conditions of the systems. Therefore the continuity conditions at $z = 0$ may be written from eqns. (18)–(21) as

$$B_1J_1(K_{01}r)\sin\beta_1D + B_2J_1(K_{02}r) + B_3J_1(K_{03}r) = C_1\phi_1(r)\sin\beta_2L + C_2\phi_2(r) + C_3\phi_3(r) \quad (22)$$

and

$$jB_1Y_{01}J_1(K_{01}r)\cos\beta_1D - B_2Y_{02}J_1(K_{02}r) - B_3Y_{03}J_1(K_{03}r) = -jC_1Y_1\phi_1(r)\cos\beta_2L + C_2Y_2\phi_2(r) + C_3Y_3\phi_3(r) \quad (23)$$

Let

$$\int_0^b r\phi_i(r)J_1(K_{0j}r)dr = A_{ij} \quad . \quad . \quad . \quad . \quad (24)$$

where i and j are integers.

On multiplying eqn. (22) by $r\phi_1(r)$, $r\phi_2(r)$ and $r\phi_3(r)$, respectively, and integrating with respect to r within the limits $r = b$ to $r = 0$, and using the orthogonal relations given in eqns. (12) and (13), the following equations are obtained:

$$C_1\sin\beta_2L = B_1A_{11}\sin\beta_1D + B_2A_{12} + B_3A_{13} \quad . \quad (25)$$

$$C_2 = B_1A_{21}\sin\beta_1D + B_2A_{22} + B_3A_{23} \quad . \quad (26)$$

$$C_3 = B_1A_{31}\sin\beta_1D + B_2A_{32} + B_3A_{33} \quad . \quad (27)$$

Similarly, using eqn. (23),

$$jC_1Y_1\cos\beta_2L = -jB_1Y_{01}A_{11}\cos\beta_1D + B_2Y_{02}A_{12} + B_3Y_{03}A_{13} \quad (28)$$

$$-C_2Y_2 = -jB_1Y_{01}A_{21}\cos\beta_1D + B_2Y_{02}A_{22} + B_2Y_{03}A_{23} \quad (29)$$

$$-C_3Y_3 = -jB_1Y_{01}A_{31}\cos\beta_1D + B_2Y_{02}A_{32} + B_3Y_{03}A_{33} \quad (30)$$

From eqns. (25)–(30), it may be shown that

$$jB_1A_{11}(Y_1\cot\beta_2L\sin\beta_1D + Y_{01}\cos\beta_1D) + B_2A_{12}(jY_1\cot\beta_2L - Y_{02}) + B_3A_{13}(jY_1\cot\beta_2L - Y_{03}) = 0 \quad . \quad . \quad . \quad . \quad . \quad (31)$$

$$B_1A_{21}(Y_2\sin\beta_1D - jY_{01}\cos\beta_1D) + B_2A_{22}(Y_2 + Y_{02}) + B_3A_{23}(Y_2 + Y_{03}) = 0 \quad (32)$$

$$B_1A_{31}(Y_3\sin\beta_1D - jY_{01}\cos\beta_1D) + B_2A_{32}(Y_3 + Y_{02}) + B_3A_{33}(Y_3 + Y_{03}) = 0 \quad (33)$$

Therefore

$$jY_{01}\cot\beta_1D = \frac{\begin{vmatrix} -jY_{11}A_{11}\cot\beta_2L & A_{12}(jY_1\cot\beta_2L - Y_{02}) & A_{13}(jY_1\cot\beta_2L - Y_{03}) \\ Y_2A_{21} & -A_{22}(Y_{02}+Y_2) & -A_{23}(Y_{03}+Y_2) \\ Y_3A_{31} & -A_{32}(Y_{02}+Y_3) & -A_{33}(Y_{03}+Y_3) \end{vmatrix}}{\begin{vmatrix} A_{11} & A_{12}(jY_1\cot\beta_2L - Y_{02}) & A_{13}(jY_1\cot\beta_2L - Y_{03}) \\ A_{21} & -A_{22}(Y_{02}+Y_2) & -A_{23}(Y_{03}+Y_2) \\ A_{31} & -A_{32}(Y_{02}+Y_3) & -A_{33}(Y_{03}+Y_3) \end{vmatrix}} \quad . \quad . \quad . \quad . \quad (34)$$

electromagnetic fields at the junction plane given by $z = 0$ in the system shown in Fig. 1. However, for simplicity it is assumed that only three modes, namely H_{01}, H_{02} and H_{03}, are needed to satisfy the continuity conditions of the electromagnetic fields at the boundary between the two regions in the cavity

This equation shows that, if the constants A_{ij}, Y_{0n} and Y_n are known, a theoretical $(D + L)/L$ curve can be plotted, thus enabling the evaluation of the required circuit parameters.

The integrals of the type A_{ij} are easily evaluated by straightforward integration. It will be seen from Section 8.1 that for

the evaluation of the wave impedances, Y_{0n} and Y_n, the corresponding cut-off constants in the empty and partially filled regions of the waveguide must be evaluated. The method for evaluating the various cut-off constants is given in Section 8.2.

(4) NUMERICAL EXAMPLE

A polystyrene rod of radius 0·633 cm and permittivity, $\epsilon_r = 2{\cdot}52$ was used in the system of Fig. 1. The various constants on the right-hand side of eqn. (34) were evaluated, when the following equation was obtained:

$$\cot \beta_1 D = \frac{53{\cdot}09 \cot \beta_2 L + 0{\cdot}085}{49{\cdot}66 - 0{\cdot}153 \cot \beta_2 L} \quad . \quad . \quad . \quad (35)$$

From this equation a theoretical $(D + L)/L$ curve was calculated, as shown, together with the experimentally determined curve, in Fig. 4.

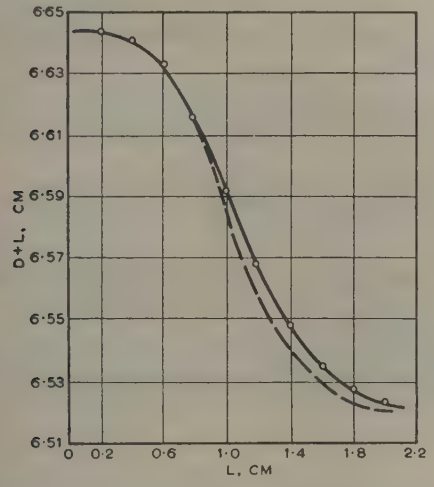

Fig. 4.—Comparison of the experimental $(D + L)/L$ curve with the theoretical curve calculated on the assumption of only three modes at the discontinuity.

——— Theoretical curve.
····· Experimental curve.

The two curves show an extremely good agreement. The slight shift of the experimental curve towards the L-axis may be explained as being due to the shift in the position of the virtual short-circuit on the partially filled side of the cavity because of the hole in the end wall to admit the dielectric rod.

On considering the existence of only two modes instead of three at the junction, the following expression was obtained:

$$\cot \beta_1 D = \frac{53{\cdot}09 \cot \beta_2 L + 0{\cdot}235}{49{\cdot}64 - 0{\cdot}19 \cot \beta_2 L} \quad . \quad . \quad (36)$$

Eqns. (35) and (36), obtained on the assumption of three and two modes, respectively, show very little difference. The equivalence of the two expressions and the satisfactory agreement between the theoretical and experimental curves shown in Fig. 4 give support to the assumption that only the first few modes are excited to satisfy the continuity conditions at the junction. Further justifications for this are given in Section 5.

The parameters D_0 and L_0 were calculated from the theoretical curve given in Fig. 4 using eqns. (2) and (3); from the maximum slope of the curve it was found that $k\sqrt{(Z_2/Z_1)} = 0{\cdot}93 \pm 0{\cdot}01$.

The characteristic impedances of the transmission lines are equal to those of the wave impedances of the corresponding waveguides, and k, the turns ratio of the ideal transformer, is found to be equal to $0{\cdot}99 \pm 0{\cdot}01$. Hence, k may be taken equal to unity within the limits of accuracy involved in the present calculations.

(5) JUSTIFICATION FOR ASSUMING ONLY A FEW EVANESCENT MODES AT THE JUNCTION

Consider the electromagnetic fields in partially filled portions of the cavity system shown in Fig. 1. For H_{0n} mode of propagation, the electric and magnetic fields are given by[12]

$$E_{\theta 1} = -jA_n \omega \mu_0 K_{1n} J_1(K_{1n} r) \varepsilon^{-\gamma_n z} \quad . \quad . \quad . \quad . \quad . \quad (37)$$

$$H_{r1} = A_n \gamma_n K_{1n} J_1(K_{1n} r) \varepsilon^{-\gamma_n z} \quad . \quad . \quad . \quad . \quad . \quad . \quad (38)$$

$$H_{z1} = A_n K_{1n}^2 J_0(K_{1n} r) \varepsilon^{-\gamma_n z} \quad . \quad . \quad . \quad . \quad . \quad . \quad . \quad (39)$$

$$E_{\theta 2} = -j\omega \mu_0 K_{2n} [B_n J_1(K_{2n} r) + C_n Y_1(K_{2n} r)] \varepsilon^{-\gamma_n z} \quad (40)$$

$$H_{r2} = \gamma_n K_{2n} [B_n J_1(K_{2n} r) + C_n Y_1(K_{2n} r)] \varepsilon^{-\gamma_n z} \quad . \quad . \quad (41)$$

$$H_{z2} = K_{2n}^2 [B_n J_0(K_{2n} r) + C_n Y_0(K_{2n} r)] \varepsilon^{-\gamma_n z} \quad . \quad . \quad . \quad (42)$$

γ_n is imaginary and equal to $j\beta_2$ for the propagating mode corresponding to $n = 1$, but it becomes real for $n \geqslant 2$ and is equal to α_n, the attenuation coefficient. The suffixes 1 and 2 refer respectively to the region inside the dielectric rod and the region between the dielectric rod and the outer conductor. A_n, B_n and C_n are amplitude constants.

The propagation coefficient γ_n is related to the cut-off constants by

$$\gamma_n^2 = K_{1n}^2 - \omega^2 \mu_0 \epsilon_1 = K_{2n}^2 - \omega^2 \mu_0 \epsilon_0 \quad . \quad . \quad (43)$$

For evanescent modes of higher order, γ_n becomes sufficiently large for the approximation $K_{1n} = K_{2n}$ to be made.

If $K_{1n} = K_{2n}$, from the continuity of the electromagnetic fields at $r = a$, it follows from eqns. (37)–(42) that

$$A_n J_1(K_{1n} a) = B_n J_1(K_{1n} a) + C_n Y_1(K_{1n} a) \quad . \quad . \quad (44)$$

$$A_n J_0(K_{1n} a) = B_n J_0(K_{1n} a) + C_n Y_0(K_{1n} a) \quad . \quad . \quad (45)$$

from which it can be seen that

$$(A_n - B_n) J_1(K_{1n} a) = C_n Y_1(K_{1n} a) \quad . \quad . \quad . \quad (46)$$

and

$$(A_n - B_n) J_0(K_{1n} a) = C_n Y_0(K_{1n} a) \quad . \quad . \quad . \quad (47)$$

Eqns. (46) and (47) are consistent only if

$$J_1(K_{1n} a) Y_0(K_{1n} a) = Y_1(K_{1n} a) J_0(K_{1n} a) \quad . \quad . \quad (48)$$

But, from the well-known properties of Bessel functions,

$$J_1(K_{1n} a) Y_0(K_{1n} a) - J_0(K_{1n} a) Y_1(K_{1n} a) = \frac{2}{\pi K_{1n} a} \neq 0 \quad (49)$$

Hence, the only solution of eqns. (46) and (47) is $A_n = B_n$ and $C_n = 0$. Also, μ has the same value anywhere in the structure, so that it is justifiable, for these high-order modes, to assume that eqns. (37)–(39) apply to both the regions 1 and 2.

Therefore, in the system of Fig. 1, the electric and magnetic fields of the higher H_{0n} modes have the same pattern on both sides of the junction. Consequently, the evanescent modes of higher order are not excited because of the principle of orthogonality, and accurate evaluation of the circuit parameters may be made by considering the existence of only the first few modes, as already demonstrated.

On the other hand, if the dielectric rod has a permeability different from that of free space, $E_{\theta 1}$ and $E_{\theta 2}$ can never be equal, even if K_{1n} is approximated to K_{2n}, as they depend on the values of permeabilities in the two regions, as shown by eqns. (37) and (40). Hence, as the electric fields on the two sides of the junction are not the same, even for very-high-order evanescent modes, the analysis made with a non-magnetic rod in the system is not applicable.

The justifications given above also follow from purely physical considerations. For high-order H modes the fields are predominantly magnetic and therefore are not affected appreciably by the non-magnetic dielectric rod, and as a result have the same values as if the rod did not exist. For a ferromagnetic rod, however, these fields are affected by the rod and have different values inside it. Hence, the method discussed in the paper for the evaluation of equivalent circuit parameters is unsuitable for asymmetric waveguide junctions having dielectrics with magnetic properties for H modes of propagation.

(6) ACKNOWLEDGMENTS

Thanks are due to Professor H. E. M. Barlow of University College, London, for providing facilities for the work described here. Particular thanks are due to Dr. J. Brown for his guidance in all stages of the work.

(7) REFERENCES

(1) SCHWINGER, J.: 'Discontinuity in Waveguides', M.I.T. Lecture Notes, edited by D. S. Saxon.
(2) MILES, J. W.: 'The Equivalent Circuit of a Plane Discontinuity in a Cylindrical Waveguide', *Proceedings of the Institute of Radio Engineers*, 1946, **34**, p. 728.
(3) LEWIN, L.: 'Advanced Waveguide Theory' (Iliffe, 1950).
(4) COLLIN, R. E., and BROWN, J.: 'The Calculation of the Equivalent Circuit of an Axially Unsymmetrical Waveguide Junction', *Proceedings I.E.E.*, Monograph No. 145 R, August, 1955 (**103** C, p. 121).
(5) BERZ, F.: 'Reflection and Refraction of Microwaves at a Set of Parallel Metallic Plates', *ibid.*, Paper No. 1038 R, January, 1951 (**98**, Part III, p. 47).
(6) WHITEHEAD, E. A. N.: 'The Theory of Parallel-Plate Media for Microwave Lenses', *ibid.*, Paper No. 1093 R, March, 1951 (**98**, Part III, p. 133).
(7) SINHA, J. K., and BROWN, J.: 'A New Cavity Resonator Method of Measuring Permittivities', *ibid.* (to be published).
(8) MONTGOMERY, C. G., DICKE, R. H., and PURCELL, E. M.: 'Principles of Microwave Circuits', Radiation Laboratory Series (McGraw-Hill, 1948), Vol. 8, Chapter 5.
(9) MARCUVITZ, N.: 'Waveguide Handbook', *ibid.* (McGraw-Hill, 1951), Vol. 10, Chapter 3.
(10) KING, R. W. P.: 'Transmission Line Theory' (McGraw-Hill, 1955), Section 3.
(11) SLATER, J. C.: 'Microwave Electronics' (Van Nostrand, 1950), Chapter 4.
(12) PINCHERLE, L.: 'Electromagnetic Waves in Metal Tubes Filled Longitudinally with Two Dielectrics', *Physical Review*, 1944, **66**, p. 118.

(8) APPENDICES

(8.1) Evaluation of $\phi_n(r)$, α_n and Y_n in the Partially Filled Portion of the Cavity

The expressions for the transverse components of the electromagnetic fields in the partially filled portion of the cavity system are given by eqns. (37), (38), (40) and (41), which involve three amplitude constants. However, it is possible,[12] by considering the continuity of electromagnetic fields at the surface of separation of two dielectrics, to use only one amplitude constant for expressing the fields in the entire region of the system.

The function $\phi_n(r)$ has also been defined to express the fields inside the waveguide system such that

$$E_\theta = \phi_n(r)\varepsilon^{-\gamma_n z} \quad . \quad . \quad . \quad . \quad . \quad (50)$$

and

$$H_r = -Y_n\phi_n(r)\varepsilon^{-\gamma_n z} \quad . \quad . \quad . \quad . \quad (51)$$

From eqns. (41), (36) and (38), it may be shown that

$$\phi_n(r) = -j\omega\mu_0 A_n K_{1n} J_1(K_{1n}r) \quad 0 < r < a \quad . \quad . \quad . \quad . \quad (52)$$

$$= -j\omega\mu_0 A_n \frac{K_{1n}^2}{K_{2n}}\left[\frac{Y_1(K_{2n}b)J_1(K_{2n}r) - J_1(K_{2n}b)Y_1(K_{2n}r)}{J_0(K_{2n}a)Y_1(K_{2n}b) - Y_0(K_{2n}a)J_1(K_{2n}b)}\right] \quad . \quad . \quad . \quad . \quad (53)$$

$$a < r < b$$

A_n must satisfy the normalization condition given by eqn. (13), i.e.

$$\frac{j\sqrt{2}}{A_n} = \omega\mu_0 K_{1n} a J_0(K_{1n}a)\left\{2\frac{J_1(K_{1n}a)}{K_{1n}aJ_0(K_{1n}a)}\left(\frac{K_{1n}^2}{K_{2n}^2} - 1\right) + 1 + \frac{K_{1n}^2}{K_{2n}^2}\left[\frac{4}{\pi^2 a^2 K_{2n}^2}\frac{1}{J_0(K_{2n}a)Y_1(K_{2n}b) - J_1(K_{2n}b)Y_0(K_{2n}a)} - 1\right]^2\right\}^{1/2} \quad . \quad . \quad . \quad . \quad (54)$$

The constants β_2, $\alpha_2 \ldots \alpha_n$ may be evaluated by substituting for K_{1n}, K_{2n}, etc., in eqn. (43), since $\gamma_n = j\beta_2$ for $n = 1$ and $\gamma_n = \alpha_n$ for $n > 2$.

The wave impedance Y_n is given by the ratio of the transverse magnetic field to that of the transverse electric field corresponding to the nth mode. Hence, from eqns. (37)–(41),

$$Y_n = \frac{\gamma_n}{j\omega\mu_0} \quad . \quad . \quad . \quad . \quad . \quad . \quad (55)$$

so that

$$Y_1 = \frac{\beta_2}{\omega\mu_0} = \beta_2\frac{Y_0}{\beta_0} \quad . \quad . \quad . \quad . \quad . \quad (56)$$

and

$$Y_n = -j\alpha_n\frac{Y_0}{\beta_0} \quad n = 2, 3 \quad . \quad . \quad . \quad . \quad (57)$$

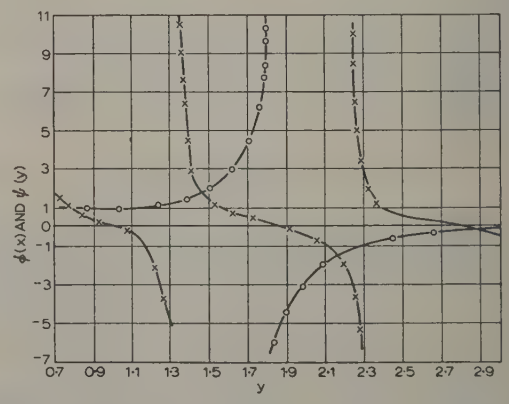

Fig. 5.—Intersections of the functions $\phi(x)$ and $\psi(y)$ plotted against the same y-axis.
—·—·— $\phi(x)$
—×—×— $\psi(y)$

(8.2) Evaluation of K_{0n}, K_{1n} and K_{2n}

The values of the cut-off constants are required for the evaluation of A_{ij}, the wave impedances and the attenuation coefficients. The evaluation of K_{0n} is straightforward and is given by

$$K_{0n}b = S_m \quad . \quad . \quad . \quad . \quad . \quad . \quad (58)$$

where $n = 1, 2 \ldots$ and $m = 2, 3$, b is the radius of the cavity and S_m is the mth root of the function $J_1(S)$.

For the evaluation of the constants K_{1n} and K_{2n}, the characteristic equation[12] of the partially filled region of the system is used:

$$\phi(x) = \psi(y) \quad . \quad . \quad . \quad . \quad . \quad . \quad (59)$$

where

$$\phi(x) = \frac{1}{x}\frac{J_1(x)}{J_0(x)} \quad . \quad . \quad . \quad . \quad . \quad (60)$$

$$\psi(y) = \frac{1}{y}\frac{J_1(y)Y_1(my) - Y_1(y)J_1(my)}{J_0(y)Y_1(my) - Y_0(y)J_1(my)} \quad . \quad . \quad (61)$$

$$x = K_{1n}a,\ y = K_{2n}a \text{ and } m = b/a.$$

Also, from eqn. (43),

$$x^2 = y^2 - \omega^2 a^2 \mu_0(\epsilon_1 - \epsilon_0) \quad . \quad . \quad . \quad . \quad (62)$$

From eqns. (61) and (62) it is possible to plot the function $\phi(x)$ and $\psi(y)$ on the same y-axis. The two functions, being oscillatory, intersect at a series of points. The various values of y, corresponding to the intersections, refer to the different H_{0n} modes. y or K_{2n}, corresponding to any H_{0n} mode having been found, K_{1n} may easily be calculated.

A plot of the functions $\phi(x)$ and $\psi(y)$ against y for the system under consideration is given in Fig. 5.

621.396.677.3 : 621.396.933.2

The Institution of Electrical Engineers
Monograph No. 382 E
May 1960
©

THE DESIGN OF CYLINDRICAL METAL-PLATE MICROWAVE LENSES FED BY NON-RESONANT SLOTTED WAVEGUIDE ARRAYS

By J. W. CROMPTON, M.E., Associate Member.

(*The paper was first received* 19*th May, and in revised form* 24*th November*, 1959. *It was published as an* INSTITUTION MONOGRAPH *in May*, 1960.)

SUMMARY

The use of a suitably modified refractive index enables cylindrical lenses with squinting linear feeds to be designed by the usual 2-dimensional methods applicable to lenses with non-squinting feeds.

An example is given of the design of a typical lens fed by a non-resonant slotted waveguide having a 20° squint angle.

LIST OF SYMBOLS

λ = Free-space wavelength.
θ = Squint angle of the linear source.
ρ = Angle of refraction in the metal-plate lens medium.
n = Refractive index of the metal-plate lens medium.
n' = Effective refractive index referred to the plane XOZ (Fig. 2).
α, β = Dimensions of the lens (defined in Fig. 5).

(1) INTRODUCTION

In certain applications of microwave aerials it is convenient to use cylindrical metal-plate lenses fed by slotted-waveguide linear arrays. A case in point is the airborne Doppler navigation equipment described by Clegg and Crompton* where two cylindrical lenses are used, each of which collimates 3 cm radiation from two slotted arrays. The isometric drawing (Fig. 1) shows the two lenses with the slotted waveguides above them. The four radiation patterns obtained from this aerial system have main lobes 3° × 6° (to 3 dB) and their centre-lines are aligned accurately in certain specified directions relative to the aircraft longitudinal axis and the horizontal plane.

The lenses have apertures approximately 24 in long by 12 in wide and, because they are fed by line rather than by point sources, they are cylindrical, being designed for a focal length appropriate to the 12 in aperture, say 12 in or less. The design of lenses of this type for use with broadside linear arrays has been discussed by Ruze.†

However, in order to obviate problems of bandwidth and matching inherent in the design of broadside arrays, the spacing of the slots is usually made less than half a wavelength. When this is done the direction of the maximum of the radiation pattern does not coincide with the normal to the length of the array. The array is then not truly broadside and is said to squint. The squint angle is, of course, dependent on the slot spacing, the frequency and the broad dimension of the waveguide, but since these are all readily controllable the squint angle may be predetermined with considerable precision. The existence of the squint angle is, in fact, of assistance in obtaining the desired beam directions from the aerial of the Doppler navigation equipment, but it somewhat complicates the design of the lenses themselves, as will now be shown.

Radiation from a microwave array is usually linearly polarized, the polarization (direction of the electric field) being either coplanar with, or perpendicular to, the length of the array. These two cases are shown in Figs. 2(*a*) and (*b*), each of which depicts diagrammatically the conical wavefront, the direction of the electric field and the orientation of the plates of the lens.

In optical work, cylindrical collimating lenses are commonly used to transform cylindrical wavefronts into plane wavefronts propagating in a direction normal to the generator of the cylinder. In the present instance, however, the incident wavefront is conical and the emergent wavefront is plane, but its direction of propagation is tilted away from the normal, as shown in Figs. 2(*a*) and (*b*).

In the system shown in Fig. 2(*a*), the source has a squint angle, θ, and its polarization is coplanar with the length of the array (e.g. a waveguide with slots in one of its narrow walls).

The origin, O, of the co-ordinate system has been taken on, and the direction of the OY axis coincident with, the phase centre-line of the linear array. The OZ direction is normal to OY and lies in the plane of symmetry of the lens. OX is normal to the plane YOZ.

The lens comprises a set of rectangular metal plates arranged parallel to each other and to the YOZ plane. Since the spacing of the plates may be varied, the phase velocity of the wave in the metal-plate medium, and hence the refractive index of the medium, is in general a discontinuous function of the distance x from the centre of the lens.

The paths of two typical rays are traced through the lens system in Fig. 3; one lies in the plane of symmetry of the system, YOZ, and the other passes through the lens between an outer pair of metal plates. In general, the refractive index of the metal-plate medium differs for the two rays, and their angles of refraction, ρ_0 and ρ_x, are not equal. This means that the ray paths through the lens are not parallel, and any attempt to design the lens by ray tracing results, in general, in very difficult 3-dimensional geometry.

Since a cylindrical lens is essentially 2-dimensional it is possible to avoid this 3-dimensional approach, and it will be shown that, by using a suitably modified refractive index, lenses of this type may be designed by the usual methods applicable to lenses fed by non-squinting arrays (see Ruze). The method is useful for both the types of lens shown in Figs. 2(*a*) and (*b*).

(2) DISCUSSION

Consider the traces of the wavefronts in a plane XOZ normal to the linear source. Between the feed and the lens the traces of the wavefronts are circles centred on the phase centre of the feed. Since the direction of propagation of the radiation from the feed is inclined everywhere at the squint angle θ to the plane XOZ, the apparent wavelength as measured by an observer confined to the plane is $\lambda \sec \theta$.

* CLEGG, J. E., and CROMPTON, J. W.: 'Low-Power C.W. Doppler Navigational Equipment', *Proceedings I.E.E.*, Paper No. 2566 R, March, 1958 (105 B, Suppl. 9, p. 258).

† RUZE, J.: 'Wide-Angle Metal-Plate Optics', *Proceedings of the Institute of Radio Engineers*, 1950, 38, p. 53.

Correspondence on Monographs is invited for consideration with a view to publication.

Mr. Crompton is at the Weapons Research Establishment, Salisbury, South Australia.

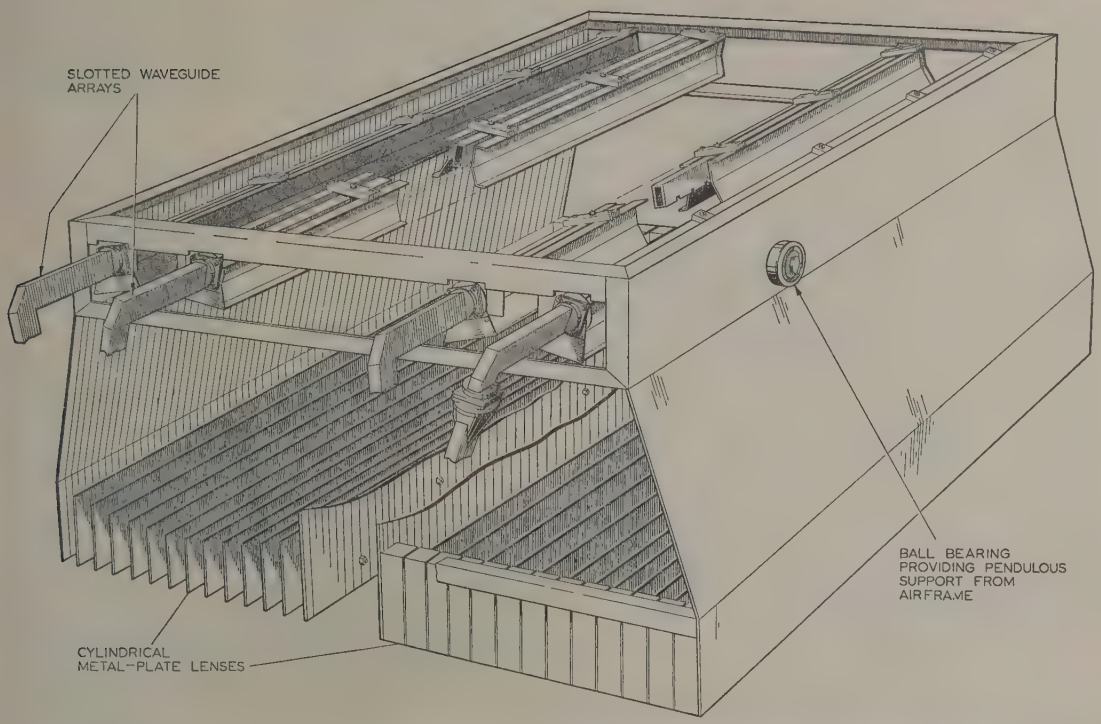

Fig. 1.—An aerial system for an airborne Doppler navigation equipment using metal-plate microwave lenses fed by squinting linear arrays.

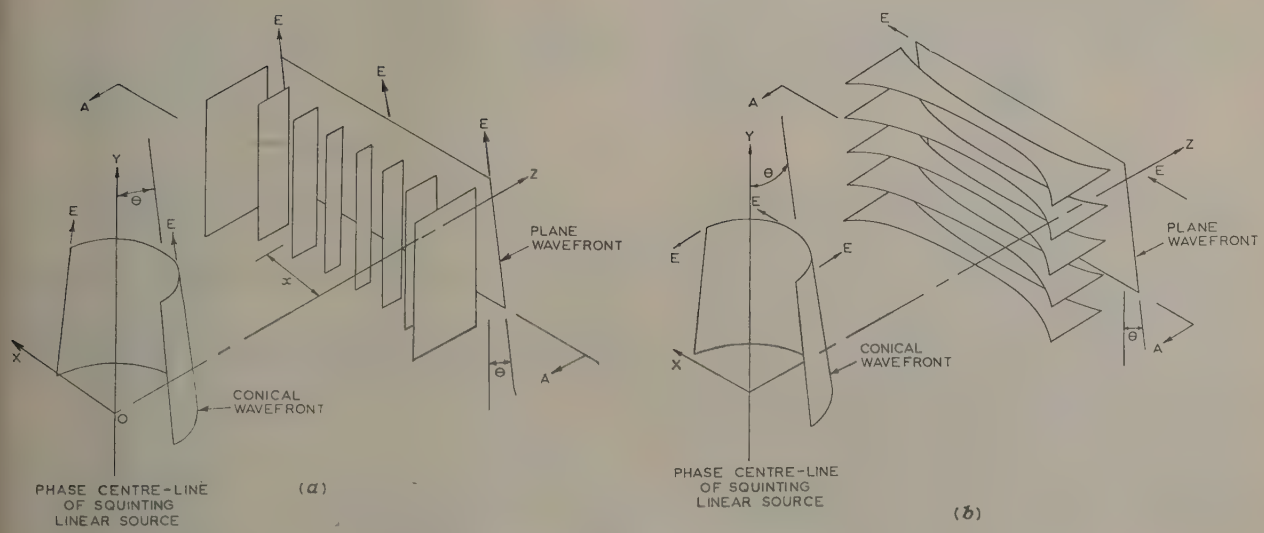

Fig. 2.—Lenses used with squinting linear sources.

(*a*) Polarization coplanar with the source.
(*b*) Polarization normal to the source.

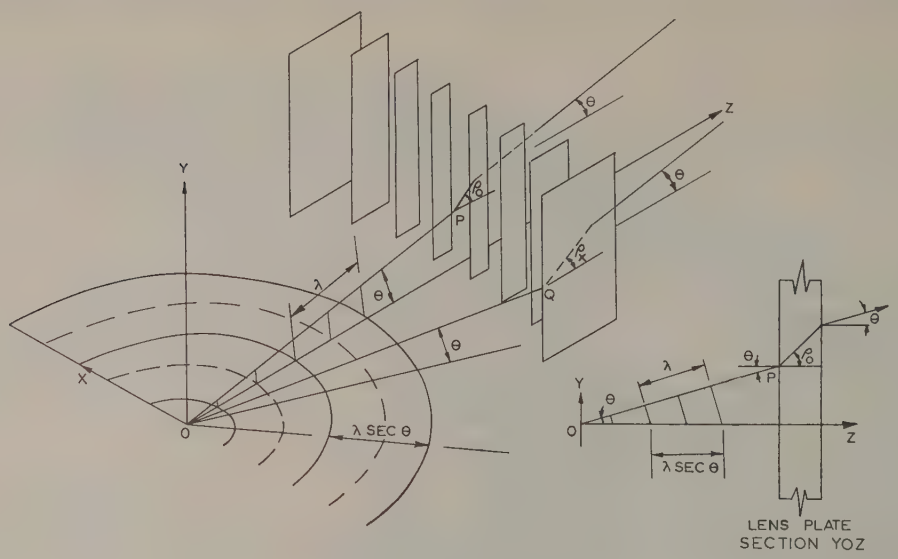

Fig. 3.—Ray paths through the lens.

On entering the lens the wavefronts are refracted, the angle of refraction being determined by Snell's law,

$$\frac{\sin\theta}{\sin\rho} = n \quad . \quad . \quad . \quad . \quad . \quad . \quad . \quad (1)$$

while the wavelength in the lens in the direction of the wave normal is λ/n. Inside the lens, therefore, the apparent wavelength in the plane XOZ is $(\lambda/n)\sec\rho$.

On the far side of the lens the direction of propagation again makes an angle θ with the plane XOZ, and the apparent wavelength in this plane is $\lambda\sec\theta$.

The effective refractive index of the lens medium as it appears to an observer confined to the plane XOZ is thus

$$n' = \frac{\text{Wavelength outside the lens}}{\text{Wavelength inside the lens}}$$

$$= \frac{\lambda\sec\theta}{(\lambda/n)\sec\rho}$$

i.e. $$n' = n\sec\theta\cos\rho$$

which, on substituting for ρ from eqn. (1), becomes

$$n' = \sec\theta\sqrt{(n^2 - \sin^2\theta)} \quad . \quad . \quad . \quad . \quad (2)$$

A graph showing the variation of n' with n for various values of θ is given in Fig. 4.

The lens may now be designed using conventional 2-dimensional formulae (see Ruze). The effective refractive indices referred to the plane XOZ having been determined, they must be converted to true refractive indices (from which the spacings of the metal plates may be calculated) by means of eqn. (2) or Fig. 4. An example of this procedure is given in Section 3.

In the case where the polarization is parallel to the plane XOZ [see Fig. 2(*b*)], the lens plates, and therefore the directions of propagation within the lens, are also parallel to XOZ. The effective refractive index referred to the plane XOZ is now

$$n' = \frac{\lambda\sec\theta}{\lambda/n} = n\sec\theta \quad . \quad . \quad . \quad . \quad . \quad (3)$$

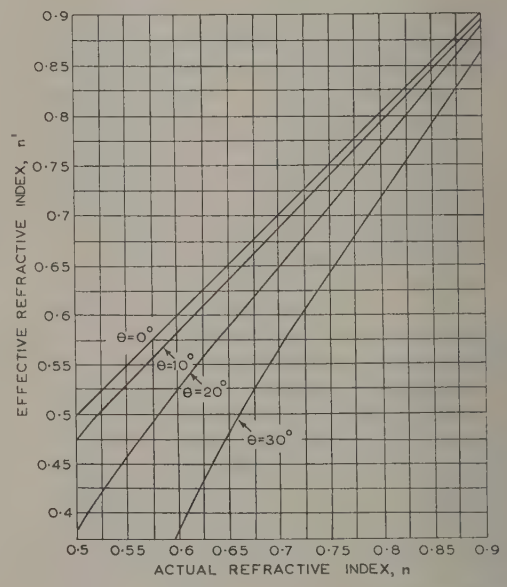

Fig. 4.—Variation of effective refractive index with squint angle.

It should be noted that in this case the lens places no constraints other than Snell's law on the directions of propagation inside the lens and parallel to the plane XOZ.

(3) DESIGN OF A STRAIGHT-FRONT-FACE LENS

The method was used to design the lens aerials for the c.w. airborne Doppler navigational aid. These lenses are fed by waveguide arrays of narrow face slots having squint angles of about 20°. The lens aperture is approximately 24 × 12 in and the focal length is 12 in. The lens was required to have good scanning properties in order that it could be used satisfactorily with two feeds disposed symmetrically 8° on either side of the

plane of symmetry. Abbé's sine condition is satisfied if the lens surface nearer the feed is a cylinder of radius equal to the focal length, and Ruze has shown that excellent scanning properties are achieved if the other surface is made plane. The shapes of the lens surfaces having thus been decided on, the object of the design is to determine the required variation of refractive index across the lens, and hence the spacing of the lens plates.

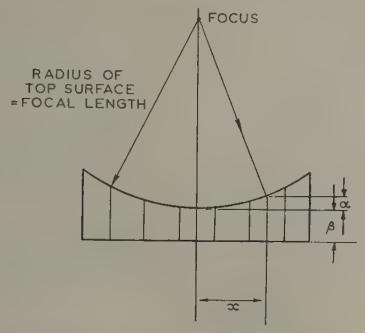

Fig. 5.—Cross-section of the lens.
The aperture dimension x is normalized with respect to the focal length of the lens.

Referring to Fig. 5, which shows a cross-section of the lens by a plane parallel to XOY, the electrical path length through the lens at any station distant x from the centre must be equal to the electrical path length at the centre. To generalize the arithmetic in accordance with normal optical practice, the aperture co-ordinate, x, has been normalized with respect to the focal length. Thus, for this example, $x = \pm 0{\cdot}5$ at the edges of the lens.

Let n_0 be the true refractive index of the metal-plate medium at the centre, and n_x the true refractive index at station x. Then, by eqn. (2), the effective refractive indices to be used in equating path lengths in the plane normal to the generator of the cylindrical lens system are

$$n_0' = \sec\theta\sqrt{(n_0^2 - \sin^2\theta)}$$

and

$$n_x' = \sec\theta\sqrt{(n_x^2 - \sin^2\theta)}$$

For equal path lengths, $n_0'\beta = n_x'(\alpha + \beta)$, where α and β are defined in Fig. 5.

Therefore

$$n_x' = n_0'\frac{\beta}{\alpha + \beta} \quad . \quad . \quad . \quad . \quad . \quad (4)$$

Since the top surface is cylindrical, α and x are related thus:

$$\alpha = 1 - \sqrt{(1 - x^2)} \quad . \quad . \quad . \quad . \quad . \quad (5)$$

To avoid tight mechanical tolerances and excessive reflection from the lens surfaces, the range of true refractive indices used was limited to $0{\cdot}5 \leqslant n \leqslant 0{\cdot}75$.

Using Fig. 4 and taking $\theta = 20°$, we have, at the centre of the lens, $x = 0$, $\alpha = 0$, $n_0 = 0{\cdot}75$ and $n_0' = 0{\cdot}71$.

At the extremities, $x = \pm 0{\cdot}5$, $\alpha = 0{\cdot}134$, $n_{0{\cdot}5} = 0{\cdot}5$ and $n_{0{\cdot}5}' = 0{\cdot}39$.

Therefore

$$\beta = \frac{n_x'\alpha}{n_0' - n_x'} = \frac{0{\cdot}39 \times 0{\cdot}134}{0{\cdot}71 - 0{\cdot}39} = 0{\cdot}17$$

i.e. the central thickness of the lens must be 0·17 times its focal length.

The value of β having been determined, the effective index, n_x', may be calculated for any value of x using eqns. (4) and (5). This relationship is shown in Fig. 6. The curve is next corrected

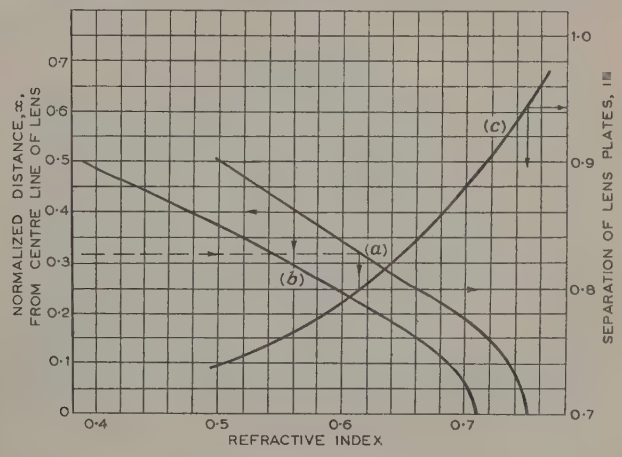

Fig. 6.—Method of obtaining the required plate separation at a given distance from the lens centre-line.
(*a*) True refractive index.
(*b*) Effective refractive index.
(*c*) Plate separation for given refractive index ($\lambda = 3{\cdot}2$ cm).

using eqn. (2), or Fig. 4, to show the true refractive index as a function of x.

Curves showing the relationship between true refractive index and the separation of the lens plates for a particular operating frequency are also plotted in Fig. 6. The final design information needed is a curve showing the required plate separation at any distance from the centre. This is simply obtained from Fig. 6 by entering at the required value of x, reading off the true refractive index required at this distance from the centre and hence the appropriate plate separation for the frequency for which the lens is to be used. The process is indicated by the arrow heads on Fig. 6.

(4) CONCLUSION

A simple method for the design of microwave metal-plate lenses for use with squinting line sources is described and this avoids the difficulties of 3-dimensional ray tracing. An example of the design of a lens for a specific application is given.

Tests on lenses designed in this way have shown that their performance is in good agreement with theoretical expectation.

(5) ACKNOWLEDGMENT

The paper is published by permission of the Chief Scientist, Australian Defence Scientific Service.

621.318.4:518

The Institution of Electrical Engineers
Monograph No. 383 M
June 1960
©

EXTENSION OF THE DUAL-INPUT DESCRIBING-FUNCTION TECHNIQUE TO SYSTEMS CONTAINING REACTIVE NON-LINEARITY

By R. M. HUEY, B.Sc., B.E., O. PAWLOFF, Dipl.Ing., and T. GLUCHAROFF, Dipl.Ing., M.E.

(*The paper was first received 28th September, 1959, and in revised form 15th February, 1960. It was published as an* INSTITUTION MONOGRAPH *in June, 1960.*)

SUMMARY

Kochenburger's describing function and also the dual-input describing function due to West, Douce and Livesley are well known. These techniques enable the graphical solution of non-linear differential equations in which the non-linear coefficient is associated with the first-order differential term to be obtained. The paper describes an extension of these methods, allowing the non-linear coefficient to be associated with any term in the differential equation.

It is shown that the typical non-linearity presented by an iron-cored inductor or by a ferro-electric capacitor may be resolved into a simple feedback system containing a single non-linear element which is independent of frequency, together with elements possessing linear transfer functions. The resulting equivalent block diagram is suitable for analysis by either of the describing-function techniques. As an example, the dual-input technique is used to predict accurately jump phenomena in an iron-cored ferroresonant circuit, and the validity of the equivalent block diagram suggested is also checked by simulation on an analogue computer.

LIST OF SYMBOLS

$N(a)$ = A non-linear, non-reactive output/input ratio.
$\psi(j\omega)$ = Frequency response function.
v_o = Output voltage.
v_i = Input voltage.
ω = Angular frequency.
a = Amplitude at frequency ω.
b = Amplitude at frequency $n\omega$.
n = Integer or integral fraction.
θ = Phase angle.
i = Instantaneous current (with subscripts referring to equivalent or actual circuit elements).
v = Instantaneous voltage (with subscripts referring to equivalent or actual circuit elements).
Φ = Magnetic flux.
R, L, C = Linear circuit parameters.
$R(i), L(i), C(i)$ = Non-linear circuit parameters.
G = An amplitude-dependent, frequency-independent gain.
p = The Heaviside operator in Section 2; elsewhere, the Laplace complex variable.
B = Magnetic flux density.
H = Magnetic field intensity.
M = Intensity of magnetization.
μ = Real part of a complex permeability.
D = Electric displacement.
E = Electric field intensity.
P = Electric polarization.
ϵ = Real part of a complex permittivity.
σ = Surface charge density.
l = Length of a magnetic path.
d = Thickness of dielectric, Section 2; a distance on the complex plane, Appendix.
q = Electric charge.
N = Number of turns.
k = Constants in a power series.
R_S = Equivalent resistance simulating copper loss.
R_H = Equivalent resistance simulating core losses.
α = Phase angle used to define a complex permeability μ ($\cos\alpha - j\sin\alpha$).

Capital letters are used to indicate the Laplace transform of a time-dependent variable, except that the Laplace transform of magnetic flux Φ is indicated by the symbol $\tilde{\Phi}$. The rationalized M.K.S. system of units is employed.

(1) INTRODUCTION

The describing-function technique developed by Kochenburger[1] and others allows the frequency-response method of analysis to be applied to stability investigations in feedback

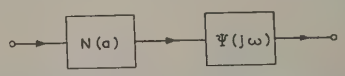

Fig. 1.—Separation of the response of a non-linear system into independent amplitude- and frequency-dependent functions.

systems containing non-linear elements. It is best applied graphically by plotting the open-loop frequency response, $\psi(j\omega)$, on a Nyquist diagram in which the critical point $(-1, j0)$ has been replaced by a plot of $-1/N(a)$ or describing function. Instability is indicated by an enclosure of, or an intersection with the plot of $-1/N(a)$ by the plot of $\psi(j\omega)$. The principal limitations to the describing-function analysis are:

(*a*) The input to the non-linear device must be very nearly sinusoidal.

(*b*) The amplitude-dependent characteristics of the system must be capable of being isolated into a non-linear block, $N(a)$ in Fig. 1, which must be completely separable from the frequency-dependent characteristics of the system which, in turn, must be lumped into a block $\psi(j\omega)$.

Requirement (*b*) also applies to the dual-input describing-function technique evolved by West, Douce and Livesley[2] and one of their two main examples* describes a 'simple' non-linear element ($v_o = v_i^3$) followed by a linear frequency-dependent network whose response falls with increasing frequency. The first requirement, however, has been transformed, in their case, to read

(*c*) The input to the non-linear element must be representable, very nearly, by a dual-frequency signal

$$v_i = a\cos(\omega t + \theta) + b\cos n\omega t \quad . \quad . \quad . \quad . \quad (1)$$

where a, b and n are real.

* Reference 2, p. 467.

Correspondence on Monographs is invited for consideration with a view to publication.
Messrs. Huey and Pawloff are in the Electrical Engineering School, University of New South Wales.
Mr. Glucharoff is in the Electrical Engineering School, Newcastle University College, University of New South Wales.

Their technique is valuable, and their suggested analysis involves an examination of the system response to a small (or incremental) signal at a frequency $n\omega$ in the presence of a main signal or excitation (of which the amplitude, a, may be either large or small) at a frequency ω. In general, a separate analysis is required for each selected value of n over adequate ranges of the two parameters a and θ in eqn. (1). In the case of forced oscillations, it enables prediction of instabilities at either harmonic or sub-harmonic frequencies of the fundamental excitation (n = integer or integral fraction), and also of jump phenomena ($n = 1$). In the case of free oscillations of feedback systems it is shown to predict certain instabilities of conditionally stable systems.

It is the purpose of the present paper to show that their technique may be extended to include other functions in addition to those they have exemplified, all of which may be described as resistive non-linearities in which $N(a)$ can be specified by a non-linear gain quite independently of $j\omega$. It is shown that, by the introduction of a suitably chosen intermediary variable, a typical reactive non-linearity may be represented by a simple equivalent block diagram in which the non-linearity is defined by a block from which all reactive effects have been removed. The resulting equivalent block diagram for the system will, in general, contain feedback loops additional to any already present in the physical system being analysed.

(2) SPECIFICATION OF A NON-LINEAR REACTANCE BY AN EQUIVALENT FEEDBACK SYSTEM

In the most general case of a circuit branch with non-linear elements, shown in Fig. 2, we may write

$$v = \int \frac{i}{C}dt + Ri + \frac{d(Li)}{dt} \quad . \quad . \quad . \quad . \quad (2)$$

where any or all of the quantities C, R and L are to be considered as non-linear rather than as the usual linear circuit elements.

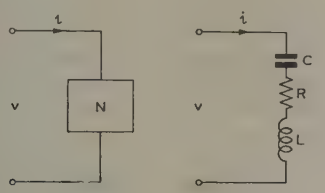

Fig. 2.—A generalized non-linear circuit-element.

For the moment, let these quantities be considered as functions of i, although it is easy to see later that any other reasonable specification will suffice. Using $C(i)$, $R(i)$ and $L(i)$ to define the non-linear capacitance, resistance and inductance, eqn. (2) may be re-written

$$v = \frac{1}{p}\left[\frac{i}{C(i)}\right] + R(i)i + p[L(i)i] \quad . \quad . \quad . \quad (3)$$

Here v and i are time-varying quantities and p is the Heaviside operator. The sort of operational process by which one may remove quantities from the square-bracketed terms in eqn. (3) is not at all obvious and even when such processes are devised they are unlikely to be very generally applicable.[3]

Dealing with each in turn, non-linear resistive terms such as $v_R = R(i)i$ do not require any special comment.[2]

Non-linear inductive terms such as $v_L = p[L(i)i]$ may be treated by the introduction of an intermediary variable:

$$\Phi = \frac{1}{p}v_L \quad . \quad . \quad . \quad . \quad . \quad . \quad . \quad (4)$$

The new variable, Φ, is connected linearly with the original variable, v_L, and is immediately recognizable as magnetic flux. It is not essential, however, that the intermediary variable be chosen to have any particular physical existence. A suitable relationship (Fig. 3) between the original variable, i, and Φ will

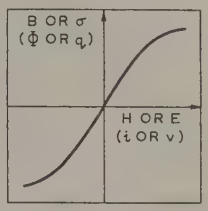

Fig. 3.—Non-linear induction in a magnetic field, or non-linear polarization in an electric field.

be considered at length in the example set out in the following Sections. The new definition of $L(i)$ may be shown as an equivalent block diagram (Fig. 5) using the normal transfer-function and describing-function notation of capital letters. Here G is a gain due to the non-linear relationship between i and Φ and is dependent only on amplitude. It is shown in the following Sections that iron and copper losses may be defined to a good approximation by additional and separate linear blocks (Fig. 7).

Non-linear capacitive terms such as $v_C = \frac{1}{p}\left[\frac{i}{C(i)}\right]$ may be treated in a similar way. The analogy between the two cases is obvious from Fig. 3 and the corresponding equations[4, 5]

$$\left.\begin{aligned} B &= \mu_0 H + M \\ \mu &= \frac{B}{H} \end{aligned}\right\} \quad . \quad . \quad . \quad . \quad . \quad (5a)$$

and

$$\left.\begin{aligned} D &= \epsilon_0 E + P \\ \epsilon &= \frac{D}{E} = \frac{\sigma}{E} \end{aligned}\right\} \quad . \quad . \quad . \quad . \quad . \quad (5b)$$

Where one wrote $L = \Phi/(Hl) = \Phi/I$ the analogous relation is $C = q/(Ed) = q/v$ (l and d are length of magnetic circuit and thickness of dielectric, respectively). If the B/H curve or the σ/E curve is practically linear, L and C reduce to the usual linear circuit constants. The obvious intermediary variable for a non-linear capacitance is q, defined by

$$q = \int i_c dt = \frac{1}{p}i_c \quad . \quad . \quad . \quad . \quad . \quad . \quad (6)$$

The equivalent block diagram to represent $C(i)$ is shown in Fig. 4, V_c being written in place of V. Specification of the non-linear circuit parameters may be achieved most conveniently

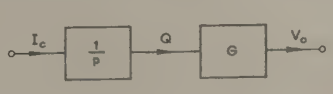

Fig. 4.—Equivalent block diagram for the term $\frac{1}{p}\left[\frac{i}{C(i)}\right]$ of eqn. (3).

by rescaling the curve of Fig. 3 with the variables $q - v$ (or $\Phi - i$).

When more than one kind of non-linearity is present in a system, manipulation of equivalent block diagrams in the manner suggested can be helpful in determining sensible approximations to deal with such awkward cases. In the following Sections the example used is that of the iron-cored inductor and the steps used for the computation of G follow the method set out in Reference 2. It is clear, however, that the process used is equally applicable to a capacitor with a non-linear dielectric.

(3) DERIVATION OF EQUIVALENT BLOCK DIAGRAM OF AN IRON-CORED INDUCTANCE

The derivation will be divided into three sections, an ideal (lossless) inductance, a non-linear inductance with copper loss, and a non-linear inductance with copper and iron losses. Throughout, variables denoted by lower-case symbols refer to time-varying quantities, while corresponding capital symbols refer to the Laplace transforms of these quantities. The analysis is normalized to a one-turn coil, so that $N\Phi = \Phi$.

(3.1) Pure Inductance

In a lossless non-linear inductance, L, as shown in Fig. 5(a), we have $v = d\Phi/dt$ or $\Phi = \int v dt$, whence $\tilde{\Phi} = V/p$. This simple relation is shown in block-diagram form in Fig. 5(b),

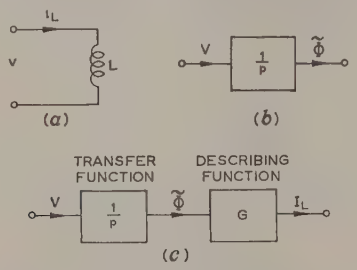

Fig. 5.—Circuit and equivalent block diagrams of a non-linear pure inductance, i.e. the term $p[L(i)i]$ of eqn. (3).

whence the transfer function between input voltage and flux is $\tilde{\Phi}/V = 1/p$ and this relationship holds for any inductance, whether linear or non-linear.

To obtain the transfer function between input voltage and current, consider the equation $i_L = f(\Phi)$. In general, i is a multi-valued function of Φ, but the assumption of an ideal inductance implies that $f(\Phi)$ is single-valued. The assumption of symmetry for positive and negative currents is not an undue restriction, so that the function may be written as a power series with odd terms only:

$$i_L = \frac{1}{L}(\Phi + k_1\Phi^3 + k_2\Phi^5 + \ldots) \quad . \quad . \quad . \quad (7)$$

where L, k_1, k_2, etc., are constants.

From eqn. (7) a describing function (either the normal or the dual-input kind) connecting flux and current may readily be calculated. The function so calculated will exhibit a gain which is independent of frequency but dependent on amplitude. The resulting equivalent block diagram for a non-linear ideal inductance is shown in Fig. 5(c).

(3.2) Inductance with Copper Loss

In this case the non-linear element is shown first in circuit form [Fig. 6(a)] as the ideal non-linear inductance, L, of Fig. 5(a) in series with a winding resistance, R_s. The behaviour of this circuit may be described by the relations

$$v = v_R + v_L \qquad v_R = iR_s$$

and $$v_L = \frac{d\Phi}{dt} \qquad i = f(\Phi) \text{ as for Fig. 5}(a)$$

These four relations may be formed into blocks for assembly into a block diagram in the normal way [Fig. 6(b)]. The assembly is shown in Fig. 6(c). From this diagram either of the usually desired transfer functions, $\tilde{\Phi}/V$ or I/V, may be obtained.

(3.3) Inductance with Core and Copper Losses

Proceeding as before, first the circuit representation of Fig. 7(a) is drawn, L and R_s being as in Fig. 5(a). The core losses are represented by a linear resistance, R_H, in parallel with the ideal non-linear inductance L. Justification for this representation is given on pp. 17–20 of Reference 4, where it is shown that the energy loss per cycle, if B is sinusoidal, is given by

$$\int_0^{2\pi/\omega} H\frac{dB}{dt}dt = \pi B_{max}^2 \frac{\sin\alpha}{\mu} \quad . \quad . \quad . \quad . \quad (8)$$

where α and μ are constants defining a complex permeability, and the equation has been rewritten for rationalized M.K.S. units. Since by definition the flux is sinusoidal the peak value of v_L is proportional to B_{max}, and the loss in eqn. (8) may be simulated by a dissipation (peak $v_L)^2/2R_H$ in a constant resistance R_H placed across the voltage v_L. The reasonableness of assuming v_L and Φ to be sinusoidal is mentioned in Section 6(d). It is important to notice that this assumption should be justified

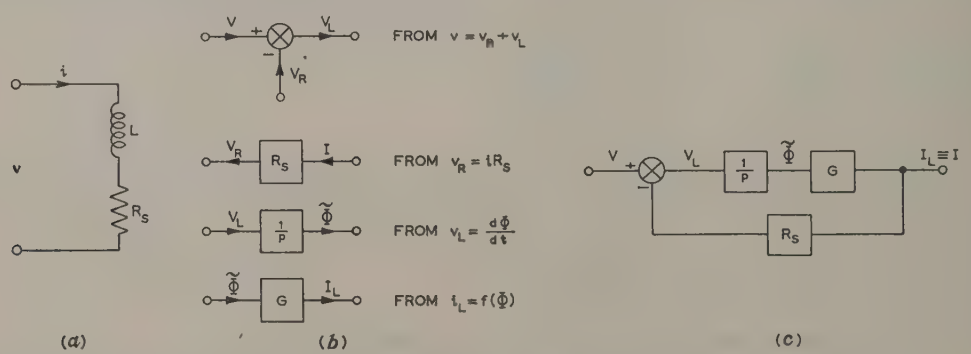

Fig. 6.—Circuit and equivalent block diagrams of a non-linear inductance with copper losses.

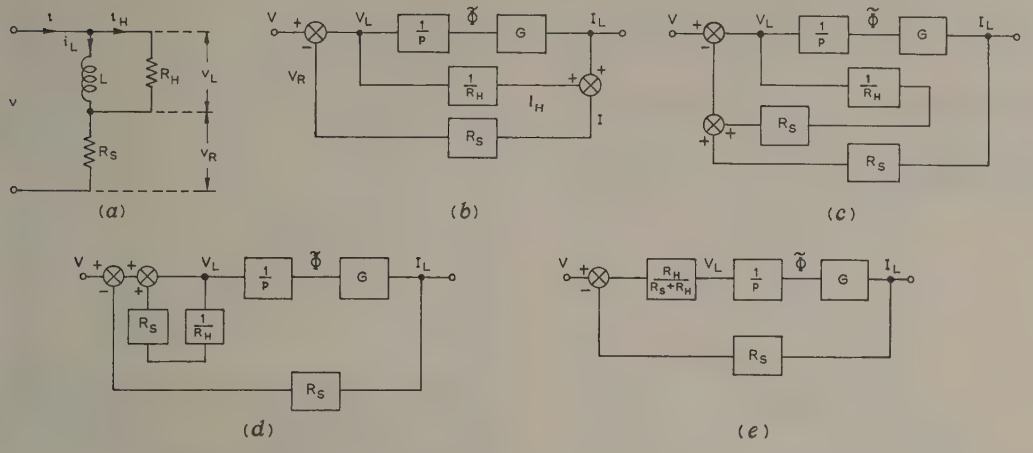

Fig. 7.—Circuit and equivalent block diagrams of a non-linear inductance with copper and core losses.

afresh for each particular system or circuit which comes under study.

An analysis of ferroresonant circuits by Plotkin[6] utilizes an equivalent series resistance to account for core losses. Such a resistance must be amplitude-dependent with respect to current and is less convenient for the present purpose than a fixed parallel resistance.

In addition to the four relations in Section 3.2 it is necessary to write $i = i_L + i_H$ and $i_H/v_L = 1/R_H$, which may be represented in block-diagram form by a summation and a block of transfer function $1/R_H$, respectively. These are added to Fig. 6(*c*) to form the equivalent block diagram of Fig. 7(*b*), from which transfer functions for I_L/V, I/V or $\tilde{\Phi}/V$ may be obtained.

In the case when only I_L/V or $\tilde{\Phi}/V$ is required, the diagram may be simplified. Applying the principle of superposition to the linear portions of Fig. 7(*b*), one may derive Fig. 7(*c*) and thence Fig. 7(*d*).

The minor loop consisting of R_s and $1/R_H$ in Fig. 7(*d*) may be treated as a single series element having a transfer function

$$\frac{1}{1+\dfrac{R_S}{R_H}} = \frac{R_H}{R_S + R_H}$$

and this indicates the hysteresis losses as simply reducing the loop gain by a factor $R_H/(R_S + R_H)$. The final simplification is to the block diagram in Fig. 7(*e*). It should be noted that i_L is not available for physical measurement in the actual circuit; it represents the current through the idealized inductance component L of Fig. 7(*a*).

(4) THE NON-LINEAR ELEMENT *N*

A large number of non-linearities are of the general form shown in Fig. 3, having a linear portion for small inputs and then a gradual reduction in slope, and being symmetrical in the first and third quadrants. In many cases two terms of the series in eqn. (7) suffice to describe the non-linearity, and non-linear inductance and capacitance may be described by

$$\left.\begin{aligned} i &= \frac{1}{L}(\Phi + k\Phi^3) \\ \text{or} \qquad v &= \frac{1}{C}(q + kq^7) \end{aligned}\right\} \quad . \quad . \quad . \quad . \quad . \quad (9)$$

where L and C are the (normalized) small-signal or initial inductance and capacitance respectively.*

For the inductance which is being considered, write $Li = \Phi + k\Phi^3$.

The procedure described by West, Douce and Livesley[2] was followed in order to calculate the necessary describing function for a dual-frequency input $\Phi = a\cos(\omega t + \theta) + b\cos n\omega t$.

The actual derivation is set out in Appendix 11, and the results for the incremental gain of the non-linearity are:

For all values of n except $n = 1$

$$G_2 = 1 + \frac{3}{2}ka^2$$

For $n = 1$

$$G = 1 + \frac{3}{2}ka^2 + \frac{3}{4}ka^2\frac{\cos(\omega t + 2\theta)}{\cos \omega t}$$

The corresponding dual-input describing function for $n = 1$ is given by

$$-\frac{1}{\text{incremental gain}} = -\frac{1}{G}$$

$$= -\frac{4}{3ka^2}\frac{1}{\left(\dfrac{4}{3ka^2} + 2 + \varepsilon^{j2\theta}\right)}$$

The single-input describing function for the same (fundamental) frequency is

$$-\frac{1}{\text{gain function}} = -\frac{1}{1 + \frac{3}{4}ka^2}$$

The dual-input describing function may be plotted on the complex plane.[2] This has been done for the particular iron-cored coil whose measured characteristics are shown in Section 6. Here $Li = \Phi + 10^{-5}\Phi^3$ and a series of circles is obtained, as shown in Fig. 13.

For very small amplitudes the loci degenerate into the critical point $(-1, j0)$ of normal linear analysis. For very large amplitudes the envelopes of the loci become asymptotic with the 30° lines in Fig. 10 of Reference 2 which was plotted for a simple cubic non-linearity.

* The two terms $q + kq^7$ appear to fit the knee of a typical ferro-electric non-linearity[7] better than the two terms $q + kq^3$.

If the open-loop frequency response of the linear part of the system enters the region of instability enclosed by the dotted lines in Fig. 9, instability characterized by a jump (since $n = 1$) will occur.

(5) EQUIVALENT BLOCK DIAGRAM OF A FERRORESONANT CIRCUIT

Consider the *LCR* series circuit of Fig. 8(*a*) in which the inductance L is non-linear. The equivalent block diagram for this circuit may readily be drawn, utilizing the theory presented in Section 3.

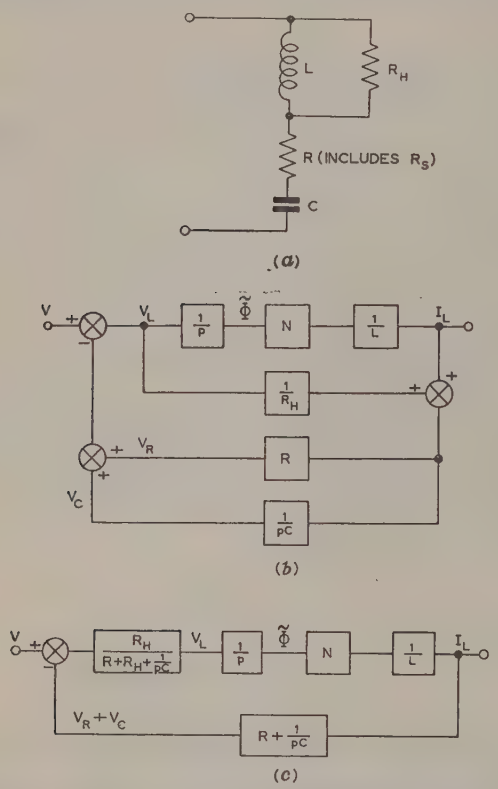

Fig. 8.—Circuit and equivalent block diagrams of a ferroresonant circuit.

The appropriate transfer function for the capacitor is $V_c/I = 1/C_p$ while the circuit relation may be written as $V_L = V - V - V_R - V_c$, and in turn this may be shown on the block diagram as a summation with output V_L and inputs $+V$, $-V_R$ and $-V_c$. The complete block diagram is shown in Fig. 8(*b*). An alternative form, Fig. 8(*c*), combines R and $1/C_p$ into one block of transfer function $(pCR + 1)/pC$. For either kind of describing-function analysis, the system is separated into the resistive non-linearity N and the frequency-dependent linear portion whose transfer function is

$$\frac{(pCR + 1)R_H}{pLpC(R + R_H) + 1}$$

The latter is then plotted (Fig. 9) on the same diagram as $-1/G$ (see Fig. 13) in the way described in Reference 2. The region of instability for $n = 1$ (i.e. jumps) may be seen directly from this plot.

(6) MEASUREMENTS ON NON-LINEAR INDUCTANCES

To enable computations, as suggested in the previous Sections, to be made of the response or stability of a circuit including an iron-cored inductance, the following quantities must be measured (V and I are r.m.s. values in this Section).

(*a*) *Series resistance, R_S.*—At low frequencies where skin effect is inappreciable, the d.c. resistance of the coil may be taken as R_S.

(*b*) *Equivalent parallel loss resistance, R_H.*—By measuring the total losses with a wattmeter and subtracting the loss in R_S, the iron losses, W_H, are obtained and thence $R_H = V_L^2/W_H$ [Fig. 7(*a*)].

In our experience a plot of R_H versus input voltage will give a fairly flat straight line, i.e. the equivalent resistance, R_H, is very nearly independent of input voltage except for small input voltages. This agrees with the statements quoted from Reference 4. Together they have been taken as justifying the use of a fixed value of R_H in the equivalent circuit, Fig. 7(*a*). It is convenient, therefore, to make this measurement at voltages about half way up to the knee of the saturation curve. The input voltage, V, and total current, I, are measured in order to compute V_L and I_L by linear circuit theory.

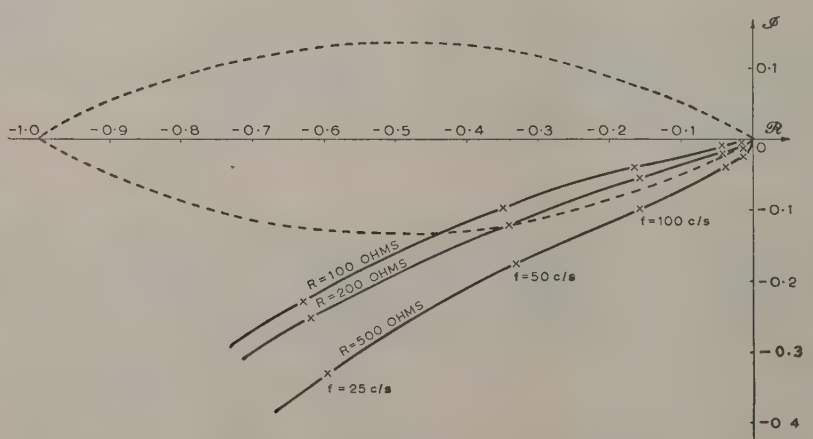

Fig. 9.—Nyquist diagram showing separated frequency response and negative reciprocal of amplitude-dependent response of the system in Fig. 8.

(*c*) *Initial inductance, L.*—The same set of measurements serve to determine L. Thus $L = V_L/\omega I_L$ where $I_L = \sqrt{(I^2 - I_R^2)}$.

(*d*) $i_L = f(\Phi)$ *curve.*—Determination of this curve from published B/H curves for the steel used is not particularly satisfactory, since any air-gap which may be present will alter the shape of the Φ/i curve. A fluxmeter may be used, but the authors' experience indicates that the curve can best be plotted from measured values of I_{max} and V_{max} for a sinusoidal applied voltage v.

$$\text{If } \frac{d\Phi}{dt} = v_L = \cos \omega t, \ \Phi = \int v_L dt = \frac{\sin \omega t}{\omega}$$

It is easy to show that, provided that R_s is small, $v_L \simeq v$, while even for moderate values of R_s the distortion created in the waveform of v_L is not large although numerically we must take $V_L = \sqrt{(V^2 - V_R^2)}$.

The measured initial inductance L, the V_{max}/I_{max} curve and the equivalent hysteresis resistance, R_H, should be considered when fitting together graphically to obtain a suitable numerical choice of constants L and k to fit best the equation $Li_L = \Phi + k\Phi^3$.

In their investigation the authors obtained the following values using an inductance with a conventional Stalloy laminated core without air-gap—actually, a filament-transformer primary winding:

$$R_S = 46 \text{ ohms} \qquad L = 22 \text{ H}$$
$$R_H = 8\,000 \text{ ohms} \qquad k = 10^{-5}$$

The resulting simulation of hysteresis loss on an analogue computer appears to be novel and a paper elaborating this aspect is in course of preparation.

(7) AGREEMENT BETWEEN JUMPS FOUND IN ACTUAL AND SIMULATED MODEL OF AN IRON-CORED *LC* CIRCUIT

A ferroresonant circuit, Fig. 8(*a*), was made up using the iron-cored inductor whose characteristics are given at the end of Section 6. The occurrence of jumps in such non-linear circuits may be displayed very precisely for one frequency at a time by plotting families of v/i characteristics.

This form of presentation will be used to compare the jumps found by measurement on an actual iron-cored LC circuit with those found by simulation on an analogue computer of the proposed equivalent block diagrams (Fig. 8) for the same circuit.

A comparison is shown in Fig. 10 at one frequency (50 c/s) for results of measurements on the actual model and measurements on the simulated model with the real time scale slowed by a factor of 50. The jump on the actual model disappeared at somewhat below $R = 500$ ohms, and on the simulated model at just over $R = 500$ ohms. The agreement between the amplitudes at which jumps occurred, both upward and downward, is seen to be very close. It is concluded that this comparison demonstrates

(*a*) The validity of the equivalent block diagram shown in Fig. 7 for the non-linear inductor with both copper and core losses.
(*b*) That the methods used to measure the parameters of the iron-cored inductor were correctly chosen.
(*c*) That the simulation used in the analogue computer is valid over a wide range of amplitudes.

These conclusions will be valid over a range of frequency which includes significant harmonics and sub-harmonics.

(8) AGREEMENT BETWEEN REGIONS OF INSTABILITY FOUND FROM ACTUAL MODEL AND FROM EQUIVALENT BLOCK DIAGRAM

For arrangements such as the ferroresonant circuit of Fig. 8(*a*) characteristics may be plotted in terms of parameters other than

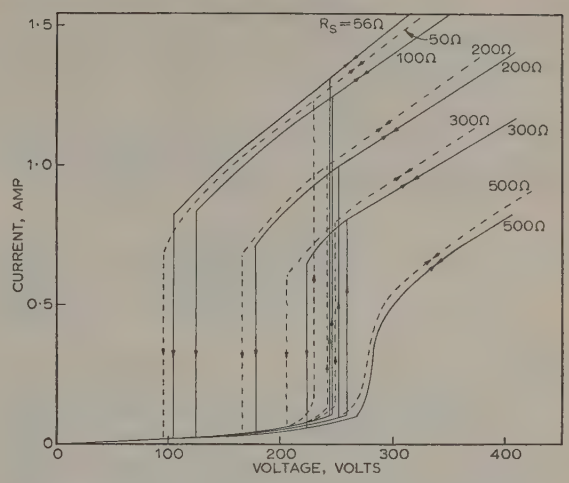

Fig. 10.—Comparison of jumps displayed by actual model and observed on computer-simulated model of Fig. 8(*c*).

—— Actual model.
---- Computer-simulated model.

v and i in order to display the jumps. One such obvious parameter is the excitation frequency, and it is also appropriate to choose one of the circuit parameters for this purpose. In the present investigation the circuit parameter chosen is the series resistance, R.

A comparison is displayed in Fig. 11 for the results of measurements on the simulated model and those extracted from the

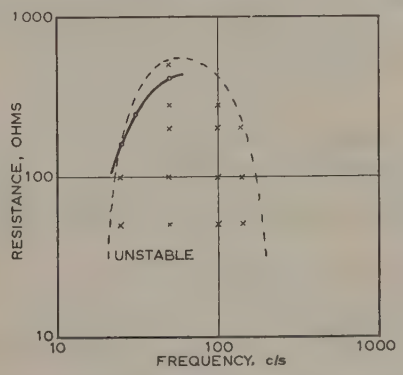

Fig. 11.—Plot of stable and unstable regions on a frequency series-resistance plane, comparing jumps in actual model and jumps predicted by dual-input describing function of Fig. 9.

× Simulated.
O Calculated.

calculation of the region of jumps using the dual-input describing function (see Fig. 9). In each case a marked point indicates instability. Approximate contours have been drawn separating the unstable or jump region (with the cloud of points) from the stable region. The agreement appears reasonable.

It is concluded that this comparison and that of Section 7 demonstrate that the equivalent block diagram of Fig. 7 for an iron-cored inductor, together with the use of simulation or computation by the dual-input describing-function technique, can predict its circuit behaviour over wide ranges of amplitude and frequency.

(9) CONCLUSIONS

A technique has been presented whereby methods of non-linear analysis which are valid only for resistive non-linearities may be extended to reactive non-linearities.

Application of this technique to devices possessing non-linear inductance and/or non-linear capacitance is suggested. For a particular non-linear inductor used in a ferroresonant circuit, experimental results verify the theoretical analysis.

(10) REFERENCES

(1) KOCHENBURGER, R. J.: 'A Frequency Response Method for Analysing and Synthesising Contactor Servomechanisms', *Transactions of the American I.E.E.*, 1950, **69**, Part I, p. 1270.

(2) WEST, J. C., DOUCE, J. L., and LIVESLEY, R. K.: 'The Dual-Input Describing Function and its Use in the Analysis of Non-Linear Feedback Systems', *Proceedings I.E.E.*, Paper No. 1877 M, July, 1955 (**103** B, p. 463).

(3) PRESS, A.: 'Treatment of Harmonics in Alternating Current Theory by means of a Harmonic Algebra', *University of California Publications in Engineering*, 1919, **2**, p. 141.

(4) ASTBURY, N. F.: 'Industrial Magnetic Testing' (Institute of Physics, London, 1952).

(5) FROHLICH, H.: 'Theory of Dielectrics' (Oxford University Press, 1950).

(6) PLOTKIN, S.: 'Discontinuous Transition Time between Unstable States in Ferroresonant Circuits', *Transactions of the American I.E.E.*, 1957, **76**, Part I, p. 410.

(7) VON HIPPEL, A.: 'Dielectric Materials and Applications' (Wiley, 1954), p. 187.

(11) APPENDIX

Derivation of the Describing Functions given in Section 4

Let the non-linear characteristic be $Li = \Phi + k\Phi^3$ and let there be a dual-frequency input given by

$$\Phi = a\cos(\omega t + \theta) + b\cos n\omega t \quad . \quad . \quad . \quad (10)$$

Then substituting and expanding:

$$\begin{aligned} Li = {} & a\cos(\omega t + \theta) + b\cos n\omega t \\ & + k\frac{3a}{4}(a^2 + 2b^2)\cos(\omega t + \theta) + k\frac{3b}{4}(2a^2 + b^2)\cos n\omega t \\ & + k\frac{a^3}{4}\cos 3(\omega t + \theta) + k\frac{b^3}{4}\cos 3n\omega t \\ & + k\frac{3a^2b}{4}\{\cos[(n+2)\omega t + 2\theta] + \cos[(n-2)\omega t - 2\theta]\} \\ & + k\frac{3ab^2}{4}\{\cos[(2n+1)\omega t + \theta] + \cos[(2n-1)\omega t - \theta]\} \end{aligned}$$

$$. \quad . \quad . \quad . \quad (11)$$

For easy identification let the terms of eqn. (11) be numbered ① to ⑩ (see also Table 1 of Reference 2).

(*a*) *Normal Describing Function* (*Frequency* $= \frac{\omega}{2\pi}$).

When n has any value except $\frac{1}{3}$, 1 or 3 the output component of angular frequency ω is

$$① + ③ = a\cos(\omega t + \theta) + k\frac{3a}{4}(a^2 + 2b^2)\cos(\omega t + \theta)$$

The input signal of this frequency is $a\cos(\omega t + \theta)$ and the apparent gain is therefore $1 + k\frac{3}{4}(a^2 + 2b^2)$ and there is no phase shift.

If the second input is removed (i.e. $b = 0$), the apparent gain for the single-frequency input reduces to

$$G_1 = 1 + k\tfrac{3}{4}a^2 \quad . \quad . \quad . \quad . \quad . \quad (12)$$

which is the negative reciprocal of the normal describing function for this non-linear characteristic. Further, even if b is present (provided it is small so that $2b^2 \ll a^2$) the apparent gain at angular frequency ω is still $1 + k\frac{3}{4}a^2$.

(*b*) *Incremental Describing Function* (*Frequency* $= \frac{n\omega}{2\pi}$; $n \neq 1$ or 3).

When n has any value except 1 or 3 the output component of angular frequency $n\omega$ is

$$② + ④ = b\cos n\omega t + k\frac{3b}{4}(2a^2 + b^2)\cos n\omega t$$

The input signal at this frequency is $b\cos n\omega t$ and the apparent gain is therefore $1 + k\frac{3}{4}(2a^2 + b^2)$.

For b small so that $b^2 \ll 2a^2$ this expression reduces to

$$G_2 = 1 + k\frac{3a^2}{2} \quad . \quad . \quad . \quad . \quad . \quad . \quad (13)$$

which may be termed the incremental gain of the non-linearity at angular frequency $n\omega$ and which is valid except for $n = 1$ or 3. The incremental describing function is the negative reciprocal of the above gain.

(*c*) *Incremental Describing Function* (*Frequency* $= \frac{n\omega}{2\pi}$; $n = 3$).

When $n = 3$ the output components of frequency $n\omega$ are

$$② + ④ + ⑤ = b\cos 3\omega t + k\frac{3b}{4}(2a^2 + b^2)\cos 3\omega t + k\frac{a^3}{4}\cos 3(\omega t + \theta)$$

However, the term ⑤ was initially present due to the input $a\cos(\omega t + \theta)$, and hence the incremental gain for the signal $b\cos 3\omega t$, where b is small, reduces to $1 + k\frac{3a^2}{2}$, the same expression as in (*b*). As far as incremental gain is concerned, therefore, we need consider only the two cases set out in (*b*) and (*d*).

(*d*) *Incremental Describing Function* (*Frequency* $= \frac{n\omega}{2\pi}$; $n = 1$).

When $n = 1$ the output component of angular frequency $n\omega$ is ① + ② + ③ + ④ + ⑧ + ⑩. Of these, the terms ① and ③ were initially present due to the input $a\cos(\omega t + \theta)$, before the second signal $b\cos\omega t$ was injected (provided that $2b^2 \ll a^2$).

The incremental gain for the second signal is thus the ratio of the terms ② + ④ + ⑧ + ⑩ to the input $b\cos\omega t$, and on the further assumption that b is sufficiently small so that $b \ll 2a$ (enabling term ⑩ to be neglected) the incremental gain reduces to

$$G = 1 + k\frac{3a^2}{2} + k\frac{3a^2}{4}\frac{\cos(\omega t + 2\theta)}{\cos\omega t} \quad . \quad . \quad (14)$$

The locus of the incremental gain as the arbitrary angle θ is varied from 0 to 2π is a circle with centre $1 + k\frac{3a^2}{2}$ and radius $k\frac{3a^2}{4}$ [see Fig. 8 of Reference 2].

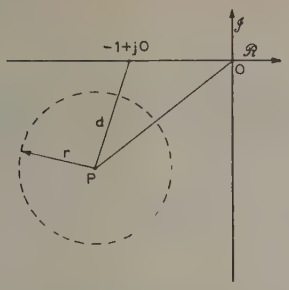

Fig. 12.—Condition for enclosure of the $(-1, j0)$ point.
P is the point $(1 + k\frac{3}{2}a^2)(x + jy)$

It is clear that the value of G is independent of b so long as b is kept small. The incremental open-loop gain (for small signals of frequency $n\omega$; $n = 1$) for the whole system may thus be defined as the product of G and the frequency response $\psi(j\omega)$ of the linear part of the system. The function $G\psi(j\omega)$ may thus be treated as linear with regard to small signals of frequency $n\omega$; $n = 1$. Following the argument in Section 3.1 of Reference 2, let $\psi(\omega j) = x + jy$ be the frequency response of the linear part of the system. The incremental open-loop gain for this frequency is thus a circle at centre $(1 + k\frac{3}{2}a^2)(x + jy)$ and radius $k\frac{3a^2}{4}(x^2 + y^2)^{1/2}$. The condition for this circle to enclose the $(-1, j0)$ point on the frequency-response complex plane may be derived from Fig. 12.

The distance d of P from the $(-1, j0)$ point is given by

$$d^2 = (1 + k\tfrac{3}{2}a^2)^2y^2 + (1 + k\tfrac{3}{2}a^2)^2x^2 - 2(1 + k\tfrac{3}{2}a^2)x + 1 \quad (15)$$

The limiting condition for stability may be obtained by equating d^2 to r^2 and solving for a:

$$(1 + k\tfrac{3}{2}a^2)^2y^2 + (1 + k\tfrac{3}{2}a^2)^2x^2 - 2(1 + k\tfrac{3}{2}a^2)x + 1 = k^2\tfrac{9}{16}a^4(x^2 + y^2) \quad (16)$$

Alternatively, it is convenient to plot the frequency-response function, $\psi(j\omega)$, and the incremental describing function, $-1/G$, on the same complex plane. A detailed plot of $-1/G$ is shown in Fig. 13 and the combined plot in Fig. 9. These two Figures should be compared with Figs. 10 and 12(*a*), respectively, of Reference 2.

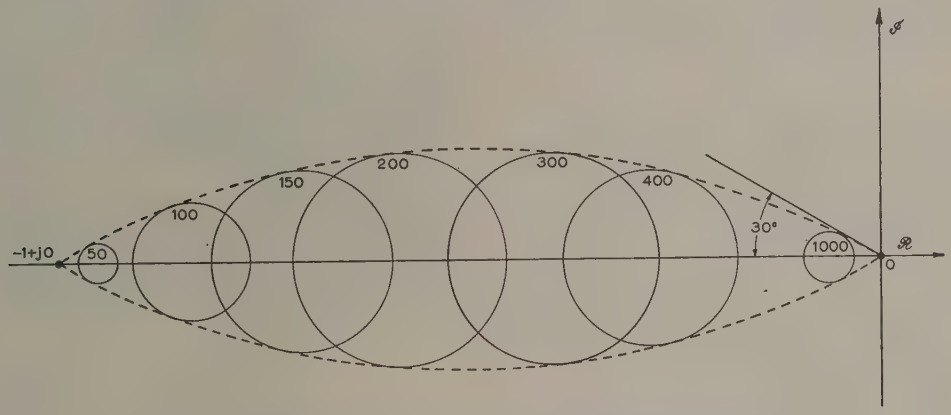

Fig. 13.—Plot on the complex plane of the incremental describing function

$$-\frac{1}{G} = \frac{4}{3ka^2}\,\frac{-1}{\left(\frac{4}{3ka^2} + 2 + \varepsilon^{j2\theta}\right)} \quad \text{for } k = 10^{-5}$$

Circles are for various amplitudes, a.

621.391.827.42: 621.395.2

The Institution of Electrical Engineers
Monograph No. 384 E
June 1960
©

INTERMODULATION ON AMPLITUDE-MODULATED MULTI-CHANNEL LINE LINKS

By J. C. H. DAVIS, M.A., and H. O. FRIEDHEIM, B.Sc., Associate Member.

(*The paper was first received 7th May, in revised form 16th November*, 1959, *and in final form 4th March*, 1960. *It was published as an* INSTITUTION MONOGRAPH *in June*, 1960.)

SUMMARY

The paper develops a method for estimating the total intermodulation noise power falling into any channel in the transmission band of an a.m. multi-channel line system with many repeater sections in tandem. These sections may be composed of widely varying lengths of cable imperfectly equalized by non-identical amplifiers whose in-band feedback, output load impedance and output network response all vary with frequency. The whole system is loaded in such a way that the signal levels at each intermodulation source are also functions of frequency.

After developing the basic theory, methods are given for estimating the system performance before building an amplifier and also when a model amplifier is available. These methods are more general than those previously published and are illustrated by examples.

LIST OF PRINCIPAL SYMBOLS

c = Number of regulated r.f. links in a system (at the ends of which frequency translation occurs).
D_1, D_n = Vectors representing an intermodulation product after the first and nth amplifier, respectively.
f = Frequency.
F_r = Effective feedback for an rth-order intermodulation product.
g_r = Coefficient of v^r in the characteristic valve equation.
k = Psophometric weighting factor.
m = Number of speech channels in the system.
M = Multi-channel peak factor.
n = Number of repeaters in tandem in a system.
p_0 = Speech factor (mean speech power divided by standard test-tone power).
P_r = Psophometrically weighted intermodulation noise power of rth-order products of one type falling into a disturbed channel at a 0 dBm0 point.
Q = Link addition function.
t_r = rth-harmonic margin of distorting valve, measured in a resistive load with voltage V_d between grid and cathode without feedback.
$u_r = V_r/V_d$ = Normalized voltage.
V = Fundamental signal voltage between grid and cathode of the distorting valve.
z_r = Distribution function (containing quantities to be summed when evaluating P_r).
β = Transmission phase between corresponding points in successive repeater sections.
ν = Product phase—a phase angle associated with each intermodulation product.
σ = Standard deviation.
$\rho = (f - f_1)/(f_2 - f_1)$ = Normalized frequency.
τ = Constant time delay.
$\phi = \beta - \tau\omega$ = Difference phase.
ω = Angular frequency.

Correspondence on Monographs is invited for consideration with a view to publication.
Mr. Davis and Mr. Friedheim are with British Telecommunications Research Ltd.

(1) INTRODUCTION

An a.m. communication system is non-linear if various signals interact with each other to produce new signals, i.e. if harmonic and intermodulation terms are present which appear as noise in the channels.

Several authors[1–5] have examined special cases of the problem of intermodulation. This paper re-examines some aspects of the problem for a more general practical case and shows how a more detailed knowledge of the system may ease its design.

The general system discussed here consists of repeater sections of widely different lengths whose losses are imperfectly equalized by passive networks and feedback amplifiers of unequal non-linear behaviour. Their in-band feedback, output load impedance and output network response all vary with frequency, and they may contain more than one predominant source of intermodulation. The general system is loaded in such a way that the nominal signal levels at each intermodulation source are also functions of frequency.

The problem divides into three main parts: the calculation of the amplitude of a particular intermodulation product in one amplifier (the generation problem); the effect of connecting many such amplifiers in tandem (the transmission problem); and the summation of all products of one type falling into a given channel (the summation problem).

(2) TRANSMISSION PROBLEM

(2.1) Phase Functions

Every communication system is non-linear, but, in fact, the intermodulation products are kept several orders of magnitude below speech signals. A first-degree non-linear system is assumed, where the intermodulation products of one source do not themselves generate further intermodulation products at a later source. Such a system can in theory be replaced by a completely linear system with sources of signal-dependent intermodulation noise appearing at each amplifier. The sequence of addition of these signals is immaterial.

This first-degree non-linear system does not fully describe a practical system, and exceptions will be discussed later.

For the purpose of noise intermodulation planning, multi-channel speech signals can be represented by white noise in each channel of the same mean power over a prescribed time interval as an equivalent sinusoidal test signal.[1, 10]

Consider fundamental signals of the form $v_r = A_r \cos(\omega_r t + \gamma_r)$ at an intermodulation source, giving, amongst many others, a product of angular frequency ω_0, where ω_0 is the sum of p positive and q negative frequency terms.

$$\omega_0 = (\omega_1' + \omega_2' + \ldots + \omega_p') - (\omega_1'' + \omega_2'' + \ldots + \omega_q'') = \sum_p \omega' - \sum_q \omega'' \quad \ldots\ldots\ldots \quad (1)$$

The full expression for this intermodulation signal is

$$\eta_1 = k_1(A_1'A_2' \ldots A_p')(A_1''A_2'' \ldots A_q'') \cos(\omega_0 t + \gamma_0) \quad (2)$$

where $\gamma_0 = \sum_p \gamma' - \sum_q \gamma''$ and k_1 is a constant depending only on the properties of the intermodulation source. Both the fundamental signals and the product undergo transmission phase changes $\beta(\omega_r)$ and $\beta(\omega_0)$, respectively, before reaching the next corresponding intermodulation source in the next amplifier. Here a new product η_2 of angular frequency ω_0 is formed from the same speech signals, the phase difference between η_2 and η_1 being the product phase ν, where

$$\nu = \sum_p \beta' - \sum_q \beta'' - \beta(\omega_0) \quad . \quad . \quad . \quad . \quad (3)$$

In a practical cable system, the transmission phase function $\beta(\omega)$ is the sum of a small non-linear phase frequency characteristic $\phi(\omega)$ and a large linear phase frequency characteristic $\tau\omega$, corresponding to a constant time delay, τ. After substituting $\beta(\omega) = \phi(\omega) + \tau\omega$ in eqn. (3),

$$\nu = \sum_p \phi' - \sum_q \phi'' - \phi(\omega_0) \quad . \quad . \quad . \quad . \quad (4)$$

For intermodulation calculations, the transmission phase β, which is awkward to handle, can be replaced by the difference phase ϕ, which is much easier to handle. Typically, in a 6-mile repeatered 0·375 in coaxial cable, β at 4 Mc/s is about 300π. Section 11.1 shows how this angle can be measured to $\pm 4°$, but a curve of β against frequency cannot be read to such accuracy. Instead, by choosing a convenient slope τ and subtracting $\tau\omega$, the difference phase ϕ can be plotted. A typical ϕ curve is shown in Fig. 1. By using eqn. (4), the product phase v can be calculated quickly for any combination.

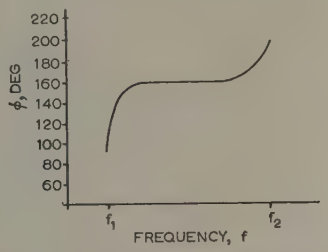

Fig. 1.—Typical difference phase function ϕ_f.

It has been found that, for a given system, fully equalized repeater sections of whatever lengths have practically identical $\phi(\omega)$ functions, although very different values of τ must be chosen for each case. Although the cable and the variety of equalizers or simulators have very different loss characteristics above the band, this introduces an in-band phase change which is very nearly proportional to frequency.[6] However, below the band, lines and equalizers have very similar loss characteristics. This is just as well, since dissimilar characteristics would produce in-band phase characteristics inversely proportional to frequency.[6]

Extensive measurements on actual repeatered coaxial-line links have confirmed that the difference phase function $\phi(\omega)$ is surprisingly invariant (about $\pm 5°$) between widely varying equalized repeater sections for a given system.

(2.2) Ideal System

An ideal system has the following properties: it is first-degree non-linear; all sections have the same difference phase function $\phi(\omega)$, although the transmission phase function $\beta(\omega)$ varies widely between sections: all sections are perfectly amplitude equalized at all in-band frequencies; and all repeaters have identical intermodulation generation characteristics.

In this ideal system a new individual product of frequency f_0, due to the same fundamentals, is generated at every successive amplifier, all of the same amplitude but displaced from each other by the product phase ν. Assuming an initial product of amplitude D_1, the resultant vector D_n, after n repeaters, is given by

$$\frac{D_n}{D_1} = \frac{\sin \frac{1}{2}n\nu}{\sin \frac{1}{2}\nu} \varepsilon^{j(n-1)\nu/2} \quad . \quad . \quad . \quad . \quad (5)$$

The amplitude of this function is given in Fig. 2.

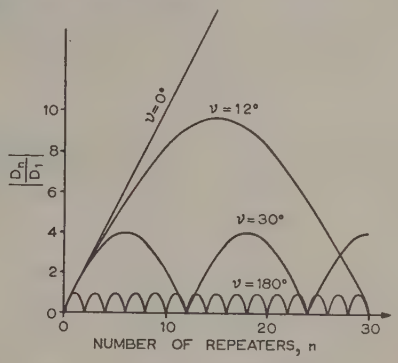

Fig. 2.—Ideal link addition function.

If $\nu = 0$, $D_n/D_1 = n$, i.e. algebraic addition takes place. If $\nu = \pm \pi$, there is cancellation at successive repeaters.

For all other values of ν, $|D_n/D_1|$ has a maximum of cosec $\frac{1}{2}\nu$. If an ideal system can be so designed that $\frac{1}{2}\pi \leqslant \nu \leqslant \frac{3}{2}\pi$, D_n will never exceed D_1 by more than 3 dB at any point.

For second-order and some third-order products a system can be thus designed by making the ϕ/frequency curve approximate to a constant value near $\phi = \pi$. This is best achieved by introducing an odd number of inverting stages in each amplifier, rather than by poling successive amplifiers.

The so-called group 3/1 products (see Section 4.3) of the form

$$f_0 = f_1 + f_2 - f_3 \quad . \quad . \quad . \quad . \quad . \quad . \quad (6)$$

all frequencies being positive, have a product phase

$$\nu = \phi_1 + \phi_2 - \phi_3 - \phi_0 \quad . \quad . \quad . \quad . \quad (7)$$

This important group tends to $\nu = 0$ and it is usually difficult to prevent their algebraic addition.

(2.3) The Practical System

The above analysis has considered primary products formed directly from the intermodulation of fundamentals only. In a practical system these in turn intermodulate at successive amplifiers with both fundamentals and other products, giving secondary products. All are negligible except those secondary third-order products which are formed by intermodulation of fundamentals and primary second-order products, which may be of a magnitude not very different from identical primary third-order products. If the system is designed so that $\nu = 0$ both for the primary third-order product and for the primary second-order products which form it, D_n/D_1 is proportional to $n(n-1)$. In a long system so designed, secondary products of the type $f_0 = f_1 + f_2 - f_3$ will predominate over the same primary type. This can easily be avoided by designing the system to avoid $\nu = 0$ for primary second-order products, in which case the secondary products are swamped by primary products after a few repeaters.

Effects of variations in ϕ, which are rarely more than 5°, are entirely negligible.

In all modern coaxial systems, actual signal levels must not

vary by more than ± 2 dB from nominal at any point in the system at any transmission band frequency due to any cause, including ageing. It is prudent to allow a safety factor of 1·25 for the whole link, owing to imperfect equalization and higher-degree non-linearity effects for those products for which ν is within 5° of zero. For all other values of ν, the overall effect is negligible.

The major difference between ideal and practical systems is the variation in amplifier intermodulation amplitudes. This changes with old and new valves and feedback, but the phase remains almost constant. Differences of 10 dB in amplitude are common between third-order products from similar amplifiers with new valves under standard test conditions.

The vector representing an intermodulation product in any amplifier can be considered as the sum of a mean and an error vector. It is assumed that individual links are equipped with amplifiers chosen at random from a very large population with a mean vector D_1 and a standard deviation of σD_1. D_1 satisfies eqn. (5). A number of links, each equipped with a sufficiently large number, n, of amplifiers will have resultant error vectors of indeterminate phase, whose amplitudes,[7] usually of Gaussian distribution, have a standard deviation $\sigma D_1 \sqrt{n}$.

Assuming algebraic addition of mean and error vectors, but neglecting any other previously discussed practical effects,

$$\frac{D_n}{D_1} = \operatorname{cosec} \tfrac{1}{2}\nu + \sigma\sqrt{n} \quad . \quad . \quad . \quad . \quad (8)$$

With a system divided into c r.f. equalized links, at the ends of which frequency translation occurs, each with a large number of amplifiers, and taking the safety factor 1·25 into account, the link addition function Q can therefore be written as

$$Q = \left|\frac{D_n}{D_1}\right| \quad . \quad . \quad . \quad . \quad . \quad . \quad (9)$$

When $\nu = 0$,

$$Q = \frac{1{\cdot}25n}{\sqrt{c}} \quad . \quad . \quad . \quad . \quad . \quad . \quad (10)$$

and when $\nu = \pi \pm \pi/2$,

$$Q = \sigma\sqrt{n} \quad . \quad . \quad . \quad . \quad . \quad . \quad (11)$$

These results differ from those of Brockbank and Wass[2] by the significant factor σ.

We have insufficient information about the amplitude distribution of these error vectors in aged systems under different maintenance conditions, except that for all products σ is less than 0·5, and perhaps much less.

Figs. 3–6 show that eqns. (5), (10) and (11) form a reliable description of a practical system. They are the result of measure-

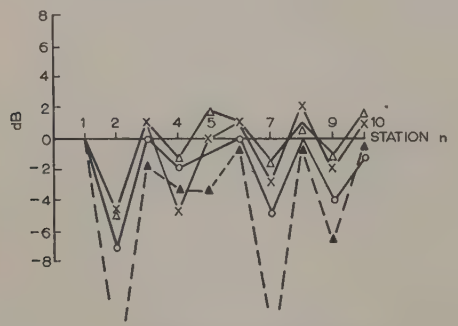

Fig. 3.—Measured link addition function.

Second-order products in a white noise loaded system.
○ Measured at 534 kc/s.
× Measured at 1 002 kc/s.
△ Measured at 2 438 kc/s.
▲ Calculated, $\nu = 160°$.

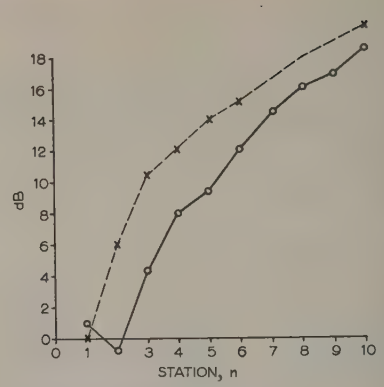

Fig. 4.—Third-order product; $\nu = 2°$.
○ Measured.
× Calculated.

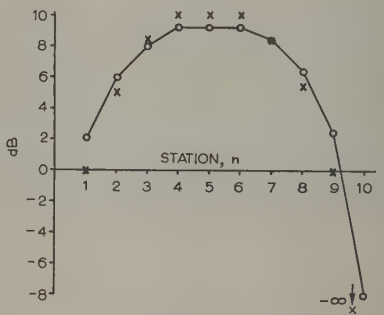

Fig. 5.—Third-order product; $\nu = 36°$.
○ Measured.
× Calculated.

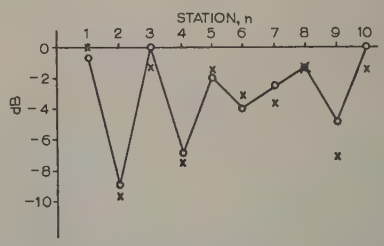

Fig. 6.—Second-order product; $\nu = 168°$.
○ Measured.
× Calculated.

ments on a route containing 10 repeaters which were normal production models and had been running for 5 months. Fig. 3 shows second-order products on the system loaded with white noise. Even at the tenth amplifier the error component is small compared with the resultant of the mean vectors.

Fig. 4 shows a third-order product of the $f_0 = f_1 + f_2 - f_3$ type. The anomaly at the second amplifier is assumed to be due to secondary intermodulation terms.

(3) GENERATION PROBLEM AND DESIGN FORMULA

If full advantage is to be taken of eqns. (10) and (11), they must be included in the design formula from which the sum of all products of any type falling into a given channel at the end of the route can be calculated. It is therefore most convenient not to sum at the output of each amplifier but to find the amplitudes of the various vectors when they reach the system audio output point and to sum them there. In discussing the general

case described in Section 1 one must return to first principles, i.e. the characteristic equation of the non-linear device.

An ideal pentode is assumed to be the intermodulation source in each amplifier. The signal output current, i, is related to the grid-cathode voltage v by the characteristic equation:

$$i = g_0 + g_1 v + g_2 v^2 + g_3 v^3 + \ldots + g_r v^r \quad . \quad . \quad (12)$$

where g_r are measurable positive real constants independent of the anode circuit.

Consider an rth-order r-tone product of amplitude I_r and frequency f_0 resulting from the intermodulation of sinusoidal signals of frequencies $f_1, f_2, f_3 \ldots f_r$, and having grid-cathode voltages $V_1, V_2, V_3 \ldots V_r$. These voltages are assumed to be those corresponding to 0 dBr test tone levels. It has been shown[2] that

$$I_r = \frac{r!}{2^{r-1}} g_r V_1 V_2 V_3 \ldots V_r \quad . \quad . \quad . \quad . \quad (13)$$

This product has a frequency of

$$f_0 = \pm f_1 \pm f_2 \pm f_3 \pm \ldots \pm f_r \quad . \quad . \quad . \quad (14)$$

The signal V_0 at frequency f_0 produces a fundamental output current $g_1 V_0$, so that the ratio of product to signal current (the product margin) at f_0 is

$$\frac{r!}{2^{r-1}} \frac{g_r}{g_1} \frac{V_1 V_2 V_3 \ldots V_r}{V_0}$$

This ratio is independent of the anode circuit and is the same at any point of the repeater section, i.e. at the anode, at the output terminals of the output network, anywhere along the line and at the grid of the next distortion source.

In a feedback amplifier this ratio will be reduced by the effective feedback F_r at frequency f_0. For any second-order product, the effective feedback is practically the same as the return difference on the distortion source, but for third-order products the effective feedback is less than the return difference[8, 9] by about 10 dB in the case of pentode-type valves.

After n successive amplifiers the various products of the same kind have added up in the way described in Section 2.3, so that the margin will be

$$\frac{r!}{2^{r-1}} \frac{g_r}{g_1} \frac{V_1 V_2 V_3 \ldots V_r}{V_0} \frac{Q_r}{F_r}$$

The signal is now assumed to be demodulated and brought to the 0 dBm0 audio point without distortion.

The mean-speech voltage[1] is a fraction, $\sqrt{p_0}$, of the standard test level voltage. p_0 is a function of the number of speech channels, m, and is at present taken to be[10]

$$10 \log_{10} p_0 = -15 \text{ dB} \quad m \geqslant 240 \quad . \quad . \quad . \quad . \quad . \quad (15)$$

$$10 \log_{10} p_0 = -(1 + 6 \log_{10} m) \text{ dB} \quad 12 \leqslant m \leqslant 240 \quad (16)$$

Strictly speaking, eqns. (15) and (16) apply to the case where all values of $V_1, V_2 \ldots V_r$ are of equal amplitude, but there is reason to believe that they also apply to any practical system where V is a function of frequency.

By using this speech factor p_0, the various sets such as $(V_1\sqrt{p_0}, V_2\sqrt{p_0}, V_3\sqrt{p_0} \ldots V_r\sqrt{p_0})$ modulating into frequency f_0 can be assumed to be unrelated in time, so that they add like powers.

Finally, a summation must be made of all products of the same order and type yielding frequency f_0, indicated symbolically by Σ_r below. Details of the summation processes are given in Section 4.

Introducing a psophometric weighting factor, k, at present defined as

$$10 \log_{10} k = -4 \text{ dB for a 4 kc/s channel} \quad . \quad (17)$$

and remembering that at the 0 dBm0 point the speech power is not 1 but p_0 milliwatts, the psophometrically weighted intermodulation noise power due to all permissible products of one possible type of rth order falling into a disturbed channel of transmission frequency f_0 at the 0 dBm0 audio output point is given by

$$P_r = \frac{k p_0^r}{F_r^2} \left(\frac{r! g_r}{2^{r-1} g_1} \right)^2 \sum_r \left(\frac{V_1 V_2 V_3 \ldots V_r}{V_0} Q_r \right)^2 \text{ milliwatts} \quad . \quad (18)$$

It is convenient to refer all grid voltages to one arbitrary voltage V_d, and to define a normalized voltage u by

$$u_r = \frac{V_r}{V_d} \quad . \quad . \quad . \quad . \quad . \quad . \quad . \quad (19)$$

At a grid-cathode voltage, V_d, the ratio of the rth harmonic power to the fundamental power into any resistive anode load is given by

$$t_r = \left(\frac{g_r}{2^{r-1} g_1} \right)^2 V_d^{2(r-1)} \quad . \quad . \quad . \quad . \quad (20)$$

It is an interesting fact (Section 9), not quite following from the 3/2 power law, that for all pentode-type valves the average values of the factor $(g_r/2^{r-1}g_1)^2$ are

$$10 \log_{10} \left(\frac{g_2}{2g_1} \right)^2 = -13 \text{ dB} \quad . \quad . \quad . \quad . \quad (21)$$

$$10 \log_{10} \left(\frac{g_3}{4g_1} \right)^2 = -24 \text{ dB} \quad . \quad . \quad . \quad . \quad (22)$$

It is also convenient (Section 4) to express the summation in the form of a distribution factor z_r defined by

$$\sum_r \left(\frac{u_1 u_2 u_3 \ldots u_r}{u_{f0}} Q_r \right)^2 = \frac{m^{r-1} z_r}{r!^2} \quad . \quad . \quad . \quad (23)$$

where m is the number of speech channels in the system. Substituting in eqn. (18) gives

$$P_r = \frac{k t_r p_0^r m^{r-1} z_r}{F_r^2} \text{ milliwatts} \quad . \quad . \quad . \quad (24)$$

This is the desired design formula. A detailed system design example is given in Section 11.2.

It is essential that both t_r and z_r be referred to the same reference level. Should either t_r or z_r be given referred to V_d or u_d, and z_r' or t_r' be given referred to V_d' or u_d', they must be brought to the same reference level by the following relationship obtained from eqns. (19), (20) and (23):

$$\left(\frac{u_d'}{u_d} \right)^{2(r-1)} = \left(\frac{V_d}{V_d'} \right)^{2(r-1)} = \frac{z_r'}{z_r} = \frac{t_r}{t_r'} \quad . \quad . \quad (25)$$

In the special case where anode load, output network response and feedback are all constant over the transmission band, eqn. (24) is identical in form with the Brockbank and Wass formula.[2]

Should a repeater contain multiple sources of intermodulation, it is advisable to carry out separate calculations for each source.

In the case of transistors, even allowing for multiple intermodulation sources in each transistor, it is not strictly sufficient to replace grid voltage by base or emitter current in eqn. (12). The non-linear behaviour of transistors and medium internal impedance devices, such as triodes, is more complex and has been expressed by a characteristic equation containing derivatives and powers of derivatives of the input excitation.[11] However, line amplifiers of a 60 kc/s to 1·4 Mc/s transistor system using either diffused base or Mesa transistors have behaved like valve amplifiers.

(4) SUMMATION PROBLEM

(4.1) Conventions

Before the summation in eqn. (23) can be performed, all possible combinations of the frequencies involved must be found. Only two-tone second-order and three-tone third-order products will be considered, since all other products have been shown[2] to be negligible in comparison.

Each channel is referred to by its transmission frequency f and has a bandwidth b. All frequencies are taken to be positive. f_a, f_b and f_c are signal frequencies, f_0 the resulting product frequency, and f_1 and f_2 the lowest and highest frequencies of the transmission band respectively. In all cases $0 \leqslant f_1 \leqslant f_a, f_b, f_c, f_0 \leqslant f_2$ and $f_a > f_b$.

(4.2) Second-Order Products

With the above restrictions there are only two groups, namely

$$f_a + f_b - f_0 = 0 \quad . \quad . \quad . \quad . \quad . \quad (26)$$

$$f_a - f_b - f_0 = 0 \quad . \quad . \quad . \quad . \quad . \quad (27)$$

All other combinations are equivalent to these two. Fig. 7 shows a model of eqns. (26) and (27) to find the required ranges of f_a and f_b for given f_1, f_2 and f_0. All values of f_a and f_b contributing to eqn. (26) lie on ST, and those contributing to eqn. (27) lie on UV. The inclusion of the boundary line MR given by $f_a = f_b$ introduces negligible errors. It is obvious that

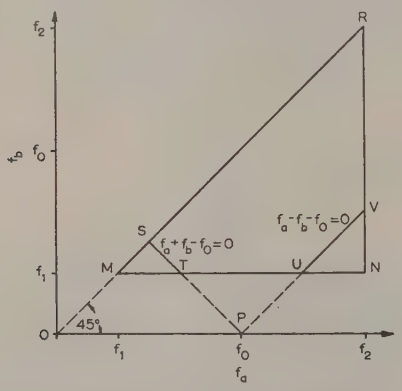

Fig. 7.—Second-order group model.

Co-ordinates

Point	f_a	f_b
M	f_1	f_1
N	f_2	f_1
R	f_2	f_2
P	f_0	0
S	$\frac{1}{2}f_0$	$\frac{1}{2}f_0$
T	$f_0 - f_1$	f_1
U	$f_0 + f_1$	f_1
V	f_2	$f_2 - f_1$

these ranges depend upon the ratio f_1/f_2. If $f_2 < 2f_1$, no second-order products fall within the band.

Assuming u_f and Q_f to be known, and taking f_b to be the dependent variable, it is easy, for any one disturbed channel f_0, to find the products $(u_a u_b Q_{a,b,-f_0})^2$ and $(u_a u_b Q_{a,-b,-0})^2$ for all permissible values of f_a for $(f_a + f_b - f_0 = 0)$ and $(f_a - f_b -$

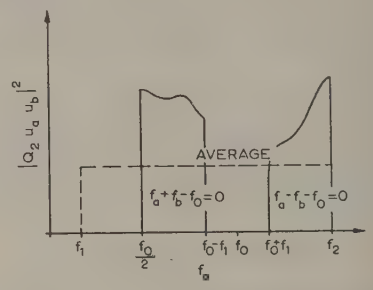

Fig. 8.—Second-order products for groups $f_a \pm f_b - f_0 = 0$.

$f_0 = 0$) products respectively. They can be plotted against f_a as in Fig. 8. From eqn. (23),

$$z_2 = \frac{4b \times \text{area under curve}}{u^2_{f_0}(f_2 - f_1)} \quad . \quad . \quad . \quad . \quad (28)$$

(4.3) Third-Order Products

With the above conventions there are only three groups as shown in Table 1.

Its restrictions and other useful information can easily be obtained from Fig. 9, which is a geometrical model for finding required ranges of f_a, f_b and f_c for the equations of Table 1 and for given f_1, f_2 and f_0. The f_a and f_b scales are linear and identical, and $\sqrt{2}$ times the length of the sliding linear f_c scale. For any value of f_c, lines at $-45°$ inside MNR represent the locus of f_a and f_b. The f_c-cursors of groups 3/1 and 3/2 carry the complete f_c scale, the limits of f_c being given by their coincidence with point M. The f_c-scale on the group 3/3 cursor is limited between f_1 and $\frac{1}{3}f_0$, which may be a more severe restriction than that imposed by the point M. For groups 3/2 and 3/3, the number of products falling into a channel f_0 depends upon $f_2 - f_1$ and the ratio f_2/f_1, but for group 3/1 it depends only upon $f_2 - f_1$.

Assuming Q_f and u_f to be known, and taking f_b to be the dependent variable, it is easy to find the product $(u_a u_b u_c Q_{a,b,\pm c,\pm f_0})^2$ for any one group for all permissible combinations modulating into f_0. This product can be plotted as in the 3-dimensional models of Fig. 10, over the base in the $f_a f_c$ plane corresponding to the f_a and f_c ranges of Fig. 9. From eqn. (23)

$$z_3 = \frac{36b^2 \times \text{volume over the } f_a f_c \text{ plane}}{(f_2 - f_1)^2 u^2_{f_0}} \quad . \quad . \quad (29)$$

For all cases, z can thus be found by numerical, graphical or, in simple cases, analytical integration (see Sections 11.3 and 11.4).

Table 1

THIRD-ORDER GROUPS

Group	Equation	Typical product phase, ν	Permitted range of f_c for given f_0	Limits of f_a for given f_c and f_0
3/1	$f_a + f_b - f_c - f_0 = 0$	0°	$f_1 < f_c < f_2$	$\frac{1}{2}(f_0 + f_c) < f_a \leqslant f_0 + f_c - f_1$ if $f_1 \leqslant f_c \leqslant f_1 + f_2 - f_0$ $\frac{1}{2}(f_0 + f_c) < f_a \leqslant f_2$ if $f_1 + f_2 - f_0 \leqslant f_c \leqslant f_2$
3/2	$f_a + f_b - f_c + f_0 = 0$	$\pm 30°$	$f_0 + 2f_1 < f_c < f_2$	$\frac{1}{2}(f_c - f_0) < f_a < f_c - f_0 + f_1$
3/3	$f_a + f_b + f_c - f_0 = 0$	$\pm 30°$	$f_1 \leqslant f_c < \frac{1}{3}f_0$ $f_c < f_0 - 2f_1$	$f_a > f_b > f_c$ $\frac{1}{2}(f_0 - f_c) < f_a < f_0 - f_1 - f_c$

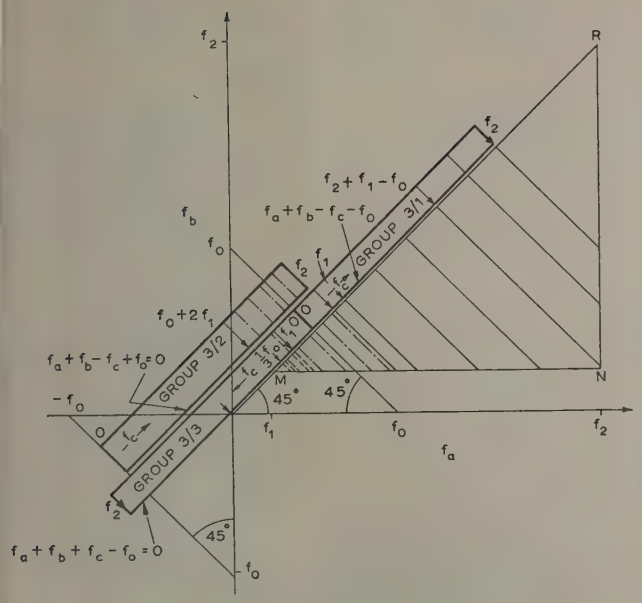

Fig. 9.—Third-order group model.

Co-ordinates

Point	f_a	f_b
M	f_1	f_1
N	f_2	f_1
R	f_2	f_2

(5) EXPERIMENTAL LABORATORY TEST METHOD

By using up to three oscillators, a model amplifier and a good wave analyser, the integrated signal/intermodulation-noise power ratio of one type falling into a disturbed channel f_0 can be found experimentally by adjusting output levels to the required nominal levels, measuring the nominal-signal/actual-noise ratios of a carefully selected combination of test frequencies and following the summation procedure of the previous Section. A certain Q function must be assumed.

Normally, for a given disturbed channel f_0, about 4 and 16 measurements suffice to find the total second-order and group 3/1 products, respectively. The graphical error is usually of the order of $\pm 10\%$ (or 1 dB), the same order as the experimental error. This method gives an excellent knowledge of the amplifier's non-linear performance, is very versatile and is much more reliable during design than any single harmonic or two-tone measurement. The complete system is best tested with a noise loading set,[12, 13] which is of limited usefulness when testing a single amplifier. Overloading tends to occur before third-order products can be separated out, and, even if this is not the case, there is no known method of separating group 3/1 from groups 3/2 and 3/3 products.

(6) TOTAL POWER LAW

Starting from the characteristic equation (12), a much used law—the total power law—has been demonstrated[2] for the special case where in-band feedback, anode load and output network response are all constant. It states that the total rth-order output power at frequencies both inside and outside the transmission band is proportional to the total fundamental output power raised to the power r, irrespective of the frequency characteristics of the fundamental output power.

In the general case considered here, this law no longer applies

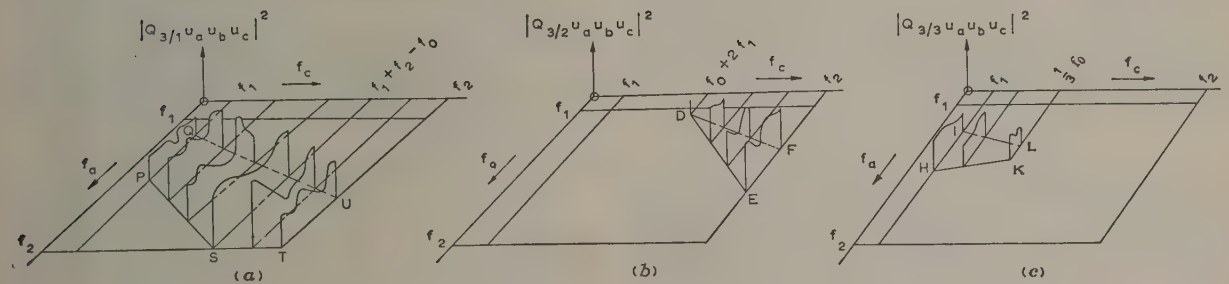

Fig. 10.—Three-dimensional model of Fig. 9.

(a) Group 3/1: $f_a + f_b - f_c - f_0 = 0$.

Point	Co-ordinate f_a	Co-ordinate f_c	f_b
Q	$\frac{1}{2}(f_0+f_1)$	f_1	$\frac{1}{2}(f_0+f_1)$
P	f_0	f_1	f_1
S	f_2	$f_1+f_2-f_0$	f_1
T	f_2	f_2	f_0
U	$\frac{1}{2}(f_0+f_2)$	f_2	$\frac{1}{2}(f_0+f_2)$

(b) Group 3/2: $f_a + f_b - f_c + f_0 = 0$.

Point	Co-ordinate f_a	Co-ordinate f_c	f_b
D	f_1	f_0+2f_1	f_1
E	$f_2-f_0-f_1$	f_2	f_1
F	$\frac{1}{2}(f_2-f_0)$	f_2	$\frac{1}{2}(f_2-f_0)$

(c) Group 3/3: $f_a + f_b + f_c - f_0 = 0$.

Point	Co-ordinate f_a	Co-ordinate f_c	f_b
H	f_0-2f_1	f_1	f_1
I	$\frac{1}{2}(f_0-f_1)$	f_1	$\frac{1}{2}(f_0-f_1)$
K	$\frac{1}{3}(2f_0-3f_1)$	$\frac{1}{3}f_0$	f_1
L	$\frac{1}{3}f_0$	$\frac{1}{3}f_0$	$\frac{1}{3}f_0$

when referred to output power. By arguments identical with those of Reference 2 the following general law is derived:

$$\sum_{f=0}^{\infty} (I_r F_r)^2 = k_r \left(\sum_{\lambda=1}^{m} V_\lambda^2 \right)^r \quad . \quad . \quad . \quad . \quad (30)$$

where V_λ = Fundamental grid-cathode test voltage of an in-band channel.
k_r = Constant.
F_r = Effective return difference on the grid at the frequency of I_r.
I_r = rth-order anode current of frequency f with feedback applied.

Again this summation is independent of the frequency characteristic of V. Of course, $\sum_{\lambda=1}^{m} (V_\lambda^2)$ is the mean-square of the complex fundamental grid-cathode voltage.

The modified total power law of eqn. (30) is useful in system planning.

It is possible to derive the system design formula (24) for the general case from the total power law, but difficulties arise when trying to specify a reference level for t_r [eqn. (20)].

(7) POWER-HANDLING CAPACITY

The amplifier must be able to handle without overloading an output power corresponding to a sinusoidal grid-cathode voltage V_{max}(r.m.s.) given by

$$V_{max}^2 = mp_0 M (V^2)_{av} \quad . \quad . \quad . \quad . \quad . \quad (31)$$

Here, M is the multi-channel peak factor, defined in Reference 1, and $(V^2)_{av}$ is the mean-square grid test voltage. From eqn. (19),

$$(V^2)_{av} = \left(\frac{u^2}{u_d^2} \right)_{av} (V_d)^2 \quad . \quad . \quad . \quad . \quad (32)$$

Eqn. (31) applies to systems of 60 or more channels where the nominal equivalent grid power varies smoothly over the transmission band by not more than 10 dB. This overall excursion can be increased as the number of channels increases. Eqn. (31) may or may not apply to other systems.

(8) CONCLUSIONS

The theory and methods described give an accurate description of practical multi-channel a.m. repeatered coaxial-cable systems carrying speech. At each stage in the development of a system, they provide as accurate an estimate of the intermodulation noise in each channel as the practical available information warrants.

Examples have been worked in order to obtain a measure of the sensitivity of the total noise to changes in the many parameters. While, of course, each design must be treated on its own, the following rules of thumb have emerged. The in-band frequency characteristics of both feedback and output network response can be left largely to the amplifier designer's convenience, provided that they approach the practical maximum efficiency. Pre-emphasis can usually be applied to compensate for both. It is usually easier to choose a pre-emphasis characteristic to suit a given amplifier than to make an amplifier suit a preconceived pre-emphasis characteristic. Once it has been chosen, the total noise is not significantly affected by deviations of ± 2 dB or so. Pre-emphasis can only redistribute the total thermal and intermodulation noise powers to give a rather indeterminate optimum. If in a first theoretical design run, after flat level adjustment, the mean total noise power over the transmission band exceeds the specification value, neither changes in the achievable feedback nor the pre-emphasis characteristics will usually bring it into specification all over the band.

(9) ACKNOWLEDGMENTS

The authors wish to express their thanks to the Director of Research of British Telecommunications Research Ltd. for permission to publish the paper, to many of the firm's staff for their help, to the L.M. Branch of the General Post Office for the loan and operation in the field of a noise loading set, and to Mr. D. Turner of the Post Office Research Station for the information of eqns. (21) and (22).

(10) REFERENCES

(1) Holbrook, B. D., and Dixon, J. T.: 'Load Rating Theory for Multi-Channel Amplifiers', *Bell System Technical Journal*, 1939, **18**, p. 624.
(2) Brockbank, R. A., and Wass, C. A. A.: 'Non-Linear Distortion in Transmission Systems', *Journal I.E.E.*, 1945, **92**, Part III, p. 45.
(3) Bennett, W. R.: 'Cross Modulation in Multi-Channel Systems below Overload', *Bell System Technical Journal*, 1940, **19**, p. 587.
(4) Jacobsen, B. B.: 'The Effect of Non-Linear Distortion in Multi-Channel Amplifiers', *Electrical Communication*, 1940, **19**, p. 29.
(5) Thomson, W. E.: 'The Response of a Non-Linear System to Random Noise', *Proceedings I.E.E.*, Monograph No. 106 R, September, 1954 (**102** C, p. 46).
(6) Bode, H. W.: 'Network Analysis and Feedback Amplifier Design' (Van Nostrand, 1945), p. 308.
(7) Lord Rayleigh: 'Theory of Sound' (Macmillan, 1894), Vol. 1, Paragraph 42a.
(8) Duerdoth, W. T.: 'The Design of Amplifiers for the Birmingham–Manchester Coaxial Cable', *Proceedings I.E.E.*, Paper No. 1288 R, April, 1952 (**99**, Part IIIA, p. 385).
(9) Ketchledge, R. W.: 'Distortion in Feedback Amplifiers', *Bell System Technical Journal*, 1955, **34**, p. 1265.
(10) International Telegraph and Telephone Consultative Committee, Geneva, December, 1958, Study Group 1, Question 32.
(11) Jones, D. H.: 'Intermodulation Distortion in an Experimental Group Amplifier using Transistors', *Proceedings I.E.E.*, Paper No. 2878 E, May, 1959 (**106** B, Suppl. 15, p. 472).
(12) Golding, J. F.: 'The White-Noise Method of Measuring Crosstalk and Noise Interference in Multi-Channel Telephone Link Systems', *Electronic Engineering*, 1958, **30**, p. 349.
(13) White, R. W., and Whyte, J. S.: 'Equipment for Measurement of Inter-Channel Crosstalk and Noise on Broadband Multi-Channel Telephone Systems', *Post Office Electrical Engineers' Journal*, 1958, **48**, p. 127.

(11) APPENDICES

(11.1) Measurement of the Transmission and Difference Phase Functions

The transmission phase of a typical repeater section changes by 2π some hundreds of times over the transmission frequency band. Looping back after the first repeater, or in experimental installations using one normal section-length loop, puts the transmit and receive terminals a few feet apart. If an output signal is compared with the input signal, a cancellation will

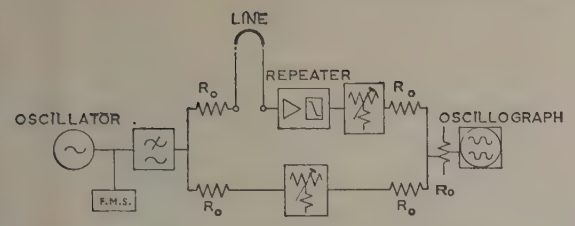

Fig. 11.—Circuit for the measurement of transmission phase.

occur at all frequencies corresponding to a transmission phase of $(2n - 1)\pi$, provided that the loop is equalized.

Fig. 11 shows the schematic of the experimental layout. The first balance point slightly below the transmit band is found and its frequency monitored accurately. Balance frequencies are obtained at intervals of 2π. A straight-line fit of the measured phase/frequency characteristic is estimated. At each of the balance frequencies the difference in phase shift between the straight line value and the measured value is calculated, giving a first difference phase $\phi'(f)$, with a total range of less than π. This can now be plotted, and a straight line can be fitted by eye, the difference being the required difference phase function $\phi(f)$.

This method, given correct earthing arrangements, showed up spurious resonances of 3°–4° very clearly at a total transmission phase angle of some 50000°. By using the low-pass filters, balance points were readily repeated by different operators to ±8 c/s at 4 Mc/s.

(11.2) Detailed System Design Example

System Specification.

Transmission band: $f_1 = 0{\cdot}2$ Mc/s; $f_2 = 6$ Mc/s.
Number of channels: $m = 1450$.
Channel bandwidth: $b = 4$ kc/s.
Number of regulated r.f. links: $c = 9$.
Number of repeaters: $n = 252$.
Number of repeaters per regulated r.f. link: $n/c = 28$.
Difference phase function: ϕ = constant = 164°.
Psophometric weighting factor: $k = 0{\cdot}4$, or −4 dB.
Speech coefficient: $p_0 = 0{\cdot}03$, or −15 dB.
Multi-channel peak factor: $M = 20$, or +13 dB.

Pentode-Type Output Valve Characteristics.

Slope: $g_1 = 15$ mA/volt.
At 1 volt (r.m.s.) grid voltage:
2nd harmonic margin: $10 \log_{10} t_{2\,(V=1\,\text{volt})} = -13$ dB; deviation, $\sigma_2 = \sqrt{0{\cdot}2}$.
3rd harmonic margin: $10 \log_{10} t_{3\,(V=1\,\text{volt})} = -24$ dB.

Amplifier Characteristic (see Table 2).

Bode-type output network (Fig. 12): anode load at 200 kc/s: $R_0 = 300$ ohms.

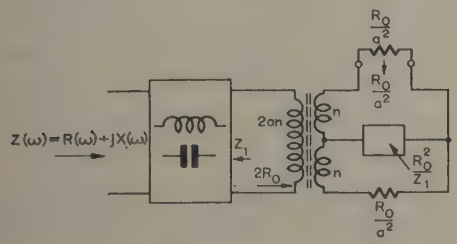

Fig. 12.—Bode network.

Table 2

Amplifier Characteristics

Frequency f	Insertion gain of output network α_i	Effective feedback 2nd-order F_2^2	Effective feedback 3rd-order F_3^2	Provisional transmit level S_1	Normalized frequency $(f - f_1)/(f_2 - f_1) = \rho$
Mc/s	dB	dB	dB	dBr	
0·2	0	44	34	−25	0
1·2	0	42	32	−23·3	0·17
2·1	0·2	37	27	−21·5	0·33
4	2	32	22	−16·3	0·67
5	4	29	19	−12·7	0·83
6	6	28	18	−7	1

The problem is to find the total intermodulation noise in the above channels at a 0 dBm0 audio point at the end of the system, adjusting the transmission levels, if necessary, for a better noise distribution, and to find the required overload point.

Step 1.—Fix a reference channel. The lowest frequency at $\rho_1 = 0$ will be taken as the reference channel.

Step 2.—Find the harmonic margins t_2 and t_3 at the reference channel $\rho_d = 0$ and reference voltage V_d.

In a Bode network, half the available output power flows into the load.

Fundamental power output for 1-volt grid voltage
$= \frac{1}{2}g_1^2 R_0$ milliwatts.
$= 34$ mW or +15·3 dBm.

Nominal output power S_1 for V_d grid voltage
$= -25$ dBm.

Ratio of these powers $= 40{\cdot}3$ dB.

From eqn. (20) and the above,

$10 \log_{10} t_2 = 10 \log_{10} t_{2\,(V=1\,\text{volt})} - 40{\cdot}3 = -53{\cdot}3$ dB.

$10 \log_{10} t_3 = 10 \log_{10} t_{3\,(V=1\,\text{volt})} - 2 \times 40{\cdot}3 = -104{\cdot}6$ dB.

Step 3.—Find u_ρ^2, the squared normalized grid-voltage characteristics. The reference channel is given by $\rho_d = 0$; at this frequency $u_d^2 = 1$, by definition, corresponding to an output level of $S_1 = -25$ dBr and a network insertion gain of $\alpha_i = 0$ dB; at any other frequency, therefore,

$$10 \log_{10} u_\rho^2 = S_1 + 25 - \alpha_i \text{ decibels.}$$

This is shown in Table 3.

Table 3

ρ	$10 \log_{10} u_\rho^2$
	dB
0	0
0·17	1·7
0·33	3·3
0·67	6·7
0·83	8·3
1	10

Step 4.—Find the distribution functions z_2 and $z_{3/1}$.

Since ϕ_ρ is constant and nearly 180°, the line transmission function Q_r^2 is constant and can be taken through the summation sign of eqn. (23). In this example, the variation of the u_ρ^2/frequency characteristic with frequency, ρ, is linear. Although the system has band-pass characteristics, little error is introduced

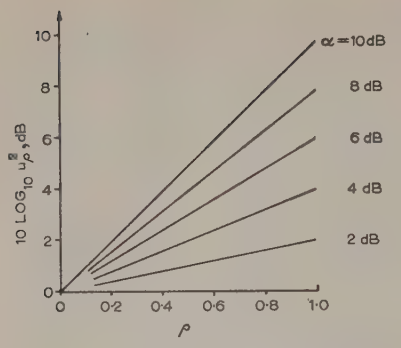

Fig. 13.—Grid loading function $u_\rho^2 = 10^{0 \cdot 1 \alpha \rho}$.
Reference point: $u_d = 1$ at $\rho = 0$.

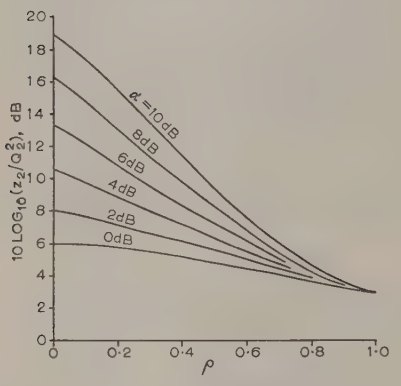

Fig. 14.—Distribution function z_2/Q_2^2 of Fig. 13.

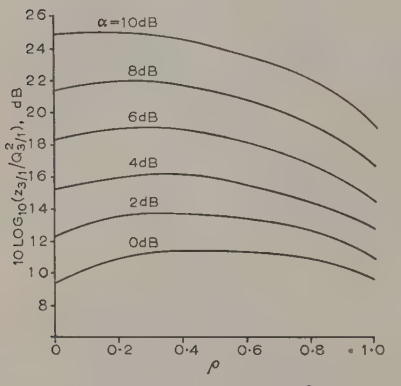

Fig. 15.—Distribution function $z_{3/1}/Q_{3/1}^2$ of Fig. 13.

by using the low-pass templates of Figs. 13–15. They too have been drawn relative to a reference level $\rho = 0$ so that no level correction is necessary (Table 4).

If templates for this u_ρ^2 characteristic are not available, the distribution functions z_2 and $z_{3/1}$ must now be obtained (see Sections 11.3 and 11.4).

Step 5.—Find the total second-order noise, P_2. For all second-order terms $\nu = \pm 164°$. From eqns. (11) and (24),

$$Q_2^2 = n\sigma_2^2 \quad . \quad . \quad . \quad . \quad . \quad . \quad . \quad (33)$$

Table 4

ρ	$10 \log_{10} \frac{z_2}{Q_2^2}$	$10 \log_{10} \frac{z_{3/1}}{Q_{3/1}^2}$
0	18·8	24·8
0·17	16·0	25·0
0·33	12·8	24·7
0·67	6·5	23·0
0·83	4·3	21·7
1	3·0	19·0

$$10 \log_{10} P_2 = 10 \log_{10} \frac{t_2 k p_0^2 m n \sigma_2^2 z_2}{F_2^2 Q_2^2}$$

$$= -38 \cdot 5 + 10 \log_{10} \frac{z_2}{Q_2^2 F_2^2} \text{dBm0} \quad (34)$$

Step 6.—Find the total group 3/1 noise, $P_{3/1}$.

For all group 3/1 products, $\nu = 0$. From eqns. (10) and (24),

$$Q_{3/1}^2 = \frac{(1 \cdot 25n)^2}{c} \quad . \quad . \quad . \quad . \quad . \quad (35)$$

$$10 \log_{10} P_{3/1} = 10 \log_{10} \frac{t_3 k p_0^3 m^2 (1 \cdot 25)^2 n^2 z_{3/1}}{c F_3^2 Q_{3/1}^2}$$

$$= -49 \cdot 5 + 10 \log_{10} \frac{z_{3/1}}{Q_{3/1}^2 F_3^2} \text{dBm0} \quad . \quad (36)$$

Step 7.—Find any other intermodulation noise. None was thought to be significant.

Step 8.—Find the thermal noise, P_a, per channel at the 0 dBm0 point.

Formulae for doing so are well known and need not be reproduced here. In this case, a knowledge of the arrival levels at the input of the amplifier panel and the characteristics of the input valve, etc., is required. Feedback has no effect. For this example we assume that P_a, the psophometrically weighted thermal noise power per channel at the 0 dBm0 output audio point, is as given in Table 5.

Table 5

f	P_2	$P_{3/1}$	P_a
Mc/s	dBm0	dBm0	dBm0
0·2	−63·7	−58·7	−74
1·2	−64·5	−56·5	−70
2·1	−62·7	−51·8	−64
4	−64·0	−48·5	−62
5	−63·2	−46·8	−62
6	−63·5	−48·5	−63

Step 9.—Find the total noise, P, per channel.

The noise powers being unrelated, add like powers. Thus the total noise per channel is given by

$$10 \log_{10} P = 10 \log_{10} (P_a + P_2 + P_{3/1} + \ldots) \text{dBm0} \quad (37)$$

Step 10.—Level adjustment.

It is required, say, to keep P below −51 dBm0. In this example, third-order noise predominates. Lowering all transmit levels by 4 dB, i.e. at an output level of $S_2 = (S_1 - 4)$ dBr, Table 6 is obtained.

Table 6

f	P_a	P_2	$P_{3\,1}$	P	S_2
Mc/s	dBm0	dBm0	dBm0	dBm0	dBr
0·2	−70	−67·7	−66·7	−63·4	−29
1·2	−66	−68·5	−64·5	−61·5	−27·3
2·1	−60	−66·7	−59·8	−56·3	−25·5
4	−58	−68·0	−56·5	−54·0	−20·3
5	−58	−67·2	−54·8	−52·3	−16·7
6	−59	−67·5	−56·5	−54·2	−11·0

It is seen that P is below the required level everywhere in the band. There is no appreciable total noise change between transmit levels S_2 and $(S_2 - 5)$ dBr in any channel, P_a predominating over $P_{3/1}$ as the transmit level is lowered. This is quite a typical result.

Step 11.—Overload point.

By simple integration of the u_ρ^2 characteristic it is found that its average value is given by $10\log_{10}(u^2/u_d^2)_{av} = +5{\cdot}9$ dB above the reference point at frequency $\rho = 0$.

The amplifier must be able to handle the grid voltage V_{max}. From eqns. (31) and (32),

$$V_{max}^2 = mp_0 M\left(\frac{u^2}{u_d^2}\right)_{av} V_d^2 \quad . \quad . \quad . \quad . \quad (38)$$

From Step 3, at $f_d = 200$ kc/s the value $u_d^2 = 1$ corresponds to an output level $S_{1f_d} = -25$ dBr. After the level adjustment of Step 10, it corresponds to an output level of $S_{2f_d} = -29$ dBr. The overload point at 200 kc/s, therefore, corresponds to an output level of $10\log_{10}[mp_0 M(u^2/u_d^2)_{av}] + S_{2f_d}$ decibels relative to 1 mW. At all other frequencies, the minimum overload point α_c at the output of the repeater is, therefore, given by (Table 7)

Table 7

f	α_c
Mc/s	dBm
0·2	6·7
1·2	6·7
2·1	6·9
4	8·7
5	10·7
6	14·7

$$\alpha_c = 10\log_{10}\left[mp_0\left(\frac{u^2}{u_d^2}\right)_{av} M\right] + S_{2f_d} + \alpha_i$$
$$= +6{\cdot}7 + \alpha_i \text{ decibels relative to 1 mW} \quad . \quad (39)$$

(11.3) Calculation of Distribution Functions z_r by Analytical Integration

(11.3.1) Second-Order Products.

For a given f_0, if $f_a = x$, $f_b = (f_0 - x)$ or $(x - f_0)$ for an $(f_a + f_b - f_0 = 0)$ or an $(f_a - f_b - f_0 = 0)$ product, respectively. The limits of f_a can be read off Fig. 8. From eqn. (28),

$$z_2 = \frac{4b \times \text{area under the curve of Fig. 8}}{u_{f_0}^2(f_2 - f_1)}$$
$$= \frac{4b}{u_{f_0}^2(f_2 - f_1)}\left(\int_{f_0/2}^{f_0 - f_1} u_x^2 u_{f_0 - x}^2 Q_{x,\,f_0 - x,\,-f_0}^2\,dx + \int_{f_0 + f_1}^{f_2} u_x^2 u_{x - f_0}^2 Q_{x,\,x - f_0,\,-f_0}^2\,dx\right) \quad . \quad . \quad . \quad . \quad . \quad (40)$$
$$0 \leqslant f_1 \leqslant f_0,\ x \leqslant f_2$$

Each integral must be taken as zero if its lower limit exceeds its upper.

(11.3.2) Group 3/1 Products.

If $f_c = x$ and $f_a = y$, f_b takes a value $w = x + f_0 - y$. The limits on f_a and f_c can be read off Fig. 10(*a*). For a given f_0, from eqn. (29),

$$z_{3/1} = \frac{36b^2 \times \text{volume } V \text{ of Fig. 10(}a\text{)}}{u_{f_0}^2(f_2 - f_1)^2}$$

where
$$V = \int_{x_2}^{x_1}\int_{y_2}^{y_1} \lambda\,dy\,dx + \int_{x_4}^{x_3}\int_{y_4}^{y_3} \lambda\,dy\,dx \quad . \quad . \quad . \quad (41)$$

$$\lambda = u_y^2 u_{x+f_0-y}^2 u_x^2 Q_{y,\,x+f_0-y,\,-x,\,-f_0}^2 \quad . \quad . \quad (42)$$

$$x_1 = f_1 + f_2 - f_0 \qquad y_1 = x + f_0 - f_1$$
$$x_2 = f_1 \qquad y_2 = \tfrac{1}{2}(x + f_0)$$
$$x_3 = f_2 \qquad y_3 = f_2$$
$$x_4 = f_1 + f_2 - f_0 \qquad y_4 = \tfrac{1}{2}(x + f_0)$$

and
$$0 \leqslant f_1 \leqslant f_0,\ x,\ y \leqslant f_2$$

(11.3.3) Example.

A low-pass system of normalized passband frequencies $\rho_1 = 0$ and $\rho_2 = 1$ has a constant difference phase $\phi(\rho)$. The normalized grid voltage u_ρ is given by

$$u_\rho^2 = \varepsilon^{2A\rho} = 10^{0{\cdot}1\alpha\rho} \quad . \quad . \quad . \quad . \quad . \quad (43)$$

i.e. the plot of $10\log_{10} u_\rho^2$ against linear frequency, ρ, is a straight line with a total rise of α decibels or A nepers over the band (Fig. 13).

Find expressions for z_2 and $z_{3/1}$ for a disturbed channel, ρ, where $0 \leqslant \rho \leqslant 1$. The reference level is $u_d^2 = 1$ at $\rho = 0$. Since $\phi(\rho)$ is constant for all frequencies, Q^2 can be taken outside the integration signs.

From eqn. (40),

$$\frac{u_\rho^2(\rho_2 - \rho_1)}{4Q_2^2} z_2 = \int_{\frac{1}{2}\rho}^{\rho} \varepsilon^{2Ax}\varepsilon^{2A(\rho - x)}dx + \int_{\rho}^{1} \varepsilon^{2Ax}\varepsilon^{2A(x-\rho)}dx$$
$$\frac{z_2}{Q_2^2} = 2\rho + \frac{1}{A}[\varepsilon^{4A(1-\rho)} - 1] \quad . \quad . \quad . \quad . \quad (44)$$

When $A = 0$

$$\frac{z_2}{Q_2^2} = 4\left(1 - \frac{\rho}{2}\right) \quad . \quad . \quad . \quad . \quad . \quad (45)$$

Eqn. (44) is plotted in Fig. 14.

Finding $z_{3/1}$.

From eqns. (41) and (42),

$$\frac{u_\rho^2(\rho_2 - \rho_1)^2 z_{3/1}}{36Q_{3/1}^2} = \int_0^{1-\rho}\int_{(x+\rho)/2}^{x+\rho} \lambda\,dy\,dx + \int_{1-\rho}^{1}\int_{(x+\rho)/2}^{1} \lambda\,dy\,dx$$

where $\lambda = \varepsilon^{2Ay}\varepsilon^{2A(x+\rho-y)}\varepsilon^{2Ax}$
$= \varepsilon^{2A(\rho+2x)}$

Solving

$$\frac{z_{3/1}(\rho)}{Q_{3/1}^2} = \frac{9}{8A^2}[1 - 4A\rho + (4A - 4A\rho + 1)\varepsilon^{4A} - 2\varepsilon^{4A(1-\rho)}] \quad . \quad . \quad . \quad . \quad (46)$$

When $A = 0$, $$\frac{z_{3/1}(\rho)}{Q^2_{3/1}} = 9[1 + 2\rho(1 - \rho)] \quad . \quad . \quad . \quad . \quad (47)$$

Eqn. (46) is plotted in Fig. 15.

(11.4) Finding Distribution Functions by Graphical Integration

The method of finding the distribution functions by graphical integration will be illustrated by an example.

Given that a system of normalized band frequencies $x = f/f_2$ has:
transmit band: $x_2 = 1$, $x_1 = 0{\cdot}1$
phase characteristic: $\phi_{(x)} = 160°$
squared normalized grid-voltage characteristic u_x^2:

$$0{\cdot}1 \leqslant x \leqslant 0{\cdot}5\text{: } 10 \log_{10} u_x^2 = 0 \text{ decibels} \quad . \quad . \quad . \quad . \quad (48)$$

$$0{\cdot}5 \leqslant x \leqslant 1\text{: } 10 \log_{10} u_x^2 = 20\,(x - 0{\cdot}5) \text{ decibels} \quad . \quad (49)$$

Find z_2 and $z_{3/1}$ at $x = 0{\cdot}8$.

Since ϕ_x is constant, Q_2^2 and $Q_{3/1}^2$ can be taken outside the integration signs. The reference level is $u_1^2 = 1$ at $x = 0{\cdot}1$.

Finding z_2.

Table 8 is derived from Fig. 8 and eqns. (48) and (49).

Table 8

x_0	Frequency		Level			
	x_a	x_b	$10 \log_{10} u_a^2$	$10 \log_{10} u_b^2$	$20 \log_{10} u_a u_b$	$(u_a u_b)^2$
0·8	0·4	0·4	0	0	0	1
	0·5	0·3	0	0	0	1
	0·6	0·2	+2	0	+2	1·58
	0·7	0·1	+4	0	+4	2·5
	0·9	0·1	+8	0	+8	6·3
	1·0	0·2	+10	0	+10	10

Graphical integration of $(u_a u_b)^2$ over the x_a range from 0·4 to 0·7 and 0·9 to 1·0 gives an area of 1·2 scaled units. From eqn. (28),

$$\frac{z_2}{Q_2^2} = \frac{4 \times 1{\cdot}2}{(x_2 - x_1)u^2_{(0{\cdot}8)}} = \frac{4 \times 1{\cdot}2}{0{\cdot}9 \times 4} = 1{\cdot}3$$

Finding $z_{3/1}$.

Choosing 4 values of x_c, the ranges of x_a are given in Table 9.

Table 9

x_0	x_c	$x_{a\,max}$	$x_{a\,min}$
0·8	0·5	1·0	0·65
	0·8	1·0	0·8
	0·9	1·0	0·85
	1·0	1·0	0·9

As long as the integration is performed over these ranges, the test frequencies need not include the limiting values of x_a.

Table 10

Frequency			Level				
x_c	x_a	x_b	u_c^2	u_a^2	u_b^2	$(u_a u_b u_c)^2$	
			dB	dB	dB	dB	Ratio
0·5	0·7	0·6	0	4	2	+6	4
	0·9	0·4	0	8	0	+8	6·3
	1·0	0·3	0	10	0	+10	10
0·8	0·8	0·8	6	6	6	+18	63
	0·9	0·7	6	8	4	+18	63
	1·0	0·6	6	10	2	+18	63
0·9	0·9	0·8	8	8	6	+22	160
	1·0	0·7	8	10	4	+22	160
1·0	0·9	0·9	10	8	8	+26	400
	1·0	0·8	10	10	6	+26	400

It is obvious from Table 10 that values for x_c below 0·5 are negligible. By graphical integration over the base of Fig. 10(*a*), the volume is 7·2 scaled units. Hence, from eqn. (29),

$$\frac{z_{3/1}}{Q^2_{3/1}} = \frac{36 \times \text{volume}}{(x_2 - x_1)^2 u^2_{(0{\cdot}8)}} = \frac{36 \times 7{\cdot}2}{(0{\cdot}9)^2 \times 4} = 80$$

(11.5) Effects of Non-Linear Difference Phase Functions

In most practical coaxial systems the difference phase ϕ can be made to lie within the range $180° \pm 40°$ over the transmission band. In these cases negligible errors in the total group 2 and group 3 noise powers are introduced by taking $\phi = 180°$.

In the general case, however, every factor $(u_a u_b)^2$ or $(u_a u_b u_c)^2$, etc., in a summation must be weighted by its relevant Q^2 function, found from eqns. (4), (8), (9), (10) and (11), before the final summation is undertaken.

621.313.1.017.31 : 621.3.013.23

The Institution of Electrical Engineers
Monograph No. 385 U
June 1960
©

EQUIVALENT CIRCUIT AND EVALUATION OF EDDY-CURRENT LOSS IN SOLID CORES SUBJECTED TO ALTERNATING AND ROTATING MAGNETIC FIELDS

By Prof. N. KESAVAMURTHY, M.A., B.E., M.Sc.(Tech.), Graduate, and P. K. RAJAGOPALAN, B.E., M.S., Ph.D.

(*The paper was first received* 28*th October*, 1959, *and in revised form* 11*th March*, 1960. *It was published as an* INSTITUTION MONOGRAPH *in June*, 1960.)

SUMMARY

In the study of eddy-current distribution in solid cores subjected to a pulsating or rotating magnetic field a general 2-dimensional current distribution exists and is created by a magnetizing winding that restricts the current flow through it in only one direction. Under such situations, the method of evaluation of the equivalent impedance of the system as a whole is difficult to visualize and has not so far been attempted in the literature. Such an evaluation calls for a concept of the power factor of the magnetizing winding. This is the special feature of the paper.

The paper further examines the usefulness of this concept for the evaluation of eddy-current loss in solid cores and thus offers an alternative method.

To give more validity to several of the formulae deduced in the paper, the analysis is applied to compute the performance characteristics of a solid-rotor induction machine and certain conclusions are drawn.

(1) LIST OF PRINCIPAL SYMBOLS

The rationalized M.K.S. system of units is used throughout the paper.

B_x, B_y, B_z = x-, y- and z-components of the magnetic flux density at the point (x, y, z), Wb/m^2.
$\hat{B}_x, \hat{B}_y, \hat{B}_z$ = Amplitudes of the components of the magnetic flux density, Wb/m^2.
E_x, E_y, E_z = x-, y- and z-components of the electrical intensity at the point (x, y, z), V/m.
$\hat{E}_x, \hat{E}_y, \hat{E}_z$ = Amplitudes of the components of electrical intensity, V/m.
H_x, H_y, H_z = x-, y- and z-components of the magnetizing force, AT/m.
$\hat{H}_x, \hat{H}_y, \hat{H}_z$ = Amplitudes of the components of magnetizing force, AT/m.
J_x, J_y, J_z = x-, y- and z-components of the current density, amp/m^2.
$\hat{J}_x, \hat{J}_y, \hat{J}_z$ = Amplitudes of the components of current density, amp/m^2.
$\omega = 2\pi f$ = Angular frequency, rad/s.
ρ = Resistivity, ohm-m.
μ_0 = Permeability of free space.
μ = Permeability of the iron core, H/m.
τ = Pole pitch.
s = Fractional slip, ω/ω_0.

(2) INTRODUCTION

In the study of the eddy-current distribution in solid cores subjected to a pulsating or rotating magnetic field, the following cases are of special importance:

(*a*) An infinite half-space of solid iron subjected to a pulsating magnetic field in one direction.
(*b*) A toroid of solid iron of circular section subjected to a pulsating field.
(*c*) A solid-iron core of infinite width subjected to a travelling wave on its surface.
(*d*) A solid-iron core of finite width subjected to a travelling field on its surface.
(*e*) Case (*c*) subjected to a pulsating field.
(*f*) Case (*d*) subjected to a pulsating field.

For all these cases a magnetizing winding is necessary. Consequently, we must obtain relationships between the e.m.f. induced in the winding and the current through it. The problem is thus one of determining the equivalent circuit of the system as a whole in terms of impedance and power factor.

For each of the cases, the field distribution inside the core is created by a magnetizing winding that restricts the current through it in only one direction. For cases (*a*) and (*b*) the directions of the eddy currents are all parallel to the current in the magnetizing winding, although they have an attenuation and a phase shift in the direction normal to the winding. It is still possible to determine[1, 2] the relative phase shift between an 'equivalent current' in the exciting winding and the e.m.f. induced in it. For the other cases, the unidirectional current in the exciting winding creates a 2-dimensional current-density distribution in planes parallel to the plane of the magnetizing winding. The method of evaluating the equivalent impedance of the system as a whole is then difficult to visualize and has not so far been attempted. It calls for the concept of a power factor of the magnetizing winding. This is the special feature of the paper.

The paper further examines the usefulness of this concept for the evaluation of eddy-current loss in solid cores and thus offers an alternative method.

Lastly, in order to give more validity to several of the formulae deduced in the paper, the analysis is applied to compute the performance characteristics of a solid-rotor induction machine assuming linear range of operation.

The analysis is based on the assumption of constant permeability of the core.

(3) FIELD EQUATIONS

Consider the co-ordinate system in which the surface of the iron is in the xy-plane, the z-direction extending into the material normal to the surface. Without loss of generality the magnetizing winding is assumed to be uniformly distributed on the surface. The current through the winding is confined to directions parallel to the x-axis, inducing a pulsating or travelling magnetic field in the y-direction.

The equations that govern the magnetizing force $\boldsymbol{H}$, the flux density $\boldsymbol{B}$ and the current density $\boldsymbol{J}$, at any point inside the medium (ignoring the displacement current) are the characteristic equations of Maxwell:

$$\left.\begin{aligned} \text{curl } \boldsymbol{H} &= \boldsymbol{J} \\ \text{curl } \boldsymbol{E} &= -\frac{\partial \boldsymbol{B}}{\partial t} \\ \text{div } \boldsymbol{B} &= 0 \end{aligned}\right\} \quad \ldots\ldots (1)$$

Correspondence on Monographs is invited for consideration with a view to publication.
Prof. Kesavamurthy is Professor of Electrical Engineering, and Dr. Rajagopalan is in the Electrical Engineering Dept., at the Indian Institute of Technology, Kharagpur.

The equations take this form using the system of units referred to in Section 1. Also, $\boldsymbol{E} = \rho \boldsymbol{J}$ and $\boldsymbol{B} = \mu \boldsymbol{H}$ are the equations that govern the electric and magnetic properties of the material. For the assumption of constant permeability, these equations reduce to the form

$$\text{curl curl } \boldsymbol{H} = -\frac{\mu}{\rho}\frac{\partial \boldsymbol{H}}{\partial t} \quad . \quad . \quad . \quad . \quad (2)$$

(4) FIELD DISTRIBUTION IN SOLID MAGNETIC CORES DUE TO TIME-VARYING FIELDS

The solution of the differential eqn. (2) is obtained from a knowledge of the boundary, namely the geometrical configuration, of the core and the nature of the time-varying field acting on it.

(4.1) Distribution due to a Pulsating Field on an Infinite Half-Space of Solid Iron

The half-space of solid iron extending to infinity in the x, y and z directions is subjected to a pulsating field at the surface in the y-direction having the form

$$H_{y0} = [H_y]_{z=0} = H_0 \varepsilon^{j\omega t}$$

Obviously $H_x = H_z = 0$, and H_y alone exists and is independent of x and y. Hence, from eqn. (2),

$$\frac{d^2 H_y}{dz^2} = j\left(\frac{\omega\mu}{\rho}\right) H_y \quad . \quad . \quad . \quad . \quad . \quad (3)$$

leading to the solution:

$$\left.\begin{aligned} & H_x = H_z = 0 \\ & H_y = H_0 \exp(j\omega t - \lambda' z) \\ \text{and} \quad & J_x = \lambda' H_0 \exp(j\omega t - \lambda' z) \\ & J_y = J_z = 0 \\ \text{where} \quad & \lambda'^2 = j\frac{\omega\mu}{\rho} \end{aligned}\right\} \quad . \quad . \quad . \quad . \quad (4)$$

(4.2) Field Distribution in an Infinitely-Long Solid Cylindrical Core of Circular Section subjected to a Pulsating Field

Choosing the cylindrical co-ordinate system (r, θ, z) with z-axis coaxial with that of the cylinder and making use of the symmetry of the system, it is seen that H_z alone exists and is independent of θ and z. Using eqn. (2), we finally have

$$\frac{1}{r}\frac{d}{dr}\left(r\frac{dH_z}{dr}\right) = j\left(\frac{\omega\mu}{\rho}\right) H_z$$

This leads to the distribution:

$$\left.\begin{aligned} & H_r = H_\theta = 0 \\ & H_z = cJ_0[j(\sqrt{j})\beta r]\varepsilon^{j\omega t} \\ \text{and} \quad & J_r = J_z = 0 \\ & J_\theta = j(\sqrt{j})\beta c J_0'[j(\sqrt{j})\beta r]\varepsilon^{j\omega t} \\ \text{where} \quad & \beta^2 = \frac{\omega\mu}{\rho} \end{aligned}\right\} \quad . \quad . \quad . \quad . \quad (5)$$

c = Constant determined by the magnetizing force at the surface.

(4.3) Field Distribution due to a Travelling Magnetic Field on an Infinite Half-Space of Solid Iron

Consider an infinite half-space of iron with a sinusoidally distributed magnetic field on its surface defined by:

$$H_{z0} = [H_z]_{z=0} = H_0 \exp j\left(\frac{\pi y}{\tau} - \omega t\right)$$

Clearly $H_x = 0$, and H_y and H_z alone exist and are independent of x. Hence, from eqn. (2),

$$\frac{\partial^2 H_y}{\partial y^2} + \frac{\partial^2 H_y}{\partial z^2} = -j\left(\frac{\omega\mu}{\rho}\right) H_y$$

$$\frac{\partial^2 H_z}{\partial y^2} + \frac{\partial^2 H_z}{\partial z^2} = -j\left(\frac{\omega\mu}{\rho}\right) H_z$$

Solving the above equations,

$$\left.\begin{aligned} & H_x = 0 \\ & H_y = -j\left(\frac{\tau\lambda}{\pi}\right) H_0 \exp\left[j\left(\frac{\pi y}{\tau} - \omega t\right) - \lambda z\right] \\ & H_z = H_0 \exp\left[j\left(\frac{\pi y}{\tau} - \omega t\right) - \lambda z\right] \\ \text{and} \quad & J_x = -\frac{\tau}{\pi}\frac{\omega\mu}{\rho} H_0 \exp\left[j\left(\frac{\pi y}{\tau} - \omega t\right) - \lambda z\right] \\ & J_y = J_z = 0 \\ \text{where} \quad & \lambda = \left(\frac{\pi^2}{\tau^2} - j\frac{\omega\mu}{\rho}\right)^{1/2} = \alpha - j\beta, \text{ say} \end{aligned}\right\} \quad . \quad (6)$$

One can recognize, at this stage, that the expression for J_x for this 1-dimensional case can be obtained in a more straightforward manner by using the principle that the induced e.m.f. is the rate of cutting of flux; the direction of this e.m.f. is governed by the right-hand rule, i.e. $E_x = -B_z v$. Hence, $J_x = -(v\mu/\rho)H_z$. Since $v = \omega\tau/\pi$ and substituting for H_z we are led to the same expression for J_x as in eqn. (6).

(4.4) Field Distribution due to a Travelling Magnetic Field on the Surface of a Block of Iron (see Reference 2)

Consider the block of iron extending to infinity in both y- and z-directions and bounded by the planes $x = \pm \frac{1}{2}h$. In general, the magnetic field travelling at the surface may be of the form

$$H_{z0} = [H_z]_{z=0} = \mathrm{f}(x) \exp j\left(\frac{\pi y}{\tau} - \omega t\right)$$

where $\mathrm{f}(x)$ defines the distribution along the x-direction at the surface. If H_{z0} at the surface is independent of x, then $\mathrm{f}(x)$ defines a rectangular distribution along the x-direction. Consequently, the expression for H_{z0} becomes

$$H_{z0} = \sum_{r=0}^{\infty} \frac{4}{\pi}(-1)^r \frac{1}{(2r+1)} H_0 \cos(2r+1)\frac{\pi x}{h} \exp j\left(\frac{\pi y}{\tau} - \omega t\right)$$

$$= Y \sum_{r=0}^{\infty} c_r \cos(2r+1)\frac{\pi x}{h}$$

where $Y = \exp j\left(\frac{\pi y}{\tau} - \omega t\right)$; and $c_r = \frac{4}{\pi}(-1)^r \frac{1}{(2r+1)} H_0$

For this type of field, inside the material, H_z is of the form

$$H_z = Y \sum_{r=0}^{\infty} c_r \cos(2r+1)\frac{\pi x}{h} \varepsilon^{-\lambda_r z}$$

where $\lambda_r^2 - (2r+1)^2 \frac{\pi^2}{h^2} - \frac{\pi^2}{\tau^2} = -j\frac{\omega\mu}{\rho}$

satisfying eqn. (2).

The condition $\text{div } \boldsymbol{H} = 0$ necessitates the choice of H_x and H_y in the forms:

$$H_x = Y \Sigma a_r \sin(2r+1)\frac{\pi x}{h} \varepsilon^{-\lambda_r z}$$

$$H_y = Y \Sigma b_r \cos(2r+1)\frac{\pi x}{h} \varepsilon^{-\lambda_r z}$$

satisfying the relationship

$$(2r+1)\frac{\pi}{h}a_r + j\left(\frac{\pi}{\tau}\right)b_r - \lambda_r c_r = 0$$

Knowing the constants c_r, the problem is one of determining the constants a_r and b_r. Clearly, $J_z\,(=J_{z0})$ at the surface should be zero. Furthermore, for the type of boundary condition assumed and since the medium is homogeneous and isotropic involving one mode of attenuation in the z-direction, J_z must be zero everywhere inside the medium. As a consequence,

$$-(2r+1)\frac{\pi}{h}b_r - j\left(\frac{\pi}{\tau}\right)a_r = 0$$

Solving for a_r and b_r we finally have

$$\left.\begin{aligned}
H_x &= \sum_{r=0}^{\infty} a_r \sin\left[(2r+1)\frac{\pi x}{h}\right]\exp\left[j\left(\frac{\pi y}{\tau}-\omega t\right)-\lambda_r z\right]\\
H_y &= \sum_{r=0}^{\infty} b_r \cos\left[(2r+1)\frac{\pi x}{h}\right]\exp\left[j\left(\frac{\pi y}{\tau}-\omega t\right)-\lambda_r z\right]\\
H_z &= \sum_{r=0}^{\infty} c_r \cos\left[(2r+1)\frac{\pi x}{h}\right]\exp\left[j\left(\frac{\pi y}{\tau}-\omega t\right)-\lambda_r z\right]\\
J_x &= \sum_{r=0}^{\infty} d_r \cos\left[(2r+1)\frac{\pi x}{h}\right]\exp\left[j\left(\frac{\pi y}{\tau}-\omega t\right)-\lambda_r z\right]\\
J_y &= \sum_{r=0}^{\infty} f_r \sin\left[(2r+1)\frac{\pi x}{h}\right]\exp\left[j\left(\frac{\pi y}{\tau}-\omega t\right)-\lambda_r z\right]\\
J_z &= 0
\end{aligned}\right\} \quad (7a)$$

where

$$\left.\begin{aligned}
a_r &= \frac{4}{\pi h}(-1)^r \frac{\lambda_r}{(2r+1)\left[(2r+1)^2\frac{\pi^2}{h^2}+\frac{\pi^2}{\tau^2}\right]}H_0\\
b_r &= j\frac{4}{\pi}(-1)^r\frac{\pi}{\tau}\frac{\lambda_r}{(2r+1)\left[(2r+1)^2\frac{\pi^2}{h^2}+\frac{\pi^2}{\tau^2}\right]}H_0\\
c_r &= \frac{4}{\pi}(-1)^r\frac{1}{2r+1}H_0\\
d_r &= j\frac{\pi}{\tau}c_r + \lambda_r b_r\\
&= 4\frac{\omega\mu}{\rho}(-1)^r\frac{1}{(2r+1)\left[(2r+1)^2\frac{\pi^2}{h^2}+\frac{\pi^2}{\tau^2}\right]}H_0\\
f_r &= (2r+1)\frac{\pi}{h}c_r - \lambda_r a_r\\
&= j\frac{4}{h}\frac{\omega\mu}{\rho}(-1)^r\frac{1}{\left[(2r+1)^2\frac{\pi^2}{h^2}+\frac{\pi^2}{\tau^2}\right]}H_0
\end{aligned}\right\} \quad (7b)$$

and $\lambda_r = \left[(2r+1)^2\frac{\pi^2}{h^2}+\frac{\pi^2}{\tau^2}-j\frac{\omega\mu}{\rho}\right]^{1/2}$

$= (\alpha_r - j\beta_r)$, say

(4.5) Field Distribution due to a Pulsating Field Sinusoidally Distributed in Space on a Block of Iron

Consider the block of iron referred to in Section 4.4. The pulsating magnetic field at the surface may be defined as

$$H_{z0} = [H_z]_{z=0} = \frac{4}{\pi}H_0\sum_{r=0}^{\infty}(-1)^r\frac{1}{2r+1}\cos\left[(2r+1)\frac{\pi x}{h}\right]\sin\frac{\pi y}{\tau}\varepsilon^{j\omega t}$$

Following the procedure outlined in Section 4.4 we finally have

$$\left.\begin{aligned}
H_x &= \sum_{r=0}^{\infty} a_r' \sin\left[(2r+1)\frac{\pi x}{h}\right]\sin\frac{\pi y}{\tau}\exp(j\omega t-\nu_r z)\\
H_y &= \sum_{r=0}^{\infty} b_r' \cos\left[(2r+1)\frac{\pi x}{h}\right]\cos\frac{\pi y}{\tau}\exp(j\omega t-\nu_r z)\\
H_z &= \sum_{r=0}^{\infty} c_r' \cos\left[(2r+1)\frac{\pi x}{h}\right]\sin\frac{\pi y}{\tau}\exp(j\omega t-\nu_r z)\\
J_x &= \sum_{r=0}^{\infty} d_r' \cos\left[(2r+1)\frac{\pi x}{h}\right]\cos\frac{\pi y}{\tau}\exp(j\omega t-\nu_r z)\\
J_y &= \sum_{r=0}^{\infty} f_r' \sin\left[(2r+1)\frac{\pi x}{h}\right]\cos\frac{\pi y}{\tau}\exp(j\omega t-\nu_r z)\\
J_z &= 0
\end{aligned}\right\} \quad (8a)$$

where

$$\left.\begin{aligned}
a_r' &= \frac{4}{\pi}\frac{\pi}{h}(-1)^r\frac{\nu_r}{\left[(2r+1)^2\frac{\pi^2}{h^2}+\frac{\pi^2}{\tau^2}\right]}H_0\\
b_r' &= -\frac{4}{\pi}\frac{\pi}{\tau}(-1)^r\frac{\nu_r}{(2r+1)\left[(2r+1)^2\frac{\pi^2}{h^2}+\frac{\pi^2}{\tau^2}\right]}H_0\\
c_r' &= \frac{4}{\pi}(-1)^r\frac{1}{2r+1}H_0\\
d_r' &= -j\left(\frac{4}{\pi}\right)\frac{\pi}{\tau}\frac{\omega\mu}{\rho}(-1)^r\frac{1}{(2r+1)\left[(2r+1)^2\frac{\pi^2}{h^2}+\frac{\pi^2}{\tau^2}\right]}H_0\\
f_r' &= -j\left(\frac{4}{\pi}\right)\frac{\pi}{h}\frac{\omega\mu}{\rho}(-1)^r\frac{1}{(2r+1)^2\frac{\pi^2}{h^2}+\frac{\pi^2}{\tau^2}}H_0
\end{aligned}\right\} \quad (8b)$$

and

$$\nu_r = \left[(2r+1)^2\frac{\pi^2}{h^2}+\frac{\pi^2}{\tau^2}+j\frac{\omega\mu}{\rho}\right]^{1/2}$$

Note that $\nu_r = \overline{\lambda}_r = \alpha_r + j\beta_r$ [eqn. (7b)].

(4.6) Field Distribution due to an Alternating Field Sinusoidally Distributed in Space on an Infinite Half-Space of Iron

Clearly, for this case, $H_x = 0$ everywhere and $J_y = J_z = 0$. Furthermore, H_y and H_z inside the medium are independent of x. The type of field at the surface can be defined as

$$H_{z0} = [H_z]_{z=0} = H_0 \sin\frac{\pi y}{\tau}\varepsilon^{j\omega t}$$

Hence, inside the medium, H_z is of the form:

$$H_z = H_0 \sin \frac{\pi y}{\tau} \exp [(j\omega t - \nu z)]$$

where $$\nu^2 = \frac{\pi^2}{\tau^2} + j\frac{\omega\mu}{\rho}$$

Following the steps outlined in Section 4.3, we finally have

$$\left.\begin{aligned} H_x &= 0 \\ H_y &= -\frac{\tau}{\pi}\nu H_0 \cos \frac{\pi y}{\tau} \exp (j\omega t - \nu z) \\ H_z &= H_0 \sin \frac{\pi y}{\tau} \exp (j\omega t - \nu z) \\ J_x &= -j\left(\frac{\omega\mu}{\rho}\right)\frac{\tau}{\pi} H_0 \cos \frac{\pi y}{\tau} \exp (j\omega t - \nu z) \\ J_y &= 0 \\ J_z &= 0 \end{aligned}\right\} \quad . \quad . \quad (9)$$

where

$$\nu = \left(\frac{\pi^2}{\tau^2} + j\frac{\omega\mu}{\rho}\right)^{1/2} = \bar{\lambda} \text{ [eqn. (6)]}$$

Alternatively, as in Section 4.3, for this 1-dimensional case where all the currents are axial, the expression for J_x can be obtained by making use of the principle that the induced e.m.f. is the rate of change of flux linkages; the direction of the e.m.f. being governed by Lenz's law.

Now

$$\Phi_y = -\frac{\tau}{\pi}\mu H_0 \cos \frac{\pi y}{\tau} \exp (j\omega t - \nu z)$$

Hence $$E_x = -\frac{\partial \Phi_y}{\partial t} = \rho J_x$$

Therefore $$J_x = -j\left(\frac{\omega\mu}{\rho}\right)\frac{\tau}{\pi} H_0 \cos \frac{\pi y}{\tau} \exp (j\omega t - \nu z)$$

as in eqn. (9).

(5) THE CONCEPT OF POWER FACTOR OF THE MAGNETIZING WINDING AND ITS IMPLICATIONS

Two methods of approach are possible for the evaluation of eddy-current loss in the core.

Method 1.

$$P_e = \frac{1}{T}\iiint_v \int_0^T \rho |J|^2 dv dt$$

where P_e is the average loss over one cycle of period T. The integration is over the volume v of the material. For a harmonic variation of J, the above expression simplifies to

$$P_e = \tfrac{1}{2}\iiint_v \rho(\hat{J}_x^2 + \hat{J}_y^2 + \hat{J}_z^2) dv$$

Method 2.

The energy flow in the interval of time T into the material of volume v, bounded by the surface S is, using the Poynting vector,

$$W_e = \iint_S \int_0^T [(\boldsymbol{E} \times \boldsymbol{H}) \,.\, d\boldsymbol{S}] dt$$

The average flux of energy per cycle of period T, i.e. the power loss, is

$$P_e = \frac{1}{T}\iint_S \int_0^T [(\boldsymbol{E} \times \boldsymbol{H}) \,.\, d\boldsymbol{S}] dt$$

where $\boldsymbol{E}$ and $\boldsymbol{H}$ are the vectors on the plane of the surface $d\boldsymbol{S}$. If

$$E = \hat{E}_0 \sin \omega t$$

$$H = \hat{H}_0 \sin (\omega t - \psi)$$

it follows that

$$P_e = \frac{1}{2}\iint_S \hat{E}_0 \hat{H}_0 \sin \theta \cos \psi \, dS$$

where θ = Angle between the vectors $\boldsymbol{E}$ and $\boldsymbol{H}$.
ψ = (Time) phase difference between $\boldsymbol{E}$ and $\boldsymbol{H}$.

In all the cases discussed in Section 4 the power transfer by the magnetizing winding must appear as the total loss in the core. This power is equal to the product of the voltage required to balance the induced e.m.f. in the winding, the current through the winding and the power factor of the winding. In general, the problem is one of determining the induced e.m.f. and the current in the winding.

(5.1) Concept of Power Factor for 1-Dimensional Distribution

Consider first the distribution outlined in Section 4.1 and defined by eqn. (4). The e.m.f. induced in the winding per unit length in the x-direction is the same as the electrical intensity E_{x0}, at the iron surface. Thus

$$E_{x0} = \rho J_{x0} = \lambda' \rho H_0 \varepsilon^{j\omega t}$$

Therefore $-E_{x0}$ is the voltage applied per unit length of the magnetizing winding. The current in the magnetizing winding per unit length in the y-direction is $-H_{y0}$ $(=H_0\varepsilon^{j\omega t})$. Thus the average power loss per unit surface area is

$$\begin{aligned} P_{e1} &= \tfrac{1}{2}\hat{E}_{x0}\hat{H}_{y0} \cos (E_{x0}, H_{y0}) \\ &= \tfrac{1}{2}(\rho|\lambda'|H_0)H_0 \cos \left(\frac{\pi}{4}\right) \\ &= \frac{\rho}{2\sqrt{2}}|\lambda'|H_0^2 \end{aligned} \quad . \quad . \quad . \quad . \quad . \quad . \quad (10)$$

the power factor being $\cos \pi/4$.

Consider, next, the case examined in Section 4.2. Clearly, using eqn. (5), the induced e.m.f. per unit axial length of the magnetizing winding is given by

$$(2\pi a)E_{\theta 0} = 2j\sqrt{(j)}\pi a \rho \beta c J_0 [j\sqrt{(j)}\beta a]\varepsilon^{j\omega t}$$

where a = Radius of the section.

Also,

$-H_{z0}$ = Current per unit length in the z-direction, when the magnetizing winding is replaced by an equivalent current sheet,

$$= -cJ_0[j\sqrt{(j)}\beta a]\varepsilon^{j\omega t}$$

Hence the loss per unit axial length is

$$P_{e2} = \tfrac{1}{2}(2\pi a \hat{E}_{\theta 0})\hat{H}_{z0} \cos \psi_0$$

where ψ_0 = Phase angle between $E_{\theta 0}$ and H_{z0}.
$\cos \psi_0$ = Power factor of the winding.

It is worth examining certain practical situations in which the field distributions derived in Section 4.3–4.6 may be assumed

to exist. Consider, for example, an induction machine with a solid-iron rotor. The distributed winding on the stator can be made to produce a sinusoidally distributed magnetic field rotating in space or alternating along one axis depending upon the type of connections employed. The problem of primary concern in such machines is the evaluation of rotor power factor and its impedance. Without loss of generality we can neglect the effect of air-gap. This 1 : 1 correspondence between the practical machine and the cases examined in Sections 4.3–4.6 will be helpful for the future development of the concept of the power factor of the magnetizing winding.

The case examined in Section 4.3 refers to a situation in which the rotor currents are all axial. Using eqns. (6), the induced e.m.f. per axial length of the magnetizing winding is $V_{x0} = \rho J_{x0}$. Also, $-H_{y0}$ is the current per unit length in the y-direction. From the arguments employed earlier, ψ_0, the phase angle between J_{x0} and H_{y0}, is arg $(j\lambda)$ where $\lambda = \alpha - j\beta$.

i.e. $$\cos\psi_0 = \frac{\omega\mu}{2\alpha\rho|\lambda|} \quad . \quad . \quad . \quad . \quad (11a)$$

If π/τ is small, $\cos\psi_0 \to 1/\sqrt{2}$ and corresponds to the power factor for the case dealt with in Section 4.1.

Also P_{e3} = Loss per unit surface area

$$= \tfrac{1}{2}E_{x0}H_{y0}\cos\psi_0$$

$$= \frac{1}{4\alpha}\left(\frac{\tau}{\pi}\right)^2\left(\frac{\omega\mu}{\rho}\right)^2\rho H_0^2 \quad . \quad . \quad . \quad . \quad . \quad . \quad (11b)$$

(5.2) Concept of Power Factor for a 2-Dimensional Distribution—Rotating Field

From the previous Section we have gathered enough ideas to develop the concept of the power factor of the magnetizing winding for the general case discussed in Section 4.4. In practice, this refers to the distribution in the solid rotor having finite axial length without end-rings.

(5.2.1) Evaluation of Loss.

For the field distribution defined by eqns. (7*a*) and (7*b*) the evaluation of the power loss may be based on the Poynting vector. Since E_x and H_y are each sinusoidally distributed in space along the x-axis, the loss per unit surface area is

$$P_{e4} = \tfrac{1}{4}\Sigma\,(\hat{E}_{x0r}\hat{H}_{y0r}\cos\psi_{10r} - \hat{E}_{y0r}\hat{H}_{x0r}\cos\psi_{20r})$$

where ψ_{10r} and ψ_{20r} are the phase angles between E_{x0r} and H_{y0r}, and between E_{y0r} and H_{x0r}, respectively. In other words,

$$P_{e4} = \frac{p}{4}\mathscr{R}\,\Sigma\,(d_r\bar{b}_r - f_r\bar{a}_r)$$

where the bar stands for the conjugate.

Making use of the relationships between the coefficients given in eqn. (7*b*) we have finally

$$P_{e4} = \tfrac{1}{4}\Sigma - \frac{\omega\tau}{\pi}\mu c_r\bar{b}_r \quad . \quad . \quad . \quad . \quad (12)$$

(5.2.2) Physical Interpretation of Eqn. (12).

Eqn. (12) could have been deduced from physical considerations as follows: Clearly, the current-carrying winding could be considered in terms of a current sheet on the surface of the iron, all currents being axial, i.e. along the x-direction. The e.m.f. induced in such a sheet will have only one direction and hence will be given by the product of radial flux density and the velocity of the travelling field at the surface, i.e.

$$-\left(\frac{\omega\mu\tau}{\pi}\right)H_{z0}$$

This induced e.m.f. has a sinusoidal distribution in the x-direction. Hence the average power transferred per unit surface area of the winding is

$$\tfrac{1}{4}\mathscr{R}\,\Sigma - \frac{\omega\mu\tau}{\pi}c_r\bar{b}_r$$

which is the same as in eqn. (12).

(5.2.3) Concept of Power Factor of the Magnetizing Winding.

For the case examined in Section 4.4, H_{z0} is independent of x. Therefore, the e.m.f. induced in the equivalent current sheet is also independent of x, and is given by

$$V_0 = -\frac{\omega\mu\tau}{\pi}H_{z0} \quad . \quad . \quad . \quad . \quad . \quad (13)$$

Furthermore, H_{y0} is sinusoidally distributed in the x-direction and has the significance of the current in the sheet per unit peripheral length. The average power transferred per unit surface area due to the $(2r+1)$th harmonic of this current, $-H_{y0r}$, is given by

$$\frac{1}{2h}V_0\left(\int_{-h/2}^{h/2}\hat{H}_{y0r}dx\right)\cos\psi_{0r} \quad . \quad . \quad . \quad (14)$$

where ψ_{0r} is the phase angle of $\hat{H}_{y0r}$. Hence the total loss is

$$P_{e4} = \tfrac{1}{2}\mathscr{R}\left[V_0\Sigma\frac{2}{\pi}\frac{(-1)^r}{2r+1}\bar{b}_r\right]$$

$$= \tfrac{1}{2}\mathscr{R}(V_0\dot{H}_{av}), \text{ say}$$

where $$\dot{H}_{av} = \Sigma\frac{2}{\pi}\frac{(-1)^r}{2r+1}b_r$$

$$= -\frac{8}{\pi^2}H_0\Sigma\frac{j\frac{\pi}{\tau}\lambda_r}{(2r+1)^2\left[(2r+1)^2\frac{\pi^2}{h^2}+\frac{\pi^2}{\tau^2}\right]} \quad (14)$$

One can recognize that $\dot{H}_{av}$ has the physical significance of the current in the magnetizing winding. The reasoning is as follows: The current in the sheet per unit length in the y-direction is $-H_{y0}$ and is sinusoidally distributed in the x-direction. Hence the current drawn from the source per unit length is given by

$$-\frac{1}{h}\int_{-h/2}^{h/2}\hat{H}_{y0}dx$$

which results in the same expression as in eqn. (14).

In a similar manner, for a boundary condition when H_{y0} is independent of x, it can be shown that

$$P_{e4} = -\frac{1}{2}\frac{\omega\mu\tau}{\pi}\mathscr{R}\left[H_{y0}\Sigma\frac{2}{\pi}(-1)^r\frac{1}{2r+1}c_r\right]$$

$$= \frac{1}{2}\mathscr{R}(H_0\bar{V}_{av}) \quad . \quad . \quad . \quad . \quad . \quad . \quad . \quad . \quad (15)$$

where $$\dot{V}_{av} = -\left(\frac{\omega\mu\tau}{\pi}\right)\Sigma\frac{2}{\pi}\frac{(-1)^r}{2r+1}c_r \quad . \quad . \quad . \quad . \quad (16)$$

For this case $\dot{V}_{av}$ has the physical significance of the e.m.f. induced per unit axial length of the winding. This follows from the fact that the e.m.f. induced per unit axial length is

$$-\frac{1}{h}\int_{-h/2}^{h/2}\left(\frac{\omega\tau\mu}{\pi}\right)H_{z0}dx$$

which leads to the same expression as in eqn. (16) on substitution for H_{z0}.

Eqns. (12) and (13) can be rewritten in the vector form as

$$\dot{H}_{av} = H_{av} \angle \psi_0$$

$$\dot{V}_0 = -\left(\frac{\omega\mu\tau}{\pi}\right) H_0$$

Hence $-\cos\psi_0$ is the power factor of the magnetizing winding. In a similar manner, the power factor when H_{y0} is independent of x can be evaluated using eqns. (15) and (16).

(5.2.4) Evaluation of Loss based on the Concept of Power Factor.

Let $$\lambda_r = \alpha_r - j\beta_r = |\lambda_r|\varepsilon^{-j\phi_r}, \text{ say}$$

Then $$\sin\phi_r = \frac{\beta_r}{|\lambda_r|} \text{ and } \beta_r = \frac{\omega\mu}{2\rho\alpha_r}$$

The phase angle between the individual terms of $\dot{V}_0$ and $\dot{H}_{av}$ is, $\arg(j\lambda_r) = \left(\frac{\pi}{2} - \phi_r\right)$; i.e. the rth term in the series for $\dot{H}_{av}$ [eqn. (13)] lags $\dot{V}_0$ by $\frac{\pi}{2} - \phi_r$. Therefore the power factor will be $\cos\left(\frac{\pi}{2} - \phi_r\right) = \sin\phi_r$. In order to evaluate the loss per unit surface area we use the formula

$$P_{e4} = \tfrac{1}{2} V_0 \sum_{r=0}^{\infty} |\dot{H}_{av}| \sin\phi_r \ (r\text{th term})$$

Using eqns. (14) and (7*b*), on simplification and reduction it is seen that

$$P_{e4} = \frac{\rho}{8}\left(\frac{4}{\pi}\right)^2 \left(\frac{\omega\mu}{\rho}\right)^2 H_0^2 \sum_{r=0}^{\infty} \frac{1}{\alpha_r(2r+1)^2\left[(2r+1)^2\frac{\pi^2}{h^2} + \frac{\pi^2}{\tau^2}\right]} \quad . \quad . \quad . \quad . \quad (17)$$

The same expression for loss can also be obtained by making use of the Poynting vector. Alternatively, use of eqn. (12) leads to an identical expression. The same expression has been deduced by Carter[2] using method 1, as indicated earlier.

(5.2.5) Impedance of the Exciting Winding.

The equivalent impedance per unit length in the x- and y-directions will be given by

$$\dot{Z} = \frac{\bar{V}}{\bar{H}_{av}}$$

The conjugates of the quantities are chosen for reasons stated below.

If $$\dot{E} = E_0\varepsilon^{j\theta_1}\varepsilon^{j\omega t}$$

$$\dot{I} = I_0\varepsilon^{j\theta_2}\varepsilon^{j\omega t}$$

then $$\dot{Z} = \frac{E_0}{I_0} \angle \theta_1 - \theta_2 = \frac{\dot{E}}{\bar{I}}$$

On the other hand, if

$$\dot{E} = E_0\varepsilon^{j\theta_1}\varepsilon^{-j\omega t}$$

$$\dot{I} = I_0\varepsilon^{j\theta_2}\varepsilon^{-j\omega t}$$

then $$\dot{Z} = \left(\frac{E_0}{I_0}\right) \angle \theta_2 - \theta_1 = \frac{\bar{E}}{\bar{I}}$$

The type of field considered is of the form $\exp\left[j\left(\frac{\pi y}{\tau} - \omega t\right)\right]$

Using eqns. (14) and (7*b*)

$$\frac{1}{\dot{Z}} = -j\left(\frac{8}{\pi^2}\right)\left(\frac{\pi^2}{\tau^2}\right)\left(\frac{1}{\omega\mu}\right) \Sigma \frac{\bar{\lambda}_r}{(2r+1)^2\left[(2r+1)^2\frac{\pi^2}{h^2} + \frac{\pi^2}{\tau^2}\right]}$$

where . . . . (18)

$$\bar{\lambda}_r = \alpha_r + j\beta_r$$

Let

$$\dot{Z} = R + jX = Z \angle \psi_0$$

Then $\cos\psi_0$ is the overall power factor of the iron.

So far as the authors are aware an interpretation of a general field distribution leading finally to the concept of the power factor of the magnetizing winding has not so far been attempted.

(5.3) Concept of Power Factor for a General 2-Dimensional Field Distribution—Alternating Field

In this Section, we shall develop the concept of power factor and associated quantities for the type of field distribution discussed in Section 4.5. Following the method outlined in Section 5.2, the loss based on the Poynting vector is given by

$$P_{e5} = \frac{1}{8}\sum_{r=0}^{\infty}(\hat{E}_{x0r}\hat{H}_{y0r}\cos\psi_{10r} - \hat{E}_{y0r}\hat{H}_{x0r}\cos\psi_{20r})$$

when the quantities have the significance stated earlier. It may be borne in mind that E_x and H_y are each sinusoidally distributed in space along both the x- and y-directions.

Using eqns. (8),

$$P_{e5} = \frac{\rho}{8}\mathscr{R}\sum_{r=0}^{\infty}(d_r'\bar{b}_r' - f_r'\bar{a}_r)$$

$$= \frac{1}{8}\Sigma -j\left(\frac{\omega\mu\tau}{\pi}\right)c_r'\bar{b}_r'$$

Here $-j\left(\frac{\omega\mu\tau}{\pi}\right)c_r'$ has the significance of an induced e.m.f.

Using the method outlined in Section 5.2, we finally have:

$$P_{e5} = \tfrac{1}{4}\mathscr{R}(V_0\bar{H}_{av}), \text{ say}$$

where $$\dot{H}_{av} = \sum_{r=0}^{\infty}\left(\frac{2}{\pi}\right)(-1)^r\frac{1}{(2r+1)}b_r' = H_{av} \angle \pi + \phi_0 \quad (19)$$

and $$\dot{V}_0 = -j\left(\frac{\omega\mu\tau}{\pi}\right)H_0 \quad . \quad . \quad . \quad . \quad . \quad . \quad . \quad (20)$$

Hence $\psi_0 = \left(\frac{\pi}{2} - \phi_0\right)$, and $\cos\psi_0$ is the power factor of the magnetizing winding. Also, H_{av} and V_0 have the significance of current and e.m.f., respectively, of the winding.

To evaluate the loss based on the concept of power factor we can see that

$$\nu_r = \bar{\lambda}_r = \alpha_r + j\beta_r = |\lambda_r|\varepsilon^{j\phi_r}$$

Also, $$P_{e5} = \tfrac{1}{4}V_0\sum_{r=0}^{\infty}|H_{av}|_{r\text{th term}}\sin\phi_r \quad . \quad . \quad . \quad (21)$$

On simplification and reduction it is seen that

$$P_{e5} = \tfrac{1}{2}P_{e4}$$

This same expression giving identical values of loss and power factor could have been deduced from Section 5.2 directly by considering two rotating fields, each of amplitude $\frac{1}{2}H_0$, and rotating in opposite directions.

Enough has been said to pass over without much discussion on the evaluation of loss and the parameters of the exciting winding for the case referred to in Section 4.6.

(6) EQUATIONS OF PERFORMANCE OF AN INDUCTION MACHINE WITH SOLID IRON ROTOR (LINEAR THEORY)

We will now apply the results of the foregoing analysis to determine the performance of an induction machine with solid-iron rotor. The basic assumptions are as follows:

(*a*) The polyphase induction machine has balanced windings and operates on a balanced polyphase system of voltages applied to the stator.

(*b*) Because of chording and distribution of the windings the stator current is assumed to establish a sinusoidal distribution of the magnetostatic potential at the stator surface. This implies that the harmonic voltages induced by the space harmonics of the air-gap flux-density distributions are ignored.

(*c*) The magnetizing force at the rotor surface is also a sinusoidal function in space.

(6.1) Method 1: Based on Field Distribution due to Pulsating Flux on Infinite Half-Space (cf. Section 4.1)

A simple approach to the analysis of this machine is to treat this as a 1-dimensional problem where the currents are all axial. We can analyse the performance of this machine on the basis of an infinite half-space of iron subjected to a pulsating field having a frequency f, equal to the slip frequency of the rotor; i.e. $f = sf_0$.

Choose the co-ordinate system as in Section 3, with the surface of the rotor in the xy-plane, the z-axis normal to it, the pulsating field being along the y-direction. Clearly, since the flux per pole divides itself into two equal parts, the pulsating flux normal to any xz-plane is one half the flux per pole. Thus this is $h\Phi_0$, say, where h is the axial length of the rotor. Knowing Φ_0 it is a simple matter to fix the magnetizing force, H_{y0}, at the surface using eqn. (4).

$$\Phi_0 = \frac{H_0}{|\lambda|} = \left(\frac{\rho\mu}{\omega}\right)^{1/2} H_0$$

(i) *Power Factor.*

The rotor power factor is $1/\sqrt{2}$, as discussed in Section 5.

(ii) *Equivalent Rotor Current referred to the Stator.*

The magnetizing force at the rotor surface has an amplitude H_0 and is sinusoidally distributed in the y-direction. Hence the magnetostatic potential (which has the significance of ampere-turns per pole in this case) at the rotor surface will be

$$\left(\frac{\tau}{2}\right) H_{y0}\,(\text{average}) = \left(\frac{\tau}{\pi}\right) H_0$$

The ampere-turns/pole due to an equivalent stator current will be

$$\frac{1}{2}\,\frac{m}{p}\,\frac{4}{\pi} N_{eff} I_{eff} \sqrt{2}$$

where m = Number of stator phases.

p = Number of poles,

N_{eff} = Effective number of stator turns per phase.

Equating these two expressions we have

$$I_{eff} = I_r'\,(\text{say}) = \frac{H_0 p\tau}{2\sqrt{(2)} m N_{eff}} = \frac{H_0 \pi D}{2\sqrt{(2)} m N_{eff}}$$

where D is the rotor diameter.

Alternatively, the equivalent current of the rotor referred to the stator can be deduced as follows: The rotor may be considered to consist of πD 'conductors', each of unit width and carrying a current whose amplitude is H_0. The transformation ratio is then $2mN_{eff}/\pi D$. Since $H_0/\sqrt{2}$ is the r.m.s. current per rotor 'conductor' of unit width, the equivalent current of the rotor referred to the stator is

$$I_r' = \frac{\pi D H}{2\sqrt{(2)} m N_{eff}} \text{ amperes per phase}$$

(iii) *Stator Current.*

The stator current per phase could be determined by adding vectorially I_r' to the no-load current, I_0.

(iv) *Torque.*

The torque in synchronous watts can be evaluated on the basis of loss calculations or from the total power input to the rotor. In either case,

$$T = \frac{m V_1 I_r'}{\sqrt{2}} \text{ synchronous watts}$$

where V_1 = Air-gap voltages/phase $= 2h\omega_0\Phi_0 N_{eff}$.

(v) *Rotor Impedance.*

The equivalent impedance of the rotor referred to the stator is given by

$$\dot{Z}_r' = \left|\frac{V_1}{I_r'}\right| \angle 45°$$

$$= \frac{4m\omega_0 h \Phi_0 N_{eff}^2}{\pi D H_0} \angle 45°$$

Alternatively, the rotor can be considered to have m 'conductors' of width $\pi D/m$ carrying a current of amplitude $(\pi D/m)H_0$. The impedance of each conductor of axial length h is

$$\frac{mh\omega_0\Phi_0}{\pi D H_0} \angle 45°$$

Since $\omega = s\omega_0$ and the ratio of transformation is now $2N_{eff}$, the impedance referred to the stator becomes

$$\dot{Z}_r' = \frac{mh\omega\Phi_0(2N_{eff})^2}{s\pi D H_0} \angle 45°$$

which yields the same expression as before. Knowing Φ_0, the relevant quantities could be computed for any assumed values of s.

(6.2) Method 2. Based on Field Distribution due to a Travelling Flux on Infinite Half-Space (cf. Section 4.3)

The preceding analysis refers to a 1-dimensional problem. We will now examine the nature of the expressions based on the field distribution due to a travelling field on the surface of an infinite half-space of iron where only the x-component of the currents exist (see Sections 4.3 and 5.1). Using steps identical to those of method 1, the results could be summarized as follows:

For assumed values of H_0 and s the following quantities could be computed.

(i) *Equivalent Rotor Current referred to the Stator.*

$$I_r' = \frac{\tau}{\pi}\,\frac{\lambda\pi D}{2\sqrt{(2)} m N_{eff}} H_0 \text{ amp/phase}$$

(ii) *Air-gap Voltage per Phase.*

$$V_1 = 2\frac{\tau}{\pi}\omega_0 \mu h H_0 N_{eff}$$

(iii) *Equivalent Rotor Impedance per Phase.*

$$\dot{Z}_r' = \frac{4j\omega_0 \mu h m N_{eff}^2}{\bar{\lambda}\pi D}$$

$$= |Z_r'| \angle 90 - \phi_0$$

where $\bar{\lambda} = |\lambda| \varepsilon^{j\phi_0} = \alpha + j\beta$

(iv) *Rotor Power Factor.*

$$\cos\left(\frac{\pi}{2} - \phi_0\right) = \sin\phi_0 = \frac{\omega\mu}{\rho}\frac{1}{2\alpha|\lambda|}$$

(vi) *Torque in Synchronous Watts.*

$$T = mV_1 I_r' \sin\phi_0 = \frac{\pi D h}{s} P_{e3}$$

where P_{e3} is given by eqn. (11*b*).

(6.3) Method 3. Based on a General 2-Dimensional Field Distribution (cf. Section 4.4)

The analysis could be based on a more generalized field distribution as discussed in Sections 4.3 and 5.2. The following are based on assumed values of H_0 and s.

(i) *Equivalent Rotor Current.*

$$I_r' = \frac{\pi D}{2\sqrt{(2)} m N_{eff}} H_{av} \text{ amperes per phase}$$

where H_{av} is defined by eqn. (13).

(ii) *Air-Gap Voltage/Phase.*

$$V_1 = 2\frac{\tau}{\pi}\omega_0 \mu h N_{eff} H_0$$

(iii) *Equivalent Rotor Impedance referred to the Stator.*

Making use of eqn. (18), for an impedance $\dot{Z}$ of a rotor 'conductor' of unit length in the x- and y-directions, we have

$$\dot{Z}_r' = \frac{hm(2N_{eff})^2}{\pi D s}\dot{Z}$$

$$= |Z_r'| \angle \psi_0, \text{ say}$$

(iv) *Rotor Power Factor.*

The rotor power factor is $\cos\psi_0$.

(v) *Torque in Synchronous Watts.*

$$T = \frac{\pi D h}{s} P_{e4}$$

where P_{e4} is defined by eqn. (17).

For a proper application of these results the following steps are suggested:

(*a*) Choose H_0 and a particular value of s.
(*b*) Keeping s constant vary H_0 over a range and obtain V_1, I_r', $\dot{Z}_r'$, T and $\cos\psi_0$.
(*c*) Choose other values of s and repeat the calculations.

By cross reference to the family of curves relating V_1 and H_{av} in terms of the parameter, s, we could compute the performance of the machine.

Two particular cases arise in the performance of the machine:

(i) When it operates under a given induced e.m.f. (air-gap voltage) V_1.
(ii) When it operates under a constant applied voltage V at the stator terminals.

Table 1

PERFORMANCE CALCULATIONS FOR SOLID-ROTOR INDUCTION MACHINE

Slip	0·05	0·1	0·15	0·2	0·4	0·6	0·8	1·0
Method 1 $H_{y0} \times 10^{-2}$	110	152·5	184	209·7	285	339	381·2	418
I_r'	1·328	1·847	2·22	2·531	3·44	4·09	4·60	5·05
V_1	363·1	356	350·5	346	332·6	323	315·1	308·5
$\cos\psi_0$	0·707	0·707	0·707	0·707	0·707	0·707	0·707	0·707
T	1022	1394	1651	1857	2426	2803	3075	3301
Method 2 $H_{z0} \times 10^{-2}$	19·9	19·49	19·19	18·92	18·18	17·65	17·22	16·87
I_r'	1·331	1·844	2·224	2·531	3·44	4·09	4·608	5·05
V_1	363·8	356·3	350·8	345·9	332·3	322·6	314·8	308·4
$\cos\psi_0$	0·683	0·696	0·700	0·702	0·705	0·705	0·706	0·707
T	992·4	1372	1639	1843	2417	2790	3071	3303
Method 3 $H_{z0} \times 10^{-2}$	20·6	20·56	20·33	20·23	19·93	19·20	19·52	19·35
I_r'	0·481	0·676	0·821	0·943	1·312	1·59	1·815	2·01
V_1	376·6	375·8	371·6	369·8	364·3	360·0	356·8	353·7
$\cos\psi_0$	0·68	0·707	0·707	0·707	0·707	0·707	0·707	0·707
T	369·6	538·8	647·1	739·6	1014	1214	1374	1508

Specifications and Constants.

3 h.p. 400-volt 3 phase delta-connected; 4 poles; 50 c/s; stator winding factor, 0·9%; effective number of turns per phase, 426·2; stator impedance (8·88 + *j*12·33) ohms; rotor diameter, 0·139 m; pole pitch, 0·109 1 m; active axial length, 0·092 7 m; magnetizing current (phase), $1{\cdot}31 \angle -81°$.

Mild-steel rotor of resistivity $18{\cdot}5 \times 10^{-8}$ ohm-m, and permeability of 300×10^{-6} (assumed).

I_r' = Equivalent rotor current referred to the stator, amp/phase.
V_1 = Induced e.m.f. in the stator winding.
$\cos\psi_0$ = Rotor power factor.
T = Torque, synchronous watts.

In the first case, the method outlined so far can directly be applied. In the second case we make use of the relationship

$$\dot{V} = \dot{V}_1 + (\dot{I}_m + \dot{I}'_r)(R_1 + jx_1)$$

where the quantities have the usual significance, or

$$V \simeq V_1 + I_m x_1 + I'_r \cos\psi_0 (R_1 + x_1 \tan\psi_0$$

Bearing in mind the relationships that exist between I'_r and H_0 and between V_1 and H_0, it is a simple matter to fix V_1 and I'_r for an assumed slip.

(7) EXAMPLE

In order to give more validity to several of the formulae deduced in the paper, computations are made to determine the performance of an induction machine with a mild-steel solid rotor. The relevant quantities pertaining to the machine and a summary of the results of the calculations are given in Table 1.

(8) CONCLUSIONS

For the cases discussed in the paper it has been possible to determine the equivalent circuit of the system as a whole in terms of impedance and power factor. This determination has been based on a concept of power factor for the magnetizing winding which is responsible for a general 2-dimensional field distribution in the core. Furthermore, this concept has proved extremely useful for the evaluation of eddy-current loss in solid cores, and hence, in particular, for determining the characteristics of a solid-rotor induction machine when operating in the linear range of the magnetization curve.

The performance calculations of this machine, based on methods 1 and 2, yield substantially the same results for the range of operations considered. This justifies the conclusion that, without loss of generality, the analysis of such machines can be based on the simpler method 1. Referring next to the performance calculations based on method 3, it may be noted that the power factor, for the range of operation considered, is 0·707, which is the same as obtained by using the infinite half-space analysis. However, the equivalent rotor current and torque are reduced, and the ratio of reduction with respect to the other two methods is substantially a constant. Consequently, these quantities can be obtained directly by using either of the first two simple methods with a suitable alteration in the resistivity of the specimen.

The rotors of solid-rotor induction machines may have extensions exceeding the active length of the stator iron. Also, copper or steel end-rings may be provided on both sides for such types of construction to improve the performance. Judging from the results of Table 1, it may be concluded that the infinite half-space analysis with a modified resistivity of the rotor material must suffice for determining the machine performance.

Finally, it should be understood that the analysis of solid-rotor induction machines has been chosen mainly to serve as an illustration and to give validity to the various formulae developed in the paper and not with a view to offering an analysis of the performance of such machines. These machines operate under conditions of extreme saturation, even at low slips, and hence their analysis is a separate and distinct problem, calling for the evaluation of eddy-current loss, under saturation conditions, in solid ferromagnetic cores subjected to an alternating or rotating magnetic field.[3, 4]

(9) ACKNOWLEDGMENT

The authors wish to express their thanks to the Director, Indian Institute of Technology, Kharagpur, for the facilities offered.

(10) REFERENCES

(1) POHL, R.: 'Electromagnetic and Mechanical Effects in Solid Iron due to an Alternating or Rotating Field', *Journal I.E.E.*, 1944, **91**, Part II, p. 239.

(2) CARTER, G. W.: 'A Note on the Surface Losses in a Laminated Pole-Face', *Proceedings I.E.E.*, Monograph No. 123, March, 1955 (**102** C, p. 217).

(3) KESAVAMURTHY, N., and RAJAGOPALAN, P. K.: 'Eddy Currents in Solid Iron due to Alternating Magnetic Flux', *ibid.*, Monograph No. 339, June, 1959 (**105** C, p. 207).

(4) KESAVAMURTHY, N., and RAJAGOPALAN, P. K.: 'The Polyphase Induction Machine with Solid Iron Rotor', *Transactions of the American I.E.E.*, 1959, **78**, 1092.

621.396.677: 621.372.825

The Institution of Electrical Engineers
Monograph No. 386 E
June 1960
©

THE RESONANCE EXCITATION OF A CORRUGATED-CYLINDER ANTENNA

By J. R. WAIT, M.A.Sc., Ph.D., and A. M. CONDA, B.A.

(*The paper was first received 7th December, 1959, and in revised form 24th March, 1960. It was published as an* INSTITUTION MONOGRAPH *in June, 1960.*)

SUMMARY

Radiation from an axial magnetic line or slot source on the surface of a corrugated cylinder is considered. It is indicated that the power radiated in a given mode for the structure depends critically on the surface reactance and the circumference of the cylinder. In fact, for certain values of these parameters, particular modes are strongly excited and contain most of the radiated power. Numerical results are presented for several interesting cases.

The analysis is extended to an elliptic cylinder whose surface also possesses an inductive reactance. In order to facilitate the solution it is necessary to assume a special azimuthal variation of the surface reactance. For the model as chosen, strong resonance characteristics are again obtained. This model may be adapted to study the problem of a corrugated panel on a flat metallic ground plane which is excited by a parallel slot source.

(1) INTRODUCTION

It is now well known that a corrugated surface or a dielectric-coated metallic plane will support a wave which propagates along the interface and does not radiate.[1] At the risk of over-simplification, this wave will be called a surface wave if for TM waves the surface is purely inductive and if for TE waves the surface is purely capacitive. Even if the surface is partly curved, it has been shown[2, 3] that the wave excited on the structure, by a dipole for example, bears a close resemblance to that on a lossless surface. The bending of the guiding surface tends to produce leakage of energy in the normal direction. The structure of the field in the case of large radii of curvature is not appreciably changed near the surface.

When the radius of curvature is not large, it is expected that leakage from the structure will play a major role. An example is a corrugated or dielectric-coated cylinder with a circumference of only a few wavelengths. Such a model was studied by the authors[4] for a slot or magnetic current excitation, where it was shown that the radiation patterns exhibit enhanced lobes as a result of resonance phenomena. The case of a circular cylinder with anisotropic boundary conditions under electric dipole excitation has also been considered.[5] Recently, Cullen[6] has indicated that such a cylinder excited by an axial (electric) line source may be strongly resonated if the (capacitive) surface reactance is chosen in a certain fashion. It is the purpose of the present paper to pursue these matters further.

(2) THE CIRCULAR CYLINDER MODEL

A circular cylinder of radius a whose surface impedance (looking inward) is purely inductive is considered first. To make the problem completely 2-dimensional in nature, the source is taken to be a magnetic line source of strength K volts and is located at $r = a$, which is the surface of the cylinder with respect to a cylindrical co-ordinate system (ρ, ϕ, z). The electric field of this structure has only a ϕ-component in the far zone (i.e. $\rho \gg \lambda$) and is given by[4, 7]

$$E_\phi = 60\epsilon_0\omega K\left(\frac{2}{\pi k\rho}\right)^{1/2} \varepsilon^{-j(k\rho+\pi/4)} Q(\phi) \quad . \quad . \quad (1)$$

where ϵ_0 = the permittivity of free space $\simeq 8{\cdot}854 \times 10^{-12}$
$\omega = 2\pi \times$ frequency
$k = 2\pi/$wavelength

$$Q(\phi) = \frac{1}{x}\sum_{m=0}^{\infty} \frac{\epsilon_m \cos m\phi \; \varepsilon^{jm\pi/2}}{\mathrm{H}_m'(x) + G_c\mathrm{H}_m(x)} \quad . \quad . \quad . \quad (2)$$

$G_c = X/\eta_0$
X = Surface reactance
η_0 = Intrinsic impedance of free space $\simeq 120\pi$ ohms
$x = ka = 2\pi a/\lambda$
$\mathrm{H}_m(x)$ = (cylindrical) Hankel function of second kind, usually designated $\mathrm{H}_m^{(2)}(x)$
$\mathrm{H}_m'(x) = d\mathrm{H}_m(x)/dx$

Numerical values of $Q(\phi)$ were given by Wait and Conda[4] for ϕ in the range 0–180°, $x = 2$, 3 and 8, and several values of G_c in the range between 0 and 0·3. It was observed that in several cases the function $|Q(\phi)|$ varied in a pronounced manner with ϕ. This is not surprising, since, for certain values of m, the summand of the series representation becomes large when $\mathrm{H}_m'(x) + G_c\mathrm{H}_m(x)$ is small. Cullen[6] in an analogous problem has suggested that, if G_c were chosen in an appropriate manner, the pattern function $|Q(\phi)|$ may vary almost like $\cos m\phi$. To demonstrate this, it is noted that for real values of G_c and x,

$$|\mathrm{H}_m'(x) + G_c\mathrm{H}_m(x)|^2 = [\mathrm{J}_m'(x) + G_c\mathrm{J}_m(x)]^2 + [\mathrm{Y}_m'(x) + G_c\mathrm{Y}_m(x)]^2 \quad . \quad (3)$$

The term involving the Y functions dominates the right-hand side of eqn. (3). It is zero when

$$G_c = -\frac{\mathrm{Y}_m'(x)}{\mathrm{Y}_m(x)} \quad . \quad . \quad . \quad . \quad . \quad . \quad . \quad (4)$$

or when $$xG_c = \tan\beta_m$$

where $$\beta_m = \arctan\left[-\frac{x\mathrm{Y}_m'(x)}{\mathrm{Y}_m(x)}\right] \quad . \quad . \quad . \quad . \quad (5)$$

For example, if $x = 3$,

$$\begin{array}{lll} \beta_0 = 248{\cdot}45° & \beta_1 = 111{\cdot}94° & \beta_2 = 82{\cdot}94° \\ \beta_3 = 64{\cdot}61° & \beta_4 = 65{\cdot}92° & \beta_5 = 74{\cdot}30° \\ \beta_6 = 78{\cdot}57° & \beta_7 = 80{\cdot}81° & \beta_8 = 82{\cdot}22° \end{array}$$

and so on. If the term corresponding to $m = 6$ is to be predominant, it follows that $G_c = \frac{1}{3}\tan 78{\cdot}57° = 1{\cdot}65$, corresponding to an inductive surface reactance $X = 120\pi G_c = 622$ ohms. In this case, the pattern function, $Q(\phi)$, is almost proportional to $\cos\phi$6.

Correspondence on Monographs is invited for consideration with a view to publication.
The authors are at the National Bureau of Standards, Boulder, Colorado, U.S.A.

The total power radiated from the structure is proportional to the quantity

$$P = \int_0^{2\pi} Q^*(\phi)Q(\phi)d\phi \quad . \quad . \quad . \quad . \quad . \quad (6)$$

the asterisk denoting a complex conjugate. This can be rewritten

$$P = \sum_{m=0}^{\infty} p_m \quad . \quad . \quad . \quad . \quad . \quad . \quad (7)$$

where p_m is the power associated with each mode and is given by

$$p_m = \frac{\epsilon_m}{x^2} \frac{1}{|H_m'(x) + G_c H_m(x)|^2} \quad . \quad . \quad . \quad (8)$$

where $x = ka$.

To illustrate the relative amounts of power in the various modes for a typical resonance condition, p_m is listed for $G_c = 1{\cdot}65$ and $x = 3$:

$$\begin{aligned} p_0 &= 0{\cdot}16 \quad p_4 = 0{\cdot}27 \\ p_1 &= 0{\cdot}33 \quad p_5 = 0{\cdot}28 \\ p_2 &= 0{\cdot}32 \quad p_6 = 146 \\ p_3 &= 0{\cdot}30 \quad p_7 = 0{\cdot}033 \end{aligned}$$

with the remaining terms decreasing very rapidly beyond this point. It is noticed that most of the radiated power is in one mode.

The variation of p_m as a function of surface reactance, G_c, for several mode numbers is shown in Fig. 1 for $ka = 3$. It

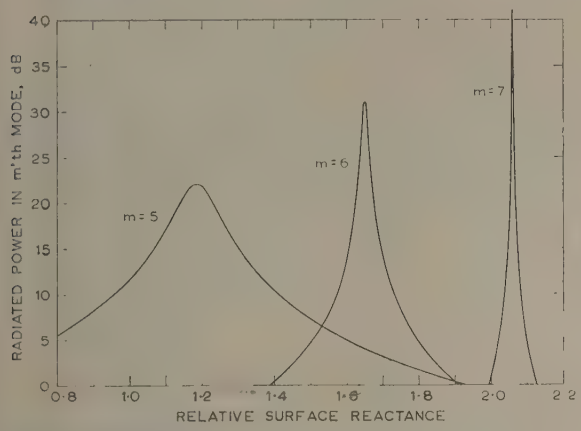

Fig. 1.—Resonance effect for a reactive cylinder with line source excitation, $ka = 3$.

may be noted that the resonance effect becomes marked for higher mode numbers. This is illustrated more effectively in Fig. 2 for a larger cylinder for which $ka = 6$.

It may be easily shown that the function $Q(\phi)$ also characterizes the azimuthal pattern of an electric current line source located on the surface of the cylinder. As mentioned, this was the model chosen by Cullen. Then $G_c = Y\eta_0$, where Y is the surface susceptance at $r = a$. Thus, the results in Figs. 1 and 2 are also applicable to this case.

The specific form of the radiation pattern function, $Q(\phi)$, is shown in Fig. 3 for $ka = 3$ and $G_c = 1{\cdot}649$ corresponding to the resonance for $m = 6$. It is seen that there is a close resemblance to the function $\cos 6\phi$. In the forward direction (i.e. near $\phi = 0°$) the other modes contaminate the ideal pattern to some extent. The effect is, however, quite small.

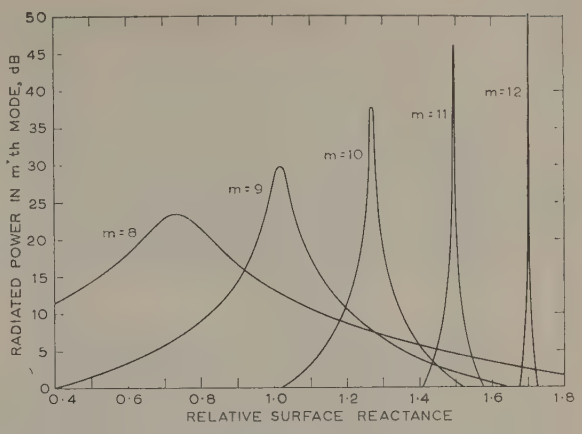

Fig. 2.—Resonance effect for a reactive cylinder with line source excitation, $ka = 6$.

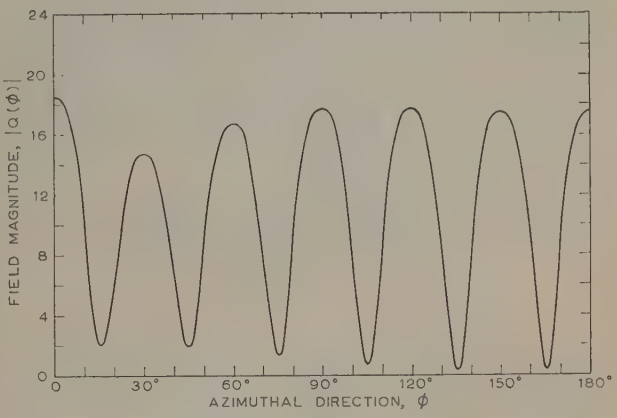

Fig. 3.—Radiation pattern for a reactive cylinder at a resonance, $G_c = 1{\cdot}649$, $ka = 3$.

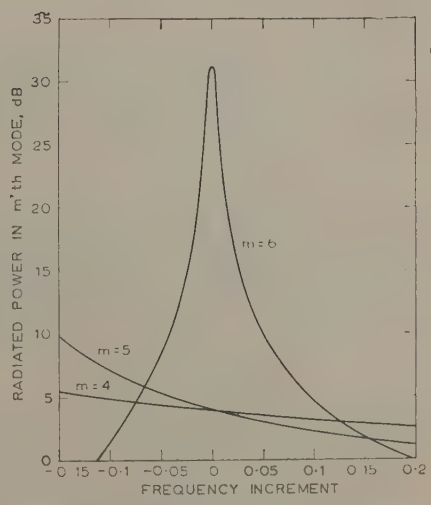

Fig. 4.—Shape of the resonance curve for the reactive cylinder, $G = 1{\cdot}649(1 + \delta)$, $ka = 3(1 + \delta)$.

The influence of a small change of frequency from its resonance value is also of interest. For example, if the relative change of frequency is δ, the value of ka changes in the first example from 3 to $3(1+\delta)$. If the cylinder is corrugated the inductive reactance will also be approximately proportional to frequency.[4] Thus, for a relative frequency change or increment, δ, the value of G_c changes from its resonance value of $1\cdot649$ to $1\cdot649(1+\delta)$. The subsequent 'de-tuning' is illustrated in Fig. 4, where the power, p_m, is plotted as a function of the frequency increment, δ. This illustrates well the sharpness of the resonance curve for $m=6$. The power in the other modes is also changed, of course, but not to the same extent.

(3) THE ELLIPTIC CYLINDER MODEL

A rather obvious extension of the previous analysis is to an elliptic cylinder with a corrugated surface. As in the case of the circular cylinder, the surface impedance of the elliptic cylinder is assumed to be specified. Unfortunately, the problem becomes very complicated if the impedance is a constant, since all the modes are then coupled by the boundary condition. The resulting equation to be solved then involves an infinite determinant. This difficulty can be circumvented if the surface impedance varies around the cylinder in a particular fashion. The method was used previously in a closely related problem,[8] so it is not necessary to go through the derivation in detail.

The specific model is an elliptic cylinder of minor axis $2a$ and major axis $2b$. If the cylinder axis is coincident with the z-axis of a rectangular co-ordinate system (x, y, z), the surface of the cylinder is specified by $x^2/b^2 + y^2/a^2 = 1$. It is now convenient to introduce elliptic cylinder co-ordinates (u, v, z) which are defined by the following transformation:

$$\begin{aligned} x &= d\cosh u\cos v \\ y &= d\sinh u\sin v \\ z &= z \end{aligned}$$

where $2d$ is the distance between the foci of the (confocal) ellipses which are located at $x=\pm d, y=0$. Then $b=d\cosh u_0$ and $a=d\sinh u_0$, where $u=u_0$ is the surface of the elliptic cylinder.

An axial magnetic line source, K, is located on the surface of the cylinder at co-ordinates $u=u_0$ and $v=v_0$. The boundary condition is then given by

$$H_z = -\frac{1}{Z(v)}E_v \text{ at } u=u_0$$

The specific form of the surface impedance function is taken to be

$$Z(v) = j\eta_0 G_s \frac{\cosh u_0}{(\cosh^2 u_0 - \cos^2 v)^{1/2}} \quad . \quad . \quad . \quad (9)$$

where $\eta_0 \simeq 120\pi$ ohms and G_s is the relative surface reactance at $v=\pi/2$. For present purposes G_s is taken real and is analogous to the relative reactance, G_c, in the circular cylinder case. For this boundary condition the field external to the elliptic cylinder is given by

$$H_z = \epsilon_0\omega K\sum_{m=0}^{\infty}\frac{\mathrm{Se}_m(k^2d^2, v_0)\,\mathrm{Se}_m(k^2d^2, v)}{\mathrm{N}_m^{e,o}(k^2d^2)} \times \frac{\mathrm{He}\,\mathrm{o}_m^{(2)}(k^2d^2, u)jT}{\mathrm{He},\,\mathrm{o}_m^{(2)}(k^2d^2, u_0) - T\,\mathrm{He},\,\mathrm{o}_m^{(2)\prime}(k^2d^2, u_0)} \quad . \quad (10)$$

where $$T = \frac{\eta_0}{Z(\pi/2)\,jkd\cosh u_0} = -\frac{1}{G_s\,kd\cosh u_0}$$

The quantities $\mathrm{Se}_m(k^2d^2, v)$ and $\mathrm{So}_m(k^2d^2, v)$ are the even and odd angular Mathieu functions[8] respectively, of argument k^2d^2 and v. $\mathrm{He}_m^{(2)}(k^2d^2, u_0)$ and $\mathrm{Ho}_m^{(2)}(k^2d^2, u_0)$ are even and odd radial Mathieu functions respectively, of the fourth kind, of argument k^2d^2 and u_0. The prime over the radial function indicates a derivative with respect to u_0. $\mathrm{N}_m^e(k^2d^2)$ and $\mathrm{N}_m^o(k^2d^2)$ are the normalization factors for even and odd angular Mathieu functions, and they are functions of k^2d^2. The summation indicated is over all integral values of m and in general includes both even and odd functions (as indicated by the double suffix e, o_m).

The power radiated per unit length is readily obtained by integrating the radial component of the Poynting vector around a concentric circular cylinder of infinite radius. That is,

$$P = \tfrac{1}{2}\eta_0 \lim_{\rho\to\infty}\int_0^{2\pi} H_z H_z^* \rho\, d\phi \quad . \quad . \quad . \quad . \quad (11)$$

in terms of cylindrical co-ordinates (ρ, ϕ, z). To perform this integration it should be noted that

$$\begin{aligned} &\int_0^{2\pi}\mathrm{Se},\,\mathrm{o}_m(k^2d^2, v)\,\mathrm{Se},\,\mathrm{o}_n(k^2d^2, v)\,dv \\ &\quad = \mathrm{Ne},\,\mathrm{o}_m(k^2d^2) \quad \text{if} \quad m=n \\ &\quad = 0 \quad \text{if} \quad m\neq n \quad . \quad . \quad . \quad . \quad . \quad . \quad . \quad (12) \end{aligned}$$

and $$\lim_{u\to\infty}|\mathrm{He},\,\mathrm{o}_m^{(2)}(k^2d^2, u_0)|^2 = \frac{1}{k\rho} \quad . \quad . \quad . \quad (13)$$

Thus,

$$\frac{P}{V^2} = \frac{\epsilon_0\omega}{2}\sum_{m=0}^{\infty}\frac{1}{\mathrm{N}_m^{e,o}(k^2d^2)}\frac{T^2[\mathrm{Se},\,\mathrm{o}_m(k^2d^2, v_0)]^2}{|\mathrm{He},\,\mathrm{o}_m^{(2)} - T\,\mathrm{He},\,\mathrm{o}_m^{(2)\prime}|^2} \quad . \quad (14)$$

where the argument of the radial functions is understood to be (k^2d^2, u_0). The source is now located at the centre of the broad face (i.e. $v_0=\pi/2$). Furthermore, the elliptic cylinder is allowed to degenerate into a strip (i.e. $b\to0$ and $a\to d$) of width $2d$. The equation for the radiated power now reduces to

$$\frac{P}{V^2} = \frac{\epsilon_0\omega}{2}\sum_{m=0}^{\infty}p_m \quad . \quad . \quad . \quad . \quad . \quad (15)$$

where $$p_m = \frac{1}{\mathrm{N}_m^e\left[\left(\frac{kdG_s}{g_{em}}\right)^2 + \left(g_{em} - kdG_s\frac{f_{em}}{g_{em}}\right)^2\right]} \quad . \quad (16)$$

for $m=0, 2, 4\ldots$

and $$p_m = \frac{1}{\mathrm{N}_m^o\left[\left(\frac{1}{g_{om}}\right)^2 + \left(\frac{f_{om}}{g_{om}} - kdG_s g_{om}\right)^2\right]} \quad . \quad . \quad (17)$$

for $m=1, 3, 5\ldots$ The functions f_{em}, f_{om}, g_{em} and g_{om} are the 'joining factors' and are tabulated as a function of k^2d^2. They are related to the radial Mathieu functions of argument $(k^2d^2, 0)$ in the following manner:[9]

$$\left.\begin{aligned} \mathrm{He}_m^{(2)} &= \frac{1+jf_{em}}{g_{em}} & \mathrm{He}_m^{(2)\prime} &= -jg_{em} \\ \mathrm{Ho}_m^{(2)} &= +jg_{om} & \mathrm{Ho}_m^{(2)\prime} &= \frac{1-jf_{om}}{g_{om}} \end{aligned}\right\} \quad . \quad . \quad (18)$$

The function p_m is thus a measure of the power which goes into the m'th mode. Taking $(kd)^2 = 12$ and 36, p_m is plotted as a function of the relative surface reactance, G_s, for various

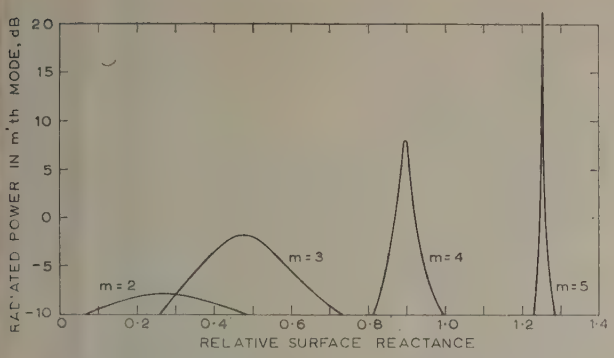

Fig. 5.—Resonance effect for a reactive strip with line source excitation, $(kd)^2 = 12$, $v_0 = \pi/2$.

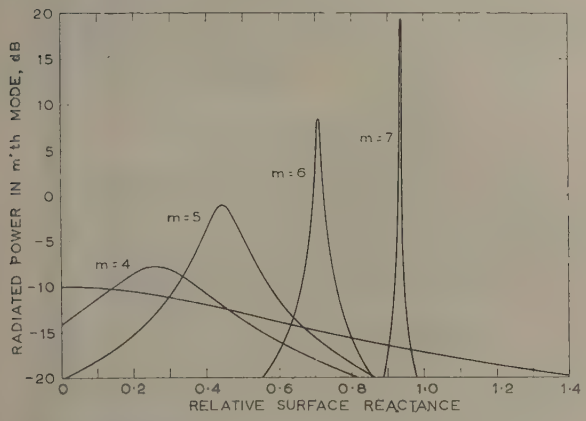

Fig. 6.—Resonance effect for a reactive strip with line source excitation, $(kd)^2 = 36$, $v_0 = \pi/2$.

values of m. The curves shown in Figs. 5 and 6 are very similar to those for the circular cylinder. For certain values of G_s the radiated power tends to be concentrated in a particular mode. For this limiting case of a strip, the surface impedance should have the functional form

$$Z(x) = j\eta_0 G_s\left(1 - \frac{x^2}{d^2}\right)^{-1/2} \quad . \quad . \quad . \quad . \quad (19)$$

which is a special case of eqn. (9) when $u_0 = 0$. The relative surface reactance thus rises from its central value, G_s, to infinity at the edge. Physically, such a behaviour is not realizable, but if the elliptic cylinder has a small but finite thickness the singularity at the edge is removed.

The azimuthal behaviour of the field in a given mode number is proportional to the function $\mathrm{Se}_m(k^2d^2, v)$. In the far field, v may be replaced by the azimuth angle ϕ. Furthermore, since the source is located at the centre of the broad face, the even-order modes are associated only with the function $\mathrm{Se}_m(k^2d^2, \phi)$ and the odd-order modes are associated only with $\mathrm{So}_m(k^2d^2, \phi)$.

The preceding discussion has been limited to a magnetic line source on the surface of a reactive elliptic cylinder. The same solution is applicable to an electric line source if the surface admittance of the cylinder has the form

$$Y(v) = (j/\eta_0)G_s\frac{\cosh u_0}{(\cosh^2 u_0 - \cos^2 v)^{1/2}} = \frac{1}{Z(v)} \quad . \quad (20)$$

Thus, G_s is the relative surface susceptance at $v = \pi/2$. In the case of the strip, the above simplifies to

$$Y(x) = (j/\eta_0)G_s\left(1 - \frac{x^2}{d^2}\right)^{-1/2} = \frac{1}{Z(x)} \quad . \quad . \quad (21)$$

For G_s real and positive, the surface thus exhibits a capacitive reactance.

A particularly interesting situation exists if, instead of an isolated elliptic cylinder, we consider a semi-elliptical boss on a perfectly conducting ground plane. For example, in terms of elliptic-cylinder co-ordinates the ground plane is defined by $v = 0$ and π, and $u > u_0$. The elliptical boss is defined by $u = u_0$ and $0 < v < \pi$. The solution for this problem is a very simple extension of the preceding. In the case of a magnetic line source, K, at $v = v_0$ the formula for the external field, H_z, is identical with eqn. (10) for the isolated elliptic cylinder, except that K is replaced by $2K$ and the odd Mathieu functions are discarded. This comes about because the boundary condition requires that the normal derivative of H_z be zero on the ground plane. On the other hand, the corresponding solution for the electric current I contains only odd Mathieu functions, since E_z is to be zero on the ground plane.

The limiting case of the elliptical boss when the minor axis approaches zero is a panel of width $2d$ on the flat ground plane. The surface reactance varies across this panel in a special way. For the magnetic line source it must vary as $(1 - x^2/d^2)^{-1/2}$ as x ranges from 0 to $\pm d$. A physical structure which may approximate to the required variation of surface reactance for the magnetic line source is shown in Fig. 7. The structure

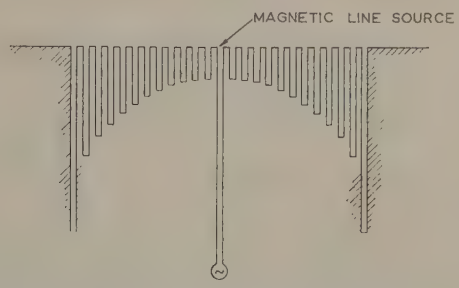

Fig. 7.—Cross-section of a corrugated panel which provides a variable surface reactance.

consists essentially of a number of parallel grooves of depth l cut in a metal plate. The periodicity, d, and the width, w, of the grooves are taken to be very small compared with the wavelength. It is known that such a structure may be macroscopically represented by a surface whose average surface reactance is given by

$$X(x) = \eta_0\frac{w}{d}\tan kl$$

In obtaining this simple formula it is assumed that l is a constant. In this case it varies with x; however, this should not modify the argument to any extent if the relative variation of l from one groove to the next is small.

Now the required variation of $X(x)$ is specified by

$$X(x) = \eta_0 G_s\left(1 - \frac{x^2}{d^2}\right)^{-1/2}$$

Thus, the required depth of the grooves is obtained from the relation

$$kl = \arctan\left[\frac{d}{w}G_s(1 - x^2/d^2)^{-1/2}\right] \quad . \quad . \quad (22)$$

This would indicate that l has some nominal value at the centre of the panel and increases to near $\lambda/4$ at the edges. A corrugated structure of this kind should exhibit the desired form of the reactance variation to any desired degree of precision if the number of grooves is sufficiently large.

The corresponding structure for the case of an electric line source is not as simple to synthesize. An approximate form might be a dielectric panel whose thickness varied from a maximum at the centre to a small value at the edges.

(4) CONCLUSIONS

On the basis of the results presented here, it appears that a cylindrical structure which has a reactive surface may be strongly resonated by an axial source. While the models chosen here are 2-dimensional in form, similar effects can be demonstrated for 3-dimensional structures. For example, a sphere which has latitudinal corrugations may be strongly resonated by a centrally located electric dipole source. The resulting pattern of these modes is described by the Legendre polynomial $P_n(\cos\theta)$ in analogy to $\cos n\phi$ for the circular cylinder model. The results for the spherical corrugated model will be contained in a subsequent paper.

(5) ACKNOWLEDGMENT

We would like to thank Prof. A. L. Cullen for his suggestions and for making available a copy of his paper[6] before publication.

The work in the present paper was supported by the Air Force Cambridge Research Center through Contract CSO and A 58–40.

(6) REFERENCES

(1) WAIT, J. R.: 'Excitation of Surface Waves on Conducting, Stratified Dielectric-Clad, and Corrugated Surfaces', *Journal of Research of the National Bureau of Standards*, 1957, **59**, p. 365.

(2) WAIT, J. R.: 'Guiding of Electromagnetic Waves by Uniformly Rough Surfaces', Proceedings of the Symposium on Electromagnetic Theory, University of Toronto, 1959.

(3) BARLOW, H. E. M.: 'Surface Waves supported by Curved Boundaries', *ibid.*, and 'The Power Radiated by a Surface Wave Circulating around a Cylindrical Surface', *Proceedings I.E.E.*, Paper No. 2771 E, March, 1959 (**106** B, p. 180).

(4) WAIT, J. R., and CONDA, A. M.: 'Radiation from Slots on Dielectric-Clad and Corrugated Cylinders', *Journal of Research of the National Bureau of Standards*, 1957, **59**, p. 307.

(5) WAIT, J. R.: 'Radiation from an Electric Dipole in the Presence of a Corrugated Cylinder', *Applied Science Research*, 1955, **6B**, p. 117.

(6) CULLEN, A. L.: 'Surface Wave Resonance Effect in a Reactive Cylindrical Structure excited by a Line Source', *Journal of Research of the National Bureau of Standards*, 1960, **64D**, p. 13.

(7) WAIT, J. R.: 'Electromagnetic Radiation from Cylindrical Structures' (Pergamon Press, 1959).

(8) WAIT, J. R.: 'Scattering of Electromagnetic Waves from a "Lossy" Strip on a Conducting Plane', *Canadian Journal of Physics*, 1955, **33**, p. 383.

(9) National Bureau of Standards, 'Tables Relating to Mathieu Functions' (Columbia University Press, 1951).

DISCUSSION ON 'TRANSIENT RESPONSE OF BAND-PASS FILTERS TO MODULATED SIGNALS'*

Messrs. J. W. Head and **C. G. Mayo** (*communicated*): We congratulate Mr. Mayne on his use of operational calculus, as opposed to symbolic calculus, but feel that his attention should be drawn to two papers on the more general subject of frequency modulation, which includes Mr. Mayne's suddenly-applied carrier as a special case.

Frequency modulation was discussed in a concise and elegant manner by van der Pol,[A] and more recently various methods of dealing with the subject were compared by the writers,[B] who found that the operational approach had significant advantages of conciseness and clarity; this approach made it possible to distinguish clearly between distortion and mere delay in the general case.

We also consider that Caqué's operational calculus (principally known through the work of Jeffreys) based on the operators

$$\mathrm{Qh}(t) = \int_0^t \mathrm{h}(\tau)d\tau \quad \mathrm{p} = \mathrm{Q}^{-1} \quad . \quad . \quad . \quad \text{(A)}$$

is significantly different from Heaviside's operational calculus (based on $\mathrm{p} \equiv d/dt$), and that the differences are to the disadvantage of the former. Eqn. (A) implies two processes: integration and selection of what has to be integrated. It is preferable to have these processes explicitly disentangled, and to write eqn. (A) in Heaviside's language:

$$\mathrm{Qh}(t) = \int_{-\infty}^t \mathrm{h}(\tau)\mathrm{H}(\tau)d\tau \quad . \quad . \quad . \quad . \quad \text{(B)}$$

where $\mathrm{H}(\tau)$ is Heaviside's unit step, zero for $\tau < 0$ and unity for $\tau > 0$, so that the integration sign is used only for integrating all of the intergrand that there is up to a particular time, t, and the integrand itself carries the information that it happens to be zero for t negative. When this is done, however, eqn. (B) makes clear that the operand of Q is not $\mathrm{h}(\tau)$ but $\mathrm{h}(\tau)\mathrm{H}(\tau)$. If the integrating operator p^{-1} has lower limit $-\infty$ as in eqn. (B) instead of zero as in eqn. (A), all algebraic manipulations of functions of p are reversible and can be carried out in any order, whereas the corresponding operations with the operator Q in eqn. (A) may or may not involve the values of $\mathrm{h}(\tau)$ and its derivatives when $\tau = 0$ according to the order in which they are carried out.

Mr. D. Q. Mayne (*in reply*): The monograph by Messrs. Head and Mayo[B] which I have read with interest, has a more general aim than that of mine, which was mainly concerned with suitable approximations for the modulation function and the application of these to a particular type of filter. No restrictions were placed on the modulation function of the input signal, and in fact the rather severe case of step modulation was considered, whereas Head and Mayo, by stipulating that the modulation function can be expanded in terms of its derivatives, derive further useful results in a simple and illuminating way. However, I fully concur with the opinion expressed in their monograph that the operational calculus has been discarded rather prematurely in favour of symbolic calculus on the mistaken ground of lack of rigour. Dalton (Reference 11 in my monograph) has shown how the

* MAYNE, D. Q.: Monograph No. 331 E, March, 1959 (see **106** C, p. 144).

operational calculus may be rigorously applied to ordinary and partial differential equations.

The first problem in the use of operational calculus is the choice of the primary operator. Jeffrey has used Q, defined in eqn. (A). The resultant equation in Q incorporates all the initial constants and can be manipulated as desired, provided only that the Q operator or any part of it is not interchanged in order with the operand which is a function of t. The final solution is obtained by expanding in powers of Q or by a partial-fraction expansion.

For convenience in setting up the operational equations $p \equiv 1/Q$ may be used ($p \neq d/dt$). Thus $Qf'(t) = f(t) - f(0)$, so that $pQf'(t) = f'(t) = pf(t) - pf(0)$. Higher derivatives will be correspondingly replaced by functions of p which include the values of the function and of the appropriate derivatives at $t = 0$, as is done in symbolic calculus. If p is understood as $D \equiv d/dt$, however, the comment made by Head and Mayo is true as Q and D are not commutative.

Head and Mayo, if I understand their contribution correctly, propose a different primary operator p, where $\frac{1}{p}h(t) = \int_{-\infty}^{t} h(\tau)\,.\,d\tau$.

Now $$D \times \frac{1}{p} f(t) = f(t); \quad \text{i.e. } D \times \frac{1}{p} = 1$$

Also $$\frac{1}{p} \times Df(t) = f(t) - f(-\infty)$$

i.e. $1/p \times D = 1$ only if $f(-\infty) = 0$. If this is so $1/p$ and D are commutative and we can replace D by p where we understand $p = d/dt$ and $1/p = \int_{-\infty}^{t} (\,)d\tau$. The use of this operator would seem to give a solution suitable for those cases where the forcing function can be regarded as a stationary time series. Expansion in positive powers of p is also permissible. The difference between the various approaches can be illustrated briefly.

Let $$v = iR + L\frac{di}{dt}$$

Using operator D,

$$i = \frac{1}{R + LD} \cdot v = C \exp(-\alpha t) + \exp(-\alpha t) \int \frac{v}{L} \exp(\alpha\tau) dt$$

$\alpha = R/L$, C = an arbitrary constant.

Using the operator $Q = \int_0^t (\,)d\tau$, $p = 1/Q$,

$$v = iR + L\,.\,p\,.\,i - L\,.\,p\,.\,i(0)$$

Therefore

$$i = \exp(-\alpha t) \int_0^t \frac{v}{L} \exp(\alpha\tau) d\tau - i(0) \exp(-\alpha t)$$

Using the operator $1/p = \int_{-\infty}^{t} (\,)d\tau$, $p = d/dt$

$$i = \frac{1}{R + Lp} v = \exp(-\alpha t) \int_{-\infty}^{t} \frac{v}{L} \exp(\alpha\tau) d\tau$$

The last two approaches are complementary, the former being an extension of the latter whereby v in the latter is split up into $v\,.\,H(-t) + v\,.\,H(t)$. The response to $v\,.\,H(-t)$ gives the terms involving the initial conditions in the former approach.

References

(A) VAN DER POL, B.: 'The Fundamental Principles of Frequency Modulation', *Journal I.E.E.*, 1946, **93**, Part III, p. 153.

(B) HEAD, J.W., and MAYO, C. G.: 'The Response of a Network to a Frequency-Modulated Input Voltage', *Proceedings I.E.E.*, Monograph No. 305 R, May, 1958 (**105** C, p. 509).

EXPLICIT FORM OF F.M. DISTORTION PRODUCTS WITH WHITE-NOISE MODULATION*

EXTENSION AND CORRECTION

By R. G. MEDHURST, B.Sc., and J. H. ROBERTS, B.Sc.

(*Communication received* 11*th May*, 1960.)

Monograph No. 352 presented formulae for the distortion/signal ratio in the top channel of a trunk radio system employing f.d.m. frequency modulation when the signal passes through a transmission network whose characteristics (amplitude and/or phase) are non-linear with frequency. The formulae apply when the amplitude and phase characteristics are expressed as power series in frequency (measured from the carrier frequency). This information is important for the design of amplifiers and demodulators.

The formulae given covered amplifier phase characteristics and discriminator amplitude characteristics up to sixth degree; amplifier amplitude characteristics and discriminator phase characteristics were, however, covered only up to fourth degree, which will not be adequate for many purposes. The data required to fill this gap have now been evaluated using the methods already described in the Monograph. It is seen from expression (7) of the Monograph that, by considering the same orders of distortion as in the earlier work, formulae are obtained giving the distortion due to amplifier amplitude and discriminator phase characteristics up to the seventh degree. During the course of this further analysis (which was again carried out with the help of an Hec 2M digital computer), programming and computational errors were discovered in the earlier work. These invalidate certain of the entries in Table 1 of Monograph 352; in consequence, all of the original formulae have been recomputed. Table 1 on pages 368 and 369 shows the complete set of formulae, including those already published in the Monograph, corrected where necessary, the symbols having the same significance as before.

Extensive checks have been applied to all the formulae shown in the Table, and they are now believed to be error-free. In a private communication, Dr. R. Magnusson, of Chalmers University of Technology, Götebog S, Sweden, has very kindly informed us of the results of his independent derivation (by a different method) of the formulae for amplifier phase and discriminator amplitude characteristics up to sixth degree, and also for amplifier amplitude and discriminator phase characteristics to the same degree. The former agree exactly with the formulae in the Table, as also do the latter with the portions of the present formulae remaining after equating the seventh-degree coefficients to zero.

The authors wish to thank Mr. F. W. Parker and Miss Christine Gregory of the G.E.C. Computer Service for carrying through the very extensive digital computer work.

* Monograph No. 352 E, January, 1960 (see 107 C, p. 120).

This note is a communication from the Staff of the Research Laboratories of the General Electric Company Limited, Wembley, England.

Table 1

DISTORTION/SIGNAL (VOLTAGE RATIO) IN THE TOP CHANNEL (WHITE-NOISE FREQUENCY MODULATION)

Order of distortion	Phase-modulation distortion due to amplifier characteristic	Amplitude-modulation distortion due to discriminator characteristic
Second	*Amplitude characteristic* $\frac{\omega_\Delta \hat{\omega}_m^2}{\sqrt{2}}\left\{\left(\frac{b_7}{\omega_c^7}\right)^2\left[\frac{2\,233}{180}\hat{\omega}_m^8 + \frac{2\,429}{4}\hat{\omega}_m^6\omega_\Delta^2 + \frac{36\,309}{4}\hat{\omega}_m^4\omega_\Delta^4 + \frac{77\,175}{2}\hat{\omega}_m^2\omega_\Delta^6 + \frac{99\,225}{2}\omega_\Delta^8\right]\right.$ $+\left(\frac{b_5}{\omega_c^5}\right)^2\left[\frac{35}{4}\hat{\omega}_m^4 + 125\hat{\omega}_m^2\omega_\Delta^2 + 450\omega_\Delta^4\right]$ $+\frac{9}{2}\left(\frac{b_3}{\omega_c^3}\right)^2 + \left(\frac{b_5}{\omega_c^5}\right)\left(\frac{b_7}{\omega_c^7}\right)\left[\frac{83}{4}\hat{\omega}_m^6 + \frac{1\,981}{3}\hat{\omega}_m^4\omega_\Delta^2 + \frac{9\,975}{2}\hat{\omega}_m^2\omega_\Delta^4 + 9\,450\omega_\Delta^6\right]$ $+\left(\frac{b_3}{\omega_c^3}\right)\left(\frac{b_7}{\omega_c^7}\right)\left[\frac{147}{10}\hat{\omega}_m^4 + \frac{735}{2}\hat{\omega}_m^2\omega_\Delta^2 + 945\omega_\Delta^4\right]$ $\left.+\left(\frac{b_3}{\omega_c^3}\right)\left(\frac{b_5}{\omega_c^5}\right)\left[\frac{25}{2}\hat{\omega}_m^2 + 90\omega_\Delta^2\right]\right\}^{1/2}$	*Amplitude characteristic* $\frac{1}{\sqrt{2}}\frac{\omega_c}{B_1}\omega_\Delta\left\{\left(\frac{b_6'}{\omega_c^6}\right)^2\left[\frac{13\,387}{1\,260}\hat{\omega}_m^8\omega_\Delta^2 + \frac{6\,263}{21}\hat{\omega}_m^6 + 2\,526\hat{\omega}_m^4\omega_\Delta^4\right.\right.$ $\left.+5\,850\hat{\omega}_m^2\omega_\Delta^6 + 4\,050\omega_\Delta^8\right] + \left(\frac{b_4'}{\omega_c^4}\right)^2\left[\frac{101}{15}\hat{\omega}_m^4 + 44\hat{\omega}_m^2\omega_\Delta^2 + 72\omega_\Delta^4\right] + 2\left(\frac{b_2'}{\omega_c^2}\right)^2$ $+\left(\frac{b_2'}{\omega_c^2}\right)\left(\frac{b_6'}{\omega_c^6}\right)\left[\frac{137}{15}\hat{\omega}_m^4 + 130\hat{\omega}_m^2\omega_\Delta^2 + 180\omega_\Delta^4\right] + \left(\frac{b_2'}{\omega_c^2}\right)\left(\frac{b_4'}{\omega_c^4}\right)\left[\frac{22}{3}\hat{\omega}_m^2 + 24\omega_\Delta^2\right]$ $\left.+\left(\frac{b_4'}{\omega_c^4}\right)\left(\frac{b_6'}{\omega_c^6}\right)\left[\frac{1\,768}{105}\hat{\omega}_m^6 + \frac{4\,402}{15}\hat{\omega}_m^4\omega_\Delta^2 + 1\,110\hat{\omega}_m^2\omega_\Delta^4 + 1\,080\omega_\Delta^6\right]\right\}^{1/2}$
Third	$2\omega_\Delta^2\hat{\omega}_m^2\left\{\left(\frac{b_6}{\omega_c^6}\right)^2[20\hat{\omega}_m^4 + 225\hat{\omega}_m^2\omega_\Delta^2 + 675\omega_\Delta^4] + 3\left(\frac{b_4}{\omega_c^4}\right)^2\right.$ $\left.+\left(\frac{b_4}{\omega_c^4}\right)\left(\frac{b_6}{\omega_c^6}\right)[15\hat{\omega}_m^2 + 90\omega_\Delta^2]\right\}^{1/2}$	$\frac{\omega_c}{B_1}\omega_\Delta^2\left\{\left(\frac{b_5'}{\omega_c^5}\right)^2\left[\frac{305}{9}\hat{\omega}_m^4 + 200\hat{\omega}_m^2\omega_\Delta^2 + 300\omega_\Delta^4\right] + 3\left(\frac{b_3'}{\omega_c^3}\right)^2\right.$ $\left.+\left(\frac{b_3'}{\omega_c^3}\right)\left(\frac{b_5'}{\omega_c^5}\right)[20\hat{\omega}_m^2 + 60\omega_\Delta^2]\right\}^{1/2}$
Fourth	$\frac{\sqrt{2}}{8}\omega_\Delta^3\hat{\omega}_m^2\left\{\left(\frac{b_7}{\omega_c^7}\right)^2\left[\frac{156\,345}{4}\hat{\omega}_m^4 + 386\,610\hat{\omega}_m^2\omega_\Delta^2 + 1\,014\,300\omega_\Delta^4\right]\right.$ $\left.+2\,300\left(\frac{b_5}{\omega_c^5}\right)^2 + \left(\frac{b_5}{\omega_c^5}\right)\left(\frac{b_7}{\omega_c^7}\right)[18\,410\hat{\omega}_m^2 + 96\,600\omega_\Delta^2]\right\}^{1/2}$	$\frac{\sqrt{2}}{4}\frac{\omega_c}{B_1}\omega_\Delta^3\left\{\left(\frac{b_6'}{\omega_c^6}\right)^2\left[\frac{75\,255}{28}\hat{\omega}_m^4 + 14\,790\hat{\omega}_m^2\omega_\Delta^2 + 20\,700\omega_\Delta^4\right]\right.$ $\left.+92\left(\frac{b_4'}{\omega_c^4}\right)^2 + \left(\frac{b_4'}{\omega_c^4}\right)\left(\frac{b_6'}{\omega_c^6}\right)[986\hat{\omega}_m^2 + 2\,760\omega_\Delta^2]\right\}^{1/2}$
Fifth	$3\sqrt{(55)}\omega_\Delta^4\hat{\omega}_m^2\left(\frac{b_6}{\omega_c^6}\right)$	$\sqrt{(55)}\frac{\omega_c}{B_1}\omega_\Delta^4\left(\frac{b_5'}{\omega_c^5}\right)$
Sixth	$\frac{7}{8}\sqrt{(5\,046)}\omega_\Delta^5\hat{\omega}_m^2\left(\frac{b_7}{\omega_c^7}\right)$	$\frac{1}{4}\sqrt{(5\,046)}\frac{\omega_c}{B_1}\omega_\Delta^5\left(\frac{b_6'}{\omega_c^6}\right)$

	Phase characteristic	*Phase characteristic*
Second	$\frac{\omega_\Delta \hat{\omega}_m}{\sqrt{2}}\left\{\left(\frac{a_6}{\omega_c^6}\right)^2\left[\frac{13\,387}{1\,260}\hat{\omega}_m^8+\frac{6\,263}{21}\hat{\omega}_m^6\omega_\Delta^2+2\,526\hat{\omega}_m^4\omega_\Delta^4+5\,850\hat{\omega}_m^2\omega_\Delta^6+4\,050\omega_\Delta^8\right]\right.$ $+\left(\frac{a_4}{\omega_c^4}\right)^2\left[\frac{101}{15}\hat{\omega}_m^4+44\hat{\omega}_m^2\omega_\Delta^2+72\omega_\Delta^4\right]+2\left(\frac{a_2}{\omega_c^2}\right)^2$ $+\left(\frac{a_2}{\omega_c^2}\right)\left(\frac{a_6}{\omega_c^6}\right)\left[\frac{137}{15}\hat{\omega}_m^4+130\hat{\omega}_m^2\omega_\Delta^2+180\omega_\Delta^4\right]+\left(\frac{a_2}{\omega_c^2}\right)\left(\frac{a_4}{\omega_c^4}\right)\left[\frac{22}{3}\hat{\omega}_m^2+24\omega_\Delta^2\right]$ $\left.+\left(\frac{a_4}{\omega_c^4}\right)\left(\frac{a_6}{\omega_c^6}\right)\left[\frac{1\,768}{105}\hat{\omega}_m^6+\frac{4\,402}{15}\hat{\omega}_m^4\omega_\Delta^2+1\,110\hat{\omega}_m^2\omega_\Delta^4+1\,080\omega_\Delta^6\right]\right\}^{1/2}$	$\frac{1}{\sqrt{2}}\frac{\omega_c\omega_\Delta\hat{\omega}_m}{B_1}\left\{\left(\frac{c_7'}{\omega_c^7}\right)^2\left[\frac{2\,233}{180}\hat{\omega}_m^8+\frac{2\,429}{4}\hat{\omega}_m^6\omega_\Delta^2+\frac{36\,309}{4}\hat{\omega}_m^4\omega_\Delta^4+\frac{77\,175}{2}\hat{\omega}_m^2\omega_\Delta^6\right.\right.$ $+\frac{99\,225}{2}\omega_\Delta^8\left]+\left(\frac{c_5'}{\omega_c^5}\right)^2\left[\frac{35}{4}\hat{\omega}_m^4+125\hat{\omega}_m^2\omega_\Delta^2+450\omega_\Delta^4\right]\right.$ $+\frac{9}{2}\left(\frac{c_3'}{\omega_c^3}\right)^2+\left(\frac{c_5'}{\omega_c^5}\right)\left(\frac{c_7'}{\omega_c^7}\right)\left[\frac{83}{4}\hat{\omega}_m^6+\frac{1\,981}{3}\hat{\omega}_m^4\omega_\Delta^2+\frac{9\,975}{2}\hat{\omega}_m^2\omega_\Delta^4+9\,450\omega_\Delta^6\right]$ $+\left(\frac{c_3'}{\omega_c^3}\right)\left(\frac{c_7'}{\omega_c^7}\right)\left[\frac{147}{10}\hat{\omega}_m^4+\frac{735}{2}\hat{\omega}_m^2\omega_\Delta^2+945\omega_\Delta^4\right]$ $\left.\left.+\left(\frac{c_3'}{\omega_c^3}\right)\left(\frac{c_5'}{\omega_c^5}\right)\left[\frac{25}{2}\hat{\omega}_m^2+90\omega_\Delta^2\right]\right\}^{1/2}$
Third	$\omega_\Delta^2\hat{\omega}_m\left\{\left(\frac{a_5}{\omega_c^5}\right)^2\left[\frac{305}{9}\hat{\omega}_m^4+200\hat{\omega}_m^2\omega_\Delta^2+300\omega_\Delta^4\right]+3\left(\frac{a_3}{\omega_c^3}\right)^2\right.$ $\left.+\left(\frac{a_3}{\omega_c^3}\right)\left(\frac{a_5}{\omega_c^5}\right)[20\hat{\omega}_m^2+60\omega_\Delta^2]\right\}^{1/2}$	$2\frac{\omega_c}{B_1}\omega_\Delta^2\hat{\omega}_m\left\{\left(\frac{c_6'}{\omega_c^6}\right)^2[20\hat{\omega}_m^4+225\omega_m^2\omega_\Delta^2+675\omega_\Delta^4]\right.$ $\left.+3\left(\frac{c_4'}{\omega_c^4}\right)^2+\left(\frac{c_4'}{\omega_c^4}\right)\left(\frac{c_6'}{\omega_c^6}\right)[15\hat{\omega}_m^2+90\omega_\Delta^2]\right\}^{1/2}$
Fourth	$\frac{\sqrt{2}}{4}\omega_\Delta^3\hat{\omega}_m\left\{\left(\frac{a_6}{\omega_c^6}\right)^2\left[\frac{75\,255}{28}\hat{\omega}_m^4+14\,790\hat{\omega}_m^2\omega_\Delta^2+20\,700\omega_\Delta^4\right]\right.$ $\left.+92\left(\frac{a_4}{\omega_c^4}\right)^2+\left(\frac{a_4}{\omega_c^4}\right)\left(\frac{a_6}{\omega_c^6}\right)[986\hat{\omega}_m^2+2\,760\omega_\Delta^2]\right\}^{1/2}$	$\frac{\sqrt{2}}{8}\frac{\omega_c}{B_1}\omega_\Delta^3\omega_m\left\{\left(\frac{c_7'}{\omega_c^7}\right)^2\left[\frac{156\,345}{4}\hat{\omega}_m^4+386\,610\hat{\omega}_m^2\omega_\Delta^2+1\,014\,300\omega_\Delta^4\right]\right.$ $\left.+2\,300\left(\frac{c_5'}{\omega_c^5}\right)^2+\left(\frac{c_5'}{\omega_c^5}\right)\left(\frac{c_7'}{\omega_c^7}\right)[18\,410\hat{\omega}_m^2+96\,600\omega_\Delta^2]\right\}^{1/2}$
Fifth	$\sqrt{(55)}\omega_\Delta^4\hat{\omega}_m\left(\frac{a_5}{\omega_c^5}\right)$	$3\sqrt{(55)}\frac{\omega_c}{B_1}\omega_\Delta^4\hat{\omega}_m\left(\frac{c_6'}{\omega_c^6}\right)$
Sixth	$\frac{1}{4}\sqrt{(5\,046)}\omega_\Delta^5\hat{\omega}_m\left(\frac{a_6}{\omega_c^6}\right)$	$\frac{7}{8}\sqrt{(5\,046)}\frac{\omega_c}{B_1}\omega_\Delta^5\hat{\omega}_m\left(\frac{c_7'}{\omega_c^7}\right)$

INDEX TO VOLUME 107, PART C

1960

ABBREVIATIONS

(P)—Paper. (D)—Discussion.

UNWIN BROTHERS LIMITED, WOKING AND LONDON

PROCEEDINGS OF THE INSTITUTION OF ELECTRICAL ENGINEERS

PART C—MONOGRAPHS, SEPTEMBER 1960

CONTENTS

Declaration on Fair Copying.—Within the terms of the Royal Society's Declaration on Fair Copying, to which The Institution subscribes, material may be copied from issues of the *Proceedings* (prior to 1949, the *Journal*) *which are out of print and from which reprints are not available.* The terms of the Declaration and particulars of a Photoprint Service afforded by the Science Museum Library, London, are published in the *Journal* from time to time.

Bibliographical References.—It is requested that bibliographical reference to an Institution paper should always include the serial number of the paper and the month and year of publication, which will be found at the top right-hand corner of the first page of the paper. This information should precede the reference to the Volume and Part.

Example.—Smith, J.: 'Reflections from the Ionosphere', *Proceedings I.E.E.*, Paper No. 4091 R, December, 1954 (102 B, p. 1234).

Published by The Institution, Savoy Place, London, W.C.2. *Telephone:* COVent Garden 1871. *Telegrams:* 'Voltampere, Phone, London.'
Printed by Unwin Brothers Limited, Woking and London.